



UNIVERSITÀ DEGLI STUDI
DI TRENTO

University of Trento - DICAM

Department of Civil, Mechanical and Environmental Engineering

**Tracing bedload transport in Alpine mountain streams by means
of PIT-tagged particles: interplay between sediment supply and
hydro-meteorological forcing**

Ph.D. Candidate

Matteo Toro

Supervisor

Prof. Luigi Fraccarollo

Co-supervisor

Prof. Francesco Brardinoni

Abstract

Conceptual models of first-order controls governing river channel dynamics in mountain streams have been rarely tested in the field. In this Ph.D. thesis we examine the effects of hydro-meteorological forcing and sediment supply on the bedload transport dynamics of mountain streams. To this purpose we select three step-pool mountain streams that share identical granitic lithology, but exhibit contrasting sediment supply and hydro-climatic conditions. The three study sites, which are located in Trentino, Eastern Italian Alps, include the Ussaia Creek (2.3 km²) in Val di Sole, and the Grigno and Tolvà Creeks (7 km²) in Valsugana. The former is characterized by high, sand-rich sediment supply delivered by some 20 m-thick glacial deposits. The latter two, which flow through glacially carved bedrock terrain, are disconnected from colluvial sediment inputs so that sediment sources are limited to channel banks and bars during high flows. Mean annual precipitation is respectively 844 mm in Ussaia Creek and 1511 mm in Grigno and Tolvà Creeks. All study streams experience, to variable extents, snowmelt and rainfall-induced bedload transporting flows.

To estimate quantitatively the effects and the interactions associated with sediment supply and hydro-meteorological forcing, we monitor precipitation and atmospheric temperature. Hydrological levels at instrumented sections are recorded via pressure transducers. Bedload transport is monitored by tagging and tracking 632 stones (b-axis: 30 to 131 mm; weight 88-4004 g). The tracking of these PIT-tagged tracers was conducted from December 2013 to December 2015 by means of an RFID portable pole antenna. Cumulatively, a total of 16, 11 and 19 bedload events were monitored respectively at Grigno, Tolvà and Ussaia Creek. We measured displacement lengths occurred during inter-survey periods, induced by peak flows associated to snowmelt, rainfall or a combination of the two (mixed-type). Active channel depth was evaluated via direct digging tests at the three study sites finding a median burial depth of 0.1 m at Grigno and Tolvà Creeks, and 0.25 m at Ussaia Creek; recent findings (Schneider et al., 2014), show that ordinary bedload events of boulder-bed streams in the Alps, active layer thickness is comprised within 0.01 and 0.22 m; Houbrechts et al. (2012) demonstrated that in mountain streams the active layer thickness is lower than D_{50} . The active layer width was evaluated via orthophoto maps obtained through Structure-from-Motion. To characterize the streambed roughness and the channel slope we conducted topographic and morphologic surveys. To evaluate event-based bedload sediment volumes we applied the virtual velocity approach (Haschenburger and Church, 1998). In particular, to assess the minimum discharge able to entrain clasts, determining the virtual transport duration of each tracer weight class, we used the competence flow method. In order to evaluate the uncertainty associated with methodology that has been customarily applied in the literature, we performed a sensitivity analysis of the evaluation of bedload transfer proposing three scenarios varying the assumptions that (i) virtual velocities are normally distributed and therefore justifying the adoption of median virtual velocities instead of the average virtual velocity, (ii) that active channel width is constant in time, hence replacing bankfull width with site-specific active widths, evaluated on the base of PIT-tagged particles displacements.

The monitoring year 2014 was characterized by a total annual precipitation two times larger than the historical mean, associated to a prolonged snowmelt and to heavy storm front events. By contrast, in 2015 we observed no snowmelt and no precipitation occurred in November and December. At Grigno and Tolvà Creeks, the majority of sediment is transported during autumn storm fronts (median travel distance: 30 m) and secondarily by summer convective storms (median travel distance: 4.5 m). At Ussaia Creek, snowmelt-related events induced 17% of the observed displacement lengths (median travel distance: 2 m), but the primary source of sediment transport is associated chiefly with prolonged storm fronts (median travel

distance: 200 m). The mass of tracers does not affect virtual velocities, that are instead affected by seasonal distribution of hydro-meteorological events. In fact, at Grigno and Tolvà Creeks we observe a stratification of velocities according to hydro-meteorological forcing, with the largest values observed during rainfall season, commonly associated to highest values of peak discharge. Variability of virtual velocities at Ussaia Creek does not depend on seasonal hydro-climatic forcing and peak discharge values, with distributions of virtual velocities partly overlapping among snowmelt- and rainfall-related events. The seasonal pattern is translated to bedload transport volumes, with Ussaia Creek transporting by the end of the snowmelt period in 2014, three times more sediment than Grigno Creek. This is testified by a prolonged autumn rainfall that hit simultaneously the study sites, caused a debris-flow that transported 1084 m³ at Ussaia Creek, a much larger quantity compared to the 32.2 m³ evaluated at Grigno and the 62.5 m³ at Tolvà Creek.

The definition of rainfall intensity-duration thresholds of precipitation events triggering bedload at our sites shows that transport-limited systems (i.e., Ussaia Creek) result sensitive to precipitation inputs characterized by low rainfall intensity (below 5 mm hr⁻¹) and large duration. Conversely, supply-limited systems (i.e., Grigno and Tolvà Creeks) exhibit armoured beds and interlocked, resilient structures that limit entrainment processes, mobilizing bedload only in response to short-duration/high-intensity rainfall (10 mm hr⁻¹). These channels preserve their morphological structure even under high flow events, triggering sediment transport processes limitedly to peaked storm hydrographs.

In the present study we show that the variability in bedload transport among different study reaches is linked to sediment supply conditions and to peculiar hydro-climatic settings. An additional study site characterized by dry conditions, Strimm Creek (Alto Adige, Italy), allows us to obtain a latitudinal transect from dry to wet conditions across the Eastern Italian Alps. By monitoring tracer displacements from 2011 to 2015 at this formerly-glaciated, high-elevation mountain basin, we observe that limited sediment-supply conditions exert a strong control on bedload, chiefly triggered by snowmelt events that account for 73% of the overall travel distances. At Grigno and Tolvà Creeks, also characterized by limited sediment supply, transport is dominated by rainfall events, responsible of driving 95% of the overall travel distances. Sediment availability at Ussaia Creek is responsible for triggering the largest observed bedload events, associated to prolonged autumn precipitation and secondarily to snowmelt events.

Table of Contents

Abstract	i
Table of Contents	iii
List of Tables	v
List of Figures	vii
1. Introduction	1
1.1 <u>Concise literature review on bedload tracers</u>	4
1.2 <u>Objectives</u>	7
2. Study area	11
2.1 <u>Geo-climatic setting of the study basins</u>	11
2.1.1 Grigno-Tolvà basin	11
2.1.2 Ussaia basin	17
2.1.3 Strimm basin	20
2.2 <u>Monitoring sites</u>	22
2.2.1 Grigno-Tolvà Creeks	22
2.2.2 Ussaia Creek	26
2.2.3 Strimm Creek	28
3. Data collection and methods	29
3.1 <u>Boundary conditions: reach scale bed topography</u>	29
3.1.1 Channel bed topography	29
3.1.2 Structure from Motion	32
3.1.3 Channel cross sections	36
3.2 <u>Downstream hydraulic geometry</u>	37
3.3 <u>Grain size distribution</u>	39
3.4 <u>Water discharge</u>	39
3.5 <u>Precipitation and atmospheric temperature</u>	42
3.6 <u>Bedload monitoring</u>	43
3.7 <u>Tracers' virtual velocities for constraining bedload volumes</u>	51
3.8 <u>Hydro-meteorological forcing and magnitude of bedload volumes transported</u>	53
4. Results	55
4.1 <u>Channel boundary conditions</u>	55
4.1.1 Channel bed topography of monitored reaches	55
4.1.1.1 Longitudinal profiles	55
4.1.1.2 Cross sections	65
4.1.2 <u>Downstream hydraulic geometry</u>	69
4.1.3 <u>Grain size distribution</u>	71
4.2 <u>Hydro-meteorological forcing</u>	75
4.2.1 Grigno Creek	75
4.2.2 Tolvà Creek	79
4.2.3 Ussaia Creek	82

4.3 <u>Travel distances of PIT-tagged stones</u>	90
4.4 <u>Tracers' virtual velocities</u>	117
4.5 <u>Distribution of tracers' travel distances and virtual velocities</u>	139
4.5.1 Distribution of tracers' travel distances	139
4.5.2 Distribution of tracers' virtual velocities	146
4.6 <u>Determination of active layer depth and active channel width</u>	153
4.7 <u>Evaluation of bedload volumes and sensitivity analysis</u>	157
4.8 <u>Linking hydro-meteorological forcing with bedload transport: rainfall intensity-duration thresholds for bedload events</u>	166
5. Discussion	173
5.1 <u>The effect of sediment supply</u>	173
5.2 <u>Comparison of seasonality of bedload transport across monitoring sites</u>	176
5.3 <u>Thresholds of rainfall intensity-duration</u>	183
5.4 <u>Timescales of investigation</u>	185
5.5 <u>Latitudinal transect</u>	192
6. Conclusions	194
Bibliography	197
Appendix	204

List of Tables

Table 1.1	Compilation of previous studies that have used PIT-tagged particles for investigating bedload sediment dynamics	5
Table 3.1	Specifics of longitudinal profile surveys at Ussaia Creek	30
Table 3.2	Specifics of SfM surveys. Ground Control Points (GCPs) are acquired by means of a total station	33
Table 3.3	Specifics of the channel cross sectional surveys	36
Table 3.4	Specifics of DHG section surveyed for each monitoring site	37
Table 3.5	Specifics of the meteorological stations	42
Table 3.6	Grain size classes and number of elements for each class of released cohorts in the monitored sites	47
Table 3.7	Summary information on tracer clasts	48
Table 3.8	Weight categories (g) of the tracer clasts	48
Table 4.1.1	Values of slope of the surveyed thalweg of all the studied reaches	62
Table 4.1.2	Descriptive statistic of pool depth and step height values analyzed at all the sites	64
Table 4.1.3	Comparative distributions of D_{16} , D_{50} and D_{84} at each monitored site	74
Table 4.3.1	List of hydro-meteorological events comparable simultaneously on the three monitoring sites	100
Table 4.3.2	Rainfall characteristics of July 26, 2014 event	101
Table 4.3.3	Rainfall characteristics of August 13, 2014 event	102
Table 4.3.4	Rainfall characteristics of October 13 th 2014 event	103
Table 4.3.5	Rainfall characteristics of November 4-8, 2014 event	104
Table 4.3.6	Rainfall characteristics of May 20, 2015 event	106
Table 4.3.7	Rainfall characteristics of September 14, 2015 event	106
Table 4.3.8	Rainfall characteristics of October 13-16, 2015 event	108
Table 4.4.1	Event dates and peak discharge for which no clasts displacement has been observed at Grigno, Tolvà and Ussaia Creek	117
Table 4.4.2	Event dates and peak discharge for which clasts displacement has been observed at Grigno Creek	118
Table 4.4.3	Event dates and peak discharge for which clasts displacement has been observed at Tolvà Creek	119
Table 4.4.4	Event dates and peak discharge for which clasts displacement has been observed at Ussaia Creek	119
Table 4.4.5	Type of forcing input for bedload events and related virtual transport duration at Grigno Creek	122
Table 4.4.6	Type of forcing input for bedload events and related virtual transport duration at Tolvà Creek	123
Table 4.4.7	Type of forcing input for bedload events and related virtual transport duration at Ussaia Creek	123
Table 4.4.8	Event dates and peak discharge for which clasts displacement has been observed at Strimm Creek	135
Table 4.4.9	Type of forcing input for bedload events and related virtual transport duration at Strimm Creek	136
Table 4.5.1	Number of observations, mean and median travel distances , peak discharge and	139

	maximum rainfall intensity at Grigno Creek for each survey	
Table 4.5.2	Number of observations, mean and median travel distances, peak discharge and maximum rainfall intensity at Tolvà Creek for each survey	140
Table 4.5.3	Number of observations, mean and median travel distances, peak discharge and maximum rainfall intensity at Ussaia Creek for each survey	140
Table 4.5.4	Number of observations, mean and median tracers' virtual velocities, peak discharge and maximum rainfall intensity at Grigno Creek for each survey	146
Table 4.5.5	Number of observations, mean and median tracers' virtual velocities, peak discharge and maximum rainfall intensity at Tolvà Creek for each survey	146
Table 4.5.6	Number of observations, mean and median tracers' virtual velocities, peak discharge and maximum rainfall intensity at Ussaia Creek for each survey	147
Table 4.6.1	Digging tests conducted on buried tracers for each site	155
Table 4.6.2	Active channel width evaluated for different scenarios	155
Table 5.1	Type of forcing input for bedload events and related virtual transport duration at Grigno Creek	177
Table 5.2	Type of forcing input for bedload events and related virtual transport duration at Ussaia Creek	178
Table 5.3	Regression equations fitted through the rainfall events and all the events combined	183
Table 5.4	Mean and median values of the travel distances (Td) derived from the actual surveys and from the seasonally lumped scenarios at the three study sites	186
Table 5.5	Mean and median values of the virtual velocities (Vv) derived from the actual surveys and from the seasonally lumped scenarios at the three study sites	187
Table A4.2.1	Characteristics of hydro-meteorological forcing events recorded at the Grigno Creek monitoring site and Malga Sorgazza weather station in 2014	266
Table A4.2.2	Characteristics of hydro-meteorological forcing events recorded at the Grigno Creek monitoring site and Malga Sorgazza weather station in 2015	266
Table A4.2.3	Characteristics of hydro-meteorological forcing events recorded at the Tolvà Creek monitoring site and Passo Brocon weather station in 2014	267
Table A4.2.4	Characteristics of hydro-meteorological forcing events recorded at the Tolvà Creek monitoring site and Passo Brocon weather station in 2015	268
Table A4.2.5	Characteristics of hydro-meteorological forcing events recorded at the Ussaia Creek monitoring site and Mezzana weather station in 2013	268
Table A4.2.6	Characteristics of hydro-meteorological forcing events recorded at the Ussaia Creek monitoring site and Mezzana weather station in 2014	269
Table A4.2.7	Characteristics of hydro-meteorological forcing events recorded at the Ussaia Creek monitoring site and Mezzana weather station in 2013	270
Table A4.3.1	Summary information on PIT surveys	270
Table A4.3.2	Recovery rates per survey at Grigno Creek	272
Table A4.3.3	Recovery rates per survey at Tolvà Creek	273
Table A4.3.4	Recovery rates per survey at Ussaia Creek	274
Table A4.3.5	Recovery rates per survey at Strimm Creek	276

List of Figures

Figure 1.1	Factors controlling the reach scale variability in the fluvial system, divided into upstream, downstream and local controls (from Kondolf and Piegay, 2002)	2
Figure 1.2	Distribution of monitored sites within the Trentino-Alto Adige region, with climatic diagrams referring to the study sites (from www.clima-alpino.eu , modified)	9
Figure 2.1	The Grigno-Tolvà Creek basin	13
Figure 2.2	Main geo-lithological units of the Grigno-Tolvà Creeks basin	14
Figure 2.3	Tectonic setting of the Valsugana – Cima d’Asta area	16
Figure 2.4	Localization of the Val di Sole (blue square)	17
Figure 2.5	Geological map of the area surrounding the Ussaia Creek watershed (from CARG sheet n. 42 “Malè”, modified)	19
Figure 2.6	Location of the Venosta Valley and its geographic borders	20
Figure 2.7	The Grigno Creek basin and the monitoring setup	22
Figure 2.8	a) Digital terrain model of the watershed; b) longitudinal profiles along the Grigno Creek valley	22
Figure 2.9	Longitudinal profile of the upper portion of the Grigno Creek	23
Figure 2.10	a) Digital terrain model of the watershed; b) longitudinal profiles along the Tolvà Creek valley	23
Figure 2.11	Longitudinal profile of the upper portion of the Tolvà Creek	24
Figure 2.12	Representative morphological structures in the Grigno Creek (plates a-b-c-d) and Tolvà Creek (plates e-f-g-h)	24
Figure 2.13	The Grigno Creek immediately downstream of the confluence with Tolvà creeks, a) after the large flood of November 1966; b) today	25
Figure 2.14	a) Digital terrain model of the watershed; b) longitudinal profile along the Ussaia mainstem	26
Figure 2.15	a) The thick glacigenic blanket acting a source of material, and the Ussaia Creek flowing at the footsteps of the talus; b) monitored reach of the Ussaia Creek: a typical step-pool sequence, characterized by highly unstability of the steps, caused by the abundant sandy fraction, visible on the lateral deposit	27
Figure 2.16	Longitudinal profile along the Strimm Creek	28
Figure 3.1	(a) Example of planar projection of collected points for the 2014/2015 surveys; (b) example of projection on the vertical plane of collected points along downstream distance for the 2014/2015 surveys	31
Figure 3.2	Points used as test for Z elevation values of the constructed DEM (example from Grigno Creek)	32
Figure 3.3	Examples of SfM-derived orthophoto mosaic in: (a) the Grigno Creek at low flow and (b) the Ussaia Creek in dry conditions. Blue arrow indicate direction of water flow	34
Figure 3.4	Example of delineation of active channel width in the Grigno Creek: (a) at bankfull flow; and (b) at low flow conditions	35
Figure 3.5	Example of cross section surveyed at Ussaia site	36
Figure 3.6	Distribution in the Grigno basin of the cross sections surveyed for downstream hydraulic geometry (UG: Upper Grigno Creek; LG: Lower Grigno Creek; T: Tolvà Creek)	38
Figure 3.7	Example of grain size distribution at Grigno site. (a) Histogram of sampled pebbles; (b) cumulative percentages curve for the same sample	39
Figure 3.8	Stage-discharge curve constructed at the Grigno Creek monitoring site. The relations for the other monitoring sites are reported in Appendix 3.1. (Q = water	40

	discharge (l s^{-1}), P = hydrostatic pressure (bar))	
Figure 3.9	Recorded water levels for significant flood events projected onto cross sections equipped with pressure sensor at a) Grigno, b) Tolvà, c) Ussaia, d) Strimm Creek	40
Figure 3.10	Bed surface and tracer cumulative grain size distribution in (a) Grigno, (b) Tolvà, (c) Ussaia, (d) Strimm Creek	45
Figure 3.11	Distribution of b-axis of sampled keystone (n , number of observations)	45
Figure 3.12	Passive Integrated Transponders consisting of a glass-encapsulated copper coil, inserted into drilled stones to allow detection after floods	46
Figure 3.13	Release of tracers at Ussaia site: ribs are spaced 2 m apart and each row spans across the entire section	46
Figure 3.14	Mobile antenna manufactured by Oregon RFID by means of which bedload monitoring surveys have been conducted. In the picture is visible the palmtop where clasts ID are displayed (yellow device), and the grey backpack, where the portable reader/datalogger is located	49
Figure 3.15	Flowchart schematizing the flow competence method adopted to individuate entrainment threshold discharges for each weight classes and determine the values of bedload transfer for each hydro-meteorological event. In brackets are reported the sections of this thesis referring to the listed topic	51
Figure 3.16	Flowchart illustrating the methods adopted to individuate hydro-meteorological thresholds for constraining bedload transported volumes	54
Figure 4.1.1	Plan view of the surveyed points along the thalweg at a) Grigno Creek, b) Tolvà Creek, and c) Ussaia Creek from 2012 to 2015. Major changes at Ussaia Creek are recognizable between each inter-survey period	57
Figure 4.1.2	a) Longitudinal profile of Grigno Creek, illustrating the main morphologies at reach scale; b) boulder-cascade in the upstream portion of the reach; c) overview of the boulder-cascade and plane bed characterizing the central-lower portion of the study reach. On the left is visible an erratic boulder; d) plane bed and channel widening 50 m downstream the end of the monitored reach	58
Figure 4.1.3	a) Longitudinal profile of Tolvà Creek, illustrating the main morphologies at reach scale; b) the distinctive boulder-cascade present at Tolvà Creek, in the central portion of the reach; c) steep cascade 30 m downstream the monitored channel reach	59
Figure 4.1.4	a) Longitudinal profiles of Ussaia Creek for the period 2012-2015. Pictures showing changes occurred after the debris flow of November 5 th , 2014: the upstream portion of the monitored reach as of b) July 27 th , 2014, c) March 28 th , 2015. Cascade reach in the central portion as of d) July 27 th , 2014, e) March 28 th , 2015	61
Figure 4.1.5	Longitudinal profile of Strimm Creek surveyed in 2012	62
Figure 4.1.6	Percent frequency distribution of step height and pool depth along the monitored portion of a) Grigno Creek, b) Tolvà Creek, c) Ussaia Creek, d) Strimm Creek	64
Figure 4.1.7	Typical cross sections surveyed at Grigno Creek: a) boulder cascade in the upstream reach, b) plane bed in the lower portion	65
Figure 4.1.8	Cross sections surveyed at Tolvà Creek: a) boulder cascade in the central reach, b) deep lateral pool in the lower portion; note the presence of a super-elevated, secondary channel on the left, separated from the rest of the channel by a large boulder plunging directly into the pool	66
Figure 4.1.9	Cross sections surveyed at Ussaia Creek: a) reach characterized by the presence of rapids, separated in the center by a stable, vegetated island (survey 2013), b) the same reach, surveyed in 2015, after the 5 November 2014 debris flow. Channel thalweg migrated rightwards	67

Figure 4.1.10	Cross sections surveyed at Strimm Creek: a) reach characterized by the presence of a well confined pool, b) Typical example of a large section at Strimm Creek, with the presence of a central bar, not vegetated	68
Figure 4.1.11	Bankfull width (median) as a function of contributing area for Grigno and Tolvà Creeks	69
Figure 4.1.12	Bankfull width (median) as a function of contributing area for Grigno and Tolvà Creeks	70
Figure 4.1.13	Wetted area (median) as a function of contributing area for Grigno and Tolvà Creeks	70
Figure 4.1.14	Bed surface non-cumulative grain size distribution at a) Grigno Creek, b) Tolvà Creek, c) Ussaia Creek, d) Upper and Lower Strimm Creek.	73
Figure 4.1.15	Comparative bed surface cumulative grain size distribution at all the sites	74
Figure 4.2.1	Monthly climograph recorded at Malga Sorgazza station for the year a) 2014, b) 2015. (TAP: Total Annual Precipitation)	76
Figure 4.2.2	Water discharge hydrograph (blue line) and hourly rainfall intensity (vertical black bars) for the year 2014 at Grigno Creek (rainfall intensity recorded at Malga Sorgazza)	78
Figure 4.2.3	Hourly precipitations, atmospheric temperature and water discharge recorded in 2014 at Grigno Creek, limited to the snowmelt period (temperature recorded at Malga Sorgazza). Black arrows are indicating snowmelt peaks	78
Figure 4.2.4	Monthly climograph recorded at Passo Brocon station for the year a) 2014, b) 2015. (TAP: Total Annual Precipitation)	79
Figure 4.2.5	Water discharge hydrograph (blue line) and hourly rainfall intensity (vertical black bars) for the year 2014 at Tolvà Creek (rainfall intensity recorded at Passo Brocon)	81
Figure 4.2.6	Hourly precipitations, atmospheric temperature and water discharge recorded in 2014 at Tolvà Creek, limited to the snowmelt period (temperature recorded at Passo Brocon). Black arrows are indicating snowmelt peaks	81
Figure 4.2.7	Monthly climograph recorded at Mezzana station for the year a) 2014; b) 2015. (TAP: Total Annual Precipitation)	82
Figure 4.2.8	Water discharge hydrograph (blue line) and hourly rainfall intensity (vertical black bars) for the year 2014 at Ussaia Creek (rainfall intensity recorded at Mezzana)	84
Figure 4.2.9	Hourly precipitations, atmospheric temperature and water discharge recorded in 2014 at Ussaia Creek, limited to the snowmelt period (temperature recorded at Mezzana). Black arrows are indicating snowmelt peaks	85
Figure 4.2.10	Hourly rainfall (vertical black bars), water discharge (blue line) and surveys (vertical purple bars) for a) 2014, b) 2015, at Grigno Creek. (S=snowmelt-dominated flood event; M=mixed-type flood event; R=rainfall dominated flood event)	86
Figure 4.2.11	Hourly rainfall (vertical black bars), water discharge (blue line) and surveys (vertical purple bars) for a) 2014, b) 2015, at Tolvà Creek. (S=snowmelt-dominated flood event; M=mixed-type flood event; R=rainfall dominated flood event)	87
Figure 4.2.12	Hourly rainfall (vertical black bars), water discharge (blue line) and surveys (vertical purple bars) for a) 2014, b) 2015, at Ussaia Creek. (S=snowmelt-dominated flood event; M=mixed-type flood event; R=rainfall dominated flood event)	88
Figure 4.2.13	Hourly rainfall (vertical black bars), water discharge (blue line) and surveys at Upper Strimm Creek (vertical purple bars) and Lower Strimm Creek (vertical blue bars). (S=snowmelt-dominated flood event; M=mixed-type flood event;	89

R=rainfall dominated flood event, from Dell’Agnese et al. (2015), modified)

Figure 4.3.1	Stacked bars showing inter-survey frequency distributions of tracer travel distances across weight categories at the Grigno Creek monitoring site for the monitoring period (May 2014 – October 2015). Numbers above bars indicate the amount of tracers released for that grain size class. No motion surveys are not included	91
Figure 4.3.2	Stacked bars showing inter-survey frequency distributions of tracer travel distances across weight categories at the Tolvà Creek monitoring site for the monitoring period (July 2014 – October 2015). Numbers above bars indicate the amount of tracers released for that grain size class. No motion surveys are not included	93
Figure 4.3.3	Stacked bars showing inter-survey frequency distributions of tracer travel distances across weight categories at the Ussaia Creek monitoring site for the monitoring period (April 2013 – October 2015). Numbers above bars indicate the amount of tracers released for that grain size class. No motion surveys are not included	96
Figure 4.3.4	Tracer travel distance as a function of tracer weight associated to the August 8 2014 event for (a) Grigno Creek, (b) Tolvà Creek, and (c) Ussaia Creek	97
Figure 4.3.5	Tracer travel distance as a function of tracer weight associated to the November 4 th – 8 th 2014 event for (a) Grigno Creek, (b) Tolvà Creek, and (c) Ussaia Creek	100
Figure 4.3.6	Comparative box plots of travel distances across weight classes at Grigno, Tolvà and Ussaia sites for the July 26, 2014 event (n= number of recovered tracers, Qmax = peak discharge in m ³ s ⁻¹)	101
Figure 4.3.7	Comparative box plots of travel distances across weight classes at Grigno, Tolvà and Ussaia monitoring sites for the August 13, 2014 event (n= number of recovered tracers, Qmax = peak discharge in m ³ s ⁻¹)	102
Figure 4.3.8	Comparative box plots of travel distances across weight classes at Grigno, Tolvà and Ussaia monitoring sites for the 13/10/2014 event (n= number of recovered tracers, Qmax = peak discharge in m ³ s ⁻¹)	104
Figure 4.3.9	Comparative box plots of travel distances across weight classes at Grigno, Tolvà and Ussaia monitoring sites for the November 4-8, 2014 event (n= number of recovered tracers, Qmax = peak discharge in m ³ s ⁻¹)	105
Figure 4.3.10	Comparative travel distances by weight classes at Grigno, Tolvà and Ussaia monitoring sites for the September 14, 2015 event (n= number of observations, Qmax = peak discharge in m ³ s ⁻¹)	107
Figure 4.3.11	Comparative travel distances by weight classes at Grigno, Tolvà and Ussaia monitoring sites for the October 13-16, 2015 event (n= number of observations, Qmax = peak discharge in m ³ s ⁻¹)	108
Figure 4.3.12	a) Tracer median travel distances as a function of weight and stratified by inter-survey peak discharge at Grigno Creek; b) Box plot showing the distribution of tracer travel distances across weight classes at Grigno Creek (n= number of observations). No motions count are not included	110
Figure 4.3.13	a) Tracer median travel distances as a function of weight and stratified by inter-survey peak discharge at Tolvà Creek; b) Box plot showing the distribution of tracer travel distances across weight classes at Tolvà Creek (n= number of observations). No motions count are not included	111
Figure 4.3.14	a) Tracer median travel distances as a function of weight and stratified by inter-survey peak discharge at Ussaia Creek; b) Box plot showing the distribution of tracer travel distances across weight classes at Ussaia Creek (n = number of observations). No motions count are not included	112
Figure 4.3.15	Stacked bars showing inter-survey frequency distributions of tracer travel	114

	distances across weight categories at the Upper Strimm Creek monitoring site for the monitoring period (September 2011 – June 2014). No motion surveys are not included (from Dell’Agnese et al., 2015)	
Figure 4.3.16	a) Tracer median travel distances as a function of weight and stratified by inter-survey peak discharge at Upper Strimm Creek; b) Box plot showing the distribution of tracer travel distances across weight classes at Upper Strimm Creek (n= number of observations). No motions count are not included	115
Figure 4.4.1	Entrainment threshold discharges (black horizontal line) for the three sites a) Grigno, b) Tolvà and c) Ussaia Creek	122
Figure 4.4.2	Box plots of the tracers’ virtual velocities in relation to corresponding inter-survey peak discharge (Q_{max}) in (a) Grigno, (b) Tolvà and (c) Ussaia Creek. The flow regime of inter-survey periods is classified into snowmelt, rainfall-induced and mixed. Mixed periods represent a combination of the first two and typically correspond to the snowmelt falling limb. At Ussaia monitored site the debris flow event is highlighted in red, triggered by a rainfall-induced event. (Black vertical arrows represent tracers’ release and the percentages above the largest whisker indicate the proportion of buried tracers, n= number of observations)	127
Figure 4.4.3	Box plots of the tracers’ virtual velocities ordered by date in (a) Grigno, (b) Tolvà and (c) Ussaia Creek. (Black vertical arrows represent tracers’ release and the percentages above the maximum whisker indicate the proportion of buried tracers, n= number of observations, Q indicates Q_{max})	128
Figure 4.4.4	Box plots of the tracers’ virtual velocities divided by hydrological forcing at a) Grigno, b) Tolvà and c) Ussaia Creek (panel (A) rainfall, panel (B) snowmelt and mixed). At Ussaia Creek the debris flow ($Q_{max} = 26.41 \text{ m}^3 \text{ s}^{-1}$) event is in black, since triggered by a rainfall event. Black vertical arrows represent tracers’ release and the percentages above the maximum whisker indicate the proportion of buried tracers, n= number of observations)	130
Figure 4.4.5	Examples of tracers’ virtual velocities as a function of weight drawn from three selected events at: (a) the Grigno Creek; and (b) the Ussaia Creek. Red squares correspond to rainfall-related velocities, green triangles to snowmelt-induced velocities, and blue diamonds to mixed events	132
Figure 4.4.6	Examples of tracers’ virtual velocities as a function of weight drawn from three selected events at Tolvà Creek. Red squares correspond to rainfall-related velocities and blue diamonds to mixed events. Snowmelt-related events are not recorded	132
Figure 4.4.7	Tracers’ virtual velocities as a function of weight for precipitation events of a) July 27 th 2014, b) August 13 th 2014, c) November 4 th -8 th 2014 and d) September 19 th 2015 at all the monitoring sites	134
Figure 4.4.8	Entrainment threshold discharges (black horizontal line) at Strimm Creek (from Dell’Agnese et al., 2015)	136
Figure 4.4.9	Box plots of the tracers’ virtual velocities in relation to corresponding inter-survey peak discharge (Q_{max}) in Strimm Creek. The flow regime of inter-survey periods is classified into snowmelt, rainfall-induced and mixed. Mixed periods represent a combination of the first two and typically correspond to the snowmelt falling limb (from Dell’Agnese et al., 2015)	138
Figure 4.4.10	Tracers’ virtual velocities as a function of weight for three selected peak discharges in Upper Strimm. Red triangles refer to rainfall-induced velocities (i.e. summer-fall 2012), blue circles to snowmelt-related velocities (i.e. spring-summer 2013), and green diamonds to mixed snowmelt-rainfall periods. Note that tracers’ virtual velocities are independent from weight (from Dell’Agnese et al., 2015)	138

Figure 4.5.1	Histograms of tracer length displacement for the event of August 13 th 2014 at a) Grigno, b) Tolvà and c) Ussaia Creek. Travel distances below the uncertainty threshold applied to field data are plotted as red bars. The black dashed line represents the threshold value of 0.2 m	143
Figure 4.5.2	Histograms of tracer length displacement for the event of November 4 th – 8 th 2014 at a) Grigno, b) Tolvà and c) Ussaia Creek. Travel distances below the uncertainty threshold applied to field data are plotted as red bars. The black dashed line represents the threshold value of 0.2 m	144
Figure 4.5.3	Histograms of tracer length displacement considering all the surveys at a) Grigno, b) Tolvà and c) Ussaia Creek. Travel distances below the uncertainty threshold applied to field data are plotted as red bars. The black dashed line represents the threshold value of 0.2 m	145
Figure 4.5.4	Histograms of virtual velocities calculated for the event of August 13 th 2014 at a) Grigno, b) Tolvà and c) Ussaia Creek	149
Figure 4.5.5	Histograms of virtual velocities calculated for the November 4-8, 2014 event at a) Grigno, b) Tolvà and c) Ussaia Creek	150
Figure 4.5.6	Histograms of virtual velocities calculated considering all the conducted surveys at a) Grigno, b) Tolvà and c) Ussaia Creek	152
Figure 4.6.1	Digging tests conducted at a) Tolvà Creek, lateral deposit formed after the November 4 th – 8 th 2014 event (burial depth: 0.25 m); b) Grigno Creek, sediment deposited on the left bank of a plane bed reach (burial depth: 0.06 m); c) Ussaia Creek, the tracer is located where the main channel was flowing before the debris flow event of November 4 th – 8 th 2014, within the alluvial fan in correspondence of the confluence with the Noce River (burial depth: 0.19 m)	154
Figure 4.7.1	Framework adopted for implementing the three bedload scenarios adopted for Grigno and Tolvà Creeks (left), and Ussaia Creek (right)	157
Figure 4.7.2	Non-cumulative (a) and cumulative (b) event representation of estimated bedload volumes transported at Grigno Creek in scenarios 1, 2 and 3. Note the efficiency of the snowmelt and ordinary rainfall events compared to heavy rainfall events of August and November 2014. In (c) is represented a close-up view of the estimated bedload volume transferred in 2015. In panel (a) we assigned the value of G equal to 0.01 to surveys where no bedload activity has been documented	159
Figure 4.7.3	Non-cumulative (a) and cumulative (b) event representation of estimated bedload volumes transported at Tolvà Creek in scenarios 1, 2 and 3. Note the efficiency of the snowmelt and ordinary rainfall events compared to heavy rainfall events of August and November 2014. In (c) is represented a close-up view of the estimated bedload volume transferred in 2015. In panel (a) we assigned the value of G equal to 0.01 to surveys where no bedload activity has been documented	161
Figure 4.7.4	Non-cumulative (a) and cumulative (b) event representation of estimated bedload volumes transported at Ussaia Creek in scenarios 1, 2 and 3. Note the efficiency of the snowmelt events in 2014 compared to 2015. In (c) is represented a close-up view of the estimated bedload volume transferred in 2015. In panel (a) we assigned the value of G equal to 0.01 to surveys where no bedload activity has been documented	163
Figure 4.7.5	Non-cumulative event representation of estimated bedload volumes transported at Upper Strimm Creek (R: rainfall season, S: snowmelt season)	164

Figure 4.8.1	Intensity-duration relationships for snowmelt, mixed-type and rainfall events that triggered bedload transport at a) Grigno, b) Tolvà, and c) Ussaia Creek. The threshold line is manually fitted, separating bedload from no bedload events (R: associated to rainfall, M: associated to mixed-type); the light grey rectangle indicates uncertainty due to overlap of bedload and no bedload events	168
Figure 4.8.2	Bedload transport in relation to rainfall intensity-duration for different forcing typologies in: (a) Grigno Creek; b) Tolvà Creek; and c) Ussaia Creek. Crosses indicate no tracer motion. Bubble size is proportional to estimated bedload transport volume (in m ³); the largest bubble is equal to bedload volume transfer of 10 m ³	171
Figure 5.1	Examples of hydrologic response to: (a) a snowmelt event (i.e., Grigno Creek); (b) a convective storm event (i.e., Grigno Creek); and (c) a mixed inter-survey period in which was recorded a snowmelt and a rainfall event (i.e., Grigno Creek)	175
Figure 5.2	Tracers' median virtual velocity as function of peak discharge at: (a) Grigno Creek; (b) Ussaia Creek. Bedload transport events are stratified by hydro-meteorological forcing typology	179
Figure 5.3	Non-cumulative (a) and cumulative (b) event representation of estimated bedload volumes transported at the study sites after applying scenarios 3a and 3b. Green and red bars mark respectively the separation between the snowmelt (S) and mixed (M) periods, and between the mixed (M) and rainfall period (R) periods. In panel a, G = 0.01 represents no-bedload periods	181
Figure 5.4	Bedload volume transfer (G) as function of peak discharge (Q _{max}) at: (a) Grigno Creek; (b) Ussaia Creek. Power-law equations refer to rainfall events only	183
Figure 5.5	Rainfall intensity-duration thresholds for bedload entrainment at Gigno, Tolvà and Ussaia Creeks (this study) in the context of prior studies conducted in the European Alps and compiled by Badoux et al. (2012)	184
Figure 5.6	Example of threshold discharges obtained from the actual field surveys (black line) and from the seasonally lumped scenario (red line) at Grigno Creek	186
Figure 5.7	Non-cumulative (a) and cumulative (b) event representation of estimated bedload volumes transported at Grigno Creek. Grey circles represent the bedload transfer as estimated from each field survey, black circles indicate the seasonally lumped counterpart	188
Figure 5.8	Non-cumulative (a) and cumulative (b) event representation of estimated bedload volumes transported at Tolvà Creek. Grey circles represent the bedload transfer as estimated from each field survey, black circles indicate the seasonally lumped counterpart	189
Figure 5.9	Non-cumulative (a) and cumulative (b) event representation of estimated bedload volumes transported at Ussaia Creek. Grey circles represent the bedload transfer as estimated from each field survey, black circles indicate the seasonally lumped counterpart	191
Figure 5.10	Mean annual precipitation (1981-2010) across the Trentino-Alto Adige region (modified from www.clima-alpino.eu) with box plots of tracers' travel distances stratified by types of hydro-meteorological forcing at: (1) Strimm Creek; (2) Ussaia Creek; and (3) Grigno Creek. Percentages indicate the ratio between travel distance for a given hydrological forcing and total travel distance	193
Figure A3.1	Stage-discharge curves constructed at Grigno, Tolvà and Ussaia Creek monitoring site. (Q = water discharge (l s ⁻¹), P = hydrostatic pressure (bar))	204
Figure A4.1.1.2	Cross sections surveyed at Grigno, Tolvà, Ussaia and Strimm Creek	205

Figure A4.1.2	Downstream hydraulic geometry sections surveyed at Grigno and Tolvà Creeks	231
Figure A5.1	Frequency distributions of tracers' travel distance obtained from the actual field surveys and from the seasonally lumped scenario) at: (a) Grigno Creek; (b) Tolvà Creek; and (c) Ussaia Creek	277
Figure A5.2	Example of threshold discharges obtained from the actual field surveys (black line) and from the seasonally lumped scenario (red line) at (a) Grigno; (b) Tolvà Creek; and (c) Ussaia Creek	279
Figure A5.3	Frequency distributions of tracers' travel distance obtained from the actual field surveys and from the seasonally lumped scenario) at: (a) Grigno Creek; (b) Tolvà Creek; and (c) Ussaia Creek	281

CHAPTER 1

Introduction

The fluvial system draining a watershed can be ideally subdivided in three zones according to Schumm (1977): the upper portion, where processes producing sediment through erosion of mountain belts prevail; the intermediate portion, where sediments are mainly transferred to lowlands, and the lower portion, where sediment is stored or exits the catchment to enter a sea basin. Anyway, these processes are acting in each portion of the subdivided catchment, especially where the stream is characterized by channel bed mobility, such that there is sediment exchange between bed and banks. This subdivision based upon dominant processes reflects also other physical characteristics of water streams such as confinement and dimension, allowing the distinction among confined streams, typical of upper-intermediate portions of the basins, semi-confined streams flowing in the piedmont belt, and non-confined streams, crossing alluvial plains. Church (1992) scales channel width according to the average diameter of elements constituting the bed, identifying three typologies. Small channels where single clasts constitute a portion of main channel morphologies, and the grain size diameter of larger elements is 1-10 times channel depth. Intermediate channels are characterized by average diameter of individual elements in the order of 0.1-1 times the channel depth, and in large channels, where pure fluvial processes dominate, the average grain diameter is typically less than 0.1 times the water depth.

Riverbeds of the most elevated portions of catchments are located in the sediment production area and generally exhibit small dimensions, high steepness and elevated degree of confinement. These streams are typical of mountainous regions, and they differ substantially from lowland streams because of the larger slope, the resistance to water flow determined by large individual elements, the discharge regime strongly influenced by seasonality and because the scale of morphological variations in space is high, whereas temporal modifications occur only after relevant events capable of imposing variations to channel bed. The morphology of such water streams is strongly connected to hillslope processes and dynamics, limiting the lateral continuity of morphologies and the downstream flux of water and sediments. A largely diffused classification of reaches in mountain drainage basins is the one proposed by Montgomery and Buffington (1997), synthesizing morphologies into colluvial, bedrock and five alluvial channel types. Within the alluvial types they distinguished among steep channels, such as cascade and step-pool, and low-gradient channels such as plane bed, pool-ripple, dune-ripple. In the first group is acknowledged an excess of transport capacity (supply limited condition), whereas the latter is dominated by a deficit of transport capacity (capacity limited condition).

The total sediment load of rivers is transported by two modes: the bedload and suspended load, and as stated by Wilcock et al. in 2009 "bedload is the basic engine of fluvial morphology". Bedload is moving nearly constantly in contact with the river bed (rolling, sliding or saltating), while the suspended load, dispersed in the flow by turbulences, is carried away for considerable distances without touching the bed (Hicks and Gomez, 2003). The modes of transport, the processes that disperse sediment within a river and factors affecting sediment supply, contribute to spatial and temporal variation in the sediment load.

In mountain environments, streams transport large amounts of coarse bed sediment, including sand, gravel and in some cases cobbles and boulders. Typically, variations of morphology in mountain channels are caused by transport events triggered by large floods able to destabilize and re-organize primary structures. Bedload in high-elevation streams plays an important role in biotic and abiotic contexts, providing riverine

habitat heterogeneity and quality (e.g., Yarnell et al., 2006; Unfer et al., 2011), interacting with hydraulic engineering infrastructures for hydropower generation and sediment transport regulation (Totschnig et al., 2011) and delivering sediment to estuarine and marine environments to equilibrate the coastal dynamics (Syvitsky and Milliman, 2007). The knowledge of bedload flux in mountain streams is therefore important for a variety of reasons in geological, engineering and ecological applications, such as natural hazard management (Badoux et al., 2014), but its quantification and prediction remains still poor (Comiti and Mao, 2012).

The fluvial system responds to changes in first-order controls such as base level, relief and tectonics, lithological properties of watershed, climatic forcing and human impacts (Figure 1.1), through morphologic adaptations and sediment load variations. Because of their degree of confinement and the strong relations with hillslope processes, mountain streams are very sensitive to geomorphic variations in the headwater catchments, suddenly adapting channel morphology to variations in lithology. The hydro-climatic regime exerts a first-order control on the frequency and duration of floods, that are the main drivers of bedload transport events. Bedload in turn is affected by local variations in morphology, and structures opposing resistance to water flow are influencing the dynamics of bedload entrainment. Another local control is represented by sediment input from hillslopes, and the frequency and magnitude of processes delivering colluvial material to the main stem, through debris flow or landslides, induce channel adjustments. On the contrary, when poor or no material is delivered to the channel, either from hillslopes or banks, bedload dynamics is inhibited creating structured and high resilient streambeds.

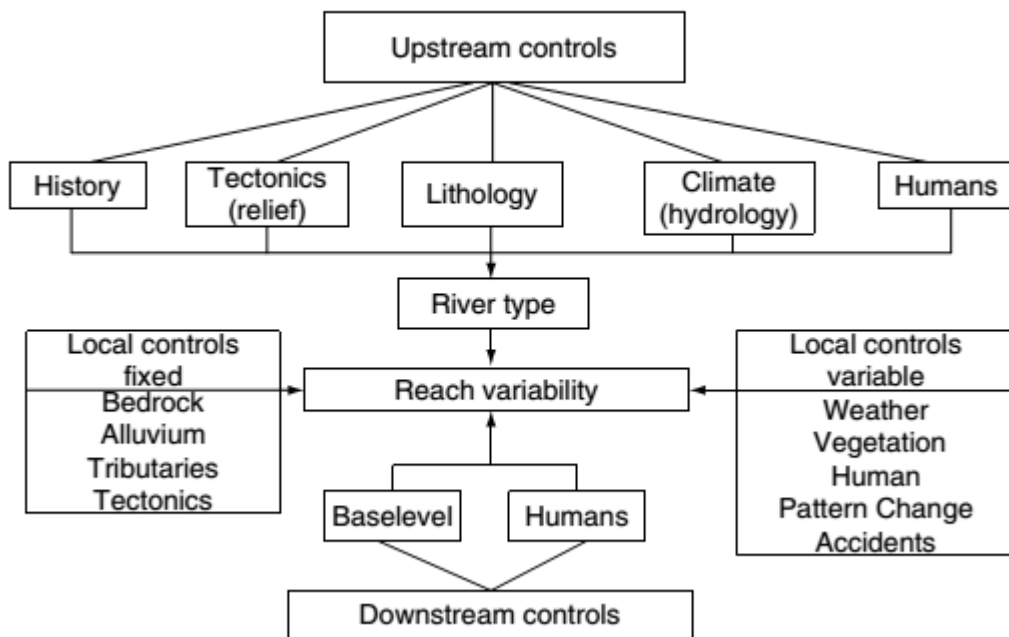


Figure 1.1. Factors controlling the reach scale variability in the fluvial system, divided into upstream, downstream and local controls (from Kondolf and Piégay, 2002).

Bedload is measured through direct or indirect methods. Direct methods aim to determine the amount of mass or volume transported in a certain time interval; indirect methods are estimating quantities that must be appropriately calibrated via direct methods to obtain bedload rate. Among direct methods, the

morphological approach is used to estimate long term variations of bedload across large spatial scales, assuming that channel bed modifications are related to sediment transport (e.g., Ham&Church, 2000; Pelpola&Hickin, 2003; Martin&Ham, 2005). Bedload quantification is obtained also estimating the amount of volume replenishing retention basins or short reaches located immediately upstream weirs, after a single flood. Through suitable equipment of such basins it is possible to obtain information on bedload intensity, installing ultrasonic sensors monitoring the variations in height of the basin floor, or pressure sensors mounted at the bottom, or via automated basket samplers located downstream a weir and crossing the channel bed. Samplers can be installed directly on the bed, such as Vortex- or Reid-type (e.g., Hayward&Sutherland, 1974; Laronne et al., 1992). Trapping the bedload within chambers equipped with pressure sensors and allowing continuous measurements of transport intensity, estimation of initiation of motion and calculation of total bedload flux at scale event. From the material collected, it is possible to measure the grain size distribution of the mobilized sediment. Mobile traps such as Helley-Smith (e.g., Vericat et al., 2006) and Bunte (e.g., Bunte and Abt, 2005) are less expensive, but require the expertise of a field operator and, when fixed to the bed, the appropriate equipment of a wadeable section. Adopting these techniques, bedload intensity and transported fractions are correctly estimated through simultaneous measurements performed across the section, via repetitions of sampling along the same vertical to characterize the temporal variability. The efficiency in sampling decreases with filling of baskets and according to the dimensions of the inlet (e.g. Vericat et al., 2006). The virtual velocity method requires the deployment in the field of geomorphic tracers (Passive Integrated Transponders, magnetic, ferric) that will be discussed more extensively in the literature review. Tracers provide a lagrangian approach to the sediment transport problem, and can be followed with mobile devices, allowing to monitor displacement lengths of particles (e.g., Lamarre et al., 2005). Their passage can be tracked via stationary antennas (e.g., Schneider et al., 2010), to establish properties such as incipient motion, virtual and real velocity of tagged-stones and rest periods. Hydraulic variables such as peak discharge, shear stress and stream power have been related to virtual velocity (e.g., Sayre and Hubbell, 1965; Hassan et al., 1992; Haschenburger and Church, 1998).

Indirect methods are considered “surrogate” techniques of bedload monitoring since they need to be calibrated via direct methods. Two main typologies of devices exist, namely the geophones and the hydrophones. Geophones are of three types, the “Swiss”, the “Japanese” and the “Swedish”. The “Swiss” measures the amplitude and the frequency of acoustic waves generated by the impacts of particles on a rectangular steel plate (e.g., Turowsky and Rickenmann, 2011), while the “Japanese” records the intensity of impacts on a metallic tube through multiple channels, thus the signal could be filtered (Mizuayama et al., 2010). The calibration depends on the modes of bedload transport, grain size of mobilized elements and sensitivity of acoustic device. The “Swedish” geophone mounts a multi-frequency (0-1000 kHz) microphone below a squared metallic plate. The hydrophone is a microphone installed in the proximity of the channel bed or close to the banks, that records acoustic signals, thus water-generated noise included. The spectral analysis conducted on frequency seems to help in discriminating the grain size of transported material (e.g., Belleudy et al., 2010). Indirect methods are generally robust but require proper stations to be equipped ensuring high degree of automation. Compared to direct methods, the advantages presented by surrogate methods are continuous and safe bedload measurements, monitoring also during large floods. Details on incipient motion conditions and temporal dynamics of bedload can be precisely investigated, without furnishing indications on active layer depth. Despite this, to correctly evaluate bedload they need proper field calibration using a direct technique, limiting the range of flood conditions in which they could be tested. Fluvial tracers, on the contrary, can be adopted in wadeable streams. Since they are recovered after

flood transit, this property makes them suitable to detect displacement characteristics related to every flood condition, enabling safe survey conditions and making them widely adopted in fluvial morphology.

1.1 Concise literature review on bedload tracers

Direct bedload measurements have been performed in the field since the beginning of the 20th century, deploying “portable” basket collectors or sediment traps directly digged within the channel bed, such as in the seminal work of Muellhofer (1933) in the River Inn. These methods have been developed until recent years, such as in Bunte and Abt (2009), where Helley-Smith sampler and sediment traps have been used to measure bedload and compare measured rates obtained using both techniques. Direct methods of sampling are usually limited to one cross section at a specific time, and are difficult to take during high-magnitude events; furthermore the sampling instruments have been highlighted to be not as accurate as proposed by theory (Habersack et al., 2001; Laronne et al., 2003; Vericat et al., 2006; Liebault et al., 2012).

Direct methods do not allow to measure the specific travel distances travelled by clasts during flood events. To overcome this problem, tracers have been deployed in fluvial geomorphology enabling displacement length of tagged particles to be tracked with different methods. The advantages of using tracers are that they are recovered after flood events, and the range and distribution of their size can adequately mimic that of reach natural conditions. Furthermore information on sediment sorting by particle size or shape can be obtained by tracers, as well as thresholds for particle entrainment, depth of the active layer (better when complemented with scour chains), sediment sources and deposition areas, and relative sediment transport rates. The largest limitation is primarily due to the recovery rate, that can affect the accuracy of measurements, especially in unusual conditions as might occur in high-elevation reaches. The first tracers used were painted rock (e.g. Einstein, 1937; Takayama, 1965; Leopold et al., 1966), used to record the track of those visible in the channel bed after flood events. This kind of tracers showed low recovery rate and buried and superficial clasts exhibit a different behaviour (Hassan and Church, 1992). A first improvement was represented by using ferric coating (Nir, 1964) or metal strips placed on the surface of clasts (Butler, 1977), but the recovery rates were generally below 35 %. To determine the movement of tracers, rivers were periodically surveyed to locate their position, revealed through a metal detector. From the comparison of the current position with the previous, the distance moved by a single particle was derived; additional information such as channel morphology and positions could be recorded, and the relationship between particle size and mobility could be inferred.

The insertion of iron cores inside the tracers represented an innovative method (Hassan et al., 1982), because of the enhanced recovery rates, up to 92 % (Schmidt&Ergenzinger, 1992). Starting from 1982 (e.g., Froehlich), magnetic tagged stones were deployed, as they ensured higher recovery rates compared to previous methods (Ferguson, 1998; Haschenburger and Church, 1998; Haschenburger, 2013). Also, a better estimation of the number of clasts moving to a subsuperficial layer was obtained, so that a greater comprehension of the active channel depth was made possible. A different system to monitor clast movements was developed by Schmidt and Ergenzinger (1992), who inserted active transponders that are recovered on the base of Radio Frequency Identification (RFID), leading to successful results (see also Chacho et al., 1989). Each of these transponders emits a wave-signal within the radio frequency range, containing its unique identification code so that monitoring and recording their positions can be done by deploying antennas in the study stream. In this way, an extended record of the tracers movements, both at high temporal and spatial resolution, is possible. Active transponders rely on an internal battery, and a signal is emitted only as long as their internal battery lasts. After the battery voltage decays, recovering these tracers is no longer possible. The deployment of Passive Integrated Transponders (PIT) became

widely adopted since they do not have an internal battery and their lifespan is theoretically unlimited. Originally developed to study the movements of fish populations via stationary antenna systems (e. g. Armstrong *et al.*, 1996; Johnston *et al.*, 2009), they were later used also to monitor bed load transport (e.g. Nichols, 2004, Lamarre *et al.*, 2005). Even though their detection range is reduced, this technique has many advantages over other methods, being relatively inexpensive, allowing easy searches and ensuring long life time of the tracers (Schneider, 2010).

PIT-tagged clast monitoring performed via portable antenna in rivers has already been applied successfully by several studies, with particle recovery rates ranging from 60 % to 100 %. These single case studies have been proposed obtaining results about recovery rates (e.g. Nichols, 2004), preliminary observations of area clustering (Lamarre *et al.*, 2005), comparison of modal distance with step-pool length (Lamarre & Roy, 2008), relations between transport characteristics and maximum peak discharge (Schneider *et al.*, 2010), relationship between transport length and tracer grain size (Camenen *et al.*, 2010), mobility of tracers released across different morphologies such as low-flow channel or bars (Liébault *et al.*, 2012), comparison of tracer transport distances in different hydrological years and model-fitting distributions of travel distances (Bradley&Tucker, 2012), quantitative field support for modelling framework based on momentum conservation at grain scale (Philips *et al.*, 2014). Considering virtual velocities of tracers, the number of studies to evaluate bedload transfer is still limited (e.g., Hassan *et al.*, 2013; Dell’Agnese *et al.*, 2015; see Table 1.1).

Table 1.1. Compilation of previous studies that have used PIT-tagged particles for investigating bedload sediment dynamics.

Authors	River	CHANNEL FEATURES			Number of tracers	Results
		Drainage area [km ²]	Length [m]	Slope [%]		
Habersack <i>et al.</i> , 2002	Waimakariri (New Zealand)	--	--	0.38	--	Distributions describing rest period/step lengths
McNamara <i>et al.</i> , 2002	Reynolds Creek (SW Idaho)	54.48	--	2.6	4	Tracers’ mobility depends from hydrograph stage
Nichols <i>et al.</i> , 2004	Lucky hill watershed (Arizona)	0.044	161	3.6	124	Recovery rates lowering in time
Lamarre <i>et al.</i> , 2005	Moras Creek (Canada)	3.2	130	2.3	204	Clustering of clasts in selected morphologies
Lamarre <i>et al.</i> , 2008a	Three reaches at Moras Creek (Canada)	3.2	14; 15; 18	3; 1; 0.7	--	Sediment storage around keystones
Lamarre <i>et al.</i> , 2008b	Spruce Creek (Quebec, Canada)	--	50	14	196	Modal distance travelled close to step-pool length
Camenen <i>et al.</i> , 2010	Arc en Maurienne (France)	1957	--	0.2-1	312	Travel length not dependent on grain size
Schneider <i>et al.</i> , 2010	Erlenbach, Riedbach (Switzerland)	0.74 (E); 18 (R)	350 (E)	17 (E); 40 (R)	425 (E); 278 (R)	Transport dependent on peak discharge
MacVicar <i>et al.</i> , 2011	Moras Creek	14	500	1.2	299	Mobility according to grain size
Liébault <i>et</i>	Bouinenc River	34.64	2000	1.6	451	Mobility of tracers enhanced

al., 2012	(France)					in low-flow channel
Bradley et al., 2012	Halfmoon Creek (Colorado)	61.5	30	1	893	Dependence of transport distance from flow levels
Houbrechts et al., 2012	17 rivers in the Ardenne Massif, Belgium	16-2910	--	0.1-1.1	--	Small events moved clasts for 3.2 m; large events moved clasts for 300 m
Biron et al., 2012	Nicolet river (Quebec, Canada)	130	300	0.15	315	Long-term maintenance of clasts within the pool
Hassan et al., 2013	10 streams investigated	--	--	--	64 field based tracers' experiments	Step-pools act as particle filter; deeply buried stones have longer rest periods.
Schneider et al., 2014	Erlenbach (Switzerland), Rio Cordon (Italy)	0.7 (E); 5 (RC)	400 (E)	17 (E); 13 (RC)	833 (E); 860 (RC)	Peak discharge has a strong influence on the distribution of travel distances
Philips et al., 2014	Mameyes River (Puerto Rico)	24.21	1200	0.078	300	Quantitative field support for modelling framework based on momentum conservation at grain scale
Dell'Agnese et al., 2015	Upper & Lower Strimm Creek (Italy)	4 (US); 7.5 (LS)	1093 (US); 1514 (LS)	8 (US); 15(LS)	259 (US); 231 (LS)	Strongly coupled conditions ensured increasing efficiency in sediment evacuation

Transport characteristics and water flow parameters are determining variations in bedload. What influences the transport distances of individual clasts are channel primary bedforms, such as step-pools or bars, and surface structures (such as imbrications). As stated before, channel structures of mountain streams are modified by large transport events able to destabilize the bed. In confined channels sediment recruitment of streams is supplied by the interactions with hillslope processes. Therefore, to understand bedload dynamics in such contexts, it is worth investigating the relations among transport parameters and other geomorphic characteristics such as bedforms, bed texture and sediment supply from adjacent slopes and low-order tributaries (Hassan and Ergenzinger, 2002).

As a matter of fact, river channel dynamics are governed by basin scale responses to variations in water and sediment supply (Montgomery and Buffington, 1997), but these conceptual models have been rarely tested in the field. A monitoring network to examine the effects of channel bed texture and morphology on bedload flux has been designed by Green et al. (2014), proving that high form resistance reaches contribute to bedload in a partial mobility fashion compared to the dimensions of available material; conversely equal mobility is achieved in reaches exhibiting reduced forms of resistance. Variations in water input and bedload estimates should be conducted simultaneously to describe quantitative cause and effect relations between sediment supply and channel morphology. Moreover the boundary conditions imposed by topography and sedimentological properties of the river bed should be adequately represented to link water and sediment fluxes to channel properties, but the mentioned quantities have not been jointly monitored in previous field works, and “the influence of sediment supply on channel morphology remains rather ambiguous in natural settings” (Mueller and Pitlick, 2013).

1.2 Objectives

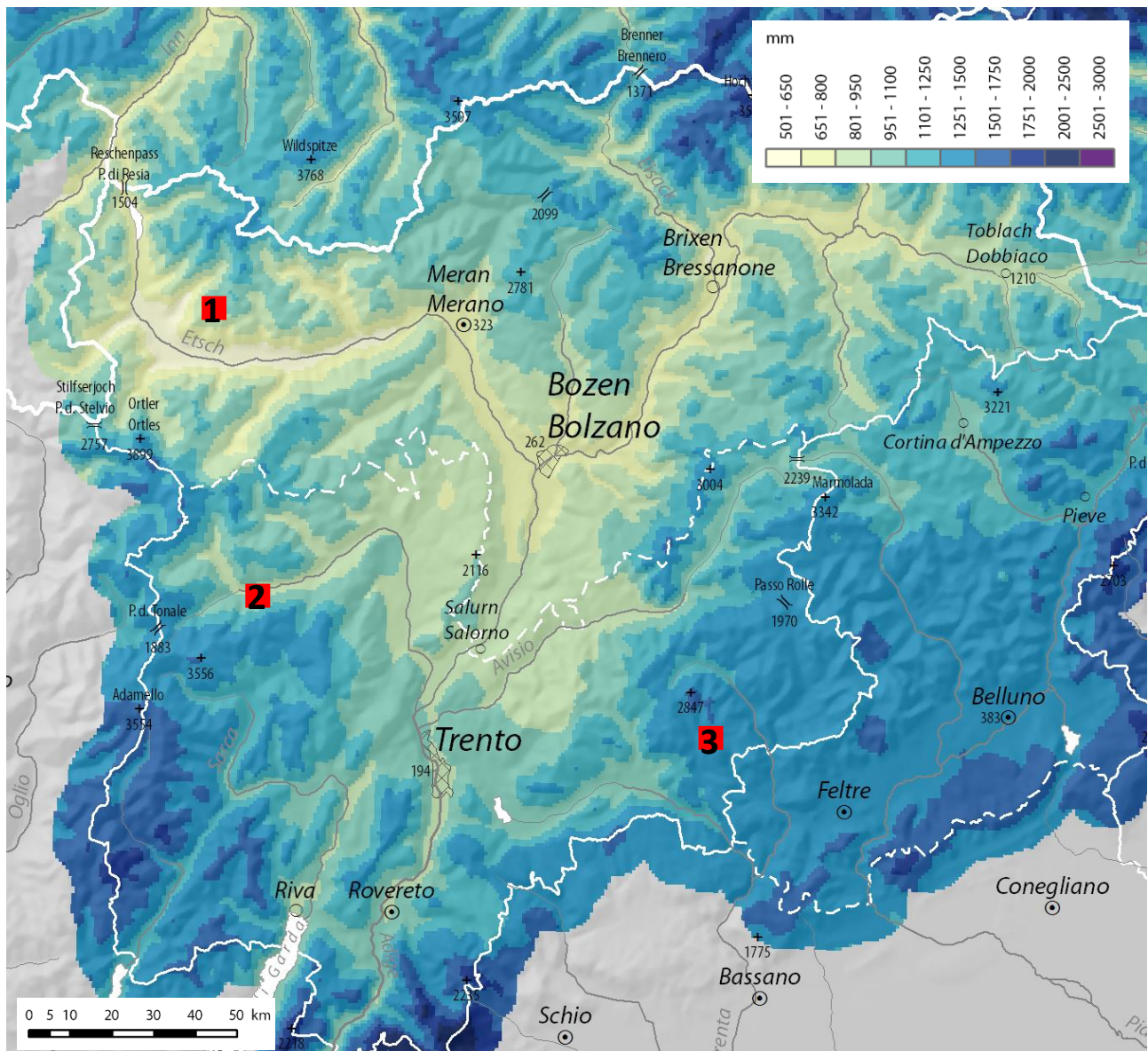
The main objective of this Ph.D thesis is linking bedload dynamics to sediment supply in mountain streams evaluating the impact of sediment sources located on hillslopes and upstream tributaries on bedload flux propagating along the main stem of the monitored catchments. To assess quantitatively the effects of this impact, we configured an experimental setup by selecting three monitoring creeks sharing identical lithology (granitoids) and alluvial morphologies (*sensu* Montgomery and Buffington, 1997), such as step-pool, plane bed and cascade, but contrasting sediment supply conditions. As will be detailed in the study area section, Grigno and Tolvà Creeks are characterized by scarce sediment supply, provided only by sediment stored in channel bed patches of mobile material. Conversely, at Ussaia Creek is present a chronic input of colluvial material from adjacent slopes, where glacial till extensively outcrops. To test the effectiveness of sediment supply or water input in determining bedload fluxes at reach scale, the Ussaia Creek is characterized by a weaker hydro-meteorological forcing compared to the Grigno and Tolvà Creeks (Figure 2). To achieve the mentioned objectives, bed sediment mobility and travel distances of pit-tagged stones are monitored from December 2013 to December 2015 at Grigno-Tolvà creeks, releasing a total of 162 clasts at Grigno Creek and 150 at Tolvà Creek. The monitoring period at Ussaia Creek extends from January 2013 to December 2015, monitoring the displacements of 446 clasts. The meteorological parameters, such as atmospheric temperature and rainfall intensity, are monitored via meteorological stations of the Trentino Provincial Meteorological Network located within 1 km from the investigated reach. The hydrologic response to meteorological forcing in the selected basins is monitored through ad hoc water gages installed within the same zones of tracer release, measuring water levels with 10 minutes time interval and opportunely calibrated via the salt dilution method. Channel boundary conditions at reach scale are monitored via total station surveys and photogrammetric methods to describe the sites in terms of slope and characteristic dimensions of macro-roughness elements such as step heights and pool depths.

To obtain the main objective, we fulfill requirements imposed by specific objectives concerning i) the impact that simultaneous meteorological event exerted on the bedload dynamics across different catchments, ii) the effects addressed on bedload by hydro-meteorological forcing peculiar of each site, iii) the destabilization of riverbed morphologic structures resulting from low-order tributary sediment supply, compared to the stability of well-organized streams depleted in colluvial inputs, iv) the definition of rainfall intensity-duration thresholds for bedload transport triggering in the investigated catchments, v) the effects of different sampling frequencies on the evaluation of bedload volume transfer.

In the present work are presented data collected in an additional field site, the Strimm Creek (see Dell'Agnese et al., 2015), to allow an exploratory comparison of bedload dynamics across a latitudinal transect in the Eastern Italian Alps. This is considered a secondary objective that benefits from displacement data coming from a cohort of 259 tracers monitored from August 2011 to October 2015. The elevation of the Strimm site (2550 m asl) and the limited accessibility allowed to monitor particle displacements only twice per year, precisely in June (after the snowmelt season) and in October (after the major rainfall events). The adoption of this style of surveying implies that bedload is monitored at different time scales compared to Grigno, Tolvà and Ussaia Creek.

The originality of the present work is the bedload monitoring conducted in parallel at four sites, surveying the displacement of tagged particles after each significant hydro-meteorological event. To explain how efforts were devoted to reach the aimed objectives we begin presenting the study areas in the second chapter. The methodologies adopted in the field are described in the third chapter. Following the order of

specific objectives, the fourth chapter is a presentations of results. Here are given details on channel boundary conditions (section 4.1), hydro-meteorological forcing events and survey frequency (section 4.2), tracers' travel distances (section 4.3) and virtual velocities (section 4.4), overall distribution of travel distances and virtual velocities (section 4.5), determination of active channel width and depth (section 4.6), evaluation of bedload volume transfer (section 4.7) and identification of rainfall thresholds for bedload triggering (section 4.8). The fifth chapter is a discussion of the results concerning seasonal variations of bedload across the different sites, effects of timescales of bedload investigation on volume transfer assessment and precipitation thresholds for bedload triggering. Finally the thesis concludes with remarks and future work perspectives.



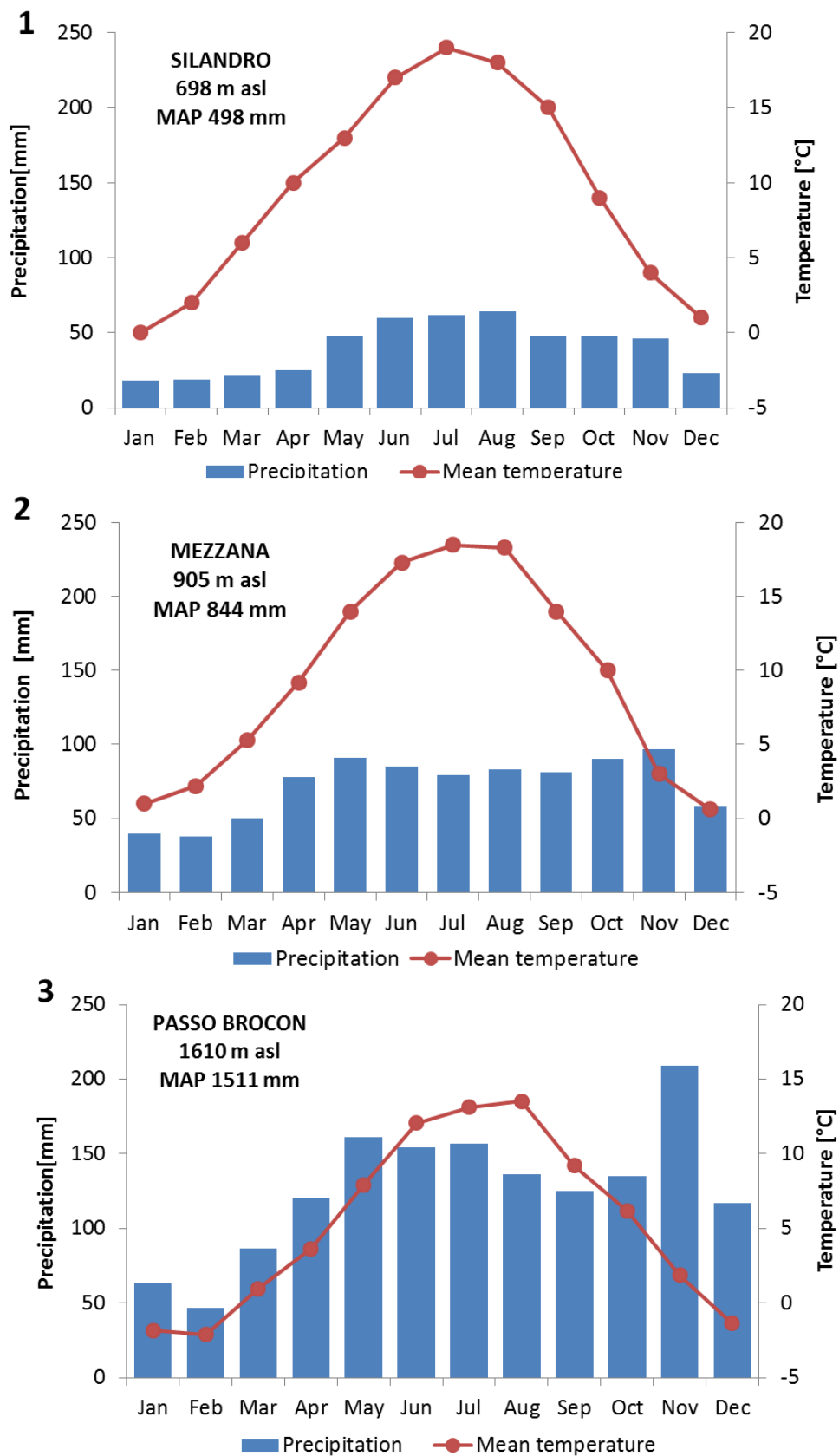


Figure 1.2. Distribution of monitored sites within the Trentino-Alto Adige region, with climatic diagrams referring to the study sites: 1) Silandro (observation period: 1990-2014); 2) Mezzana (observation period: 1990-2015); 3) Passo Brocon (observation period: 1990-2015). MAP: Mean Annual Precipitation. Basemap

colours indicate the average yearly precipitation over the 1981-2010 interval (from www.clima-alpino.eu, modified).

CHAPTER 2

Study area

2.1 Geo-climatic setting of the study basins

2.1.1 Grigno-Tolvà basin

The Grigno Creek basin (90 km²) is a mountain fluvial system belonging to the broader Brenta River basin (5840 km²), Eastern Italian Alps (Figure 2.1). The Brenta River originates from Caldonazzo and Levico lakes (450 m a.s.l.) and runs in the south-eastern sector of Trentino region. The direction of the valley is west-east between the villages of Levico and Grigno, and changes to north-south in proximity of the Veneto-Trentino border, before entering the oriental extremity of the Padana Plain. Here the direction of the valley is northwest – southeast, before being diverted in three main trunks flowing into the Venezia-Chioggia Lagoon (Adriatic Sea). In the uppermost sector the Brenta valley is bordered from Lagorai-Cima d’Asta group on the hydrographic left, and from the northernmost reliefs of Prealpi Vicentine in the hydrographic right. In correspondence of Grigno village, the Grigno Creek joins the Brenta River. Elevation of Grigno basin ranges from 243 m a.s.l. at the Grigno-Brenta confluence to 2847 m a.s.l. of the Cima d’Asta peak. Within the basin there are four main municipalities (Pieve Tesino, Castello Tesino, Cinte Tesino, Grigno), located 65 km East of Trento and 85 km North of Padova. The Grigno Creek in the central-lower portion of the basin tracks the border between the two municipalities of Castello and Pieve Tesino. The study basin which exhibits an elongated shape, originates from two main streams, Upper Grigno Creek (17 km²) and Tolvà Creek (14 km²) (Figure 2.2), that flow straight southward. Both branches stretch for approximately 6 km before joining together to form the Lower Grigno Creek. The drainage network has a dendritic pattern.

The complex physiography of the catchment is subdivided in 4 main sectors:

- a) The northernmost portion, upstream the Grigno- Tolvà confluence (GTc) at Ponte della Stua;
- b) Downstream the GTc, extending over the villages of Castello Tesino and Pieve Tesino;
- c) From the villages of Castello and Pieve Tesino until the junction with Boalon creek;
- d) From Boalon creek to Brenta river confluence

In the first sector (a), the maximum elevation is reached (Cima d’Asta – 2847 m asl). South of the main peak the Grigno creek originates from Cima d’Asta lake (2451 m asl), following a NE-SW trend. Approximately 2.5 km downstream (1615 m asl), the channel diverts to a NNW-SSE direction, until the confluence with Tolvà creek (4.9 km downstream). A N-S trending water divide (Monte Coston – Il Passetto ridge) separates the Upper Grigno valley from the Tolvà valley (13.6 km²). The Tolvà creek originates at 1950 m asl, on the eastern flank of Il Passetto peak, flowing southwards. The Tolvà creek enters the Upper Grigno creek at Ponte della Stua (1109 m asl).

The (b) sector extends from GTc, downstream to the municipalities of Pieve Tesino (843 m asl) and Castello Tesino (899 m asl). The valley has a N-S direction and collects water coming from Rio Quarazza and from a secondary valley on the hydrographic right, Val Donega. As previous, this sector is characterized by steep valley flanks, even if the height of the drain divide decreases southwards. A flattened area cuts the main valley immediately north of Monte Silana, following into Val Donega.

The (c) sector exhibit a physiographic change, with the valley widening in the E-W direction. The continuity of valley flanks is interrupted by low gradient reaches (800-850 m asl), such as those in which Governana creek and Solcena creek flow. The topography reveals a complexity that differs on the valley sides. On the hydrographic right, east of Castello Tesino, the Monte Picosta ridge (1421 m asl) is oriented NW-SE. Southwards the Eguadona valley, the main ridges are oriented N-S. On the hydrographic right, there is an arcuate topography, trending N-S (Cima La Presa – Monte Mezza).

In the (d) sector, the drainage divide of the Grigno valley on the hydrographic left (Monte Mezza – Sasso Rosso) follows a meridian trend that folds towards NW-SE direction close to Grigno village. On the hydrographic right, the general topographic trend is N-S. The Grigno creek, on this portion, flows into a deep canyon trending NNW-SSE, before entering the floodplain (260 m asl) at the junction with Brenta river (243 m asl).

The hydrological pattern in the Cima d'Asta area is closely related to the presence of the batholith, that causes a radial divergence of the network from its maximum topographic elevation. The hydrological network of the Grigno-Tolvà system originates from the southern face of granitic mass, and the main stem runs N-S. Upstream of Ponte della Stua, the network formed by Upper Grigno and Tolvà creek is V-shaped. Tributaries of the Lower Grigno Creek form angles $\leq 90^\circ$ at the confluence with the main channel. The network of Grigno tributaries is parallel, E-W oriented. Tolvà creek tributaries are subparallel, oriented NE-SW. One of the most important tributaries of the Grigno, excluding Tolvà, is represented by Quarazza creek (4.11 km²), that enters the main stem immediately south of GTC, following an E-W trend. Downstream, the only remarkable tributary is Secco Creek (6.3 km²), on the hydrographic left. On the western flank of the Grigno valley network drainage is poorly developed, and tributaries aligned E-W. Downstream, the Governana Creek (12.8 km²) enters the main stem from east, in the surroundings of Pieve Tesino and Castello Tesino villages. North of this confluence, Solcena Creek (5.6 km²) enters the Grigno channel. The former flows along a NE-SW direction, while the latter follows a NNW-SSE trend. Small tributaries, oriented E-W, enter the main watercourse in the area between Cinte Tesino and Castello Tesino. Southwards of Eguadona creek (1 km upstream Grigno village), entering the Murello Canyon, the Lower Grigno Creek shows frequent changes in direction. Once in the floodplain, the artificial channel exhibits a slight change in direction, from N-S to NW-SE.

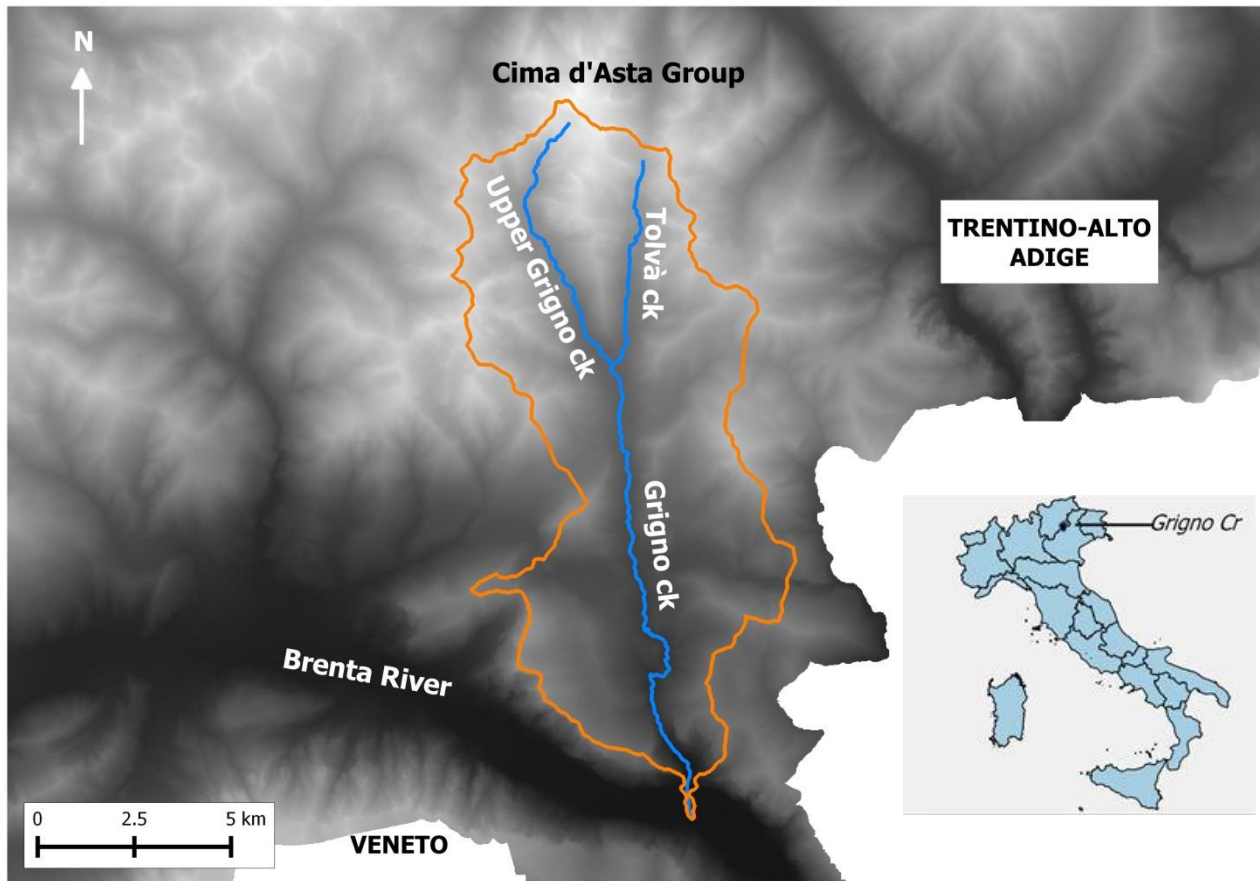


Figure 2.1. The Grigno and Tolva Creek basin.

The geology of the basin is composed by three main lithological units (Figure 2.2):

- the crystalline basement (Pre-Permian micaschysts and phillads)
- the ercinian batholith of Cima d'Asta
- the sedimentary units (Upper Triassic – Oligocene)

The upper part of the basin belongs to the Cima d'Asta Batholith that intruded during the Upper Carboniferous-Lower Permian period (275-300 My, Ferrara et al., 1962; Bertrand et al., 1965). Approximately south of the Tolva-Upper Grigno confluence. The batholith includes monzonite, monzogranite, tonalite, -granodiorite, and granite. The northwestern sector of the basin is underlain by pre-Permian micaceous schysts and phyllites, showing lateral continuity with the granitoids and intersected by porphyroids (Note illustrative della Carta Geologica d'Italia, Foglio 22 "Feltre", 1971). The mid-to-lower part of the basin is underlain by cherty limestones (Jurassic – Upper Cretacic) of Biancone and Scaglia Rossa Formations. Liassic limestones outcrop in the central portion of the basin, forming along with Upper Cretacic-Oligocene clastic carbonates, the sedimentary unit of the central-lower sector of the catchment.

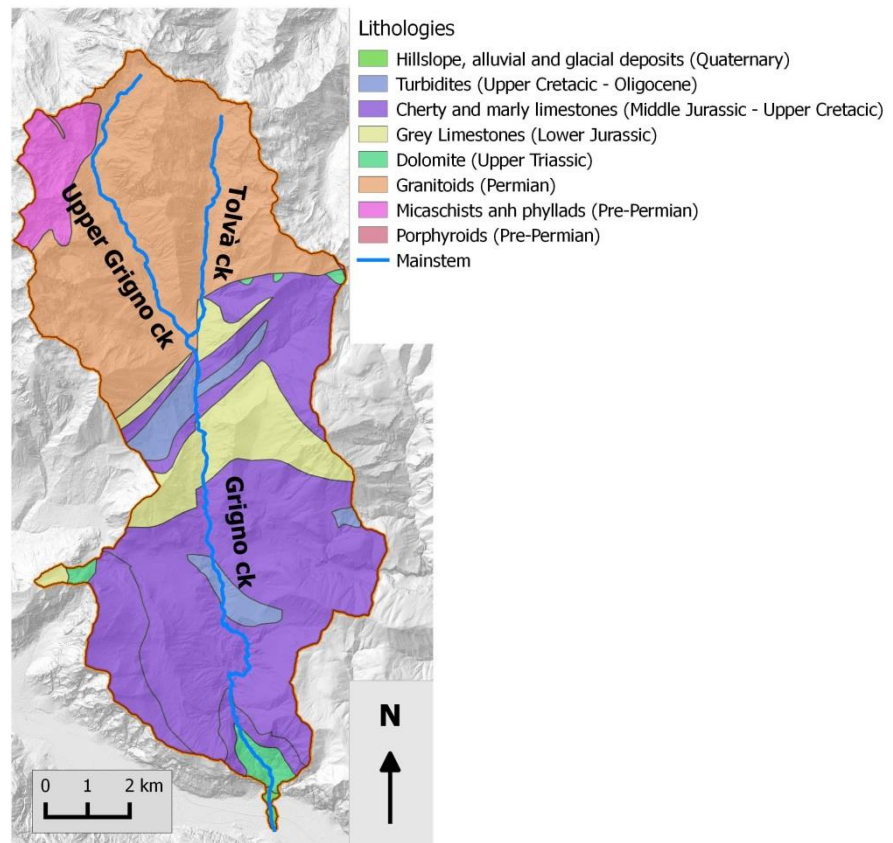


Figure 2.2. Main geo-lithological units of the Grigno-Tolvà Creeks basin.

The most important structural line in the basin is the Valsugana Line, which trends N70 and locally separates the batholith from the sedimentary sequence. The Tolvà valley is imposed along a structural discontinuity (NNE-SSW trend) that intersects the Valsugana Line, causing a sudden change in direction of this latter structure (from NE-SW to NNE-SSW) in correspondence of the Tolvà-Upper Grigno junction. The Tolvà discontinuity extends towards the central portion of the Lower Grigno basin (Note illustrative della Carta Geologica d'Italia, Foglio 22 "Feltre", 1971; Selli, 1998). The geological evolution of the area is strictly related to the geodynamic evolution of the south-eastern Alpine domain. The peculiar characteristics of this sector of Alps between Trento and Cima d'Asta are due to the presence of the Valsugana Paleoline, that bordered the Bacino Vulcanico Atesino Auct. (BVA) on its southern margin. The BVA floor is represented in this area by crystalline basement of the southern Alps domain intruded by the Permian monzogranite pluton of Cima d'Asta (CA). During the Lower Permian, the deposition of porphyry and effusive products is coeval to the intrusion of CA (Barth et al., 1994).

The Borgo Valsugana area (BVs) is a distinctive sector of the southern Alps chain since the entire sequence, from metamorphic and igneous rocks to the clastic Miocene deposits, is outcropping. Rock resistance to weathering has controlled the topographic gradient between Borgo Valsugana through and Cima d'Asta group. In the BVs area tertiary deposits and Bieno phyllites have been eroded deeper than the more tenacious granite body of CA.

Grigno basin currently constitutes an intermediate sector between the BVs and the Tesino region. Stratigraphic record from the two different areas supports the hypothesis that during the post Permian

evolution, the Grigno basin belonged to a persistent structural height. In the Chieppena Valley, adjacent to the western margin of the Grigno basin, pyroclastic material is 15 m thick and is encompassed between crystalline basement and a clastic sedimentary sequence of Lower Permian. On the other hand, in the Lagorai Mountains north of CA, the thickness of effusive deposits (riodacitic ignimbrites) exceeds 1000 m, thus indicating the Chieppena Creek as a local structural height during Lower Permian. The sequence is followed by dark clays alternating to carbonate-evaporitic layers of the Bellerophon Fm. From Lower Triassic to Carnic stage a typical peritidal sequence developed (Werfen Fm.), followed by reddish argillites and pelites overlain by quartz sandstones. During the Anisic-Ladinic time interval, dolomites have been deposited in the area (Valsugana Dolomites, Sindech Dolomites Auct.), followed by Raibl Group Fm. Rocks belonging to this latter formation are characterized by peritidal facies, interbedded by thin polychromous pelitic layers. Peritidal environment persisted during the Noric stage, where Dolomia Principale Fm. deposited. During the Liassic stage, Calcari Grigi Fm. has been deposited, denoting a general shift of the environment towards deeper areas, still highly energetic, characterized by the deposition of packstones and wackestones. From the middle Jurassic to the Paleogene the carbonatic sequence is typical of bacinal environments. The deposition of mudstones and siltites typical of the Rosso Ammonitico Fm. is the first stratigraphic evidence of this paleogeographic evolution. The presence in the upper formation (Biancone Fm.) of pure white micrites confirms the persistence of this depositional environment. Due to subsidence of the area, within the Scaglia Group are found cherty limestones and marly limestones. Following this period the differentiation of the paleogeography has been reconstructed between the sectors of BVs and Tesino. In fact, within the BVs the Scaglia Rossa Fm. (Upper Turonian) is overlain by the Calcare di Nago Fm (Upper Eocene), while in the Tesino sector is overlapped in continuity by Scaglia Cinerea Fm. (Middle-lower Eocene). The last marine sedimentary sequence outcropping in this area is represented by micaceous sandstones and conglomerates of Upper-middle Miocene, deposited during the orogenesis in Valsugana foredeep basin. The thickness of the described sequence in the BVs is about 1500 m, while in the Adige Valley the thickness amounts up to 3300 m. The Borgo Valsugana structural height was bordered in the southern sector by Val di Sella paleoline, separating the Ortigara – Altopiano di Asiago sector from more elevated areas. The northern edge was represented by the Valsugana Paleoline, while the eastern flank was bordered by the Ospedaletto-Val Tolva line. The aforementioned sequence is condensed compared to Adige Valley, excluding the Calcari Grigi Fm. that show the same thickness, indicating that faults controlling the subsidence of the structural height have been activated during Lias stage. Other evidences of the persistence of the structural height derive from limited power of Permian effusions and Biancone Fm (50 m). The sedimentary hiatus on top of Scaglia Rossa Fm. corroborates the condition of structural height at the end of Turonian stage.

The network of structural heights and lows inherited from permo-mesozoic rifting is involved by the collisional events related to the convergence of the Adriatic and European plates. Several thrusts with southern vergence were developed during the Neogene period, causing duplication of sedimentary sequences. The main direction is the Valsugana Line (N70), that from Trento across the southern-east sector of Alps extends towards the eastern portions of the Alps (Figure 2.3). Involved terranes show younger ages from W to E, including the intrusive body of CA, which larger extension is delimited by Tolva Valley and Torcegno village. The study area has been interested by tectonic uplift during the Serravallian-Tortonian interval (Castellarin et al., 2006), with compressional axis N340 that originated the Valsugana Line. This thrust accounts for 10-20 km of crustal shortening in the Southalpine Nappe System. In the Upper Messinian, foredeep deposits are characterized by the presence of granite clasts deriving from the dismantled CA intrusion. This indicates that the Valsugana hangingwall has been uplifted in the Serravallian-Tortonian interval, and the erosion already interested the CA granite body, and the drainage

network reached a foredeep basin that during the Upper Tortonian-Pliocene has been included in the orogeny.

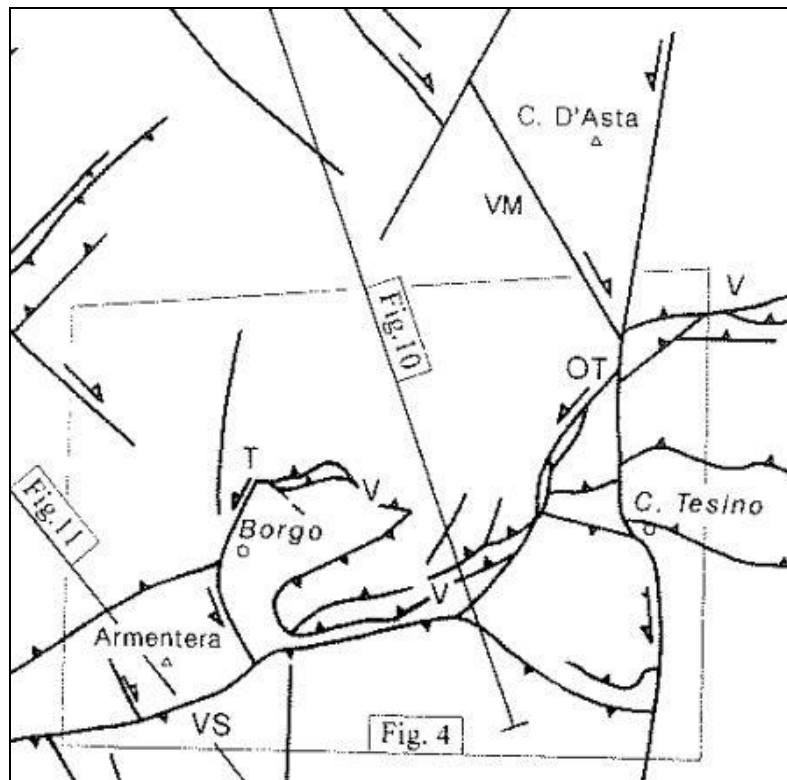


Fig. 2.3. Tectonic setting of the Valsugana – Cima d'Asta area (VM: Val Malene fault; V: Valsugana fault; OT: Ospedaletto-Val Tolva fault; T: Telve fault; VS: Val di Sella fault) (After Selli, 1998; modified) .

Quaternary geology is mainly composed by Pleistocene glacial deposits, unconsolidated slope deposits and alluvial sediments in the valley floors. Glacial blankets are outcropping discontinuously in the basin, showing with different facies. In the uppermost portion, sand-supported ablation till covers the valley flanks and flattened surfaces; here, in the valley bottom, cobbles and boulders are present, as the finer fractions of glacier-driven deposits have been washed out. In the central portion of the basin pro-glacial deposits (glaciofluvial) are hanging tens of meters above the valley bottom, feeding severe transport events during late summer rainfalls in the short tributary channels of the Grigno Creek. Slope deposits covering the flanks and the foothill of the highest reliefs are still active, due to the current evolution of rock cliffs, widely characterizing the uppermost portion of the catchment. Alluvial deposits are commonly found in the valley bottom, in the immediate surroundings of the fluvial entrenchment, forming limited flat planes that might be flooded.

Climatic conditions are typical of Alpine environments. The study area has a mean annual precipitation of 1511 mm, with maxima falling in May-June, as summer convective storms, and in October-November as Atlantic storm fronts. From May to October, monthly average rainfall is about 150 mm, while in November the yearly maximum exceeds 200 mm. Between December and March the minima of precipitation are recorded with less than 50 mm (see Figure 1.2).

Runoff is dominated by snowmelt, from late April to June, but summer and early autumn floods represent an important contribution to the flow regime. Another important contribution may be represented by rain-on-snow events, especially during May.

2.1.2 Ussaia basin

The Ussaia Creek is a right tributary of the Noce River, the main hydrological stem of western Trentino region, draining waters from the Val di Sole. This valley is located in the northwestern sector of Trentino region, bordered by Lombardia (Figure 2.4) and extending for approximately 610 km. The valley is elongated for about 50 kilometers along the direction WSW-ENE, joining downstream the Val di Non and being surrounded by several mountain ranges: the Ortles-Cevedale group by North, Brenta group at East and the Adamello-Presanella range at South. Its northern border is represented by Mount Cevedale (3764 m slm) and Cima Sternai (3443 m slm), the western border is Punta S. Matteo (3678 m) and Corno dei Tre Signori (3359 m) and the southern border is represented by Presanella (3556 m) and Monte Spinale (2104 m). Some of these mountain ranges are currently partly covered by glaciers, such as Cevedale and Presanella, or Cima Sternai, from which the most important tributaries of Noce river, origin. The main tributary valleys are Val di Peio, Val di Rabbi and Val Meledrio. The Val di Peio is cut by Rio Noce Nero, that originates from Corno dei Tre Signori (3360 m) and Rio Noce Bianco, flowing from the south-eastern face of Monte Cevedale (3769 m) covered by the glacier of Vedretta de la Mare and running by 18 km along N-S direction. Close to the Cogolo village (1172 m), the two creeks join, originating the Noce River; here, the river flows along Val di Sole and Val di Non, entering the Adige Valley, the main valley of Trentino-Alto Adige region, close to the Zambana village (206 m asl).

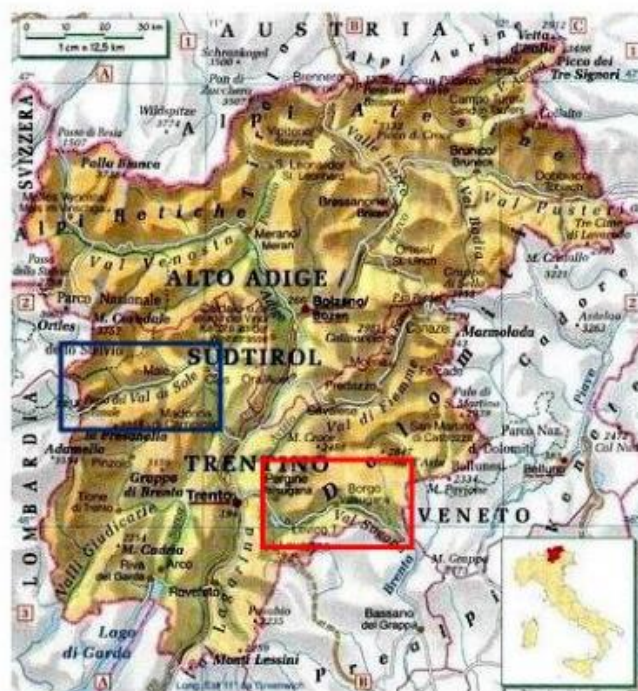


Figure 2.4. Localization of the Val di Sole (blue square).

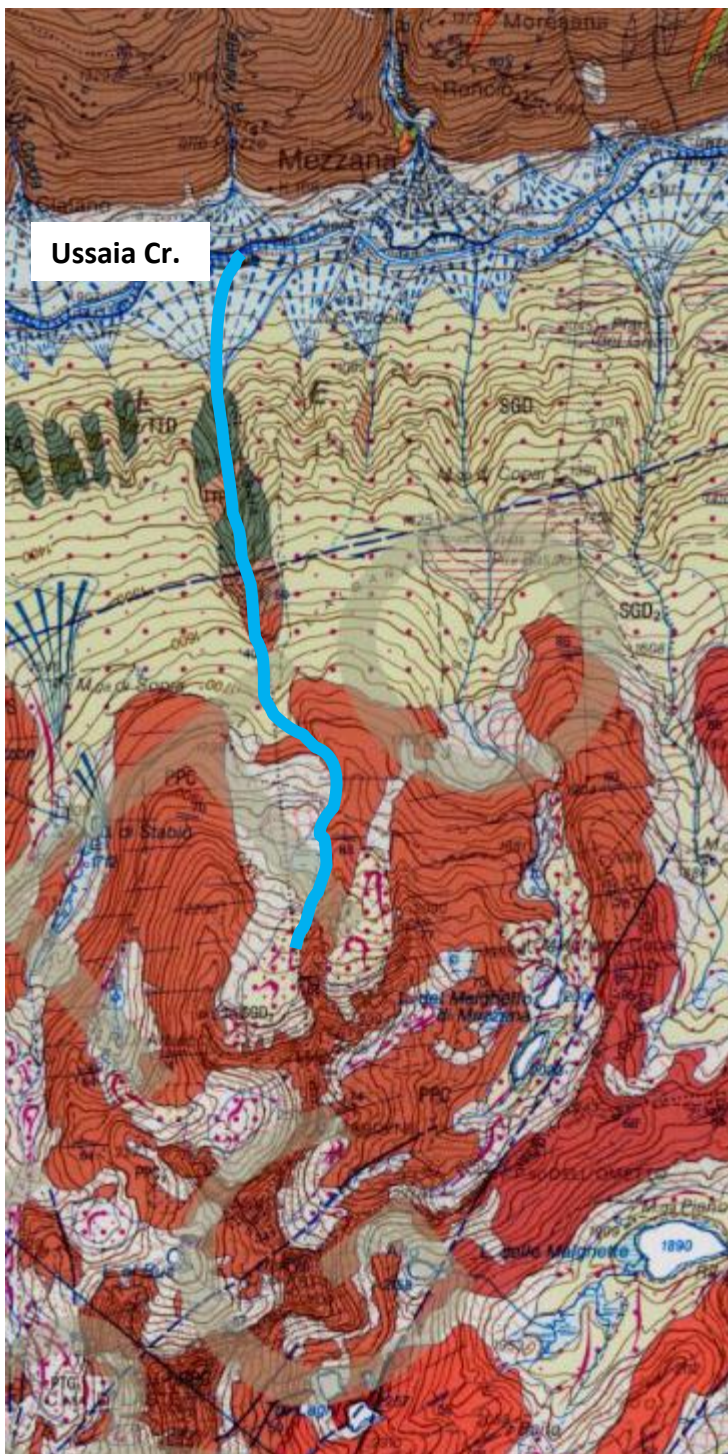
This sector is characterized by a typical alpine climate, with short and cool summer and winter characterized by abundant snow precipitations. The average monthly temperature of the hottest month (August) is about 15 °C, while during the coldest month (January) is about -2 °C. The precipitations show generally values about 1000 mm in the lowest portion of the valley, with maxima falling in springtime and autumn; snowmelt accumulation is normally extended from December until March. The climatic diagram at Mezzana (905 m slm) meteorological station shows temperature records that are referred to the period 1920 - 2014, whereas precipitations are referred to 1988- 2014 interval (see Figure 1.2).

Comparing climographs from Passo Brocon (see Figure 1.2) and from Mezzana, results that precipitations are less abundant in Val di Sole, reaching values of about 844 mm. Maxima are falling in late spring and autumn, with November showing the absolute maximum value of average monthly precipitation.

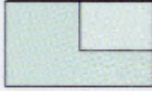
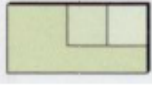
Val di Sole is a relicts glacial trough that intersects the Tonale Fault Line. It is characterized by steep flanks and a large valley bottom, filled by alluvial deposits and debris layed down during the glacial retreat. The longitudinal trend along the alpine chain, highlights the differences in the morphology and vegetation distribution of the flanks. The southern flank is characterized by the presence of glacial till and is dominated by forest trees; on the other hand the northern flank is characterized by limited amounts of glacial till. The southern flank of Val di Sole is within the Presanella massif; this sector is characterized by short and suspended glacial troughs hanging on the main valley, where limited glaciers located at the junctions of valley steps. The main glacier is Val Piana, located south of Ossana village. This side is rich of glacial cirques imposed on the intrusive complex and cover by thick blankets of glacial till (Figure 2.5). The morphology of the southern sector, comprised within the Brenta and located eastern with respect to the Presanella Massif is more morphologically complex that the other. The most frequent morphologies in the Brenta Group are cirques and glacial troughs, incised during the Tardiglacial period (Upper Pleistocene). Carbonatic rocks are extensively outcropping in this area, characterized by karst highlands where deep circulation of groundwater is dominant. The northern slope includes two important lateral valleys: Val di Peio and Val di Rabbi. In the first the metamorphic units of the Austroalpine domain are outcropping, and is divided in two: Val del Monte at east and Val de la Mare at north. Val del Monte is characterized on its northern flank by steep slopes with gullies incised by avalanches. On the other flank slopes are less steep, and are connected to the kame terrace of Pejo village. Val de la Mare is oriented along N-S direction and is characterized by steep slopes covered by forest trees is its lower portions and by alluvial and glacial deposits in its upper portions. In the Val di Rabbi the imprinting left by glaciers is still visible. The morphology is currently characterized by the presence of alluvial deposits of Rio Rabbies and by abundant colluvial material in its upper portions.

Val di Sole cuts the tectonic limit between the Austroalpine and Sudalpine domains, defined by the two segments of Periadriatic line (Linea Insubrica s.l.), Tonale and North Giudicarie Fault line (e.g. Castellarin et al., 1998; Doglioni, 1987; Prosser, 2000). In the northwestern sector of the valley outcrop the metamorphic units of the Austroalpine domain ("SVS" Schists, Figure 2.5), while the southeastern sector is underlain by the units of the Sudalpine domain. This latter is characterized by the presence of the plutonic complex of the Adamello-Presanella batholith intruded within the sedimentary sequences of Triassic-Cretacic age (e.g. Castellarin et al., 1977), bounded by the North Giudicarie Fault Line. The other main tectonic segment, is the Tonale Fault line, extended from Ponte di legno to Dimaro, and separating the Tonale-Val d'Ultimo units (Austroalpine domain), from the basement of Sudalpine domain and from the Adamello batholith. From the tectonic settings derives that the actual configuration of the Val di Sole results from three main

phases: a) the Paleogenic continental collision; b) the intrusion of the Adamello batholith (Upper Eocene – Lower Oligocene); c) the extensional regime of the overall Periadriatic sector from the Upper Oligocene. Following these phases, the more recent compressive or transpressive regimes of Neogenic age, that lead to rejuvenation or reactivation of ancestral fault lines, and the formation of the thrust of the Brenta Group. In the upper portion of the studied basin outcrop the tonalites of the Adamello batholith (“PPC” Tonalite, Figure 2.5) that intruded during Oligocene the Pre-Permian Paragneiss (“TTP” Paragneiss, Figure 2.5).



BEDROCK GEOLOGY

-  PTG - Postglacial Alpine Sythem (Upp. Pleistocene - Olocene)
-  SGD - Garda Sythem (Upper Pleistocene)
-  PPC - Tonalite (Oligocene)
-  SVS - Schist (Pre-Permian)
-  TTP - Paragneiss (Pre-Permian)
-  TTA - Amphibolite (Pre-Permian)

SURFICIAL DEPOSITS

-  Hillslope
-  Landslide
-  Alluvial
-  Swamp
-  Glacigenic
-  Right transverse fault
-  Fluvial terrace
-  Rock glacier
-  Debris flow fan

Figure 2.5. Geological map of the area surrounding the Ussaia Creek watershed (from CARG sheet n. 42 “Malè”, modified).

2.1.3 Strimm basin

The Strimm basin (area 8.5 km², maximum elevation 3197 m a.s.l., minimum elevation 1394 m a.s.l., average slope 61.8%) is located in the upper Vinschgau/Venosta valley, in South Tyrol, Italy (Figure 2.6). The Venosta valley is extended for about 1442 km², and is the most western sector of the Bolzano province. In the portion close to the study basin, the valley is oriented along E-W direction, and reaches its highest point within the Ortles range in the southwest sector. Towards north-east it is bordered from the Alpi Venoste.

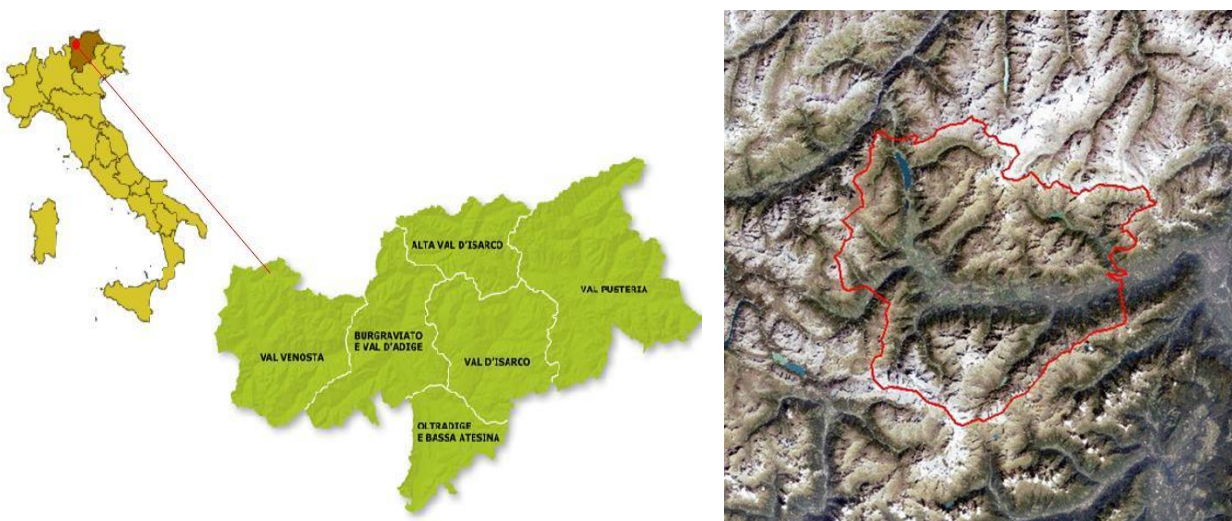


Figure 2.6. Location of the Venosta Valley (left) and its geographic borders (right).

Venosta Valley is one of the most dry sectors of the Eastern Alps, with a mean annual precipitation of 500 mm (year interval 2001-2010), well below the average of 2500-3000 mm typical of the alpine environments. Precipitation maxima fall in July (72.4 mm) and August (85.8 mm); in the same months average temperatures are about 26 and 25 °C, respectively (see Figure 1.2). The coldest months are December and January, for which monthly mean temperatures are -3.8 °C. The total number of 300 sunny days per year and the strong thermal excursions are imposing a unique, arid-steppic microclimate.

The morphological setting of the Venosta valley is determined by the glacial and periglacial processes that dominated along its flanks after the Last Glacial Maximum (LGM). The largest glacier of Late Pleistocene was the Adige glacier, that reached its maximum extension between 30,000 and 21-28,000 years before present, during the LGM (e.g. Cremaschi et al., 1987; Lambeck et al., 2002). The maximum elevation reached by its surface was between 2800 – 3000 m asl in the region of Engadina, (e.g. Florineth&Schluchter, 1998; Kelly et al., 2004). After the LGM a series of glacier advancements occurred, before the onset of Bolling-Allerod stage (Ivy-Ochs et al., 2006). The post-glacial history of Venosta valley began approximately 14,000 years before present. Between 14 e 12,5 years BP, the limit of trees cover has been positioned among 1700-1800 m asl (e.g. Heiss et al., 2005; Vescovi et al., 2007). During this time interval at altitudes higher than 2100-2550 m asl, periglacial processes dominated the slopes while the lower portions were forested. At the onset of the Olocene, the rapid warming determined an increase of

the altitude of tree cover limit, reaching values of 2400-2600 m asl (Tinner&Kaltenrieder, 2005; Aceti, 2005).

The present-day erosional activity is mainly driven by drainage network; beyond this, the macroforms of the actual landscape were clearly sculpted by glaciers. As a matter of fact there are several cirques and glaciers located in the aretes, while at lower altitudes roches moutonnées clearly testify the activity of past glaciers. The main glacial forms in the area are frontal and lateral moraines. At lower altitudes the landscape is dominated by periglacial processes and are clearly visible depositional forms such as rock glaciers, currently located between the limit of trees cover and below the ridges. In addition to these two environments, debris flow channels are very common in the landscape. The presence of mass-waste processes is testified by the presence of talus slopes and cones located at the footsteps of rocky cliffs.

From the point of view of tectonics, Venosta valley is within the Austroalpine domain. The study areas and the central portion of Venosta valley, is between the Ortles and the Campo units, close to the Engadina and Periadriatic lines (e.g. Sölva et al., 2005). These units are separated by the Vinschgau shear zone, and are mainly composed by metamorphic lithologies such as schists and gneiss associated with amphibolites and subordinately marbles and orthogneiss. The Campo and Ötztal units are characterized by fracture zones trending N, E, NE, and SW (Agliardi et al., 2009), imposing a structural control over the drainage network and lowering the strength parameters of rock formations.

2.2 Monitoring sites

2.2.1 Grigno and Tolvà Creeks

The monitored reach of the Grigno basin is located in its upper portion (basin area at monitoring site 7 km², elevation 1560 m asl, Figure 2.7) is underlain by granitic complex of the Cima d'Asta unit (Ercinic), except from the northwestern corner where pre-Permian schysts and phyllites outcrop. These two creeks flow over colluvial deposits and within its basin there several bodies of glacial till, that are covering the valley bottom in a discontinuous fashion.

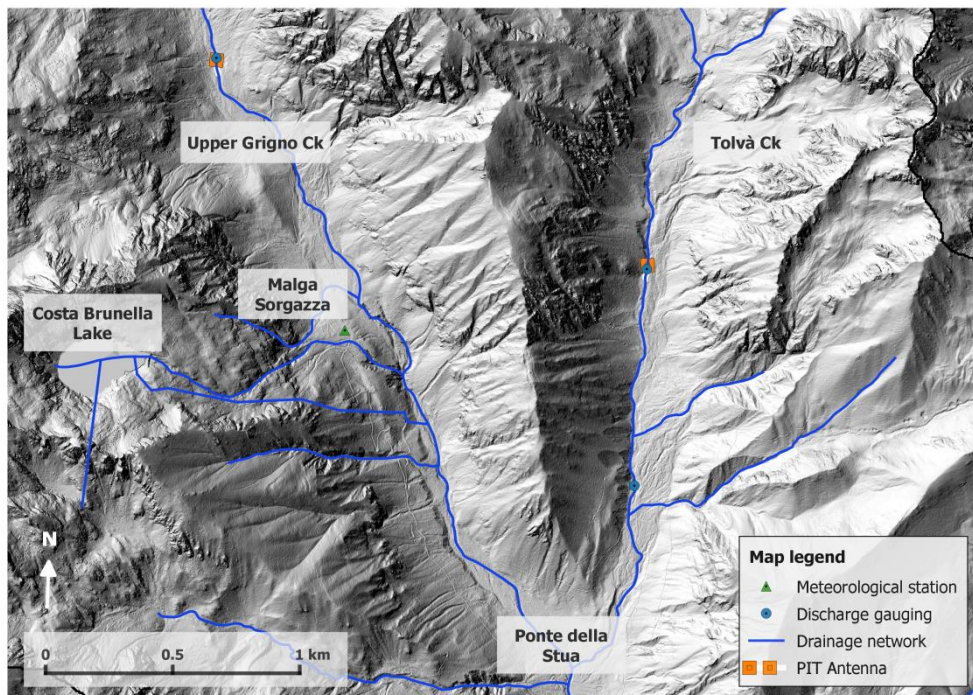


Fig. 2.7. The Grigno Creek basin and the monitoring setup.

The Grigno valley (Figure 2.8), is highly confined in its upper portions, while downstream the valley floor gradually broadens.

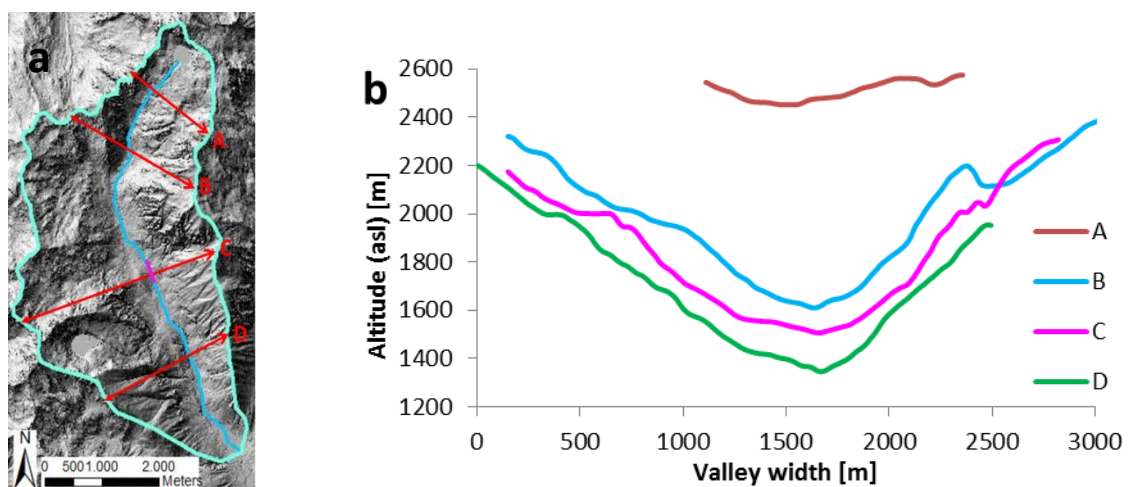


Figure 2.8. a) Digital terrain model of the watershed; b) longitudinal profiles along the Grigno Creek valley (A: headwaters; B: intermediate sector; C: monitoring area; D: lowland sector).

As shown in Figure 2.11, the headwater portions of the catchment are characterized by the presence of an overhanging cliff and a bedrock reach (Figure 2.9). Downstream, the valley gradient is reduced and located in the valley step is highlighted the monitored reach.

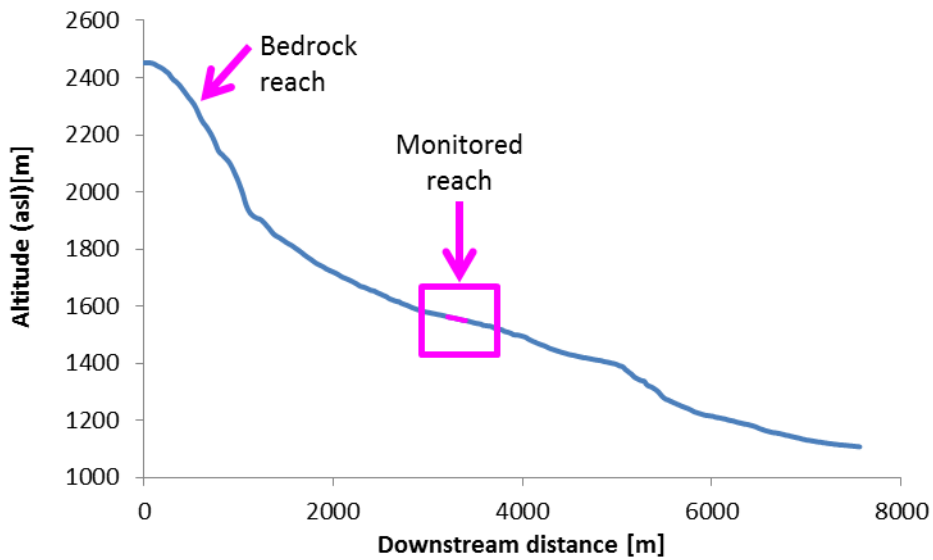


Figure 2.9. Longitudinal profile of the upper portion of the Grigno Creek.

The monitored reach of the Tolvà Creek is located in its intermediate portion (basin area at monitoring site 7 km², elevation 1405 m asl). Similarly to Grigno Creek, the transversal profiles of Tolvà Creek (Figure 2.10) are clearly showing the high value of confinement in the upper portions of the watershed, gradually decreasing downstream.

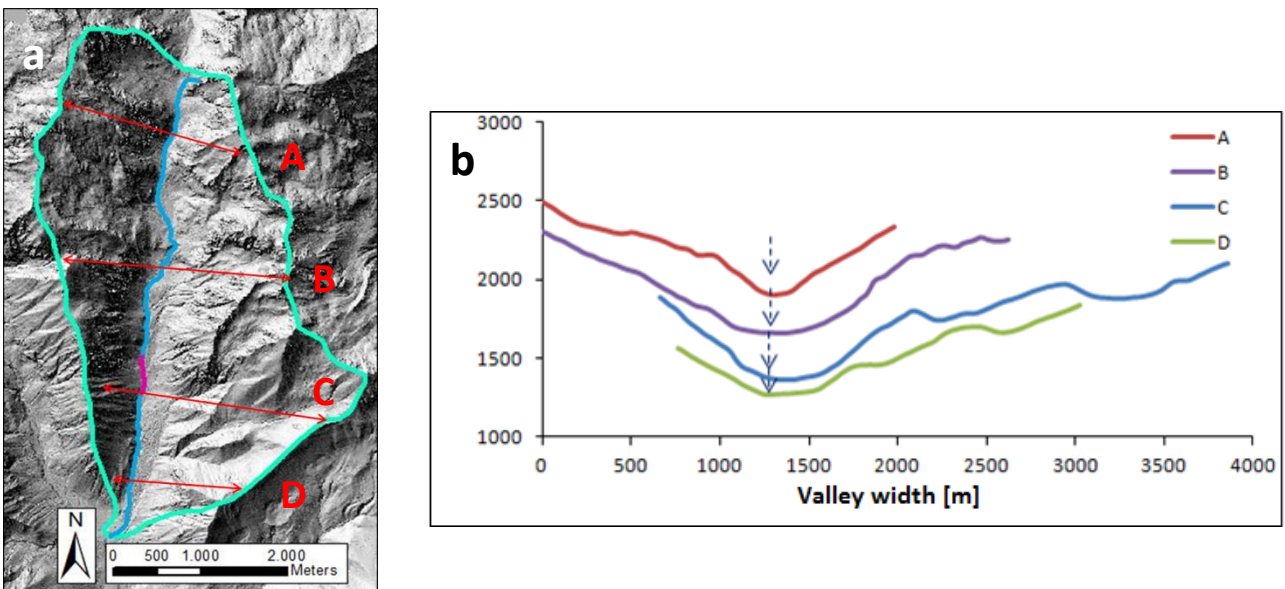


Figure 2.10. a) Digital terrain model of the watershed; b) longitudinal profiles along the Tolvà Creek valley (A: headwaters; B: intermediate sector; C: monitoring area; D: lowland sector).

Compared to Grigno, the Tolvà Creek is not characterized by rock walls in its upper portions. A fluvio-glacial, hanging valley nearly at 1700 m asl, is present upstream the monitoring site (Figure 2.11).

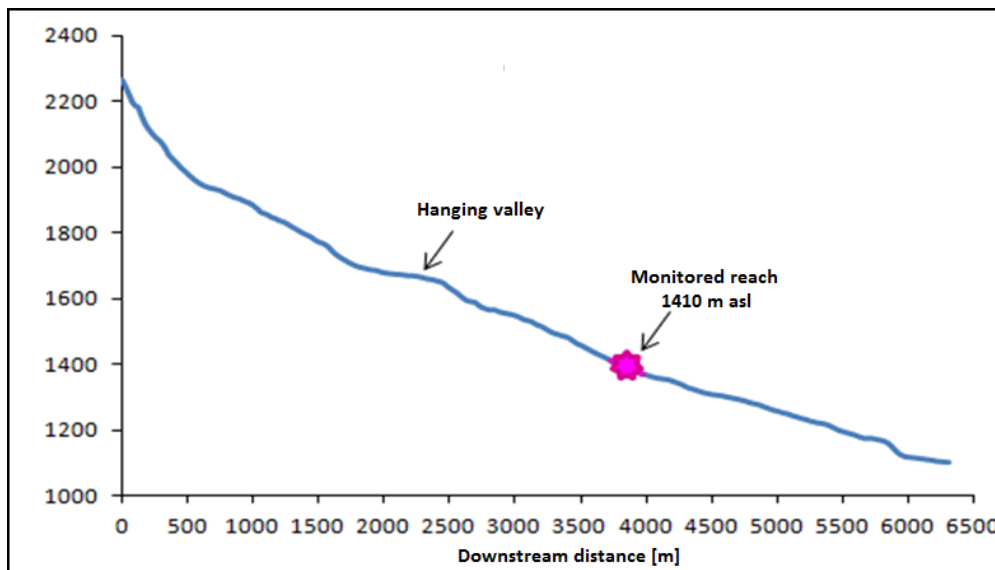


Figure 2.11. Longitudinal profile of the upper portion of the Tolvà Creek.

The Grigno and Tolvà monitoring sites (Figure 2.12) are characterized by a steep, rugged morphology. Channel reach morphology is dominated by step-pools and boulder-cascades (e.g., Montgomery and Buffington, 1997).





Figure 2.12. Representative morphological structures in the Grigno Creek (plates a-b-c-d) and Tolvà Creek (plates e-f-g-h). Grigno creek: a) step; b) deep pool; c)step – plane bed; d) plane bed - pool. Tolvà Creek: e) deep pool; f)plane bed; g)plane bed – pool; h) step .

The last adjustment of the valley floor derives from the large flood of the November 4th 1966. From written memories of locals this flood can be considered worse than the one occurred in 1882; from pictures taken immediately after the disaster it is possible to evaluate the size of the boulders transported downstream (Figure 2.13), clear evidence of the flow competence that characterized that event. For this reason check dams were built in the lowland sectors of the Grigno valley.

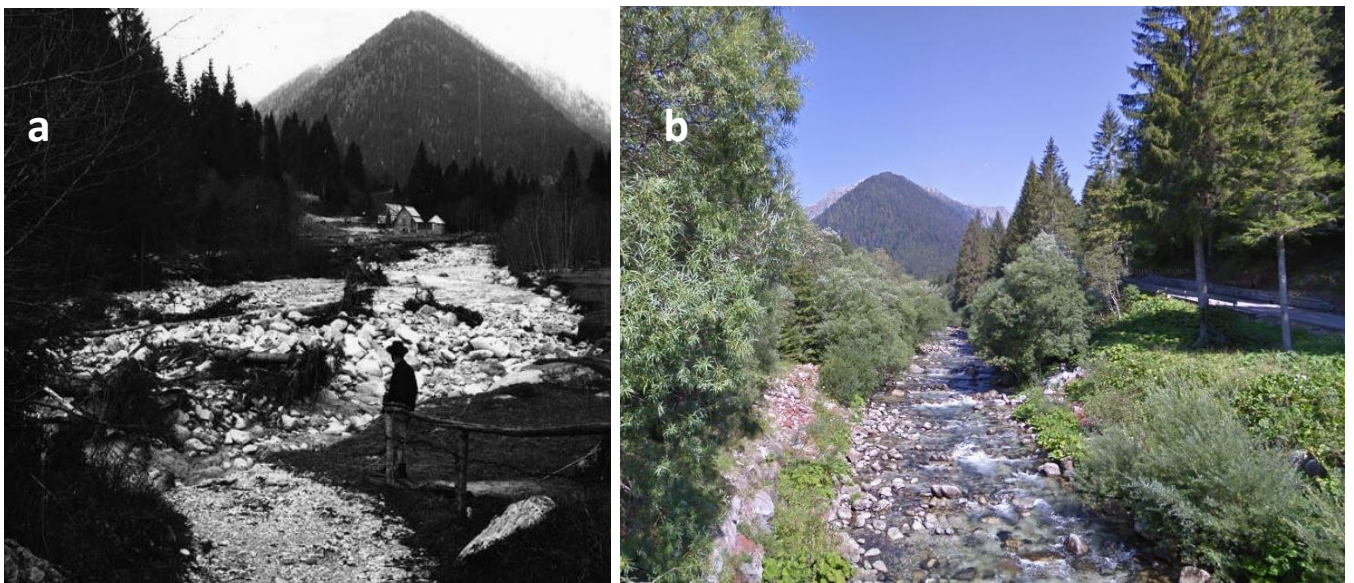


Figure 2.13. Pieve Tesino, Val Malene. The Grigno Creek immediately downstream of the confluence with Tolvà creeks, a) after the large flood of November 1966, where logs and large boulders were freshly

deposited in the floodplain (from, La Brentana: l'alluvione del 1966 nella Valsugana Orientale, modified); b) today, the same section is completely channelized, with large boulders forming the steep artificial banks.

2.2.2 Ussaia Creek

The Ussaia creek (basin area 2.3 km², max elevation 2389 m, min elevation 890 m asl) originates from a relict glacial cirque and flows, in its upper portion, on colluvial material. The glacial imprinting is evident in the upper portion, because of the presence of a relict rock glacier and also because of the sharp change in the valley gradient (Figure 2.14), due to the presence of the glacial incision. At 1900 m asl, cuts a thick glacial blanket (> 20 m), highly heterometric and characterized by the presence of large boulders (Figure 2.15), that represent the sediment source for the material transported by the Ussaia creek. In the intermediate sector (1500 m asl), the stream cuts rocks belonging to the Alpine basement, intersecting a tectonic contact between paragneiss and a lenticular body of amphibolite. In the lower portion (1100 m asl), as the valley slope decreases the bottom widens. Here is present a large debris cone, highly vegetated in its upper portion, and modeled by anthropic adjustments in its lower portion. Both deposits, glacial and alluvial, are eroded from the granitic lithology of the Adamello-Presanella batholith.

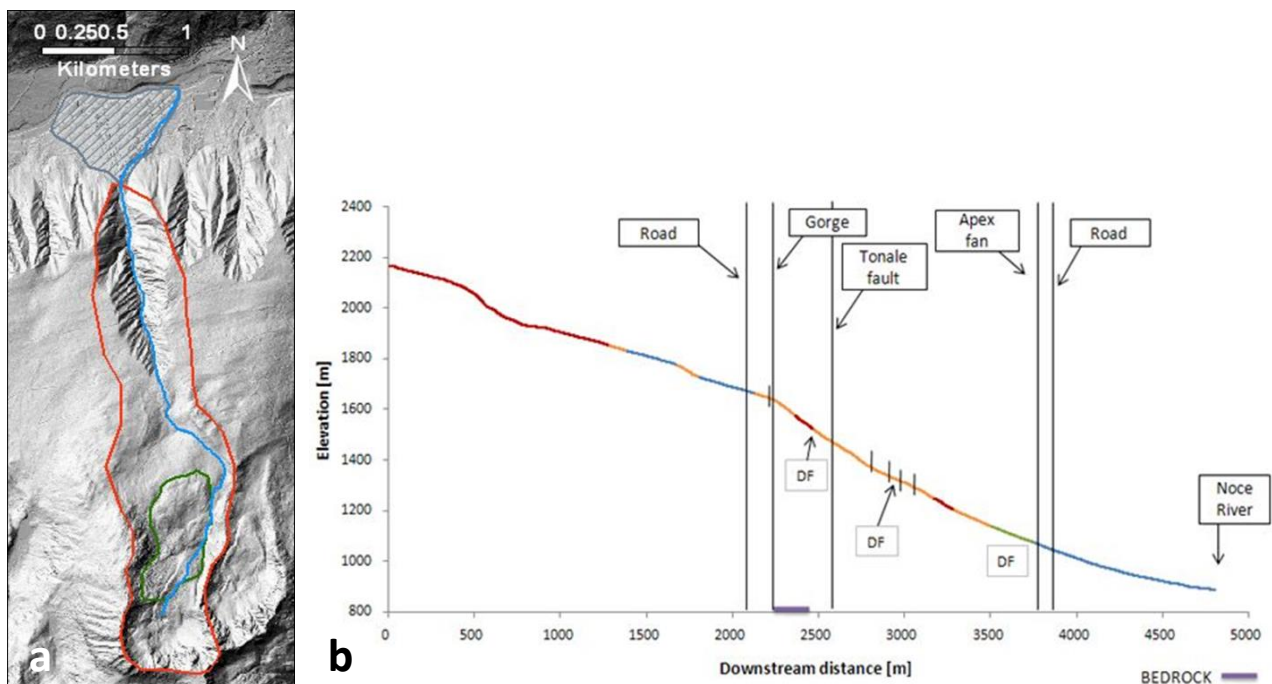


Figure 2.14. a) Digital terrain model of the watershed; b) longitudinal profile along the Ussaia mainstem.

In the headwater of Ussaia catchment, the valley exhibits a high grade of confinement. At about 1700 m asl, the presence of a tectonic limit (Tonale Fault Line) determines a deterioration of the mechanical properties of the rocks, allowing a gorge to be incised. Within the monitored reach the later confinement is reduced as the talus develops further downstream entering the Noce River.

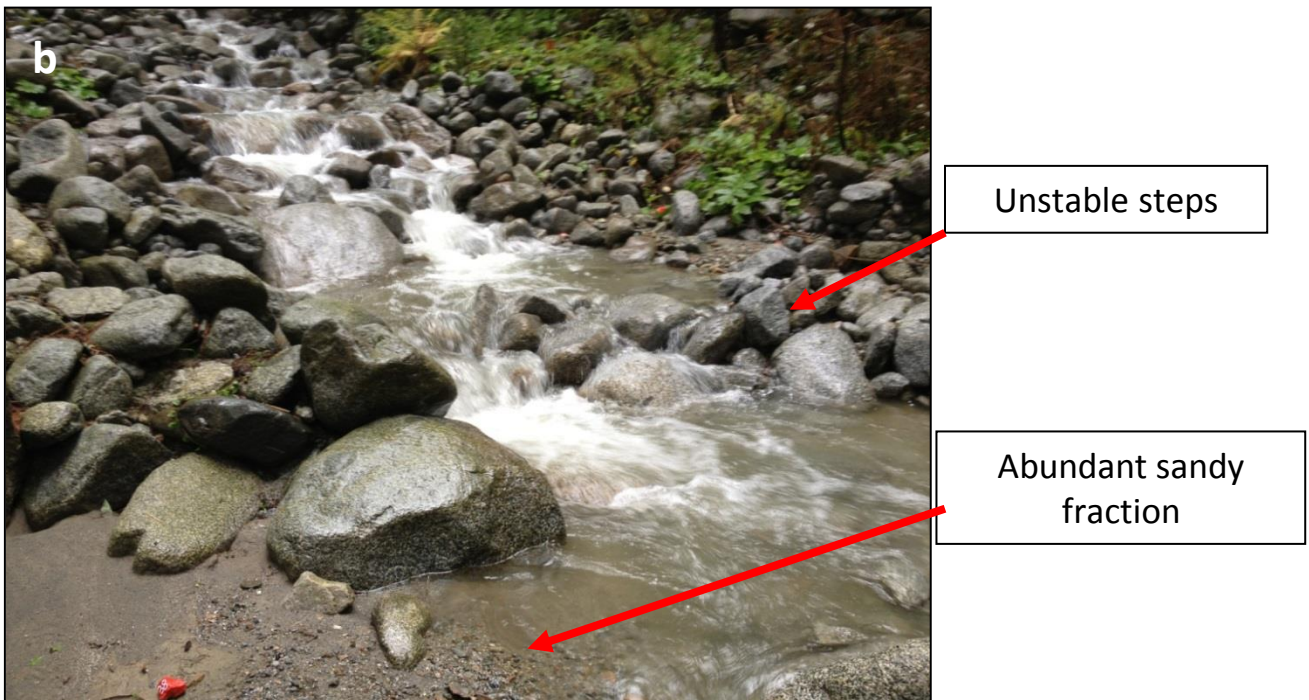


Figure 2.15. a) The thick glacigenic blanket acting a source of material, and the Ussaia Creek flowing at the footsteps of the talus; b) monitored reach of the Ussaia Creek: a typical step-pool sequence, characterized by highly instability of the steps, caused by the abundant sandy fraction, visible on the lateral deposit.

2.2.3 Strimm Creek

The Strimm Creek originates from The Allitz Lakes (2650 m asl), and joins Gatria Creek (a channel monitored for debris flows, see Comiti et al., 2014), in proximity of a filter check dam, which functions as outlet section for both basins. From the junction, the stream is called Allitz Creek and flows into the Adige / Etsch River after crossing one of the largest alluvial fans in the Alps (about 10 km²).

Most of the upper portion of the Strimm basin is underlain by paragneiss of the Mazia unit (Habler et al., 2009), except for the distal-most part of the basin, in which orthogneiss outcrops. Currently active processes include periglacial, fluvial, and colluvial transport. Periglacial activity is prevalent on the talus slopes of the upper Strimm basin (i.e., several intact rock glaciers), fluvial transport occurs along the main stem of the Strimm Creek, from the hanging valley floor down to the confluence with Gatria Creek. Colluvial processes (mostly channelized debris flows) dominate the sediment transfer from the steep hillsides and tributaries – located downstream of the rocky valley step – to main channel in the medium-lower part of the basin.

The monitoring site is located at about 2500 m asl, and from the release zone to the morphological step the stream flows for about 1.2 km. The step is comprised between 2400 and 2200 m asl, and imposes a disconnection among the US and LS.

Sediment connectivity in the Strimm and Gatria basins has been previously investigated through a geomorphometric index (Cavalli et al., 2013), which highlighted how the upper portion of the Strimm basin – corresponding to the hanging valley (Figure 2.16), hereafter called “Upper Strimm”, US – is poorly connected to the basin outlet, whereas the intermediate-lower parts (“Lower Strimm”, LS) feature much higher connectivity. Rapids and cascade units are prevalent in the US part (average 4% slope), whereas bed morphology is predominantly stepped (cascade and step-pool units) in the LS part (average 10% slope). Channel width is on average 4 m in both the upper and the lower part.

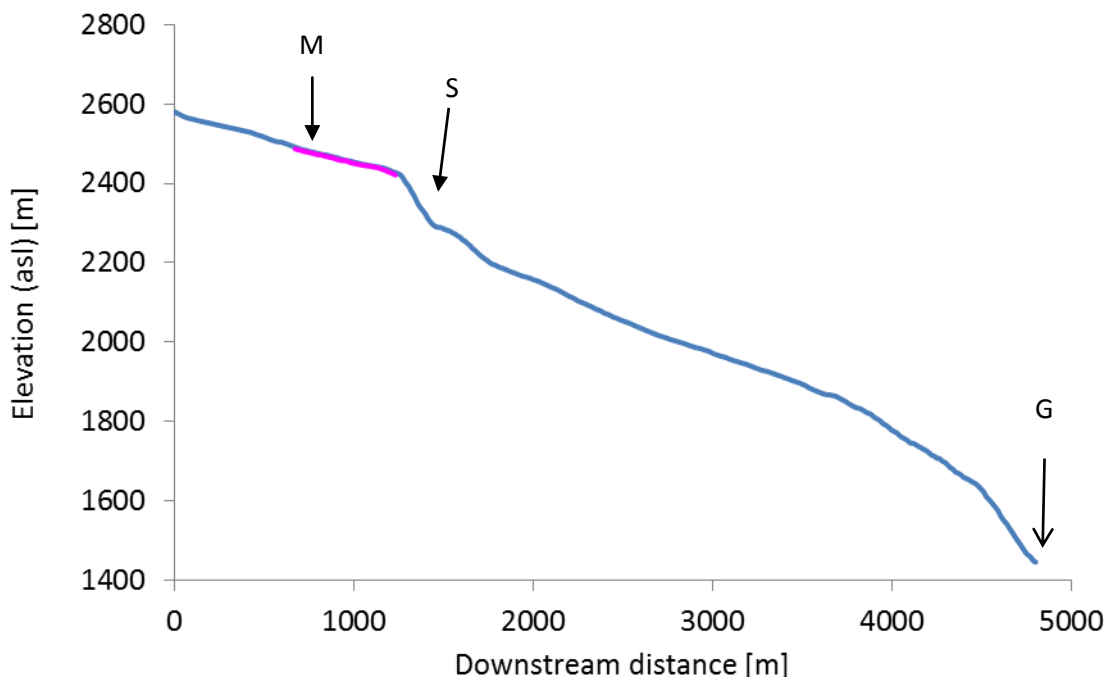


Figure 2.16. Longitudinal profile along the Strimm Creek. Highlighted the monitoring site (M, purple line), the morphological step (S) and the junction with the Gatria Creek (G).

CHAPTER 3

Data collection and methods

In the current chapter we present the methods adopted for data collection in the field. We begin focusing on the techniques adopted to survey the topography of the reaches, to describe quantitatively variables such as channel slope, width, grain size distribution and active layer depth. The Structure from Motion technique, used to determine active channel width, is also described in this section. Concerning channel sections, we first describe the cross sections surveyed at each monitored reach and successively we focus on downstream hydraulic geometry, describing cross sections surveyed at basin scale. Then we present the methods used to estimate the liquid discharge, followed by the description of the location of the meteorological stations available to obtain precipitation and atmospheric temperature data. The next section concerns the bedload monitoring technique, presenting the methods used to release the tracers and track their position after each relevant flood. Linking bedload data to discharge, and following the approach of the flow competence method, we will describe how threshold discharges are obtained, allowing to calculate the virtual velocities of tracers, and finally estimate the bedload volume transfer. At the end of the chapter rainfall intensity-duration thresholds will be linked to bedload events.

3.1 Boundary conditions: reach scale bed topography

3.1.1 Channel bed topography

Channel bed topography was surveyed at all four monitoring sites. The frequency of these surveys was dictated by the overall channel stability. Specifically, in the Ussaia Creek site, which experiences frequent morphological changes, surveys were conducted on a yearly basis. Conversely, at the Grigno, Tolvà, and Upper Strimm Creek, all characterized by immobile key stones, we conducted one topographic survey only.

The longitudinal profile of Ussaia Creek was monitored from 2012 to 2015. The monitored reach extends from the upstream section of PIT release downstream to a stable artificial cascade, for a total length of approximately 220 m. We repeated the surveys in the same period of the year, i.e. at the end of June/beginning of July. The same typology of survey has been conducted on the Grigno and Tolvà Creeks, where, due to their morphological stability the longitudinal profile along the thalweg is surveyed only once, during September 2014.

At Ussaia Creek, we used a Leica TCS705 total station that records the coordinates x,y and z of the selected topographic points along the longitudinal profile. Two operators were necessary to complete the survey in 8 hours, registering the morphologies encountered along the thalweg and describing every unique situation in the channel at the time of survey. In particular we sampled the topography at each break determined by the presence of a step and pool, collecting the highest point of the step and the immediate downstream beginning of the pool. To ensure a more detailed restitution of the morphological surface we surveyed the deepest point of each pool and we distinguished across several morphological types, such as rapid, cascade, plane bed or chutes. To repeat the topographical survey each year we installed a fixed reference

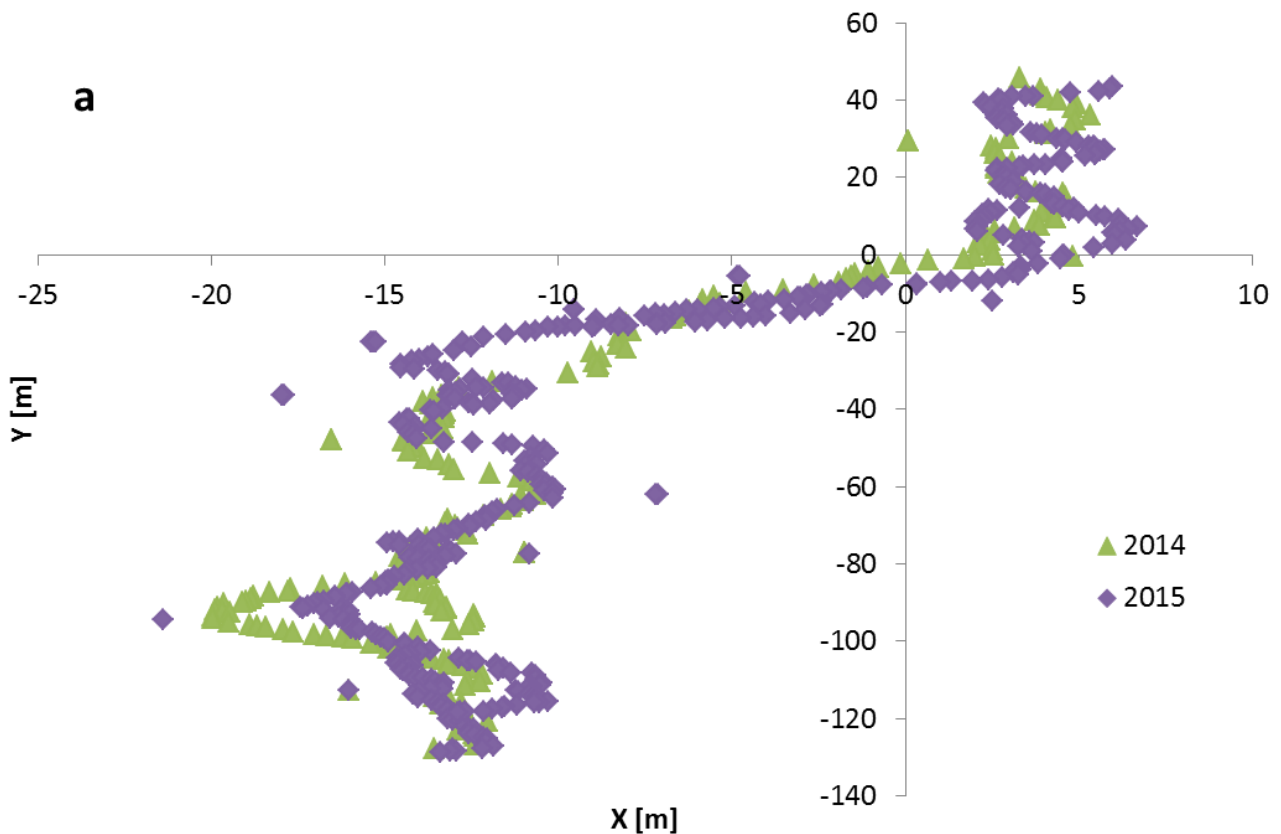
network of 5 benchmarks, alternatively placed on each bank at a distance of 30/40 m to provide full visibility from each station pointing upstream or downstream. Then we collimated the network to know the locations of the benchmarks and for each survey we repeated the measurements to know the transformations required to align each dataset.

A different number of points has been acquired during surveys (Table 3.1). The extension of surveyed reach is fixed, but the geometry of the thalweg varied through the years, resulting in a different number of points collected and different surveyed lengths.

Table 3.1. Specifics of longitudinal profile surveys at Ussaia Creek.

Survey date	Length of survey (m)	Points acquired
2/7/2012	230	125
3/7/2013	180	108
30/6/2014	195	204
29/6/2015	205	338

The output of these surveys is a plot of the vertical position of the thalweg line downstream, and a planar projection of the collected points (Figure 3.1). From such datasets it is then possible to analyze the vertical and planar variation of the thalweg configuration. As mentioned above, since the planar configuration can change between two subsequent surveys, it is not possible to directly compare the vertical variations occurred. Instead it is possible to locate subreaches that preserved a similar planar configuration, such that the vertical coordinates are overlapping and the estimate of vertical variations of the thalweg are less affected by errors.



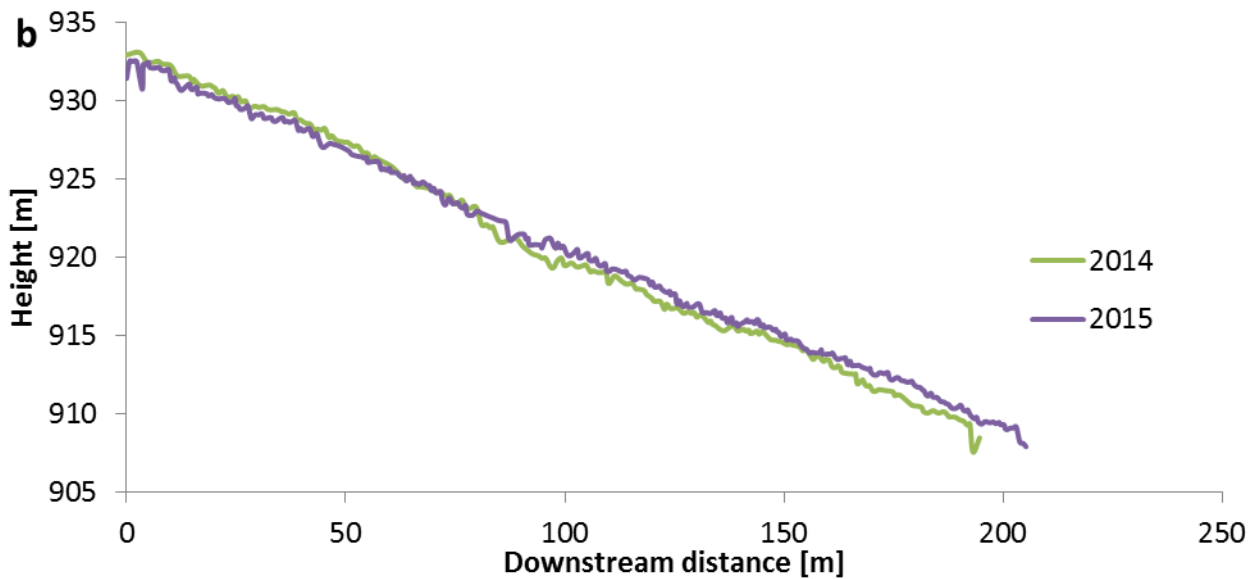


Figure 3.1. (a) Example of planar projection of collected points for the 2014/2015 surveys; (b) example of projection on the vertical plane of collected points along downstream distance for the 2014/2015 surveys.

The topography of the Grigno and Tolvà monitored sites were mapped in detail in September 2014, during low flow conditions. To reproduce bed topography, elevations and planar coordinates were measured using a Leica robotic total station (model TCR705). The total station collects x, y and z coordinates electronically and data are stored on an internal memory. The station tracks a 360° prism moved by the operator walking over the bed surface; to survey the 100 m long reaches two operators are required to complete the work in one day for each site. The accuracy of the topographic measurements is 5'' (1.5 mgon). Several benchmarks distributed along the monitored stretch are used to ensure the reproducibility of the survey for multi-temporal purposes. To map the bed, a sparse network of points was acquired firstly surveying points along the right side of the channel, including channel margin and important structures (such as pools, lateral pockets) characterizing the morphology, as well as breaks of slope. Within the pools, for example, the external shape and the position of the deepest point were surveyed. Then, the same procedure was repeated in the central (often coincident with the thalweg) and left portion of the channel.

Maps of the bed were obtained from the interpolation of the elevation data using a triangular irregular network modeling approach. This model interpolates surface defined by collected points and is considered to be appropriate when critical breaks of slope are included in the sampling scheme. The DEM of channel bed has been created through interpolation of TIN using different methods (Heritage et al., 2009), such as linear interpolation, minimum curvature, inverse distance weighted and ordinary linear kriging. DEMs created has been evaluated extracting 5% of the surveyed points dataset, used as independent points to assess the accuracy of each interpolator using metrics error indices (Williams et al., 2013).

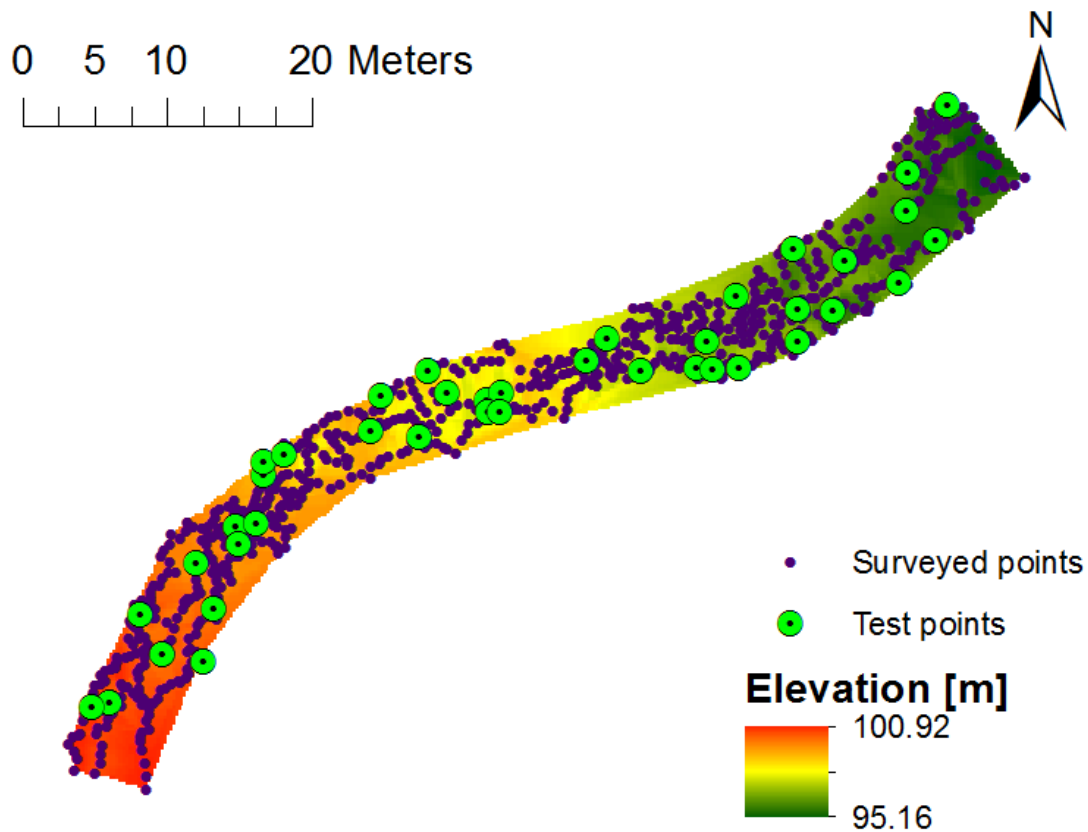


Figure 3.2. Points used as test for Z elevation values of the constructed DEM (example from Grigno Creek)

3.1.2 Structure from motion

Structure from Motion (SfM) is a photogrammetric method that allows to survey and reconstruct three-dimensional features starting from a series of partially overlapping oblique photos. Since the requirements are limited, this method is suitable for low budget projects, it requires limited operator's expertise (or training) and is suitable for scanning areas with difficult access.

The resolution of the scene is based on the automatic positioning of the point of view and camera orientation, without the need - required in conventional photogrammetry - of 3-D coordinates of ground control points (e.g., Westoby et al., 2012; Micheletti et al., 2014).

Unlike traditional photogrammetry, the scene reconstructed from SfM lack the orientation and the scale provided by ground control points. It follows that the surveyed scenes are reconstructed in a relative coordinate system, which subsequently should be aligned to an absolute one. The coordinates transformation is achieved by introducing an opportune number of Ground Control Points (GCPs) with known coordinates (i.e., points surveyed via differential GPS).

In this PhD thesis the scene reconstruction and its post-processing aimed to generate high resolution imagery orthophoto based on the source photos and reconstructed geometry of the monitored sites. To obtain the DTM, co-registration of the dense cloud has been necessary through deployment of GCPs. Once the point cloud dataset has been converted from image-space to relative coordinate system, the two sets of points were located in the same relative coordinate system. All the points populated a spatial database

from which the DTM was generated. The orthophoto will be used as base layer to map channel morphologies and portions of the channel completely immobile. Excluding such areas, active channel width will be assessed for different flow scenarios. The DTM will be the input for channel roughness maps, on which will be plotted the position of tracers, to establish relations between roughness and sediment mobility. As second output the model will be used to simulate different flood events, estimating water and sediment connectivity between each reach.

The SfM has been applied at three of the study sites: a 75 m channel stretch in the Grigno Creek, 75 m in the Tolvà Creek and 148 m in the Ussaia Creek. To ensure best channel coverage, oblique photographs were taken at low flow, or when possible (i.e., Ussaia), during dry conditions (Table 3.2).

Table 3.2. Specifics of SfM surveys. Ground Control Points (GCPs) are acquired by means of a total station.

Site	Date of image acquisition	Q (m ³ s ⁻¹)	Number of Photos	Channel length (m)	Number of GCPs		Average density [points m ⁻²]
					Subaerial	Submerged	
Grigno Cr.	25/06/2015	0.31	600	75	119	783	3.5
Tolvà Cr.	28/06/2015	0.24	666	60	141	529	3.5
Ussaia Cr.	3/11/2014	0.076	178	148	3	204	0.4
	10/04/2015	0	361	176	254	NA	0.24

To calculate active channel width, wetted areas are delimited on the orthophoto. In the case of stable channels a single survey is required for the characterization of the main structures, while in extremely unstable channels (such as Ussaia), multi-temporal datasets have to be acquired to record the morphologic changes occurred. We acquired photographs at the Grigno and Tolvà sites, during extremely low flows at the beginning of summer 2015 (Table 3.2). At the Ussaia site the first set of images was acquired in November 2014, before a debris flows event that changed the configuration of the channel bed. The second set was acquired in April 2015, when the entire channel was dry. Oblique photographs were taken with a Nikon D3300 reflex camera, mounted on a 5 m-long telescopic pole. An important piece of the procedure was to set up and install in the field the fixed reference network and the mobile reference network. Fixed network allows correct acquisition and overlapping of multi-temporal scenes. The mobile network of targets was distributed in each sub-reach for referencing purposes. This network is required for the computed model to be co-registered in the real-world coordinates.

To obtain a full topographic characterization of the channel bed, the photogrammetric survey of the subaerial portion of the channel bed was integrated with an ad hoc total station topographic survey. The latter allows to capture the submerged portions of the channel bed and provides additional subaerial GCPs to the photogrammetric survey. In particular, topographic points were taken at strategic locations characterizing the topography of the deepest parts of the pools, of the toe of the banks or places such as highly turbulent cascades, where images are not static and subsequent image reconstruction might lead to uncorrect coordinates. In the Grigno and Tolvà sites, where the average channel width spans between 5 and 9 m we surveyed 783 and 529 points respectively, with an average density of 3.5 points per m². At the Ussaia site, where wetted channel is limited (i.e., between 2 and 3 m), we surveyed the thalweg profile in

2014 (204 points over 220 m) to provide extra GCP in submerged areas; in 2015 the channel was completely exposed at the time of photogrammetric survey, hence no additional points were required (see Table 3.2). The photographic dataset has been processed with AgiSoft PhotoScan Professional. The procedure involves the manual inspection and selection of pictures, removing blurred frames or those not overlapping properly. The software then reads all the geometric features of the scene, reconstructing camera positions and orientations, aligning the pictures and finally building a sparse *point cloud*. Based on the estimated camera positions the program calculates depth information for each frame to be combined into a single dense point cloud. PhotoScan can produce dense point clouds (i.e., from $23.1 \cdot 10^6$ of Ussaia scene to $32.3 \cdot 10^6$ points of Tolvà Creek scene), which can be edited and classified at will, hence exported for further analysis.

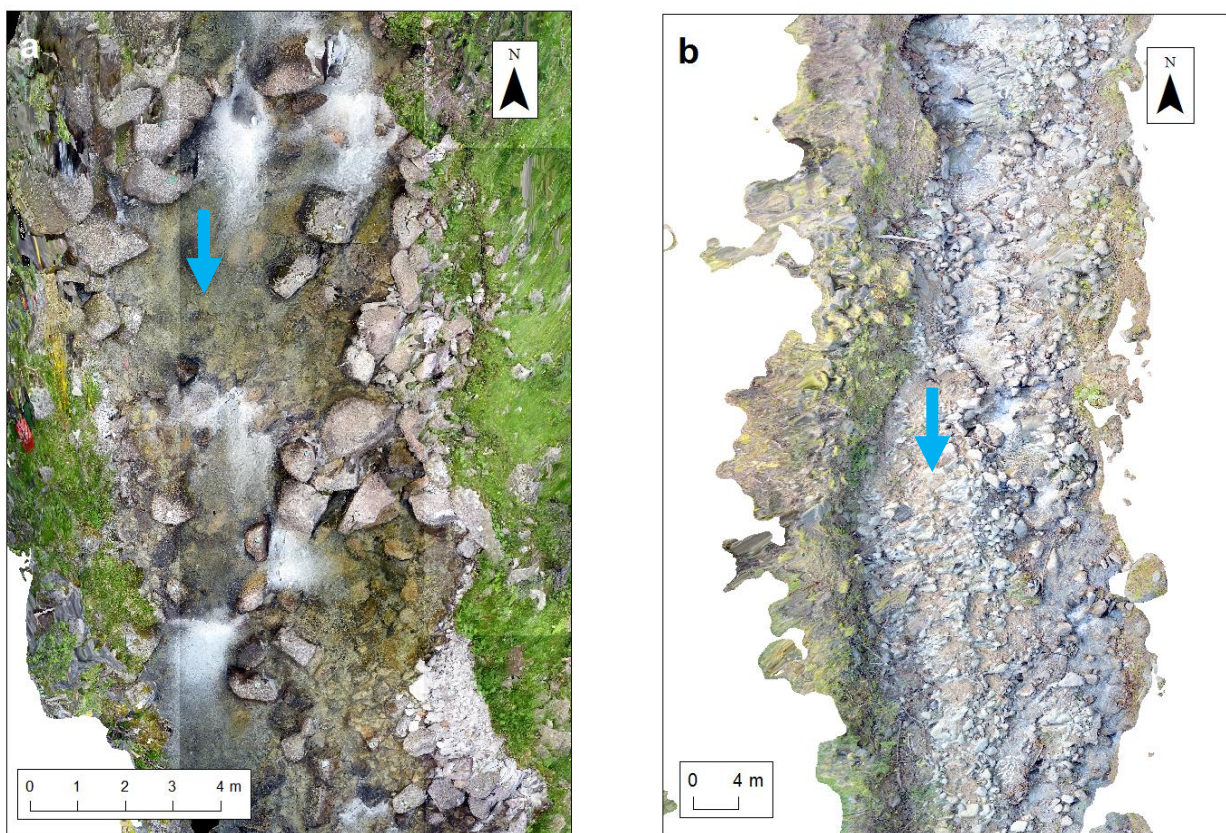


Figure 3.3. Examples of SfM-derived orthophoto mosaic in: (a) the Grigno Creek at low flow and (b) the Ussaia Creek in dry conditions. Blue arrow indicate direction of water flow.

Channel width is a parameter involved in the calculation of G . The portion of channel active during bedload transport events depends on water stage, hence the orthophoto combined with multi-temporal information from tracers (i.e., mobility of tracers along channel structures) and from water stage recording, helps in determining whether a portion is active under certain hydrological conditions. Mapping the stable areas not involved in transport processes, and establishing the portions of the channel active during flood events gives the average active channel width. Subdividing the channel into homogeneous portions of 1 to 5 m of downstream distance, the active channel area is delineated and equation 3.1 is applied to obtain the active channel width:

$$\bar{W}^{low} = \sum_{k=0}^n \frac{A_k^{low}}{L_t} \quad (\text{equation 3.1})$$

Where:

\bar{W}^{low} = average active channel width during low flow [m];

A_k^{low} = active channel area during low flow [m²];

L_t = length of thalweg [m];

This relation is applied to define the average channel width in the two scenarios – bankfull flow or low flow- (figure 3.4), and introduced in equation 3.1 for the evaluation of the bedload transport volume (G).

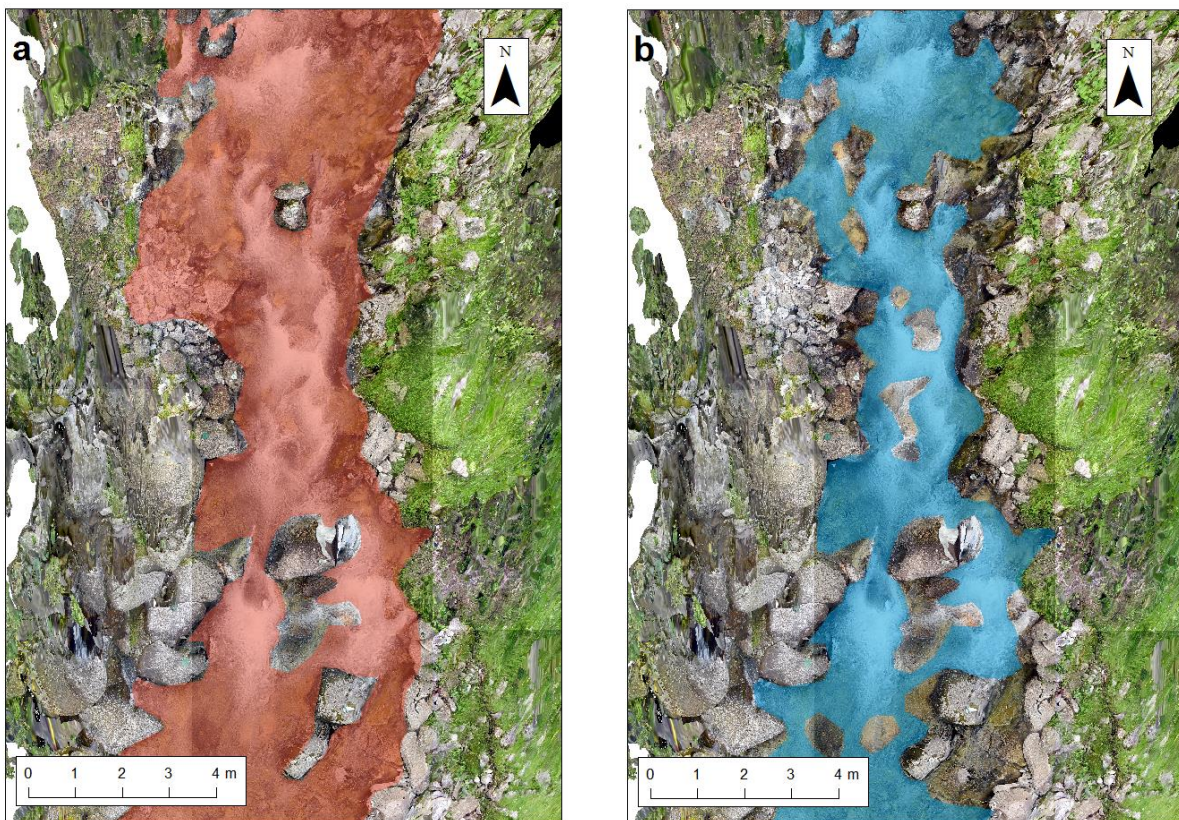


Figure 3.4. Example of delineation of active channel width in the Grigno Creek: (a) at bankfull flow; and (b) at low flow conditions.

3.1.3 Channel cross sections

To obtain information on channel morphology and downstream variation in transverse configuration, we surveyed cross sections at each site, at reach scale. Channel cross sectional surveys provide information about active channel width, depth, wetted perimeter, bank height and angle, and the presence and extension of bars and vegetation (Figure 3.5). Derived attributes for active channel include cross-sectional area, average depth, hydraulic radius and width-to-depth ratio.

Cross sections were sampled at distances based on channel morphologies rather than strictly on multiple of channel width, generally spaced from 3 to 10 meters.

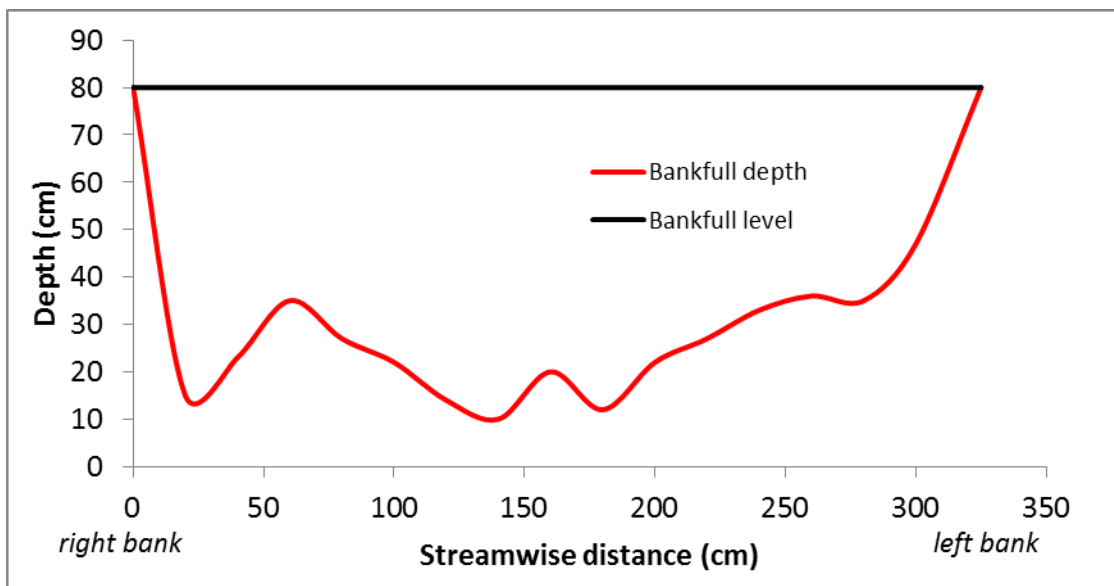


Figure 3.5. Example of cross section surveyed at Ussaia site.

At the monitored sites characterized by stability (Grigno and Tolvà Creek), we surveyed cross section during September 2014; at Ussaia Creek, characterized by larger instability of channel morphologies, surveys were repeated in July 2013 and June 2015, after the debris flow occurred in November 2014 (Table 3.3).

Table 3.3. Specifics of the channel cross sectional surveys.

Study site	Survey date	Number of X-s
Grigno Cr.	10/09/2014	12
Tolvà Cr.	12/09/2014	10
Ussaia Cr.	02/07/2013	29
Ussaia Cr.	30/06/2015	16
Strimm Cr.	30/05/2011	120

The channel cross sections are analyzed to obtain the average and maximum value of depth and width, wetted perimeter and area, required to calculate the shear stress at the bed:

$$\tau = \rho g R S \quad (\text{equation 3.2})$$

where

τ = bed shear stress [N m^{-2}];

ρ = density of fluid [kg m^{-3}];

g = gravity acceleration [m s^{-2}];

R = hydraulic radius [m];

S = slope [non-dimensional];

These cross sections will be adopted, in conjunction with other sections distributed along the mainstem, for the evaluation of the Downstream Hydraulic Geometry (see section 3.2).

3.2 Downstream hydraulic geometry

The downstream adaptations of channel characteristics, such as width, depth and wetted area, is investigated by means of Downstream Hydraulic Geometry (DHG).

DHG surveys have been conducted in 10 reaches (77 sections) of the Upper Grigno Creek and in 8 reaches (53 sections) in the Tolvà Creek. In the Lower Grigno Creek, 5 more reaches have been investigated, for a total number of 23 surveyed reaches (135 sections). In the Upper Grigno Creek the first set of cross sections (UG1) has been surveyed approximately 2.5 km downstream the water divide, while in the Tolvà Creek the uppermost section is located 1.5 km downstream the water divide. The last section, in the Lower Grigno Creek (LG5), is about 11.5 km downstream the water divide (Figure 3.6). At Ussaia Creek, 4 main reaches have been surveyed for a total of 212 sections (Table 3.4).

Table 3.4. Specifics of DHG section surveyed for each monitoring site.

Site	Number of reaches	Number of sections
Grigno Cr.	15	82
Tolvà Cr.	8	53
Ussaia Cr.	4	29

At Ussaia Creek all of the sections are within reaches in pristine conditions, as in the Upper Grigno Creek from reaches UG1 to UG6. From UG7 to approximately 50 m downstream, the channel is in dry conditions for large periods of the year due to the presence of a water intake. The UG8 section is located immediately downstream a relict subglacial canyon and upstream a hydropower plant. Sections UG9-UG10 are located 1

km downstream the restitution of the plant and the channel flows in a rectangular-shaped section, with artificial levees. The Tolvà Creek shows natural conditions in the reaches T1-T5; downstream, a water intake regulates the water flow in the lower sections (T6-T8). The Lower Grigno Creek is a channelized stream in few sections. Upstream the confluence, the presence of a settling area for sediments and a selective weir just upstream a bridge (Ponte della Stua) influences water and sediment flow in the lower portions. Between LG2 and LG4 the channel has been straightened after the 1966 flood event, showing artificial trapezoidal sections (LG2), or rectangular cross section and shallow banks (LG3-LG4).

At Grigno-Tolvà site data were acquired in September 2014, whereas at Ussaia Creek in July 2009. Representative reaches to be surveyed were selected in the field, locating the uppermost ones downstream large rock walls scoured by glacier where bedrock channels are currently imposed. For a single reach a set of 10 or less cross sections has been surveyed, spaced approximately from 3 to 7 channel widths. After establishing the bankfull level from geomorphologic evidences, such as the limit of stable riparian vegetation, with a stadia rod and a metric tape we measured from the channel floor a) the height of current water surface, b) the height of reference bankfull flow, sampling each 30 cm in a streamwise distance. A handheld GPS marked the position of each upstream section within the investigated reach.

To calculate the watershed area drained in the analyzed reaches, the hydrological model implemented in JGrass (Rigon et al., 2006) has been used.

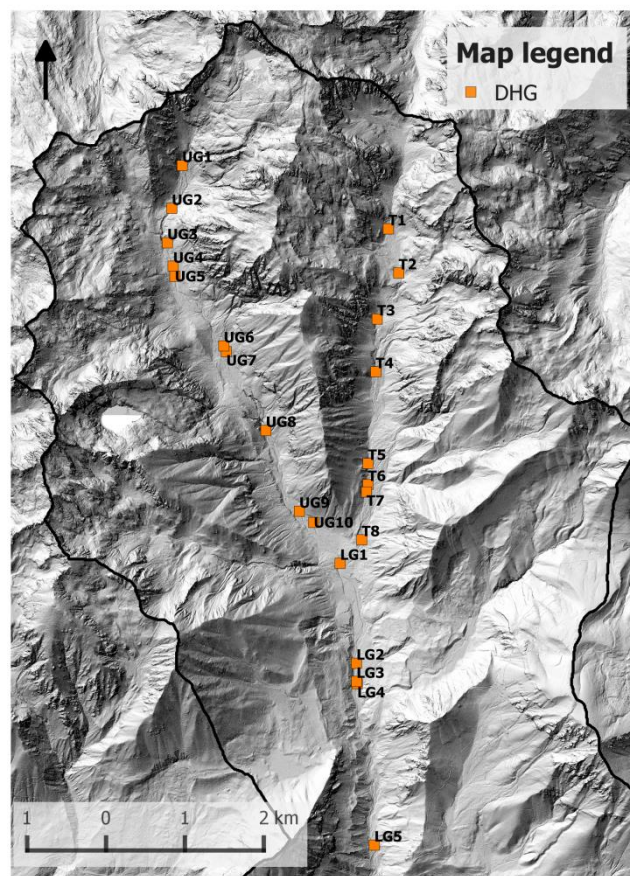


Figure 3.6. Distribution in the Grigno basin of the cross sections surveyed for downstream hydraulic geometry (UG: Upper Grigno Creek; LG: Lower Grigno Creek; T: Tolvà Creek).

3.3 Grain size distribution

The pebble count (Wolman, 1954) is a sampling of 100 stones in the river bed or a river bar, along a selected line or within an area. The stones measured are randomly chosen while walking across the bed surface. The intermediate b-axis of each selected stone is measured with a gravelometer. As the stones are sampled their sieve sizes are recorded in grain size classes (mm) that increase by powers of $2^{0.5}$, also termed “half-phi” after the phi scale of Krumbein (1938). Results are organized in histograms such that the distribution can be plotted and the cumulative percentages of each class can be calculated (Figure 3.7).

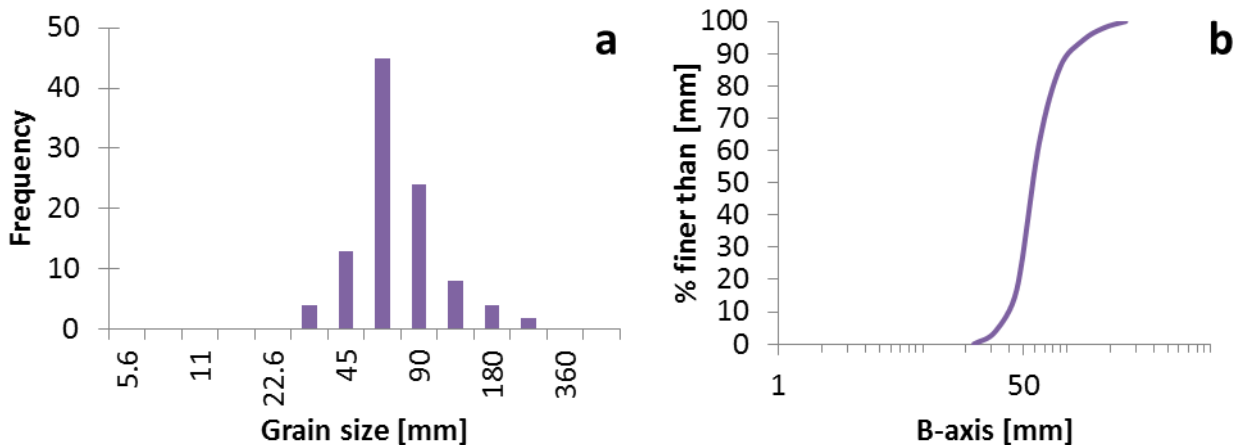


Figure 3.7. Example of grain size distribution at Grigno site. (a) Histogram of sampled pebbles; (b) cumulative percentages curve for the same sample.

3.4 Water Discharge

Each monitoring study site is equipped with a pressure transducer that measure water pressure (hence water stage) in real time with a recording frequency set to 10 minutes. In the Grigno Creek monitoring site the transducer is installed at 1562 m asl, closing a contributing area of 7.2 km^2 . It is located in the upstream portion of the monitored reach, at the transition between the downstream end of a pool and the beginning of a glide, and records water stage since 28 November 2013. In the Tolva Creek the sensor is installed at 1406 m asl (6.9 km^2). It is placed in plane bed morphology, in the central portion of the monitored reach. It records water levels since 26 November 2013. In the Ussaia Creek the pressure probe is installed at 925 m asl (1.8 km^2), in a shallow-pool/plane bed morphology, and functions since September 2012.

To determine a stage-discharge rating curve, hence translate water stage measurements into water discharge, we have used the salt dilution method (e.g., Moore, 2005) and have applied equation 3.3. Water conductivity was recorded via a WTW 340i conductivity meter. From the following relation

$$Q = \frac{c_i V_i}{\int_0^\infty c(t) dt} \quad (\text{equation 3.3}),$$

where:

C_i = initial concentration of saline solution [g L^{-1}],

V_i = volume of the mass added to the stream [L],

$C(t)$ = concentration [g L^{-1}],

Q = volumetric discharge rate [L s^{-1}];

the stage-discharge curve is constructed for every site through the relation existing among the water discharge and the pressure and applying a regression between the variables. Each value of pressure can be converted in a volumetric discharge rate (Figure 3.8) applying the regression equation of the rating curve.

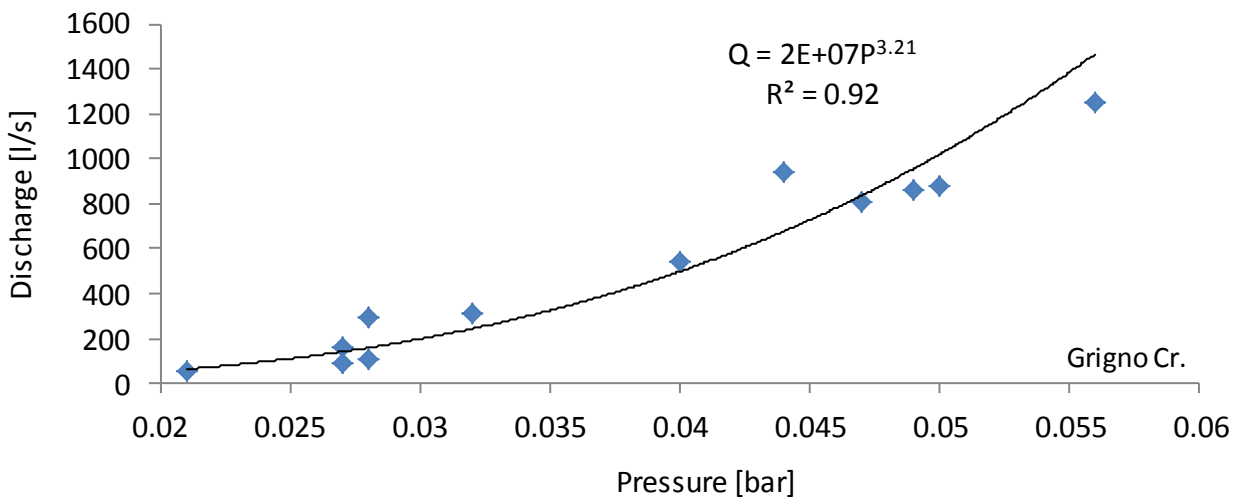
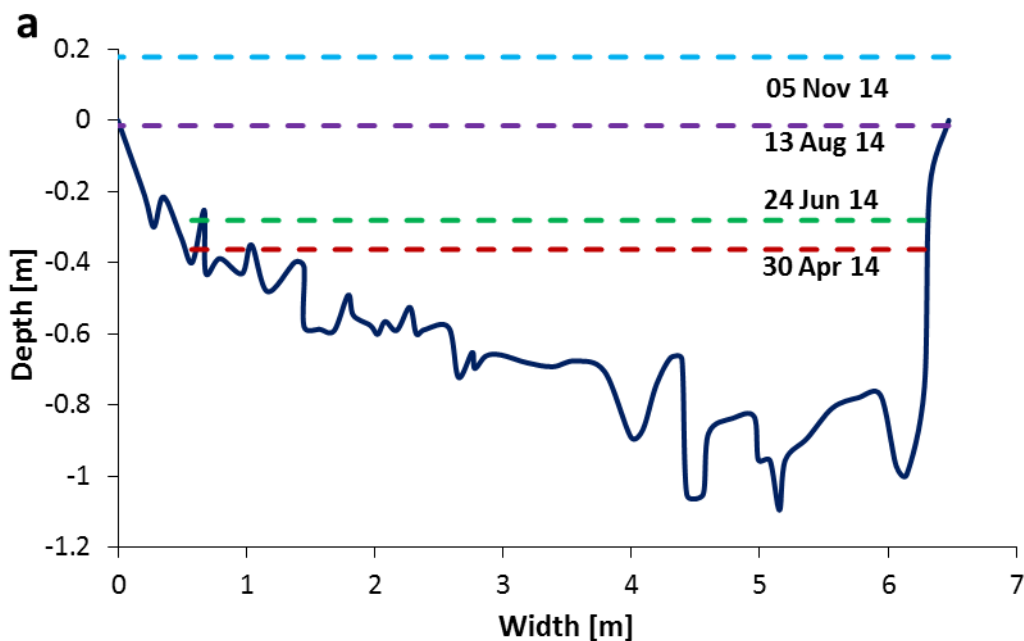


Figure 3.8. Stage-discharge curve constructed at the Grigno Creek monitoring site. The relations for the other monitoring sites are reported in Appendix 3.1. (Q = water discharge (l s^{-1}), P = hydrostatic pressure (bar)).

Water discharge data of the Strimm Creek are taken from Dell’Agnese et al. (2015). For each site the hydrometric levels of significant events are projected onto the surveyed cross-section equipped with the pressure sensors, to visualize the impact of the selected events compared to bankfull level (Figure 3.9).



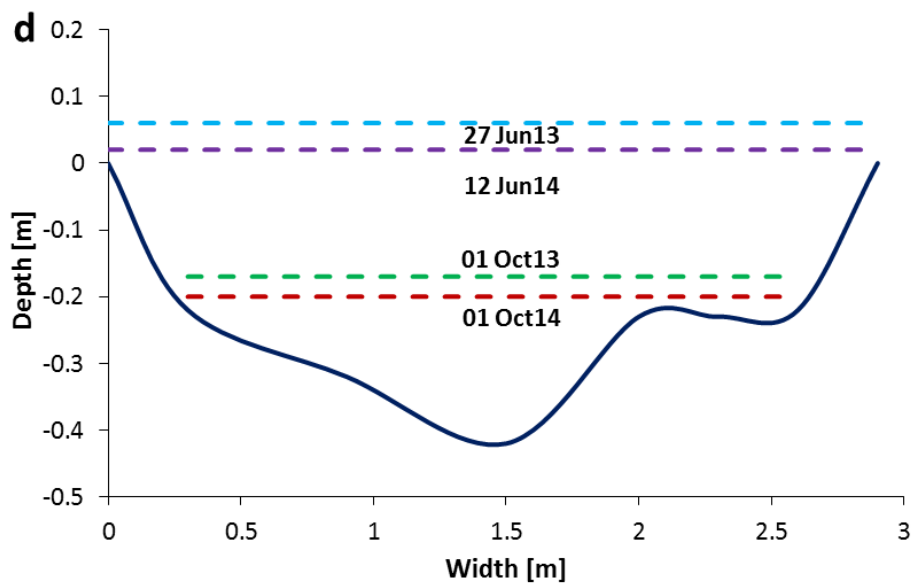
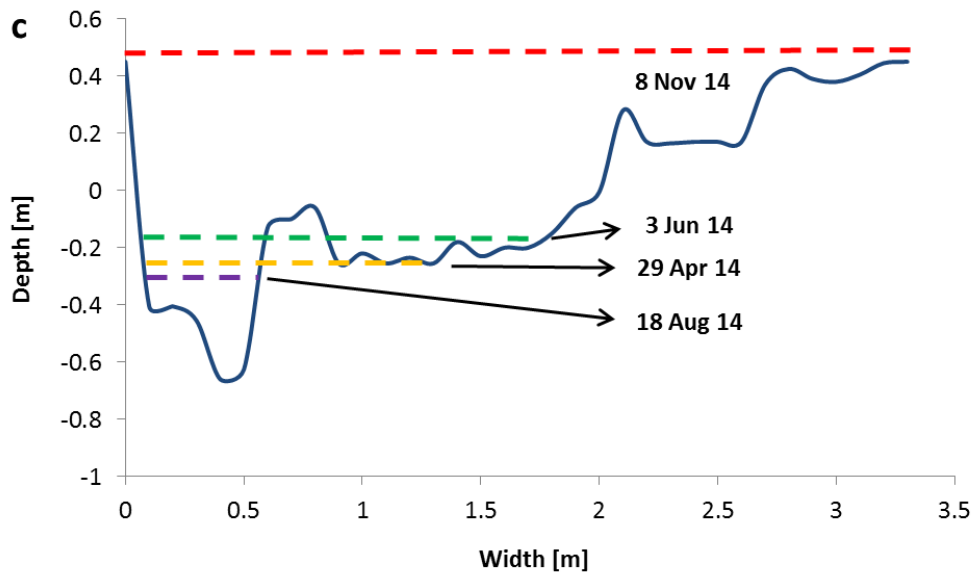
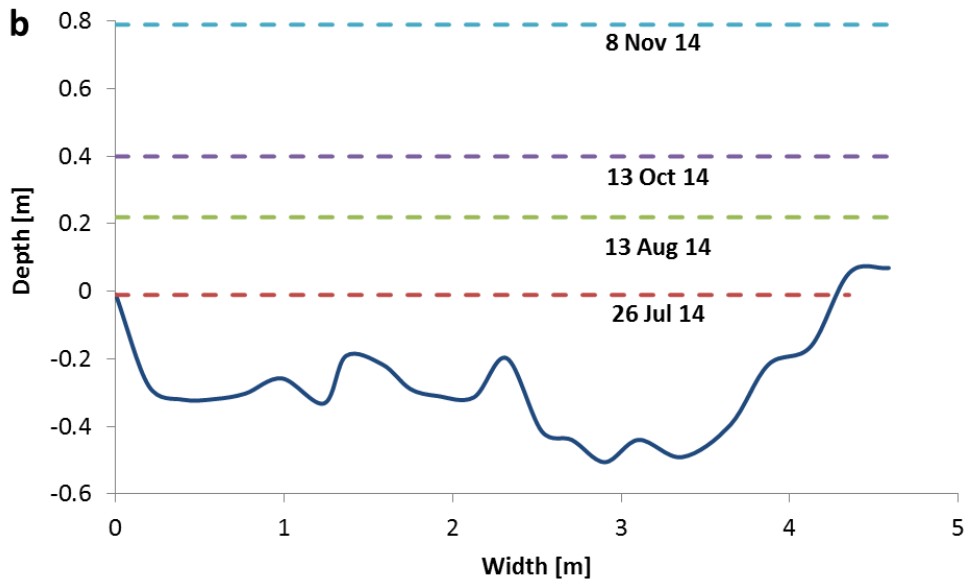


Figure 3.9. Recorded water levels for significant flood events projected onto cross sections equipped with pressure sensor at a) Grigno, b) Tolvà, c) Ussaia, d) Strimm Creek.

3.5 Precipitation and atmospheric temperature

To monitor the meteorological parameters such as atmospheric temperature and rainfall intensity, we use meteorological stations of the Trentino Provincial Meteorological Network (www.meteotrentino.it). Each monitoring site is equipped with a meteorological station located within 1 km. Specifically, for the Grigno Creek site we use the Malga Sorgazza (MS) station, located 1.8 km downvalley. The same station is used in conjunction with that located at Passo Brocon (PB) for the Tolvà Creek site, located 1.8 km East of MS and 3.5 North-West of PB. For the Ussaia Creek site we use data logged from the Mezzana (ME) station, which is located just 200 m away (Table 3.5).

Table 3.5. Specifics of the meteorological stations.

Study site	Meteorological station	Elevation [m asl]	Monitored reach elevation [m asl]	Active since
Grigno Cr.	Malga Sorgazza	1435	1562	June 2012
Tolvà Cr.	Passo Brocon	1616	1410	January 1988
Ussaia Cr.	Mezzana	935	923	January 1989
Strimm Cr.		2560	2550	July 2011

From the hydrological measurements we can obtain information about storm hydrographs, determining parameters such as peak discharge and flood duration. Analyzing meteorological data we obtain parameters such as storm duration, rainfall intensity and cumulated rainfall of each single event.

3.6 Bedload monitoring

Bedload monitoring has been conducted on four different sites: the Grigno and Tolvà creeks (Valsugana), the Ussaia Creek (Val di Sole), the Upper and Lower Strimm creeks (Val Venosta). In the present work we investigated tracers' displacements at different scales. At Grigno, Tolvà and Ussaia creeks the accessibility of sites and the relative low elevations, allowed to monitor the tracers after each meaningful rainfall event. At Upper and Lower Strimm, the limited accessibility due to the elevations of the study reaches allows to survey the tracers only at seasonal scale. More specifically, at Grigno Creek, bedload monitoring started from December 2013. At Tolvà Creek, bedload monitoring started from July 2014, thus have not been possible to evaluate the effects of the snowmelt season. At Ussaia Creek, bedload monitoring is conducted since September 2012; in the present work we consider only data collected from April 2014, to enable a direct comparison with Grigno and Tolvà creeks. At Strimm Creek, bedload monitoring started simultaneously at both upper and lower reaches in August 2011, as a project funded through "Monitor II" (EU Interreg South-East Europe), led by the University of Bolzano (e.g., Dell'Agnese et al.,2015). During my Ph.D., I have been involved in the data collection at Upper Strimm Creek, continuing to monitor tracers' displacements until October 2015.

Following this two approaches in bedload monitoring, we are able to evaluate the results at different temporal scales: at event scale for Grigno, Tolvà and Ussaia creeks, and at seasonal scale for the Strimm Creek. Each of these sites show peculiar hydro-sedimentary characteristics, so that field data on bedload have been collected along a climatic transect, that extents from NW to SE across the Eastern Alps.

The climatic transect shows a strong positive gradient in precipitation, moving from SE towards NW, where the most dry conditions are found within the Alpine chain, specifically at Val Venosta. The sites located in Valsugana exhibit the largest values in mean annual precipitation, about 1500 mm, and are located at elevations comprised within 1240-1550 m asl. Moving towards the inner portions of the chain, Val di Sole is characterized by 850 mm of mean annual precipitation, and monitored reach is at elevation of 900 m asl. As mentioned, Val Venosta exhibits the smaller amounts of mean annual precipitations, with only 500 mm of accumulated rainfall. In this context we analyzed the bedload at Strimm Creek, where the intermediate-upper portion of the basin is covered by snow from November until June. Moving towards the upstream reach the hydrological processes becomes progressively snowmelt dominated and the effects of summer storm are dumped.

Bedload transport has been tracked by the means of geomorphologic tracers. For the purposes of this thesis the Radio Frequency IDentification (RFID) technology has been adopted in conjunction with deployment of Passive Integrated Transponders (PIT).

A preliminary analysis of the transported grain size distribution (GSD) is required to release in the channel a representative portion of the clasts effectively transported under contemporary flow regime. In September 2013, depositional surfaces were sampled at Grigno and Tolvà Creek (Figure 3.10) monitored reach to evaluate the GSD via Wolman count, while at Ussaia Creek GSD was performed in June 2013 and September 2015. At Strimm Creek data collection was conducted during summer 2012 via 34 grid-by-number pebble size count samples. Surface grain-size curves were derived for each site by integrating all the samples.

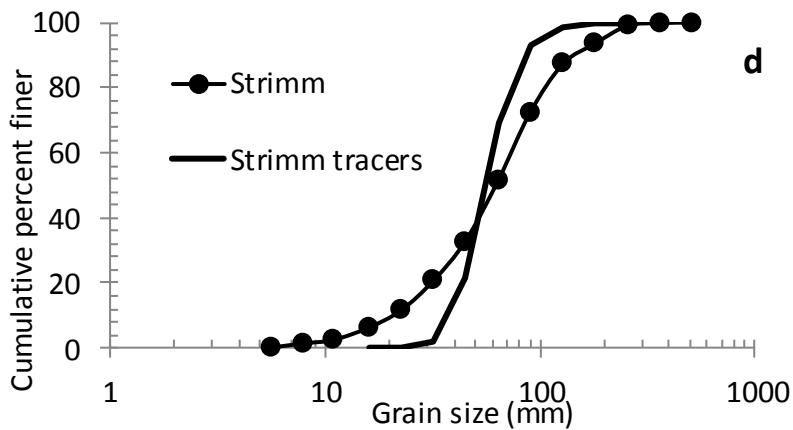
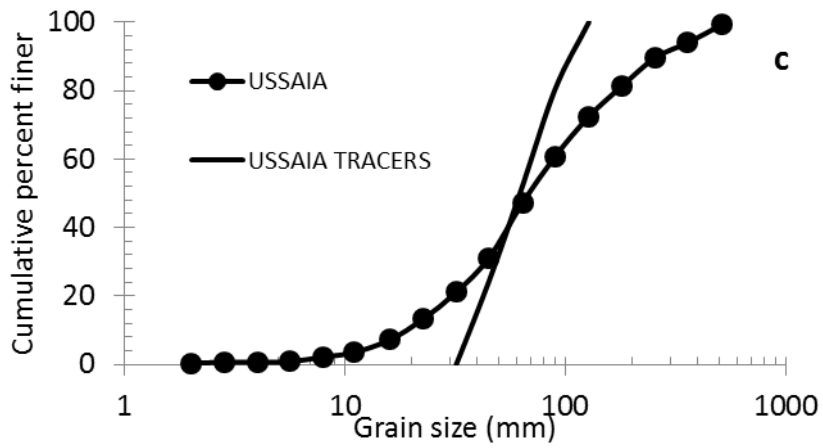
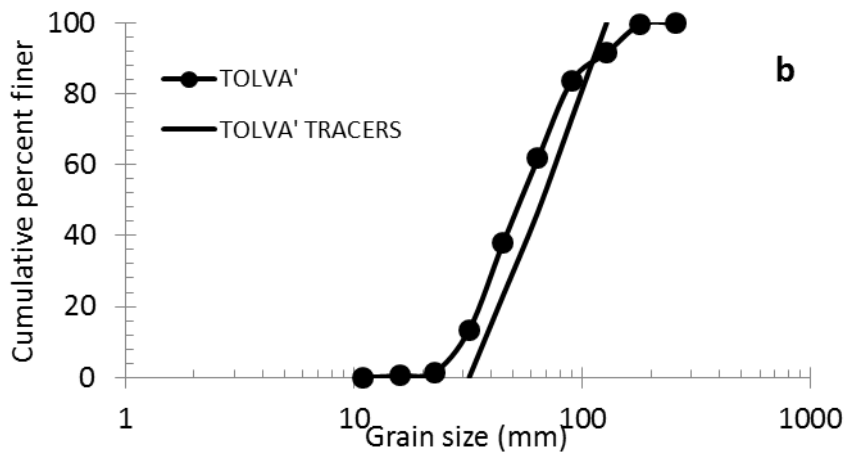
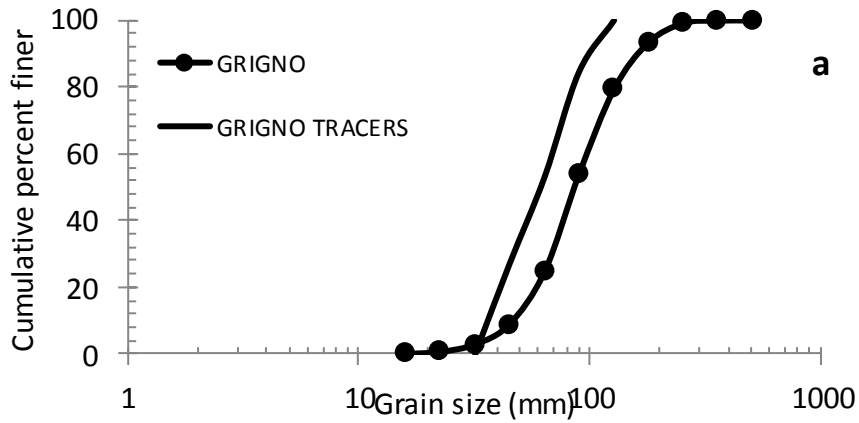


Figure 3.10. Bed surface and tracer cumulative grain size distribution in (a) Grigno, (b) Tolva, (c) Ussaia, (d) Strimm Creek.

Moreover, the b-axis dimension of keystones forming pools or steps was measured for each of the monitoring sites, to establish the dimensions of large, not-mobile clasts (Figure 3.11).

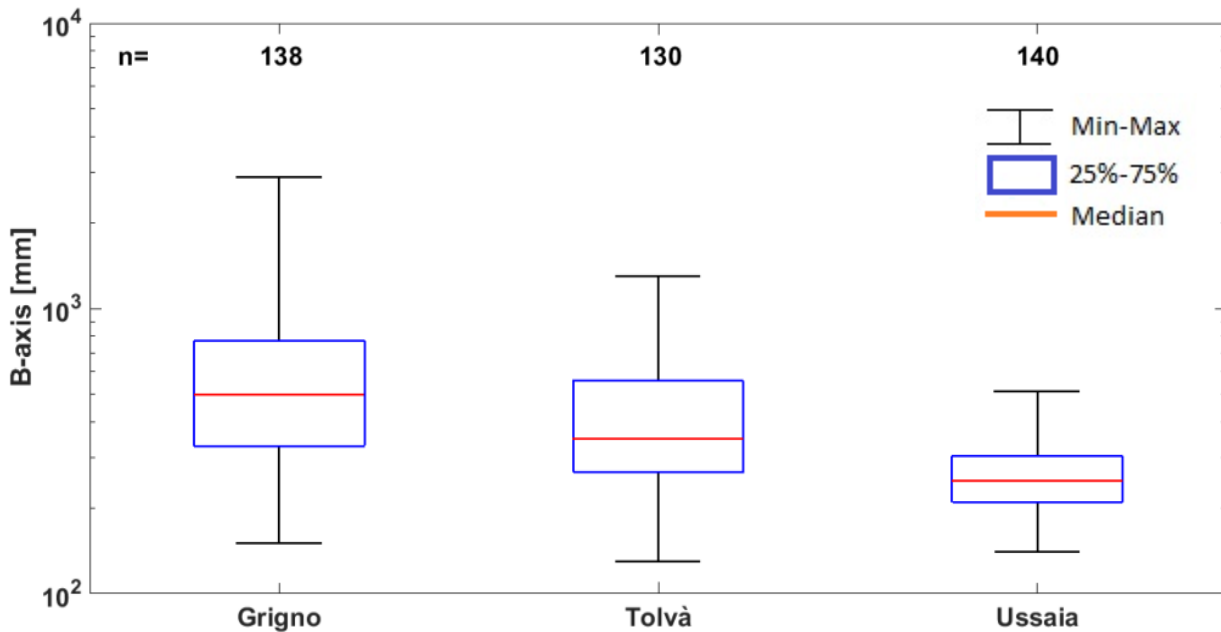


Figure 3.11. Distribution of b-axis of sampled keystones (*n*, number of observations).

To insert the transponder (PIT) into a stone is necessary drilling a hole of the dimensions of the transponder. For the purposes of this thesis work, 23.1 mm or 32 mm have been used, accordingly to the size of marked stones. Their weight is respectively 0.6 grams and 0.8 grams. Once drilled, clasts are equipped with a PIT (Oregon RFID) that consists of a glass capsule containing a solenoidal copper wire (Figure 3.12), charge capacitors and resonance capacitors (Lamarre et al., 2005). The PITs used are Half-Duplex read-only, with a 64 bit unique id; they have been tested by purchasing company to a depth of approximately 500 m (ISO 11784/11785 compatible). The hole is sealed with noncorrosive biphasic epoxidic glue, and clasts are colored with acrylic spray paint to enhance visual identification when submerged. Finally the clasts are weighted and their axes measured with a caliper, associating in a database those properties with the id code. The theoretical lifespan of these geomorphologic tracers is several decades and possible failures are related to malfunctions of the PIT itself or to the rupture of the clast containing the transponder.



Figure 3.12. Passive Integrated Transponders consisting of a glass-encapsulated copper coil, inserted into drilled stones to allow detection after floods.

The following stage consists of releasing the marked rocks within channel bed. To mark distances along the channel, several pairs of benchmarks have been placed on both sides of the creek, measuring their distance downstream. Tracing stones are located with respect to this reference frame that will be used for successive measurements after displacement. Tracers are deployed in rows perpendicular to the main direction of water flow (e.g. Leopold et al., 1966; Hassan et al., 1999). Rows are spaced approximately 3 m each downstream and clasts are distributed along the entire cross section, covering also exposed surfaces during low flow (Figure 3.13). All the morphological configurations within the reach have been crossed, to provide the opportunity of controlling clast dispersion as function of morphological starting point and channel position.



Figure 3.13. Release of tracers at Ussaia site: ribs are spaced 2 m apart and each row spans across the entire section.

Clasts have been seeded in different stages, during low flow periods (Table 3.6). At Grigno Creek clasts were released in December 2013, and after a severe snow season, the first surveys have been conducted in April 2014. During July three lines of tracers were added in the lower portion of the investigated reach. The last release was during December 2014. In the Tolva Creek (Table 3.6), tracers have been released for the first time in July 2014. After the flood event of November 2014, also in this site a new seeding of clasts has been necessary, and clasts were seeded in December 2014, summing up to a total of 150 tracers. At Ussaia Creek the first clasts were released in September 2012 and three more cohorts were seeded each consecutive year, for a total of 446 PIT tagged stones.

Table 3.6. Grain size classes and number of elements for each class of released cohorts in the monitored sites.

Grigno Cr.						
#	<i>Date of release</i>	# CLASTS	45 mm	64 mm	90 mm	128 mm
1	04/12/2013	111	28	31	35	17
2	31/07/2014	19	7	5	8	0
3	07/12/2014	32	8	8	8	8
	<i>total</i>	162	43	44	51	25

Tolva Cr.						
#	<i>Date of release</i>	# CLASTS	45 mm	64 mm	90 mm	128 mm
1	24/07/2014	98	17	26	20	35
2	06/12/2014	52	14	12	14	12
	<i>total</i>	150	31	38	34	47

Ussaia Cr.						
#	<i>Date of release</i>	# CLASTS	45 mm	64 mm	90 mm	128 mm
1	21/09/2012	126	42	42	42	0
2	12/06/2013	90	10	30	30	20
3	12/04/2014	111	26	24	24	37
4	30/04/2015	119	30	29	30	30
	<i>total</i>	446	108	125	126	87

Table 3.7. Summary information on tracer clasts.

Site	Release date	N	B axis (mm)		Weight (g)		Rib spacing (m)
			Min	Max	Min	Max	
Grigno Cr.	4 Dec 2013	111	31	128	95	3698	5
	31 Jul 2014	19	36	128	105	2752	5
	7 Dec 2014	32	37	116	121	2974	5
Tolvà Cr.	24 Jul 2014	98	36	128	88	3710	5
	6 Dec 2014	52	35	126	100	2572	5
Ussaia Cr.	21 Set 2012	126	37	109	90	1083	2
	12 Jun 2013	90	35	140	100	2009	2
	12 Apr 2014	111	35	128	108	4004	2
	30 Apr 2015	119	35	149	116	2955	2
Strimm Cr.	25 Jul 2011	101	35	229	83	6525	3
	29 Aug 2011	69	43	160	177	3085	3
	7 Jul 2013	61	49	132	179	2328	3

Table 3.8. Weight categories (g) of the tracer clasts.

Weight category	W1	W2	W3	W4	W5	W6	
Weight range	<177	177-316	316-562	562-1000	1000-1770	>1770	
GRIGNO CR.	Clast count	39	25	26	27	22	21
	Percent	24.38	15.63	16.25	16.88	13.75	13.13
TOLVA' CR.	Clast count	35	17	21	22	25	32
	Percent	23.03	11.18	13.82	14.47	16.45	21.05
USSAIA CR.	Clast count	98	65	78	78	58	69
	Percent	21.97	14.57	17.49	17.49	13.00	15.47

Mobile antenna

PIT-tagged stones are scanned using the RFID technology. The device we used is composed by three main parts: a) a portable loop antenna, b) the RFID reader, c) a palmtop connected to the reader (Figure 3.12). The antenna is a portable device used to swipe the channel, searching for PIT-tagged stones. Its main part is a loop of conductive wire (diameter 70 cm), placed in the bottom of the structure, connected to the reader through a tuning board. Its scanning radius is 50 cm. The reader/datalogger is mounted in a backpack equipped with a bottom pocket where two 16-V batteries are located. The reader is connected to a waterproof palmtop via Bluetooth technology or serial cable. The palmtop displays PIT id codes, number of readings and total time of reading for a given PIT, current status of the batteries/antenna. Since the datalogger stores the data on an internal SD card, previously found PIT can be looked-up in the database. The reader is connected to a piezobeeper that emits a loud sound when a PIT is detected. When a tracer is found, the position is recorded reading the metric tape fasten to the operator scanning channel bed surface. Distances are referred to the benchmarks established on both sides and to increase the accuracy, the position of identified tag is evaluated with respect to the closer pair of benchmarks. Visible tracers are directly measured resting on top of it. Buried tracers are carefully inspected, and the position is located

scanning the ground from different directions to check the limit of detection, placing the tracers in the middle of this detection zone.



Figure 3.14. Mobile antenna manufactured by Oregon RFID by means of which bedload monitoring surveys have been conducted. In the picture is visible the palmtop where clasts ID are displayed (yellow device), and the grey backpack, where the portable reader/datalogger is located.

While surveying, in conjunction with the aforementioned portable antenna, a stick antenna has been used. The 70-cm loop antenna has been extensively used to scan and access quickly the entire channel surfaces. In the first surveys, when population is still widely spaced and small displacement occurred, this has been the only device used. After several displacements, and due to increasing number of tracers released, some channel bed patches became densely populated. Since detecting radius of portable antenna is 50 cm, interferences between signal emitted by close tags cause hiding effects, and clasts may not be revealed. The stick antenna has an emitting source punctual rather than ellipsoidal, and its detecting radius is within 10 cm. In densely populated patches this device has technical characteristics more apt to enhance the accuracy of tags positioning. When using this antenna it has been possible to separate the signals coming from tags closely spaced, and in some cases also buried. Due to limited detecting radius, this instrument reveals the tags only when the emitter is very near to the PIT, so a direct consequence is the decrease in the survey velocity, but on the other hand ensures an increase in survey efficiency.

The depth penetration of the portable main device have not been tested. Since the antenna has to be used in natural environments free from metallic casings and/or wirings, or magnetic sources in close contact

with the channel beds, the only materials that may disturb the antenna are flowing water, cobbles, pebbles, sands and silts. In fact, during surveys, the antenna has been submerged to 1.5 m of water without encountering difficulties in reading. Clasts that remained buried in lateral bars have been scanned in subsequent surveys and detected, but the effective depth has not been measured. In the literature detection depth for antennas ranging in diameter between 0.5-1 m ranges from 0.25 up to 1 m (Lamarre et al., 2005; Allan et al., 2006). Recent laboratory tests (Chapuis et al., 2014) highlighted as detection distances over vertically implanted PIT reduced for tests conducted at a depth of 3 inches (approximately 8 cm), increased for burial depth of 6 inches (approximately 15 cm) and finally a steady decrease has been observed for deeper depths. The same experiments conducted over horizontally buried tags revealed similar behavior of detection, with less defined patterns. The authors point out as this non-linear pattern might be related to the shape of electromagnetic field. Sediment properties do not play a role in the detection distances.

The depth penetration of the stick antenna has been tested in laboratory, burying a 45 mm tagged stone under different depths of 0.2 mm sorted sand. The value found of 10 cm is in good agreement with values between the grain b-axis and half of the vertical detection range, as found by Bradley et alii (2012).

The accuracy in locating tracers depends on the device used and on the distance measurement methods. Referring to last ones, the accuracy reached depends whether clasts are visible or not. The distance of clasts resting on the surface is measured with the metric tape, and the accuracy reached is about ± 0.10 m. In the second case the accuracy is lower, generally ± 1 m, because the position of the tagged stone has to be estimated after careful inspection.

The maximum efficiency in surveying is achieved when three operators are involved: one scans the channel bed surface, one measures distances and the last one records notes. Reach surveying is possible employing two operators only, but requires longer time and presents more difficulties when high flow impede easy walking within the channel and trees or channel bends constitute visual obstructions. Since investigated reaches span about 100 m, surveying requires 4/5 hours due to channel accessibility. Longer times have been necessary only because of equipment malfunctions or bad weather conditions.

In the monitored sites the frequency of surveying has been not the same. In the Grigno-Tolvà-Ussaia creek group in fact, survey frequency has been determined by the hydro-meteorological events. The conditions in each site, such as full site accessibility and low elevation (between 1600 and 900 m asl), allow to survey soon after significant rainfall, readily tracking particles. At Strimm site, higher elevation (2550 m asl) does not allow surveying during snowmelt season, and generally after each significant rainfall event. For this reasons in this Ph.D. thesis the effects of different inter-survey periods are evaluated. At Strimm Creek, for instance, only two surveys per year have been conducted (Table 3.4.3). Tracers displacements induced by separate hydro-meteorological events cannot be distinguished and are consequently treated as produced by a single event. In the evaluation of the amount of solid transport per event (G), the reduced inter-survey frequency adopted in the Grigno-Tolvà-Ussaia creeks, and the possibility to link each displacement to a single storm hydrograph, leads to better estimates of G.

3.7 Tracers' virtual velocities for constraining bedload transport volumes

To assess bedload transport volumes we adopted the approach of virtual velocities of tracers. This methodology involves the knowledge of the displacement length travelled by each tracer after a given flood, and the magnitude and duration of the flood, i.e. the storm hydrograph, to calculate tracers' virtual velocities and obtain transported bedload volumes (Figure 3.15). These displacements, as shown in previous sections (cf. Table A4.3), have been monitored after each relevant hydro-meteorological event at Grigno, Tolvà and Ussaia Creek, whereas at Strimm Creek we conducted two surveys per year.

Monitoring tracers' displacement length allows to determine the flow transport capacity, identifying which weight classes have been entrained for a flood of a given magnitude. Basing on this method, known as the flow competence approach (e.g., Andrews, 1983), we identified the minimum discharge able to entrain clasts of each weight class.

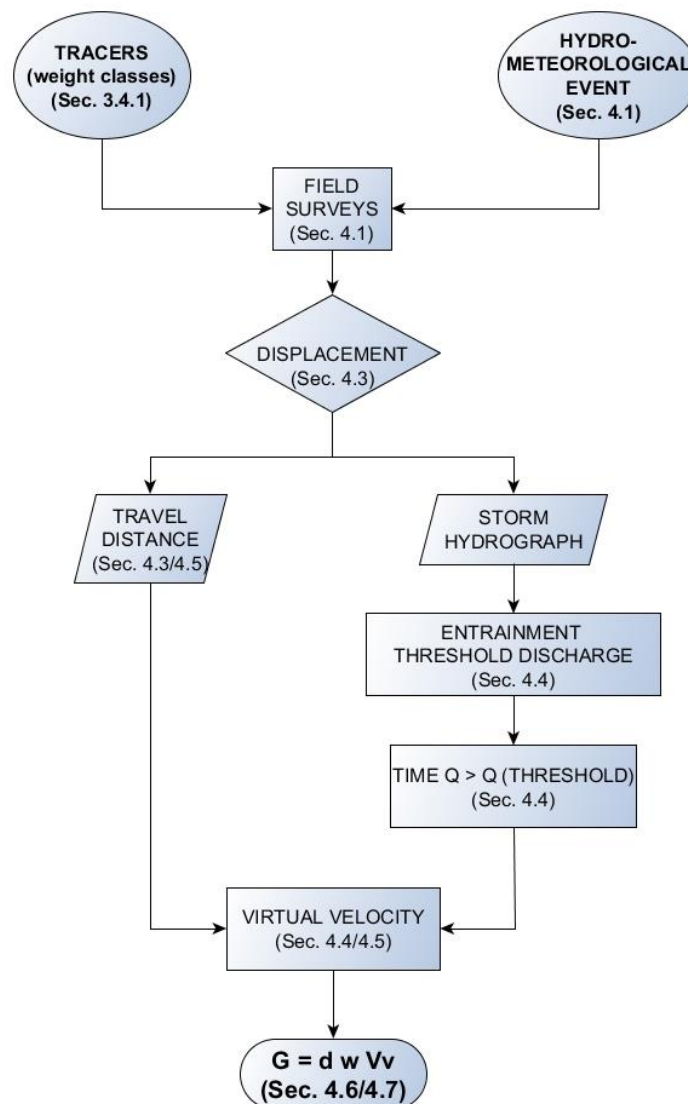


Figure 3.15. Flowchart schematizing the flow competence method adopted to individuate entrainment threshold discharges for each weight classes and determine the values of bedload transfer for each hydro-meteorological event. In brackets are reported the sections of this thesis referring to the listed topic.

The discharge value related to motion threshold that has been applied to each monitored flood, is defined as:

$$Q_t = \min \{ \max(Q_i); \min(\bar{Q}_i) \} \quad (\text{equation 3.4})$$

where:

\bar{Q}_i = discharge values for which clasts of the i -th weight class moved;

Q_i = discharge values for which clasts from the i -th weight class remained immobile.

After having defined the threshold discharge for each weight class, for all the events we calculated the virtual velocity as the ratio between the duration over threshold of the storm hydrograph between two surveys and the length travelled by a single tracer. Following Liébault and Laronne (2008) among others, the volumetric bedload transport rate G_i [$\text{m}^3 \text{s}^{-1}$] for each weight class i , is expressed as:

$$G_i = d_s w_s v_i (1-p), \text{ for } i=1..6 \quad (\text{equation 3.5})$$

where:

d_s = depth of active layer [m];

w_s = mean width of the active channel bed [m];

v_i = mean virtual velocity of the i -th class of transported clasts [m s^{-3}];

p = fractional porosity of channel sediment [non-dimensional].

Here, the value of p is assumed to be equal to 0.3 (following Bunte and Abt, 2001). The volumetric transport rate of each class was then multiplied by the integral by the integral transport time (i.e., the time for which the threshold discharge value was reached or trespassed). To derive the total volumetric inter-survey transport rate, we calculate:

$$G = \sum_{i=1}^6 G_i \quad (\text{equation 3.6})$$

The depth of the active layer was estimated based on digging tests performed at each site (see Table 4.6.1).

To evaluate the w_s , i.e. the mean active channel depth, we used different scenarios. Adopting the orthophotomaps obtained from the SfM technique, we mapped the active zones of sediment transport, considering kestones mobile or not, defining in the first case the active channel width as a bankfull width (e.g., Liebault et al., 2008; Dell’Agnese et al., 2015). To evaluate the active channel width also in reaches not covered by SfM method, we surveyed 12 downstream sections at Grigno Creek and 16 at Tolvà Creek respectively. This method provides a better estimate of active mean width values, especially in channels that did show cross-sectional variability of tracer travel distances across single transverse ribs, such as Grigno and Tolvà creeks. In this sites in fact, ordinary events are mainly transporting along the central (thalweg) portion of the channel, while during larger events (such as November 2014), also lateral zones are activated, determining an enlargement of the active channel width (see Table 4.6.2). At Ussaia Creek, since channel bed material is highly mobile (including kestones), the photogrammetric method has been adopted to evaluate the active channel width in ordinary flow conditions or during extreme events.

Virtual velocities were quantified considering the displacement length and the time the flows trespassed the threshold between two consecutive surveys; furthermore were used to evaluate the sediment transported during the inter-survey period. Due to complex channel geometry this method is preferable compared to a shear stress-based approach, where the estimate of water depth is a fundamental parameter hardly measurable in such sections (Comiti and Mao, 2012).

3.8 Hydro-meteorological forcing and magnitude of bedload volumes transported

Channel discharge is the primary control of sediment entrainment and transport rates in mountain streams. In the monitored basins the simultaneous presence of precipitation measurement network and water gages allows the connection between meteorological-driven events and hydrological basin response. The water input into a river basin (rainfall conditions and/or snowmelt) can strongly influence the initiation of phenomena such as landslides and debris flow (e.g. Diakakis, 2012). In the last years attention has been directed to prediction of severe fluvial bedload events in mountain streams (e.g., Badoux et al., 2012). To establish the empirical intensity-duration thresholds requires continuous information on the occurrence and magnitude of sediment transport in a water stream. In this thesis we investigate rainfall thresholds for bedload transport activity for each monitoring site, considering storm duration and rainfall intensity (Figure 3.16). The magnitude of sediment transport activity at single survey scale is described via three parameters: 1) the number of mobilized clasts; 2) average step length weighted over tracers’ mass; 3) total volumetric inter-survey bedload transfer G (m^3).

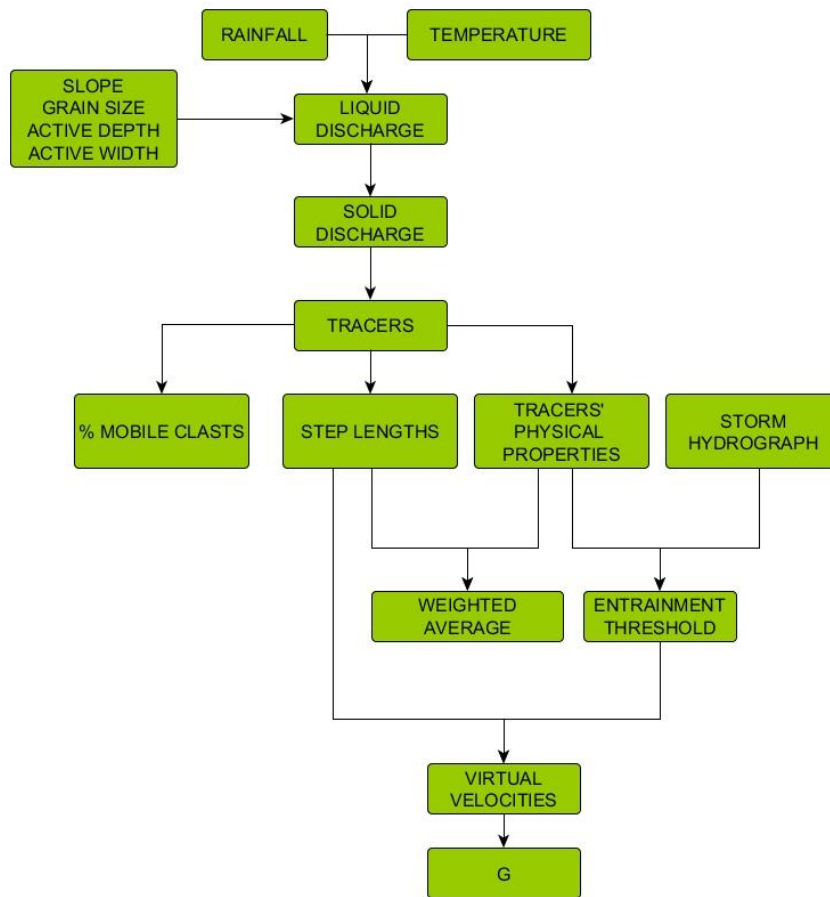


Figure 3.16. Flowchart illustrating the methods adopted to individuate hydro-meteorological thresholds for constraining bedload transported volumes.

Adopting these three parameters we are able to compare the results obtained via implementation of other methodologies for bedload transport evaluation. Specifically the number of mobilized clasts could be obtained releasing painted clasts. Tracers allow to estimate the step lengths, thus the average of travel distance weighted over mass simulate mimics the information deriving from magnetic or pit-tagged stones. Finally, approaching the problem of sediment transport via flow competence method, we introduce the threshold discharges for entrainment and the virtual velocities' events.

CHAPTER 4

Results

The results chapter presents channel boundary condition data, hydro-meteorological events described in chronological order and sediment transport data. More specifically, sediment transport will be described as tracer travel distances first. Then, via the flow competence method, characteristics of storm hydrographs are linked to clast displacements to obtain the virtual velocities. The distribution of the travel distances and virtual velocities will be analyzed to gain further insights concerning the statistical properties of the collected data. In this way we establish the differences between mean and median of these distributions, such that we will be able to perform a comparison of the bedload transfer formula using both terms. In the last results section, we will compare the parameters of hydro-meteorological forcing to the bedload transfer volumes, analyzing the effects on bedload by different hydrological inputs.

4.1 Channel boundary conditions

Concerning boundary conditions at reach scale, the longitudinal profile and the distribution of morphometric parameters such as step height and pool depth will be analyzed. Then the channel cross sections will be analyzed, that are linked to a wider perspective of channel transverse properties through the downstream hydraulic geometry surveyed at basin scale. After having analyzed the longitudinal and transverse topographic features of each reach, the grain size distributions will be presented, offering a complete overview of channel physical properties, fundamental to explain the behavior of bedload transport processes.

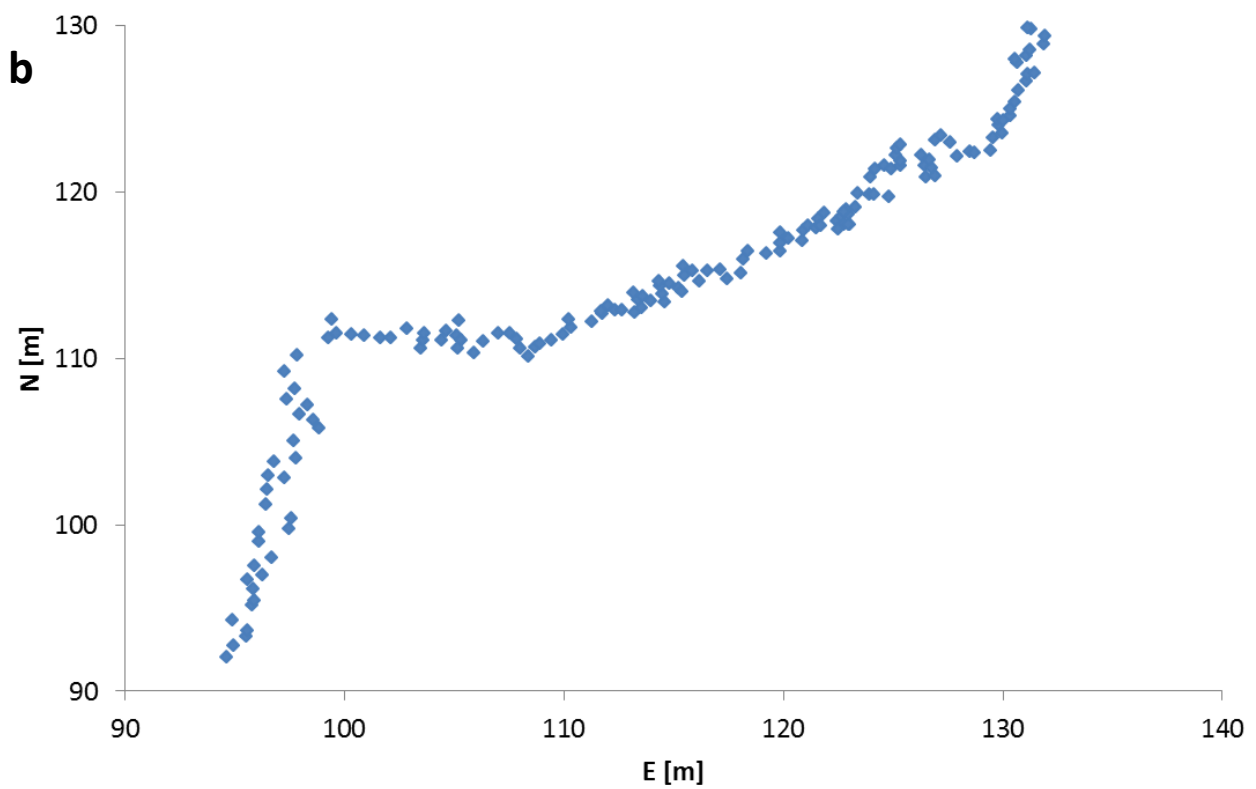
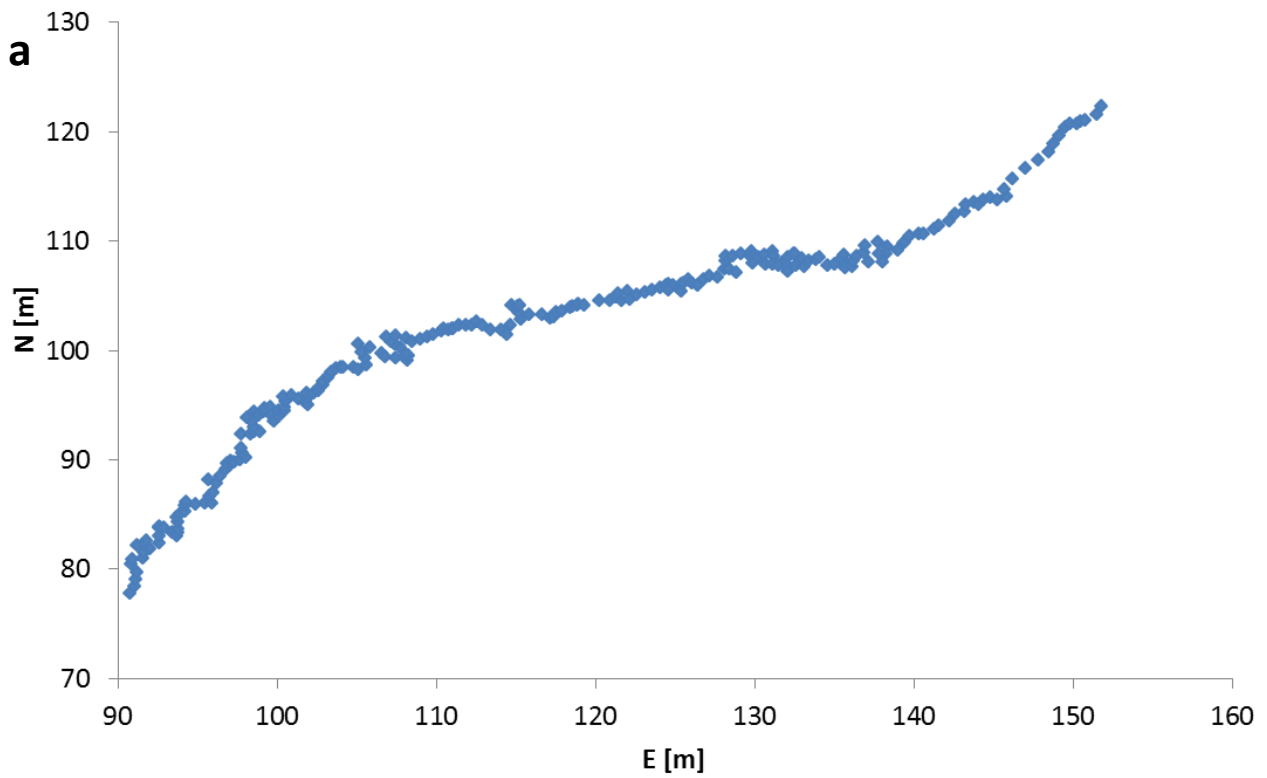
4.1.1 Channel bed topography of the monitored reaches

The frequency of these surveys was dictated by the overall channel stability. In the Ussaia Creek site, which experiences frequent morphological changes, surveys were conducted on a yearly basis. Conversely, at the Grigno, Tolvà, and Upper Strimm Creek, all characterized by immobile key stones, we conducted only one longitudinal profile survey.

4.1.1.1 Longitudinal profiles

At Grigno and Tolvà Creeks the longitudinal profiles have been surveyed one time, in September 2014. The surveys have been conducted by means of a total station, such that the planview of collected points can be plotted (Figure 4.1.1). At Ussaia Creek the longitudinal profile of the thalweg was surveyed for four consecutive years, from 2012 to 2015. The results obtained are: a) the planar distribution of the surveyed points, and b) the corresponding longitudinal profile. From the plan view it is possible to determine the lateral stability of the thalweg through time. As shown in Figure 4.1.1c, major changes occurred between each inter-survey period. This can be directly linked to the sequence of bedload events that imposed drastic rearrangements in local morphologies. For example, changes occurred between 2014 and 2015 surveys are due to the debris-flow event of November 5, 2014. The longitudinal profile at Strimm site has been

surveyed by means of a monopod laser range finder acquiring the horizontal distance and vertical angles, hence the plan view is not plotted.



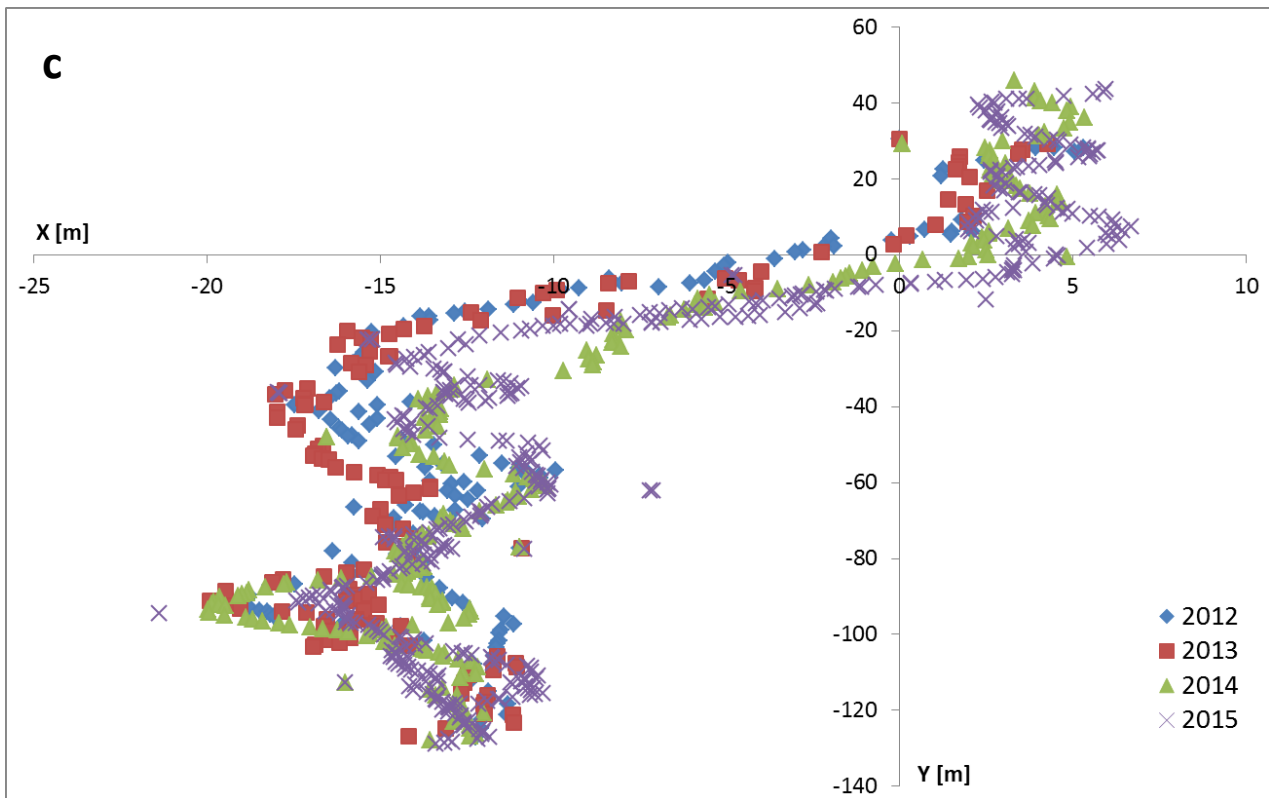


Figure 4.1.1. Plan view of the surveyed points along the thalweg at a) Grigno Creek, b) Tolvà Creek, and c) Ussaia Creek from 2012 to 2015. Major changes at Ussaia Creek are recognizable between each inter-survey period.

As shown in Figure 4.1.1c, the lateral variations of the thalweg recorded at Ussaia Creek are not allowing to compare the differences in elevations observed between two consecutive years of homologous points, thus it is not possible to quantify the thickness due to erosion or deposition along the profile. In figure 4.1.2 we present the longitudinal profiles of Grigno, Tolvà, Ussaia and Strimm creeks, to show differences in slope values among the various sites, and the morphological attributes peculiar of each profile.

At Grigno Creek the surveyed reach is 80 m, and two breaks of slope represented by cascades are clearly distinguishable. Cumulatively the drop in height is 5 m (Figure 4.1.2). At Tolvà Creek the surveyed reach extends for approximately 60 m, and the drop in height is about 6 m (Figure 4.1.3). Therefore the average slope is larger than Grigno Creek. The distinctive feature is represented by a boulder cascade located in the middle of the reach, that extends for 20 m and accounts for a drop in height of 3.5 m. The monitored reach begins with a typical step-pool sequence followed downstream by a plane bed. The channel bends towards the hydrographic right as the boulder cascade develops further downstream and entering a plane bed. The last sub-reach located on the profile is again a cascade. All the described reaches show large stability, flowing across boulders laid down by glacier activity. This situation is typical at Tolvà Creek, where also downstream the monitored reach the channel is steep, narrow and well confined, whereas at Grigno Creek, downstream the surveyed reach, the slope decreases as the channel widens (Figure 4.1.2d).

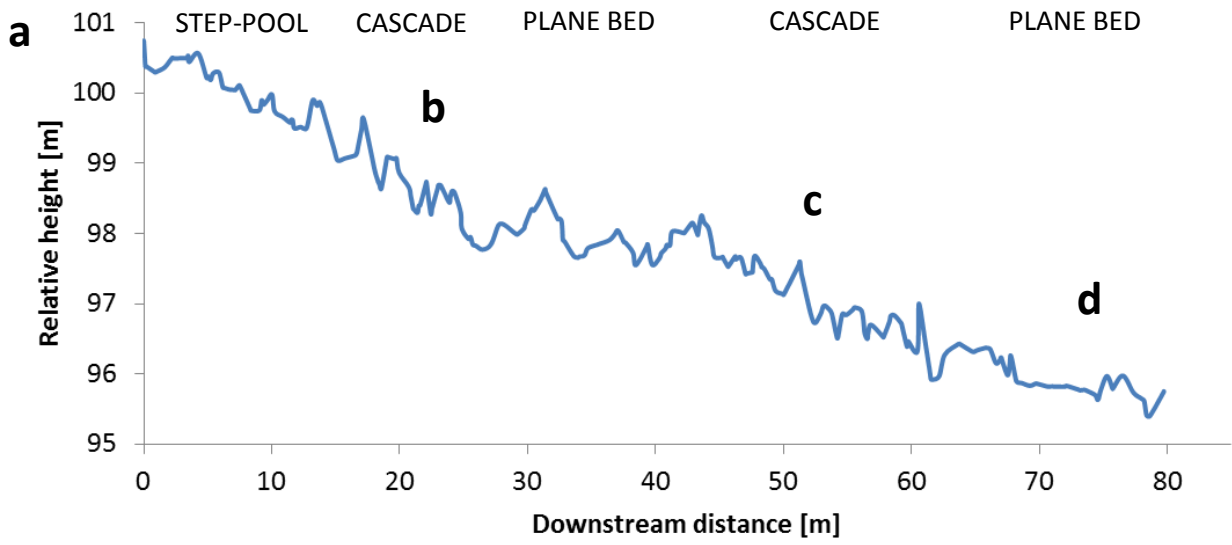


Figure 4.1.2. a) Longitudinal profile of Grigno Creek, illustrating the main morphologies at reach scale; b) boulder-cascade in the upstream portion of the reach; c) overview of the boulder-cascade and plane bed

characterizing the central-lower portion of the study reach. On the left is visible an erratic boulder; d) plane bed and channel widening 50 m downstream the end of the monitored reach.

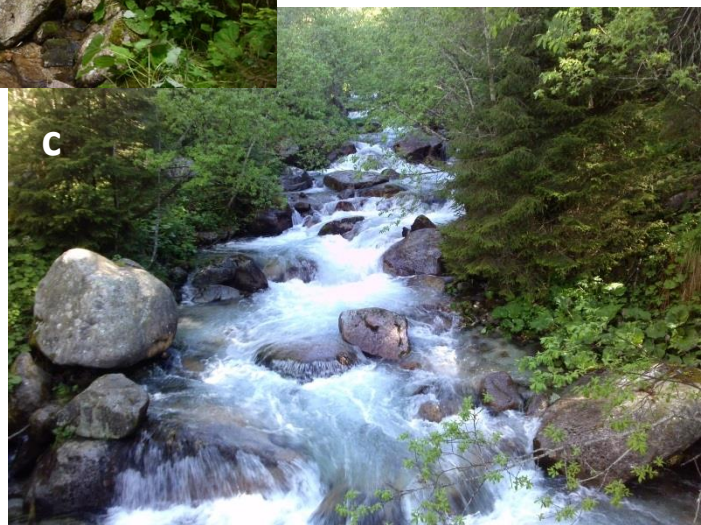
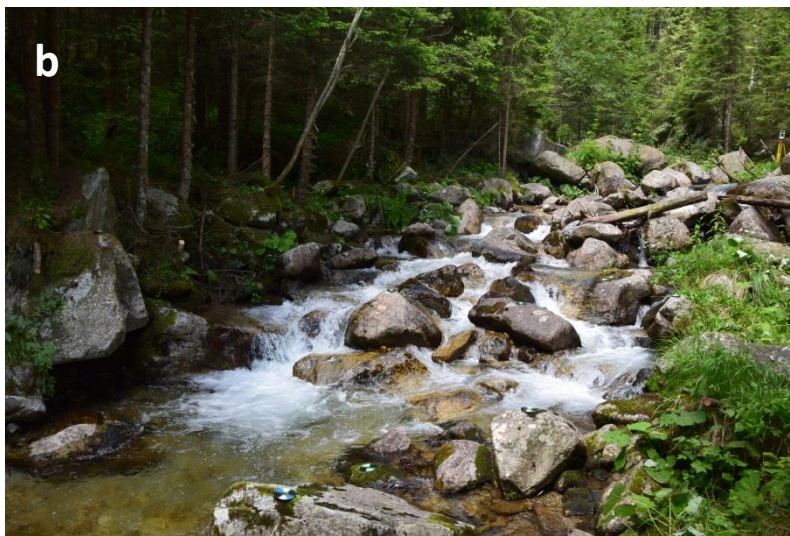
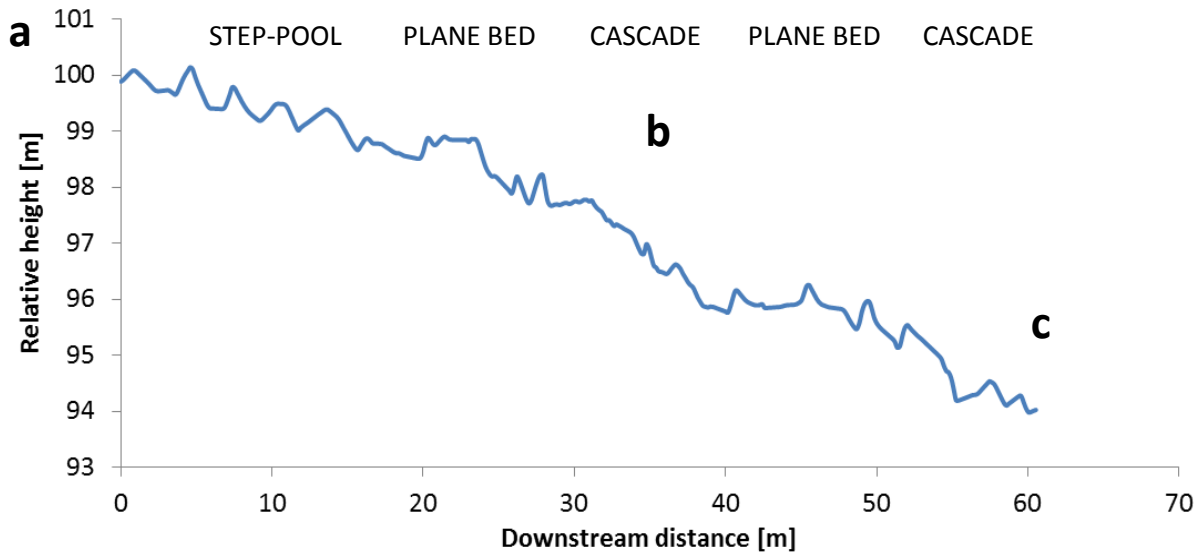


Figure 4.1.3. a) Longitudinal profile of Tolvà Creek, illustrating the main morphologies at reach scale; b) the distinctive boulder-cascade present at Tolvà Creek, in the central portion of the reach; c) step cascade 30 m downstream the monitored channel reach.

At Ussaia Creek the profiles surveyed through the years exhibit different thalweg length, due to its lateral migration. the channel is extremely unstable, with major changes in channel morphologies discernible from longitudinal profile of Figure 4.1.4. An example of the variations occurred in this channel is represented by the erosion of a vegetated central bar, due to the event of November 5, 2014.

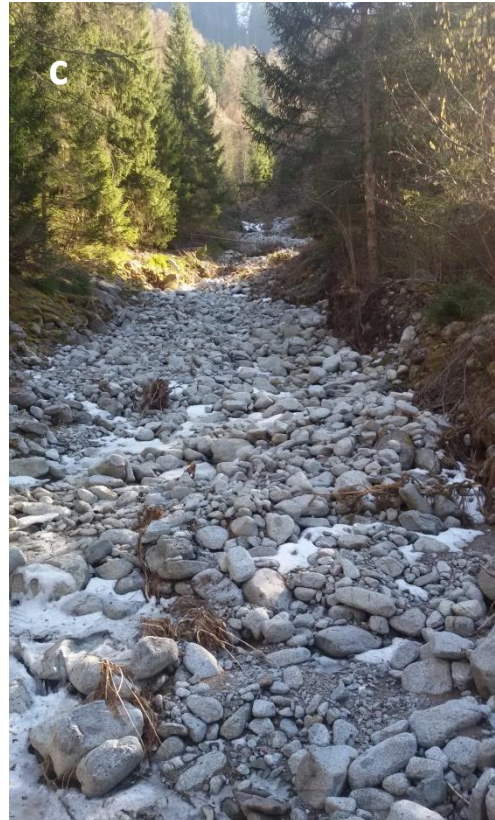
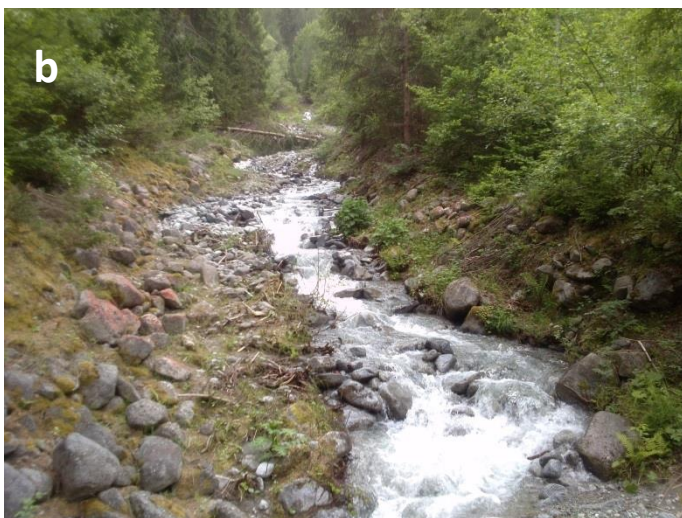
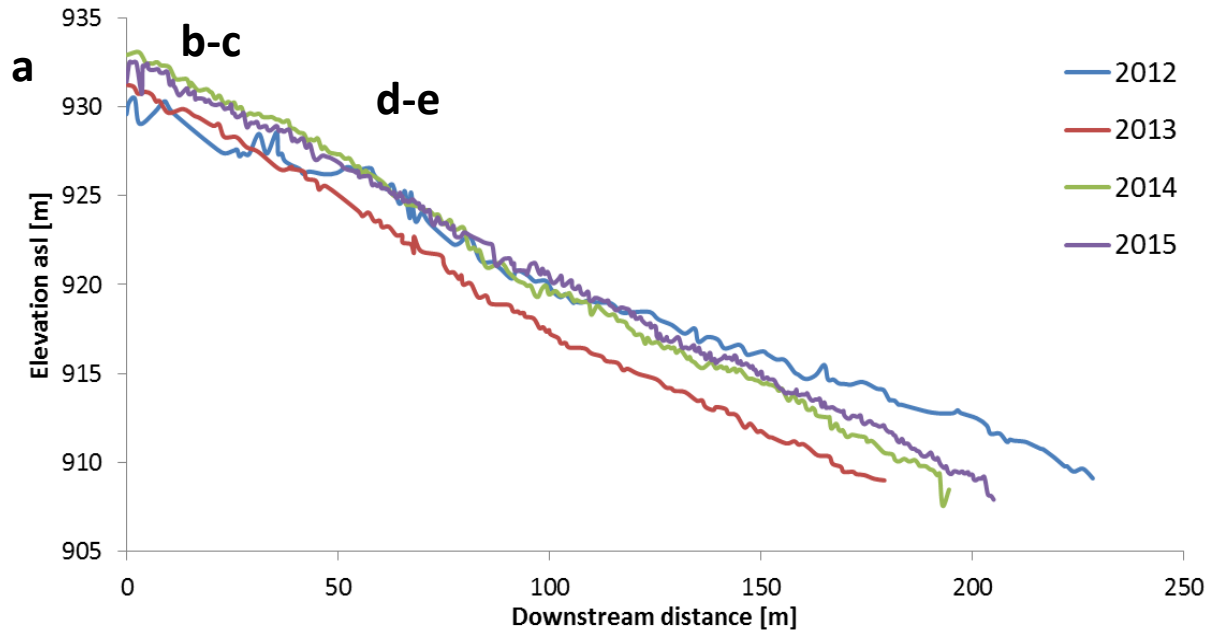




Figure 4.1.4. a) Longitudinal profiles of Ussaia Creek for the period 2012-2015. Pictures showing changes occurred after the debris flow of November 5th, 2014: the upstream portion of the monitored reach as of b) July 27th, 2014, c) March 28th, 2015. Cascade reach in the central portion as of d) July 27th, 2014, e) March 28th, 2015.

At Strimm Creek the longitudinal profile of the monitored reach was surveyed in summer 2012 (Figure 4.1.5). The average slope is 17%. The profile is homogeneous, without a single, important break of slope in the central portion (i.e., relative position 170 m downstream from beginning of profile) where a large cascade is followed downstream by a pool.

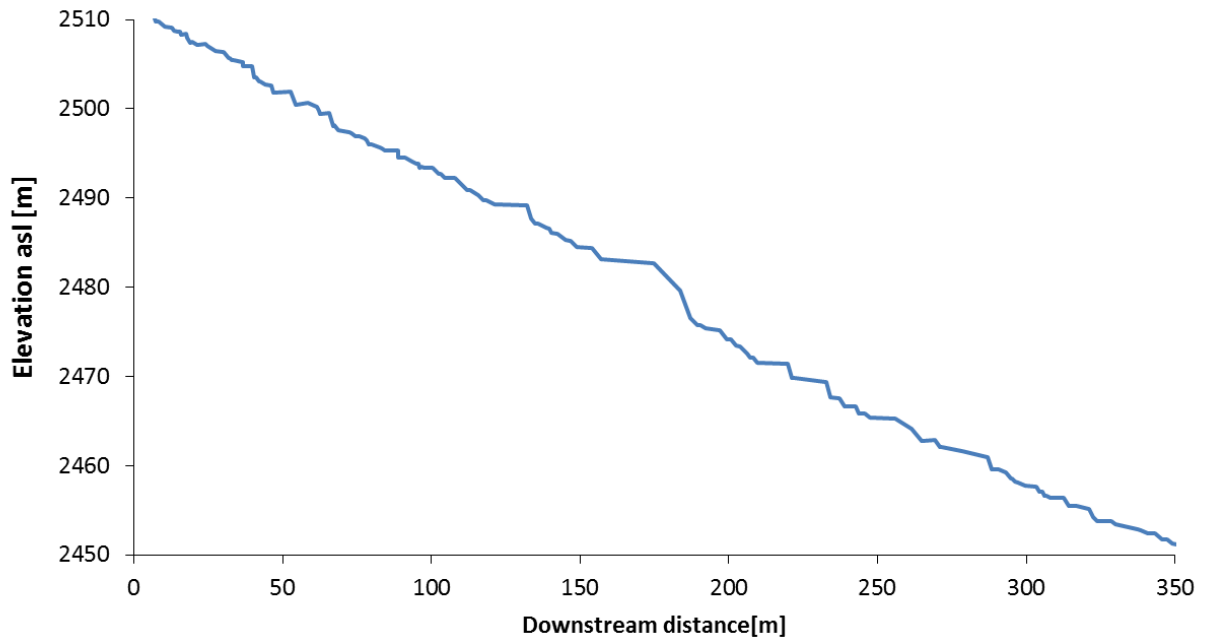


Figure 4.1.5. Longitudinal profile of Strimm Creek surveyed in 2012.

Table 4.1.1. Values of slope of the surveyed thalweg of all the studied reaches.

Site	Year	Slope			
		Mean (%)	Median (%)	Std.Dev.	Std.Error
Grigno Cr.	2014	7.5	6.4	0.16	0.08
Tolvà Cr.	2014	10	8.6	0.13	0.06
	2012	9	6.1	0.06	0.67
Ussaia Cr.	2013	12.4	9.6	2.63	0.25
	2014	12.5	8.4	0.34	0.02
	2015	11.5	7.5	0.65	0.04
Strimm Cr.	2012	17	13.5	0.31	0.09

To obtain a quantitative description of the dimensions of the channel morphological units, we compare the longitudinal profile surveyed in 2014 for Grigno, Tolvà and Ussaia Creeks and the profile surveyed in 2012 at Strimm Creek, focusing on the distribution of step heights and pool depths (Figure 4.1.6). This values can be considered an indirect measure of channel bed roughness. At Grigno and Tolvà Creek step height and pool depth are not normally distributed, but result both strongly skewed towards low values, with medians showing similar values at both sites, of 0.3 and 0.32 m respectively. Step height medians are also very similar, with comparable values of 0.4 and 0.44 m respectively. In both sites the range of variability of pool

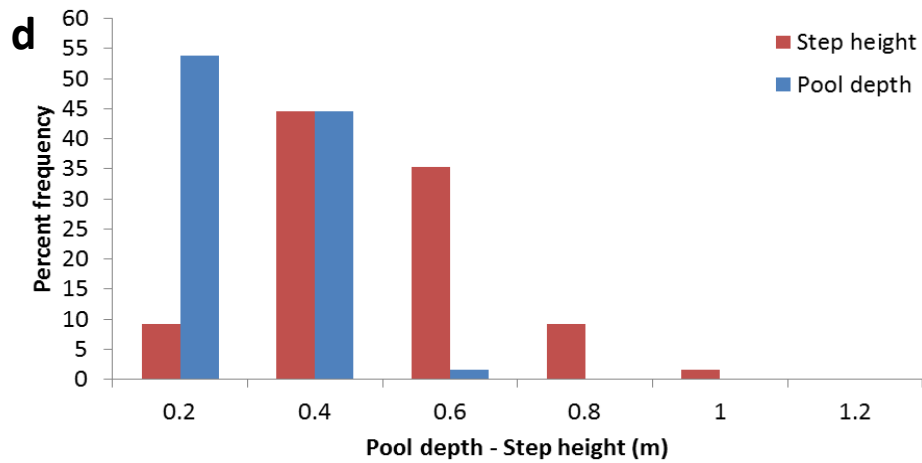
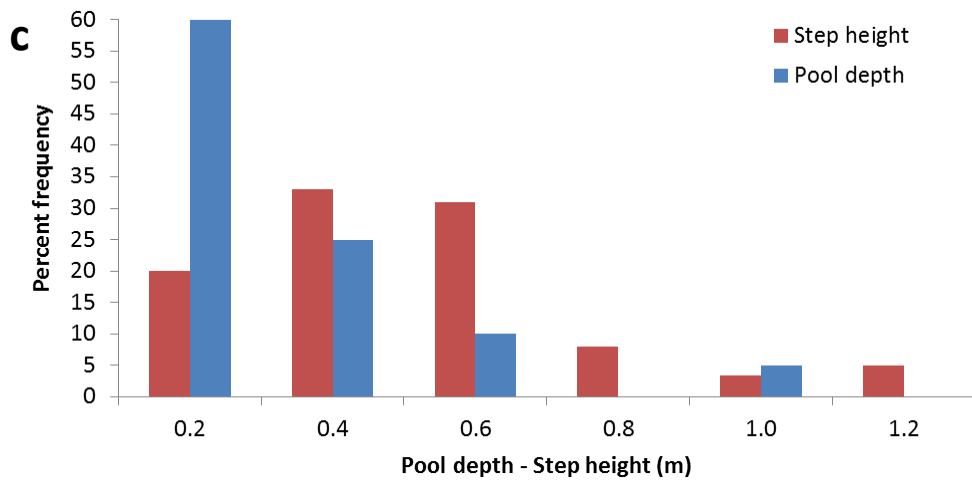
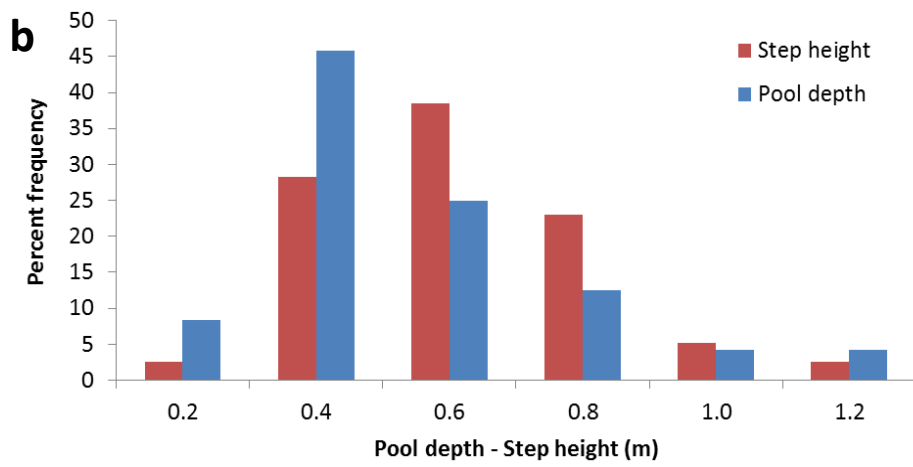
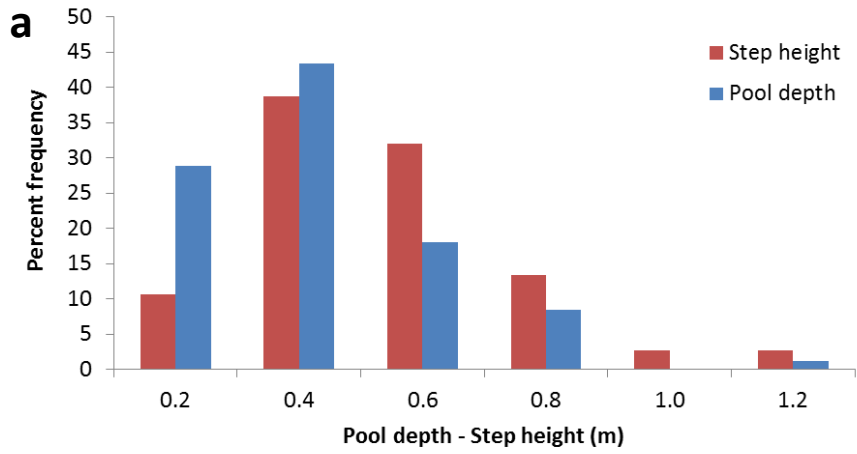


Figure 4.1.6. Percent frequency distribution of step height and pool depth along the monitored portion of a) Grigno Creek, b) Tolvà Creek, c) Ussaia Creek, d) Strimm Creek.

depths and step heights are the same, ranging from few centimeters up to 1 meter. The difference is that the mode of step height at Tolvà Creek is 0.6 m, larger than 0.4 m at Grigno Creek. This values are reflected by the larger roughness at reach displayed by Tolvà Creek, where the main boulder cascade (cf. Figure 4.1.3) and the larger presence of stepped subreaches contribute to higher relative roughness.

At Ussaia Creek the distribution of step height and pool depth are not normally distributed, but result both strongly skewed towards low values, with medians equal to 0.37 and 0.13 m respectively. Step height displays a much wider range of variability, from 0.05 to 1.02 m, compared to pool depth (Table 4.1.2).

At Strimm Creek, the mode of step heights is 0.4 m, followed by the 0.6 m class. The pool depth mode is 0.20 m. The thalweg of Strimm Creek in fact is characterized by pools of limited depths, considering that the largest pool depth is about 0.2 m, whereas the largest step height is 0.82 m. Also in this case the distribution is not normal, with both morphological parameters being skewed towards low values, with medians equal to 0.09 m for pool depth, and 0.38 m for step height. The variability of pool depth is restricted to the range 0.02-0.61 m, while step height shows larger variability, from 0.07 to 1 m.

All the values for each site are summarized in Table 4.1.3.1, reporting at first pool depth and then step height. Comparing the pool depths among various sites it is evident that median of pool depths are 0.3 m at Grigno Creek and 0.32 m at Tolvà Creek, values that are larger to 0.13 m and 0.09 m obtained at Ussaia and Strimm Creek respectively. This condition is less evident for step heights, where differences among median values various sits are less pronounced.

Table 4.1.2. Descriptive statistic of pool depth and step height values analyzed at all the sites.

	POOL DEPTH (m)			
	Grigno Cr.	Tolvà Cr.	Ussaia Cr.	Strimm Cr.
Maximum	1.07	1.01	0.85	0.61
Minimum	0.08	0.02	0.02	0.02
Mean	0.33	0.34	0.16	0.09
Median	0.30	0.32	0.13	0.09
Mode	0.4	0.4	0.2	0.2
Standard deviation	0.19	0.26	0.14	0.05
Standard error	0.19	0.06	0.03	0.12

	STEP HEIGHT (m)			
	Grigno Cr.	Tolvà Cr.	Ussaia Cr.	Strimm Cr.
Maximum	1.06	1.15	1.02	0.82
Minimum	0.08	0.11	0.05	0.07
Mean	0.43	0.50	0.4	0.41
Median	0.40	0.44	0.37	0.38
Mode	0.4	0.6	0.4	0.4
Standard deviation	0.20	0.22	0.27	0.16
Standard error	0.17	0.07	0.05	0.16

4.1.1.2 Cross sections

In this section are presented some examples of representative cross sections for each site. The main difference among the various sites is that Grigno and Tolvà Creek generally exhibit single channels in the monitored reaches, with diversions of main flux and secondary channels created by stepped morphological structures such as boulder cascades. At Ussaia and Strimm Creek is noted the presence of central bar or vegetated island, in restricted portions of the channel, generally extending 20-40 m.

In Figure 4.1.7 is presented a cross section of a typical boulder-cascade at Grigno Creek (cf. Figure 4.1.2b), where is clearly illustrated how stable boulders are responsible for main flow bifurcation, creating zones of tranquil flow on one side (e.g. pools) and steep rapids on the other side. This condition is found in the upper portion of the investigated reach, whereas in the lower portion, as shown in Figure 4.1.2a, morphologies are less stepped such as pools or plane bed and is noted the presence of a single thread channel.

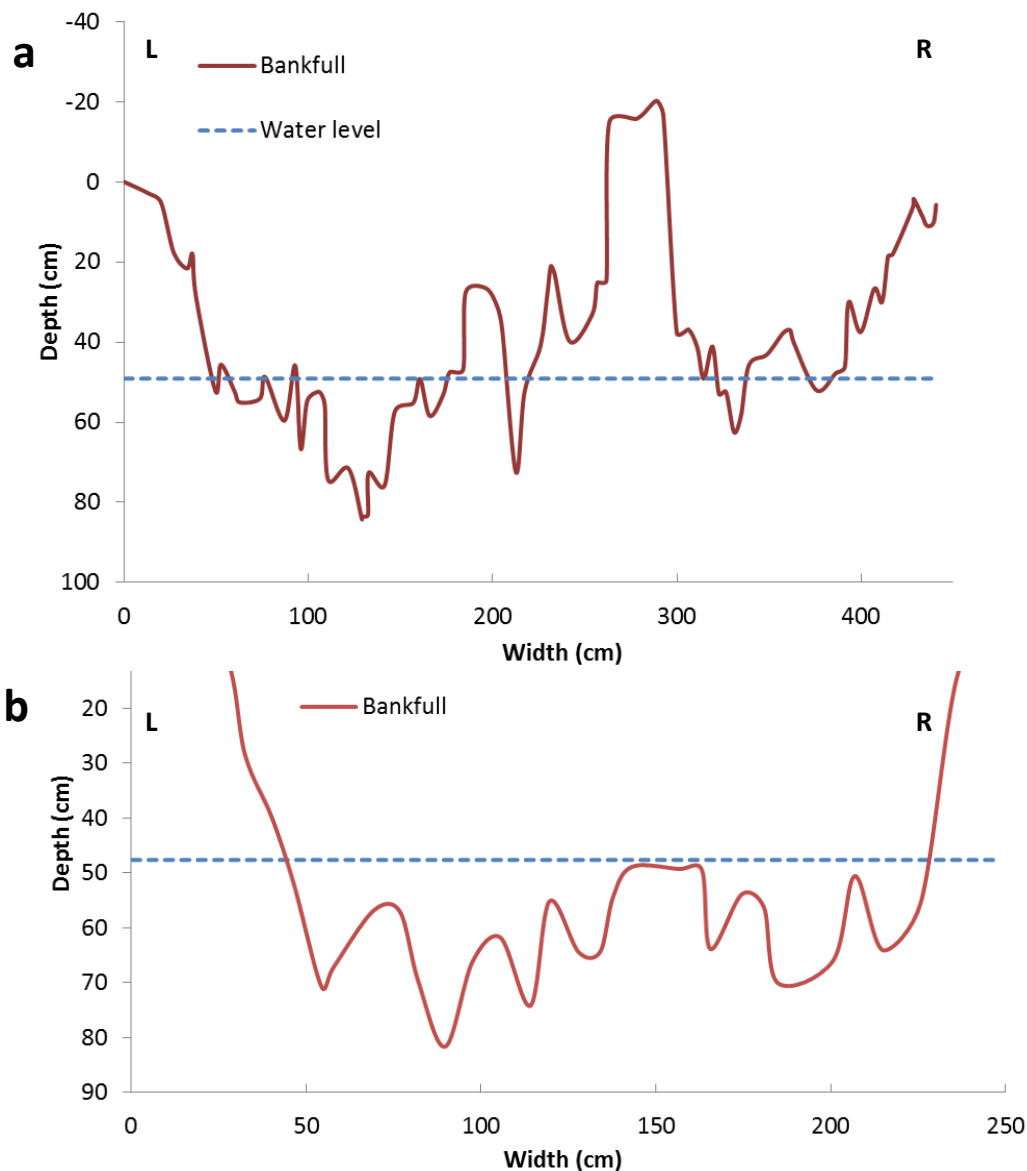


Figure 4.1.7. Typical cross sections surveyed at Grigno Creek: a) boulder cascade in the upstream reach , b) plane bed in the lower portion.

At Tolvà Creek the morphological configuration of transversal section is comparable with Grigno Creek; in Figure 4.1.8 are presented two sections of a boulder cascade (see Figure 4.1.3b) and of a pool.

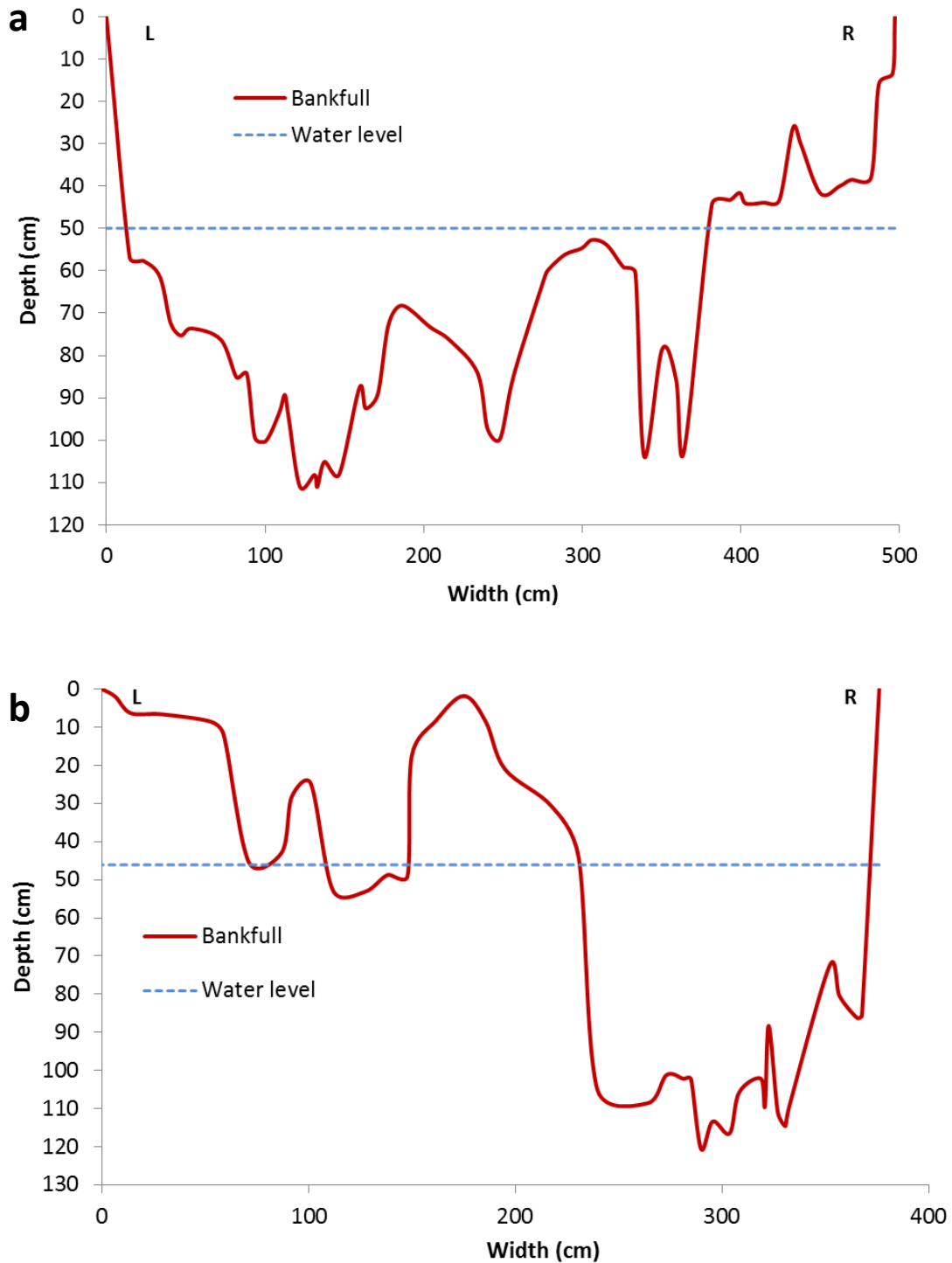


Figure 4.1.8. Cross sections surveyed at Tolvà Creek: a) boulder cascade in the central reach , b) deep lateral pool in the lower portion; note the presence of a super-elevated, secondary channel on the left, separated from the rest of the channel by a large boulder plunging directly into the pool.

At Ussaia Creek the water depth and channel configuration are very different from those shown above. Moreover the channel is characterized by the presence of a vegetated island in the period 2012-2014, eroded in 5 November 2014 by a debris flow. For this channel in Figure 4.1.9 are presented cross sections

of the same reach, characterized by rapids in 2013, that has been strongly modified after the debris flow, as shown by 2015 survey.

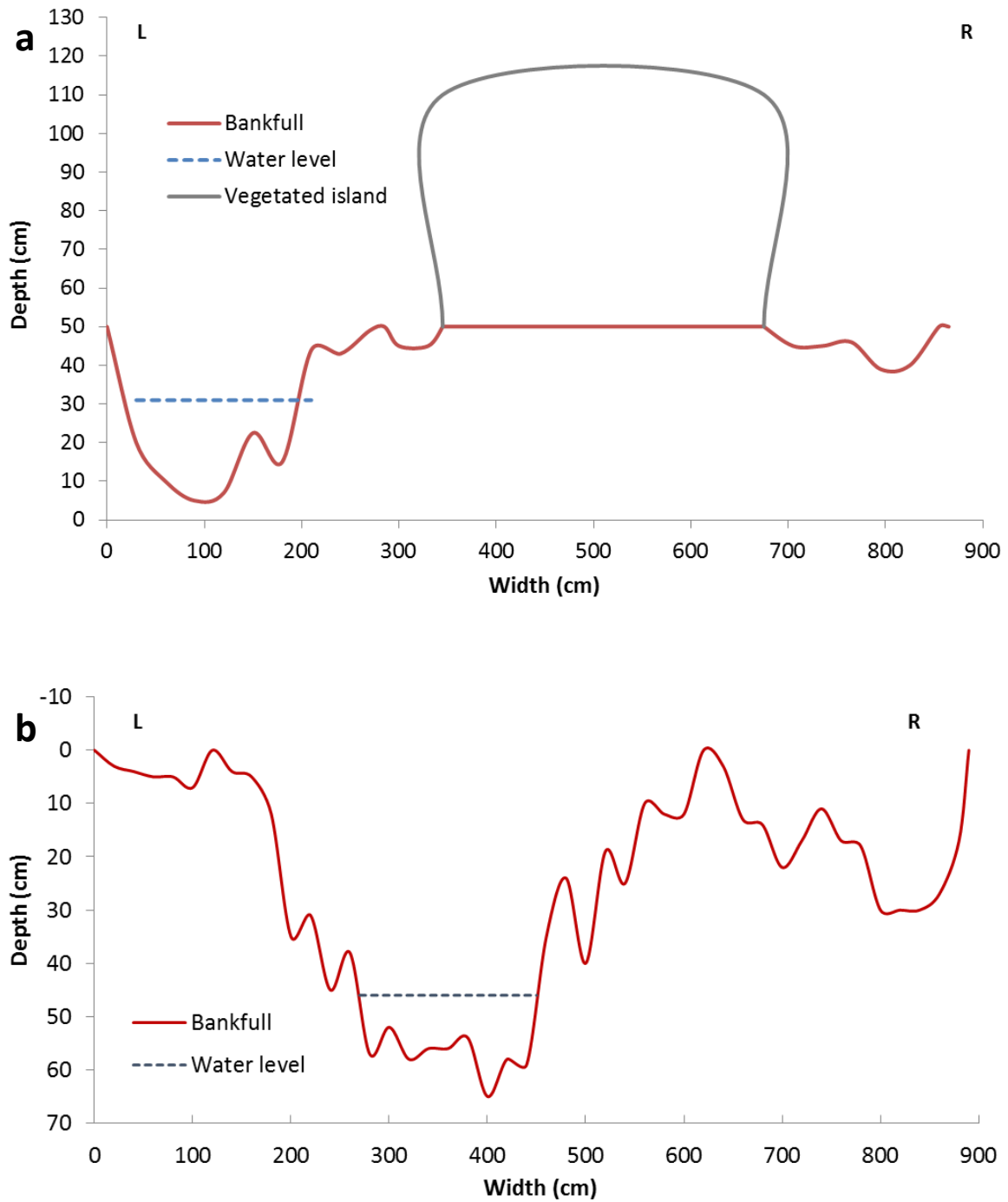


Figure 4.1.9. Cross sections surveyed at Ussaia Creek: a) reach characterized by the presence of rapids, separated in the center by a stable, vegetated island (survey 2013) , b) the same reach, surveyed in 2015, after the 5 November 2014 debris flow. Channel thalweg migrated rightwards.

At Strimm Creek the channel is characterized by a transversal configuration that varies moving downstream (Figure 4.1.10). In the upstream sections the channel is wide and there is the presence of a non-vegetated central island. From here downstream a more confined channel develops, with the presence of the deepest pools among those studied.

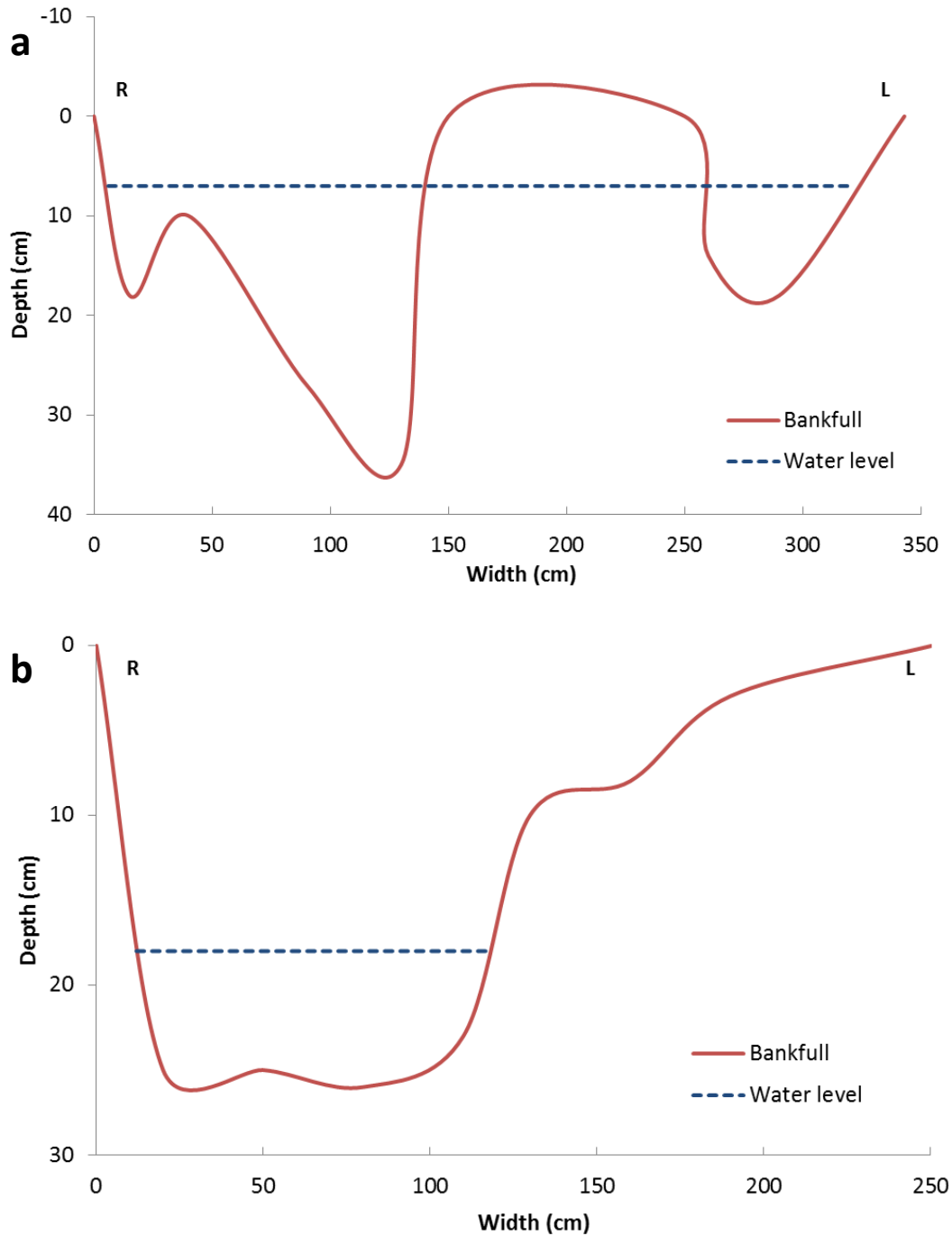


Figure 4.1.10 Cross sections surveyed at Strimm Creek: a) reach characterized by the presence of a well confined pool, b) Typical example of a large section at Strimm Creek, with the presence of a central bar, not vegetated.

All the surveyed cross sections at each site are reported in the Appendix A4.1.1 .

4.1.2 Downstream hydraulic geometry

In the Grigno-Tolvà Creek 23 reaches have been surveyed to analyze the relations between channel width, depth and wetted and contributing area. In the following panels the points plotted are distinguished between sections surveyed at Upper Grigno Creek, Lower Grigno Creek and Tolvà Creek. The lower Grigno Creek represents the reach downstream the confluence between Upper Grigno Creek and Tolvà Creek. The following exponential relations existing among these parameters is evaluated at the bankfull stage, giving:

$$\text{Width} = aA^b \quad (\text{eq. 4.1})$$

$$\text{Depth} = cA^f \quad (\text{eq. 4.2})$$

$$\text{Wetted area} = kA^m \quad (\text{eq. 4.3}),$$

where A is a proxy for water discharge Q, as in the seminal theory of Leopold and Maddock (1953).

Bankfull width displays a moderate positive dependence on contributing area ($R^2 = 0.68$) (Figure 4.1.11) with a scaling exponent ($b = 0.48$) in agreement with published values for fluvial stream channels (Knighton, 1998).

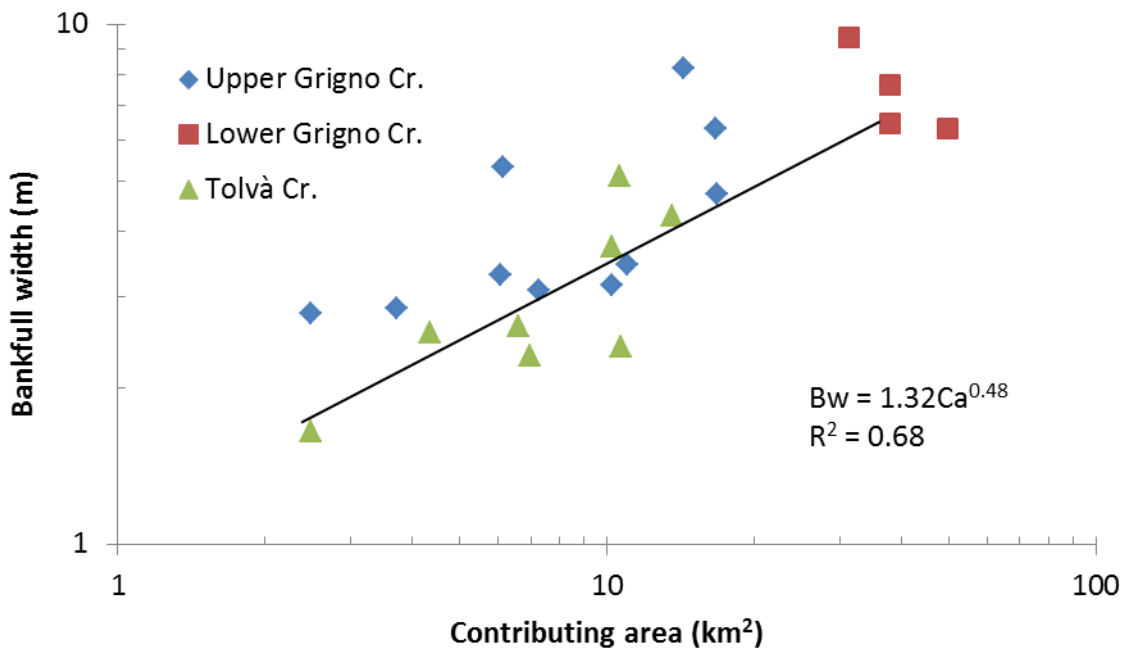


Figure 4.1.11. Bankfull width (median) as a function of contributing area for Grigno and Tolvà Creeks.

Bankfull depth exhibits a much more scattered positive dependence from contributing area (Figure 4.1.12, $R^2 = 0.13$), yet displaying a scaling exponent ($f = 0.19$) that sets within the published values for fluvially-dominated channels (Knighton, 1998). In other words, as the Grigno and Tolvà Creeks become wider, their

corresponding bankfull depth increases to a lesser extent. The points with the maximum channel depth represent channel depth in the sections UG5, UG8 and LG2, while points with the minimum channel depth are located in the sections T1, T2 and LG3 (see Figure 3.6).

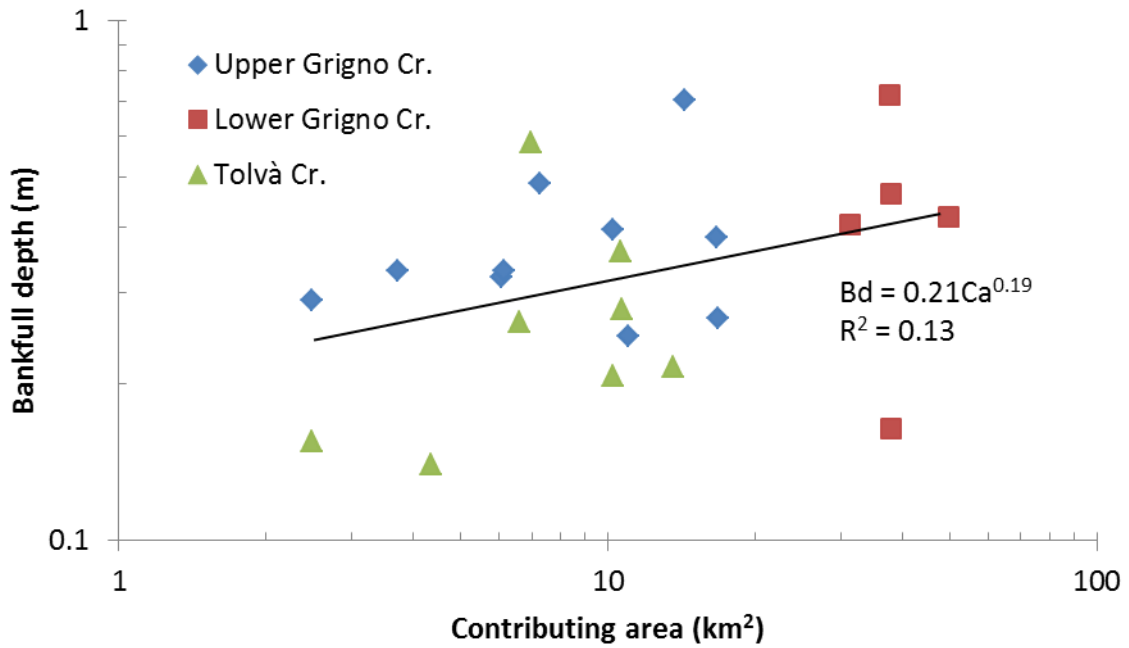


Figure 4.1.12. Bankfull width (median) as a function of contributing area for Grigno and Tolvà Creeks.

The correlation between the wetted area at bankfull stage and the drainage area (Figure 4.1.13) shows value of correlation $R^2 = 0.57$. The section T2 shows the lowest value of wetted area (0.26 m^2), with the largest variance from the regression. The value of drainage area is three times larger, considering the first and the last point from left to right, while the dependent variable does not show abrupt changes. The considered values are from the sections T6, UG8 and LG1. All of the considered sections are immediately downstream a water intake (T6, UG8) or a hydro power plant (LG1).

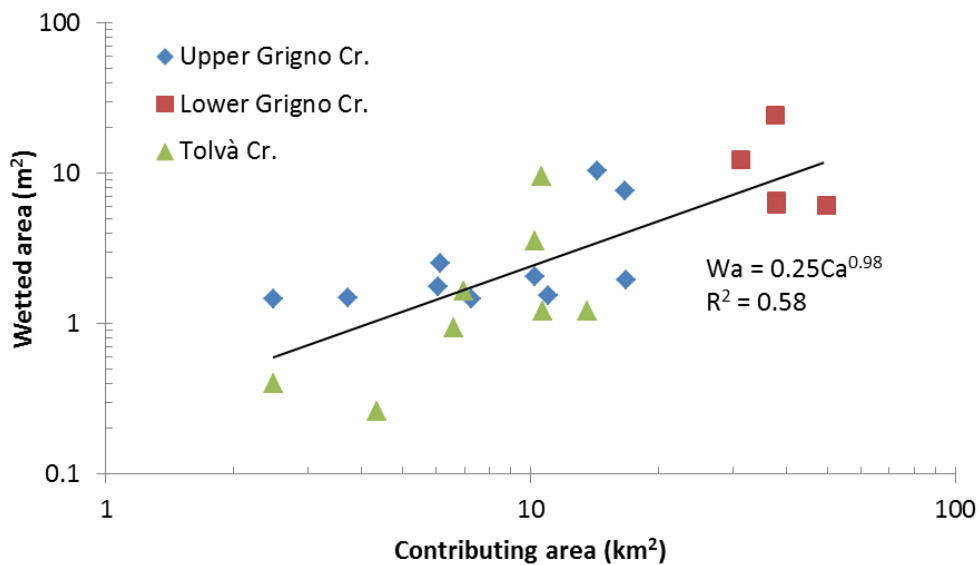


Figure 4.1.13. Wetted area (median) as a function of contributing area for Grigno and Tolvà Creeks.

A similar behavior is present also for points lying between 1 and 2 m² of wetted area. Of the 23 investigated reaches in fact, 9 are within this interval, showing a drainage area variation comprised between 1.5 and 20 km².

Downstream hydraulic geometry sections are reported in Appendix A4.1.2.

4.1.3 Grain size distribution

To characterize the grain size distribution, the results presented in this section show the distribution of grain size by plotting a histogram for each site (Figure 4.1.14). Table 4.1.3 summarizes the main properties of the distributions for each site, and the cumulative curves will be plotted together to allow a better comparison of the characteristics.

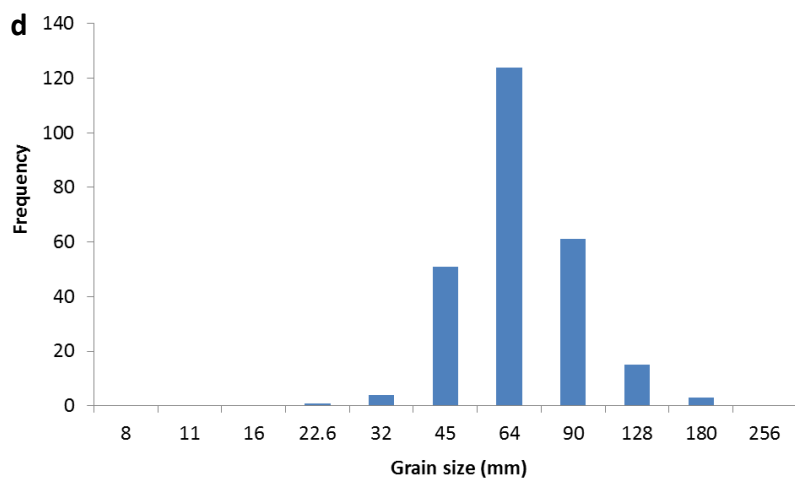
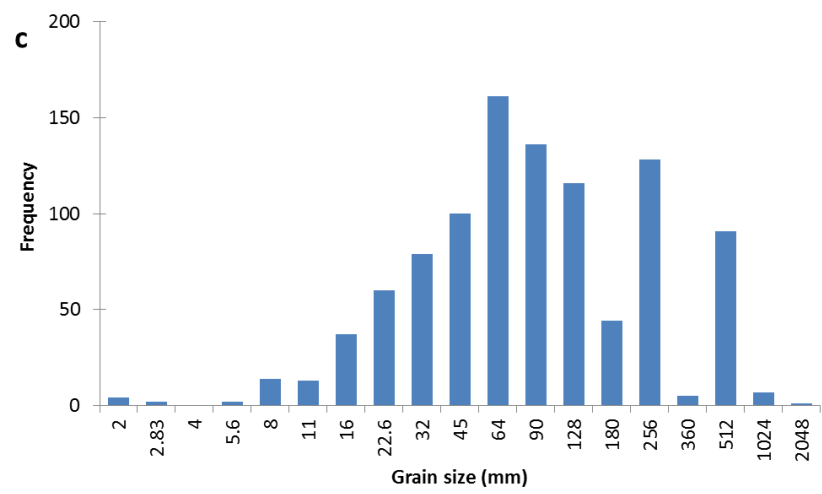
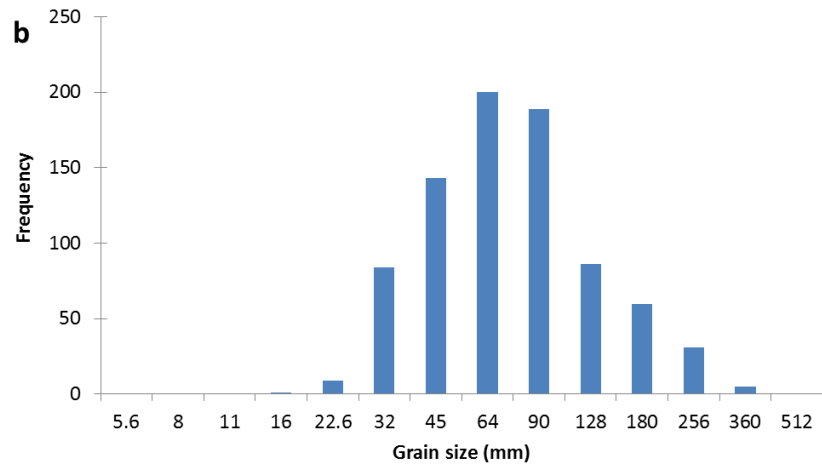
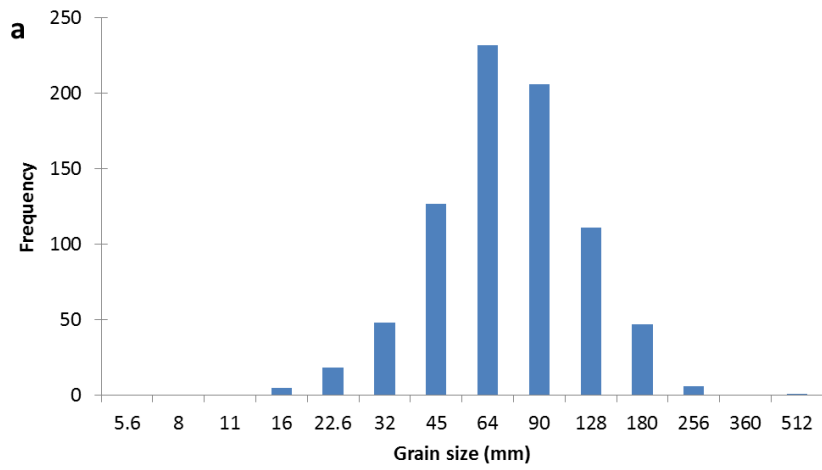


Figure 4.1.14. Bed surface non-cumulative grain size distribution at a) Grigno Creek, b) Tolvà Creek, c) Ussaia Creek, d) Upper and Lower Strimm Creek.

The distribution at Grigno Creek is homogeneous and sediment ranged from 16 to 256 mm, with $D_{16} = 37.3$ mm, $D_{50} = 61.2$ mm and $D_{84} = 101.2$ mm. The distribution at Tolvà Creek shows very similar characteristics to the Grigno Creek, ranging from 16 to 360 mm, with $D_{16} = 34.8$ mm, $D_{50} = 60.4$ mm and $D_{84} = 111.7$ mm. Sediment distribution at Ussaia Creek is skewed towards larger values of grain size, with remarkably high clast count in the 256 and 512 ϕ -axis classes. They range from 2 to 2048 mm, with $D_{16} = 25.6$ mm, $D_{50} = 68.9$ mm and $D_{84} = 219$ mm. In the Strimm Creek sediments ranged from 4 to 512 mm, with $D_{16} = 26.7$ mm, $D_{50} = 62.3$ mm and $D_{84} = 118.6$ mm.

Cumulatively Grigno and Tolvà Creeks distributions are comparable (Figure 4.1.15), but for Grigno site it is shifted towards larger grain size. The Ussaia Creek exhibits the widest range among all the distributions (Table 4.1.3), since the distribution includes more finer fraction and is also characterized by the presence of large particles. An intermediate configuration is present at Strimm Creek, where the lower half of the distribution is very close to that of Ussaia Creek, while in the upper half it resembles that of Tolvà Creek. These discrepancies in the distributions are reflected in the size and dimension of the material transported in all these sites. At Grigno and Tolvà Creeks in fact, the largest boulders are immobile (cf. Figures 3.8-3.9) and only fractions below 256-360 mm are commonly found as lateral deposits or mobile sediments constituting the channel bed. At Ussaia Creek, conversely, the largest elements forming the main channel structures, are stable at short timescales (seasonal or annual), and lateral bars are commonly composed by gravels, pebbles and boulders supported by sandy matrix. We are analyzing systems (i.e. Grigno and Tolvà Creek) characterized on one hand by limited sediment supply, and a high degree of hydrological connection between hillslopes and channels; on the other hand systems such as Ussaia Creek, characterized by transport-limited conditions and limited amounts of hydro-meteorological inputs due to its geo-climatic setting. Within this context the Strimm Creek can be view as a transport-limited system, due to its hydro-meteorological conditions imposing low-annual and summer precipitations. Observing the grain size distribution we could expect sediment transport at Strimm Creek to be comparable with the Ussaia Creek, but here conditions imposed by landscape (slope and sediment sources) are dictating the differences on bedload transport discussed in this thesis.

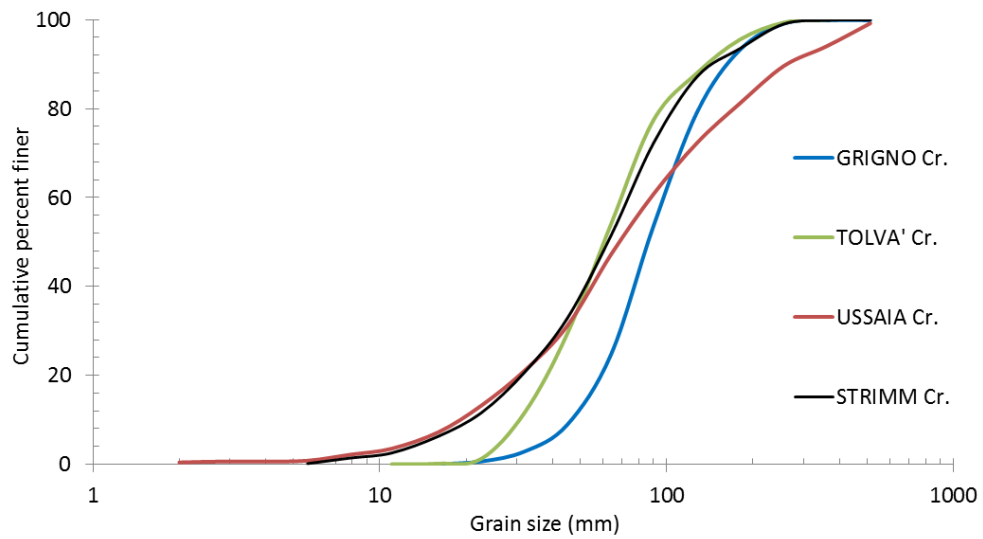


Figure 4.1.15. Comparative bed surface cumulative grain size distribution at all the sites.

Table 4.1.3. Comparative distributions of D_{16} , D_{50} and D_{84} at each monitored site.

SITE	Range [mm]	D_{16} [mm]	D_{50} [mm]	D_{84} [mm]
Grigno Cr.	16 – 256	37.3	61.2	101.2
Tolvà Cr.	16 – 360	34.8	60.4	111.7
Ussaia Cr.	2 – 2048	25.6	68.9	219
Upper Strimm Cr.	4 - 512	26.7	62.3	118.6

4.2 Hydro-meteorological forcing

The results of the datasets acquired with the methodologies illustrated in section 3 are presented in this chapter. In section 4.2 we described the channel boundary conditions for each monitored site, presenting the results of longitudinal profiles and cross-sections. For each reach the grain size distributions of the transported sediments have been characterized besides the dimensions of the b-axis of the keystones forming the main structures of the channel. In section 4.2 we illustrate the hydro-meteorological events recorded at each sites for the two year period 2014-2015. As a matter of fact, the hydro-meteorological forcing represents the independent variable that causes variations on the hydrological level measured by means of water pressure sensors at each sites. These variations are associate to two principal factors, namely precipitation and the temperature. The first directly affects the liquid discharge measured in the channel, whereas the second exerts its strongest impact during the snowmelt season, inducing variations on the thermal properties of the snowpack accumulated on the hillslopes; in turn meltwater is delivered to the main stem of the watershed, inducing variations in the hydrological regime of the mountain streams and possibly sorting impacts on bedload transport. In this section we focus on the temporal scales at which these phenomena are produced and to what extent they influence the hydrological properties of the basin.

The 2014 presented a climatic trend markedly different from 2015, and globally, the two-year period significantly differs from the historical trend. This situation is clearly recognizable for each site, and will be illustrated in the current section by comparing the 2014-2015 climographs with the historical ones. Each year will be described at seasonal scale, giving details for the most relevant hydro-meteorological events that triggered bedload transport.

4.2.1 Grigno Creek

The climographs of Figure 4.2.1 are illustrating the average monthly precipitation and temperature recorded at Malga Sorgazza. The 2014 climograph is characterized by a considerable amount of precipitation (2730 mm), reaching two maxima in January (440 mm) and October (430 mm). During January precipitation accumulated in form of snow, while in autumn precipitations are mainly in form of rainfall. A secondary maxima is registered in August, with 340 mm of rainfall accumulated. Monthly average temperatures are below zero only in January and February, reaching the minimum of $-0.8\text{ }^{\circ}\text{C}$. During March is registered a sudden increase, with the average rising to $3.8\text{ }^{\circ}\text{C}$, and reaching the maximum in July ($13\text{ }^{\circ}\text{C}$). The 2015 total annual precipitation is 1357 mm (Figure 4.2.1b), about half of the 2014. During November and December no precipitation is recorded, and also comparing the monthly averages of two-year period climographs results evident that the 2015 has been more dry that 2014. The monthly maximum is recorded in October, summing to 244 mm. In January and February little precipitation occurred as snow, and this determines the limited or absent snowmelt pulses observed in the hydrology of the monitored streams. The minimum average temperature is recorded during February ($-2\text{ }^{\circ}\text{C}$), and it rises almost constantly until July reaching $17\text{ }^{\circ}\text{C}$, more than $4\text{ }^{\circ}\text{C}$ when compared to the previous year.

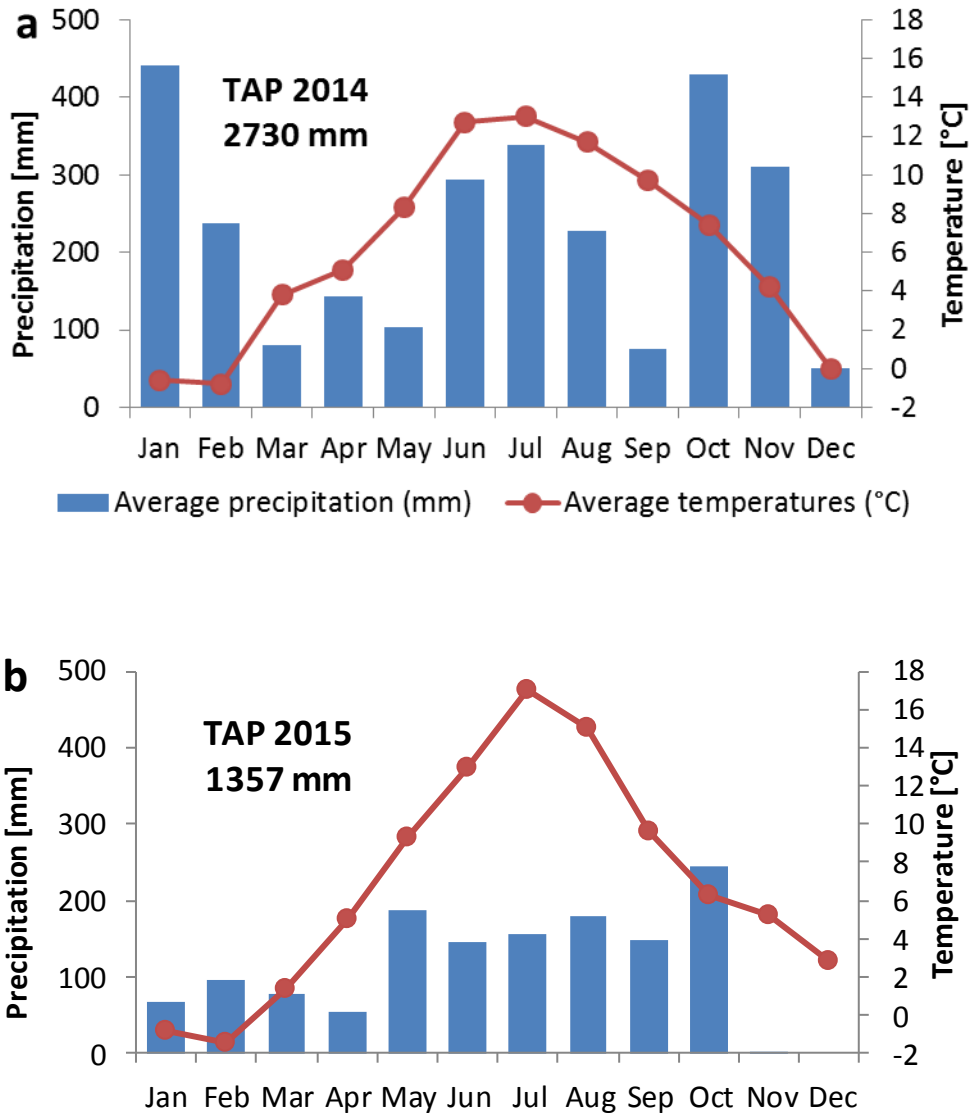


Figure 4.2.1. Monthly climograph recorded at Malga Sorgazza station for the year a) 2014, b) 2015. (TAP: Total Annual Precipitation).

Comparing the 2014 climograph with the historical one (cf. Figure 2.4), we observe anomalous positive net precipitation, whereas the seasonal distribution is similar. Specifically, the snowmelt period was exceptionally long, causing a protracted period of high flows until the end of July. In Grigno Creek we recorded a winter and spring net precipitation equal to 1300 mm, which sets well above the average historical record (632 mm) (cf. Figure 2.4). Considering the 2015 climograph, we recognize a distribution of precipitations similar to the historical record, whereas there is a net precipitation of 150 mm less than the historical value.

In the 2014-15 period were recorded a total of 27 hydro-meteorological forcing events, 15 in 2014 and 12 in 2015 respectively. In 2014, snowmelt extended from April to June, with precipitations characterized by mean intensity of 2.5 mm/h. In the summer period the mean intensity of events increase, reaching 8.4

mm/h for the event of August 13, 2014, that we consider an extreme event, characterized by a maximum rainfall intensity of 17.8 mm/h, the highest recorded during 2014 (cf. A4.2.1). In autumn a major event determined the largest peak discharge recorded at Grigno Creek, with a mean intensity of 5 mm/h and accumulated rainfall of 325 mm in 66 hours. In 2015 snowmelt is limited from April to May, and rainfall events are characterized by their restricted duration, except considering the event of October 13-16, 2015, that lasted for 88 hours, with an average rainfall intensity of 1.6 mm/h (cf. A4.2.2). Cumulatively, the relevant events of 2014 generated a total precipitation of 675 mm, compared to 296 mm of 2015 events, and are characterized by prolonged duration, lower mean and median values with respect to 2015.

Analyzing the hydrograph trend and comparing it to the distribution of precipitations for the year 2014 a direct effect on hydrograph oscillations is discernible for summer and autumn meteorological events (Figure 4.2.2). During summer, maxima hourly rainfall intensity are recorded, but their extent in time is limited; autumn events are less peaked but more prolonged. Summer floods are limited in time and are characterized by rising and falling steep limbs, while the recession of autumn floods is more extended and the continuance of rainfall sustains higher baseflow. This condition is capable of generating large autumn floods, with peak values of $Q = 19.17 \text{ m}^3\text{s}^{-1}$ (November 4-8, 2014). The synchronicity among precipitations and fluctuations in discharge is not recognizable during spring and winter periods. During winter, precipitations accumulate to the ground in form of snow. During springtime on one side the presence of the snowpack limits the surficial waterflow, while on the other hand influences directly the hydrological level in the stream accordingly to the atmospheric temperature. This relation is well illustrated in Figure 4.2.3, where the 2014 snowmelt period is presented, comparing precipitations, atmospheric temperatures and water discharge. The lack of relationship between precipitation and discharge from February until the end of July at Grigno Creek, can be explained by considering the effect of atmospheric temperature. Specifically, we observe a remarkable temporal correlation between temperature and water stage variations (Figure 4.2.3), which is evident at each monitoring site. In Grigno Creek are clearly distinguishable six cycles of temperature change that are mirrored by extended increase in water discharge. The event that marks the transition between snowmelt- and rainfall-dominated period, occurred the 24/06/2014. Before this event, peak duration is typically comprised between 100 and 550 hours, while is 320 hours for the considered event. After that, flood duration is limited to 30-85 hours for the summer period and soon after the beginning of autumn increases to 120 and 400 hours for the events of October 13-14 and November 4-8, 2014, respectively.

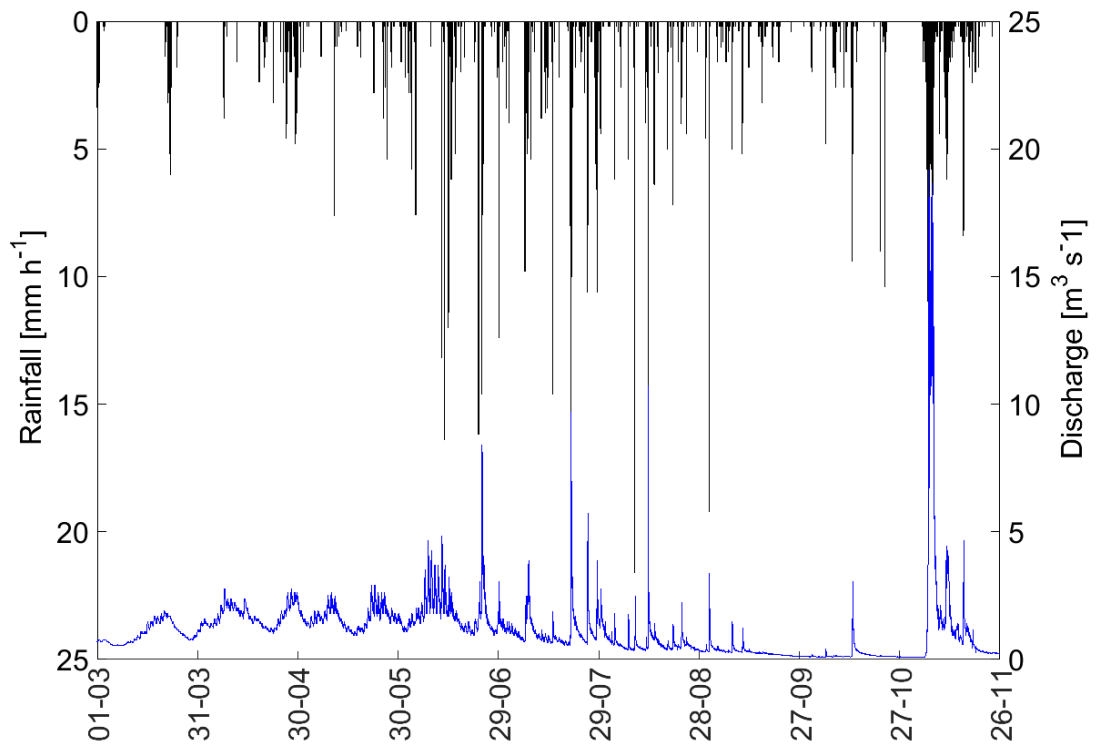


Figure 4.2.2. Water discharge hydrograph (blue line) and hourly rainfall intensity (vertical black bars) for the year 2014 at Grigno Creek (rainfall intensity recorded at Malga Sorgazza).

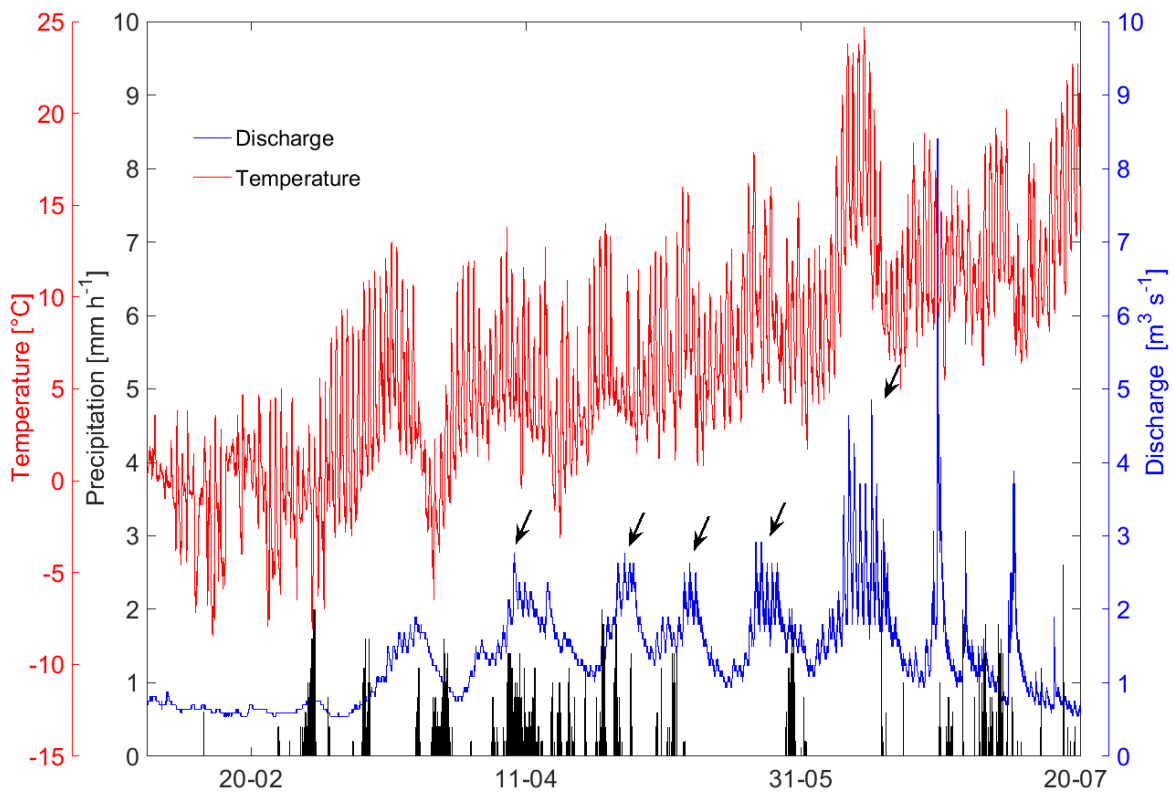


Figure 4.2.3. Hourly precipitations, atmospheric temperature and water discharge recorded in 2014 at Grigno Creek, limited to the snowmelt period (temperature recorded at Malga Sorgazza). Black arrows are indicating snowmelt peaks.

4.2.2 Tolvà Creek

In the climographs of Figure 4.2.4 are illustrated the average monthly precipitation and temperature recorded at Passo Brocon. The 2014 is characterized by a total annual precipitation of 2790 mm, reaching a primary maximum in October, with 550 mm of accumulated rainfall. Two secondary maxima are registered January and July (360 mm). As for the Grigno site, January precipitations accumulated in form of snow, while during summer precipitations events are in form of rainfall. Monthly average temperatures are below zero only in January and February, reaching the minimum of $-0.8\text{ }^{\circ}\text{C}$. From March temperatures are increasing, reaching the maximum value of $12.8\text{ }^{\circ}\text{C}$ in July. The year 2015 (Figure 4.2.4b) recorded a total annual precipitation of 1154 mm. As recorded by Malga Sorgazza, no precipitation occurred in November and December at Passo Brocon, and cumulatively the 2015 has been more dry than 2014. The monthly maximum is recorded in October, reaching 279 mm. In January and February little precipitation occurred as snow, determining limited or absent snowmelt pulses in the monitored stream. The minimum average temperature is recorded in February ($-1.6\text{ }^{\circ}\text{C}$), and from this month rises constantly until July reaching $17\text{ }^{\circ}\text{C}$, its maximum. Besides the precipitations, also temperatures recorded in November and December are anomalous. As a matter of fact, October and November share identical average temperature, and during December the average recorded is $3.7\text{ }^{\circ}\text{C}$, compared to $0.5\text{ }^{\circ}\text{C}$ of the year 2014.

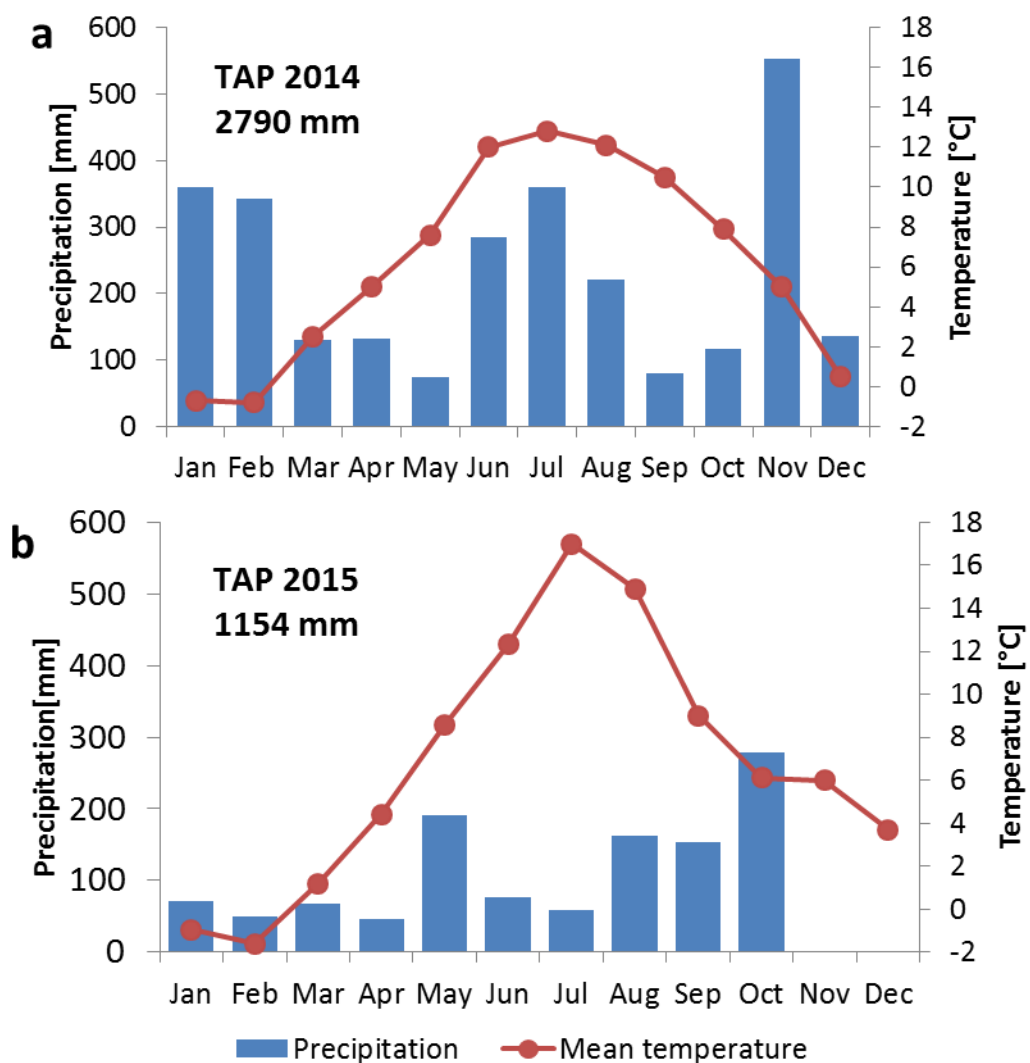


Figure 4.2.4. Monthly climograph recorded at Passo Brocon station for the year a) 2014, b) 2015. (TAP: Total Annual Precipitation)

The 2014 climograph shows a distribution of monthly average precipitation similar to the historical climograph (cf. Figure 2.4). In particular we observe an anomalous positive net precipitation, with a total accumulated precipitation of 2790 mm registered in 2014, compared to 1511 mm recorded historically. Specifically, the snowmelt period was exceptionally long, causing a protracted period of high flows until the end of July. Winter and spring net precipitation is equal to 1300 mm, which sets well above the average historical record (632 mm) (cf. Figure 2.4). Considering the 2015 climograph, the distribution of precipitations is similar to the historical record, with two maxima falling in May and October, but the strong anomaly is represented by the absence of precipitations during late autumn. As a consequence, net quantities of precipitation are 360 mm less than the historical value. Considering the temperatures, the overall trend in 2015 is similar to the historical, with a minimum in February and an increase that extends until July, where the maximum value is reached. Historically the maximum at Passo Brocon the maximum was set during August, with a value of 13.5 °C, instead the 2015 reached the considerable value of 17 °C during July. Strong differences are recorded also in the months of November and December. Historically, the average temperature in this two months was 1.9 and -1.4 °C respectively. During 2015, in November is recorded an average value of 6 °C and in December 3.7 °C.

At Tolvà Creek 17 hydro-meteorological events are observed in total, 8 in 2014 (from July to December) and 9 in 2015 (from January to October). In 2014 all the monitored events are induced by rainfall, while in 2015 we observed one snowmelt event (April), 3 mixed events in April-May and 5 rainfall events. In 2014 there is a clear difference in the duration of precipitation during summer of autumn periods. Typical events of summer period are lasting few hours (2-5), with mean values of rainfall intensity of 8-10 mm/h (cf. Table A4.2.3). The largest average intensity is recorded in the event of August 13, 2014, with a value of 13.3 mm/h. This event represents an extreme, and as a matter of fact its maximum intensity is 26.6 mm/h. Typical duration of precipitations of autumn are comprised within 11 and 60 hours. Being more prolonged, mean intensities are lower compared to the summer period (4-6.6 mm/h), but the total rainfall accumulated are considerably larger. In this period an extreme is represented by the event of November 4-8, 2014, that lasted 60 hours and a total rainfall of about 380 mm, values that are comparable with those recorded at Malga Sorgazza. For this site, the 2015 begins with a limited snowmelt that extends from April to May, and rainfall period is observed from 23 June to 16 October. Duration of precipitation in the snowmelt period are generally comprised between 9 and 24 hours (cf. Table A4.2.4), but are characterized by low mean intensities (1.1-3.5 mm/h). Rainfall events typical of summer period are restricted in time, with durations comprised within 3 and 8 hours, but exhibiting larger mean intensities, comprised between 5 and 10 mm/h. The only event recorded in autumn 2015 shows the largest duration (88 hours), and mean intensity of 1.3 mm/h, with a total rainfall of 120 mm. Similarly to Grigno Creek, a direct effect on hydrograph oscillations is discernible for summer and autumn meteorological events recorded in 2014 (Figure 4.2.5). The synchronicity among precipitations and fluctuations in discharge is not recognizable during spring and winter periods (Figure 4.2.6), when the lack of relationship between precipitation and discharge from March until the end of July at Tolvà Creek, can be explained by considering the effect of atmospheric temperature. Specifically, we observe a remarkable temporal correlation between temperature and water stage variations. As shown for Grigno Creek, also at Tolvà Creek are clearly distinguishable six cycles of temperature change that are mirrored by extended increase in water discharge. The duration of peak discharge induced by snowmelt is comprised between 4 and 12 days. From the event of June 21, 2014 the baseflow sustained by snowmelt decreases, as showed in Figure 4.2.6, where is visible that after each peak discharge values are decreasing towards the baseflow, going from 0.76 to 0.46 and to 0.43 m³s⁻¹ by July 20th. After that event, floods are rainfall-driven, peak-shaped and lasting typically 10-13

hours in the summer period and increasing to 400 hours for the event recorded in November 4-8, 2014 (Figure 4.2.5).

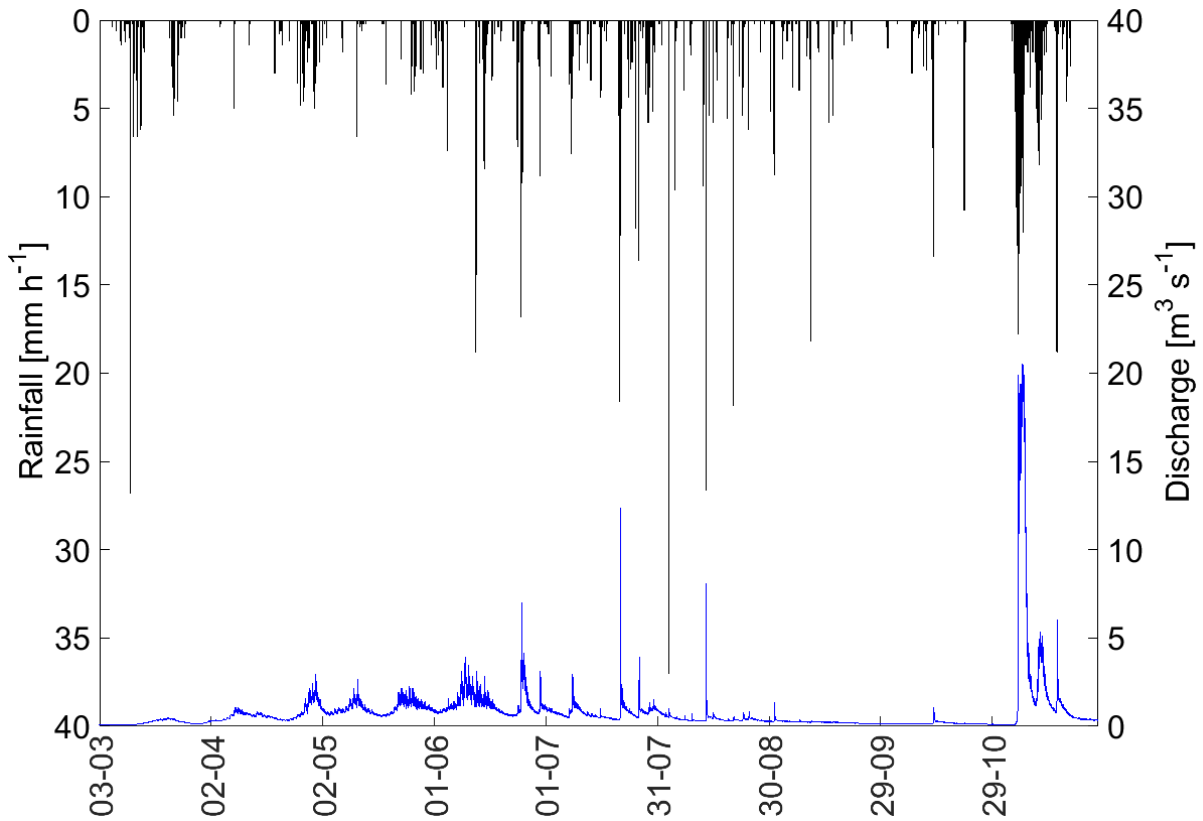


Figure 4.2.5. Water discharge hydrograph (blue line) and hourly rainfall intensity (vertical black bars) for the year 2014 at Tolva Creek (rainfall intensity recorded at Passo Brocon).

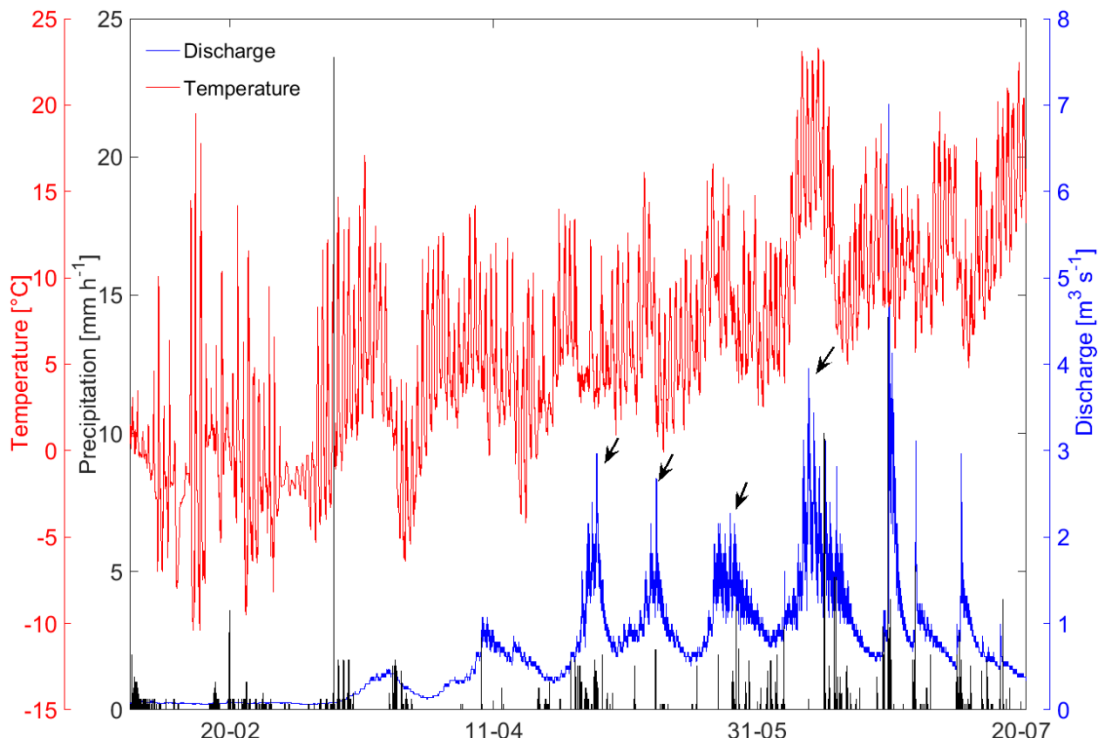


Figure 4.2.6. Hourly precipitations, atmospheric temperature and water discharge recorded in 2014 at Tolva Creek, limited to the snowmelt period (temperature recorded at Passo Brocon). Black arrows are indicating snowmelt peaks.

4.2.3 Ussaia Creek

At Ussaia Creek the year 2014 is characterized by a large net quantity of accumulated rainfall, reaching the value of 1541 mm (Figure 4.2.7a). The maximum is recorded in November (293 mm) and a secondary peak of 230 mm of rainfall is recorded during January. Other wet periods are recorded in February (170 mm) and in July-August, characterizing the total annual precipitation of this year to be double compared to the historical (844 mm). The maximum average temperature is in July (17 °C) and the minimum is reached in January. Comparably to Grigno-Tolvà sites, the year 2015 (Figure 4.2.7b) is drier than the 2014. The total annual precipitation is 853 mm, a value very close to the historical (844 mm), but no precipitation occurred in November and December at Mezzana. The monthly maximum is recorded in September, reaching 141 mm. In January and February little precipitation occurred as snow, determining limited or absent snowmelt pulses in the monitored stream. A secondary maximum is recorded in the months of May and October, with values comprised between 120-130 mm. In Ussaia Creek the snowmelt period extended to middle June, with winter and spring net precipitation amount to 738 mm, definitely above the average historical record (387 mm).

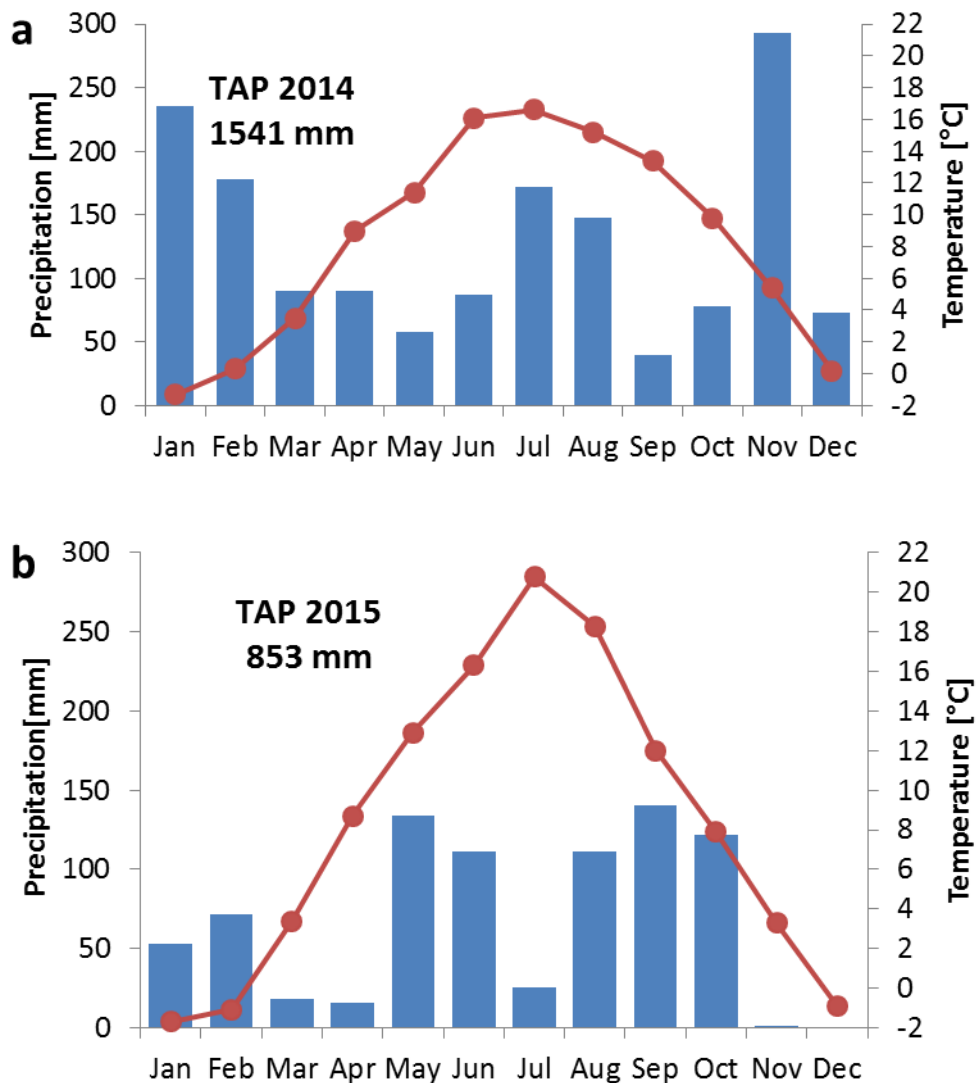


Figure 4.2.7. Monthly climograph recorded at Mezzana station for the year a) 2014; b) 2015. (TAP: Total Annual Precipitation).

The distribution of temperatures along the year is similar when analyzing the 2014 and the 2015, but their value differ. In both years the average maximum is recorded in July, but with more than 4°C of difference among the two years. The minimum average temperature of 2015 is recorded in January (-1.7 °C), and from this month rises constantly until July, in a manner that resembles that of 2014. Despite the precipitation values, temperatures recorded in November and December are similar for the two-year period. Comparing the 2015 climograph and the historical (cf. Figure 2.6), the similarity of total annual precipitation is evident, but there is a strong difference in the distribution of precipitations. As typical of the alpine climate, the historical trend shows two maxima, in May and November (100 mm); during 2015 the maxima fall in May, but no precipitations occurred in November, but is recognizable a maxima located in the period September-October, with values of 150 mm. The distribution of temperature is comparable, even if the 2015 diagram is more peaked and the maximum reached in July is 20.8 °C in 2015 and 18.3 °C for the historical record. During the dry months of November and December 2015, temperatures are comparable with the historical series.

At Mezzana a total of 39 hydro-meteorological events were observed, 13 during 2013, 18 during 2014 and 8 during 2015. Among 2013 events, were recorded 3 mixed events in April, and 10 rainfall events until November. In 2014, were recorded 3 snowmelt events from April to June. From June until July 3 mixed type events were registered, and 12 rainfall episodes were recorded until November. In 2015 were recorded 2 mixed events limited during May, and 6 rainfall events from June to late October.

In 2013 an exceptional rainfall event is recorded during the snowmelt period, with a total rainfall of 95 mm in 49 hours, imposing major changes in the channel morphology by April 25, 2013 (cf. Table A4.2.5). This type of event was never recorded again at Ussaia Creek, and represents a mixed type event. Following events recorded during summer are limited in duration (4-6 hours), exhibiting the largest values of mean intensity for that year, comprised between 2 and 4 mm/h, and total rainfall lower than 25 mm. During autumn events are more prolonged, with durations of about 25-30 hours, and total rainfall large than 50 mm, clearly showing the seasonal variation of the type of precipitation input. In 2014 are registered events more prolonged than previous year. From the comparison of durations at seasonal scale, is evident (Table A4.2.6) that the seasonal trend is replied, with limited events typically falling in summer, but the duration in 2014 are larger. The 2014 has been characterized also here at Ussaia Creek, by a snowmelt period that has extended from middle April to the end of June, and a wet summer, characterized by frequent rainfall events until the end of August. An extreme event that imposed major morphological changes, comparable to that of April 25, 2013, is recorded in the days of November 4-8, 2014. This precipitation occurred extensively in Trentino, and as observed for Grigno and Tolva Creeks, determined the largest values of peak discharge recorded. At Ussaia Creek was triggered a debris flow, hence the value of $Q = 24 \text{ m}^3 \text{ s}^{-1}$ is more realistically determined by a mix of liquid-solid discharge. In the Table A4.2.7 are listed the rainfall events of 2015, a year characterized by a restricted snowmelt period, recorded during the month of May, a by a general scarcity of precipitations. As a matter of fact, from June rainfall events succeeded with monthly frequency, but the total accumulated rainfall for single events was never larger than 55 mm. Differently from Grigno-Tolva system, here in September two events are recorded. The last event of October 2015, that spread over the Trentino region simultaneously, extended for 44 hours (the maximum value for this year) accumulating a total rainfall of about 50 mm.

Also at Ussaia Creek, a direct effect on hydrograph oscillations is discernible for summer and autumn meteorological events recorded in 2014 (Figure 4.2.8) and the lack of relationship between precipitation and discharge from April until the end of June at can be explained by considering the effect of atmospheric temperature. Specifically, we observe a remarkable temporal correlation between temperature and water

stage variations (Figure 4.2.9). As shown for the previous sites, also at Ussaia Creek are discernible daily cycles of temperature change that are mirrored by extended increase in water discharge. Here are clearly distinguishable three cycles of discharge increase occurring in May.

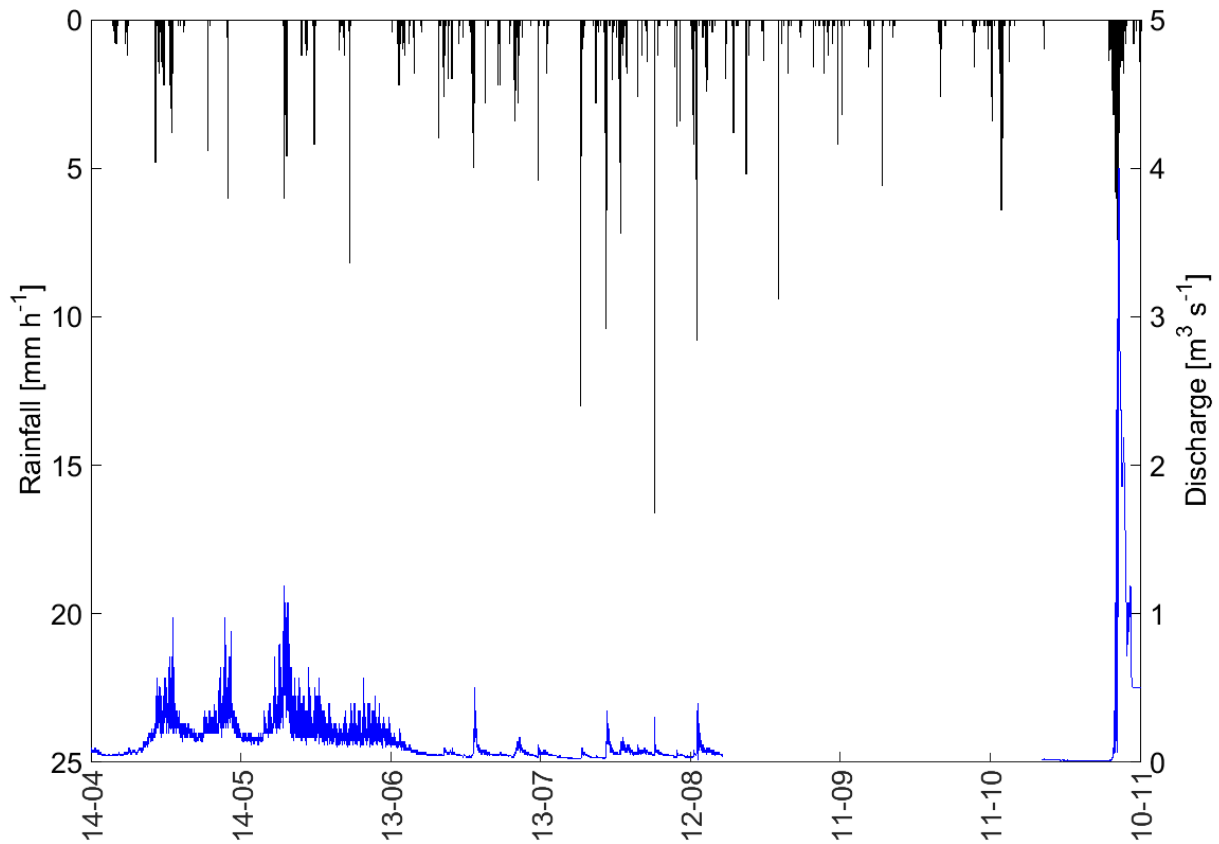


Figure 4.2.8. Water discharge hydrograph (blue line) and hourly rainfall intensity (vertical black bars) for the year 2014 at Ussaia Creek (rainfall intensity recorded at Mezzana).

The duration of these discharge peaks is typically of 4 days, reaching the maximum of 7 days by the third week of May, with values up to $1 \text{ m}^3 \text{ s}^{-1}$. The first decade of June is characterized by a sudden temperature increase, with maximum values of $25 \text{ }^\circ\text{C}$ (at Mezzana meteorological station), producing only a limited increase in liquid discharge, recording fluctuations and peak discharge generally below $0.5 \text{ m}^3 \text{ s}^{-1}$. This is clearly indicating the exhaustion of the process, and by June 20, 2014 the baseflow sustained by snowmelt is approaching to its minimum values of $0.1 \text{ m}^3 \text{ s}^{-1}$. From the event of June 21, 2014 the baseflow sustained by snowmelt decreases, as illustrated in Figure 4.2.9, where is visible that after each peak discharge values are decreasing towards the baseflow, going from 0.76 to 0.46 and to $0.43 \text{ m}^3 \text{ s}^{-1}$ by the 20th July. After that event, floods are rainfall-driven, peak-shaped and lasting typically 10-13 hours in the summer period and increasing to 400 hours for the event recorded in November 4-8, 2014 (Figure 4.2.8).

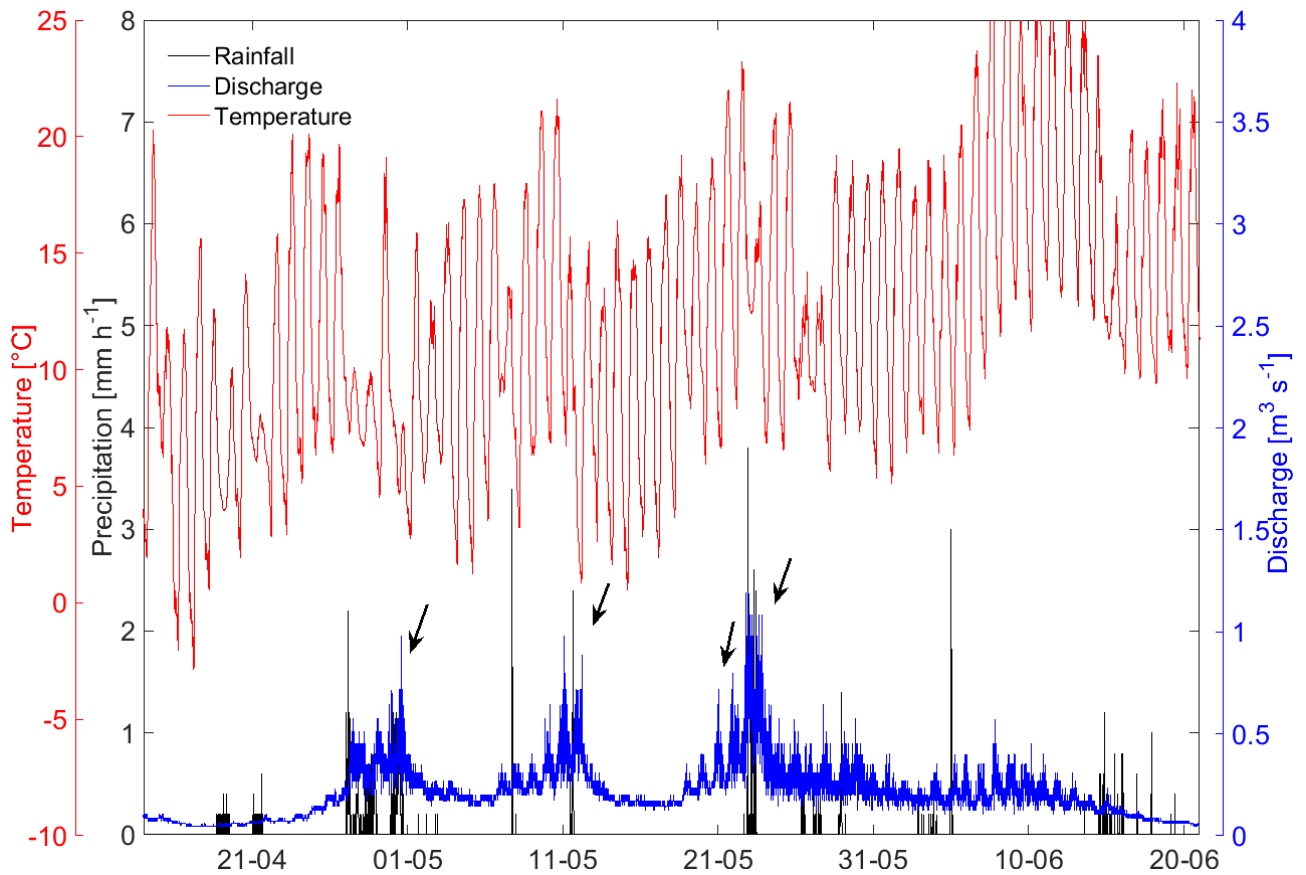


Figure 4.2.9. Hourly precipitations, atmospheric temperature and water discharge recorded in 2014 at Ussaia Creek, limited to the snowmelt period (temperature recorded at Mezzana). Black arrows are indicating snowmelt peaks.

We have shown that differences in terms of shapes, duration and intensity of hydrographs are characterizing the events that we classified so far as snowmelt, rainfall or mixed, and that have been recognized and registered at each monitored site. The relations existing among the two driving variables (precipitation and temperature), and the dependent variable (water discharge), are extended to the whole period 2014-2015, enabling to distinguish among the various typologies of hydro-meteorological forcing that generated the bedload events surveyed. According to this classification we defined snowmelt-dominated events, rainfall-dominated events and mixed-type events, that represent a combination of the two. These are typically individuated during the falling limb of the snowmelt, and water discharge is increased as a consequence of a rainfall-driven event. This classification scheme follows the specifics proposed by Dell’Agnese et al (2015) in Strimm Creek. In the following hydrographs (Figures 4.2.10-4.2.11-4.2.12-4.2.13) are plotted rainfall intensities recorded at each reference meteorological station, and vertical bars represent the temporal distribution of tracers surveys.

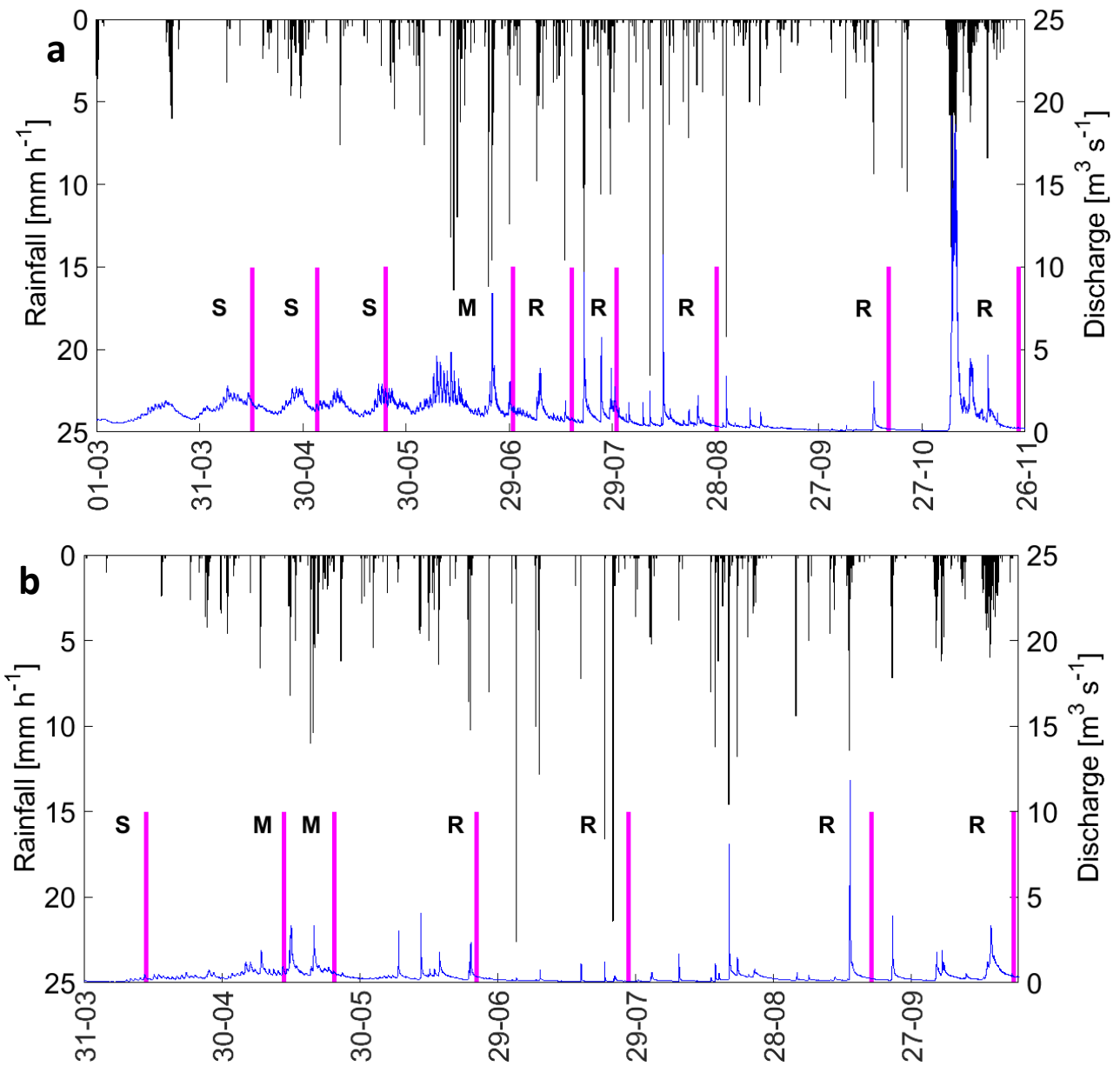


Figure 4.2.10. Hourly rainfall (vertical black bars), water discharge (blue line) and surveys (vertical purple bars) for a) 2014, b) 2015, at Grigno Creek. (S=snowmelt-dominated flood event; M=mixed-type flood event; R=rainfall dominated flood event).

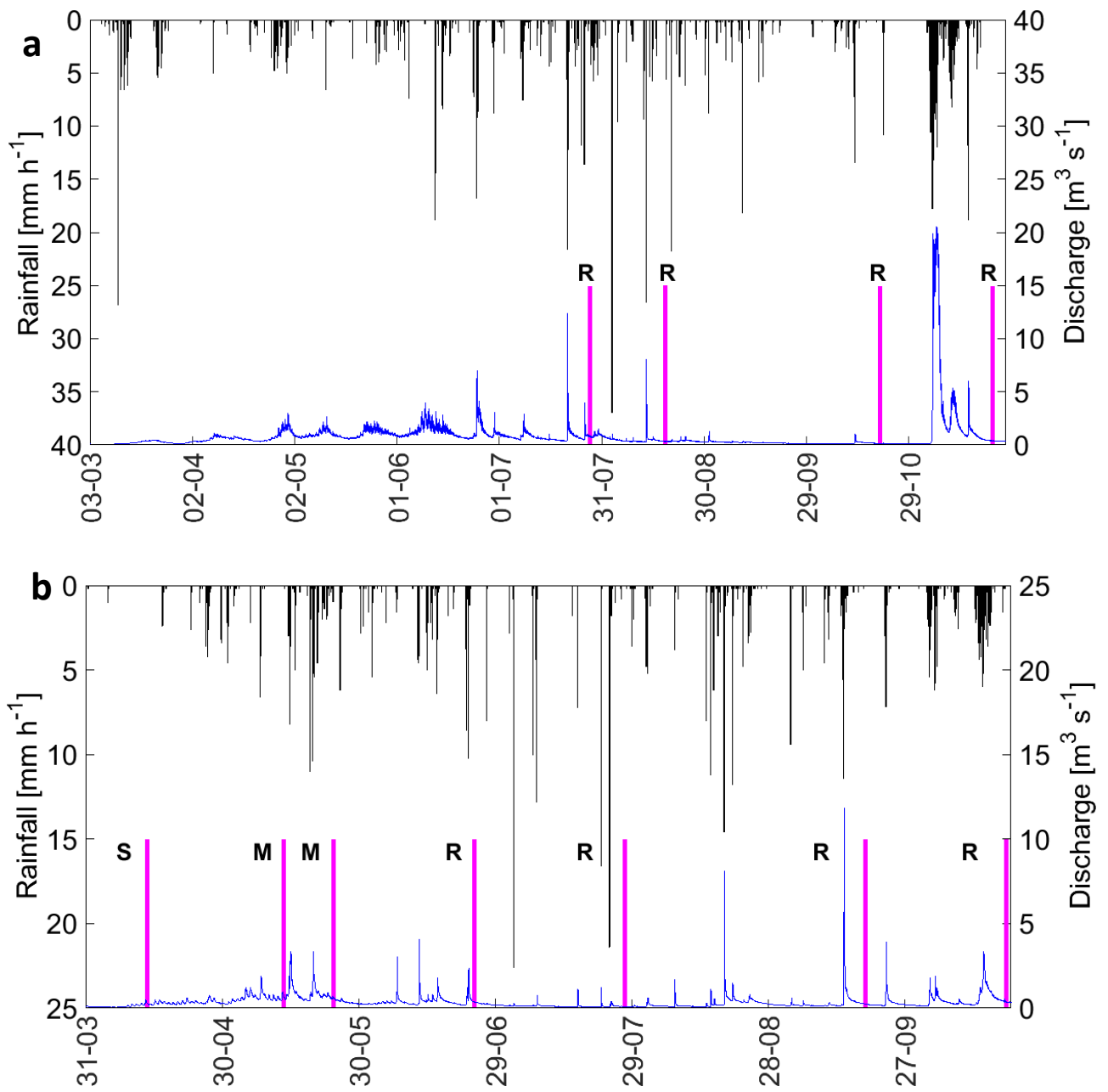


Figure 4.2.11. Hourly rainfall (vertical black bars), water discharge (blue line) and surveys (vertical purple bars) for a) 2014, b) 2015, at Tolva Creek. (S=snowmelt-dominated flood event; M=mixed-type flood event; R=rainfall dominated flood event).

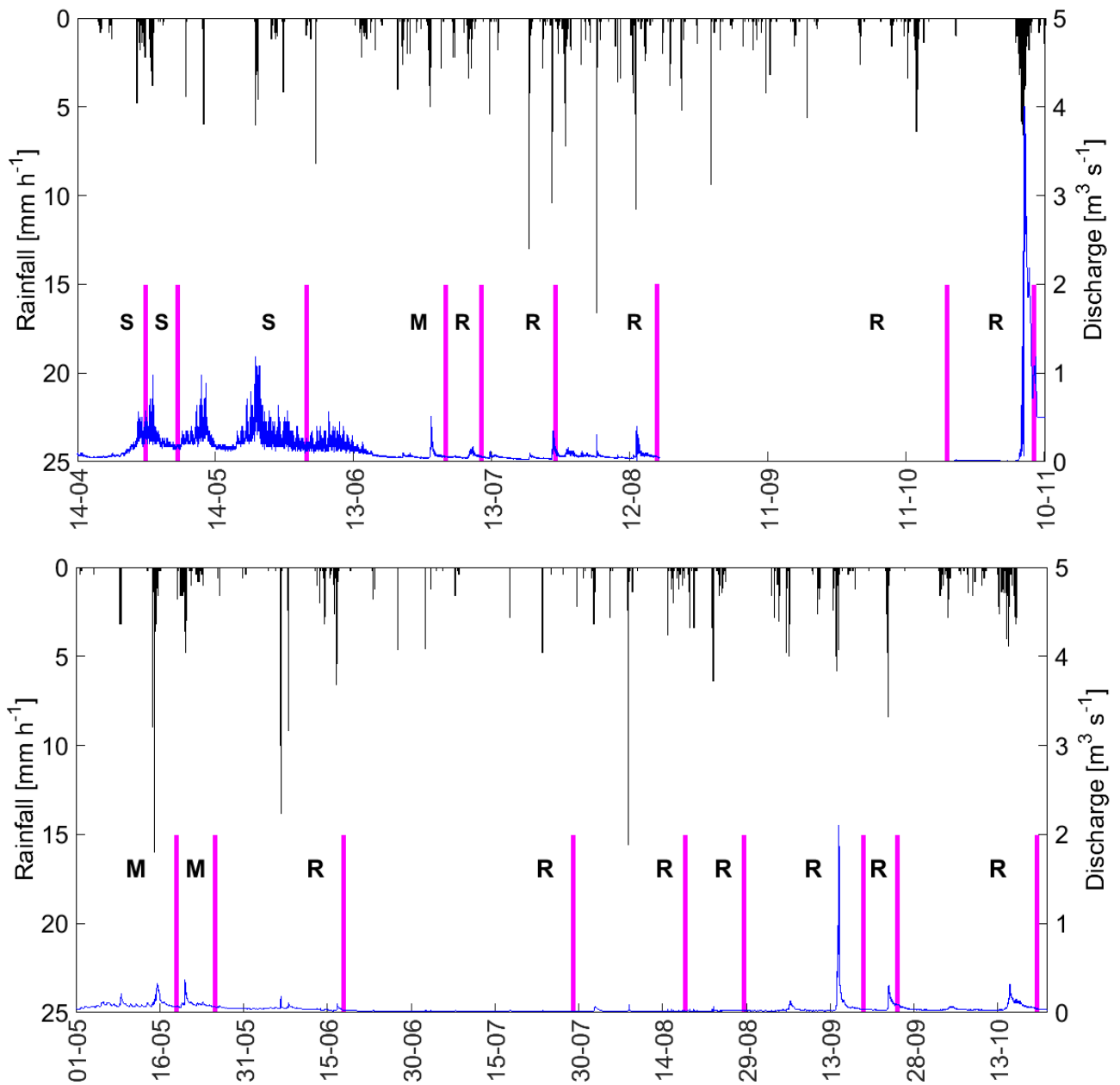


Figure 4.2.12. Hourly rainfall (vertical black bars), water discharge (blue line) and surveys (vertical purple bars) for a) 2014, b) 2015, at Ussaia Creek. (S=snowmelt-dominated flood event; M=mixed-type flood event; R=rainfall dominated flood event).

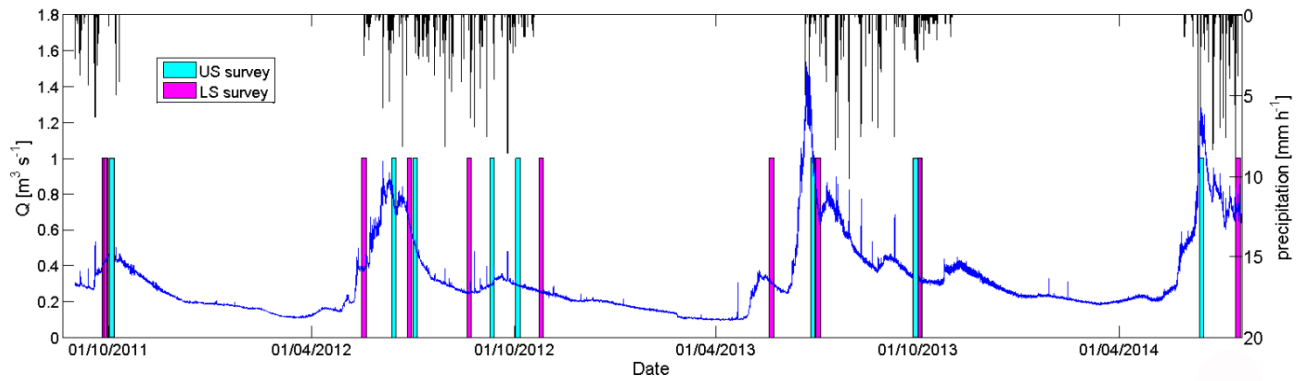
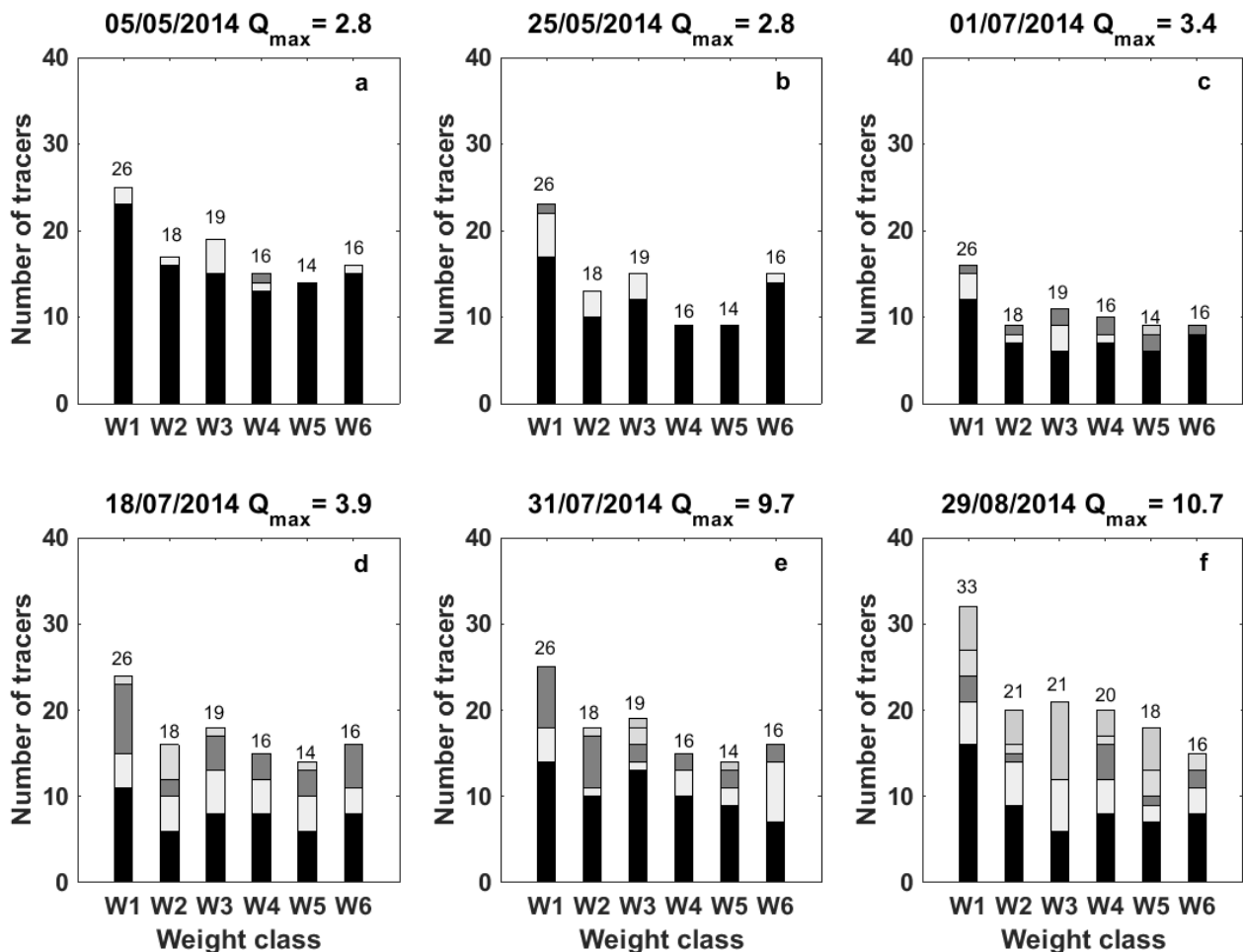


Figure 4.2.13. Hourly rainfall (vertical black bars), water discharge (blue line) and surveys at Upper Strimm Creek (vertical purple bars) and Lower Strimm Creek (vertical blue bars). (S=snowmelt-dominated flood event; M=mixed-type flood event; R=rainfall dominated flood event, from Dell’Agnese et al. (2015), modified).

4.3 Travel distances of PIT-tagged stones

The first step for evaluating bedload transport with PIT-tagged stones (hereafter termed “tracers”) is to record, and subsequently analyze, the tracers’ travel distances associated with each inter-survey period. We begin by presenting particle displacement in Grigno, Tolvà and Ussaia Creeks, where field surveys were conducted at the event scale. We then continue with the Strimm Creek data, which were collected at the seasonal scale (Dell’Agnese et al., 2015).

To provide a comprehensive view of the field surveys at Grigno, Tolvà and Ussaia monitored sites we present histograms of clasts displaced stratified by five travel distance categories (Figure 4.3.1-4.3.2.-4.3.3) and by tracer weight classes (see Table 3.8). Since this representation illustrates how clasts are moving after each flood, it is useful to recall that tracers were released at Grigno Creek in December 4th 2013 and in December 7th 2014. The panels (Figure 4.3.1) clearly show how the largest proportions of clasts are moved by rainfall-induced events. During 2014, from July 18th 2014 pure rainfall-induced events started, and the number of immobile clasts decreased notably compared to previous events.



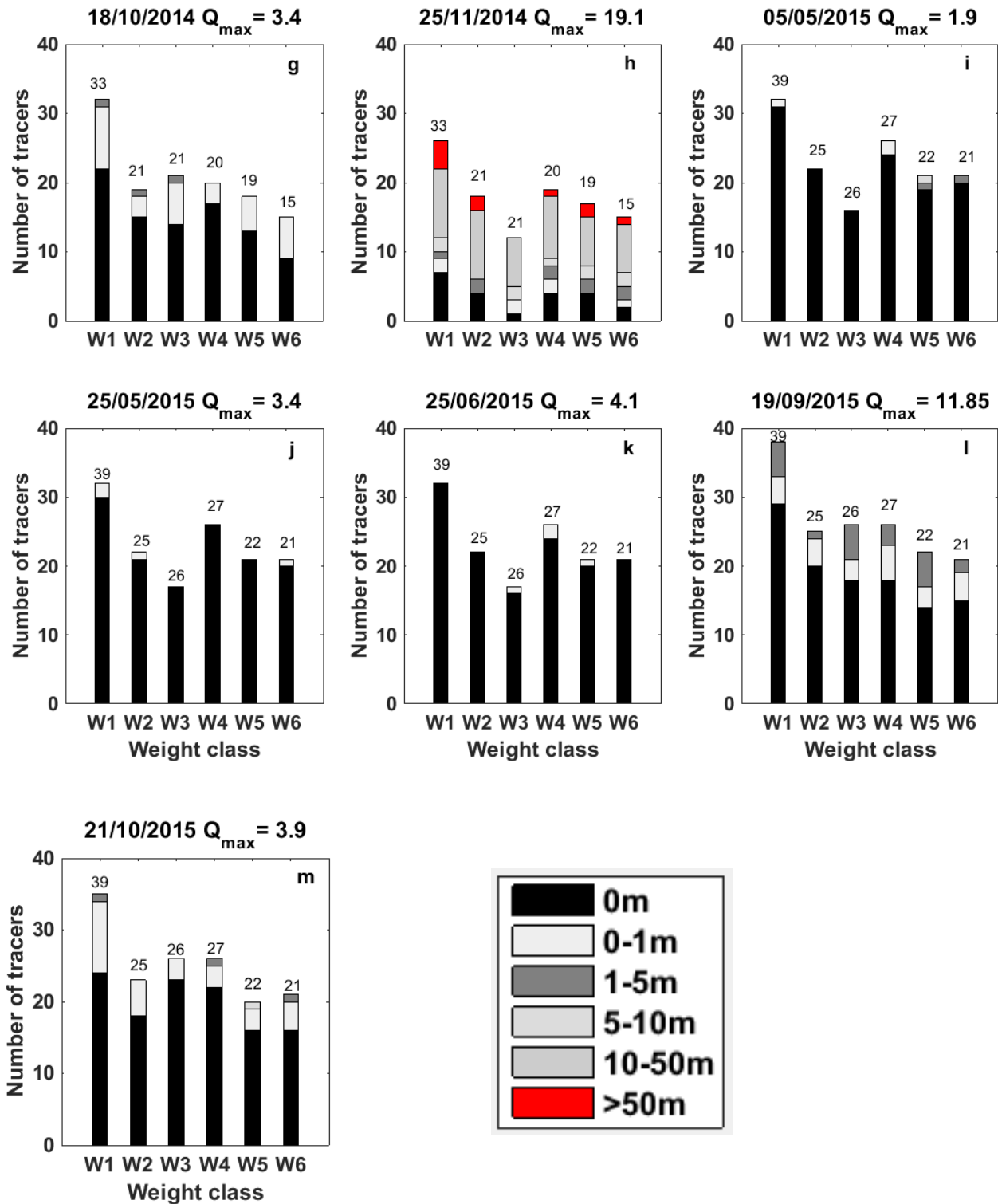
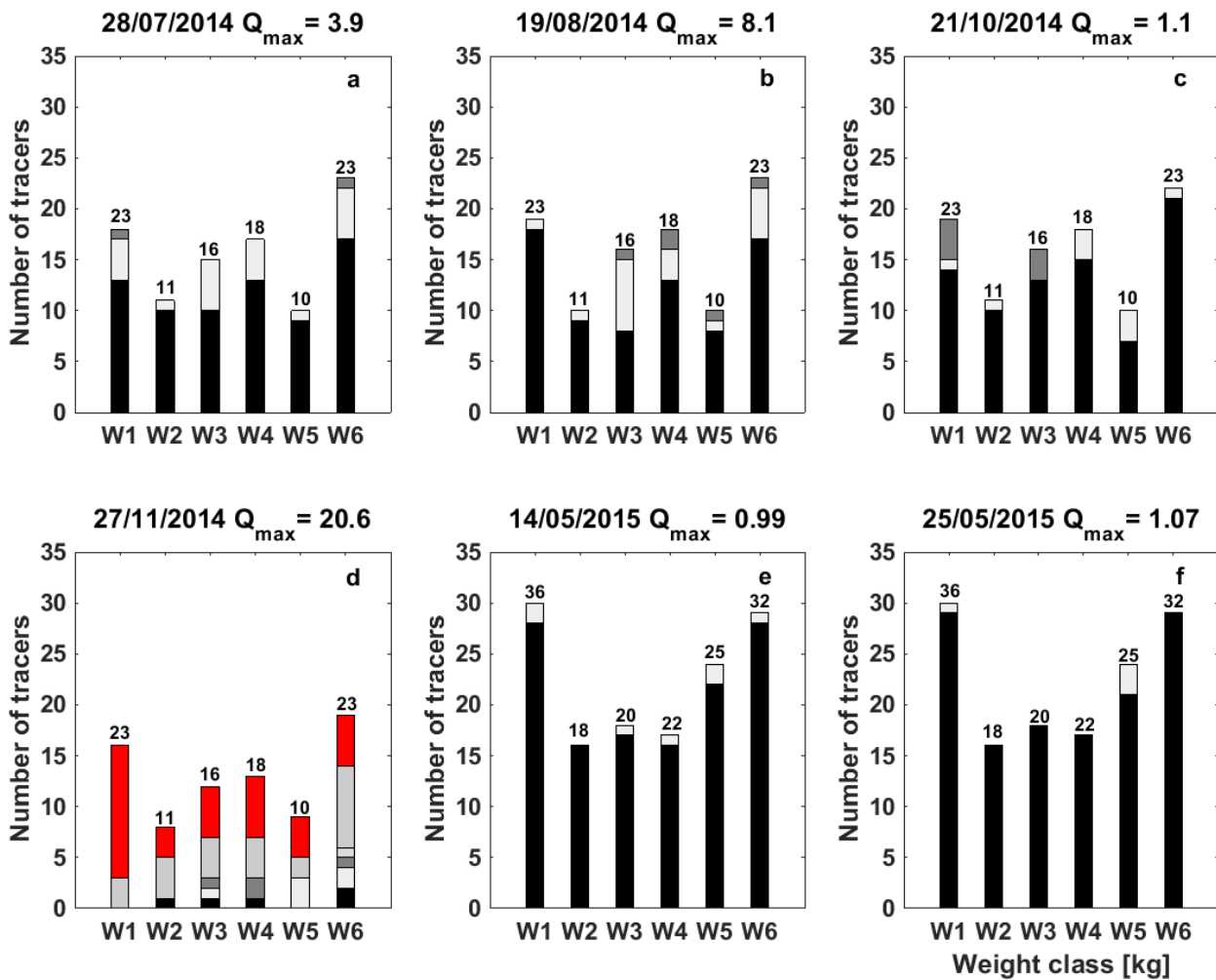


Figure 4.3.1. Stacked bars showing inter-survey frequency distributions of tracer travel distances across weight categories at the Grigno Creek monitoring site for the monitoring period (May 2014 – October 2015). Numbers above bars indicate the amount of tracers released for that grain size class. No motion surveys are not included.

The survey conducted by November 25, 2014 shows largest proportions of mobile clasts as well as larger travel distances. During 2015, the proportion of immobile clasts remains high, and this is exemplified by

the first three surveys where several weight classes did not move. Only after largest events (19/09/2015, $Q_{\max} = 11.85 \text{ m}^3 \text{ s}^{-1}$ and 21/10/2015 $Q_{\max} = 3.9 \text{ m}^3 \text{ s}^{-1}$) the proportions of mobile clasts increased. At Tolva Creek (Figure 4.3.2), despite the smaller number of events recorded, the proportion of mobile clasts is similar to the one shown in the Grigno Creek. At this site both tracers' cohorts were released in 2014, the first in July 24th and the second in December 6th. In 2014, only rainfall-induced events have been recorded and all the weight classes were always mobile. For the largest event ($Q_{\max} = 20.57 \text{ m}^3 \text{ s}^{-1}$) the number of mobile clasts and the travelled distances exhibit higher values. In the year 2015, lower events ($Q_{\max} = 0.99 \text{ m}^3 \text{ s}^{-1}$, $Q_{\max} = 1.07 \text{ m}^3 \text{ s}^{-1}$) show substantial immobility; as in the Grigno Creek, events of September 19th 2015 ($Q_{\max} = 4.32 \text{ m}^3 \text{ s}^{-1}$) and October 20th 2015 ($Q_{\max} = 1.92 \text{ m}^3 \text{ s}^{-1}$) were able to displace each weight class.



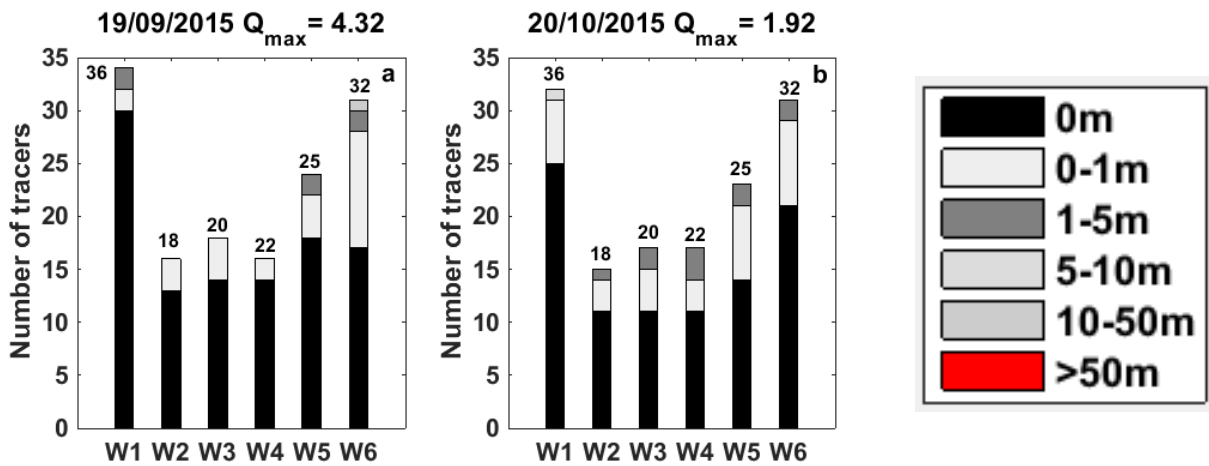
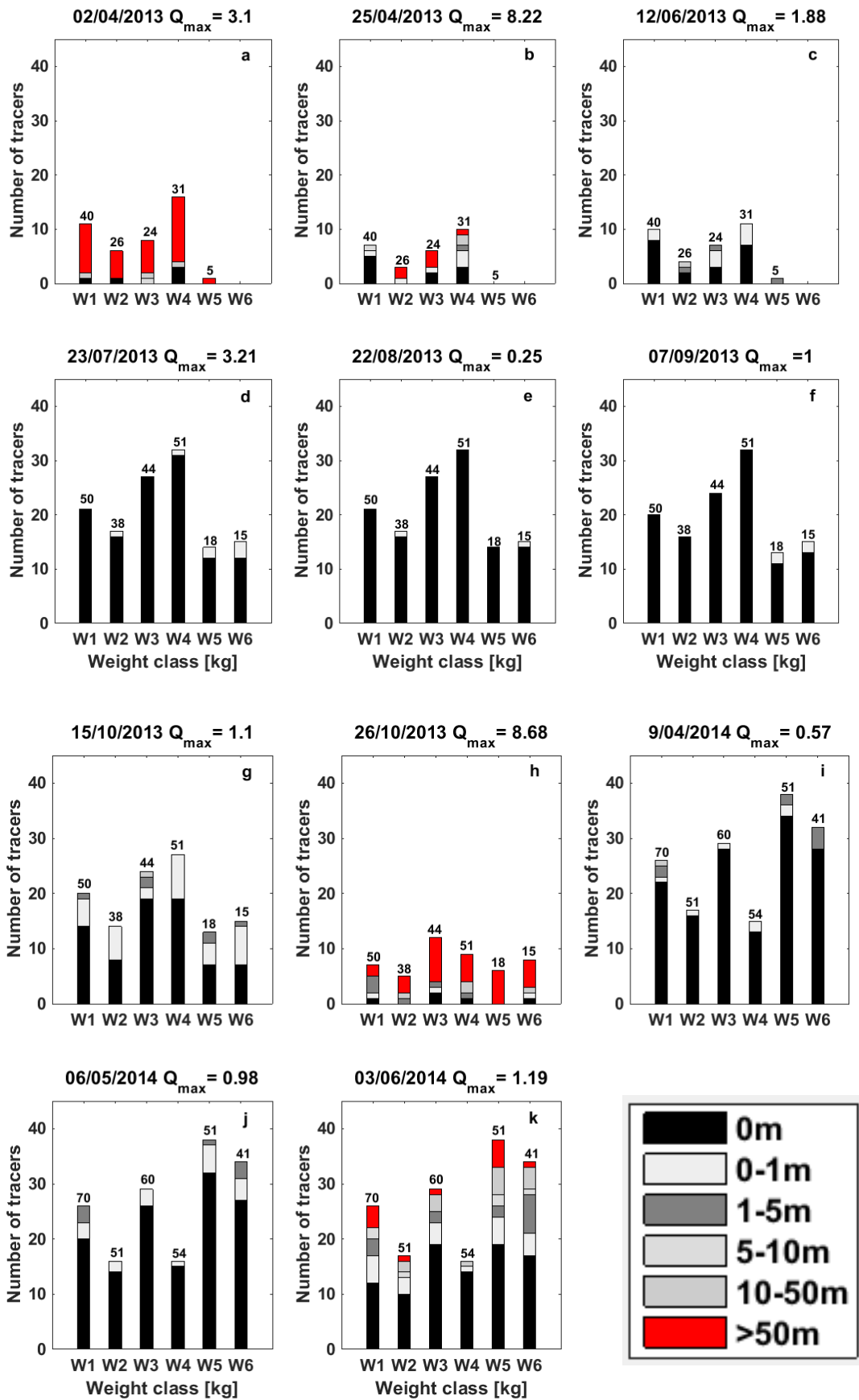


Figure 4.3.2. Stacked bars showing inter-survey frequency distributions of tracer travel distances across weight categories at the Tolva Creek monitoring site for the monitoring period (July 2014 – October 2015). Numbers above bars indicate the amount of tracers released for that grain size class. No motion surveys are not included.

At Ussaia Creek, tracers' have been released for the first time in September 21st 2012, and successively in June 12th 2013. In 2013, the April 2nd ($Q_{max} = 3.1 \text{ m}^3 \text{ s}^{-1}$) and April 25th ($Q_{max} = 8.22 \text{ m}^3 \text{ s}^{-1}$) events displaced large numbers of clasts with a considerable proportion, particularly in the former case, that travelled distances larger than 50 m. Even though the July 23rd event ($Q_{max} = 3.21 \text{ m}^3 \text{ s}^{-1}$) shows a peak water discharge of the same order of magnitude observed in the April 2nd one, in this case only few clasts experienced displacement with W1, W2 and W3 classes remaining immobile. Furthermore, the October 15th event of October 15th 2013 ($Q_{max} = 1.1 \text{ m}^3 \text{ s}^{-1}$) was able to displace a larger number of clasts compared to the July 23rd event, despite a lower peak discharge. The second event in October 2013 documents an enhanced clast mobility, with a considerable proportion of clasts from every weight class that traveled distances larger than 50 m, and the exceptional situation that all recovered clasts from W5 class traveled farther than 50 m.

In 2014 tracers' have been released in April 4th and all documented events led to displacements. In particular, the June 3rd ($Q_{max} = 1.19 \text{ m}^3 \text{ s}^{-1}$) and the debris-flow event occurred on November 5th ($Q_{max} = 26.41 \text{ m}^3 \text{ s}^{-1}$) were found to move the largest proportions. In this context, the August 18th event ($Q_{max} = 0.4 \text{ m}^3 \text{ s}^{-1}$) is the exception, in which the discharge was relatively low, but distances travelled by clasts were significantly high, up to 50 m for the W1 class. The debris-flow event displaced all the clasts, many of which reached the basin outlet at the confluence with the Noce River. This explains the abrupt drop in recovery rate observed in Figure 4.3.3q.

In 2015 tracers' have been released in April 30th, but this year has been characterized by a substantial stability of the clasts, exception due to the May 19th 2015 ($Q_{max} = 0.33 \text{ m}^3 \text{ s}^{-1}$) and September 15th 2015 ($Q_{max} = 2.11 \text{ m}^3 \text{ s}^{-1}$) events. The former was the first event after the 2015 new tracer cohort had been seeded on the channel bed, while the latter represents the largest 2015 event, with travel distances up to 50 m.



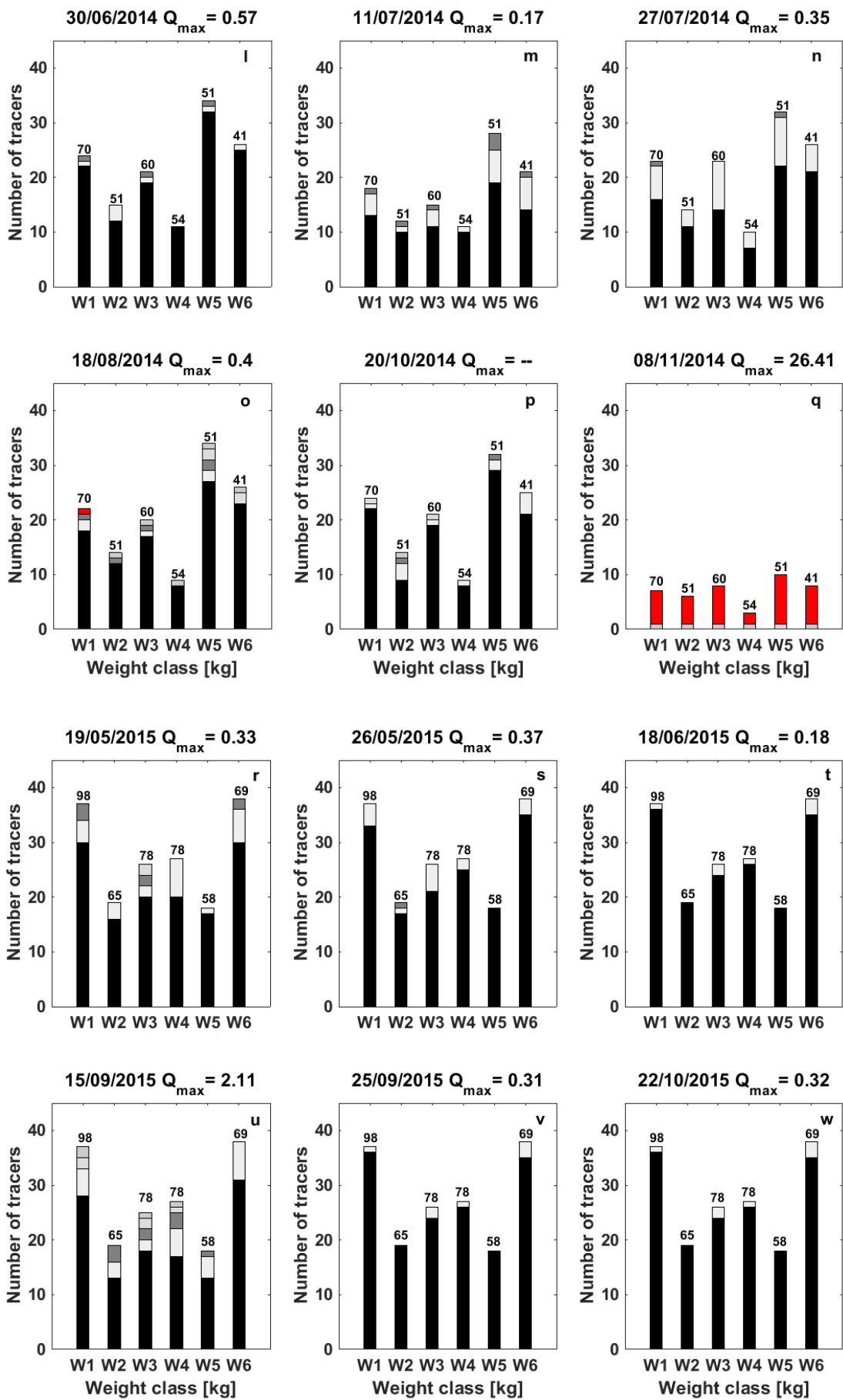


Figure 4.3.3. Stacked bars showing inter-survey frequency distributions of tracer travel distances across weight categories at the Ussaia Creek monitoring site for the monitoring period (April 2013 – October 2015). Numbers above bars indicate the amount of tracers released for that grain size class. No motion surveys are not included.

From the shown panels is evident that clast mobility is enhanced at Ussaia Creek, with respect to the sites located in Valsugana. As a matter of fact at Grigno and Tolva Creeks snowmelt events recorded by the beginning of July 2014 exhibit large portions of immobile clasts. Conversely at Ussaia Creek in the same time interval (09/04/2014 – 11/07/2014) the mobility of tracers is high, especially for events such as May 5th and June 3rd. In the first case a comparison of mobility is possible between Ussaia (Figure 4.3.3j) and Grigno (Figure 4.3.1a) Creek, with 19 clasts moved in the first site and only 9 moved at Grigno Creek. Each of the weight classes displaced at Ussaia Creek showed distances up to 5 m, whereas at Grigno Creek only the W4 class was displaced by an identical amount. In 2015, the snowmelt pulses were capable to move few clasts at all the sites (Figure 4.3.1i-j, 4.3.2e-f), but Ussaia Creek (Figure 4.3.3r-s) always displays larger amounts of number of mobilized stones and distances travelled.

When analyzing and comparing rainfall events, bedload transport at Ussaia Creek is more efficient than the other sites. This can be directly compared considering the same hydro-meteorological events, that simultaneously occurred at all the sites.

In order to provide a first preliminary appraisal of how hydro-meteorological forcing and tracer size can interact during bedload transporting events, we report six scatterplots showing tracer travel distance as a function of tracer weight associated with two selected storm events that have hit both the Grigno and Ussaia Creeks. These include the flashy convective event of August 13, 2014 (Figure 4.3.4, and the prolonged cyclonic event of November 4-8, 2014 (Figure 4.3.5).

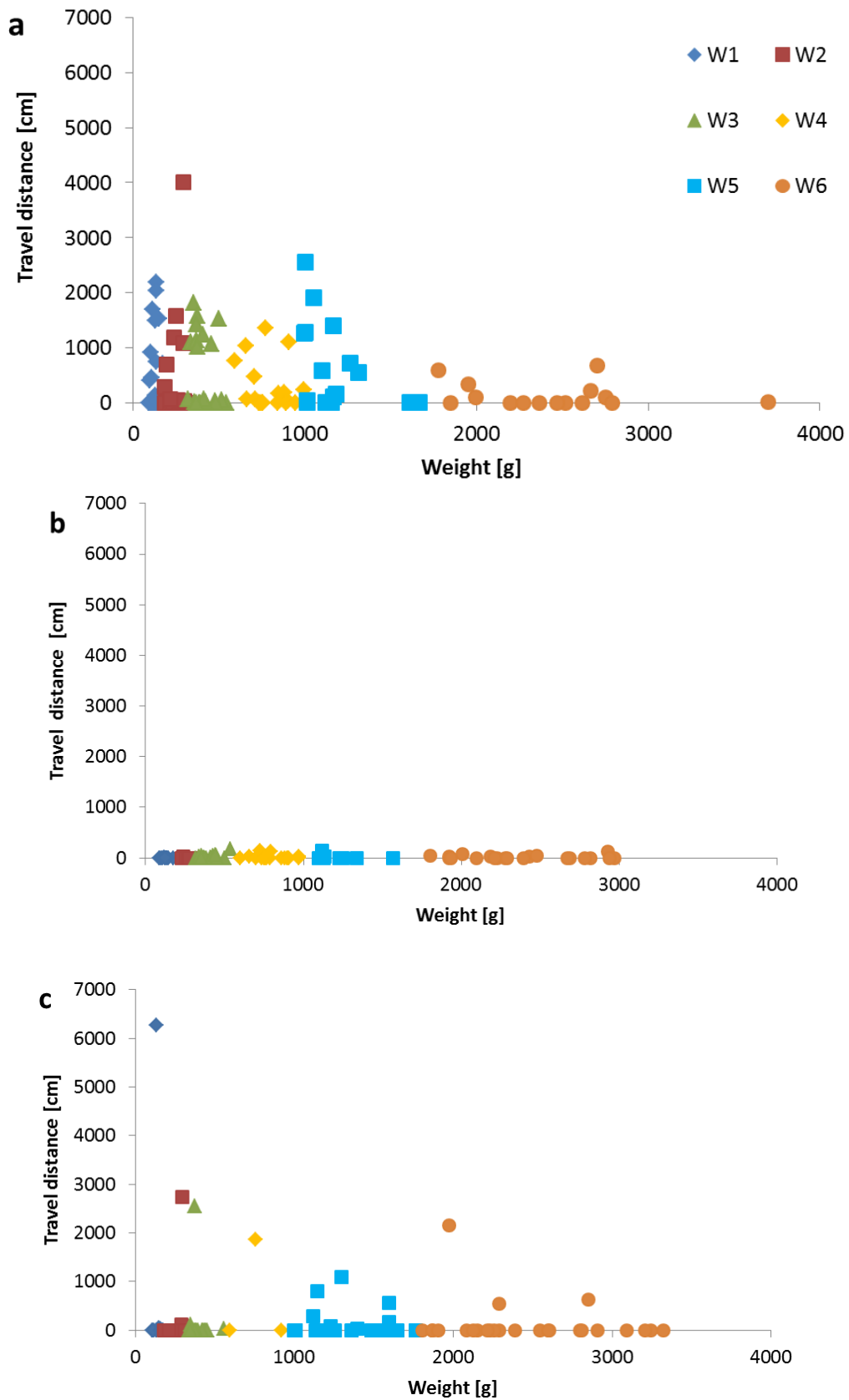


Figure 4.3.4 Tracer travel distance as a function of tracer weight associated to the August 8 2014 event for (a) Grigno Creek, (b) Tolva Creek, and (c) Ussaia Creek.

At Grigno and Ussaia sites we observe that the range of tracer travel distance tends to decline with increasing tracer weight, conversely at Tolvà Creek there are no relations among weight and distance travelled. This pattern is particularly evident in the Grigno Creek case (Figure 4.3.4a), where we observe an abrupt drop in travel distance for the heaviest tracer category W6 (>1770 g), possibly suggesting the onset of a weight-selective bedload transport.

At the same three sites, a different behavior of travel distances is observed following the November 8th 2014 extreme event (Figure 4.3.5). In this case at Grigno and Ussaia creeks the range of variability in travel distances remains constant throughout the entire weight range of tagged stones, implying that tracer weight during this event was not a clear limitation to bedload transport, in line with so called equimobility conditions (e.g., Parker et al., 1982). At Tolvà Creek, the W6 class limits the range of variability, showing a decrease in the maximum travel distances.

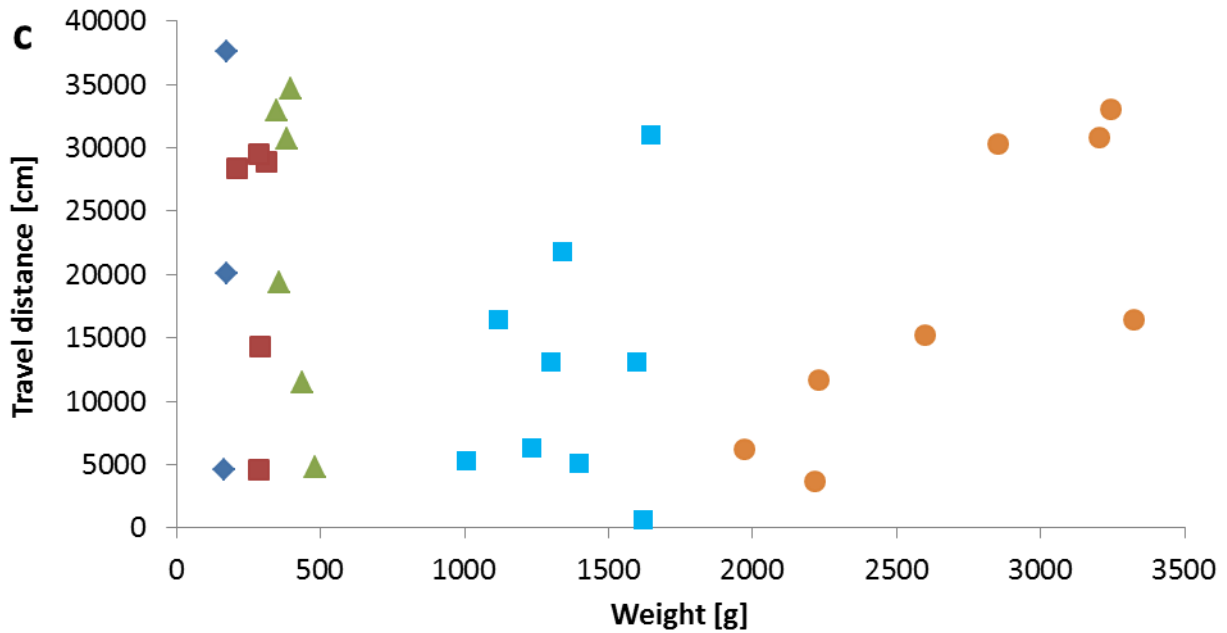
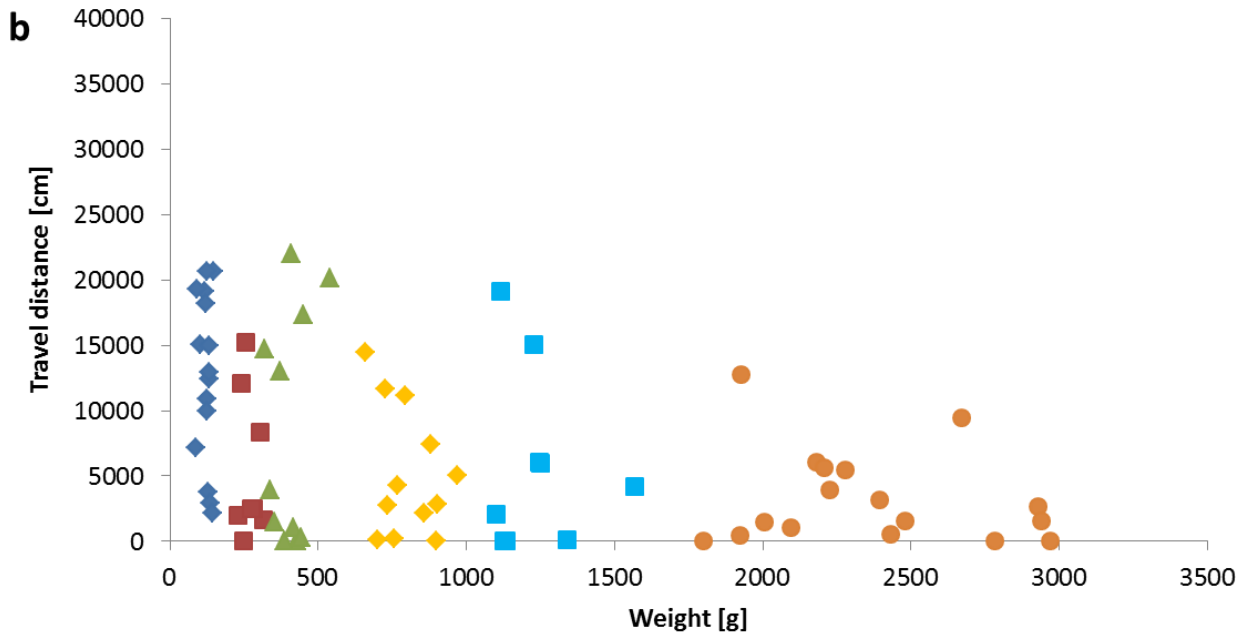
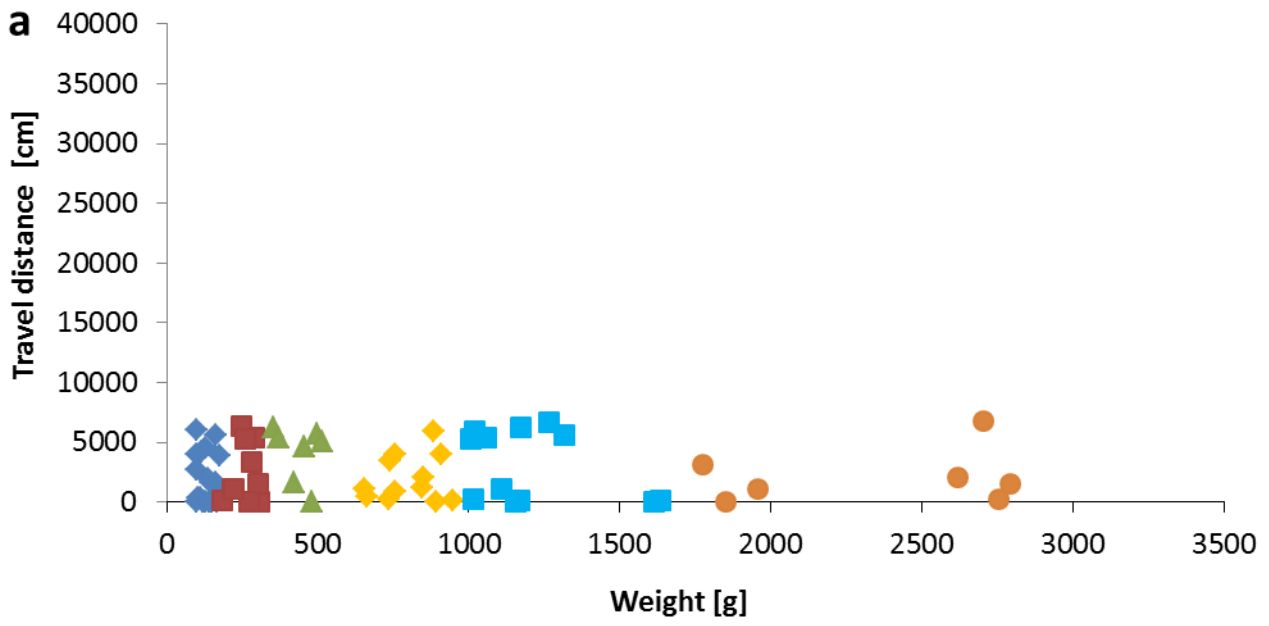


Figure 4.3.5. Tracer travel distance as a function of tracer weight associated to the November 4th – 8th 2014 event for (a) Grigno Creek, (b) Tolva Creek, and (c) Ussaia Creek.

A subset of hydro-meteorological forcing events that have affected all the three monitoring sites to explore differences in bedload transport efficiency (i.e., travel distances) by location. In Table 4.3.1 is presented a list of comparable events. The list starts in late July that represents the date since the monitoring was conducted in parallel in the three sites, Grigno, Tolva and Ussaia Creek. Due to the limited spatial extent of convective storms, this type of event was never recorded simultaneously at the three sites. Therefore we can compare only events induced by cyclonic rainfall events.

Table 4.3.1. List of hydro-meteorological events comparable simultaneously on the three monitoring sites. Since tracers have been released for the first time at Tolva Creek in July 21, 2014, events before this date are not listed.

Grigno Cr.	Tolva' Cr.	Ussaia Cr.	
21-22/07/2014	26/07/2014	26/07/2014	Not comparable
13/8/2014	13/8/2014	13/8/2014	Comparable
13/10/2014	13/10/2014	13/10/2014	Comparable
4-8/11/2014	4-8/11/2014	4-8/11/2014	Comparable
14/04/2015	15/04/2015	--	Not comparable
08/05/2015	08/05/2015	14/05/2015	Not comparable
20/05/2015	20/05/2015	20/05/2015	Comparable
12-13/06/2015	23-24/06/2015	16/06/2015	Not comparable
14/09/2015	14/09/2015	14/09/2015	Comparable
16/10/2015	16/10/2015	16/10/2015	Comparable

For each comparable event will be presented a box plot showing the distribution of tracers' travel distance at each monitoring site. Boxplots are not drawn for each comparable event because in some cases the number of recovered tracers, or the number of mobilized clasts for a specific weight class, is too small to attain any statistical significance.

Event July 26, 2014

The event of July 26th 2014 is a summer front. Malga Sorgazza and Passo Brocon meteorological station recorded identical characteristics of this rainfall episode, with a maximum intensity in the order of 10-13 mm/h and a cumulative precipitation of 40 mm. At Grigno Creek the Q_{max} recorded is $5.74 \text{ m}^3 \text{ s}^{-1}$, whereas at Tolvà Creek is $3.95 \text{ m}^3 \text{ s}^{-1}$. Mezzana meteorological station recorded a rainfall event that lasted 9 hours, with lower maximum intensity compared to Grigno-Tolvà creek (6.4 mm/h) and lower total rainfall of 31 mm.

Table 4.3.2. Rainfall characteristics of July 26, 2014 event.

Monitoring site	Duration [h]	Max intensity [mm/h]	Cumulative precipitation [mm]	Q max [$\text{m}^3 \text{ s}^{-1}$]
Grigno Cr. (Malga Sorgazza)	5	10.5	41.2	5.74
Tolvà Cr. (Passo Brocon)	5	13.6	40.4	3.95
Ussaia Cr. (Mezzana)	9	6.4	31.6	0.35

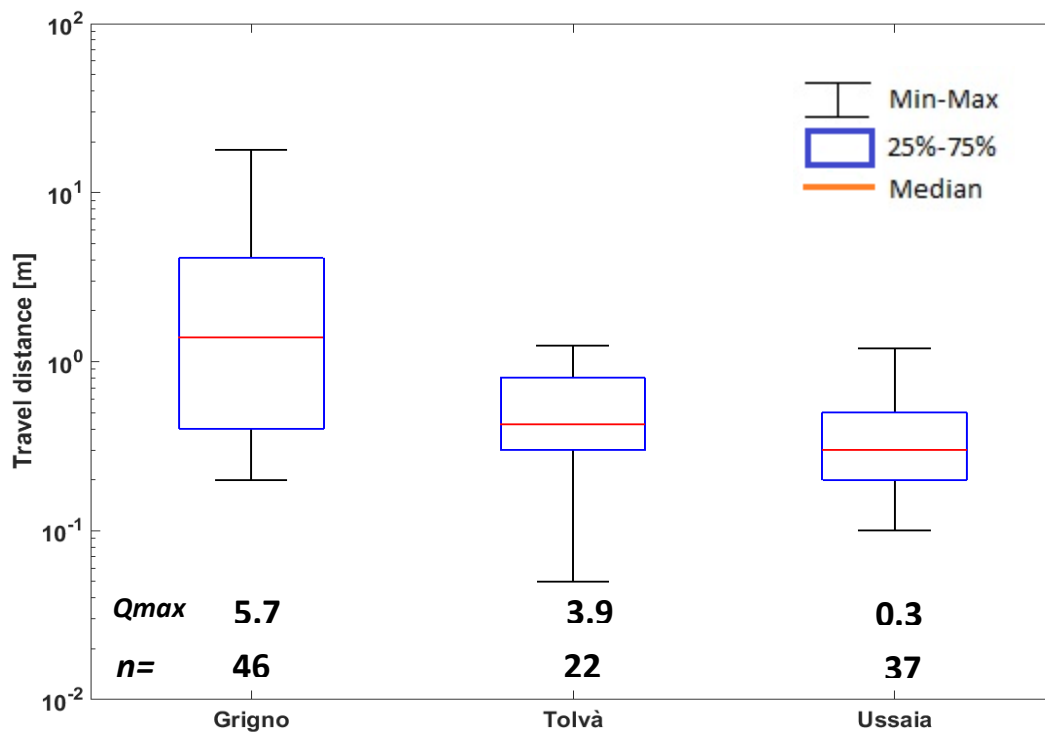


Figure 4.3.6. Comparative box plots of travel distances across weight classes at Grigno, Tolvà and Ussaia sites for the July 26, 2014 event (n = number of recovered tracers, Q_{max} = peak discharge in $\text{m}^3 \text{ s}^{-1}$).

The slight difference in peak discharge determined markedly different response in bedload triggered by the same hydro-meteorological event at Grigno and Tolvà Creek (Figure 4.3.6). The peak discharge differs by $1.8 \text{ m}^3 \text{ s}^{-1}$ at the two sites, but at Grigno Creek 46 clasts moved, with a median value of 1.5 m; conversely at Tolvà Creek only 22 tracers moved, with lower median of displacement of about 0.5 m. At Ussaia Creek 37 clasts moved with median value comparable to Tolvà Creek (0.2 m).

Event August 13, 2014

The event of August 13th 2014 is a summer front. Malga Sorgazza meteorological station recorded 4 hours of precipitation, with a maximum intensity of 17.8 mm/h and a cumulative precipitation of 33.6 mm. At Grigno Creek the recorded $Q_{\text{max}} = 10.73 \text{ m}^3 \text{ s}^{-1}$. The precipitation event recorded at Passo Brocon meteorological station shared similar characteristic, but a maximum intensity of 26.6 mm/h (Table 4.3.3). The same event recorded at Mezzana lasted 6 hours, with lower maximum intensity (8.8 mm/h) and lower total rainfall (24 mm).

Table 4.3.3. Rainfall characteristics of August 13, 2014 event.

Monitoring site	Duration [h]	Max intensity [mm/h]	Cumulative precipitation [mm]	Q max [$\text{m}^3 \text{ s}^{-1}$]
Grigno Cr. (Malga Sorgazza)	4	17.8	33.6	10.73
Tolvà Cr. (Passo Brocon)	3	26.6	39.8	8.11
Ussaia Cr. (Mezzana)	6	8.8	24	0.4

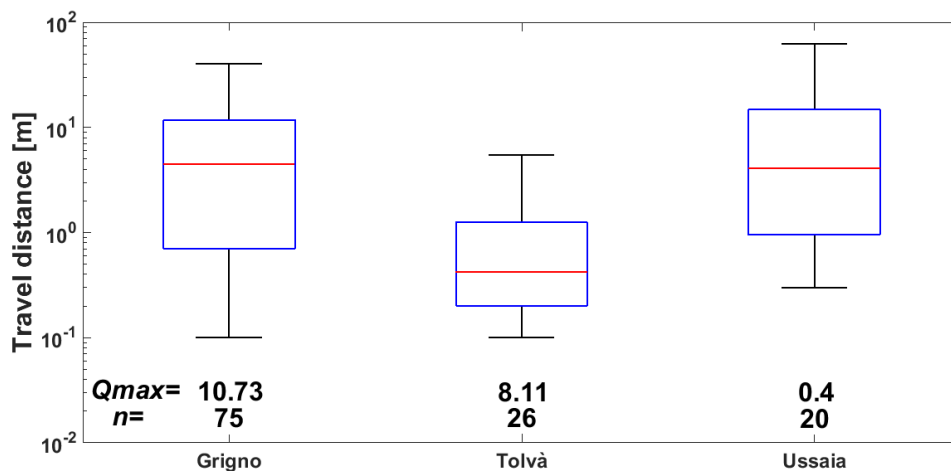


Figure 4.3.7. Comparative box plots of travel distances across weight classes at Grigno, Tolvà and Ussaia monitoring sites for the August 13, 2014 event (n = number of recovered tracers, Q_{max} = peak discharge in $\text{m}^3 \text{ s}^{-1}$).

The rainfall event shares similar characteristics across the Grigno and Tolvà basins but bedload transport efficiency is larger at Grigno than at Tolvà Creek (Figure 4.3.7). Median travel distances recorded at Grigno Creek are 4.5 m, ten times larger than those recorded at Tolvà Creek (0.45 m). At Ussaia Creek the median is 4 m, despite the value of peak discharge equal to $0.4 \text{ m}^3 \text{ s}^{-1}$, very low compared to Grigno Creek ($Q_{\text{max}} = 10.73 \text{ m}^3 \text{ s}^{-1}$). Ussaia Creek exhibits a value of maximum travel distance of about 70 m, whereas is 40 m at Grigno and only 4 m at Tolvà Creek.

Event October 13, 2014

The event of October 13, 2014 is an early autumn cyclonic front. Malga Sorgazza and Passo Brocon meteorological stations recorded 10 hours of precipitation, with a maximum intensity larger at Passo Brocon (13.4 mm/h) than at Malga Sorgazza (9.4 mm/h). In both cases cumulative precipitation is slightly more than 40 mm (Table 4.3.4). At Mezzana the precipitation has been more prolonged (21 hours), with lower maximum intensity (6.4 mm/h) but larger total rainfall (46.5 mm). For this event the water gauge at Ussaia Creek did not record the hydrometric level due to malfunctioning.

Table 4.3.4. Rainfall characteristics of October 13th 2014 event.

Monitoring site	Duration [h]	Max intensity [mm/h]	Cumulative precipitation [mm]	Q max [$\text{m}^3 \text{ s}^{-1}$]
Grigno Cr. (Malga Sorgazza)	10	9.4	40.8	3.38
Tolvà Cr. (Passo Brocon)	11	13.4	43.2	1.32
Ussaia Cr. (Mezzana)	21	6.4	46.5	-

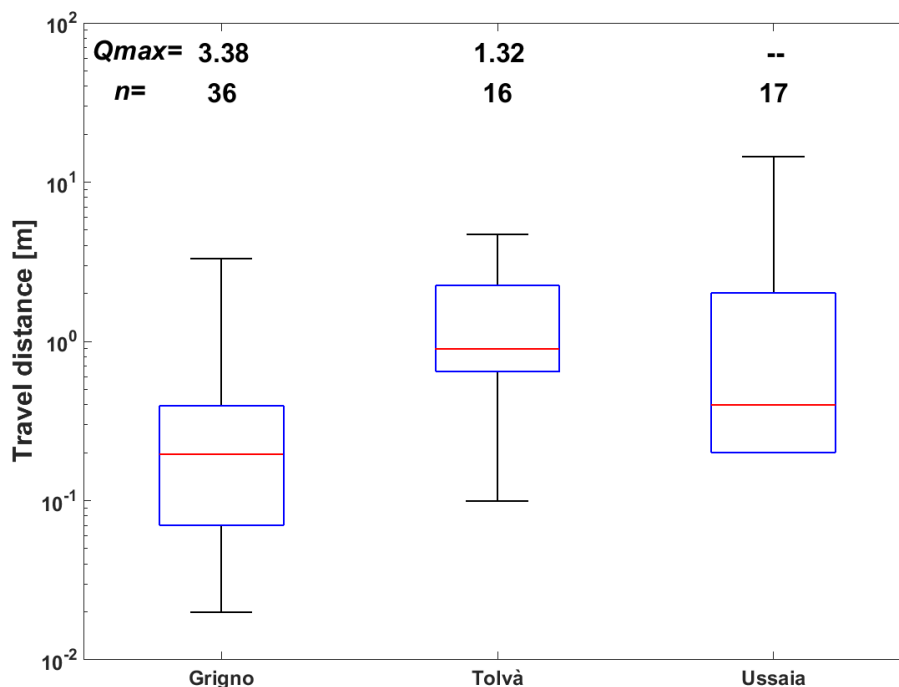


Figure 4.3.8. Comparative box plots of travel distances across weight classes at Grigno, Tolvà and Ussaia monitoring sites for the 13/10/2014 event (n= number of recovered tracers, Qmax = peak discharge in $\text{m}^3 \text{s}^{-1}$).

Comparing Grigno and Tolvà Creeks we note a discrepancy in the hydrological response of the two basins (Figure 4.3.8), that have been hit by a rainfall event with the same characteristics, but in a similar manner of the event of August 13th, at Grigno Creek peak discharge is $3.38 \text{ m}^3 \text{ s}^{-1}$ while at Tolvà Creek is $1.32 \text{ m}^3 \text{ s}^{-1}$. This would explain the different number of mobile tracers recorded for both sites even though the overall distribution of travel distances recorded at Tolvà Creek is shifted towards larger values with respect to Grigno Creek. Median values at Grigno Creek are in the order of 0.2 m, while at Tolvà Creek the median travel distance is about 1 m.

At Ussaia Creek there is a limited number of observations and the median value is 0.4 m; the largest maximum travel distance among all the sites is recorded at Ussaia Creek (10.5 m), whereas at the other two sites are below 5 m.

Event November 4th - 8th 2014

The event of November 4-8, 2014 is a prolonged autumn front. Malga Sorgazza and Passo Brocon meteorological stations recorded 60 and 66 hours of precipitation, respectively (Table 4.3.5). The maximum of precipitation intensity has been larger at Passo Brocon (17.8 mm/h) than at Malga Sorgazza (13.4 mm/h). Cumulative precipitation is 378.4 mm at Passo Brocon, while is 325.4 mm at Malga Sorgazza. At Mezzana the cumulative precipitation rainfall (158 mm). In this case the water gauge at Ussaia Creek recorded the hydrometric level of a debris flow event, leading to an exceptional high volumetric discharge.

Table 4.3.5. Rainfall characteristics of November 4-8, 2014 event.

Monitoring site	Duration [h]	Max intensity [mm/h]	Cumulative precipitation [mm]	Q max [$\text{m}^3 \text{s}^{-1}$]
Grigno Cr. (Malga Sorgazza)	66	13.4	325.4	19.17
Tolvà Cr. (Passo Brocon)	60	17.8	378.4	20.51
Ussaia Cr. (Mezzana)	75	7.4	158	26.41

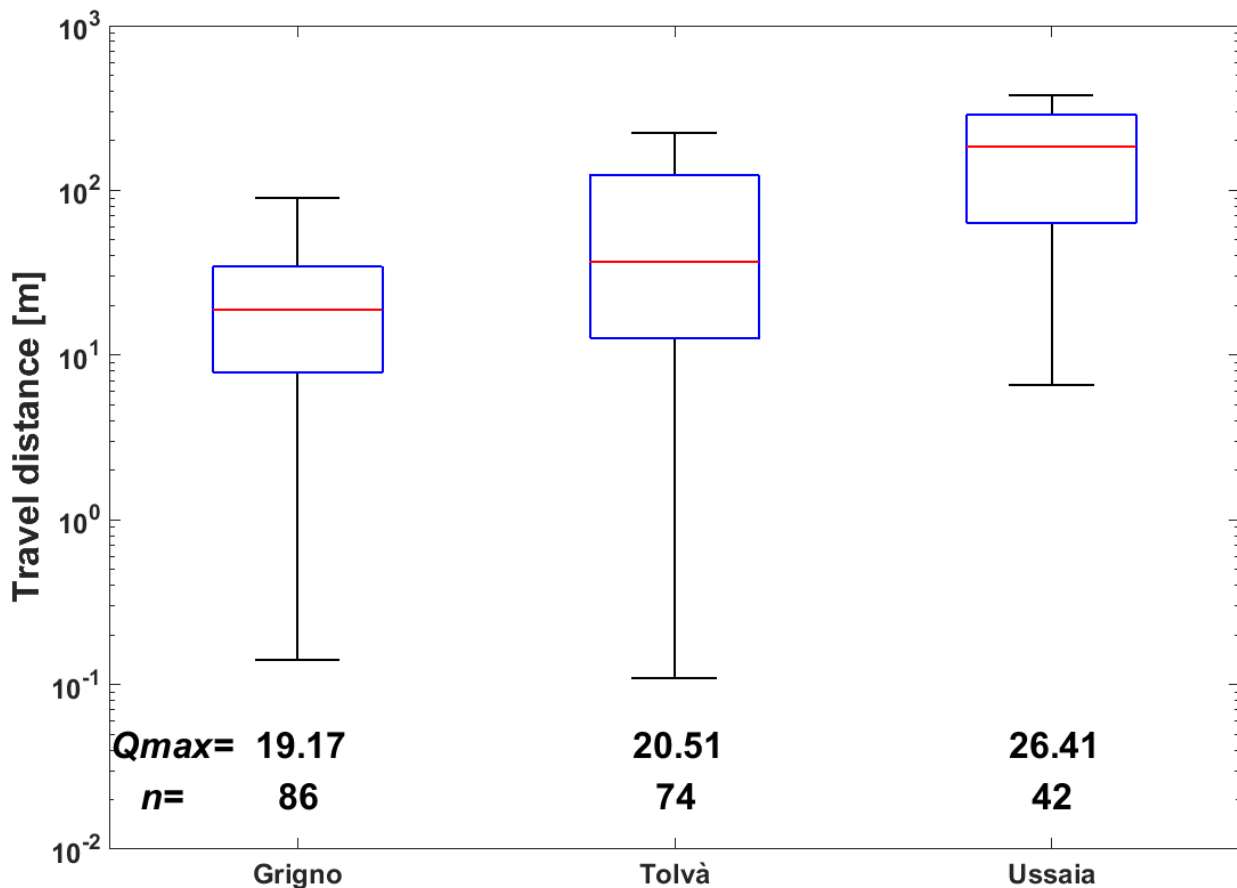


Figure 4.3.9. Comparative box plots of travel distances across weight classes at Grigno, Tolvà and Ussaia monitoring sites for the November 4-8, 2014 event (n = number of recovered tracers, Q_{max} = peak discharge in $m^3 s^{-1}$).

The conspicuous number of mobilized tracers, 86 at Grigno and 74 at Tolvà Creek, is opposed by the low recovery rate at Ussaia Creek (34%), where 42 clasts have been found, due to burial or exit from the surveyed reach. At Grigno Creek median travel distance is about 19 m (Figure 4.3.9), while maximum is 89 m. At Tolvà Creek the median the maximum travel distance are higher than Grigno Creek, with clasts that travelled up to 230 m. At Ussaia Creek the median are larger than the maximum travel distances recorded in both sites located in Valsugana, with a value of 185 m. Distances travelled by tracers in this event at Ussaia Creek are ranging between 7 and 376 m.

Event May 20, 2015

The event of May 20th 2015 is a mixed type event, recorded across all the three sites (Table 4.3.6). Interestingly, at Grigno and Tolvà Creek, the event is hydrologically characterized by a double peak, the first occurring the 15th and linked to snowmelt, and the second occurred the 20th, following a rainfall event. Also at Ussaia Creek this event is composed by a double peak, but the rainfall event is more prolonged but less intense compared to Grigno –Tolvà monitored sites.

Table 4.3.6. Rainfall characteristics of May 20, 2015 event.

Monitoring site	Duration [h]	Max intensity [mm/h]	Cumulative precipitation [mm]	Q max [m ³ s ⁻¹]
Grigno Cr. (Malga Sorgazza)	9	12.4	31	3.38
Tolvà Cr. (Passo Brocon)	8	7.2	29	1.07
Ussaia Cr. (Mezzana)	20	7	34.8	0.37

This event triggered limited bedload at Grigno and Tolvà creek, where moved only 4 tracers at both sites, with recorded distances up to 0.5 m. At Ussaia Creek bedload is more efficient, with 16 clasts moved, travelling distances up to 2.2 m and a median length of 0.25 m.

Event September 14, 2015

The event of September 14th 2015 is a short late summer front. Malga Sorgazza and Passo Brocon meteorological stations recorded 8 hours of precipitation, sharing also maximum of precipitation intensity (11 mm/h). Cumulative precipitation is 49 mm at both sites. At Mezzana the cumulative precipitation is 42.6 mm, a value comparable to Grigno and Tolvà creeks, accumulated in 16 hours of precipitation (Table 4.3.7). This event generate an important flood at Ussaia monitoring site, with peak discharge of 2.11 m³ s⁻¹, the second largest discharge recorded at this site.

Table 4.3.7. Rainfall characteristics of September 14, 2015 event.

Monitoring site	Duration [h]	Max intensity [mm/h]	Cumulative precipitation [mm]	Q max [m ³ s ⁻¹]
Grigno Cr. (Malga Sorgazza)	8	11	49.4	11.85
Tolvà Cr. (Passo Brocon)	8	11.8	49.7	4.32
Ussaia Cr. (Mezzana)	16	5.4	42.6	2.11

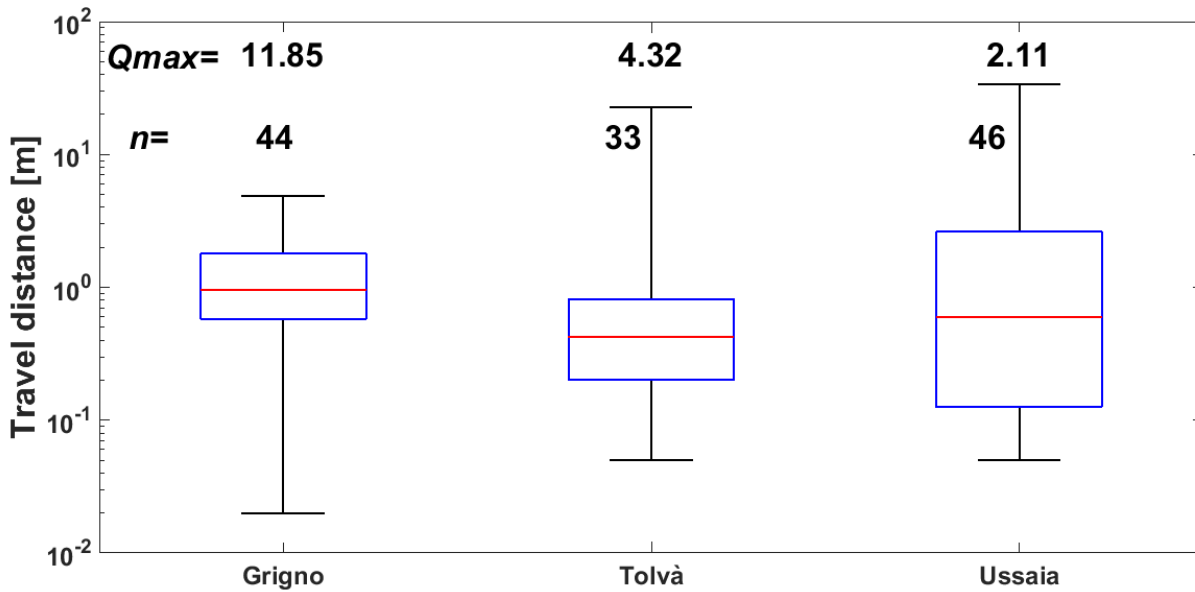


Figure 4.3.10. Comparative travel distances by weight classes at Grigno, Tolvà and Ussaia monitoring sites for the September 14, 2015 event (n= number of observations, Q_{max} = peak discharge in m³ s⁻¹).

As for previous events, also in this case the rainfall characteristics are shared between Grigno and Tolvà basins, but the hydrological response in the first has produced a larger flood in the first watershed. At Grigno Creek this event mobilized 44 clasts which median travel distances about 1 m, while at Tolvà Creek median value is 0.4 m (Figure 4.3.10). Despite the lower values of peak discharge, Tolvà Creek exhibits the largest maximum distance among the two sites, 22.6 m, while at Grigno Creek is limited to 5 m. At Ussaia Creek the duration of precipitation has been double compared to the other two sites, and the peak discharge is 2.11 m³ s⁻¹. Despite this, at Ussaia Creek moved 46 clasts, a number comparable with displacements recorded at Grigno Creek (Q_{max}= 11.85 m³ s⁻¹); the median travel distance is 0.6 m, while the largest distance is 34 m.

Event October 13-16, 2015

The event of October 10-13, 2015 is an autumn cyclonic front (Table 4.3.8). Malga Sorgazza and Passo Brocon meteorological stations recorded 88 hours of precipitation and identical maximum of precipitation intensity of 6.4 mm/h. Cumulative precipitation is 120 mm at both sites, while at Mezzana the same time meteorological input caused the cumulated rainfall to be limited to 49 mm, with maximum intensity of 4.2 mm/h.

Table 4.3.8. Rainfall characteristics of October 13-16, 2015 event.

Monitoring site	Duration [h]	Max intensity [mm/h]	Cumulative precipitation [mm]	Q max [$\text{m}^3 \text{s}^{-1}$]
Grigno Cr. (Malga Sorgazza)	88	6.4	120	3.89
Tolvà Cr. (Passo Brocon)	88	6.4	118.1	1.9
Ussaia Cr. (Mezzana)	44	4.2	49.2	0.32

The number of moved clasts at Grigno and Tolvà Creek is comparable, whereas at Ussaia Creek only 4 clasts moved, thus this data have limited statistical significance (Figure 4.3.10).

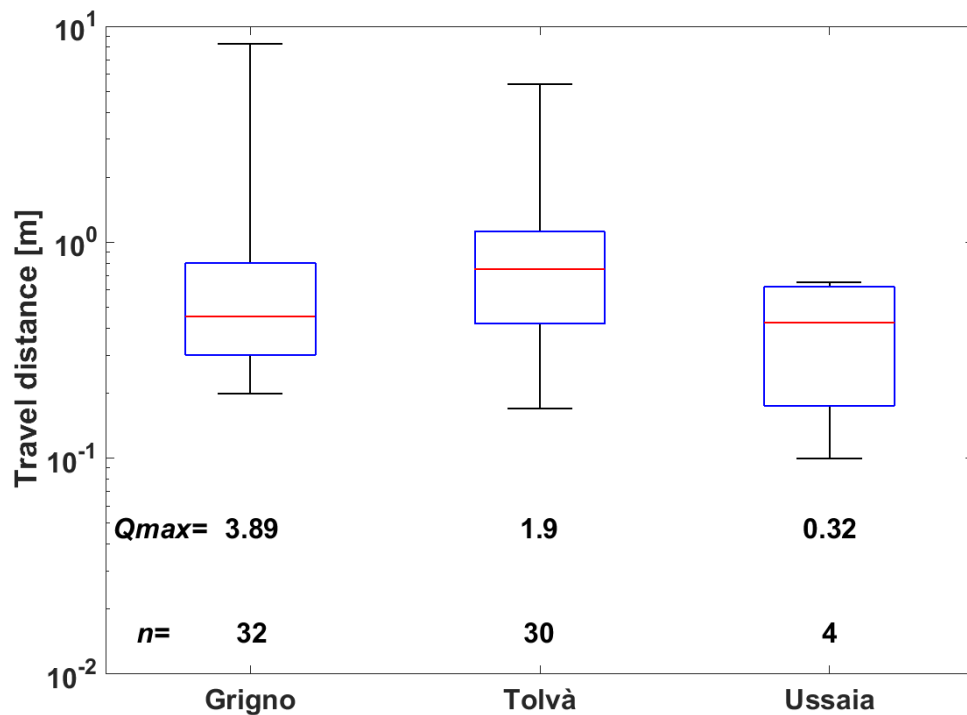


Figure 4.3.11. Comparative travel distances by weight classes at Grigno, Tolvà and Ussaia monitoring sites for the October 13-16, 2015 event (n = number of observations, Q_{max} = peak discharge in $\text{m}^3 \text{s}^{-1}$).

At Grigno Creek the median value of displacement is 0.5 m, slightly lower than Tolvà Creek, where the median is 0.7. Maximum travel distances are comparable at both sites, and are 8 m at Grigno Creek and 5 m at Tolvà Creek.

When considering the overall displacements at single event scale, Ussaia Creek is more efficient in bedload transport than Grigno and Tolvà monitored sites. This is well explained in the panels above (Figure 4.3.6-4.3.7-4.3.8-4.3.9-4.3.10-4.3.11) where, for selected events, the extremes (i.e. minimum and maximum) of the distribution of travel distances at Ussaia Creek are always larger compared to the other sites. In the event of October 13th, 2014, the maximum value exceeds by one order of magnitude the values of the other sites. In the event of November 4-8th, 2014 the overall distribution of displacements at Ussaia Creek is shifted towards larger values and is comprised between 6.6 m and 375 m, whereas the distribution at Tolvà Creek is comprised between 0.1 m and 225 m, and also the Grigno Creek lies within this range.

For each inter-survey values of Q_{max} , weight classes were plotted against the median travel distance during that period. These plots suggest that at Grigno Creek median transport distances are influenced by Q_{max} , lying within 3 orders of magnitude (Figure 4.3.12a). Specifically, within the range $2.77 \text{ m}^3 \text{ s}^{-1}$ and $3.89 \text{ m}^3 \text{ s}^{-1}$, medians lie 0.1 m and 1 m. Values are increasing as $Q_{max} = 8.41 \text{ m}^3 \text{ s}^{-1}$, where, all classes lie above 1 m, with the exception of W1 class that stands below 1 m. As Q_{max} increases to $10.73 \text{ m}^3 \text{ s}^{-1}$, median values lie between 1 m and 10 m, standing above the median values observed for $Q_{max} = 8.41 \text{ m}^3 \text{ s}^{-1}$. For $Q_{max} = 11.85 \text{ m}^3 \text{ s}^{-1}$ there is a decrease of median values, where each class plots regularly between 0.3 m and 0.5 m. This is a flood event of October 10-13, 2015, where the value of peak discharge is larger than event of August 13, 2014 ($Q_{max} = 10.73 \text{ m}^3 \text{ s}^{-1}$) but plots one order of magnitude below. The largest event recorded, of November 4-8, 2014 ($Q_{max} = 19.17 \text{ m}^3 \text{ s}^{-1}$), stands above the others and median values of W1-W5 classes are regularly plotting between 19 m and 24 m, while median values of W6 class is 13.6 m.

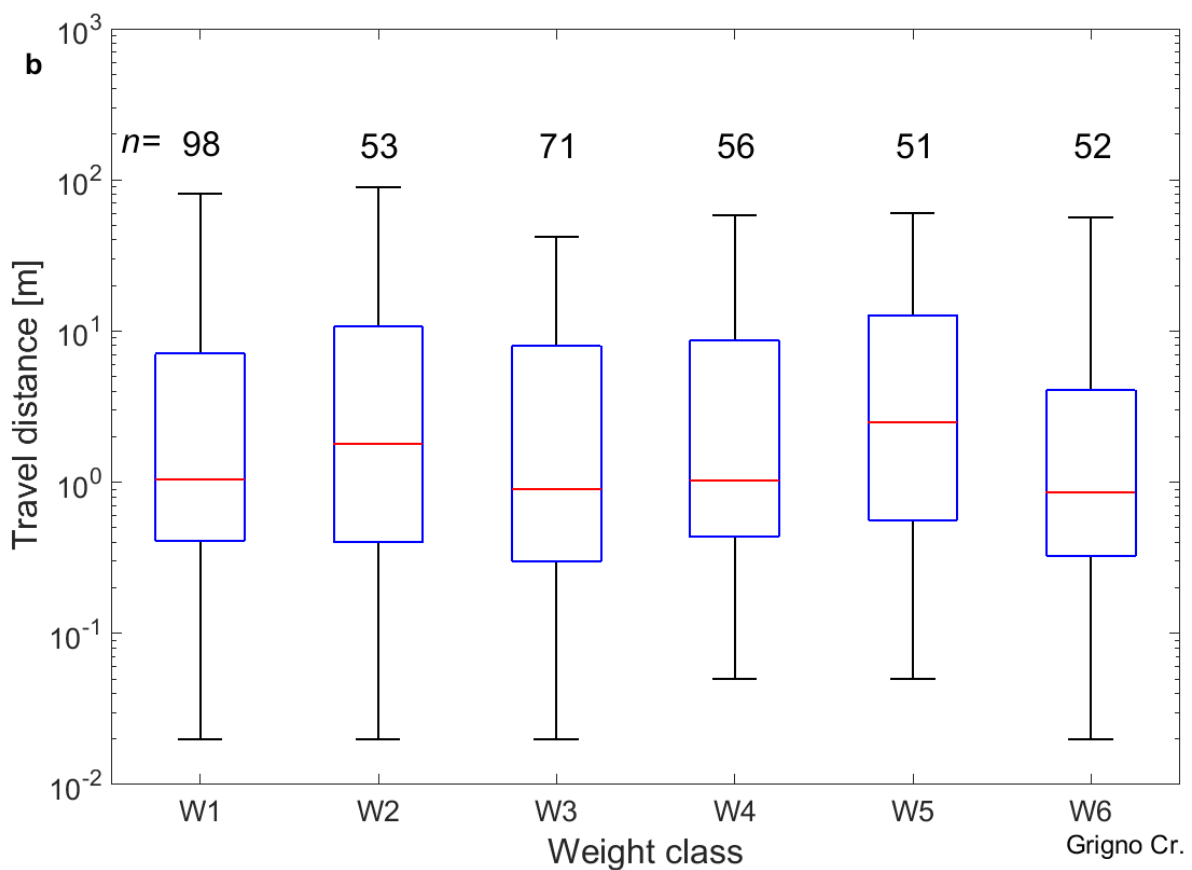
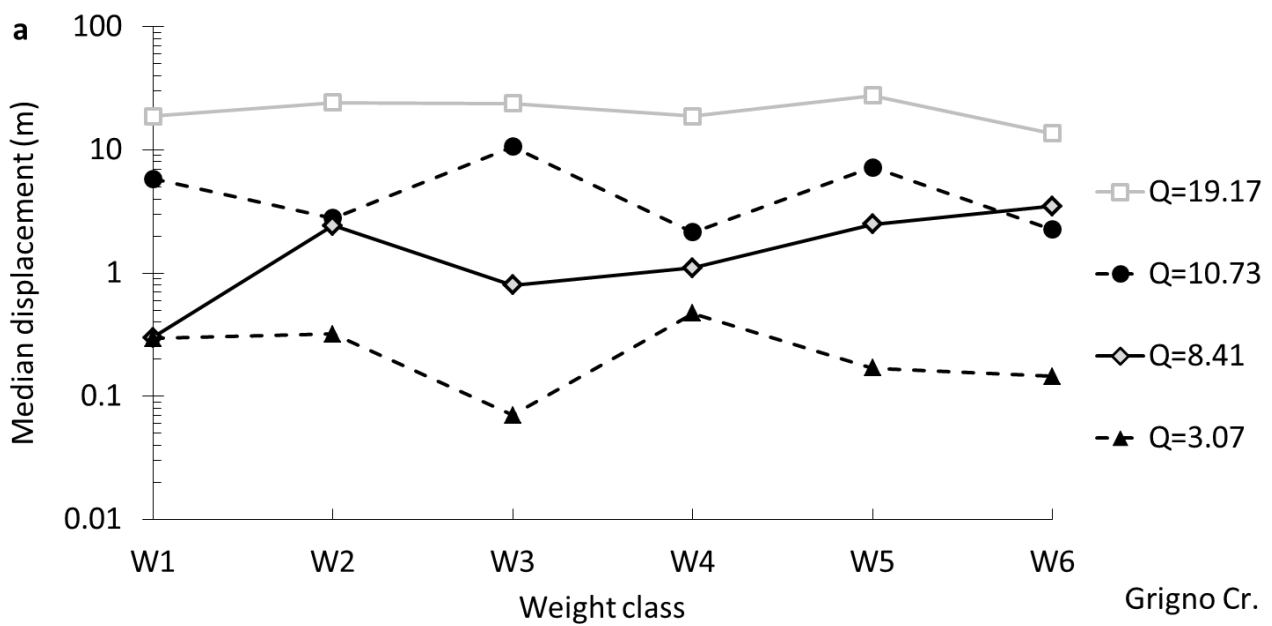


Figure 4.3.12. a) Tracer median travel distances as a function of weight and stratified by inter-survey peak discharge at Grigno Creek; b) Box plot showing the distribution of tracer travel distances across weight classes at Grigno Creek (n = number of observations). No motions count are not included.

The decrease in travel distance (in terms of maximum, median and quartiles) with increasing particle weight is poorly pronounced at Grigno Creek. Median values range between 0.85 m (W6 class) and 1.8 m (W2 class); W5 class exceptionally has the highest value of 2.5 m (Figure 4.3.12b).

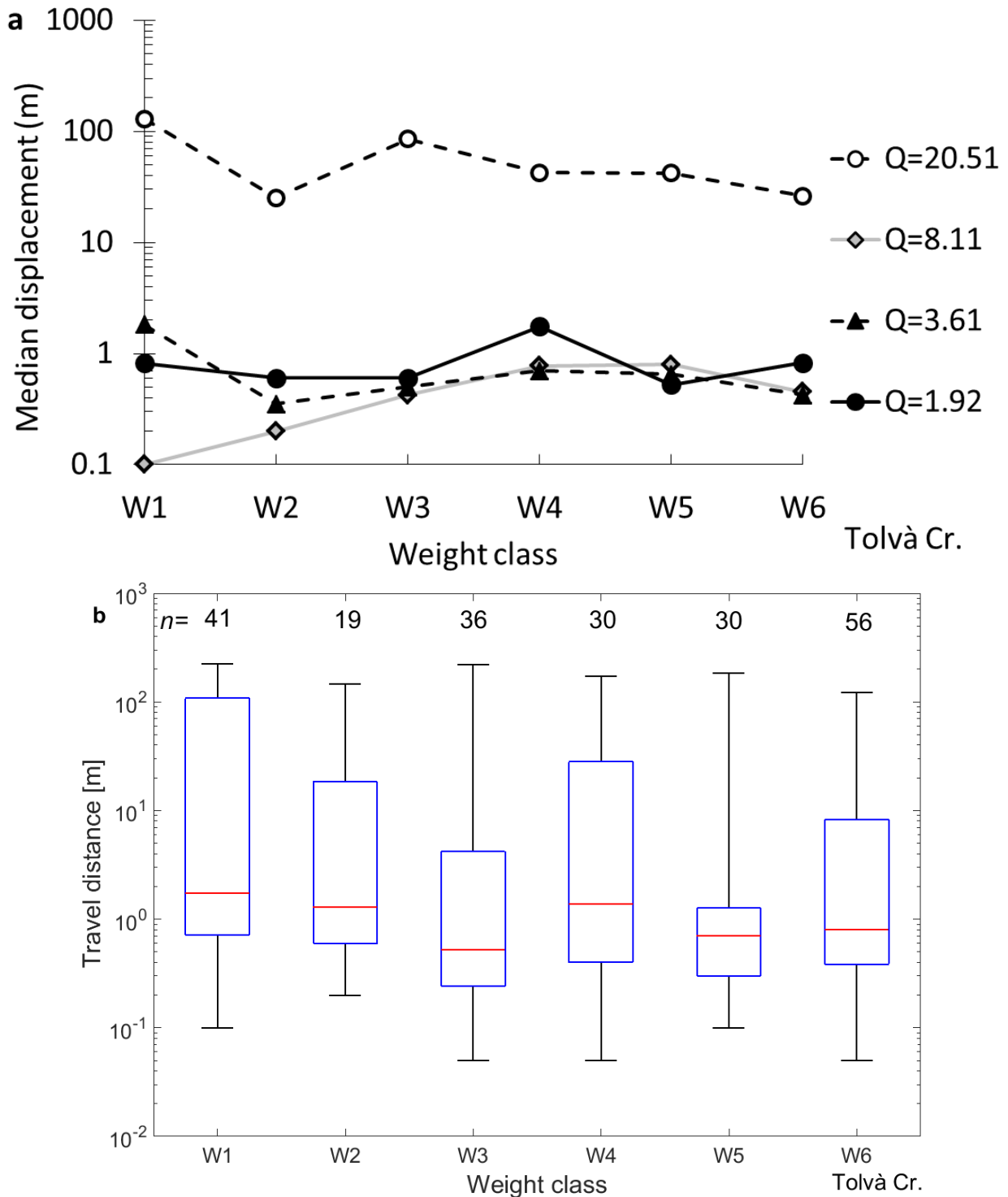


Figure 4.3.13. a) Tracer median travel distances as a function of weight and stratified by inter-survey peak discharge at Tolvà Creek; b) Box plot showing the distribution of tracer travel distances across weight classes at Tolvà Creek (n= number of observations). No motions count are not included.

Median displacements at Tolva Creek exhibit less sensitivity to Q_{\max} than observed at Grigno Creek (Figure 4.3.13a). In fact for a given flow condition, clasts generally tend to move for the same distances when considering the peak discharges between $0.99 \text{ m}^3 \text{ s}^{-1}$ and $8.11 \text{ m}^3 \text{ s}^{-1}$, clustering around median values of 1 m. At high discharge rates of $20.51 \text{ m}^3 \text{ s}^{-1}$ there is an increase of 1-2 orders of magnitude, especially if considering the W1 and the W3 classes .

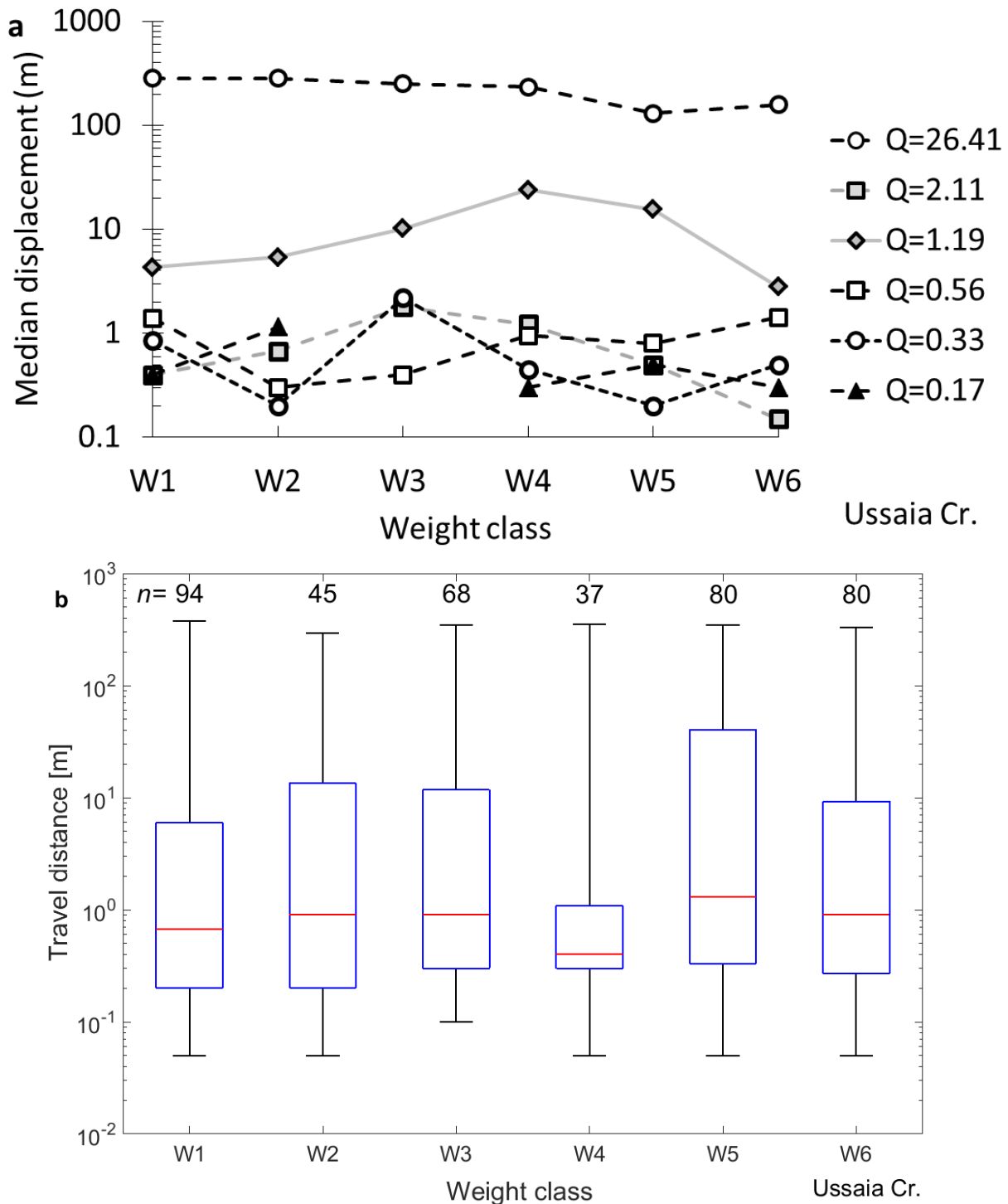


Figure 4.3.14. a) Tracer median travel distances as a function of weight and stratified by inter-survey peak discharge at Ussaia Creek; b) Box plot showing the distribution of tracer travel distances across weight classes at Ussaia Creek (n = number of observations). No motions count are not included.

At Ussaia Creek, the relation among median displacements and peak discharge is not clear (Figure 4.3.14a). As a matter of fact, there are four peak discharges ($Q_{\max} = 0.17, 0.33, 0.56$ and $2.11 \text{ m}^3 \text{ s}^{-1}$) clustering in the interval 0.1 – 1 m, while the $Q_{\max} = 1.19 \text{ m}^3 \text{ s}^{-1}$ stands in the order 5-10 m of median displacement. The debris flow event shows median displacements across weight classes in the order of 300 m, and is clearly distinguished by equimobility conditions. Concerning the other events, there are not selective transport nor equimobility conditions. Only for the events $Q_{\max} = 1.19 \text{ m}^3 \text{ s}^{-1}$ and $Q_{\max} = 2.11 \text{ m}^3 \text{ s}^{-1}$, there are some hints of size-selective events for weight classes larger than W3 and W4 respectively. Generally we note that also at Ussaia Creek heavier classes are not travelling less than lighter ones. Instead there is a generalized trend of median values around 10^0 m. Maximum travel distances are not significant because the debris flow event of 5th November 2014 imposed travel distances equal across weight classes.

Strimm Creek

At Strimm Creek the surveys have been conducted seasonally in the period from September 2011 to June 2014. Here we monitored the distances travelled by tracers in the same periods of the year throughout the mentioned time interval, in order to get information about the efficiency that rainfall events and snowmelt pulses are imposing to bedload transport. Displacement data of the Upper Strimm Creek are taken from Dell'Agnese et al. (2015). To summarize the mobility of tracers' across all the surveys conducted, we plotted stacked bars of clasts divided by tracers' weight and stratified by lengths travelled from September 2011 to June 2014. Generally surveys conducted after snowmelt periods indicate that largest displacements occur within this period (Figure 4.3.15b-d), when the hydrological input deriving from melting of the snowpack is more effective compared to rainfall events determined by convective summer storms (Figure 4.3.15a-c). This is largely verified in the survey of June 27, 2013, when due to a thick snowpack extensively covering hillslopes in springtime 2013, the snowmelt runoff has been more prolonged and sustained higher discharges, causing entrainment of each weight class, with travel distances of the W2 to W4 classes comprised within 10-30 m and for W1 class within 30-50 m (Figure 4.3.15f). In the survey of October 1st 2013 (Figure 4.3.15g) we recorded the largest amount of clasts moved (91) and the largest travel distances for each weight class, considering all the surveys conducted by the end of summertime. Globally, at Upper Strimm we note how larger proportions of tracers are systematically displaced by snowmelt flows compared to rainfall induced ones.

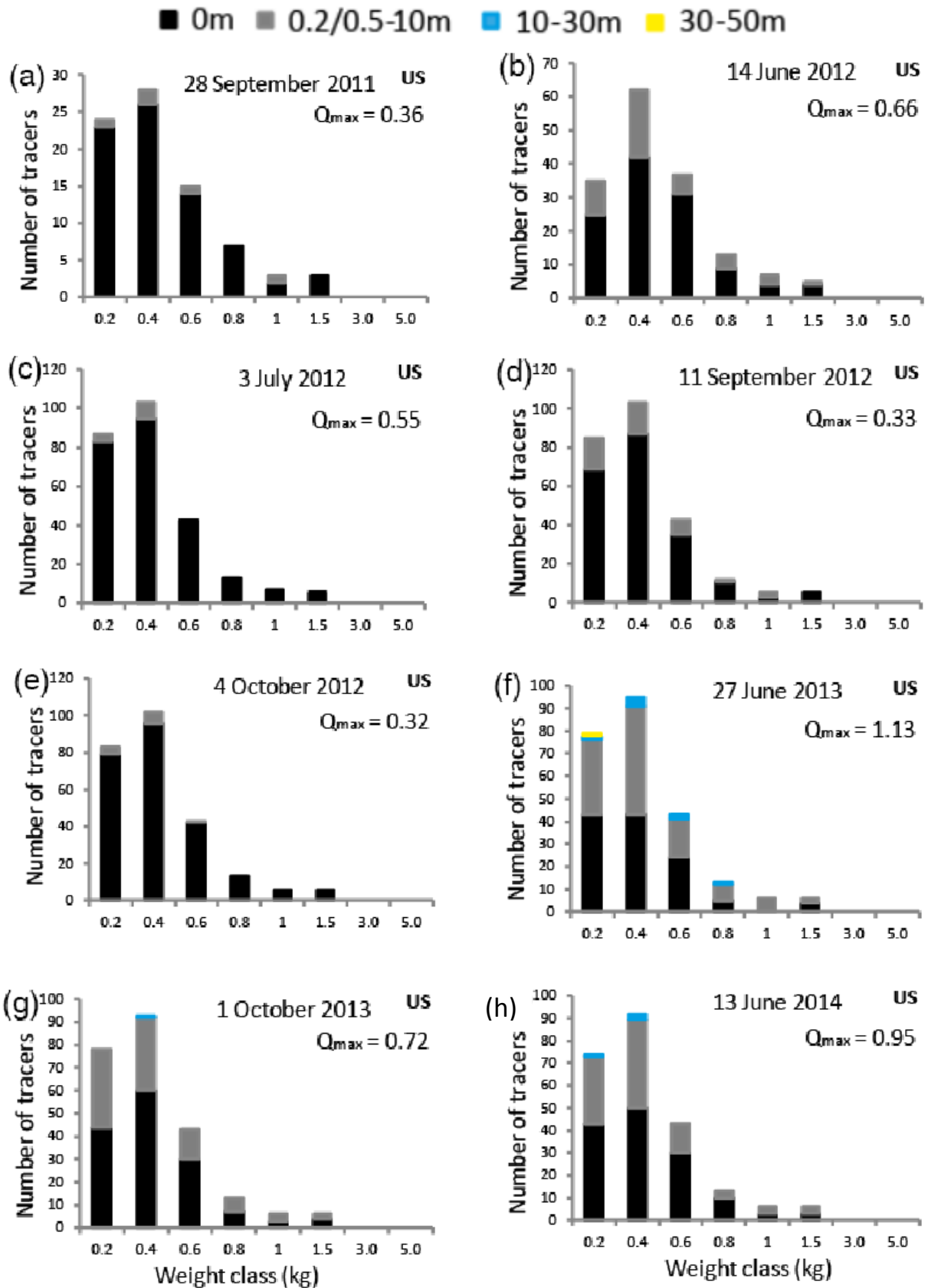


Figure 4.3.15. Stacked bars showing inter-survey frequency distributions of tracer travel distances across weight categories at the Upper Strimm Creek monitoring site for the monitoring period (September 2011 – June 2014). No motion surveys are not included (from Dell’Agnese et al., 2015).

For each inter-survey peak discharge weight classes are plotted against the median travel distance covered during that period. Travel distances appear to be weakly sensitive to changes in Q_{max} , lying all within one order of magnitude (Figure 4.3.16a). There are hints of size-selective transport sensu Parker (1982) for all the considered events, exception due for the event of $Q_{max} = 0.95 \text{ m}^3 \text{ s}^{-1}$, where a decrease in the median displacements is verified from 1.4 to 0.38 m of W1 and W6 class respectively.

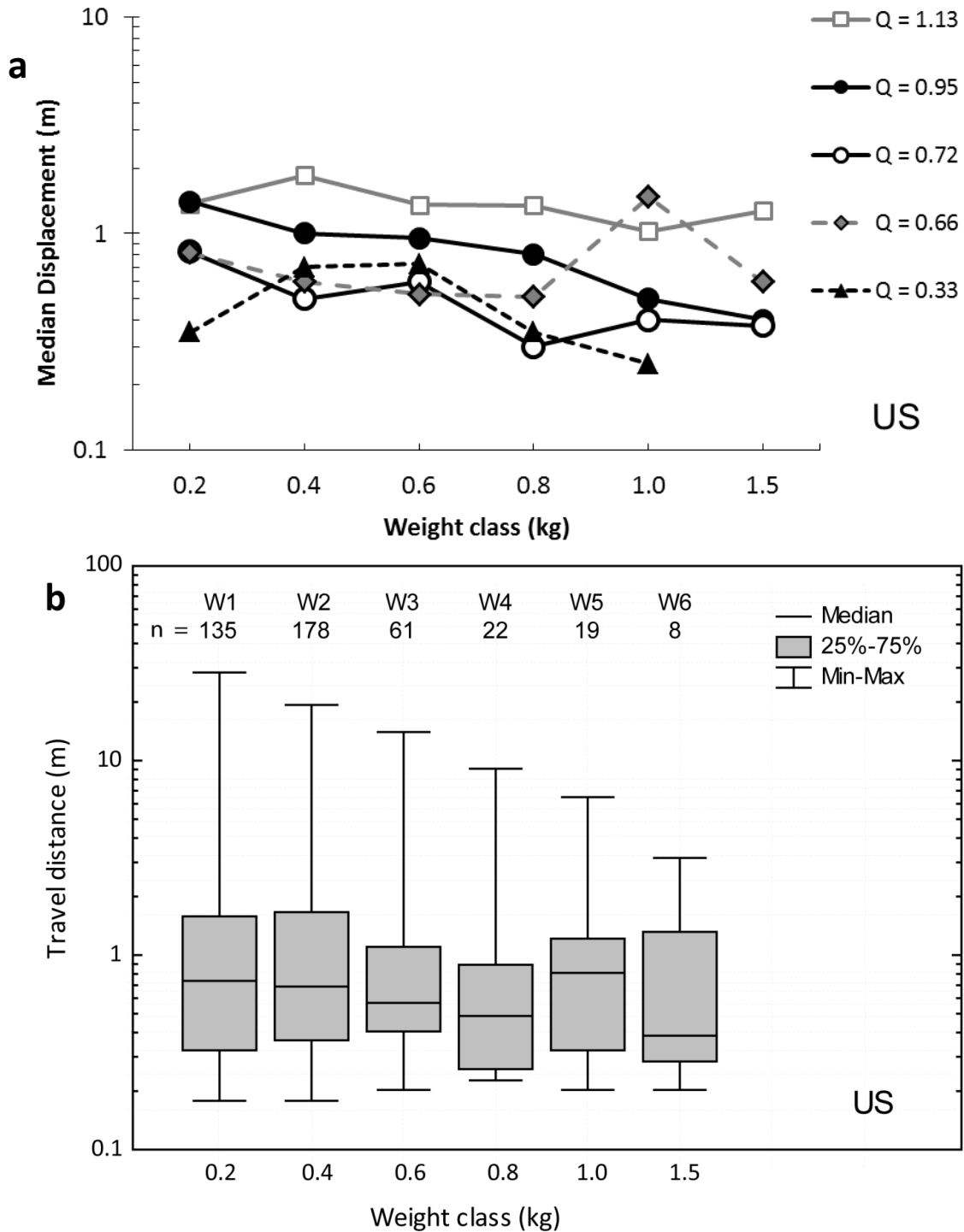


Figure 4.3.16. a) Tracer median travel distances as a function of weight and stratified by inter-survey peak discharge at Upper Strimm Creek; b) Box plot showing the distribution of tracer travel distances across weight classes at Upper Strimm Creek (n = number of observations). No motions count are not included.

At this site median values of travel distance decrease progressively considering heavier particles (Figure 4.3.16b). The only exception is represented by W5 class, probably caused by the low number of observations, compared the classes W1-W2-W3. A regular decrease is denoted in the maximum travel distances, where d_{max} decreases from 35 m (W1) to 3.9 m (W6) indicating that heavier tracers' are less mobile than lighter , in agreement with what is observed in Figure 4.3.16a.

Cumulatively, there is a profound difference in bedload transport across the monitored sites. Considering Grigno and Tolva Creek, sites characterized by disconnection from valley slopes, high roughness of bed macroforms and supply-limited conditions, the impact of snowmelt and mixed type events is lower compared to bedload triggered by rainfall events. As a matter of fact, if we consider at Grigno Creek the snowmelt events that imposed larger efficiency in bedload transport, such as May 5th or June 24th 2014, the number of displaced tracers is 15 with median distances below 1.0 m. Avoiding to consider the event of November 4-8, 2014, we observe that median travel distances are generally comprised between 0.2-5 m, and the number of mobilized clasts is between 25 and 75. While Tolva Creek shares a similar behavior, the Ussaia Creek is denoting a strong impact of snowmelt and mixed-type events on travel distances. Considering the ordinary snowmelt-related event of May 5th 2014, the median value of displacement is 0.4 m, but moving 28 clasts, double than at Grigno Creek. More striking effects have been imposed by the snowmelt-induced peak occurred on May 22-23, 2014, moving 77 clasts with median value of the overall displacements equal to 3.7 m. To better compare bedload events triggered by rainfall events, we refuse to consider the debris flow of November 4-8, 2014, focusing on events occurred in summertime or early autumn. In this case the variability of clasts displaced is high (from 4 to 44 clasts mobilized), and the median ranges in the interval 0.2-4 m. Compared to Grigno Creek, the number of displacements is reduced, but the order of magnitude of median displacement is comparable. Finally, the event of November 4-8, 2014 marks a transition in processes, since at Grigno and Tolva Creek was triggered ordinary bedload, conversely at Ussaia Creek we registered a debris flow. The efficiency in bedload transport at Strimm Creek exhibits a larger dependency from snowmelt-related events compared to rainfall-driven ones, showing comparable characteristics to the Ussaia Creek.

The box plots of travel distances from Grigno-Tolva-Ussaia monitored sites show no relation between weight and travel distances. Conversely the Strimm Creek, the only site where bedload monitoring is conducted at seasonal scale, there is an evident relation that heaviest particles are bounded to travel less and less, according to what observed when plotting median displacements for each weight class and stratifying it for selected discharges.

4.4 Tracers' virtual velocities

To calculate the velocity for a tracer is necessary to determine at first the entrainment thresholds for each weight class. Thresholds are obtained determining for each weight class, discharges capable to move a single element. From the set of discharges selected, is finally chosen the lowest value, that represents the entrainment threshold for all the floods experienced by tracers corresponding to that weight interval. Then we calculate the virtual duration, that corresponds to the theoretical time deployed by the tracer to travel the length measured between two consecutive field surveys. The final step involves the calculation of the ration among the traveled distance and the virtual duration. In the current chapter we show the entrainment thresholds, presenting discharge values responsible of tracer displacement and discharge values that not affected mobility of tracers. Box plots of the distribution of virtual velocities are illustrated considering at first all the events for each monitored site. Then, to understand how hydro-meteorological input affects virtual velocities across the different sites, we show scatterplots of similar events occurred after comparable inter-survey periods, such as snowmelt events monitored at Grigno and Ussaia creeks in 2014, considering the lack of synchronicity that governs snowmelt-related events. Mixed-type events will be compared in the same manner. Conversely, when considering rainfall-induced events, we can directly observe the effects triggered on bedload at different sites by synchronous episodes of precipitation. Particularly, by means of comparison among synchronous events, we can obtain further details on the weight-selective properties displayed by events characterized by different rainfall intensities.

We present tables showing the competence of the various floods at the three sites, considering at first surveys where no displacements have occurred (Table 4.4.1). Then we illustrate the surveys where clasts movement has been surveyed, indicating which weight classes were displaced and the corresponding magnitude of flood (Table 4.4.2-4.4.3-4.4.4).

Table 4.4.1. Event dates and peak discharge for which no clasts displacement has been observed at Grigno, Tolvà and Ussaia Creek.

Grigno Cr.	$Q_{\max} [m^3 s^{-1}]$	Tolvà Cr.	$Q_{\max} [m^3 s^{-1}]$	Ussaia Cr.	$Q_{\max} [m^3 s^{-1}]$
28/07/15	1.24	25/06/15	0.85	29/07/15	0.1
		28/07/15	1.24	18/08/15	0.1
				28/08/15	0.07

Table 4.4.2. Event dates and peak discharge for which clasts displacement has been observed at Grigno, Creek.

Grigno Creek	Q_{max} [m³ s⁻¹]	Mobilized classes
16 Apr 2014	2.7	W1, W3,W6
5 May 2014	1.6	W1 to W4, W6
25 May 2014	2.5	W1 to W3, W6
1 Jul 2014	8.4	W1 to W6
18 Jul 2014	3.9	W1 to W6
31 Jul 2014	9.7	W1 to W6
29 Aug 2014	10.7	W1 to W6
18 Oct 2014	3.1	W1 to W6
25 Nov 2014	19.1	W1 to W6
14 Apr 2015	1.9	W1, W4 to W6
14 May 2015	3.4	W1, W2, W6
25 May 2015	4.1	W3, W4, W5
25 Jun 2015	4.07	W2, W4
19 Sep 2015	11.85	W1 to W6
21 Oct 2015	3.89	W1 to W6

Table 4.4.3. Event dates and peak discharge for which clasts displacement has been observed at Tolvà Creek.

Tolvà Creek	Q_{max} [m³ s⁻¹]	Mobilized classes
28 Jul 2014	1.3	W1 to W6
19 Aug 2014	8.1	W1 to W6
21 Oct 2014	1.32	W1 to W6
27 Nov 2014	28.5	W1 to W6
14 Apr 2015	0.38	W1 to W6
14 May 2015	0.99	W1 to W6
25 May 2015	1.07	W1, W5
19 Sep 2015	4.3	W1 to W6
21 Oct 2015	1.9	W1 to W6

Table 4.4.4. Event dates and peak discharge for which clasts displacement has been observed at Ussaia Creek.

Ussaia Creek	Q_{max} [m³ s⁻¹]	Mobilized classes
29/04/2014	0.7	W1 to W6
06/05/2014	1	W1 to W6
03/06/2014	1.2	W1 to W6
30/06/2014	0.5	W1 to W3, W5, W6
11/07/2014	0.2	W1 to W6
27/07/2014	0.3	W1 to W6

18/08/2014	0.4	W1 to W6
20/10/2014	--	W1 to W6
08/11/2014	26	W1 to W6
19/05/2015	0.3	W1 to W6
26/05/2015	0.4	W1 to W4, W6
18/06/2015	0.2	W1 to W4, W6
15/09/2015	2.1	W1 to W6
25/09/2015	0.31	W1 to W6
22/10/2015	0.32	W3, W4, W6

At Grigno Creek the minimum peak discharge that mobilized weight classes from W1 to W4 and W6, is $Q_{\max} = 1.6 \text{ m}^3 \text{ s}^{-1}$ of May 5th 2014; the class W5 has been mobilized by April 14th 2015 flood, $Q_{\max} = 1.9 \text{ m}^3 \text{ s}^{-1}$. At Tolv Creek the April 14th 2015 mobilized all the weight classes with a peak discharge of $0.38 \text{ m}^3 \text{ s}^{-1}$. However, since clasts were released in December 7th 2014, this flood has been discarded since that flood is the first that hit the tracers. Conversely we considered the displacements induced among all the weight classes by the following flood (May 14th 2015, $Q_{\max} = 0.99 \text{ m}^3 \text{ s}^{-1}$), to represent the minimum entrainment threshold at Tolv Creek. At Ussaia Creek the minimum discharge able to entrain all the weight classes is Q_{\max} equal to $0.17 \text{ m}^3 \text{ s}^{-1}$ registered in July 11th 2014. At Grigno and Tolv sites, entrainment discharges are determined by snowmelt events, whereas at Ussaia Creek is related to a rainfall event. As a matter of fact at Ussaia site are recorded larger discharges during the prolonged 2014 snowmelt period, that represented a major hydrological forcing compared to summertime rainfall-induced events.

For each site we determined the entrainment threshold discharge (Figure 4.4.1), so that at flood scale we determine the virtual transport duration and consequently we evaluate the virtual velocity of tracers.

According to the extension of storm hydrograph, the time over threshold discharge is larger for snowmelt events. Peaked events such as summer convective storms or quick fronts, exhibit shorter virtual transport durations (Table 4.4.4-4.4.5-4.4.6), compared to snowmelt or mixed-type events.

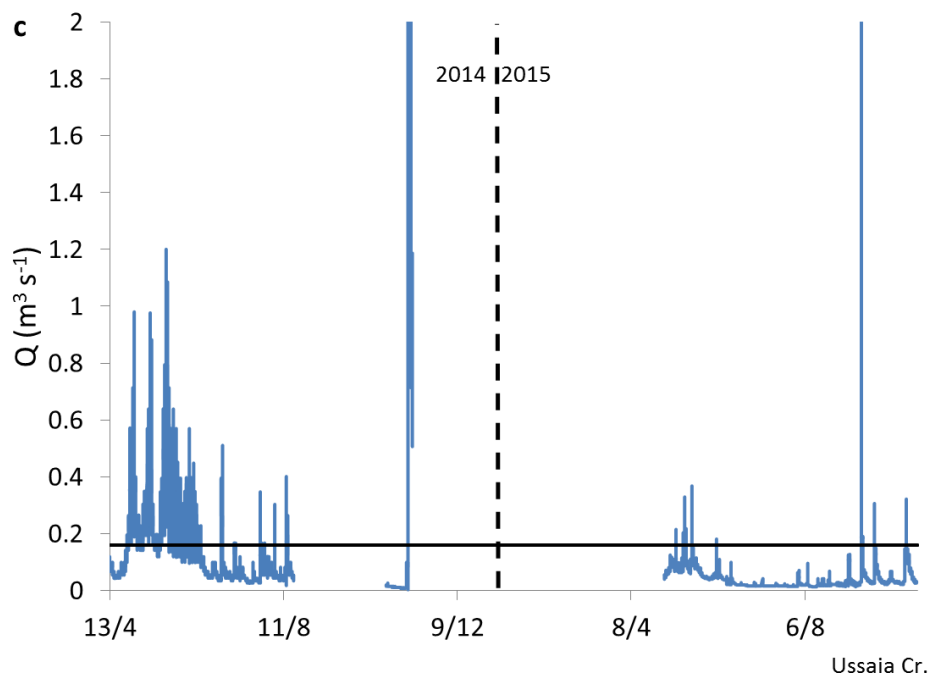
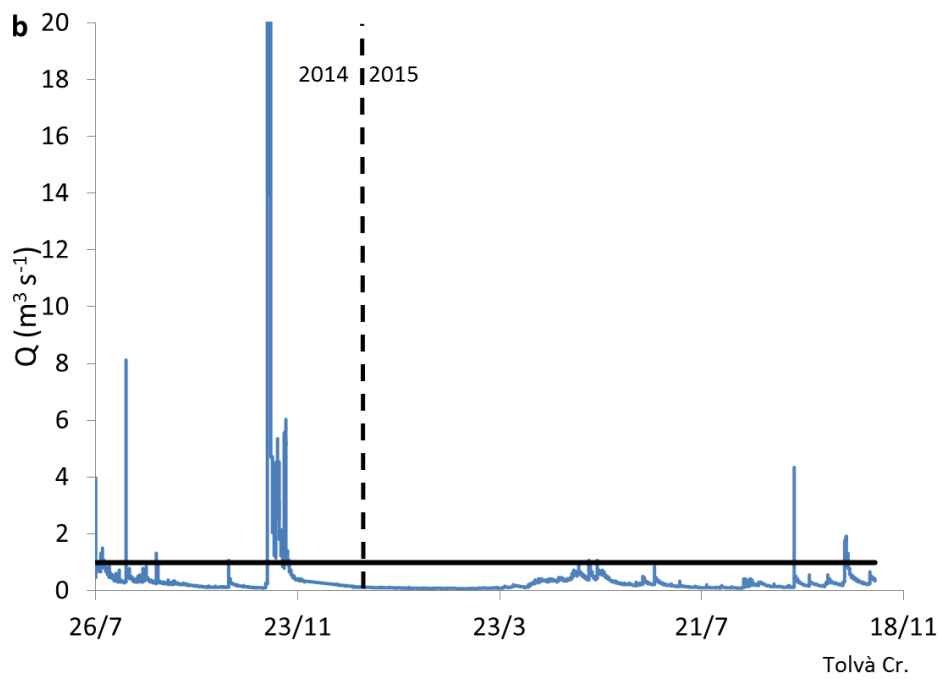
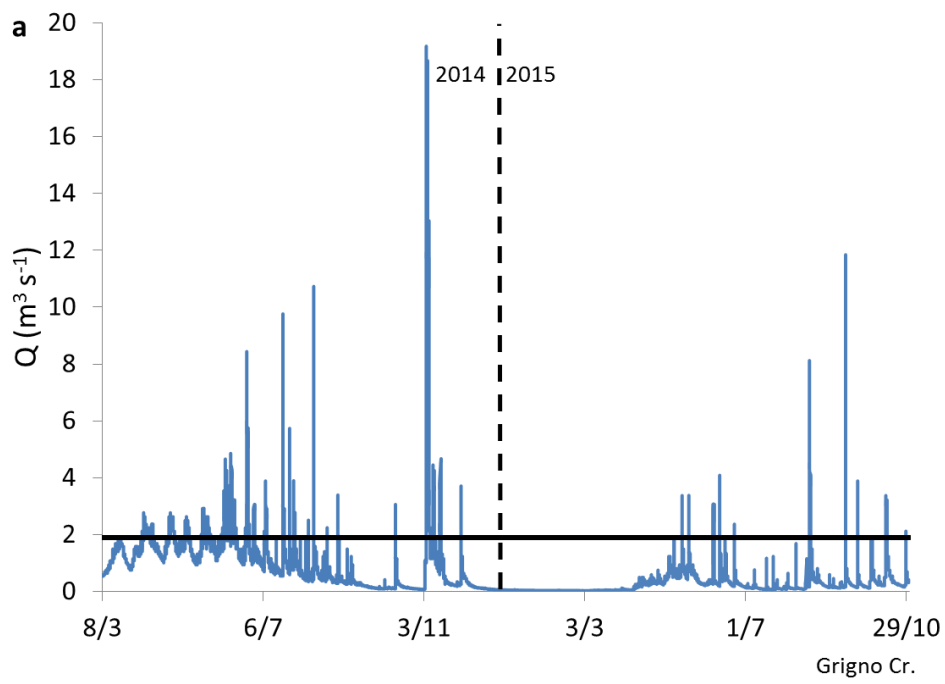


Figure 4.4.1. Entrainment threshold discharges (black horizontal line) for the three sites a) Grigno, b) Tolvà and c) Ussaia Creek.

Table 4.4.5. Type of forcing input for bedload events and related virtual transport duration at Grigno Creek.

Event date	Type	Q_{max} [m³ s⁻¹]	Inter-survey length [days]	Virtual transport duration [min]
16 Apr 2014	Snowmelt	2.7	133	7690
5 May 2014	Snowmelt	1.6	11	5430
25 May 2014	Snowmelt	2.5	20	6470
1 Jul 2014	Mixed	8.4	37	15400
18 Jul 2014	Rainfall	3.9	17	1320
28 Jul 2014	Rainfall	9.7	13	2110
19 Aug 2014	Rainfall	10.7	29	470
18 Oct 2014	Rainfall	3.1	50	270
4-8 Nov 2014	Rainfall	19.1	38	6480
14 Apr 2015	Snowmelt	3.7	140	-
14 May 2015	Mixed	1.9	30	120
25 May 2015	Mixed	4.1	11	800
25 Jun 2015	Rainfall	4.07	32	180
19 Sep 2015	Rainfall	11.85	50	640
21 Oct 2015	Rainfall	3.89	35	760

Table 4.4.6. Type of forcing input for bedload events and related virtual transport duration at Tolvà Creek.

Event date	Type	Q_{max} [m³ s⁻¹]	Inter-survey length [days]	Virtual transport duration [min]
28 Jul 2014	Rainfall	1.3	2	530
19 Aug 2014	Rainfall	8.1	22	2020
18 Oct 2014	Rainfall	1.32	63	120
4-8 Nov 2014	Rainfall	20.7	37	9450
14 Apr 2015	Snowmelt	0.38	128	-
14 May 2015	Mixed	0.99	29	350
25 May 2015	Mixed	1.07	11	1060
19 Sep 2015	Rainfall	4.3	53	280
21 Oct 2015	Rainfall	1.9	31	2390

Table 4.4.7. Type of forcing input for bedload events and related virtual transport duration at Ussaia Creek.

Event date	Type	Q_{max} [m³ s⁻¹]	Inter-survey length [days]	Virtual transport duration [min]
29/04/2014	Snowmelt	0.7	16	5170
06/05/2014	Snowmelt	1	6	9670
03/06/2014	Snowmelt	1.2	28	37230
30/06/2014	Mixed	0.5	30	12840
11/07/2014	Rainfall	0.2	8	60
27/07/2014	Rainfall	0.3	17	590
18/08/2014	Rainfall	0.4	21	730
08/11/2014	Rainfall	26	19	5140
19/05/2015	Mixed	0.3	18	1290

26/05/2015	Mixed	0.4	7	560
18/06/2015	Rainfall	0.2	23	50
15/09/2015	Rainfall	2.1	18	1200
25/09/2015	Rainfall	0.31	10	500
22/10/2015	Rainfall	0.32	27	790

The results obtained by the analysis show that at Grigno Creek typical values of virtual duration for snowmelt events range between 5500 and 7500 minutes (Table 4.4.5). A larger value (15400 minutes) is recognized for the mixed event of July 1st 2014, where the increase of hydrometric level protracted for more than ten days due to rainfall event and increased temperatures that imparted melt of a deep snowpack, sustaining a large baseflow level. Following episodes registered shorter virtual transport durations, reducing to 270 minutes of the October 18th 2014 event. A large duration is registered as a consequence of the prolonged autumn front, with value comparable to snowmelt events, 6480 minutes. In 2015 there is a drastic decrease in virtual durations, due to lesser extent of floods. For example, the unique snowmelt event of April 14th 2015 has a virtual duration of 1110 minutes, comparable to the July 18th 2014 summer convective storm. Tolva Creek shares a similar tendency with Grigno site (Table 4.4.6). Snowmelt events are registered in 2015 only, without triggering significant bedload events. The mixed events registered in 2015 show values comparable to that of Grigno Creek, while for rainfall-induced events the situation is more complex, with values of virtual transport duration that, for comparable events, tend to be larger than what observed at Grigno Creek. Since the hydrograph shape is very similar among these two sites, the factor determining this discrepancy is the different threshold discharge, that at Tolva Creek is lower than Grigno Creek.

At Ussaia Creek (Table 4.4.7) virtual transport duration for snowmelt events in 2014 is very similar to what observed at Grigno Creek. The difference at this site is determined by the short duration of summer 2014 events (60-730 minutes), whereas at Grigno Creek we recorded two events, of July 18th and 28th 2014, which transport duration exceeded 1300 minutes. In 2015 snowmelt-induced relevant bedload events are not recorded, and generally values of duration are limited compared to 2014. Beyond this, also the number of events in 2015 is reduced, and the absence of bedload-triggering events is evident especially during summertime.

At Grigno Creek there is an evident discrimination of the virtual velocities according to type of hydro-meteorological input (Figure 4.4.2a). Exception due for $Q_{\max} = 1.9 \text{ m}^3 \text{ s}^{-1}$ (first survey after the release), median values of snowmelt and mixed type events are lower compared to rainfall events. For Q_{\max} comprised between 3 and 4 $\text{m}^3 \text{ s}^{-1}$ there is a similar distribution in the velocities of the events, with median values comprised between 0.05 and 0.1 cm s^{-1} . A counterintuitive drop in the distribution of values is evident for $Q_{\max} = 8.41 \text{ m}^3 \text{ s}^{-1}$, where only 14 clasts moved, therefore the distribution can be subject to bias due to low number of observations. For $Q_{\max} = 9.69 \text{ m}^3 \text{ s}^{-1}$ the shape of the distribution is similar to those of values of discharge ranging between 3 and 4 $\text{m}^3 \text{ s}^{-1}$. This event is less peaked, with duration equal to 35 hours, a value that is larger if compared to other events of Q_{\max} below 4 $\text{m}^3 \text{ s}^{-1}$. For all these events median are comprised between 0.06 and 0.1 cm min^{-1} . By August 2014 it has been recorded a double peak discharge, that caused the distribution to be shifted towards larger values, showing a median value of

about 1 cm min^{-1} , one order of magnitude above the precedent events. Excluding this event, there is an increase in the median values from 0.06 to 0.3 cm min^{-1} considering the three peak discharges $Q_{\text{max}} = 9.69$, $Q_{\text{max}} = 11.85$ and $Q_{\text{max}} = 19.17 \text{ m}^3 \text{ s}^{-1}$.

At Tolvà Creek, the distribution of virtual velocities does not follow the increase in peak discharge (Figure 4.4.2b). The only snowmelt event recorded is biased because moved only clasts recently released. The events by October 14, 2014 and August 14, 2014 show a contrasting behavior, because they apparently not follow any relation with peak discharge. In the event of October 14th, 2014 the peak discharge is $3.61 \text{ m}^3 \text{ s}^{-1}$ and the median value is about 0.6 cm min^{-1} . This is due to the fact that event duration is 5 hours, therefore virtual velocities increase. As comparison we can consider the event of July 26th, 2014, with a peak discharge of $3.95 \text{ m}^3 \text{ s}^{-1}$, where the duration over threshold of the whole event is 36 hours, and virtual velocities are lower (median value = 0.065 cm). The event of August 14th, 2014 shows an anomalous decrease in the distribution of virtual velocities, with median value of 0.02 cm min^{-1} , despite the peak discharge $Q_{\text{max}} = 8.11 \text{ m}^3 \text{ s}^{-1}$. Also in this case, the duration over threshold of the entire event has been of 32 hours, so that the value of velocities lowered.

At Ussaia Creek the relations between virtual velocities and peak discharge are highly scattered, a feature typical of transport limited systems (Figure 4.4.2c). The striking difference with the Grigno and Tolvà creeks is the efficiency in transport of snowmelt and mixed-type events, showing values of peak discharge higher than precipitation events. The event by July 9, 2014 ($Q_{\text{max}} = 0.17 \text{ m}^3 \text{ s}^{-1}$) shows higher values of virtual velocities, compared to the event of peak discharge comprised between 0.31 and $0.37 \text{ m}^3 \text{ s}^{-1}$. The one by July 9, 2014 is the more extended in time, with 26 hours of precipitation and a mean rainfall of 26.4 mm , whereas all the others are limited to 9-13 hours but with larger mean precipitation, typically within $3 - 4 \text{ mm hr}^{-1}$. Excluding the debris flow event, the August 13, 2014 shows the highest median virtual velocity of 0.03 cm min^{-1} . Comparing the two events by April 28 and 3, 2014, the first has a peak discharge of $0.56 \text{ m}^3 \text{ s}^{-1}$, the second of $0.98 \text{ m}^3 \text{ s}^{-1}$. In the first case we recognize median velocities of 0.02 cm min^{-1} , whereas in the second case the value is limited to $0.004 \text{ cm min}^{-1}$. This anomaly is due to the fact that the survey by April 28 was conducted immediately after clasts release. Considering the debris flow event by November 7, 2014, the median value of 3.2 cm min^{-1} is well above the maximum value registered for a rainfall events (e.g., median virtual velocity 0.03 cm min^{-1} for the event of August 13, 2014), denoting the transition from the fluvially dominated transport to a debris flow.

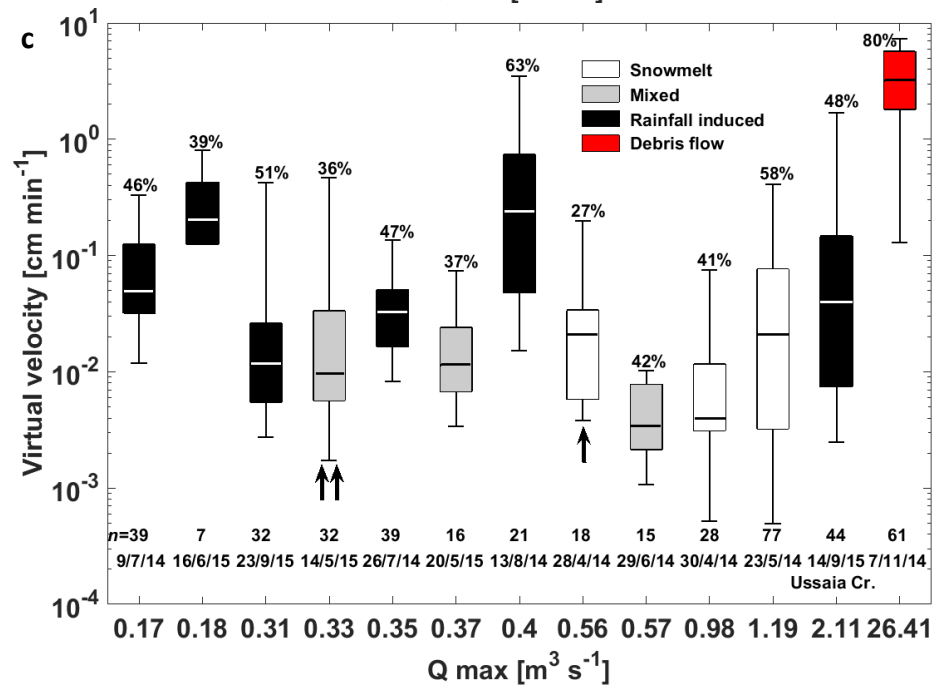
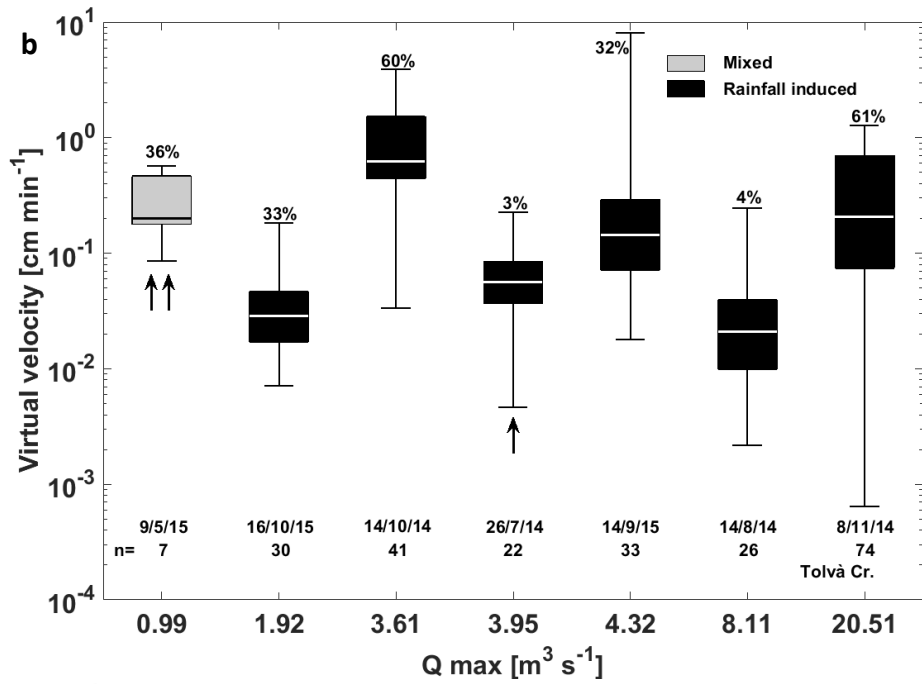
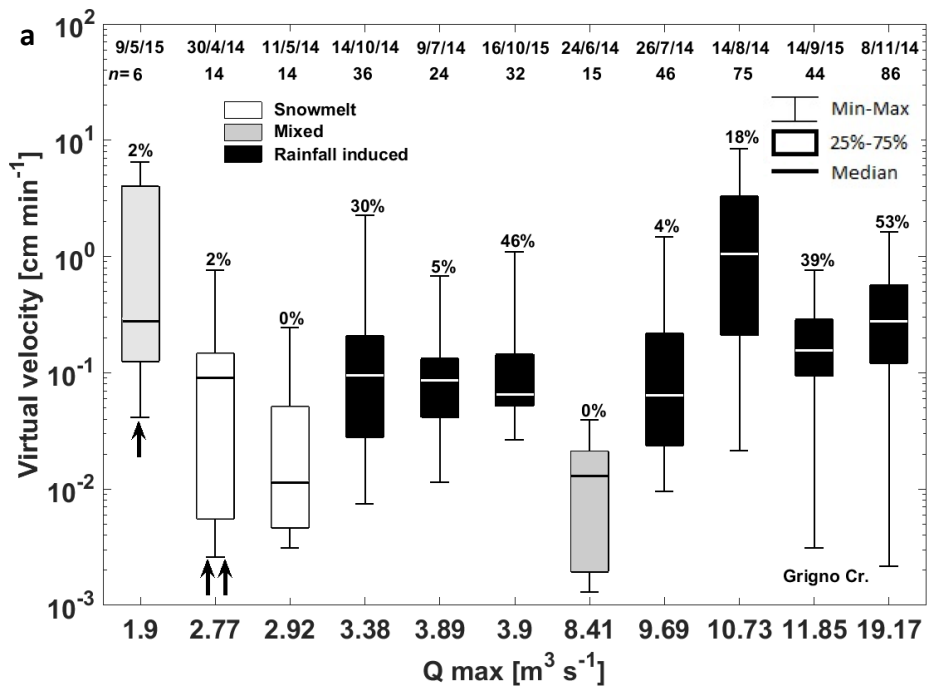
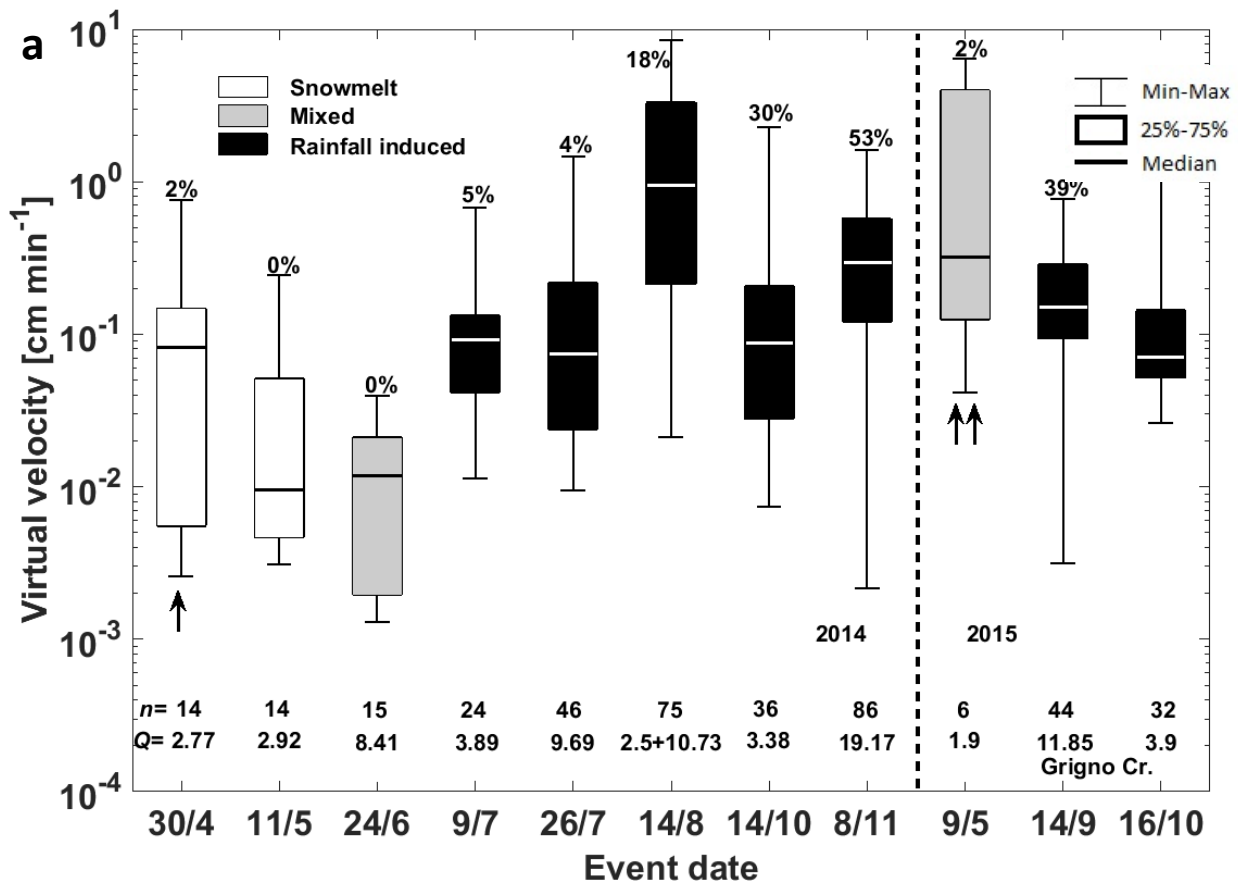


Figure 4.4.2. Box plots of the tracers' virtual velocities in relation to corresponding inter-survey peak discharge (Qmax) in (a) Grigno, (b) Tolvà and (c) Ussaia Creek. The flow regime of inter-survey periods is classified into snowmelt, rainfall-induced and mixed. Mixed periods represent a combination of the first two and typically correspond to the snowmelt falling limb. At Ussaia monitored site the debris flow event is highlighted in red, triggered by a rainfall-induced event. (Black vertical arrows represent tracers' release and the percentages above the largest whisker indicate the proportion of buried tracers, n= number of observations).

As illustrated in Figure 4.4.3, when ordered by date the boxplots of virtual velocities are showing the seasonality of bedload transport. Considering Grigno Creek, it is evident the signature of rainfall events, whose median virtual velocities are generally above the threshold of $10^{-1} \text{ cm min}^{-1}$. Snowmelt or mixed-type events velocities tend to be lower, generally 0.02 cm min^{-1} , excluding the events by April 30, 2014 and May 9, 2015 where clasts moved were recently seeded, therefore their distribution is biased. Comparing the 2014 and the 2015, it is clear a decline in transport efficiency in the last year, due to the scarcity of precipitation and a consequent limited record of tracers' displacements. At Tolvà Creek, despite the limited characterization of the site among different type of hydro-meteorological events, is possible to recognize the same distinction existing at Grigno Creek, with the 2014 characterized by an increase in efficiency of bedload events from summer to autumn, and a strong decline in virtual velocities characterizing the 2015. The event by May 9, 2015 (the only of mixed type) is biased due to displacements recorded among clasts recently seeded in the channel bed. At Ussaia Creek there is not a clear distinction between rainfall/snowmelt-mixed events. As a matter of fact the distributions of virtual velocities evaluated for rainfall by 2015 (e.g., September 14 and September 23, 2015) are similar or overlapping those of events by 2014, such as May 23, 2014. Also at Ussaia Creek is visible the decline in transport efficiency during 2015.



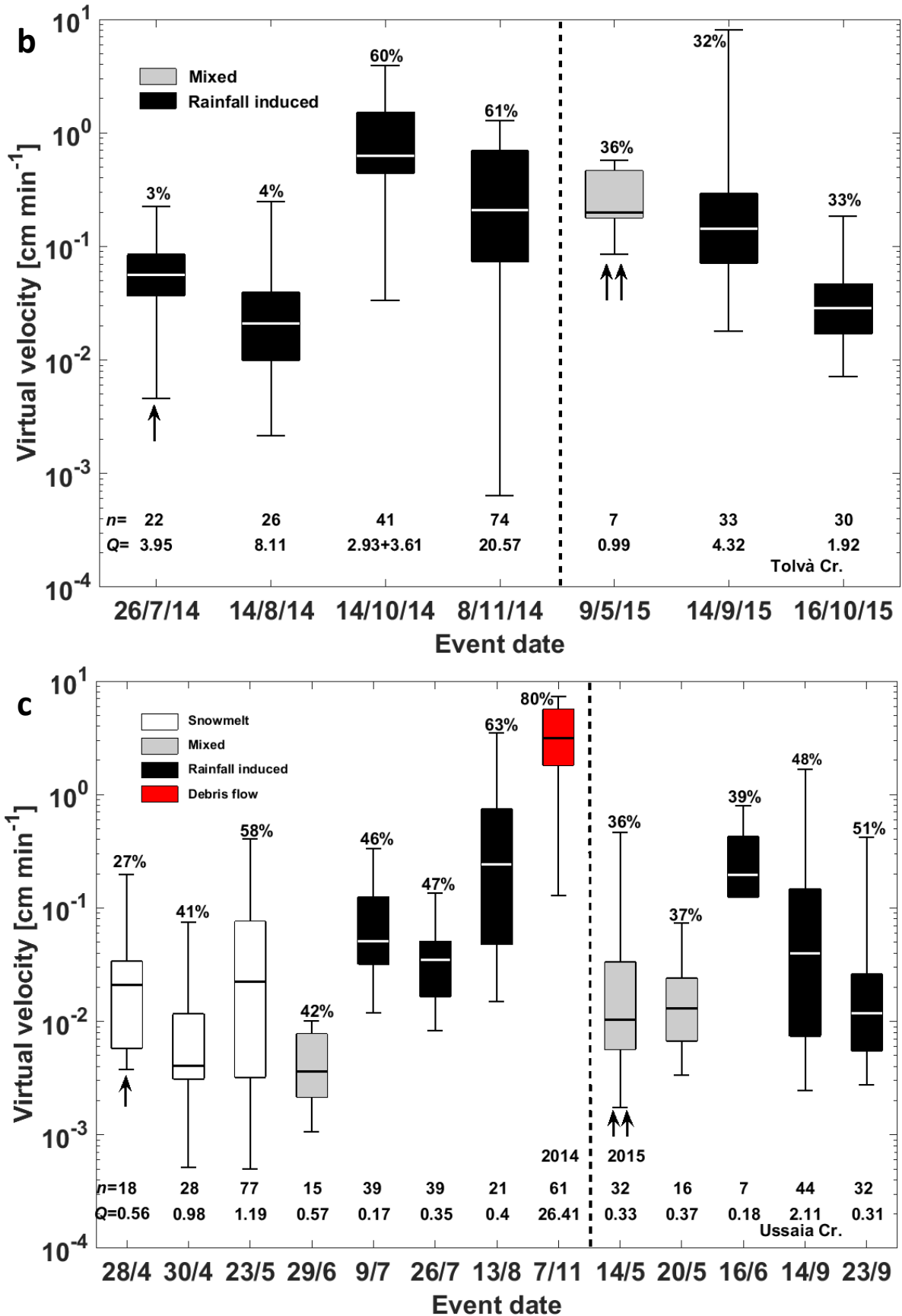
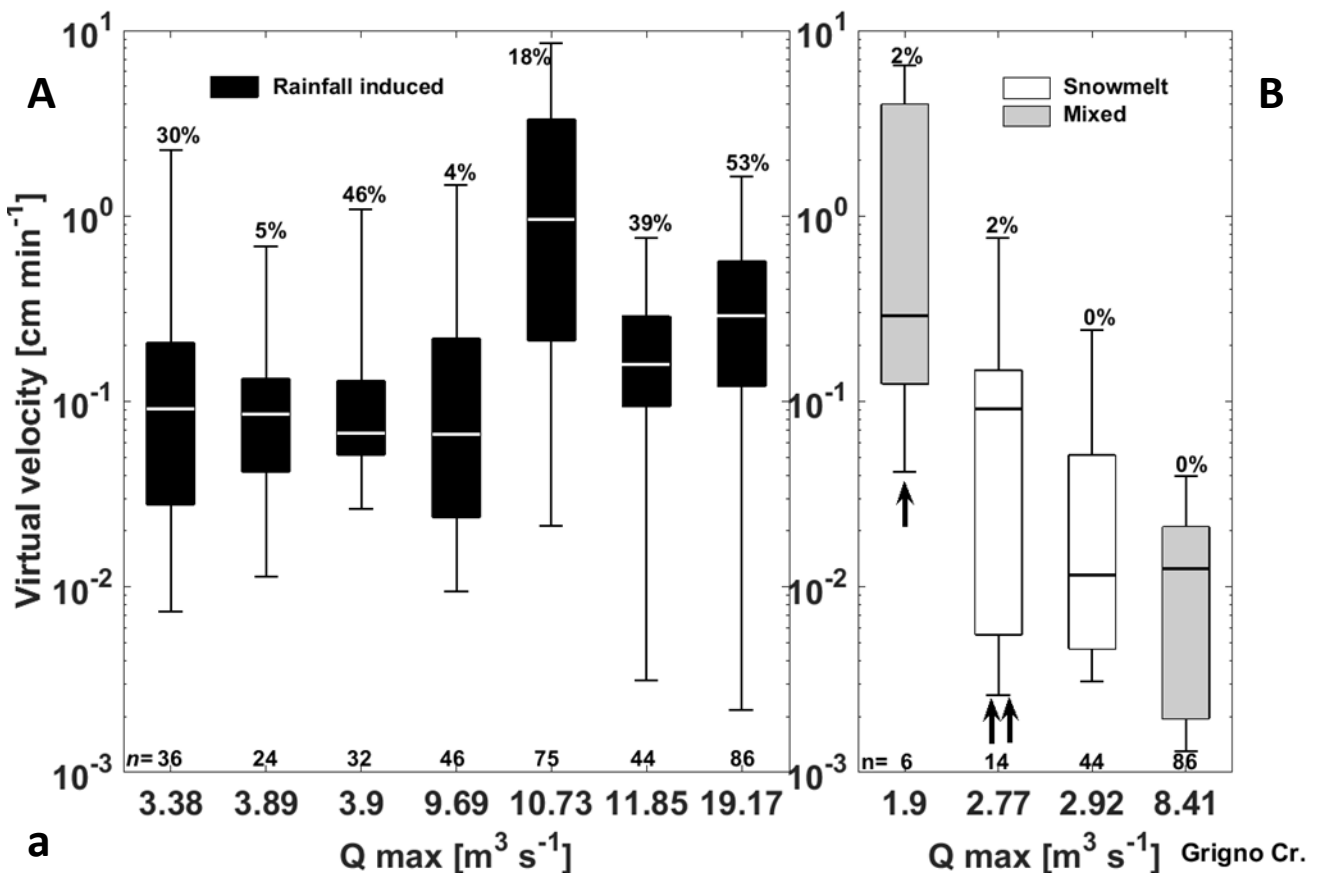


Figure 4.4.3. Box plots of the tracers' virtual velocities ordered by date in (a) Grigno, (b) Tolvà and (c) Ussaia Creek. (Black vertical arrows represent tracers' release and the percentages above the maximum whisker indicate the proportion of buried tracers, n= number of observations, Q indicates Q_{max}).

The same evaluations are corroborated if distribution of virtual velocities are plotted distinctly according to their hydrological input (Figure 4.4.4). At all the sites in fact, there are no distinct relations among peak discharge and virtual velocity. Specifically at Grigno Creek, rainfall induced events show median virtual velocities larger than 0.1 cm min^{-1} , whereas at Ussaia Creek some hints of increasing relation appear for Q_{max} larger than $0.57 \text{ m}^3 \text{ s}^{-1}$.

Cumulatively from the shown distribution is possible to understand how the enhanced mobility of clasts at Ussaia Creek, makes the relation among virtual velocities and peak discharge very unclear, with also the smaller events (e.g., $Q_{\text{max}} = 0.17 \text{ m}^3 \text{ s}^{-1}$) able to impose median velocities comparable to those of larger events.

The large number of snowmelt or mixed type events at Ussaia Creek is a clear indicator of the ability of this stream to transport even with peak discharge lower than those recorded at Grigno and Tolva creeks.



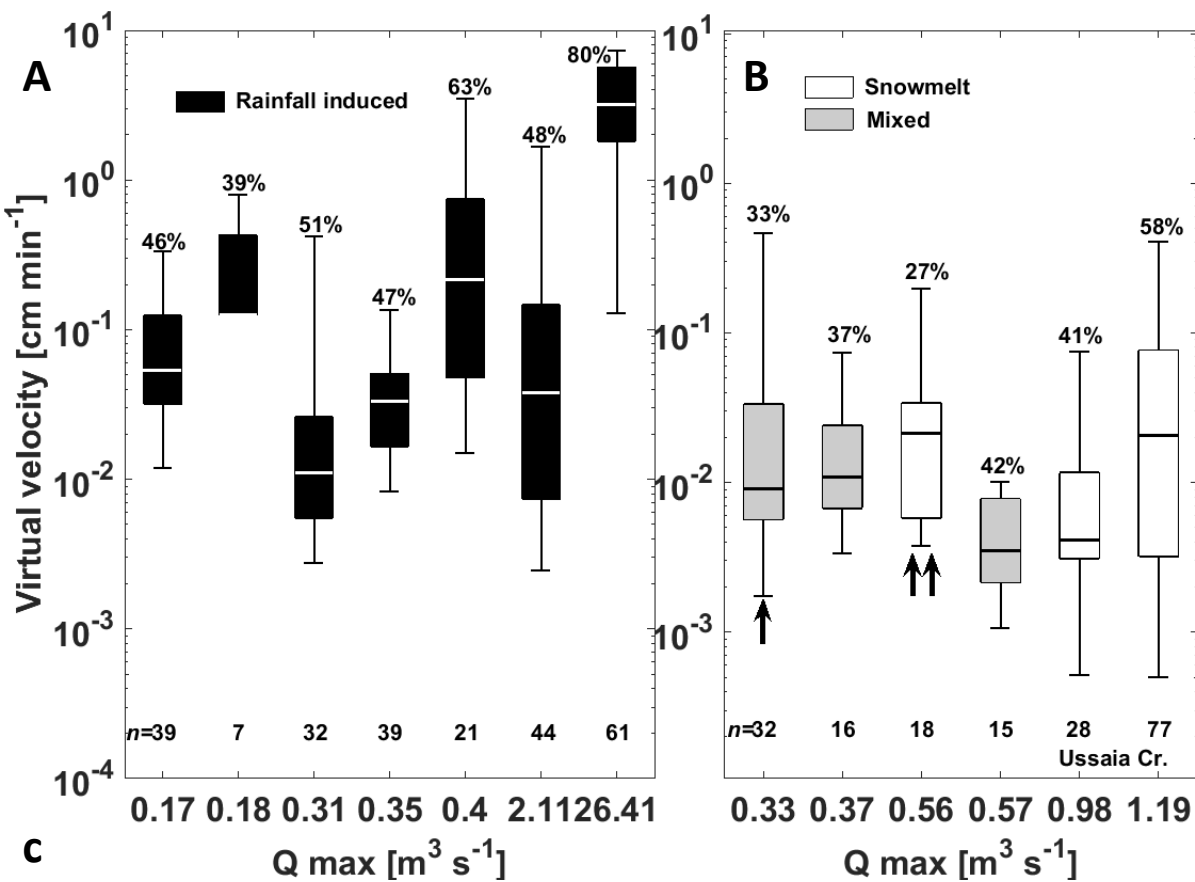
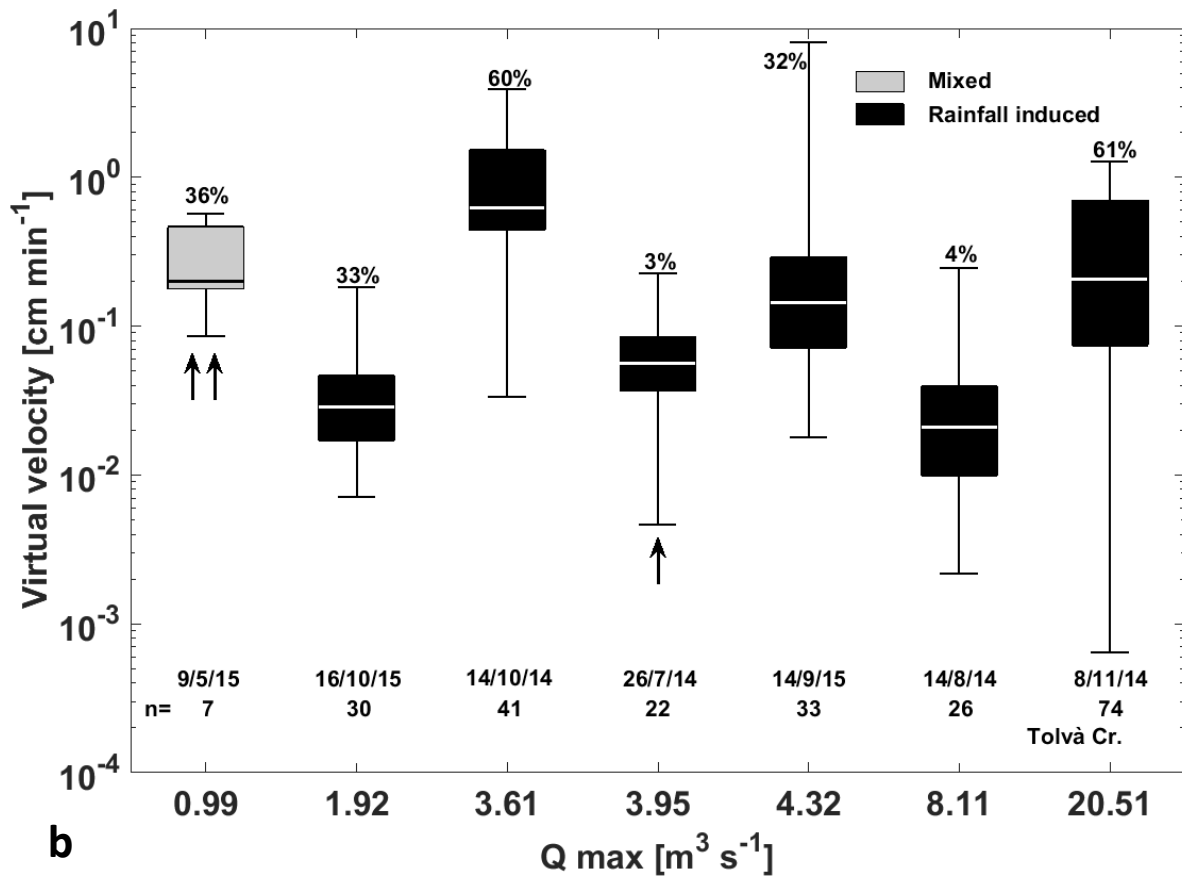


Figure 4.4.4. Box plots of the tracers' virtual velocities divided by hydrological forcing at a) Grigno, b) Tolva and c) Ussaia Creek (panel (A) rainfall, panel (B) snowmelt and mixed). At Ussaia Creek the debris flow ($Q_{max} = 26.41 \text{ m}^3 \text{ s}^{-1}$) event is in black, since triggered by a rainfall event. Black vertical arrows represent tracers'

release and the percentages above the maximum whisker indicate the proportion of buried tracers, n= number of observations).

In order to gain further insights into the effects that hydro-meteorological forcing can exert on bedload sediment transport, virtual velocities of single tracers were plotted – for selected inter-survey periods – as a function of their weight. The events are selected on the base of comparable inter-survey periods, so that we contrast the effects of snowmelt (i.e. springtime 2014), mixed (i.e. early summer 2014 and springtime 2015) and rainfall events (i.e. summer 2014) on tracers’ virtual velocity in Grigno, Tolvà and Ussaia Creek.

Starting from snowmelt events (Figure 4.4.5), we observe that at Tolvà Creek are missing events attaining statistical significance, therefore we compare only Grigno and Ussaia Creek, selecting the same snowmelt event of April 30th 2014. Considering the interval 22nd -26th April, daily temperatures recorded at Malga Sorgazza increased from 10 to 14.5 °C within five consecutive days (cf. Figure 4.2.3, the second black arrow from the left points to the considered snowmelt event), and Q_{max} reached values up to 2.78 m³ s⁻¹. At Mezzana meteorological station, the atmospheric daily temperatures reached peak values comprised between 16 and 21 °C in the same interval. Water discharge at Ussaia Creek reached $Q_{max} = 0.98$ m³ s⁻¹ (cf. Figure 4.2.9, the first black arrow from the left points to the considered snowmelt event).

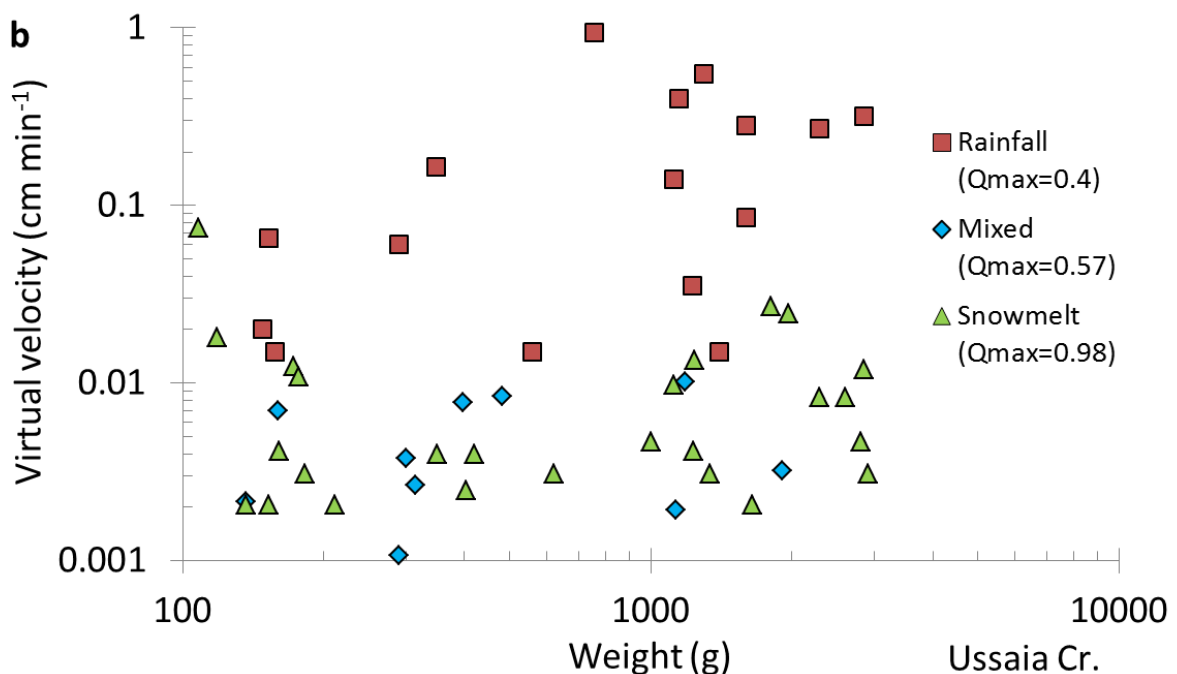
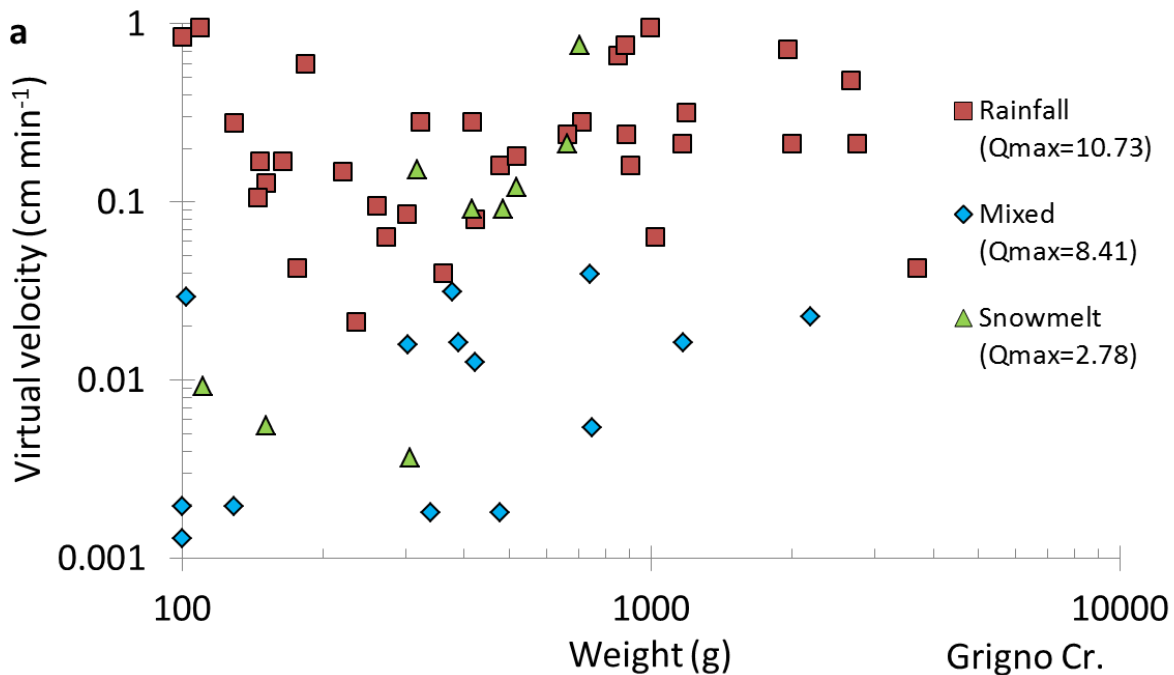


Figure 4.4.5. Examples of tracers' virtual velocities as a function of weight drawn from three selected events at: (a) the Grigno Creek; and (b) the Ussaia Creek. Red squares correspond to rainfall-related velocities, green triangles to snowmelt-induced velocities, and blue diamonds to mixed events.

The mixed type event has been characterized by regular fluctuations of daily temperatures at Malga Sorgazza, with values oscillating between 7.5 and 16 °C in the period comprised between June 26th and 30th. The precipitation event is characterized by 63 mm of accumulated rainfall in 19 hours, with a maximum intensity of 14.6 mm/h. At Grigno Creek, Q_{max} reached values up to 8.41 m³ s⁻¹. At Mezzana daily temperatures fluctuated between 7 and 23 °C, and by June 29th a precipitation of 21 hours generated 30 mm of rainfall accumulation, with a maximum intensity of 5 mm/h. At Ussaia Creek we recorded Q_{max} equal to 0.57 m³ s⁻¹. The rainfall event of August 18th 2014 occurred synchronously at all the sites, and its characteristics will be illustrated to introduce the dedicated plot. For the considered events There are no hints of weight selection. At Grigno Creek the rainfall event imposes a distribution of virtual velocities comprised between 0.03 and 1 cm min⁻¹, in agreement with what is observed at Ussaia Creek. At both sites the distribution of virtual velocities for snowmelt and mixed events overlap, but in the case of Grigno Creek snowmelt events share maximum velocities comparable with rainfall-related events, whereas at Ussaia Creek snowmelt and mixed events show lower velocities compared to rainfall.

Considering Tolvà Creek, we did not record snowmelt events attaining statistical significance, and we recorded only one mixed-type event where 7 clasts moved, by May 9th 2015. Keeping in mind the poor statistical reliability of the low number of observations for the mixed type event, the impact that this kind of event and rainfall events exert on Tolvà Creek is compared in Figure 4.4.6.

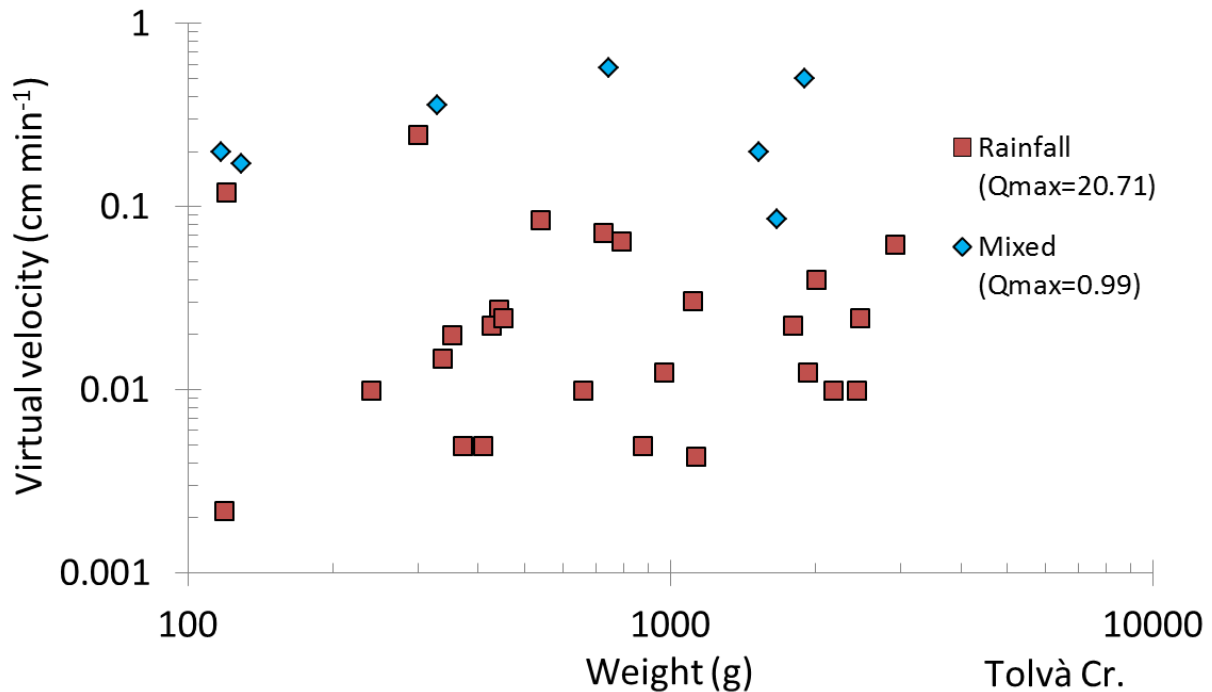
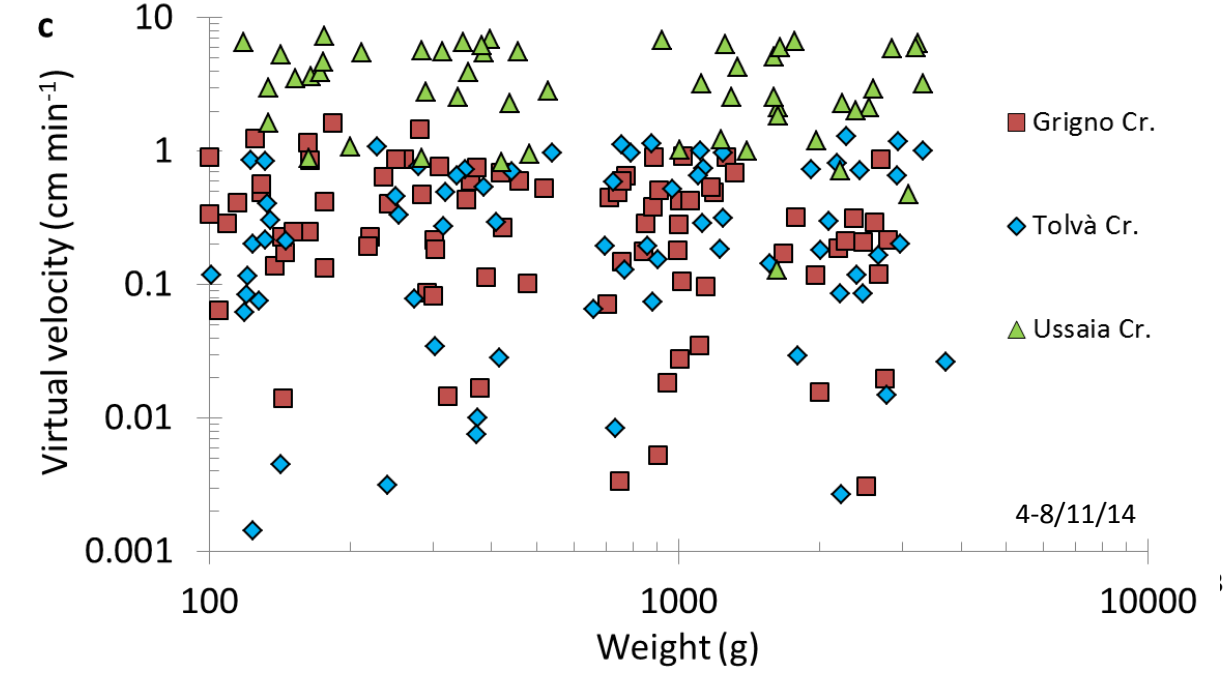
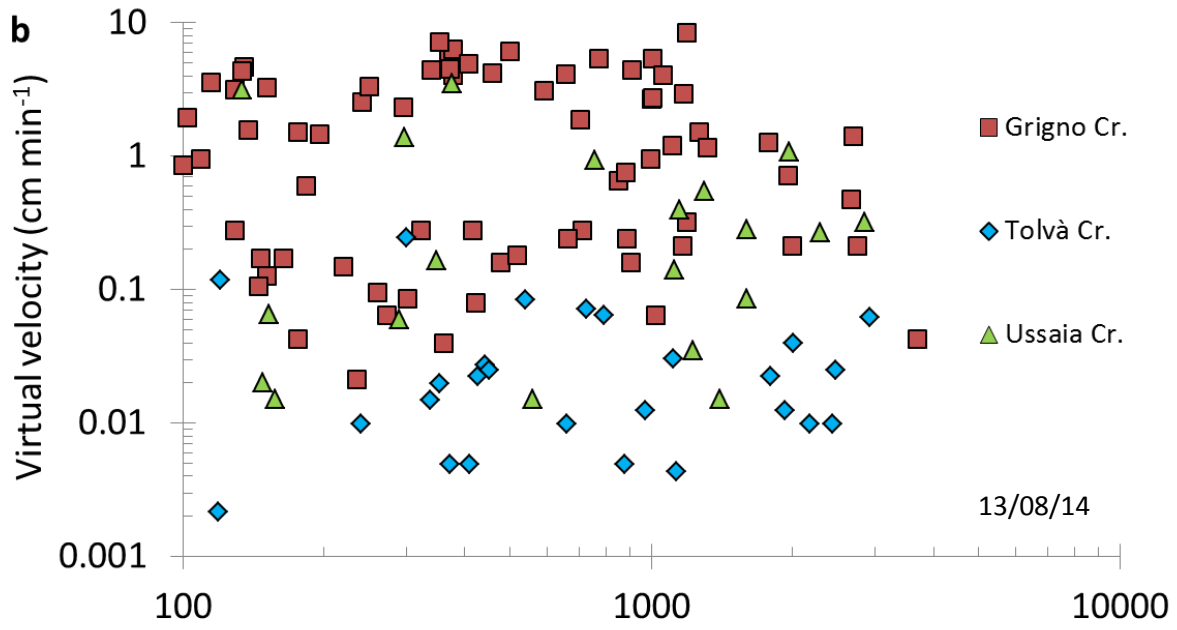
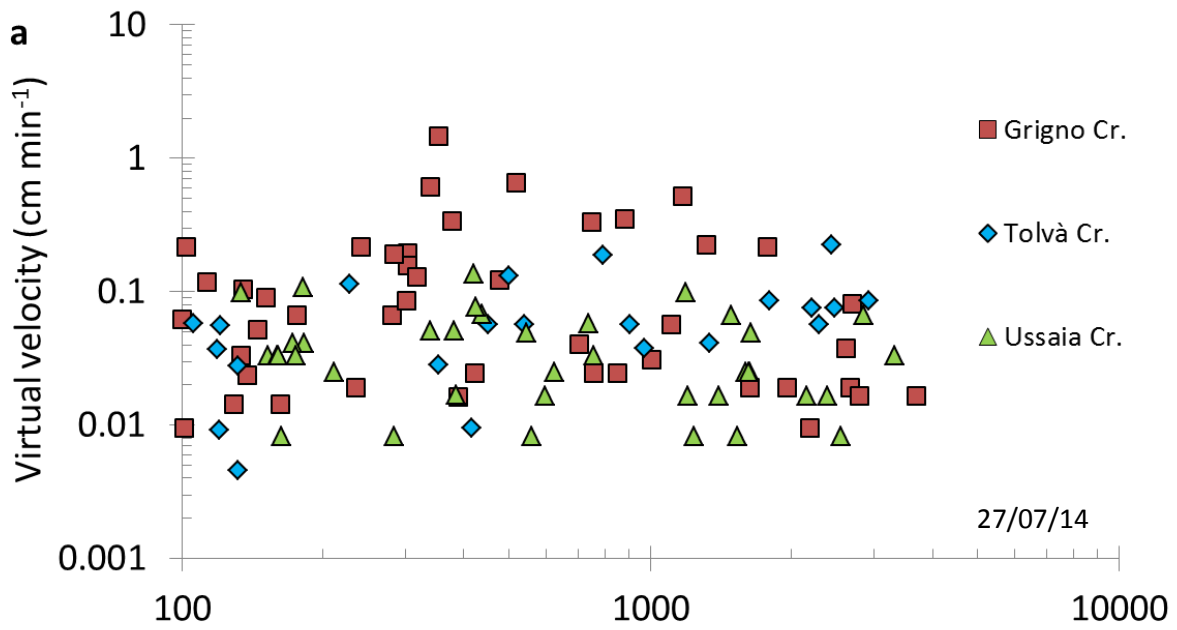


Figure 4.4.6. Examples of tracers' virtual velocities as a function of weight drawn from three selected events at Tolvà Creek. Red squares correspond to rainfall-related velocities and blue diamonds to mixed events. Snowmelt-related events are not recorded.



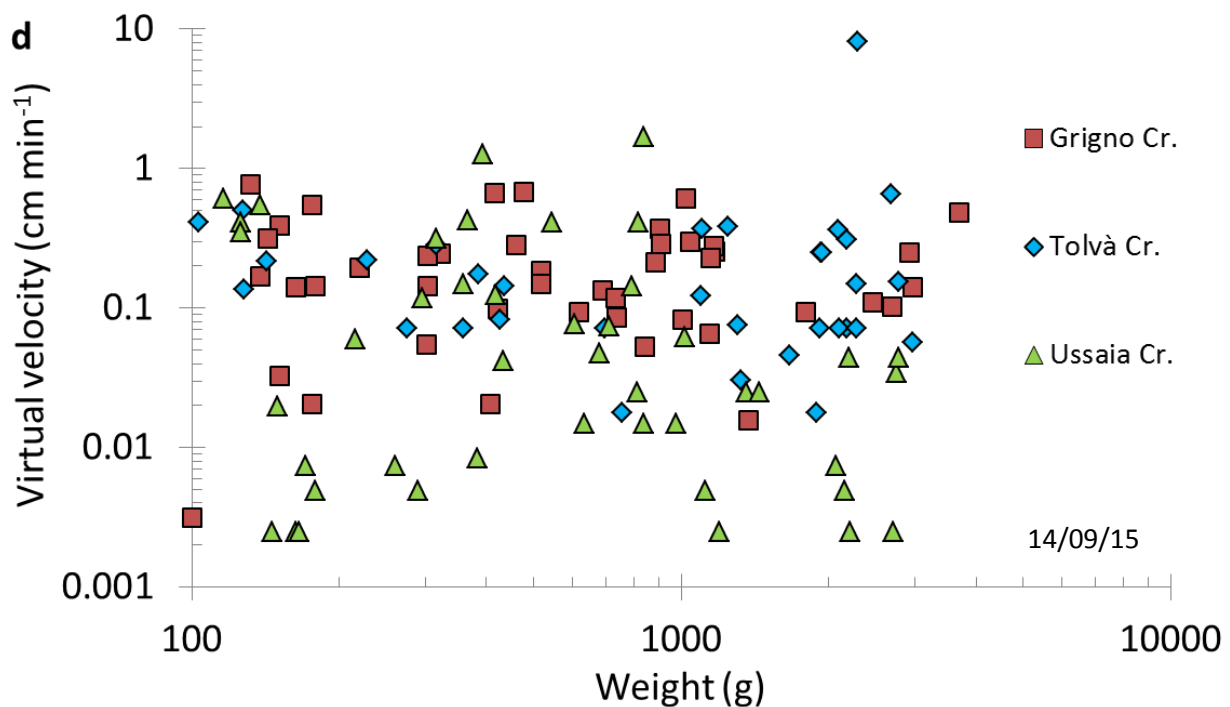


Figure 4.4.7. Tracers' virtual velocities as a function of weight for precipitation events of a) July 27th 2014, b) August 13th 2014, c) November 4th -8th 2014 and d) September 19th 2015 at all the monitoring sites.

In this case the mixed-type event impose higher virtual velocities than the rainfall event of August 13th 2014, in disagreement with which is observed at the other sites. This is determined by unusually high virtual velocities related to mixed event, larger than 0.1 cm min^{-1} , and by velocities (maximum value limited to 0.25 cm min^{-1}) imparted by rainfall event smaller in comparison to what observed at the other two sites. Also at Tolvà Creek, no hints of weight-selectivity are noted for the considered events.

When considering simultaneous events recorded at all the monitoring sites, we directly compare the effects of hydro-meteorological forcing on the virtual velocities of tracers (Figure 4.4.7). The characteristics of meteorological events considered are reported in Table 4.3.2 (event of July 27th 2014), Table 4.3.3 (event of August 13th 2014), Table 4.3.5 (event of November 4th -8th 2014) and Table 4.3.7 (event of September 19th 2015).

The event of July 27th 2014 is a summer front of moderate intensity and cumulated rainfall. Virtual velocities for this event show no dependency from weight, as all the other selected events. Velocities assessed at each of the monitored sites do not show peculiar signatures; at Tolvà and Ussaia Creek virtual velocities show an upper limit of 0.2 cm min^{-1} , whereas at Grigno Creek they are extended to 1 cm min^{-1} (Figure 4.4.7a).

The event of August 13th 2014 is a high-intensity summer front, with maximum intensity at Passo Brocon equal to 26.6 mm/h (cf. Table 4.3.3). In this case tracers' virtual velocities recorded at Grigno Creek are larger compared to the other sites (Figure 4.4.7b), with velocities up to 10 cm min^{-1} . At Tolvà Creek, despite the larger meteorological input, the Q_{max} is $8.11 \text{ m}^3 \text{ s}^{-1}$, lower than Grigno Creek and velocities are maximum 0.25 cm min^{-1} . Virtual velocities at Ussaia Creek are spread in the interval $0.01 - 5 \text{ cm min}^{-1}$.

The largest event recorded is an autumn front that hit the monitored sites from November 4th to 8th 2014, with large values of accumulated rainfall (up to 380 mm at Passo Brocon, 160 mm at Mezzana, cf. Table 4.3.5), and also large maximum intensities. For this event there is a clear segregation of the Ussaia Creek virtual velocities (Figure 4.4.7c), ranging in the interval 0.8-10 cm min⁻¹, denoting the high transport capacity characterizing the debris flow. As a matter of fact, values of 10 cm min⁻¹ have been recorded at Grigno Creek, but for that event the distribution is spread. Grigno and Tolvà Creek share similar distribution of velocities, ranging up to 1.6 cm min⁻¹.

The only comparable rainfall event of 2015 occurred in September 19th (Figure 4.4.7d). As for the event of July 27th 2014, there are not peculiar features in the distribution of virtual velocities across the three sites. Virtual velocities recorded at Ussaia Creek exhibit larger maximum values (1.68 cm min⁻¹), whereas for the two sites located in Valsugana, velocities are generally lower with values of 0.77 cm min⁻¹ recorded at Grigno Creek.

Strimm Creek

At Strimm Creek we applied the same procedures illustrated for the other sites to determine the entrainment threshold discharge, based on seasonal surveys. For every survey at least two weight classes moved, so that all peak discharges are associated to clast motion (Table 4.4.8). We found that discharges > 0.32 m³ s⁻¹ are able to mobilize clasts from any weight classes (Figure 4.4.9).

Table 4.4.8. Event dates and peak discharge for which clasts displacement has been observed at Strimm Creek.

Strimm Creek	Q_{\max} [m ³ s ⁻¹]	Mobilized classes
28/09/2011	0.36	W2, W3, W5
14/06/2012	0.66	W1 to W6
03/07/2012	0.55	W1, W2
11/09/2012	0.33	W1 to W5
04/10/2012	0.32	W1 to W3
27/06/2013	1.13	W1 to W6
01/10/2013	0.72	W1 to W6
13/06/2014	0.95	W1 to W6

02/10/2014	0.32	W1 to W6
12/06/2015	1.20	W1 to W6
09/10/2015	0.82	W1 to W6

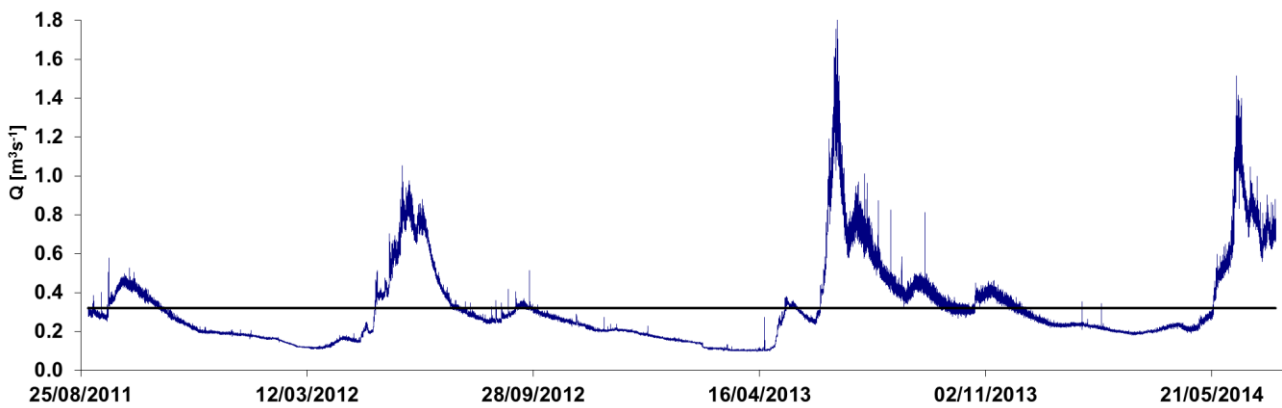


Figure 4.4.8. Entrainment threshold discharges (black horizontal line) at Strimm Creek (from Dell’Agnese et al., 2015).

Table 4.4.9. Type of forcing input for bedload events and related virtual transport duration at Strimm Creek.

Event date	Type	Q_{max} [$m^3 s^{-1}$]	Inter-survey length [days]	Virtual transport duration [min]
28/09/2011	Rain	0.36	28	60
14/06/2012	Snowmelt	0.66	260	29570
03/07/2012	Snowmelt	0.55	19	27060
11/09/2012	Rain	0.33	70	130
04/10/2012	Rain	0.32	23	10
27/06/2013	Snowmelt	1.13	266	20890

01/10/2013	Mixed	0.72	96	52370
13/06/2014	Snowmelt	0.95	255	22220
02/10/2014	Rain	0.32	111	10
12/06/2015	Snowmelt	1.20	253	19890
09/10/2015	Rain	1.82	119	44650

At Upper Strimm Creek, the box plots of virtual velocities as a function of inter-survey peak discharge (Figure 4.4.9, from Dell’Agnese et al., 2015) exhibit a markedly different behavior when considering rainfall-induced or snowmelt- and mixed-related events. Low flows ($Q_{\max} < 0.36 \text{ m}^3 \text{ s}^{-1}$) are generated by rainfall events, exhibiting peaked and restricted in time storm hydrographs. The hydrological impact of snowmelt, conversely, is characterized by a remarkable duration and generates floods with $Q_{\max} > 0.36 \text{ m}^3 \text{ s}^{-1}$. For events recorded after rainfall events in fact, velocities are comprised within 0.1 and 10 cm min^{-1} . Virtual durations evaluated for snowmelt events are generally larger than 19890 minutes (Table 4.4.8), and reach values up to 52370 for the mixed-type event and therefore the velocities are comprised within 0.001 and 0.1 cm min^{-1} . For events related to snowmelt we observe that the median of velocities varies gradually with peak flow, a feature that is clearly not recognizable for rainfall-induced events, where velocities are scattered by one order of magnitude despite similar peak discharges.

Also at this site, to gain further insights into the effects that hydro-meteorological forcing can exert on bedload sediment transport, virtual velocities of single tracers are plotted as a function of their weight for selected inter-survey periods (Figure 4.4.10).

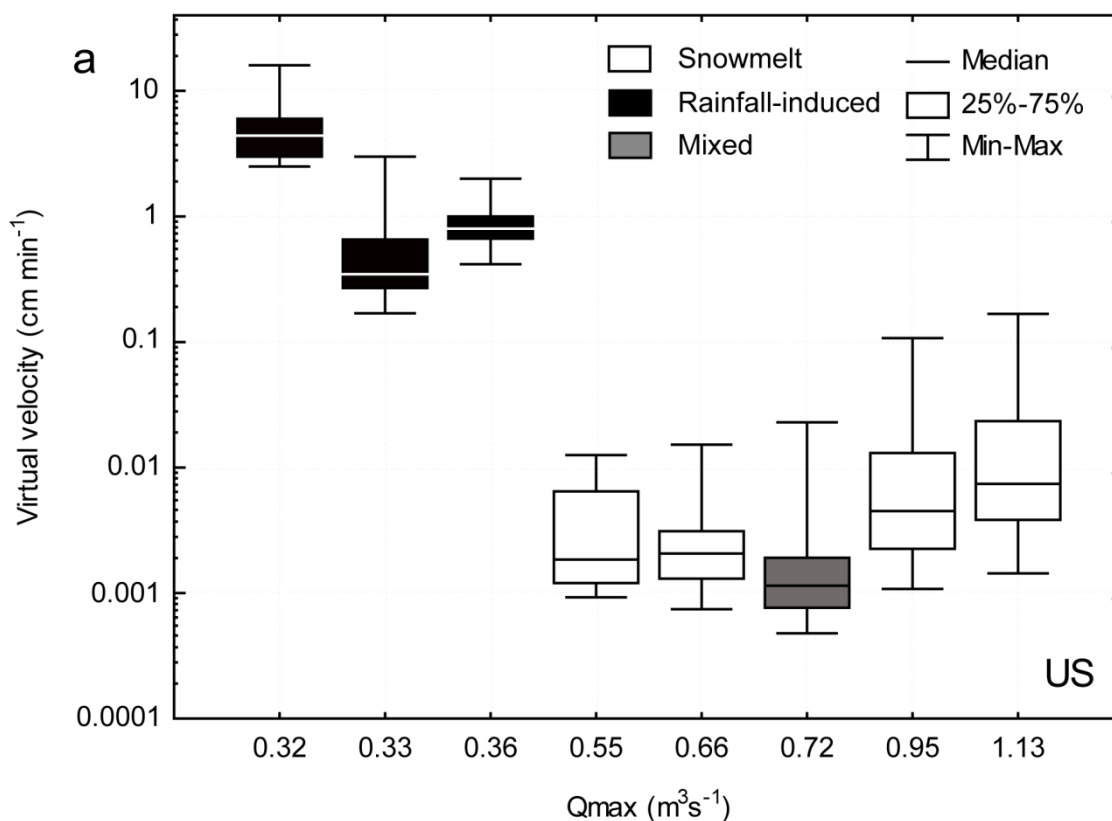


Figure 4.4.9. Box plots of the tracers' virtual velocities in relation to corresponding inter-survey peak discharge (Q_{max}) in Strimm Creek. The flow regime of inter-survey periods is classified into snowmelt, rainfall-induced and mixed. Mixed periods represent a combination of the first two and typically correspond to the snowmelt falling limb (from Dell'Agnese et al., 2015).

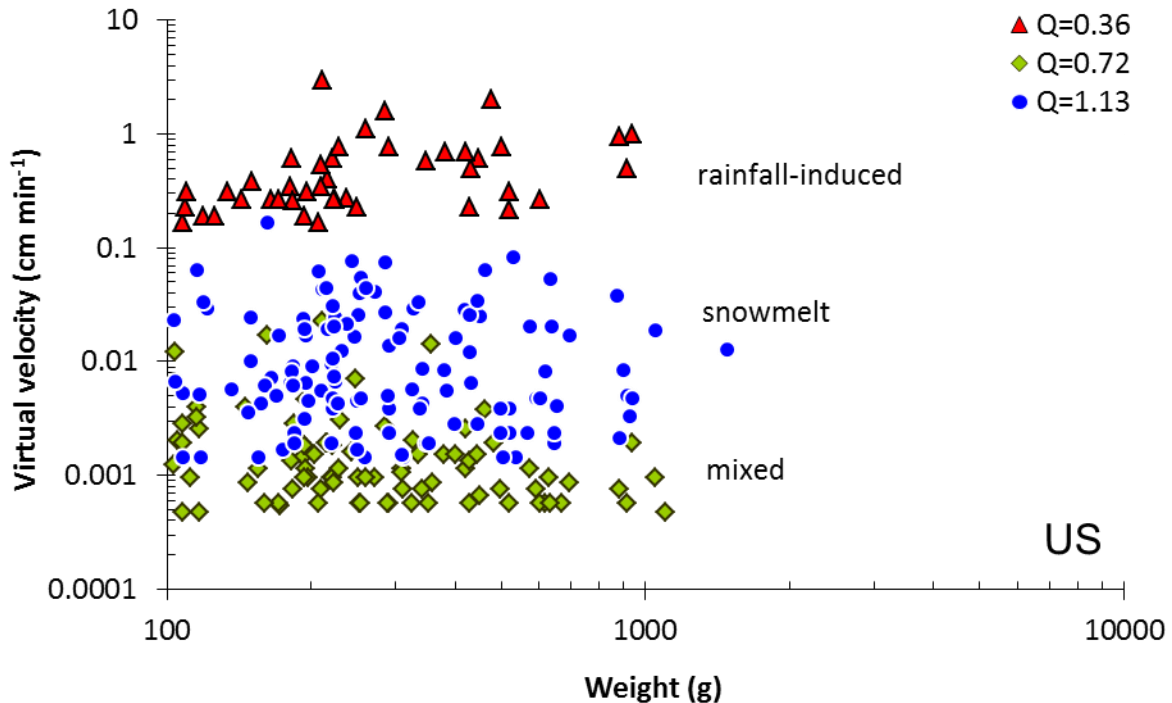


Figure 4.4.10. Tracers' virtual velocities as a function of weight for three selected peak discharges in Upper Strimm. Red triangles refer to rainfall-induced velocities (i.e. summer-fall 2012), blue circles to snowmelt-related velocities (i.e. spring-summer 2013), and green diamonds to mixed snowmelt-rainfall periods. Note that tracers' virtual velocities are independent from weight (from Dell'Agnese et al., 2015).

At this site there is an evident stratification on the virtual velocities imparted at tracers, by different type of forcings. Rainfall-induced events are capable to impart velocities comprised within 0.15 and 3 cm min⁻¹. Virtual velocities associated to snowmelt events are generally below 0.1 cm min⁻¹ but larger than 0.001 cm min⁻¹, and mixed type events are imparting the slower velocities to tracers, with the vast majority of velocities below 0.001 cm min⁻¹. No relations are observed between weight and virtual velocities, with the exception of rainfall-induced events where heavier clasts seem to travel faster compared to lighter tracers.

4.5 Distribution of travel distances and virtual velocities of tracers

4.5.1 Distribution of tracers' travel distances

The displacement length of each tracer when divided by the duration above threshold discharge determines its calculated virtual velocity. Since the net volume (or weight) of bedload transfer for a given tracer weight (or caliber) class is customarily calculated using the mean virtual velocity of that population of tracers (Liébault and Laronne, 2008; Dell'Agnese et al., 2015). However, are the virtual velocities of our tracer clasts normally distributed? And therefore, is the mean a good statistical descriptor of tracer virtual velocities? To answer these questions, we examine the frequency distributions of tracer travel distances and virtual velocities.

Table 4.5.1. Number of observations, mean and median travel distances , peak discharge and maximum rainfall intensity at Grigno Creek for each survey.

Date	Number of seeded clasts	Number of mobilized clasts	Mean travel distance [cm]	Median travel distance [cm]	Q max [$\text{m}^3 \text{s}^{-1}$]	Max rainfall intensity [mm h^{-1}]
08/04/2014	111	4	40	50	2.77	3.8
30/04/2014	111	14	63.3	40	2.77	4.8
11/05/2014	111	14	54.6	35	2.92	7.6
24/06/2014	111	15	139.1	90	8.41	14.6
9/07/2014	111	24	152.3	85	3.89	9.8
22/07/2014	111	46	266.3	140	9.69	17.4
14/08/2014	130	75	701.3	450	10.73	17.8
14/10/2014	130	36	40.5	19.5	3.38	9.4
8/11/2014	130	86	2402.2	1877.5	19.17	16.4
08/05/2015	162	6	224.2	35	1.9	6.6
20/05/2015	162	4	38.3	50	3.38	12.4
23/06/2015	162	2	30	30	4.07	10.8
14/09/2015	162	44	133.84	95.5	11.85	11

16/10/2015	162	32	78.34	45.5	3.89	6.4
------------	-----	----	-------	------	------	-----

Table 4.5.2. Number of observations, mean and median travel distances, peak discharge and maximum rainfall intensity at Tolva Creek for each survey.

Date	Number of seeded clasts	Number of mobilized clasts	Mean travel distance [cm]	Median travel distance [cm]	Q max [$\text{m}^3 \text{s}^{-1}$]	Max rainfall intensity [mm h^{-1}]
26/07/2014	98	21	53.9	42.5	3.95	13.6
13/08/2014	98	24	90.2	42.5	8.1	26.6
13/10/2014	98	16	155.9	90	1.32	13.4
8/11/2014	98	72	6838.9	3700	20.51	17.8
15/04/2015	150	9	40.75	50	0.38	0 (snow)
9/05/2015	150	7	47.1	40	1	8.2
20/05/2015	150	4	43.75	37.5	1.07	7.2
14/09/2015	150	33	122.2	42	4.32	11.8
16/10/2015	150	30	102.9	75	1.92	9.8

Table 4.5.3. Number of observations, mean and median travel distances , peak discharge and maximum rainfall intensity at Ussaia Creek for each survey.

Date	Number of seeded clasts	Number of mobilized clasts	Mean travel distance [cm]	Median travel distance [cm]	Q max [$\text{m}^3 \text{s}^{-1}$]	Max rainfall intensity [mm h^{-1}]
29/04/2014	111	18	161.4	110	0.57	4.80
06/05/2014	111	28	99.5	42.5	0.98	3.8
03/06/2014	111	77	2867.1	852	1.19	6
30/06/2014	111	15	96.7	70	0.57	5
11/07/2014	111	43	69.3	40	0.17	3.4
27/07/2014	111	39	41.4	30	0.35	6.4
18/08/2014	111	21	964.1	280	0.4	8.8
20/10/2014	111	17	1313.14	72.5	-	6.4

08/11/2014	111	61	18660	17565	26.41	7.4
19/05/2015	230	32	122.1	50	0.33	14.8
26/05/2015	230	16	39.1	22.5	0.37	7
18/06/2015	230	7	18.5	10	0.18	9.4
15/09/2015	230	44	308	60	2.1	5.4
25/09/2015	230	32	58.8	20	0.31	9.3
22/10/2015	230	4	40	42.5	0.32	4.2

Results (Tables 4.5.1-4.5.2-4.5.3) show that mean values of travel distances are larger than the median. As will be illustrated in the following panels, the distribution of travel distances is strongly left-skewed (Figure 4.5.1). As plotted in the histograms, travel distances lower than 20 cm (threshold of uncertainty of field data) were highlighted in red, to demonstrate how the shape of the distribution changes considering this threshold.

Comparing the same meteorological event of August 13, 2014 at the three sites (Figure 4.5.1), results are showing that the same event has been more efficient moving a large number of clasts at Grigno (n=75) and Tolvà Creek (n=24), than at Ussaia Creek (n=21), but at Grigno and Tolvà sites were recorded maximum travel distances larger than 50 m, whereas at Tolvà Creek maximum distances are lower than 10 m. The same happens to median travel distance, higher at Grigno Creek (4.5 m) than on the other two sites. The difference between mean and median values is consistent, being for example 964 cm (mean) and 280 cm (median), at Ussaia Creek. The difference is lower at the other two sites, but at Grigno Creek is 701 cm (mean) and 4.50 m (median), whereas at Tolvà site is 0.90 m (mean) and 0.425 m (median).

Event August 13, 2014

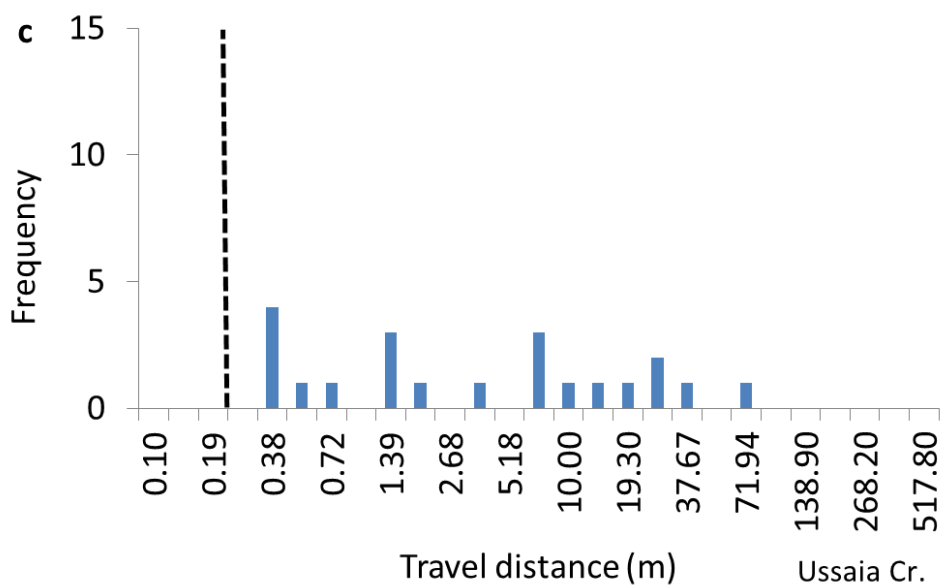
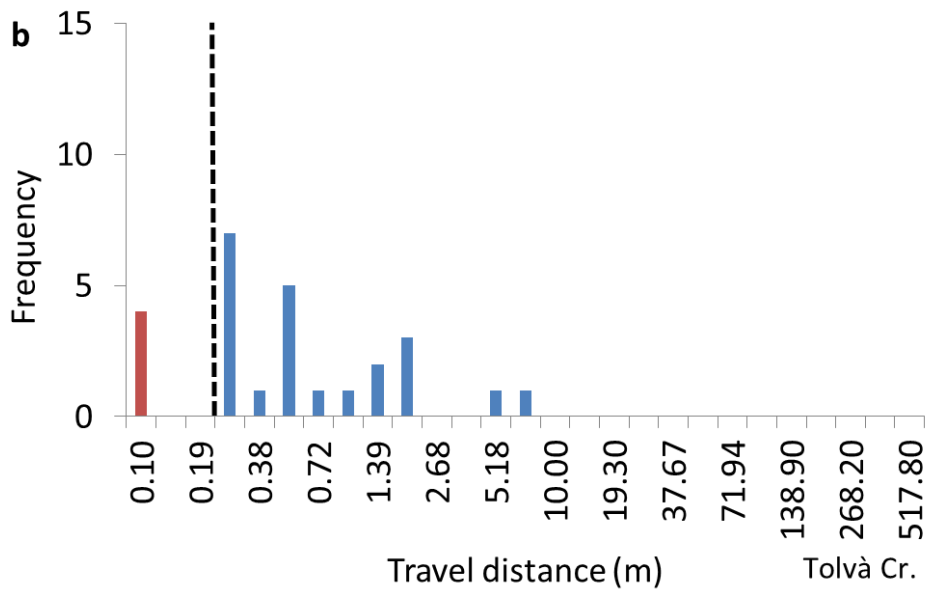
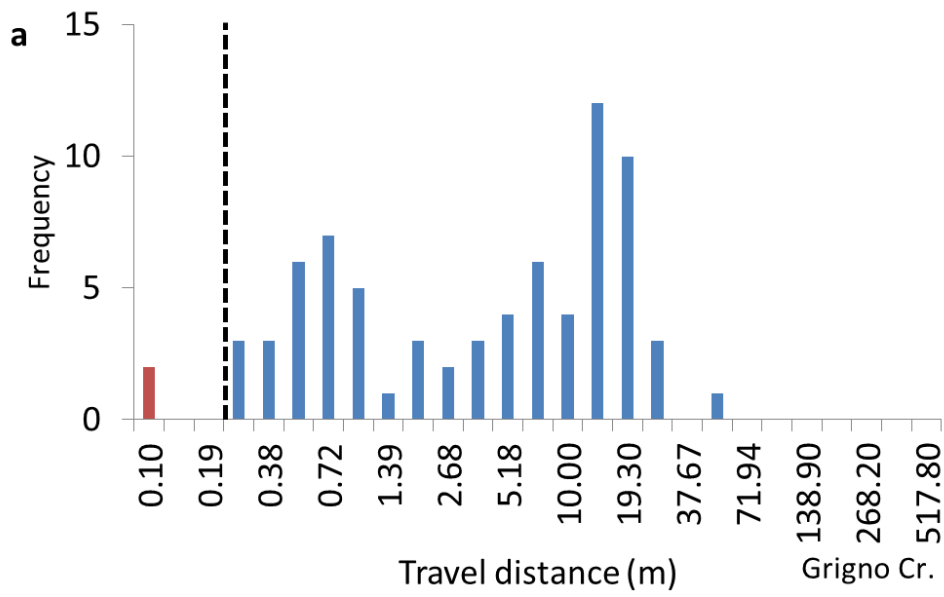
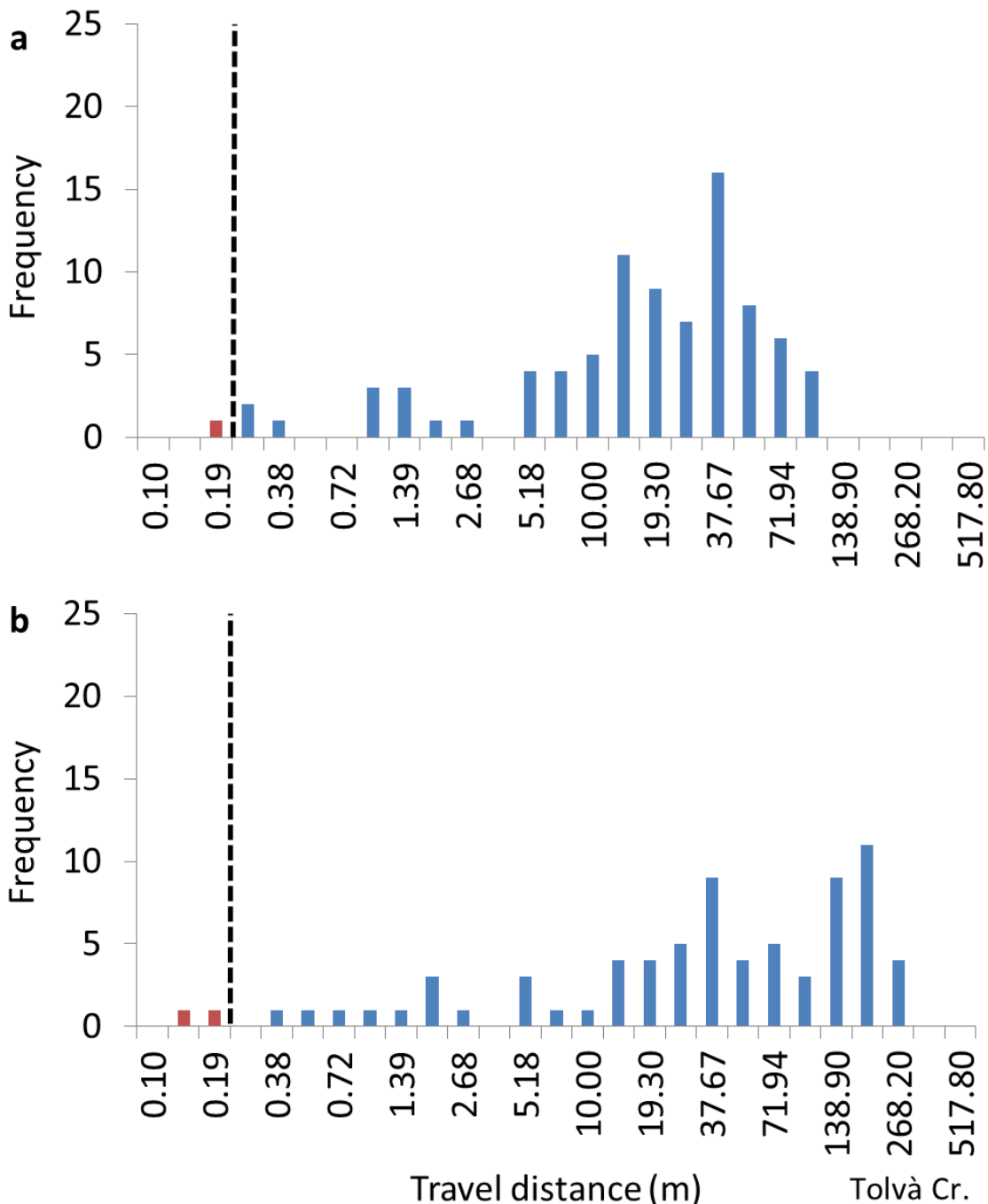


Figure 4.5.1. Histograms of tracer length displacement for the event of August 13th 2014 at a) Grigno, b) Tolvà and c) Ussaia Creek. Travel distances below the uncertainty threshold applied to field data are plotted as red bars. The black dashed line represents the threshold value of 0.2 m.

Event November 4-8, 2014

Considering the event of November 4th – 8th 2014, the number of mobilized clasts is very high (mobilized clasts n= 86 at Grigno Creek, n=72 at Tolvà Creek and n=61 at Ussaia Creek) at all the sites. The maximum travel distances were recorded at Ussaia site, with values larger than 300 m whereas at Tolvà Creek were below this limit (Figure 4.5.2). At Grigno Creek instead, values were lower than 100 m. Median are always lower than mean, remaining in the same order of magnitude. At Ussaia Creek the difference is limited (mean= 18660 cm, median=17565 cm) as well as calculated at Grigno Creek (mean= 2400 cm, median=1877 cm), but at Tolvà the mean is 6838 cm and the median 3700 cm.



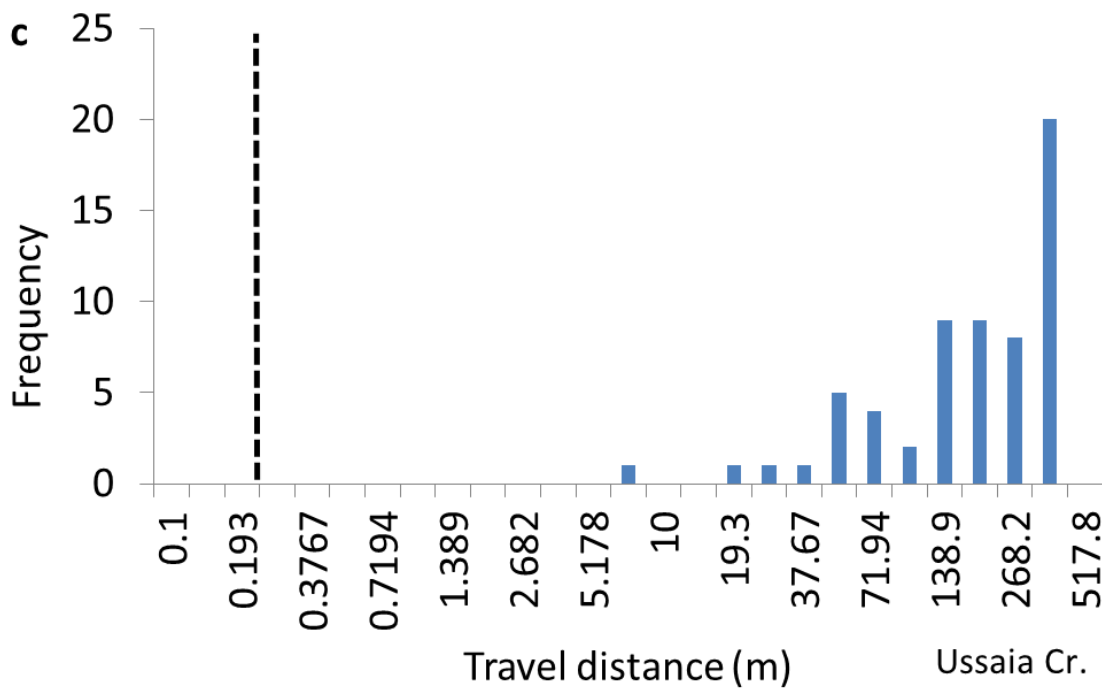


Figure 4.5.2. Histograms of tracer length displacement for the event of November 4th – 8th 2014 at a) Grigno, b) Tolvà and c) Ussaia Creek. Travel distances below the uncertainty threshold applied to field data are plotted as red bars. The black dashed line represents the threshold value of 0.2 m.

Results are clearly showing (Figure 4.5.3) that at each site, when considering the entire set of displacements, the distribution of tracers’ travel distances is not symmetrical. The maximum frequencies are registered for travel distances lower than 1.389 m in all the sites. Larger travel distances are more frequent at Ussaia Creek, where distances of 517.8 m are not present only because of the physical limit imposed by the confluence with the Noce River. Grigno and Tolvà creeks are not characterized by this constraint, and clasts are free to move downstream, but haven’t traveled such distances because of larger effects of hiding/protrusion imposed by roughness elements within the channel.

Considering the overall values of travel distances, differences are up to two orders of magnitude among the sites. At Grigno monitored site the mean is 7.3 m and the median is 1.1 m. At Tolvà and Ussaia sites, there are similar values of mean (24.5 m at Tolvà Creek, 32 m at Ussaia Creek) and identical values of median (0.9 m).

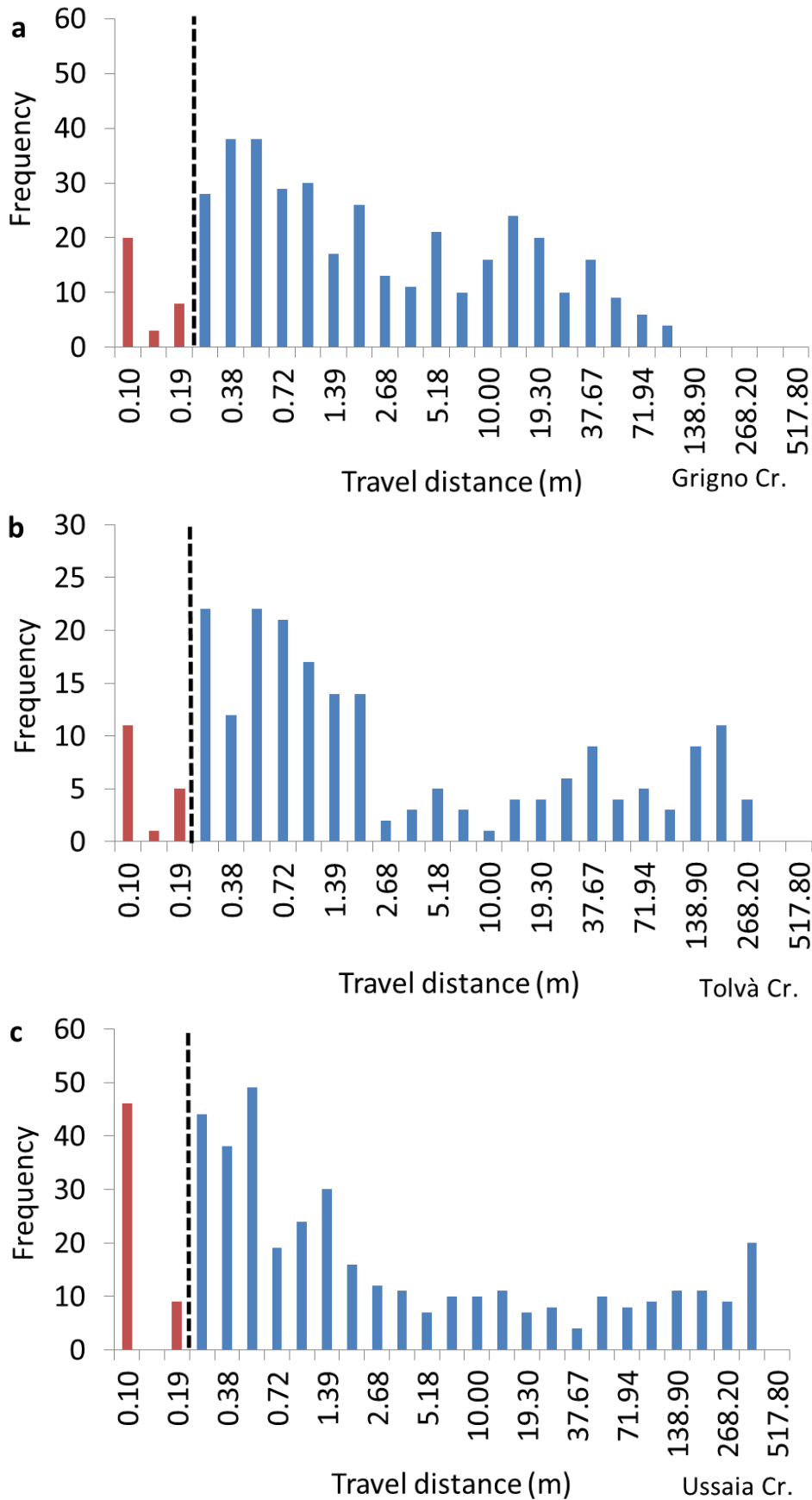


Figure 4.5.3. Histograms of tracer length displacement considering all the surveys at a) Grigno, b) Tolva and c) Ussaia Creek. Travel distances below the uncertainty threshold applied to field data are plotted as red bars. The black dashed line represents the threshold value of 0.2 m.

4.5.2 Distribution of tracers' virtual velocities

In this section are considered the distributions of the tracers' virtual velocities, introducing the mean and median values for two simultaneous events recorded on all the sites and then comparing the entire set of velocities for each site, highlighting the implications for the evaluation of the bedload transfer.

Table 4.5.4. Number of observations, mean and median tracers' virtual velocities, peak discharge and maximum rainfall intensity at Grigno Creek for each survey.

Date	Number of seeded clasts	Number of mobilized clasts	Mean virtual velocity [cm min⁻¹]	Median virtual velocity [cm min⁻¹]	Q max [m³ s⁻¹]	Max rainfall intensity [mm h⁻¹]
08/04/2014	111	4	0.06	0.01	2.77	3.8
30/04/2014	111	14	0.16	0.09	2.77	4.8
11/05/2014	111	14	0.04	0.01	2.92	7.6
24/06/2014	111	15	0.01	0.01	8.41	14.6
9/07/2014	111	24	0.14	0.09	3.89	9.8
22/07/2014	111	46	0.16	0.06	9.69	17.4
14/08/2014	130	75	1.93	0.96	10.73	17.8
14/10/2014	130	36	0.22	0.09	3.38	9.4
8/11/2014	130	86	0.39	0.29	19.17	16.4
08/05/2015	162	6	1.87	0.29	1.9	6.6
20/05/2015	162	4	0.05	0.06	3.38	12.4
23/06/2015	162	2	0.25	0.25	4.07	10.8
14/09/2015	162	44	0.22	0.16	11.85	11
16/10/2015	162	32	0.12	0.07	3.89	6.4

Table 4.5.5. Number of observations, mean and median tracers' virtual velocities, peak discharge and maximum rainfall intensity at Tolvà Creek for each survey.

Date	Number of seeded clasts	Number of mobilized clasts	Mean virtual velocity [cm min⁻¹]	Median virtual velocity [cm min⁻¹]	Q max [m³ s⁻¹]	Max rainfall intensity [mm h⁻¹]
-------------	--------------------------------	-----------------------------------	--	--	---	---

26/07/2014	98	21	0.07	0.06	3.95	13.6
13/08/2014	98	24	0.04	0.02	8.1	26.6
13/10/2014	98	16	1.15	0.63	1.32	13.4
8/11/2014	98	72	0.38	0.21	20.51	17.8
9/05/2015	150	7	0.30	0.2	1	8.2
20/05/2015	150	4	0.04	0.04	1.07	7.2
14/09/2015	150	33	0.42	0.14	4.32	11.8
16/10/2015	150	30	0.04	0.03	1.92	9.8

Table 4.5.6. Number of observations, mean and median tracers' virtual velocities, peak discharge and maximum rainfall intensity at Ussaia Creek for each survey.

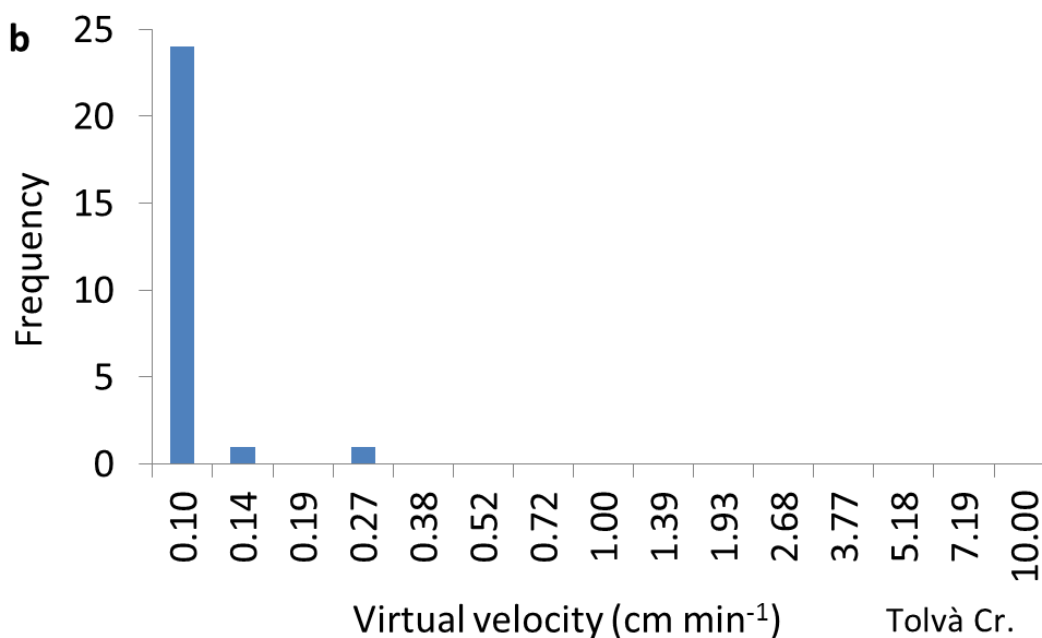
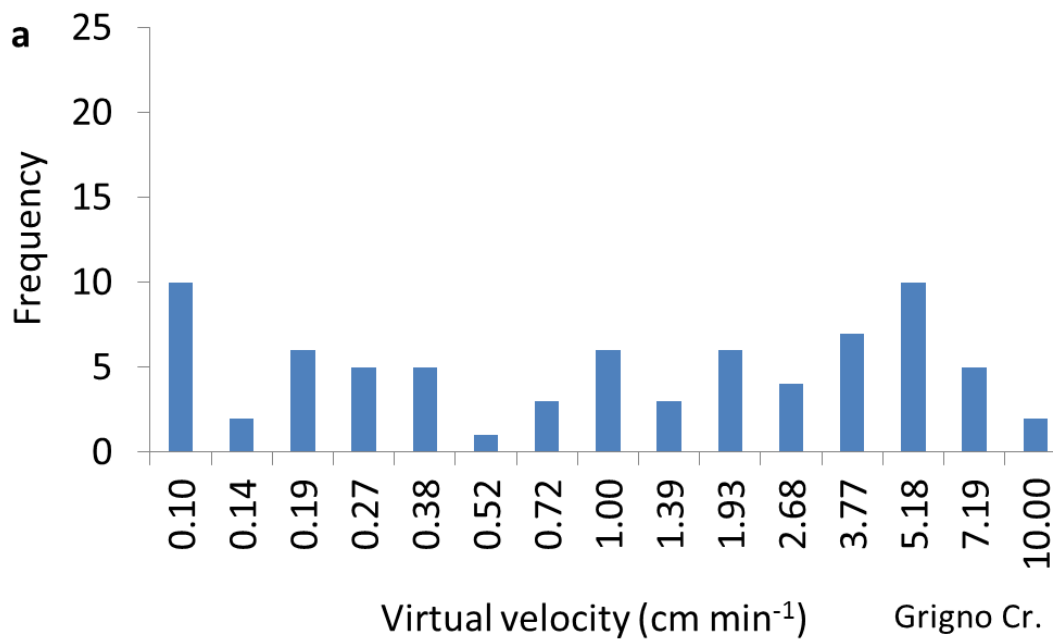
Date	Number of seeded clasts	Number of mobilized clasts	Mean virtual velocity [cm min ⁻¹]	Median virtual velocity [cm min ⁻¹]	Q max [m ³ s ⁻¹]	Max rainfall intensity [mm h ⁻¹]
29/04/2014	111	18	0.03	0.02	0.57	4.80
06/05/2014	111	28	0.01	0.004	0.98	3.8
03/06/2014	111	77	0.06	0.02	1.19	6
30/06/2014	111	15	0.005	0.003	0.57	5
11/07/2014	111	43	0.09	0.05	0.17	3.4
27/07/2014	111	39	0.04	0.03	0.35	6.4
18/08/2014	111	21	0.62	0.27	0.4	8.8
08/11/2014	111	61	3.59	3.20	26.41	7.4
19/05/2015	230	32	0.05	0.01	329	14.8
26/05/2015	230	16	0.02	0.01	367	7
18/06/2015	230	7	0.26	0.13	180	9.4
15/09/2015	230	44	0.17	0.04	2107	5.4

25/09/2015	230	32	0.04	0.01	306	9.3
22/10/2015	230	4	0.03	0.01	321	4.2

Results (Tables 4.5.4-4.5.5-4.5.6) show that the difference between mean and median values of virtual velocities ranges up to one order of magnitude.

Comparing the same meteorological event of August 13th 2014 at the three sites (Figure 4.5.4), results are showing that the event has imparted higher velocities at Grigno Creek, with values up to 10 cm min⁻¹. At Tolvà Creek the vast majority of the clasts traveled with a virtual velocity of 0.1 cm min⁻¹. The median of virtual velocities is higher at Grigno Creek (0.96 cm min⁻¹), than at Tolvà Creek (0.02 cm min⁻¹) and Ussaia Creek (0.21 cm min⁻¹). Also the mean is larger at Grigno Creek than in the other two sites, with a value of 1.9 cm min⁻¹, doubled if compared to the median; at Tolvà Creek the mean is 0.03 cm min⁻¹, whereas at Ussaia Creek the mean is three times the median.

Event August 13, 2014



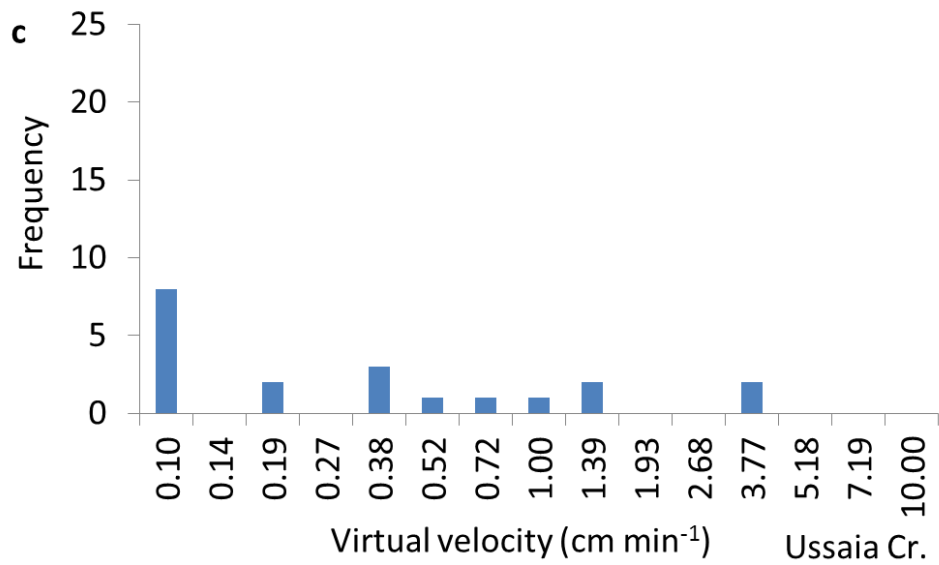


Figure 4.5.4. Histograms of virtual velocities calculated for the event of August 13th 2014 at a) Grigno, b) Tolvà and c) Ussaia Creek.

The hydro-meteorological event by November 4-8, 2014 imparted virtual velocities at Ussaia Creek larger than all the other sites (Figure 4.5.5). As a matter of fact, at Grigno and Tolvà Creek the majority of clasts shows virtual velocities of 0.1 cm min⁻¹, even if at Grigno Creek maximum values are larger than at Tolvà Creek. At Ussaia monitored site the values are comprised between 0.5 and 10 cm min⁻¹, and the majority of clasts traveled with virtual velocities of 7.194 cm min⁻¹.

Event November 4-8, 2014

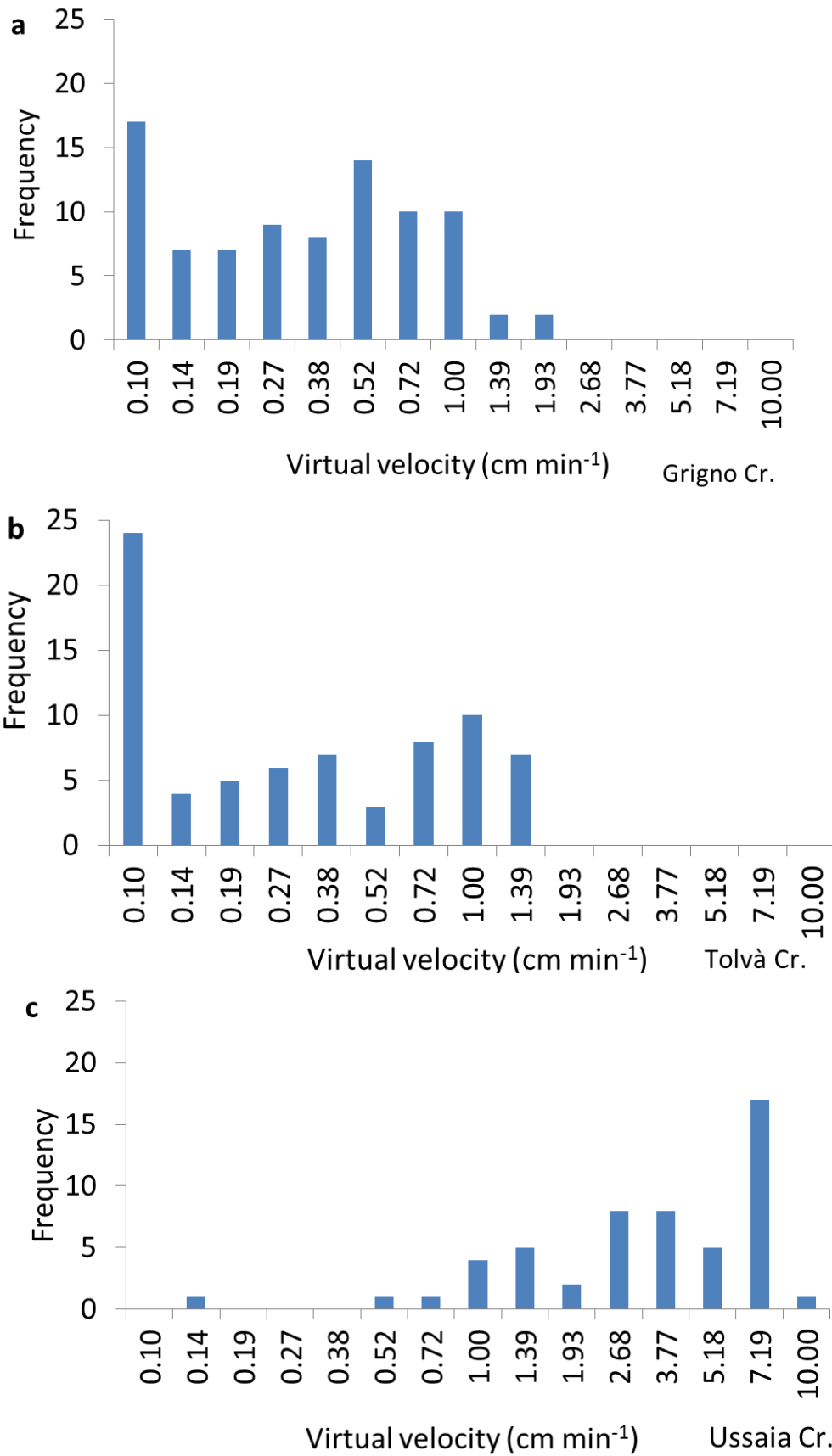


Figure 4.5.5. Histograms of virtual velocities calculated for the November 4-8, 2014 event at a) Grigno, b) Tolva and c) Ussaia Creek.

At event scale we observe that distributions are not normal, but are generally positively skewed. In particular the cases in which distributions are bi-modal are represented by virtual velocities calculated at Grigno Creek for the events of August 13th and 4th-8th November 2014, with values in both cases corresponding to the 0.1 and 5.18 cm min⁻¹. In the case of 4th-8th November 2014 event at Ussaia Creek, the distribution is negatively skewed, with the most represented value of 7.194 cm min⁻¹.

According to these observations, we suggest that for distributions analyzed in this work is more appropriate the evaluation of G by means of the median value, hence deploying values of virtual velocities smaller compared to the mean. The only cases in which we tend to overestimate the G deploying the median, are the negatively skewed cases already illustrated.

When considering all the virtual velocities, the distributions are not normal, resulting positively skewed similarly at each surveyed site (Figure 4.5.6). In all the sites the extent of the distribution of tracers' travel distances is comprised within 0.1 and 10 cm min⁻¹, but virtual velocities within 0.1 cm min⁻¹ represent the largest proportion for all the monitored creeks. At Grigno Creek represent the 41% and 68%, while at Tolvà and Ussaia Creek represent the 68% and 70% respectively. As previously illustrated in Figures 4.5.4-4.5.5 the contributions to virtual velocities larger than 0.1 cm min⁻¹ derive from events such those of August 13th, characterized by a flash flood, that triggered notable travel distances. For example at Grigno Creek the median distance is 4 m, and the maximum 40 m (cf. Figure 4.3.7), while at Ussaia Creek the median value is identical but the maximum distance is 80 m. In November 4th – 8th 2014, a prolonged floods imparted considerable travel distances, well represented by median values of about 20-30 m for the sites located in Valsugana, and 185 m for the Val di Sole site. The signature of debris flow effect is observed in the increase of frequency for the magnitude class of 7.194 cm min⁻¹ (Figure 4.5.6c).

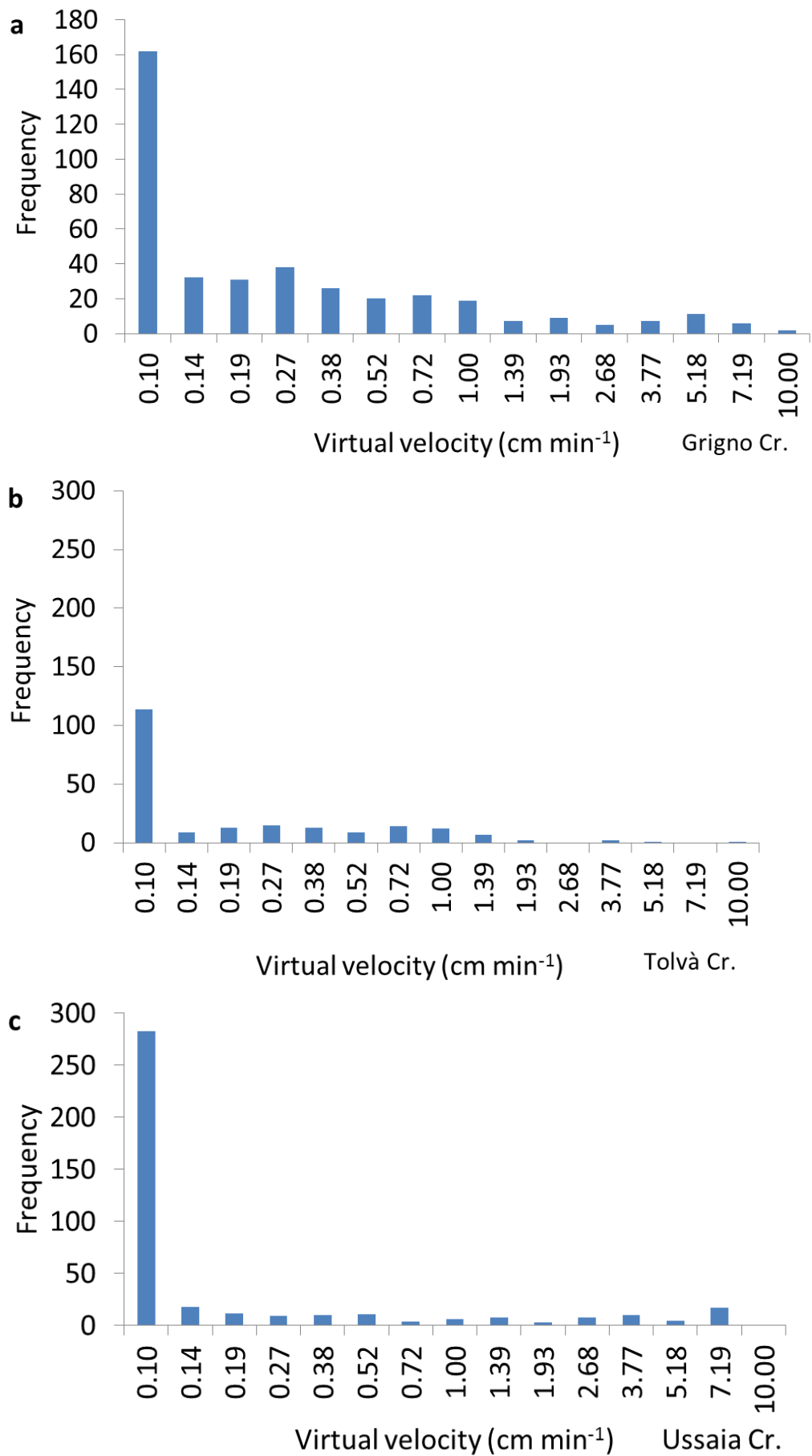


Figure 4.5.6. Histograms of virtual velocities calculated considering all the conducted surveys at a) Grigno, b) Tolv and c) Ussaia Creek.

4.6 Determination of active layer depth and active channel width

For the evaluation of G in the present work, the depth of the active layer is estimated based on digging tests performed at each site (Figure 4.6.1 and Table 4.6.1). The burial depth were at each site within the D_{50} of the surficial grain size distribution (Houbrechts et al., 2012). Therefore the values used in this thesis appear to be in agreement with those reported by literature on steep mountain streams, such as Schneider et al. (2014), which found that during ordinary events the thickness of the active layer ranges between 0.01 and 0.22 m. Moreover, Houbrechts et al. (2012) showed that the thickness of the active layer in mountain streams is typically lower than the D_{50} .





Figure 4.6.1. Digging tests conducted at a) Tolvà Creek, lateral deposit formed after the November 4th – 8th 2014 event (burial depth: 0.25 m); b) Grigno Creek, sediment deposited on the left bank of a plane bed reach (burial depth: 0.06 m); c) Ussaia Creek, the tracer is located where the main channel was flowing before the debris flow event of November 4th – 8th 2014, within the alluvial fan in correspondence of the confluence with the Noce River (burial depth: 0.19 m).

Table 4.6.1. Digging tests conducted on buried tracers for each site.

Site	Number of digging tests	Burial depth range (m)	Burial depth median (m)
Grigno Cr.	21	0.03-0.20	0.10
Tolvà Cr.	7	0.05-0.25	0.07
Ussaia Cr.	21	0.05-0.50	0.25

The methodology adopted to evaluate the active channel width to be inserted in the equation 3.5 was illustrated in section 3.7. The results presented in the Table 4.6.2 show that in the case of Grigno Creek the value obtained if considering full channel mobility is 5.7 m; isolating large boulders from the ortophotomap the active channel width reduces to 3.8 m. The Tolvà Creek is characterized by a narrower channel, and considering the full channel mobility the active width is 3.2 m. Conversely, selecting areas not characterized by the presence of large, immobile boulders, the values narrows to 1.8 m. At Ussaia Creek the distinction is between the active channel width evaluated for ordinary floods or for extreme events. In the first case the active width is 1.5 m, whereas in the latter case is 5.3 m. Differences arise because during ordinary floods mid-channel and lateral bars are immobile. Under extreme events (e.g. 4th -8th November 2014, $Q_{max}=26.51 \text{ m}^3\text{s}^{-1}$), bars and lateral deposits are involved in channel dynamics, as observed in field surveys conducted at reach scale immediately after the flood event of November 4th – 8th 2014.

Table 4.6.2. Active channel width evaluated for different scenarios.

Site	Active channel width (m)	Active channel width (m)
	(keystones mobile)	(keystones not mobile)
Grigno Cr.	5.7	3.8
Tolvà Cr.	3.2	1.8

Site	Active channel width (m)	Active channel width (m)
	(extreme events)	(ordinary floods)
Ussaia Cr.	5.3	1.5

The third parameter to be considered is the distribution of the tracers' virtual velocities. As shown in the section 4.5.2 the skewness of distributions determines variations among the mean and median values for tracers' virtual velocities at single event scale. In the present work, to give insights about the order

magnitude of variation introduced if considering full or partial channel mobility, mean or median values in the formula of G , we plotted the values of G for the previously illustrated scenarios.

At Upper Strimm Creek the values of active channel width and burial depth are taken from Dell'Agnese et al. (2015). The active channel width is considered to be coincident with the bankfull width (3.5 m), and the estimated burial depth is equal to the maximum diameter (b-axis) of the locally displaced particles. This approximation, based on digging tests conducted on a subset of buried tracers in Upper Strimm Creek results in agreement with a study conducted in the Alps, showing that during ordinary events the thickness of the active layer ranges between 0.01 and 0.22 m (Schneider et al., 2014). Also Houbrechts et al. (2012), working in Ardennian rivers, demonstrated through the use of scour chains that the active layer depth is systematically lower than D_{50} .

4.7 Evaluation of bedload volumes and sensitivity analysis

In chapter 3 we have detailed the methodology for the evaluation of bedload volume by means of the virtual velocity of PIT-tagged stones. In particular, the methodology that has been customarily applied in the literature implies a number of assumptions. These include: (i) that virtual velocities (hence travel distances) are normally distributed and therefore justifies considering the average virtual velocity, for each weight (or size) class, as a representative metric for the tracer dynamics at the event scale; (ii) that average active channel width and depth are constant through time. In order to evaluate the uncertainty associated with the foregoing assumptions and obtain a more realistic estimation of bedload volumes at the event scale, we test three working scenarios.

Scenario 1 (S1) corresponds to the classic metric configuration applied in the literature (e.g., Haschenburger and Church, 1998; Liebault and Laronne, 2008; Dell’Agnese et al., 2015), which uses average tracer virtual velocity by weight category, constant average channel width, and constant average channel depth.

Scenario 2 (S2) differs in that it uses the median tracer virtual velocity at the event scale. This choice is supported by the empirical data presented in section 4.5 (Figure 4.5.6), which shows that virtual velocities are far from being normally distributed, but exhibit a frequency distribution heavily skewed towards low values.

Scenario 3 (S3) is site-specific and differs between the Valsugana (S3a) and the Val di Sole (S3b) sites. In the former case, the calculation of average active channel width excludes the areas occupied by immobile keystones (boulder-cascades) and that do not become submerged at bankfull level. In the calculations of Ussia Creek’s bedload volumes, we use the entire average channel width for the debris-flow event (i.e., November 4-8, 2014) that mobilized the entire channel bed, and we reduce it by excluding islands and lateral bars that did not exhibit any tracer motion during floods.

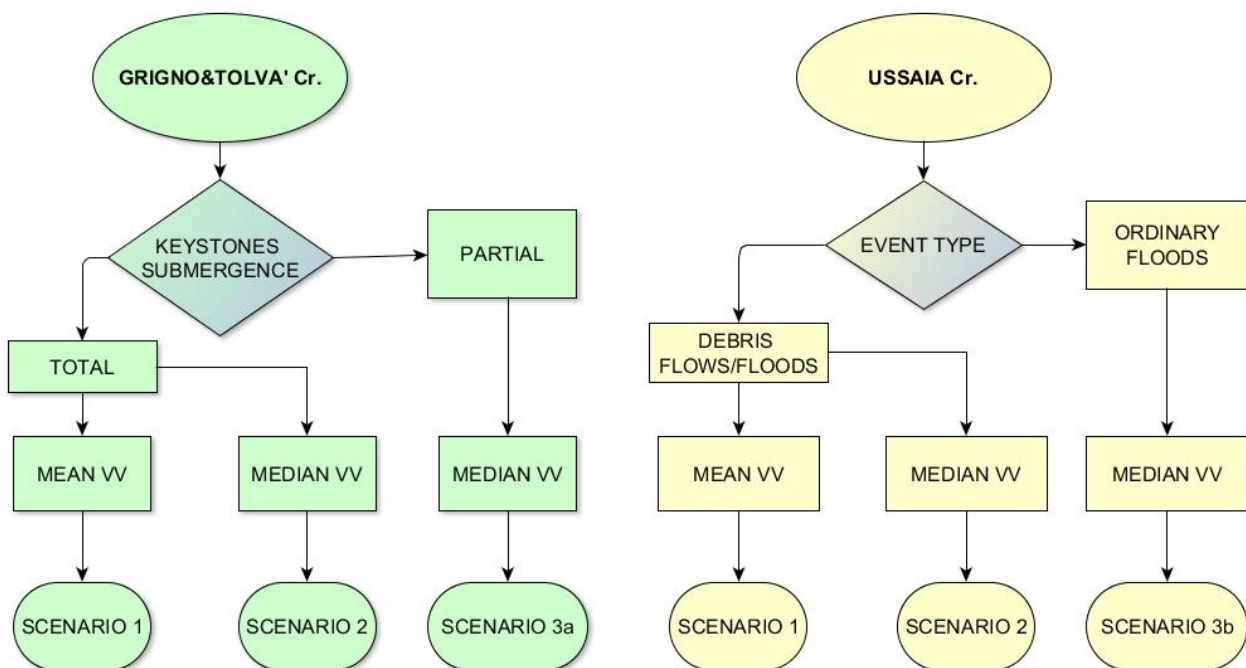
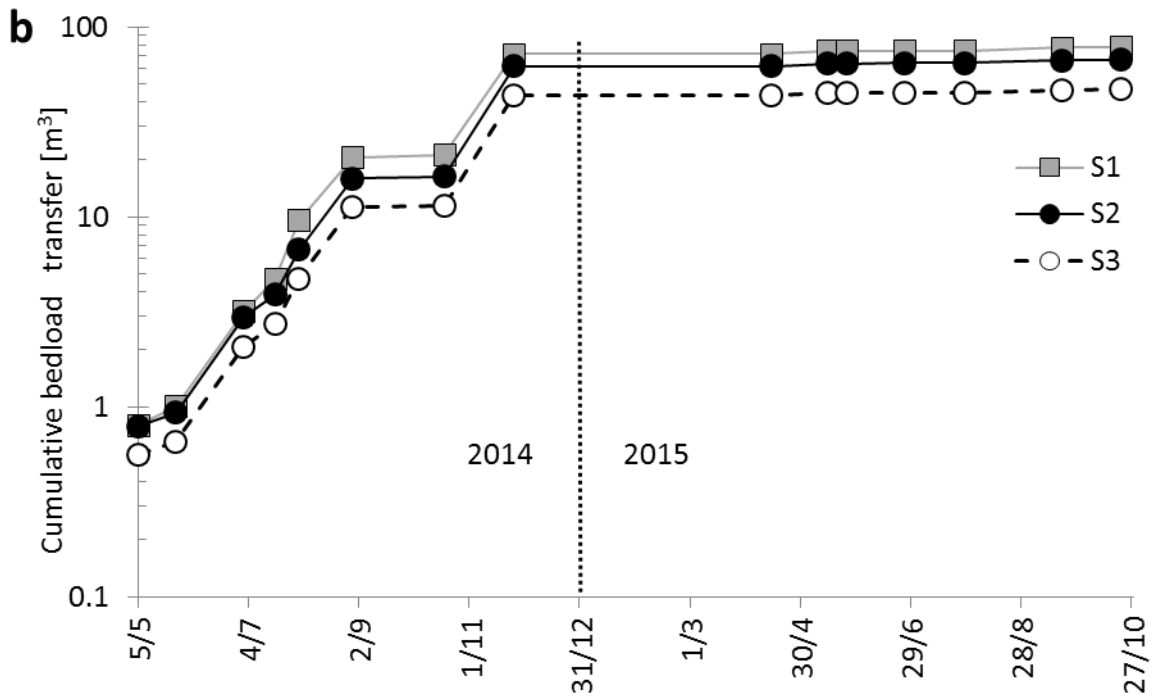
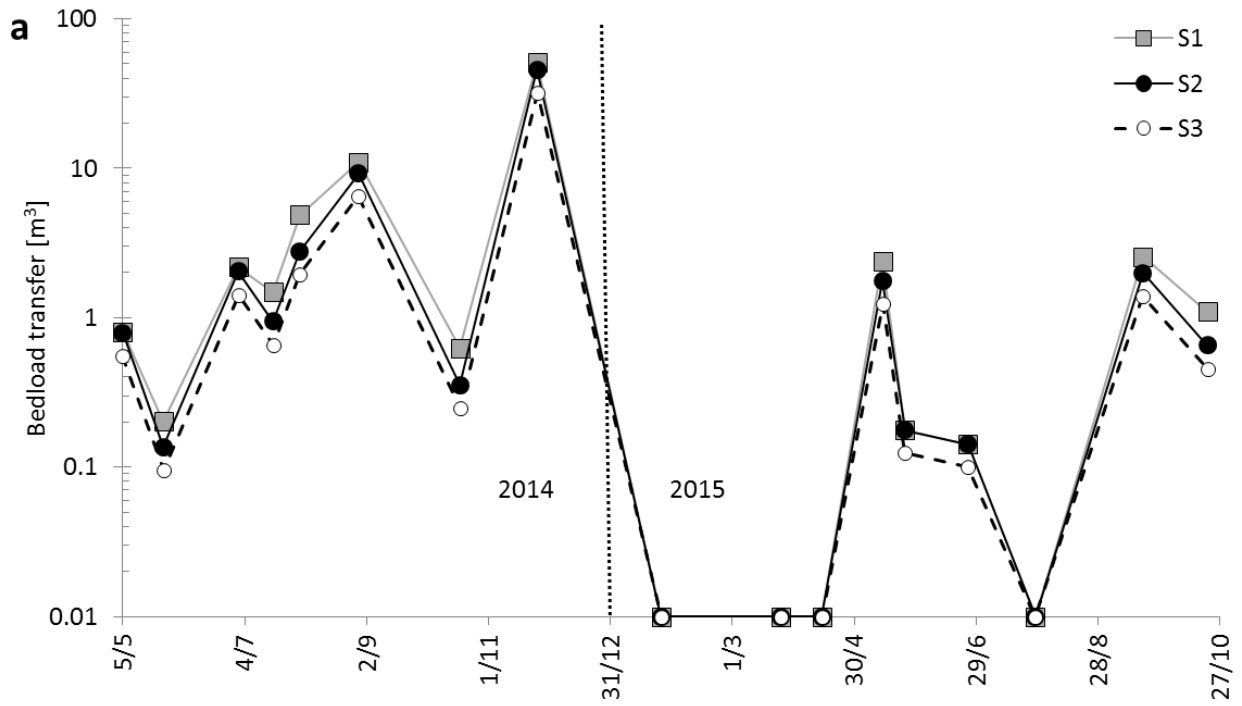


Figure 4.7.1. Framework adopted for implementing the three bedload scenarios adopted for Grigno and Tolva Creeks (left), and Ussia Creek (right).

Grigno Creek



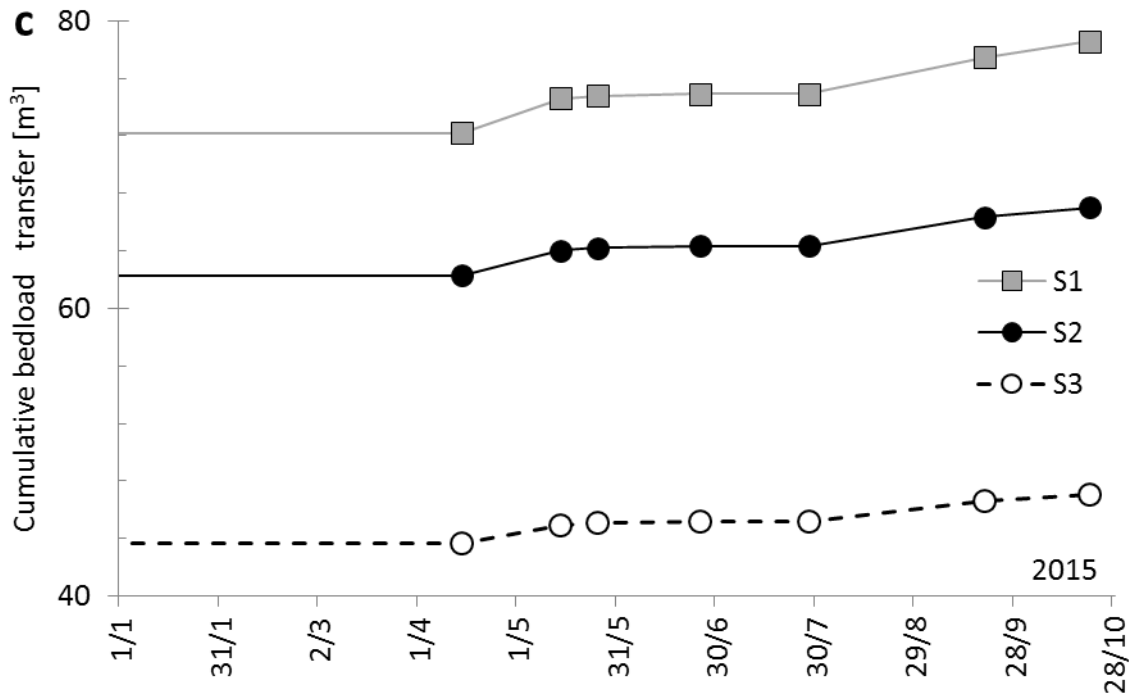
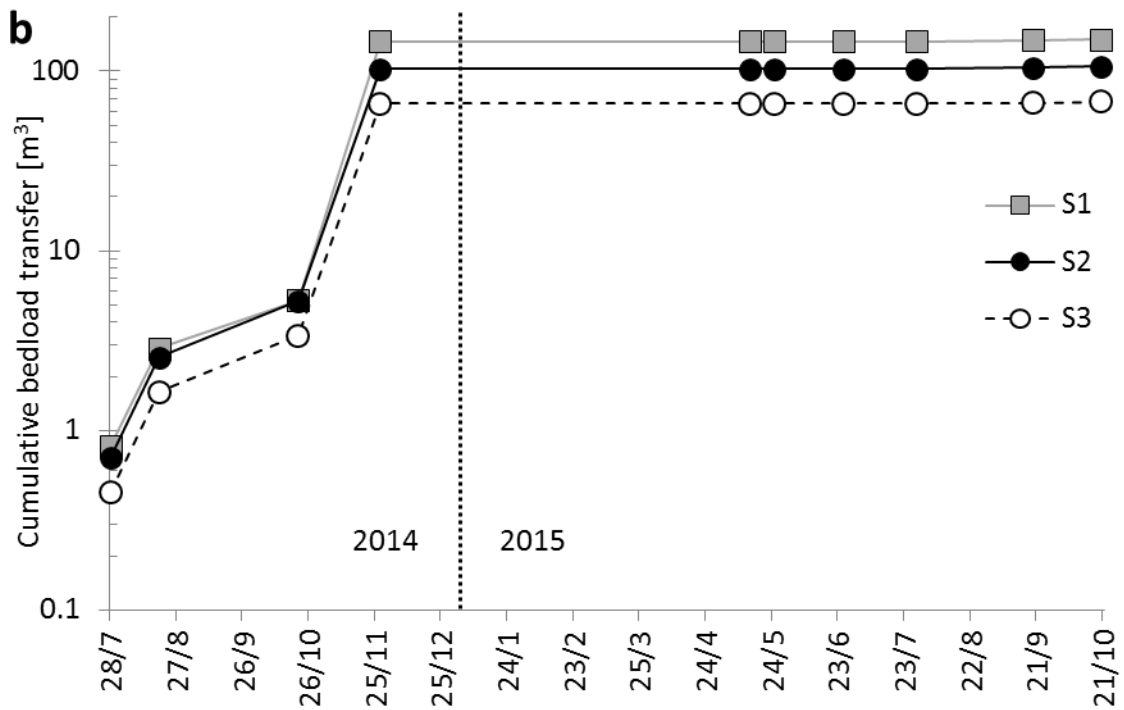
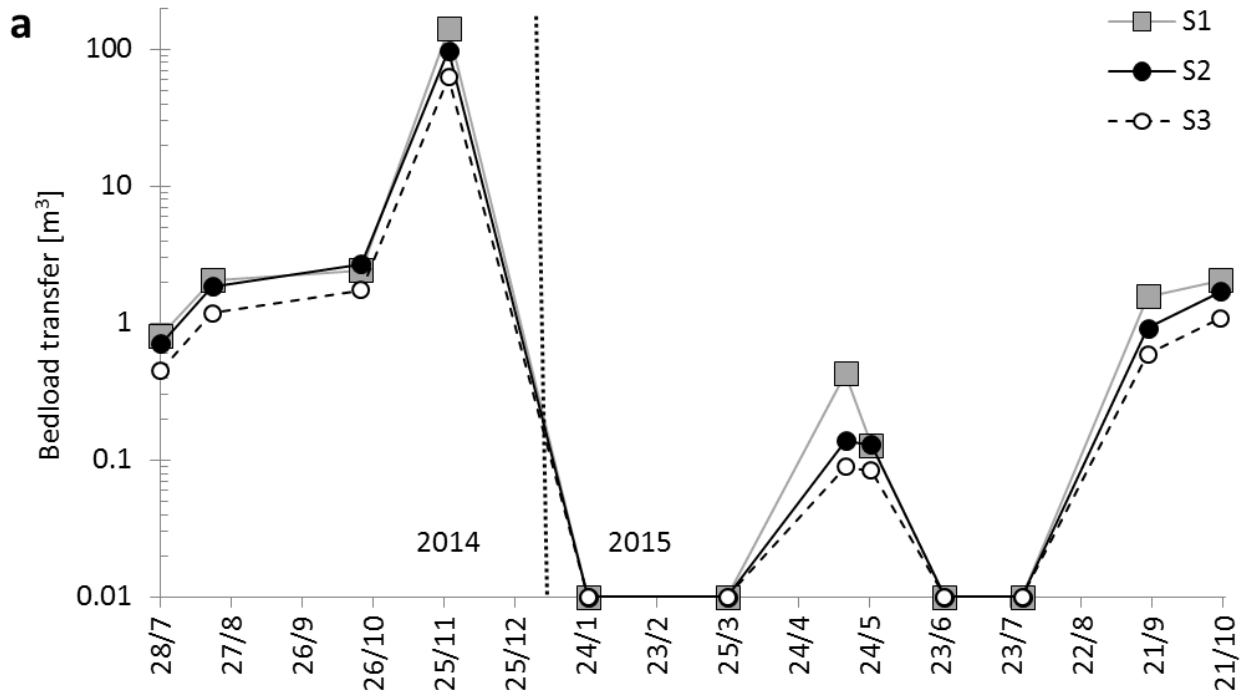


Figure 4.7.2. Non-cumulative (a) and cumulative (b) event representation of estimated bedload volumes transported at Grigno Creek in scenarios 1, 2 and 3. Note the efficiency of the snowmelt and ordinary rainfall events compared to heavy rainfall events of August and November 2014. In (c) is represented a close-up view of the estimated bedload volume transferred in 2015. In panel (a) we assigned the value of G equal to 0.01 to surveys where no bedload activity has been documented.

Results show that bedload transfer calculated by the means of the S1 and S2 is larger than the value obtained via S3 (Figure 4.7.2). When considering bedload transfer G for single surveys, the largest variations at Grigno Creek are obviously between S1 and S3. In particular the difference of G between S1 and S3 for the event of November 4th – 8th 2014 is 18.74 m³, more than the 35% of the value of S1, equal to 50.99 m³. Generally, the absolute difference between S1 and S3 is lower than 5 m³, but must be taken into account that for all the events, differences are never below the 30%, reaching values up to the 60% such as in the cases of July 31st 2014, October 13th 2014 and October 21st 2015. Differences between S2 and S3 are always below the 30% of the values of S2. The differences between S1 and S2 are comprised between 1% and 44%, with the largest values registered for all the event aforementioned, excluded the event of November 4th – 8th 2014, where the variation is about the 10% of S1.

The trend of bedload transfer differs significantly throughout the two-year period (Figure 4.7.2b). Considering the S3, by the end of snowmelt in 2014 (July 1st 2014) values of G at single event scale are generally below 2 m³. Rainfall-induced events impose a sudden increase in bedload transfer as documented in the event of August 13th 2014 when values of G increase up to 6.5 m³. The largest event recorded is that by November 4th-8th 2014, where bedload transfer has been evaluated in about 32 m³. In 2015 bedload events were never larger than 1.4 m³, recorded during the rainfall-induced event of September 19th. As shown in Figure 4.7.1c, the cumulative values of G for the year 2015 can be considered unaltered, and the overall bedload transfer is about 3 m³, one order of magnitude less compared to 40 m³ transported in 2014.

Tolvà Creek



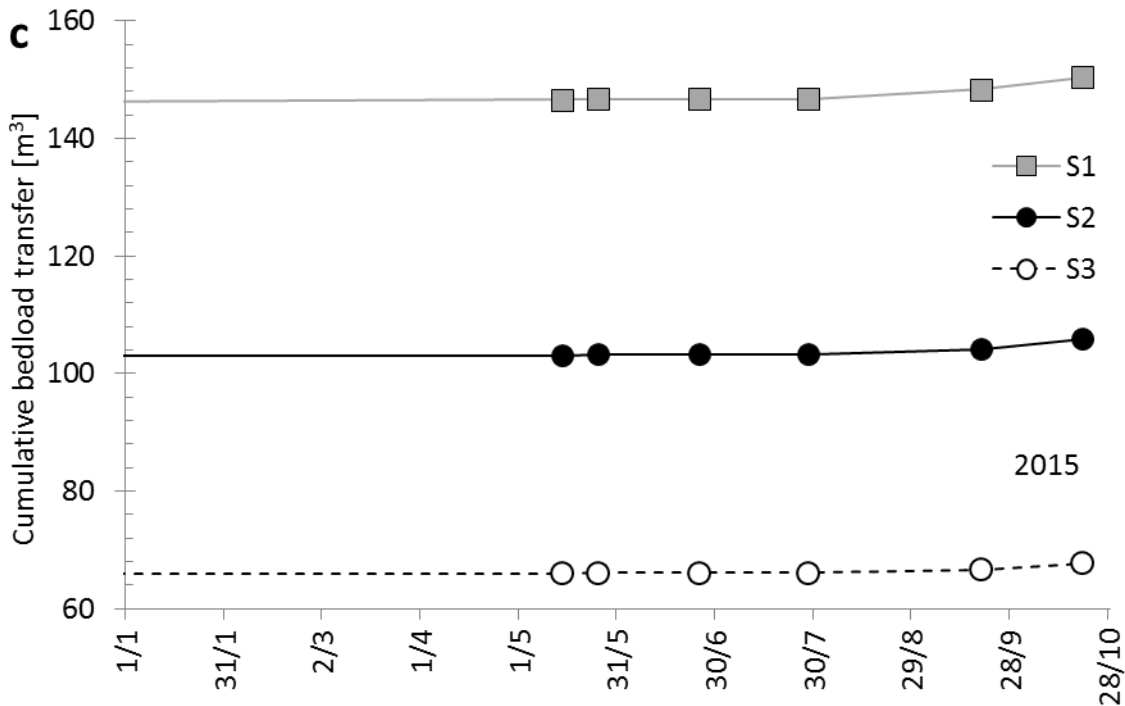
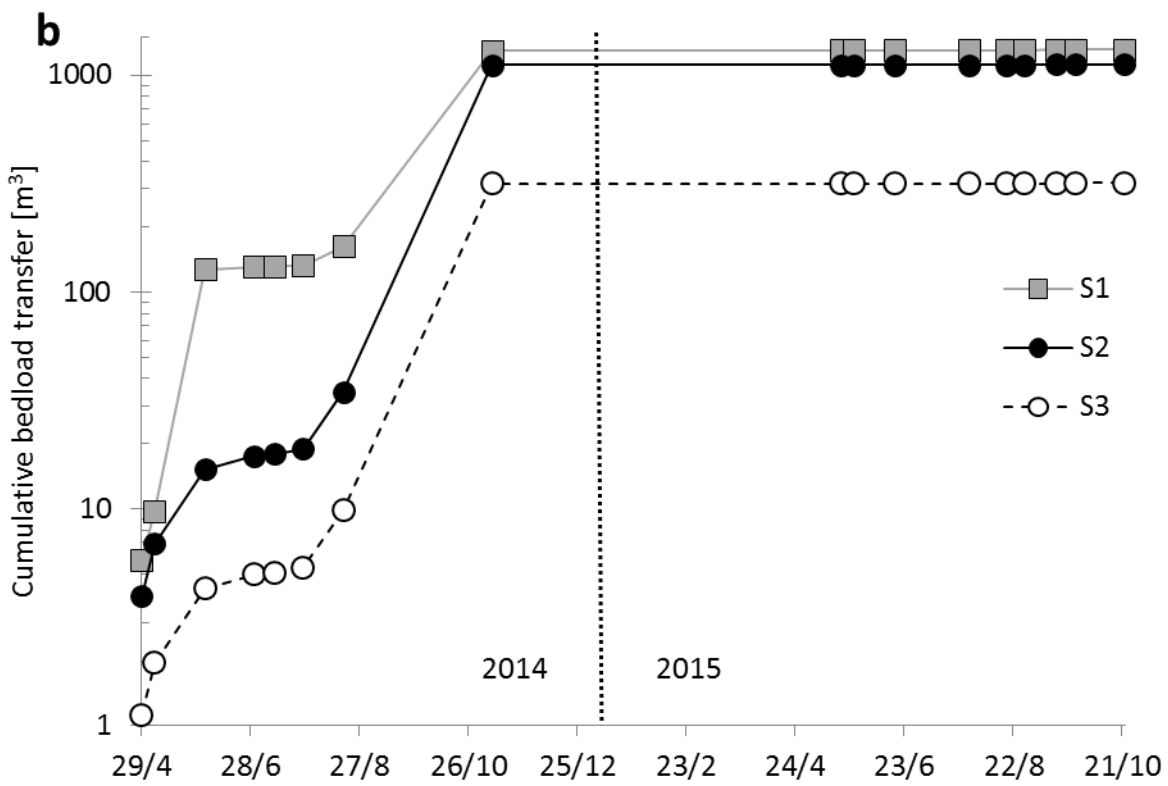
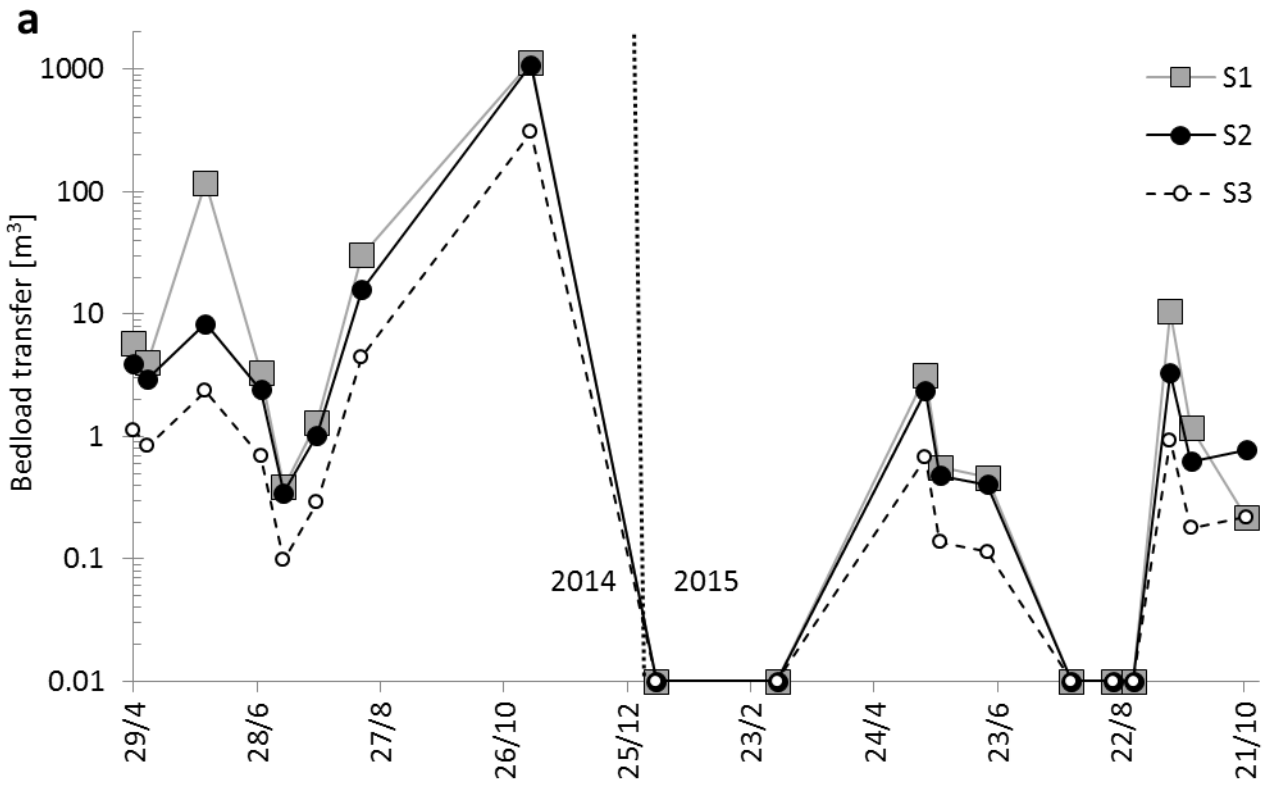


Figure 4.7.3. Non-cumulative (a) and cumulative (b) event representation of estimated bedload volumes transported at Tolvà Creek in scenarios 1, 2 and 3. Note the efficiency of the snowmelt and ordinary rainfall events compared to heavy rainfall events of August and November 2014. In (c) is represented a close-up view of the estimated bedload volume transferred in 2015. In panel (a) we assigned the value of G equal to 0.01 to surveys where no bedload activity has been documented.

Accordingly, to what observed at Grigno Creek, the largest variations between the values of G calculated by the means of the proposed scenarios at Tolvà Creek, occur between the scenarios S1 and S3 (Figure 4.7.3). In particular for the event of November 4th-8th 2014 the difference is 78 m³, about the 55% of the values of S1, that is equal to 140.87 m³. Considering the other surveys, relative differences are never below the 22% and reach values up to the 77% such as in the case of the event of May 14th 2015. Differences between S2 and S3 are reduced, and generally below the 36% of S2. The differences between S1 and S2 are comprised between 10% and 67%, with the largest values registered for the events of November 4th – 8th 2014 (30%), May 14th 2015 (67%) and September 19th 2015 (41%).

The trend of bedload transfer in 2014 differs significantly from 2015 (Figure 4.7.3b). Considering the S3, values of G during 2014 are lower than 2 m³ at single event scale. The largest bedload event recorded occurred in November 4th – 8th 2014, when transferred bedload volumes reached 63 m³. In 2015 bedload transfer never exceeded 1.09 m³ (19/09/2015). As shown in Figure 4.7.2c, cumulative G in 2015 is about 2 m³.

Ussaia Creek



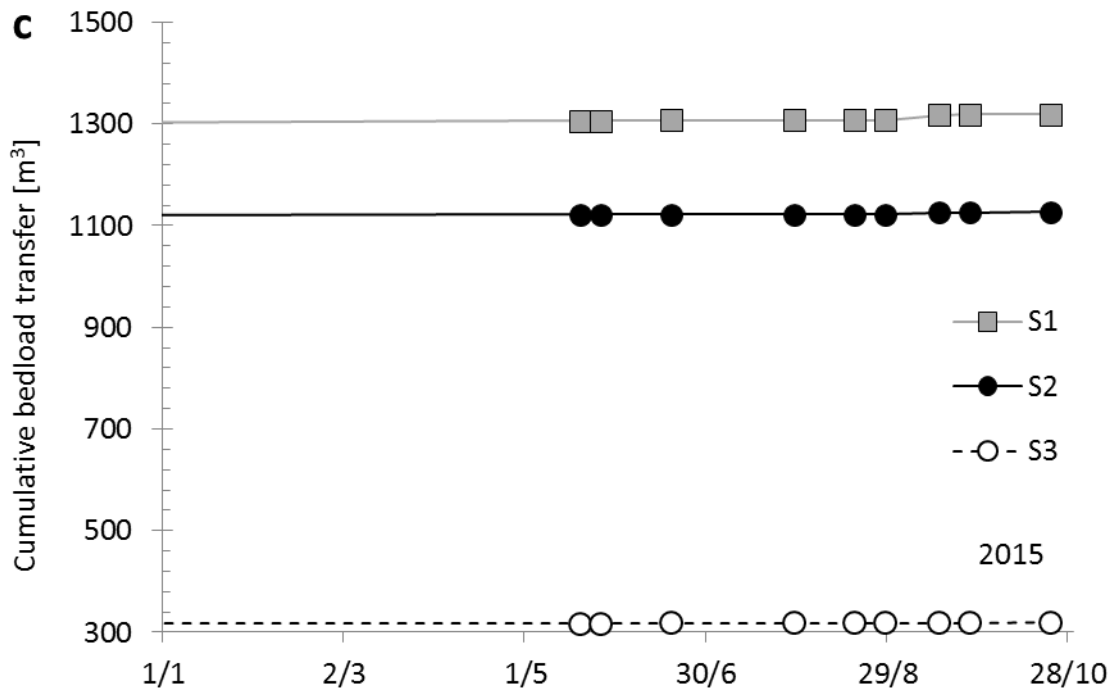


Figure 4.7.4. Non-cumulative (a) and cumulative (b) event representation of estimated bedload volumes transported at Ussaia Creek in scenarios 1, 2 and 3. Note the efficiency of the snowmelt events in 2014 compared to 2015. In (c) is represented a close-up view of the estimated bedload volume transferred in 2015. In panel (a) we assigned the value of G equal to 0.01 to surveys where no bedload activity has been documented.

At Ussaia Creek, the relative difference between S1 and S3 is always larger than 73% of S1. The critical event of November 4th – 8th 2014 is the one where the largest variations of absolute values of G are observed (Figure 4.7.4). This is due to the fact that for extreme events the active channel width increases from 1.5 m to 5.2 m (cf. Table 4.6.2). For the same event, the G evaluated through S1 or S2 exhibits a relative difference limited to 5%, due to the difference introduced adopting median and mean virtual velocities, that for this events share similar values (cf. Table 4.5.3). Differences among S1 and S2 are consistent, and their relative value ranges between 10% and 93%.

Bedload transfer in 2014 differs significantly from 2015 (Figure 4.7.4b). Considering the S3, cumulative values of G in 2014 are rapidly increasing during snowmelt period (beginning of June 2014). Within this time interval, the cumulative value of G reaches 4.3 m³, while by the beginning August is limited 5.39 m³, indicating poor efficiency of recorded event. A marked increase is due to rainfall event of August 13th, triggering a bedload event that transferred about 4.5 m³, a value comparable to what has been transported during the previous four months. In agreement with what is observed at the other sites, the largest bedload event recorded is of November 4th – 8th November 2014. This event accounts for more than 300 m³, a value that indicates the importance of this event, if we consider that the cumulative bedload transfer in 2014 is 317 m³. In 2015 bedload transfer never reached values larger than 0.9 m³, recorded in September 15th and occurred as a late summer front. As shown in Figure 4.7.3c, cumulative G for the year 2015 is about 2.5 m³.

In agreement with the observations about the distribution of tracers' velocities and selecting the value of active channel width accounting for partial submergence, in the discussion we will compare the bedload transfer at Grigno and Tolvà sites considering only the S3a. Similarly at Ussaia Creek we will consider the ordinary active channel width proposed in S3b for all the floods, with the exception of the debris flow of November 2014, where the bedload transfer will be evaluated via S2, accounting for the increase active channel width.

Strimm Creek

At Strimm Creek, since the estimate of bedload volume transferred is based on surveys conducted at the seasonal scale, we have less field information on the variability of morphological changes, including active channel width and depth. For this reason, in this case we do not perform a comparative sensitivity analysis on bedload volume scenarios, but we simply follow the literature standard (i.e., scenario 1, Figure 4.7.5).

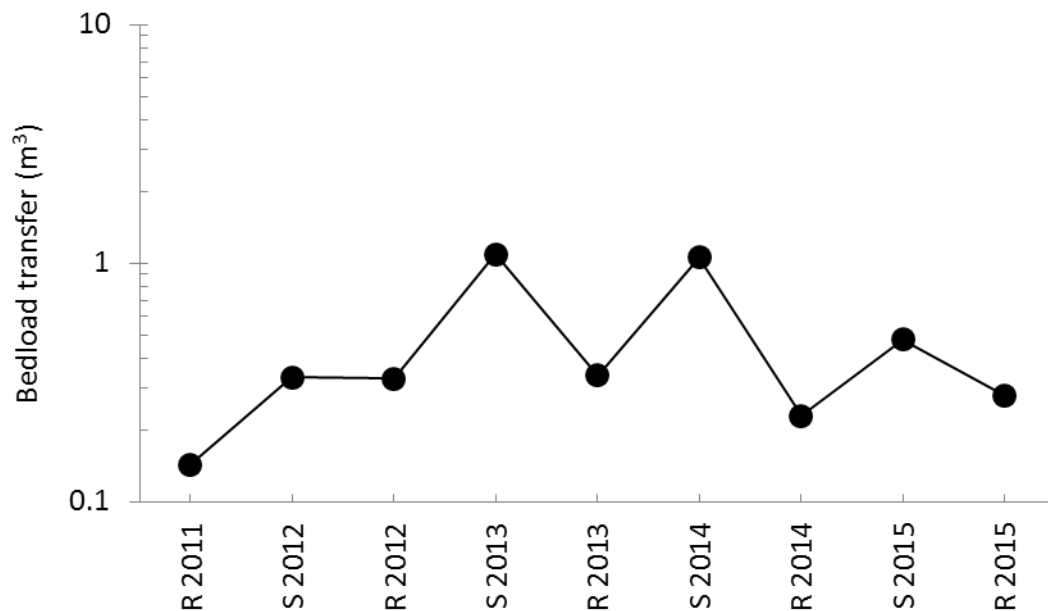


Figure 4.7.5. Non-cumulative event representation of estimated bedload volumes transported at Upper Strimm Creek (R: rainfall season, S: snowmelt season).

Bedload transport at this site exhibits low values, with snowmelt accounting for the larger bedload transfer events. The maximum values of snowmelt-related bedload events is 1 m^3 , reached in 2013 and 2014, whereas in the years 2012 and 2015 is generally lower than 0.4 m^3 . The magnitude of bedload transport events within the rainfall season is smaller compared to snowmelt across the investigated years, and exhibits values comprised between 0.15 and 0.48 m^3 . Cumulatively snowmelt accounts for the 90% of the total bedload flux, that for the investigated interval is about 4.3 m^3 , corresponding to a transport rate of about 3 tonnes per year.

Considering all the monitoring sites, the direct comparison on magnitude and frequency of bedload transfer is not allowed since the timescale of investigation of bedload are different between the group of Grigno-Tolvà-Ussaia sites, and the Strimm Creek. A direct comparison would be possible if the seasonal frequency of bedload monitoring would be applied to the aforementioned sites, such that the timing of

monitoring would be the same. To achieve this, as will be illustrated in the discussion section, at Grigno-Tolvà-Ussaia sites we will aggregate the displacement lengths to simulate that surveys are conducted with the same timing of Strimm Creek.

4.8 Linking hydro-meteorological forcing with bedload transport: rainfall intensity-duration thresholds for bedload events

The influence of the characteristics of rainfall events on triggering phenomena such as landslides or debris flows was studied by Caine in his seminal paper of 1980. Concerning fluvial transport, recently the work of Badoux et al. (2012) focused on the establishment of empirical rainfall thresholds for bedload transport activity in five Alpine experimental catchments. In this thesis, after having analyzed the hydro-meteorological forcing events (see section 4.2 and A4.2) and having estimated the bedload transfer associated to those events (see section 4.7), we investigate the effects of rainfall on bedload triggering, illustrating the relations between rainfall intensity and duration, and the magnitude of bedload volume transfer. To achieve this, at first we will determine the intensity-duration threshold associated to rainfall, that separates bedload triggering from no bedload triggering events (see Figure 4.8.1). Then, we will discriminate the effect that each type of hydro-meteorological forcing exerts on the magnitude of bedload volume transfer, adding the information about the magnitude of bedload transfer to the values plotted in the intensity-duration domain (see Figure 4.8.2).

To determine the threshold line that separates precipitation events triggering bedload transport from events that do not generate bedload activity in the monitored sites, we plotted the intensity and duration of all the analyzed rainfall events in the two-year period 2014-2015 at Grigno and Tolvà Creek (Figure 4.8.1a-b); at Ussaia Creek (Figure 4.8.1c), to have a better resolution, we plotted data collected in the time interval 2013-2015. Precipitation events are classified according to the nature of the hydro-meteorological type of forcing, hence distinguishing among precipitations occurred during snowmelt season, at the end of the snowmelt period (mixed-type events), pure rainfall events, or no bedload triggering precipitations.

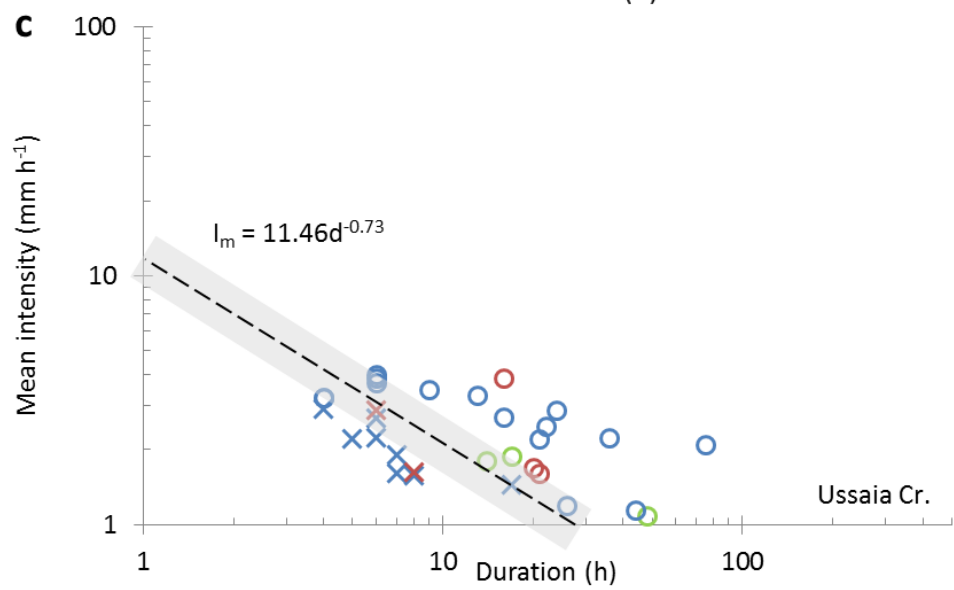
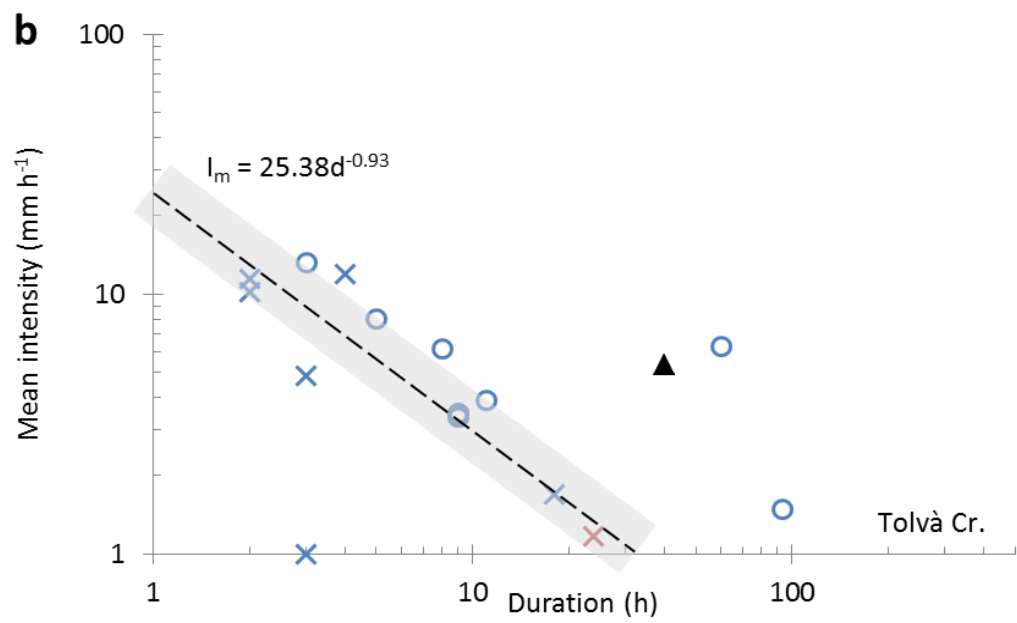
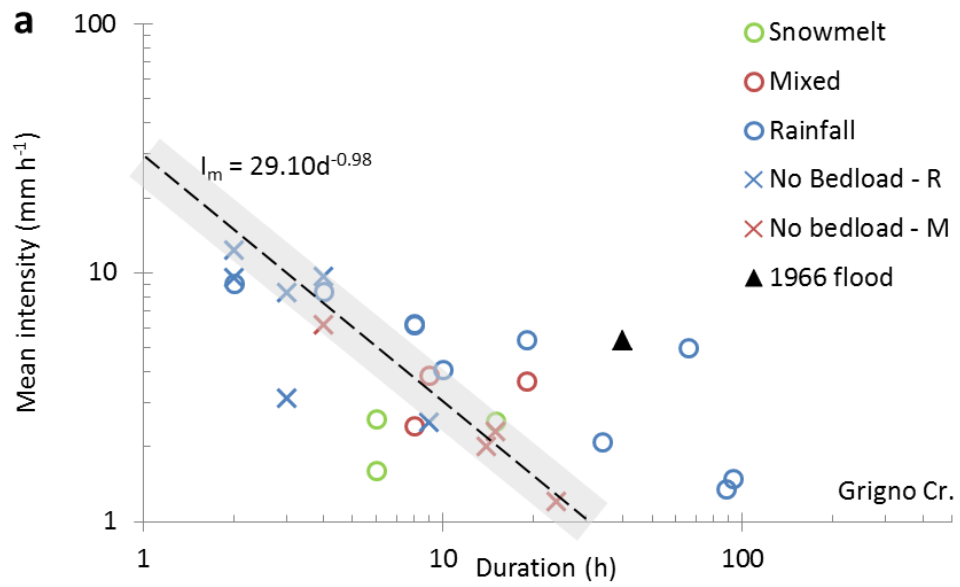


Figure 4.8.1. Intensity-duration relationships for snowmelt, mixed-type and rainfall events that triggered bedload transport at a) Grigno, b) Tolvà, and c) Ussaia Creek. The threshold line is manually fitted, separating bedload from no bedload events (R: associated to rainfall, M: associated to mixed-type); the light grey rectangle indicates uncertainty due to overlap of bedload and no bedload events.

At Grigno and Tolvà Creek (Figure 4.8.1a-b), no bedload events are characterized by high rainfall intensity and limited duration (1 hour), or by larger durations (up to 25 hours) associated to low mean intensities, below 1.2 mm hr^{-1} . Snowmelt or mixed events are generally enclosed within 20 hours of duration and limited to intensity values up to 4 mm hr^{-1} . Rainfall events are characterized by high intensity/low duration typical of summer events, or viceversa, low intensity associated to prolonged duration typical of autumn events. The overlap observed between mixed and rainfall-induced events is determined by mixed events that occurred in late snowmelt season, where the onset of the convective nature of storms typical of summer period is already visible. At Tolvà Creek we did not observe snowmelt-induced bedload, whereas the characteristics of bedload triggering events are similar to those observed at Grigno monitoring site.

The limiting curve individuated at Grigno-Tolvà sites is similar, and suggests a general threshold for bedload event; at Grigno Creek this curve has the form:

$$I_m = 29.10d^{0.98}.$$

At Tolvà Creek has the form:

$$I_m = 25.38d^{0.93},$$

Where:

I_m = mean rainfall intensity (mm hr^{-1}),

d = duration of rainfall (hr)

This curve is describing in a general way the threshold that separates the events that are not generating bedload from rainfall events generating bedload; mixed or snowmelt events apparently do not follow this line. This threshold determines the existence of two regimes common in both sites located in Valsugana. For values of $d < 4.5 \text{ hr}$ no bedload events are more frequent, whereas events characterized by $d > 4.5 \text{ hr}$ are associated to bedload. More specifically, rainfall events of $d \geq 10 \text{ hr}$ are associated to bedload.

At Ussaia Creek, even though rainfall events are overlapped with no-bedload events, we distinctly observe that rainfall events lasting less than 8 hours, with a mean intensity below 3 mm hr^{-1} , are not capable to trigger bedload transport. In few cases we observe that even for larger mean intensities no displacements occurred.

The limiting curve individuated at Ussaia Creek (Figure 4.8.1.b) is less steep compared to Grigno-Tolvà Creeks and has the form:

$$I_m = 11.46d^{-0.73}.$$

The threshold here described applies to some degree of uncertainty associated to the fact that for duration equal to 5 hours there are several overlapping precipitation events that triggered bedload or exerted any effect; for larger durations the threshold seems more appropriate. Also in this case snowmelt and mixed type events apparently do not follow the threshold. At Ussaia Creek the duration associated to rainfall events responsible of triggering bedload is larger than 8 hours, even though for these type of events we record a large bedload event (August 13th, 2014, $G = 4.46 \text{ m}^3$).

Comparing the two sites we note that at Ussaia Creek the meteorological forcing input capable of triggering bedload exhibits larger mean intensity. As a matter of fact the upper limit of intensities triggering bedload recorded at Grigno-Tolvà monitoring site is about 10 mm hr^{-1} , whereas at Ussaia site the value is sensibly lower and about 5 mm hr^{-1} .

To assess the impact that each hydro-meteorological forcing exerted on bedload volume transfer, we plot in the intensity-duration domain the precipitation events recorded in the two-year period 2014-2015 at Grigno, Tolvà and Ussaia Creeks, dimensioning the magnitude of bubbles according to transferred volume.

To snowmelt events we assigned the values of intensity/duration of short precipitations that have occurred immediately before the onset or during the discharge increase associated to increase in temperatures that determined the melt of snowpack. These precipitations are generally characterized by limited durations and mean intensities.

Considering Grigno and Tolvà Creeks as a unique system, sharing as a matter of fact identical geo-climatic settings, we observe that rainfall events associated to no bedload are characterized by strong intensity and limited duration (i.e., 2 hours and 11.5 mm hr^{-1}), or conversely by low intensity (1.2 mm hr^{-1}) and duration up to 25 hours (Figure 4.8.2a-b). The snowmelt events that triggered bedload transfer exhibit values of intensity and duration similar to those observed for no bedload and the volume of sediment mobilized is generally below 0.5 m^3 for this kind of hydrological input. Generally to these events are associated median displacements in the range of 35-50 cm, and the mobilized tracers are less of the 14%. Mixed-type events are characterized by durations comprised with 10-20 hours and intensities larger than those observed during snowmelt season, comprised within 2.5 and 4 mm hr^{-1} . The bedload volume transfer associated to these events is limited at Tolvà Creek (generally 0.1 m^3), whereas at Grigno Creek exhibits values up to 1.4 m^3 , measured after the event of June 24, 2014, where 18% of tracers have been displaced with a median of 0.9 m. Rainfall events associated to bedload show values of rainfall duration comprised between 3 and 90 hours. As expected, the largest transferred volumes (up to 60 m^3 at Tolvà Creek) are associated to rainfall characterized by prolonged duration and by large mean intensity, such as the event of 4-8 November, 2014. Considering summer events, characterized by shorter durations and larger rainfall intensities, the largest magnitude of bedload transfer is 6.5 m^3 , as occurred in August 13, 2014 at Grigno Creek (rainfall duration: 4 hours, mean intensity: 8.4 mm hr^{-1}); in the same day, Passo Brocon meteorological station recorded a

precipitation of 3 hours with an average intensity of 13.3 mm hr^{-1} , but measured bedload transport at Tolva duration: 19 hours, mean intensity: 5.4 mm hr^{-1}), or by an early autumn flood of October 13, 2014 at Tolva

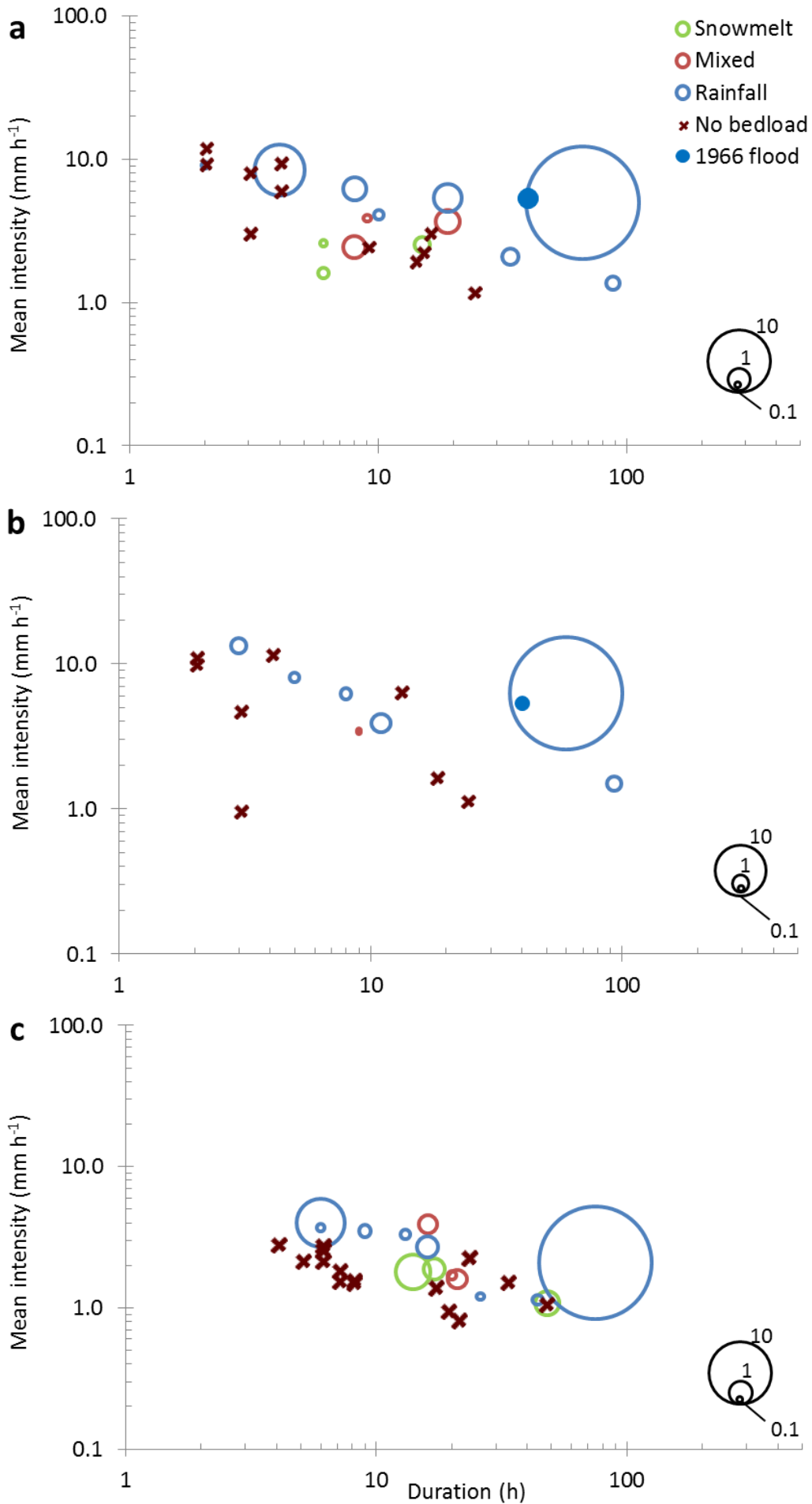


Figure 4.8.2. Bedload transport in relation to rainfall intensity-duration for different forcing typologies in: (a) Grigno Creek; b) Tolvà Creek; and c) Ussaia Creek. Crosses indicate no tracer motion. Bubble size is proportional to estimated bedload transport volume (in m^3); the largest bubble is equal to bedload volume transfer of 10 m^3 .

Creek is about 1.2 m^3 . Other rainfall events are generally capable of mobilize limited amounts of bedload, with largest values up to 2 m^3 triggered by a summer event of July 21, 2014 at Grigno Creek (rainfall duration: 11 hours, mean intensity: 3.9 mm hr^{-1}). Comparing events characterized by the same duration at Grigno Creek we observe that for a rainfall of $d = 8 \text{ hr}$ and $I_m = 6.25 \text{ mm hr}^{-1}$ the bedload transfer is comparable to a mixed event of $d = 8 \text{ hr}$ and $I_m = 2.43 \text{ mm hr}^{-1}$, showing values of G equal to 1.40 and 1.24 m^3 respectively. Even though the proportion of mobilized clasts for the mixed event is low (4.25%) compared to 28.7% associated to rainfall event, the median value of the displacement length is 2.20 m in the former case, whereas in the latter the median displacement is 0.95 m. A similar case is observed for $d = 19 \text{ hr}$. Considering events characterized by similar I_m and d , we observe comparable values of bedload across events originated by different forcing. This is the case of two bedload events, one associated to mixed-type ($d = 9 \text{ hr}$, $I_m = 3.88 \text{ mm hr}^{-1}$) and a value of $G = 0.12 \text{ m}^3$, and the other associated to rainfall ($d = 10 \text{ hr}$, $I_m = 4.08 \text{ mm hr}^{-1}$), with $G = 0.24 \text{ m}^3$, where the median displacement is 0.3 m for both events, but the proportion of mobilized clasts associated to rainfall event is 18%, whereas the mixed type event mobilized only 4% of tracers. Seems reasonable to argue that for larger precipitation intensity, the number of mobilized clasts increases, but should be taken into account also the duration. In fact, considering the two largest bedload events, the one of November 4-8 2014 ($d = 66 \text{ hr}$, $I_m = 5.01 \text{ mm hr}^{-1}$) mobilized the 80% of clasts, whereas the one of August 13, 2014 ($d = 4 \text{ hr}$, $I_m = 8.40 \text{ mm hr}^{-1}$) mobilized the 58% of clasts, with median displacement observed of 18.77 and 4.5 m respectively.

At Tolvà Creek we observe similar conditions compared to Grigno Creek (Figure 4.8.2b). There is not a clear relation between rainfall intensity and bedload volume transfer. We observe that the event of November 4-8, 2014 and the event of September 14th 2015 share identical value of I_m (6.21 mm hr^{-1}), but the former is characterized by a duration of 60 hours compared to 8 hours of the latter. This accounts for a value of G equal to 62 m^3 in the first case and 0.59 m^3 in the 2015 event.

At Ussaia Creek (Figure 4.8.2c) the maximum mean intensity is 6 mm hr^{-1} , less than the half compared to Grigno-Tolvà Creeks (maximum mean intensity: 13.30 mm hr^{-1}), whereas the range of durations is comparable across the investigated sites. Here, rainfall events that are not associated to bedload events are concentrated within a narrow window of duration, between 5 and 8 hours, reaching the largest values of intensity. Generally we observe that mixed-type and snowmelt events are capable of triggering comparable or even larger amounts of bedload transfer with respect to rainfall events. As a matter of fact bedload transfer associated to snowmelt is characterized by I_m ranging between 1 and 2 mm hr^{-1} and values of G ranging between 0.8 and 2.1 m^3 . Compared to mixed type events, where bedload transfer is below 0.69 m^3 , snowmelt events impart a larger effect on bedload activity, even if they are characterized by precipitations of limited intensity (below 2 mm hr^{-1}). Also at this site the largest bedload events are triggered by short and intense precipitations or by prolonged rainfall. A peculiarity observed at Ussaia Creek is represented by episodes with short duration (d comprised within 5 and 7 hours), and ranging between 1 and 3 mm hr^{-1} of mean intensity. These events do not affect bedload activity. Two similar events, occurred on August 13th, 2014 and June 16th, 2015 mobilized 4.45 m^3 and 0.11 m^3 respectively. The proportion of mobilized clasts is 16% for the former of 2014 and 4% for the latter, but the strongest difference appears in the median

displacement, observing a value of 4 m and 0.1 m respectively. In turn, this is related to the increase in liquid discharge, with value of peak discharge recorded in August 13th 2014 equal to $0.4 \text{ m}^3 \text{ s}^{-1}$, and equal to $0.1 \text{ m}^3 \text{ s}^{-1}$ in June 16th 2015.

Comparatively we observe that the impact generated by snowmelt and mixed-type events at Ussaia Creek is larger than at Grigno-Tolvà sites. As a matter of fact, in these two creeks the magnitude of bedload transfer triggered by those kind of hydro-meteorological inputs is limited to values below 1.4 m^3 ; conversely at Ussaia Creek snowmelt events are capable of mobilizing up to 2.4 m^3 . Moreover at Ussaia Creek, mixed-type events can trigger bedload transfer larger than values related for rainfall events. Considering rainfall events we observe that at Ussaia Creek the event of November 4-8, 2014, characterized by a duration of 75 hours and a mean intensity of 2.1 mm hr^{-1} , mobilized a volume 5 times larger than what observed at Grigno-Tolvà creek for the same episode, despite similar duration but larger mean intensities (Grigno Creek: 5 mm hr^{-1} , Tolvà Creek: 6.30 mm hr^{-1}). This is mainly due to the large sediment availability observed at Ussaia Creek, where sediment is delivered from channel bed and banks and the large proportion of finer fractions enhances bedload activity. Conversely, at Grigno and Tolvà Creek we observe a typical transport limited condition, with rainfall and hydro-meteorological forcing providing water input much larger than at Ussaia Creek, but with limited amounts of erodible sediment to be transported as bedload.

CHAPTER 5

Discussion

1. Hydro-climatic control on transport and the effect of sediment supply

Hydrographs describe the variation of liquid discharge in time, and their shape varies according to a number of controlling factors (e.g., Wilson, 1983) that can be subdivided in climatic (e.g., rainfall intensity and duration, distribution of rainfall on the basin, type of storm), topographic (e.g., catchment shape and size, direction and slope of watercourses), geologic (e.g., permeability of bedrock geology and soils), land use disturbance and vegetation cover in the drainage basin. It is well known that different types of meteorological forcing produce different hydrograph shapes (Green et al., 2013; Lenzi et al., 2004), as exemplified in our study basins too (Figure 5.1). In particular snowmelt events (Figure 5.1a) are characterized by a slow initial rising of the water level, which varies according to diurnal cycles of atmospheric temperature. Once the peak is reached, the recession limb can last for days to weeks (e.g., Figure 5.1b). Rainfall events are associated to intense convective storms or cyclonic fronts (Figure 5.1b). The rising and the falling limbs are characterized by lasting short periods, but typically, the rising limbs is steeper than the falling, with variations of several times in the magnitude of liquid discharge occurring within hours. The recession limb is characterized by a slow approach to base flow, which could be influenced by successive precipitations. What we call mixed-type events (e.g., Figure 5.1c), are inter-survey periods that host both a snowmelt and a rainfall peaks, the latter typically occurring during the recession limb of the last snowmelt hydrograph.

The effects of storm hydrographs on channel destabilization have been investigated in previous studies. Even though in field experiments it is difficult to separate the impact of flow regime from other factors affecting bedload transport, the sharp-peaked storms are less likely to develop bed armoring, and this has been recognized both in arid streams (e.g., Reid and Laronne, 1995) and in humid streams (Hassan et al., 2006). More specifically, hydrographs characterized by short falling limbs promote less bed stability and enhanced vertical exchange of particles that is reflected on the absence of vertical grain sorting. This is associated to a minimal development of bed surface armoring. On the other hand, flat hydrographs typical of snowmelt periods are promoting channel stabilization through winnowing of fines and the development of a bed armored surface, especially during the recession limb (e.g., Green et al., 2013). Transport in mountain creeks is largely affected by distribution of precipitations and typology of forcing (cf. Figure 1.2). As expected, rainfall input at Grigno Creek is the only forcing capable of displacing clasts in a boulder-dominated bed, where sediment recruitment limited to channel bed and entrainment of clasts is strongly affected by the roughness of immobile structures such as step-pools and boulder-cascades. At Ussaia Creek the mobility of primary channel structures depends on the quantities and sedimentological properties of sediment deriving from glacial till deposits dismantled in the upper portion of the basin. The supply of fine material that destabilizes step-pools and boulder-cascades permits snowmelt events to affect bedload.

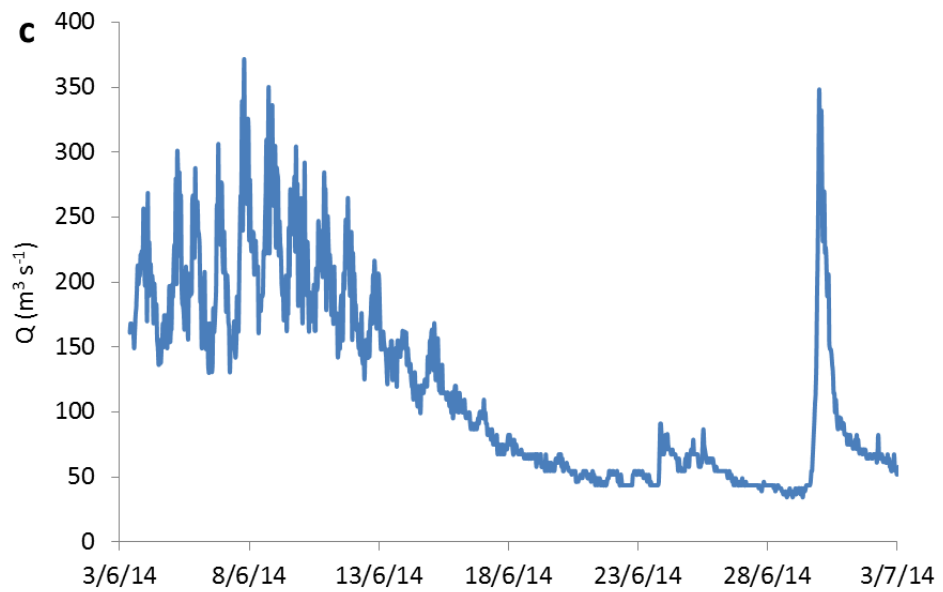
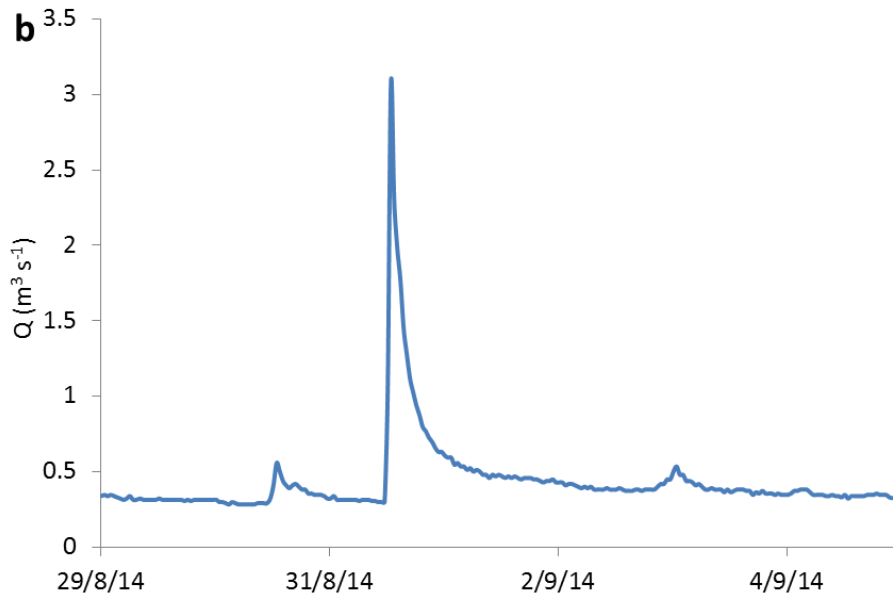
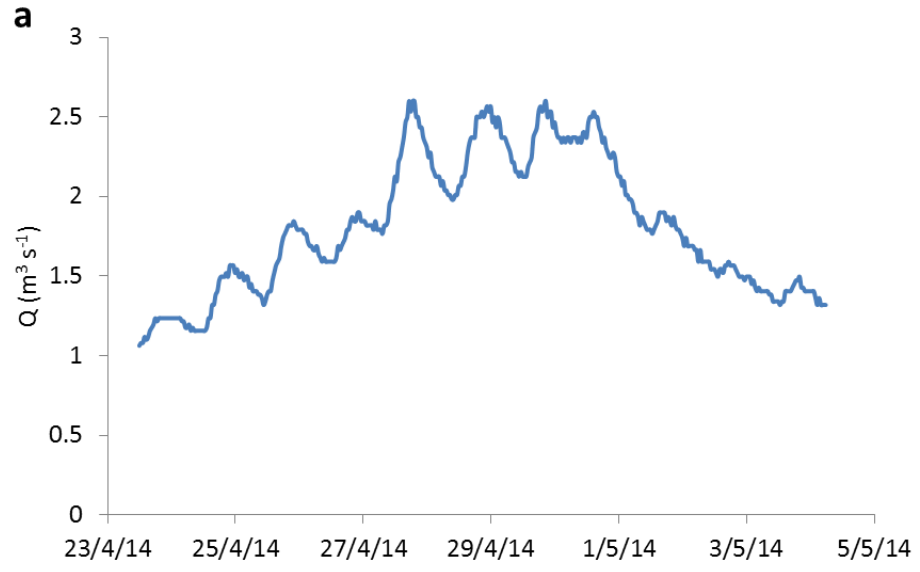


Figure 5.1. Examples of hydrologic response to: (a) a snowmelt event (i.e., Grigno Creek); (b) a convective storm event (i.e., Grigno Creek); and (c) a mixed inter-survey period in which a snowmelt and a rainfall event were recorded (i.e., Grigno Creek).

Large quantities of water input due to rainfall events are responsible for even larger bedload events. At Strimm Creek, the typology of hydrological forcing required to activate bedload is subject to the high elevation (2550 m asl) and the restricted drainage area (4 km²) of the monitoring site. As a matter of fact, only convective storms hitting the upper portion of the basin are capable of generating bedload and the most important hydrological role is played by melting of snowpack that could accumulate at these elevations. Consequently, bedload is dominated by snowmelt and only secondarily by floods caused by rainfall events.

Data comparison among Grigno and Ussaia sites allows to obtain further insights on the role played by sediment supply in the development of armoring layer. It is widely accepted that sediment-starving streams are likely to develop a high degree of armoring, as observed for Grigno Creek. In contrast, relatively high sediment supply conditions- such those described at Ussaia site- determine high exchange rates of particles within channel bed, that exhibits a lower degree of armoring.

At our study sites, recovery rates are generally high (cf. Tables A4.3.2-A4.3.3-A4.3.4-A4.3.5). At Grigno and Tolva Creeks values are exceeding the 81%, with exclusion of surveys where problems were experienced (July 1st, 2014, Grigno Creek). At Ussaia Creek the recovery rate is larger than 90%, but suddenly declines to 29% after the debris flow event of November 4-8th 2014. Successive re-injection of tracers enhances the recovery rate up to 60%, maintained throughout all the 2015, implying 100% of recovery rate for this year. Generally we can admit that recovery rate is not affected by travel distance. At Ussaia site tracers are found regardless of the travel distance. There is a physical limit imposed by the confluence with a major river, and once the clasts are trespassing the confluence they can rarely be found. At Grigno and Tolva Creek, one of the main factors affecting recovery rate is the possible hiding of tracers among the large boulders. The 20% of clasts not collected after the main flood of November 2014 probably went too far from the observation reach, even if we scanned channel bed more than 500 m downstream. These data are in agreement with Bradley and Tucker (2012), that experienced high recovery rates (70-80%) despite surveys were conducted once per year within four consecutive years. Lamarre and Roy (2005) recovered always more than the 57% of the population, a value that can be considered poor if considering that surveys were conducted after low to moderate floods. Liebault et al. (2012) reported a drastic decline in recovery rates across three years of bedload tracking from 78% to 25%, mainly due to exportation of frontrunners from the study reach.

The proportion of recovered tracers that are buried at Grigno and at Ussaia Creeks provides a description of the effects generated by sediment supply. Bearing in mind Figure 4.4.2, at Grigno and Tolva Creeks, both supply-limited, we observe very low burial rates of tracers. At Grigno values are generally below 5%, and events associated to peaked hydrographs, especially induced by precipitations falling in the period from August to November, are able to bury up to 53% of tracers (November 4-8th, 2014). The situation is similar at Tolva Creek, with a larger proportion of buried clasts (up to 61% associated to November 4-8th, 2014 flood). At Ussaia Creek, regardless the typology of event, tracers buried are always more than 30%. This is indicative of the processes of vertical mixing (see Hassan et al., 2006) occurring on the Ussaia channel bed, where the armor layer is poorly structured. At Grigno and Tolva Creeks conversely, the armor layer is well developed, thus vertical exchanges are less likely to occur, limiting burial of tracers. This fact is also evident

at Strimm Creek, where limited transport capacity and reduced sediment supply conditions are promoting a surface armor layer, inhibiting clasts' burial.

An important aspect pointed out by Bradley and Tucker (2012) concerns the mean and median travel distance. In agreement with what is observed in this study, tracers' travel distances evaluated for single surveys are generally positively skewed, so that mean are larger than median values (cf. Table 4.5.1-4.5.2-4.5.3). The exceptions to this are represented by peaked floods associated to summer convective storms (cf. Figure 4.5.1) or to prolonged autumn floods (cf. Figure 4.5.2), where distributions are right-skewed. Hassan et al. (2013), found that mobile particles occasionally show heavy tailed distributions, associated to small events. They observed thin tailed distributions during medium to large events, and this is in contrast with observation from our sites. According to Sear et al. (1996), areas that remain relatively intact during floods are promoting larger degree of mobility enhancing clasts exposure on the bed surface. At Grigno and Tolva Creeks patches of stable bed are widespread across all the study reach. As a consequence, the exposure would be greatly enhanced, and this would explain the thick-tailed distribution observed in Figure 4.5.3.

2. Comparison of seasonality of bedload transport across monitoring sites

The comparison of seasonality of bedload transport will focus on Grigno and Ussaia Creeks. This choice is dictated by the longest observation period associated to these sites, but is primarily due to the fact that we contrast two systems where main streams feature a different degree of bed structuring. Grigno Creek is characterized by rugged channel morphology, with well-developed sequences of stable step-pool or boulder cascades. This morphology is typical of regimes characterized by high discharge (e.g. Chin and Wohl, 2005), and most importantly by limited sediment supply conditions (Montgomery and Buffington, 1997). In such context, selective transport and armoring processes promote the development of step-pool sequences. Ussaia Creek is characterized by a rugged, less-structured profile, with abundant sediment supply and chronic presence of sand within channel bed. The flow regime is more subject to variations compared to Grigno Creek, with periods of limited to absent water flow observed in winter.

The approach of high survey frequency has been rarely adopted for fluvial tracers since is a time-consuming process, difficult to perform due to variable flow and site accessibility. Despite this, constraining the movement of tracers by means of repeated surveys enables to exert a large control on the definition of virtual transport durations associated to snowmelt and mixed-type events. Virtual transport durations associated to these kind of events at Grigno and Ussaia Creeks is typically in the order of 10^3 minutes, rarely exceeding 10^4 minutes. Mixed-type events show prolonged duration since they are associated to the falling limb of snowmelt hydrographs. Durations associated to rainfall events exhibit values from 10^2 to 10^3 , with flashy storms (e.g., July 11, 2014 and June 18, 2015 at Ussaia Creek) virtually transporting for 50-60 minutes. Prolonged storms associated to autumn fronts (e.g. event of November 4-8 2014) are showing the largest values of virtual transport duration associated to rainfall at all the sites.

Table 5.1. Type of forcing input for bedload events and related virtual transport duration at Grigno Creek.

Event date	Type	Q_{max} [m³ s⁻¹]	Inter-survey length [days]	Virtual transport duration [min]
16 Apr 2014	Snowmelt	2.7	133	7690
5 May 2014	Snowmelt	1.6	11	5430
25 May 2014	Snowmelt	2.5	20	6470
1 Jul 2014	Mixed	8.4	37	15400
18 Jul 2014	Rainfall	3.9	17	1320
28 Jul 2014	Rainfall	9.7	13	2110
19 Aug 2014	Rainfall	10.7	29	470
18 Oct 2014	Rainfall	3.1	50	270
4-8 Nov 2014	Rainfall	19.1	38	6480
14 Apr 2015	Snowmelt	3.7	140	-
14 May 2015	Mixed	1.9	30	120
25 May 2015	Mixed	4.1	11	800
25 Jun 2015	Rainfall	4.07	32	180
19 Sep 2015	Rainfall	11.85	50	640
21 Oct 2015	Rainfall	3.89	35	760

Table 5.2. Type of forcing input for bedload events and related virtual transport duration at Ussaia Creek.

Event date	Type	Q_{\max}	Inter-survey length	Virtual transport duration
		[$\text{m}^3 \text{s}^{-1}$]	[days]	[min]
29/04/2014	Snowmelt	0.7	16	5170
06/05/2014	Snowmelt	1	6	9670
03/06/2014	Snowmelt	1.2	28	37230
30/06/2014	Mixed	0.5	30	12840
11/07/2014	Rainfall	0.2	8	60
27/07/2014	Rainfall	0.3	17	590
18/08/2014	Rainfall	0.4	21	730
08/11/2014	Rainfall	26	19	5140
19/05/2015	Mixed	0.3	18	1290
26/05/2015	Mixed	0.4	7	560
18/06/2015	Rainfall	0.2	23	50
15/09/2015	Rainfall	2.1	18	1200
25/09/2015	Rainfall	0.31	10	500
22/10/2015	Rainfall	0.32	27	790

A direct consequence of the virtual transport duration illustrated in the Tables 5.1 and 5.2 is that larger velocities are associated to peaked events, whereas snowmelt and mixed-type events exhibit reduced velocities. This is observed at Grigno Creek (Figure 4.4.5), where larger velocities are recorded in correspondence of rainfall events, but this is not the case at Ussaia Creek, where mixed-type events (e.g., June 29th 2014 and May 14th 2015) show distributions of virtual velocities comparable to those associated with rainfall-induced events.

Plotting the values of median virtual velocities associated to the peak discharge recorded for each bedload event, we obtain a stratification according to hydrological forcing (Figure 5.2). Rainfall events at Grigno Creek are imparting the largest virtual velocities, with values comprised between 0.1 and 1 cm min^{-1} .

thus inducing larger median velocities. Median velocities associated to these two types of forcing are below 0.02 cm min^{-1} , whereas rainfall induced median velocities are plotting above this threshold, reaching 3.19 cm min^{-1} in the exceptional case of debris flow event of November 4th – 8th 2014. Comparing the two sites we observe that bedload transport efficiency at Ussaia Creek can be promoted by rainfall events but, most importantly, is also associated to snowmelt. At Grigno Creek, the stratification among rainfall and snowmelt-related events is more neat, providing an example of bedload transport efficiency largely associated to sharp-peaked rainfall events.

The timing and the amount of bedload transfer at Ussaia Creek is substantially different from that evaluated at Grigno and Tolvà Creeks for the two years investigated (Figure 5.3a). In 2014, at Ussaia we observe two main peaks, the first associated to snowmelt season and the latter occurred in November 4-8th. During snowmelt period 2014 Ussaia Creek transported about 1 m^3 of bedload. In comparison, Grigno Creek started to transport similar values of bedload only during the recession limb of hydrograph (mixed-type events). The largest impact is then observed at Grigno and Tolvà Creeks when convective summer storms are forcing flashy hydrographs peaks. An important change in those systems is associated to the large flood of 4-8 November, that simultaneously hit the monitored sites. Bedload transfer at Ussaia Creek exceeded by almost two orders of magnitude values observed at Grigno and Tolvà creeks, transporting respectively 1084 , 32.2 and 62.5 m^3 of bedload material. This is largely indicative of the efficiency in transport that characterizes Ussaia site, even though there is a clear transition between fluvial transport (Grigno and Tolvà Creeks) and debris flow that distinguished, for such hydrological input, processes affecting the Ussaia basin. In 2015, bedload transfer exhibits the same two peaks at all the sites, but the first is delayed since is associated to mixed events. What is remarkable in 2015 is the magnitude of bedload, with peak events in the order of 1 m^3 for all the sites.

The comparison between 2014 and 2015 climographs recorded at the three meteorological stations (cf. Figure 4.2.1-4.2.4-4.2.7), and the historical trend (cf. Figure 2.4-2.6), well illustrates the differences observed in terms of bedload transport. In fact, the total precipitation at Passo Brocon in 2015 is 1154 mm , a value lower than 1511 of the 1980-2010 observation period. Within November and December, and exceptional drought hit the Trentino region, with no precipitations registered at both, Malga Sorgazza and Passo Brocon. At Ussaia the precipitation accumulated in 2015 is 853 mm , a value almost identical to 844 mm of the historical, but no precipitations have been registered at Mezzana during November-December period. The scarcity of precipitation is reflected on transport regimes observed (Figure 5.3b). October rainfall triggered bedload events of comparable magnitude (about 1 m^3) across the three sites, but the lack of November precipitations, typically characterized by prolonged duration, determined the interruption of bedload transport processes at all the sites. Cumulatively, in the monitored portions of Grigno, Tolvà and Ussaia creeks, total bedload volumes amount to respectively 47.4 , 68 and 1097 m^3 (Figure 5.3b), which correspond to an average transport rate of approximately 63.2 , 120.1 and 1453.5 tonnes per year. Evaluating the transfer rate per year, we recognize that in 2014 Grigno Creek transported 43.69 m^3 , of which the 4.8% during snowmelt and 95.2% due to rainfall events. During 2015 bedload transfer is limited at 3.72 m^3 , of which the 41.4% transported due to mixed-type events and 58.6% during the remaining part of the year, triggered by rainfall events. The Tolvà Creek in the period July-December 2014 transported 65.9 m^3 , all induced by rainfall events. In 2015, at the same site the total transfer assessed is 2.39 m^3 . Mixed-type events account for the 17% , and the remaining 83% is mobilized due to rainfall events. At Ussaia Creek the total bedload transfer in 2014 is evaluated in 1094.35 m^3 . During the snowmelt period less than 0.5% is

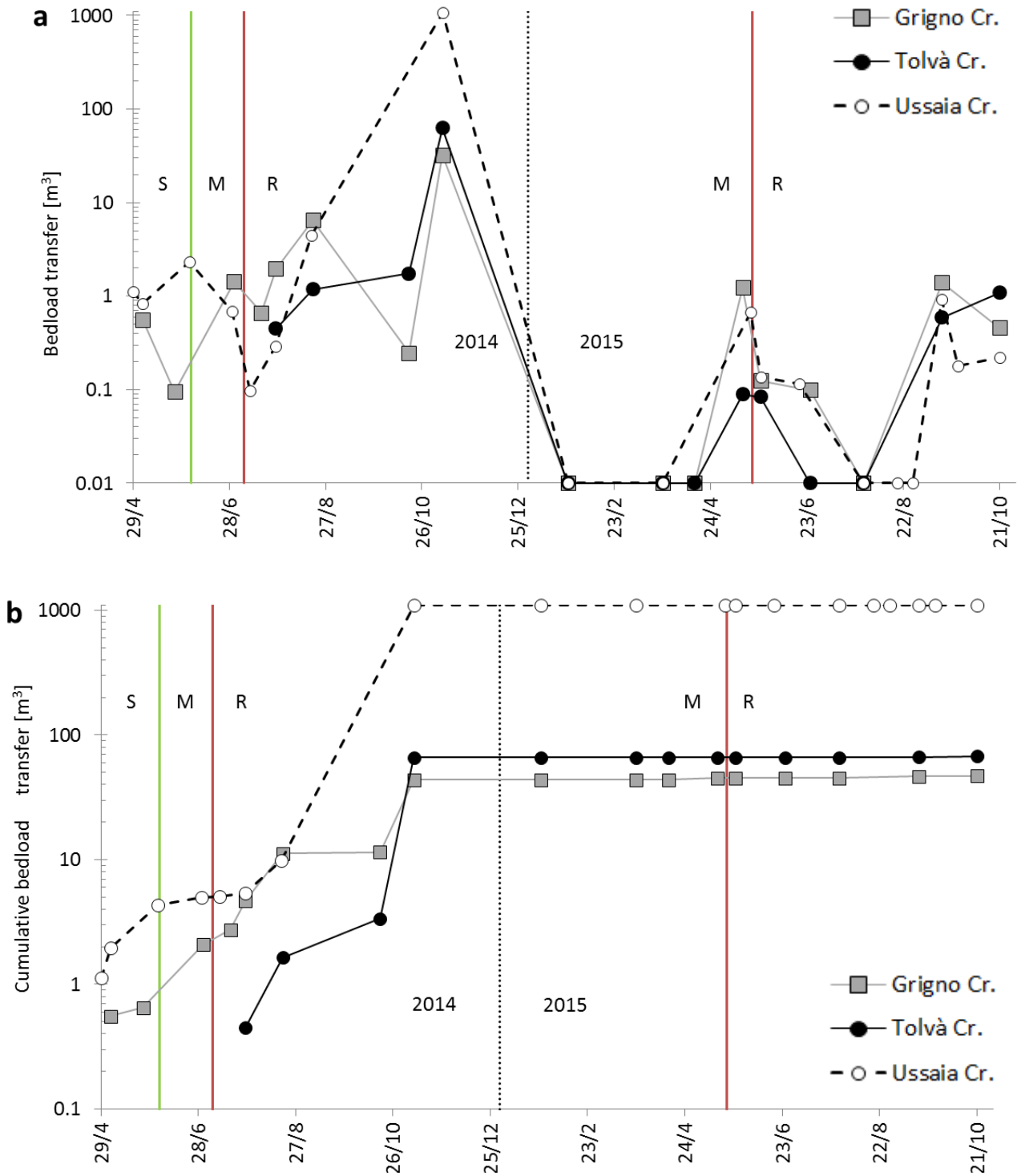


Figure 5.3. Non-cumulative (a) and cumulative (b) event representation of estimated bedload volumes transported at the study sites after applying scenarios 3a and 3b. Green and red bars mark respectively the separation between the snowmelt (S) and mixed (M) periods, and between the mixed (M) and rainfall period (R) periods. In panel a, $G = 0.01$ represents no-bedload periods.

transported; an identical proportion of material transferred is accounted by rainfall events before the debris flood of November 5th, when 99% of the observed bedload transport is concentrated. In 2015, the

total bedload transport observed at Ussaia Creek is 2.75 m³, of which the 32% due to mixed-type events and 68% triggered by rainfall events.

Analyzing the spatial variability of bedload we can contrast virtual velocities at catchment scale. In fact the Grigno watershed faces South and at monitored section covers 7 km²; conversely Ussaia Creek flows into a North-facing catchment and extends for 2 km². Direct implications on the variability of meteorological forcing and topographic factors affecting warmer period during snowmelt have been investigated by Green et al., 2013. At Ussaia monitoring site we observed that snowmelt and mixed-type events are affecting bedload more than what is observed at Grigno Creek. This spatial variability is apparently counterintuitive, since the hydrological response to snowmelt should be less pronounced at Ussaia, due to basin aspect. A key factor is therefore the sediment availability and the capacity of the stream to rework this sediment. In fact, despite facing North, and exhibiting lower water discharge compared to Grigno Creek, by the end of mixed-type events period in 2014, Ussaia Creek transported about 6 m³ compared to 2 m³ calculated at Grigno Creek. This feature is typical of transport-limited systems

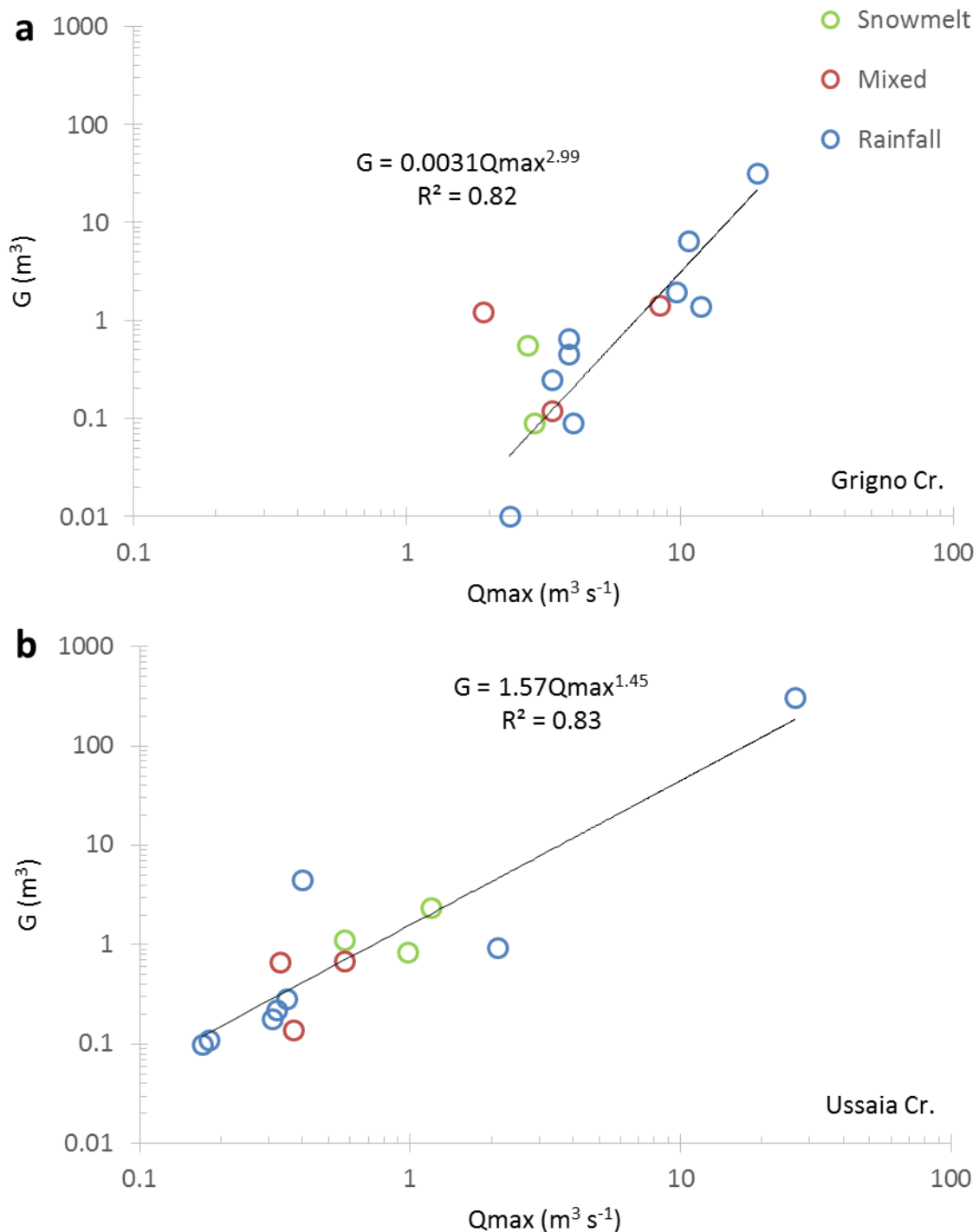


Figure 5.4. Bedload volume transfer (G) as function of peak discharge (Q_{max}) at: (a) Grigno Creek; (b) Ussaia Creek. Power-law equations refer to rainfall events only.

The relations between calculated bedload volume transfer and peak discharge are plotted, discriminating the different hydro-meteorological forcing (Figure 5.4). At Grigno site a good correlation exists among the two variables, exhibiting a value of R² equal to 0.82. An outlier is represented by the mixed event of May 14th, 2015 (Q_{max} = 1.9 m³ s⁻¹, G = 1.24 m³), represents an outlier. As a matter of fact, the lowest measured discharge is associated to a value of bedload transfer comparable to values of G obtained with Q_{max} = 9.69 m³ s⁻¹ (for the same type of hydro-meteorological input). Events sharing a similar value of Q_{max}, close to 4 m³ s⁻¹, are related to bedload transfer that significantly varies from 0.09 to 0.66 m³; a similar behavior is noted for values of Q_{max} of about 10 m³ s⁻¹, with variations of G comprised between 1.4 and 6.5 m³.

At Ussaia Creek (Figure 5.4b), values of peak discharge associated to snowmelt and mixed-type events generally exhibit larger values compared to rainfall events. The effects on bedload induced by mixed and snowmelt events is larger compared to rainfall events. Actually, we can observe that to mobilize bedload volumes larger than 0.67 m³, during snowmelt period are required peak discharges up to 1 m³. The R² value at this site is equal to 0.83, but an exception to this good correlation is represented by the event of August 13th 2014 (Q_{max} = 1.9 m³ s⁻¹, G = 1.24 m³), plotting above all the other events, and representing a peaked events caused by summer convective storm. The largest value of bedload transport is associated to debris flow event.

Table 5.3. Regression equations fitted through the rainfall events and all the events combined.

	Rainfall data		Combined data	
	Best fit equation	R ²	Best fit equation	R ²
Grigno Cr.	$G = 0.0031Q_{max}^{2.99}$	0.82	$G = 0.0181Q_{max}^{2.16}$	0.58
Ussaia Cr.	$G = 1.57Q_{max}^{1.45}$	0.83	$G = 1.54Q_{max}^{1.44}$	0.80
Strimm Cr.	$G = 0.27Q_{max}^{0.18}$	0.05	$G = 0.55Q_{max}^{0.81}$	0.48

3. Thresholds of rainfall intensity-duration

To compare rainfall intensity-duration thresholds triggering bedload individuated at our sites with previous works, we plot data from Badoux et al. (2012) jointly with trend lines of Grigno and Tolva Creeks. In this plot data from Vogelbach (Alptal, Switzerland) are missing since it is the only site for which the threshold has not been evaluated. All the other sites, namely Erlenbach (Alptal, Switzerland), Rio Cordon (Dolomites, Italy), Laval and Moulin (Draix, France) are plotted (Figure 5.5).

Duration data at Laval and Draix sites cover a wider interval compared with other sites, spanning from about 0.25 hours to nearly 80 hours, and characterized by very low intensities; at all the other sites observations range from 1 hour to 30 hours for Grigno and Ussaia Creeks, is doubled at Rio Cordon and Erlenbach (nearly 60 hours), and reaches about 80 hours at the two French sites.

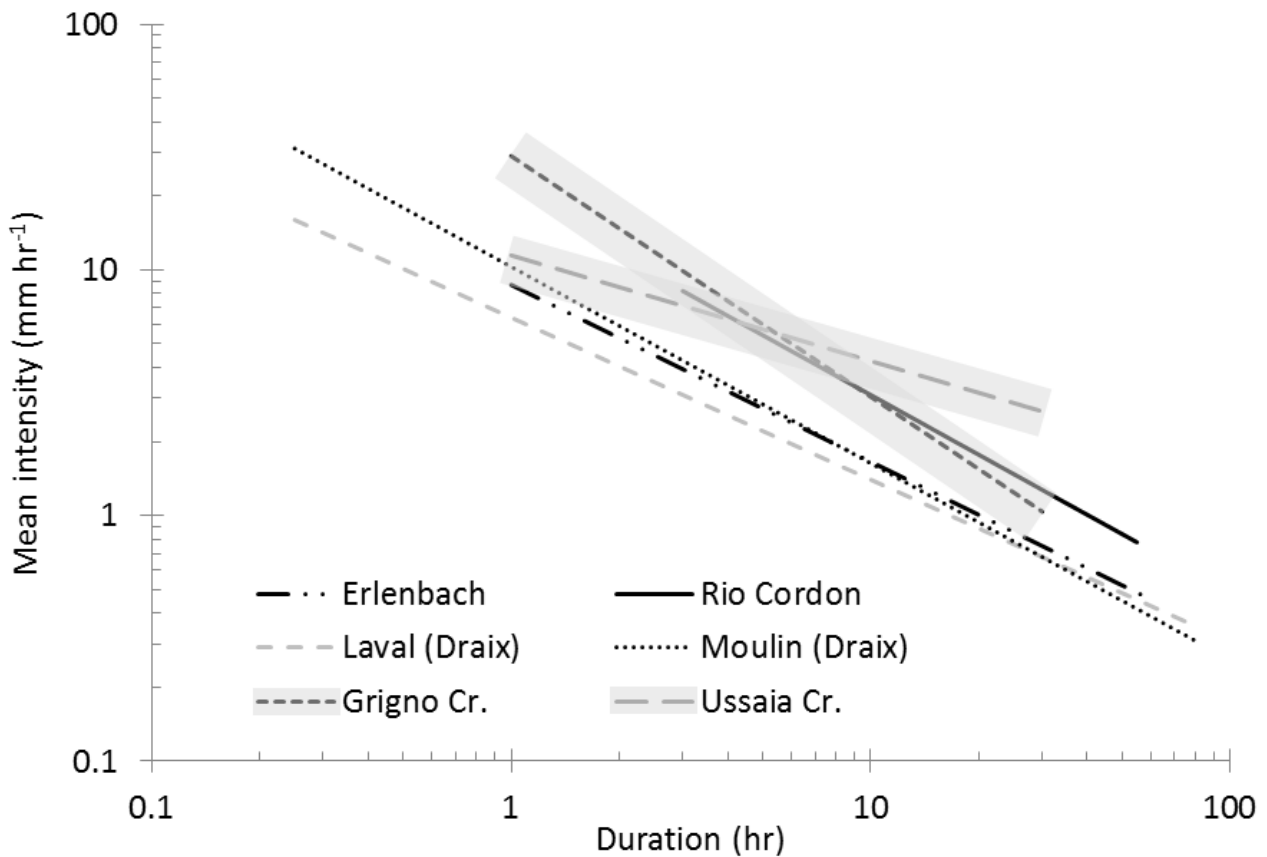


Figure 5.5. Rainfall intensity-duration thresholds for bedload entrainment at Gigno, Tolvà and Ussaia Creeks (this study) in the context of prior studies conducted in the European Alps and compiled by Badoux et al. (2012).

In the plot we generally observe that trend lines are clustering and no study site shows data isolated from the others. More specifically Erlenbach, Laval and Moulin have different slopes, but comparable intercept. Rio Cordon and Grigno Creek are located in the upper portion of plot, with Grigno Creek show the highest slopes and intercepts of all the considered data. Threshold line associated to Ussaia Creek data has the smaller slope and intercept.

The highest slope values presented by Grigno Creek and the smallest at Ussaia Creek are representative, among all the others, of the intrinsic characteristics of these two sites, where mechanisms of sediment supply and channel bed mobilization are contrasting. At Grigno Creek, interlocked step-pools and large boulder cascades are offering high resistance to bedload and are not promoting sediment recruitment from the channel itself. A comparable trend line is the one pertaining Rio Cordon, a channel characterized by boulder cascades and step-pools, where sediment supply from the upper portion of the basin is of minor relevance (Mao et al., 2009). These sites are thus characterized by higher critical rainfall to produce bedload transport, and this could be ascribed to the stable morphological conditions of their respective channel beds, and to the large grain sizes. At Ussaia Creek the strong coupling between low-order

tributaries and mainstem is responsible of frequent morphological variations associated to bedload triggered by low-intensity precipitation. For durations < 1 hour, Ussaia Creek is located between the threshold lines of Laval and Moulin sites, located in a badland morphologic context, where erosive processes are largely facilitated by the marly bedrock and the high degree of coupling between channel and hillslopes fosters bedload transport processes during floods. Ussaia Creek shows a peculiar trend, with the smallest slope. This indicates that at Ussaia Creek duration plays a major role compared to intensity, and this is corroborated by the fact that intensity-data associated to bedload are about 5 mm hr^{-1} , whereas at Grigno Creek (cf. Figure 4.8.1) the duration plays a major role compared to intensity.

Bedload entrainment in Badoux et al. is evaluated by means of different instruments; geophones with 1 minute interval resolution have been used at Erlenbach and Vogelbach for the determination begin and end of motion; at Rio Cordon an ultrasonic sensor with a resolution of 5 minutes acquired bedload data; no measurements of initiation of motion are recorded at Draix sites. In this last site sediment traps have been periodically surveyed to assess bedload transport. In this work, tracers' displacement and surveys following relevant hydro-meteorological events have been used to assess bedload transport. These methods present different thresholds to individuation of bedload. For example, geophones record the passage of particles rolling, sliding and more generally impacting a metallic plate, thus also smaller elements are contributing to define a bedload event. The dimension of the glass transponder represents a physical limit to the dimension of tracers, since it is not possible to insert it into clasts < 45 mm (b-axis). Tracers introduce a bias in the definition of bedload that encompasses only clasts larger than 45 mm. Another fundamental difference affects the definition of bedload initiation. Automated systems such as geophones allow continuous monitoring of bedload transport, with time resolution of 1 minute. Tracers' recovery is possible only after the exhaustion of the flood, thus we can only estimate a posteriori if bedload has been triggered.

4. Timescales of investigation

To examine the magnitude of bias associated to different timescales of tracers' field monitoring, we lumped all the values of travel distances recorded at single event scale, simulating that only four surveys were performed at each site during monitoring period. This is an important methodological aspect, not linked to hydrological forcing. The four "ideal" surveys are temporally distributed to mimic the investigation frequency adopted at Strimm Creek, with one survey at the end of the snowmelt period and the other by the end of November. At Tolvà Creek, since monitoring started in July 2014, the snowmelt period has not been evaluated and the first lumped survey is by November 25, 2014. As a result, the travel distance of a single tracer for a lumped survey is the sum of all the travel lengths of the actual surveys conducted in the interval occurring between two lumped surveys. These results are shown in Figure A5.1. Comparing each of the following graphs with the overall distribution of tracers' travel distances calculated for each survey (see Figure 4.5.3), we observe that the distributions are similar, but there is a difference in the frequency for each class of travel distance.

Considering the overall values of travel distances (Table 5.4), for lumped scenario at Grigno and Tolvà Creeks the values of mean are sensibly higher compared to field surveys, doubling the value as in the case of Grigno Creek (mean associated to lumped scenario is 12.99 m, 7.3 m is associated to actual surveys).

Median values for lumped scenario at Grigno and Tolvà Creek are double compared to field surveys, whereas at Ussaia Creek mean and median are almost identical.

Table 5.4. Mean and median values of the travel distances (Td) derived from the actual surveys and from the seasonally lumped scenarios at the three study sites.

Time scale	Grigno Cr.		Tolvà Cr.		Ussaia Cr.	
	Mean Td	Median Td	Mean Td	Median Td	Mean Td	Median Td
	(m)	(m)	(m)	(m)	(m)	(m)
Field surveys	7.3	1.1	24.5	0.9	32.0	0.9
Lumped scenario	13.0	2.3	35.4	1.9	33.8	1.1

Due to aggregation of surveys the condition of mobility or immobility for each weight class have changed. Using the flow competence method to assess sediment transport (see section 3.4.3), we identified the minimum discharge able to entrain clasts of each weight class, based on lumped surveys. Threshold values at each site increased after aggregation of surveys; particularly that of Grigno Creek increased from 1.9 to 3.71 m^3s^{-1} (Figure 5.6), whereas at Tolvà and Ussaia there are no significant variations. Tracers' virtual velocities have been calculated considering the new threshold discharges. Mean and median tracers' virtual velocity considering lumped surveys of field surveys are very similar (Table 5.5).

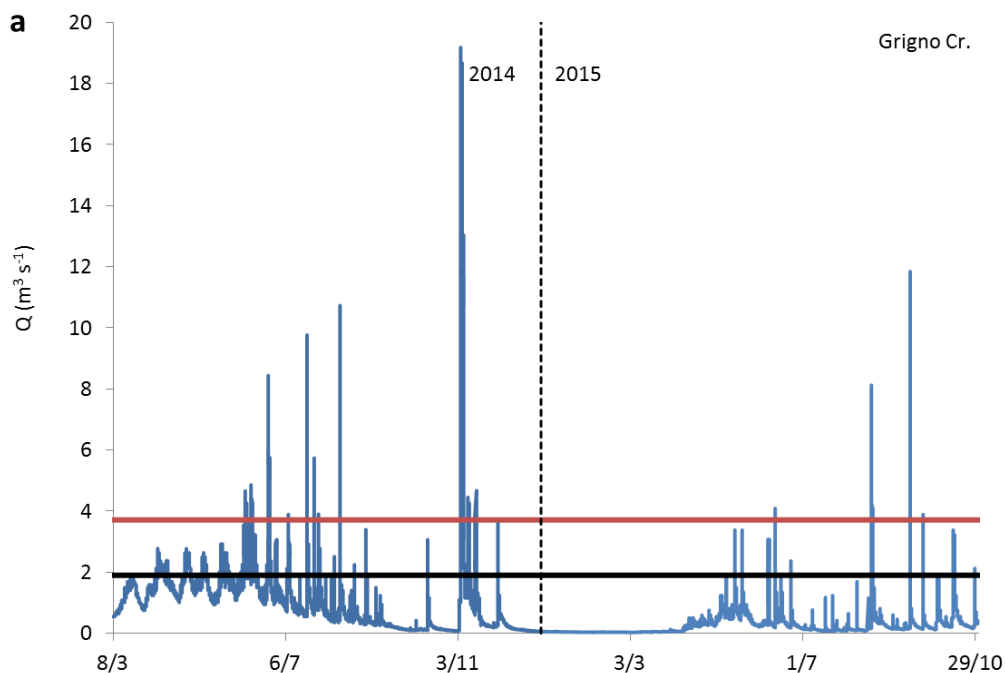


Figure 5.6 Example of threshold discharges obtained from the actual field surveys (black line) and from the seasonally lumped scenario (red line) at Grigno Creek.

Table 5.5. Mean and median values of tracers' virtual velocity (Vv) derived from the actual surveys and from the seasonally lumped scenarios at the three study sites.

Time scale	Grigno Cr.		Tolvà Cr.		Ussaia Cr.	
	Mean Vv (cm min ⁻¹)	Median Vv (cm min ⁻¹)	Mean Vv (cm min ⁻¹)	Median Vv (cm min ⁻¹)	Mean Vv (cm min ⁻¹)	Median Vv (cm min ⁻¹)
Field surveys	0.57	0.14	0.31	0.08	0.56	0.03
Lumped scenario	0.45	0.22	0.25	0.07	0.51	0.02

Bedload transfer at single event scale on Grigno Creek show comparable values for the 2014 if considering actual or lumped surveys (Figure 5.7a). For the year 2015, bedload transfer evaluated via lumped surveys is larger compared to what evaluated via actual surveys.

Cumulative values are therefore underestimated if lumped surveys are adopted in the calculation of G (Figure 5.7b). Even if at single event scale values of G are comparable, all the surveys that are lumped do not contribute to the estimate of G. As a consequence, even if single events share similar values, their cumulative value differs, as shown, by November 25, 2014 of about 15 m³, that represents the 35% of the G evaluated via non-lumped surveys.

Bedload transfer at single event scale for the period 2014-2015 at Tolvà Creek is comparable considering aggregated or not-aggregated surveys (Figure 5.8a). For the year 2015, bedload transfer obtained via lumped surveys is larger than the value calculated via actual survey and does not correspond to the actual timing of bedload events as described by considering the true surveys.

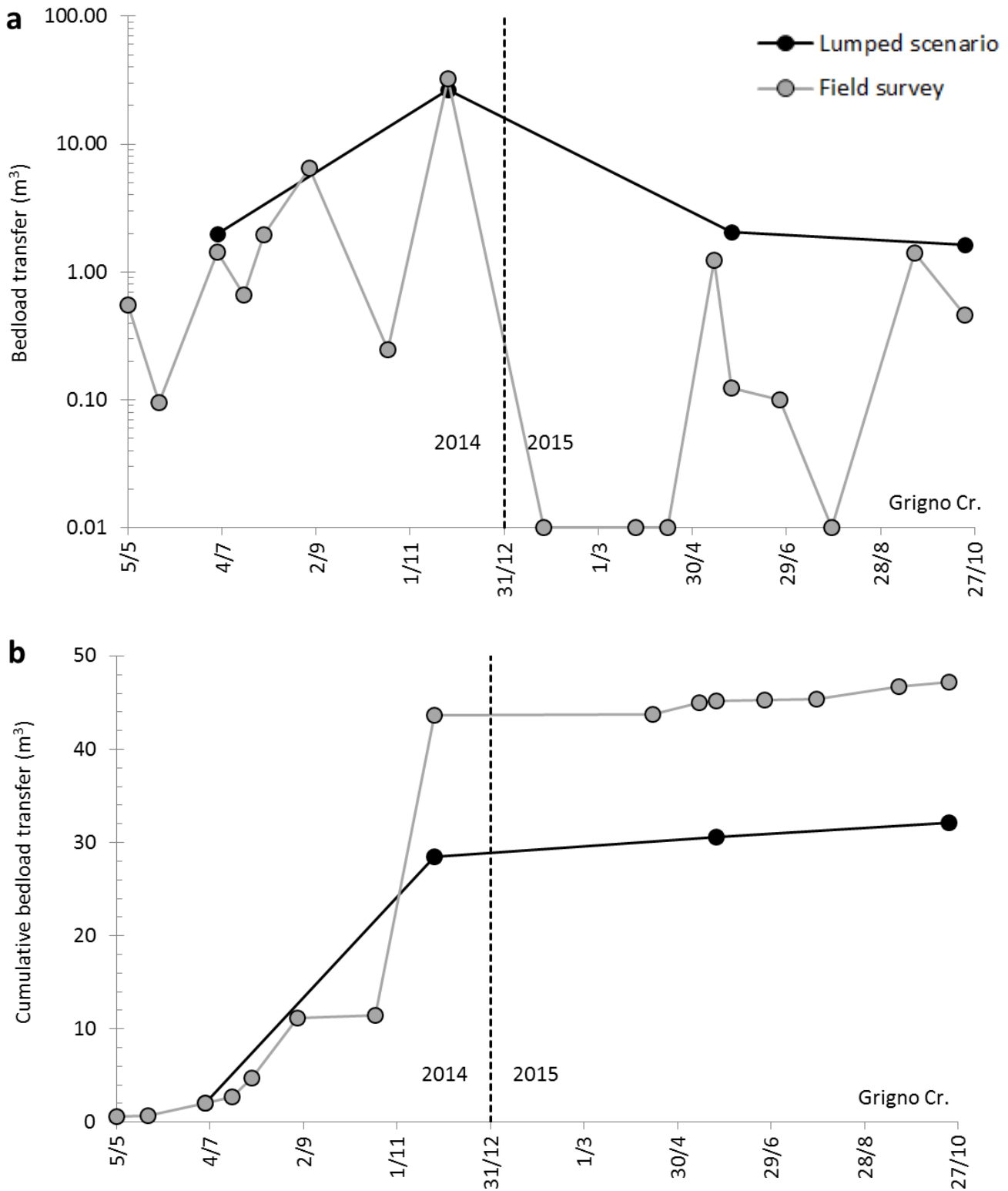


Figure 5.7. Non-cumulative (a) and cumulative (b) event representation of estimated bedload volumes transported at Grigno Creek. Grey circles represent the bedload transfer as estimated from each field survey, black circles indicate the seasonally lumped counterpart.

Cumulative values of bedload transfer are underestimated if lumped surveys are adopted in the calculation of G (Figure 5.8b). As seen in the Grigno Creek, also at Tolva Creek all the surveys that are lumped do not contribute to the cumulative value of G . As a consequence, even if single events share similar values, by November 25, 2014 the cumulative of actual surveys is 5 m^3 larger than lumped surveys, differing of about

the 9% of the G evaluated via actual surveys. Considering the cumulative values of G, the difference is constant throughout the 2015.

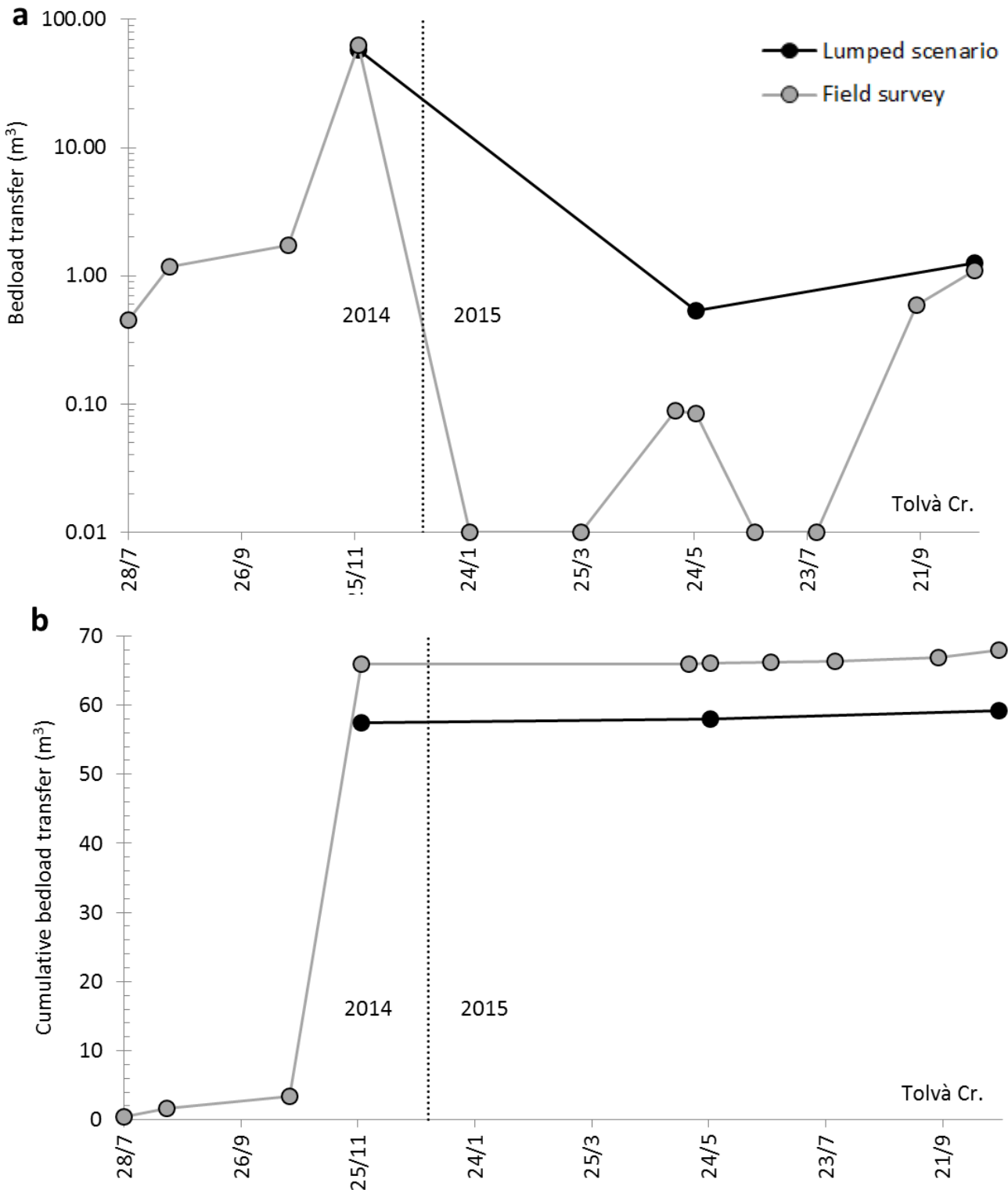


Figure 5.8. Non-cumulative (a) and cumulative (b) event representation of estimated bedload volumes transported at Tolvà Creek. Grey circles represent the bedload transfer as estimated from each field survey, black circles indicate the seasonally lumped counterpart.

At Ussaia Creek (Figure 5.9a), there are significant differences at single event scale if the evaluation of bedload is obtained aggregating or not the surveys. In 2014, considering the survey by the end of snowmelt period the difference is one order of magnitude, and by the end of November the value obtained with true surveys is 1084.50 m³ compared to 30.18 m³, obtained lumping the surveys. The reduced difference of median values of tracers' virtual velocity (Table 5.5) does not affect the evaluation of G (actual = 0.03 cm min⁻¹, lumped = 0.02 cm min⁻¹). The difference in the evaluation of G is primarily caused by the pronounced change in active channel width. For non-lumped surveys in fact, is possible to assign at single event scale the active channel width, whereas lumping the surveys would lead to an incorrect assignment of the active channel width to several lumped surveys. Considering the 2015, all the values of G have been obtained adopting the active channel width of ordinary floods (width = 1.5 m). In this case the comparison can be more direct and must be recognized that the effects of lumping the surveys are clearly visible in Figure 5.9a. Considering aggregated surveys in fact, the trend of bedload transfer seems constant, and no evident variations appear in the two surveys of May 26 and October 22, 2015. Considering the actual surveys, bedload is concentrated in two main events (May 19th and September 15th, 2015) separated by a period of relative low transport rate.

Cumulative values of bedload transfer are underestimated if lumped surveys are adopted in the calculation of G (Figure 5.9b). As seen in the other sites, all the surveys that are lumped do not contribute to the cumulative value of G. As a consequence, strong differences are recognizable by November 25, 2014.

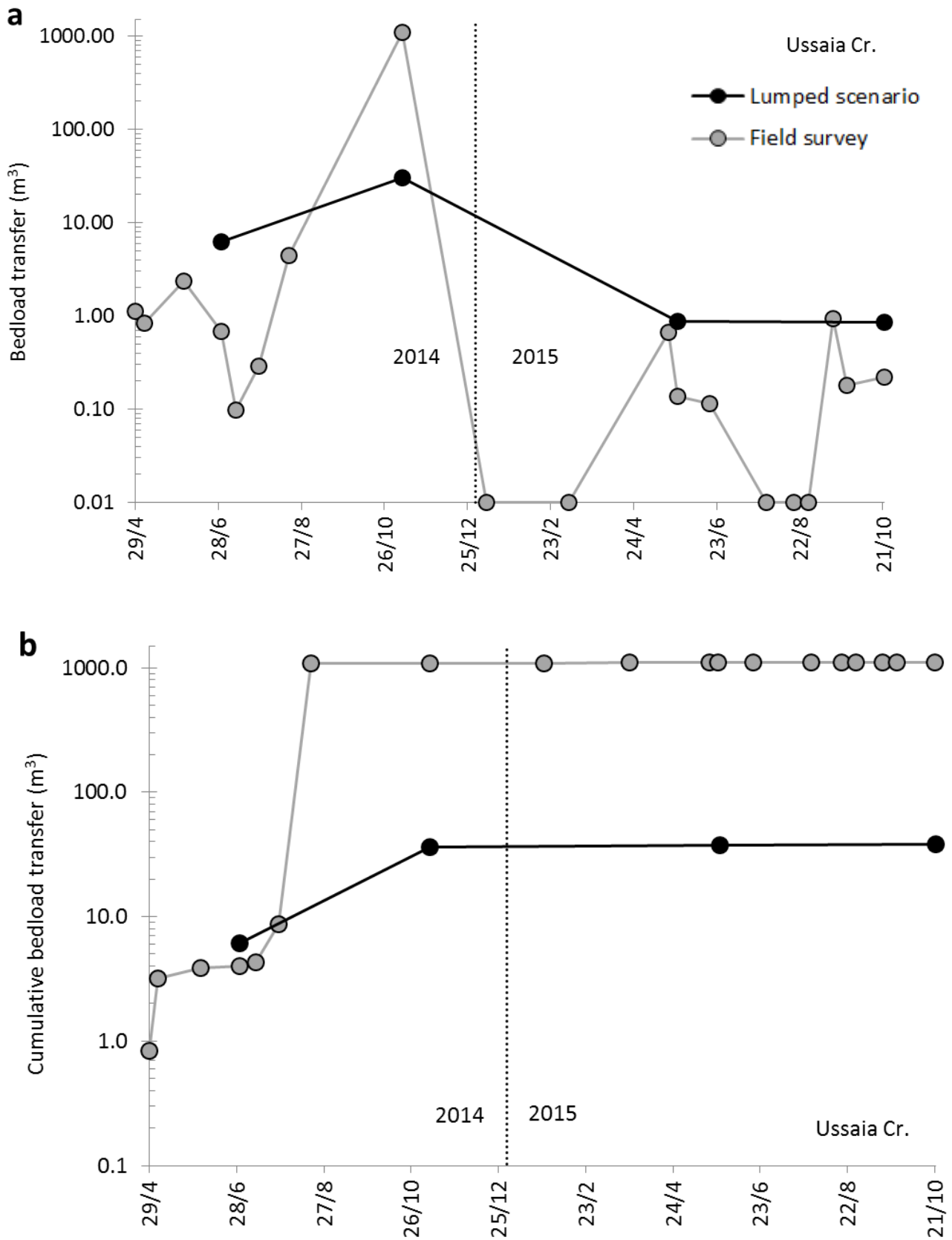


Figure 5.9. Non-cumulative (a) and cumulative (b) event representation of estimated bedload volumes transported at Ussaia Creek. Grey circles represent the bedload transfer as estimated from each field survey, black circles indicate the seasonally lumped counterpart.

5. Latitudinal transect

To compare how different forcings are affecting travel distances along a latitudinal climatic transect encompassing the Trentino-Alto Adige region, we calculated the ratio between the sum of travel distances measured for a given hydro-meteorological input and the total travel distances recorded. At Strimm Creek the 73% of tracers' travel distances are triggered by snowmelt events, whereas rainfall events account for the 20% of the total. In this site the displacements are limited and generally the median values are in the order of 1 m regardless of the forcing, even though snowmelt imparts larger travel distances. The situation is inverted at Ussaia Creek, where snowmelt is responsible for the 16% of the overall displacement and a larger role is played by rainfall, accounting for 83% of total travel distances. Median value of snowmelt-induced displacements are the largest, approximating 2 m. The distribution of rainfall-induced displacements reveals that rainfall accounts for larger travel distances. Displacements at Grigno Creek are markedly dependent from rainfall events, accounting for the 98% of travel distances.

The seasonal dominance of climatic forcing over bedload transport is linked to the transport capacity of the selected channels. We observe in fact that the sediment-starving, structured channel at Grigno (or Tolvà) Creek is responsive to flashy storms or to prolonged inputs of water, and not to flat hydrographs typical of snowmelt season. Channel roughness at the two sites located in Valsugana imposes that only sudden variations of water discharge are capable of triggering bedload. Conversely at Ussaia, channel bed is poorly structured and the roughness is relatively lower compared to Grigno and Tolvà Creeks. The sedimentological properties of bed material and the large sediment supply are responsive to snowmelt hydrographs and mixed type events. The largest transport efficiency at Ussaia Creek is also documented by the major influence on bedload triggering that is exerted by low-intensity/high duration events capable of triggering bedload. Bedload at Strimm Creek is largely dominated by snowmelt. This seems reasonable accounting for the high elevation of the basin and the limited drainage area. Compared to the other site, larger accumulation of the snowpack and subsequent water supply during melt season, is responsible for this dominance.

The limited drainage area can be ascribed as a factor limiting the impact of rainfall events, since only local convective storms would be responsible for flash floods destabilizing the armored bed surface, fostering bedload transport.

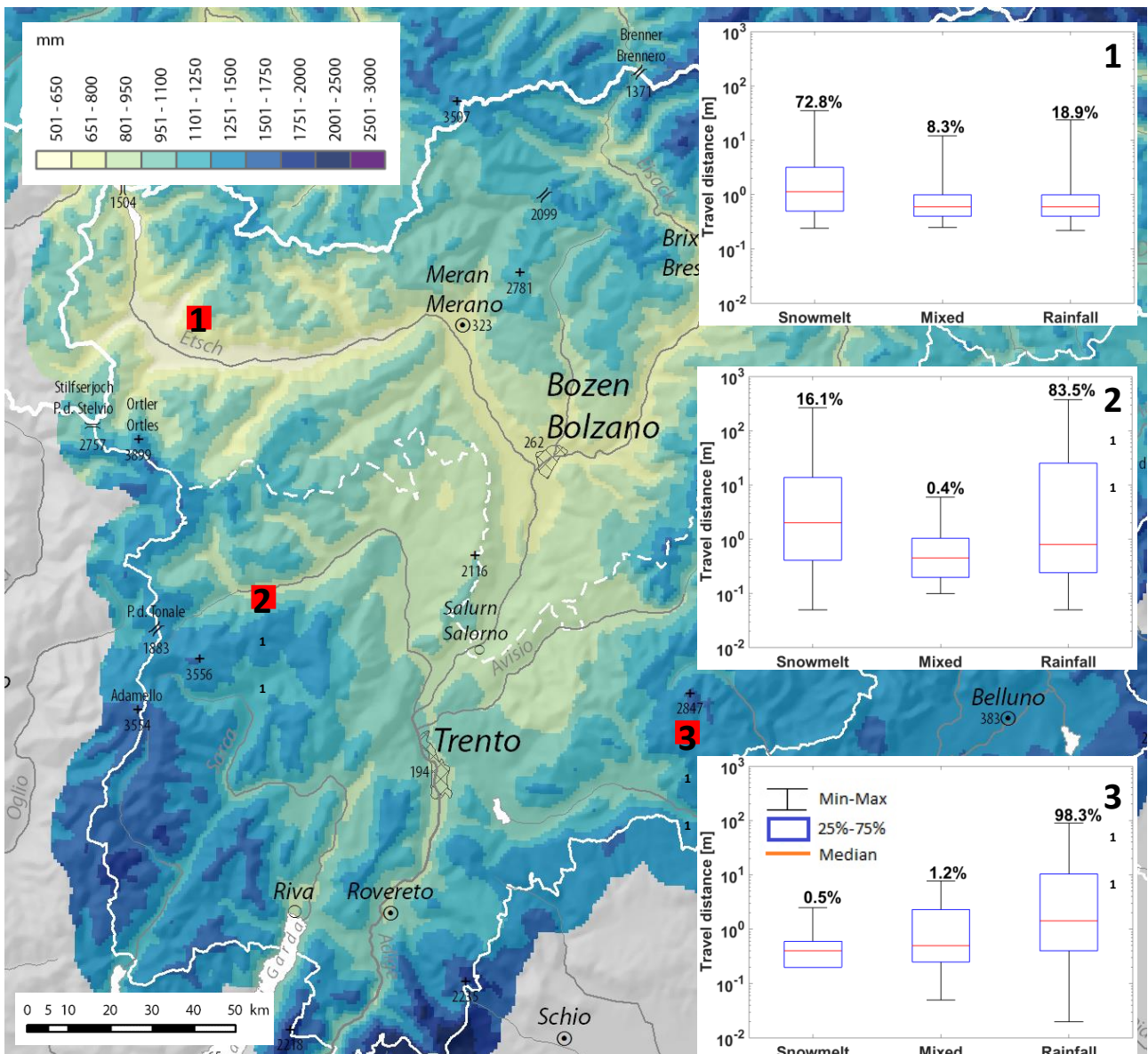


Figure 5.10. Mean annual precipitation (1981-2010) across the Trentino-Alto Adige region (modified from www.clima-alpino.eu) with box plots of tracers' travel distances stratified by types of hydro-meteorological forcing at: (1) Strimm Creek; (2) Ussaia Creek; and (3) Grigno Creek. Percentages indicate the ratio between travel distance for a given hydrological forcing and total travel distance.

CHAPTER 6

Conclusions

This thesis addressed the effects of colluvial sediment supply and hydro-meteorological forcing on reach-scale bedload morphodynamics of three step-pool/boulder-cascade mountain streams. The study streams are characterized by different channel bed roughness and stability. In Grigno and Tolvà Creeks step heights and pool depths are larger (mode: 0.6 m) compared to Ussaia (mode: 0.4 m). The comparison of grain size distribution indicates the presence of finer sediment at Ussaia Creek due to glacial till supplied by lateral inputs, promoting bed sediment mobility.

By tracking tracers' displacement after each hydro-meteorological event, we quantified the influence of sediment supply on bedload morphodynamics. In Grigno Creek, exhibiting larger channel bed stability compared to Ussaia Creek, flat-shaped hydrographs associated to snowmelt-related events poorly influence the mobility of tracers. Tracer mobility is enhanced by peak-shaped storm hydrographs occurring during the rainfall season. Travel distances in Grigno Creek are lower compared to those observed in Ussaia Creek. Sharply peaked summer events in the first site are the only forcing conditions capable to displace clasts for lengths comparable or slightly lower than those measured in Ussaia Creek. By contrast, snowmelt events are associated to median travel distance three times larger compared to those at Grigno Creek. An evident result of the effects induced by contrasting sediment supply conditions is provided by a simultaneous autumn front. Prolonged storm fronts are supplying large quantities of rainfall, enhancing the extraordinary sediment evacuation efficiency at Ussaia Creek, where the median value of travel distances associated to a November debris flow event is 200 m. The same typology of event, characterized by an even larger intensity and rainfall accumulation, promoted ordinary bedload transport at Grigno Creek, showing travel distances one order of magnitude smaller compared to Ussaia Creek.

Virtual velocities exhibit seasonal patterns and the differences observed between the two sites in terms of bedload transport can be directly linked to channel transport capacities and sediment supply conditions. In the Grigno Creek, a stratification of virtual velocities according to hydro-meteorological forcing is distinctly observed. Snowmelt-related events exhibit low discharges associated to low virtual velocities. During the rainfall season, largest water discharges are associated to the highest virtual velocities. At Ussaia there is not a distinct relation between peak discharge and virtual velocities. Events larger than $0.53 \text{ m}^3\text{s}^{-1}$ exhibit a strong positive relation between peak discharge and virtual velocities. The transition from bedload transport to debris flow is marked by an increase of median values of virtual velocities by almost two orders of magnitude.

The channel bed stability promoted by limited sediment supply is reflected also in the depth of the active layer. From the digging tests performed, we found that median tracer burial in the Grigno Creek is 0.1 m, and 2.5 time larger in the Ussaia Creek, testifying in this latter case, the vertical exchange of sediment during flood events. Moreover, in the Ussaia Creek, in the period 2013-2015, we observed three main events that radically changed the morphology of the studied reach, re-organizing main channel morphological structures, and forming lateral bars or depositional lobes. These events are associated to autumn precipitations that hit the study site in November 2013 and November 2014, and a springtime

event occurred in April 2013, when the effects of rainfall enhanced the transport capacity associated to snowmelt.

To evaluate the influence of active channel width and depth on bedload transfer, we have conducted a sensitivity analysis that is composed of three scenarios. Scenario 1 (S1) corresponds to the classic metric configuration applied in the literature (e.g., Haschenburger and Church, 1998; Liebault and Laronne, 2008; Dell’Agnese et al., 2015), which uses average tracer virtual velocity by weight category, constant average channel width, and constant average channel depth. Scenario 2 (S2) differs in that it uses the median tracer virtual velocity at the event scale. Scenario 3 (S3) is site-specific and differs between the Valsugana (S3a) and the Val di Sole (S3b) sites. In the former case, the calculation of average active channel width excludes the areas occupied by immobile keystone (boulder-cascades) and that do not become submerged at bankfull level. In the calculations of Ussaia Creek’s bedload volumes, we use the entire average channel width for the debris-flow event (i.e., November 4-8, 2014) that mobilized the entire channel bed, and we reduce it by excluding islands and lateral bars that did not exhibit any tracer motion during floods. In the Grigno Creek we observed that adopting S2, the value of cumulative bedload transfer reduces roughly by 15% compared to bedload volume evaluated using S1. Considering an active channel width calculated excluding the large immobile elements, cumulated bedload transfer is reduced by an ulterior 25%, with differences among S1 and S3a scenarios of nearly the 40%. In the case of Ussaia Creek differences are much larger, mainly due to the impact exerted by difference in channel width between ordinary and extreme events. If we adopt the entire channel mobility for ordinary events, we would overestimate the bedload transport roughly by a 4-times folder factor. By means of these simple scenarios, we demonstrated that the assumptions adopted in the methodology that has been customarily applied in the literature, could lead to less realistic evaluation of bedload volume transfer.

Linkages between rainfall properties and bedload transport have been explored. Results show that channel beds characterized by large stability are less sensitive to prolonged, low-intensity precipitations, and this is in good agreement with what observed in other Alpine catchments (Badoux et al., 2012). Conversely, highly mobile beds, such as in the Ussaia Creek, are more prone to trigger bedload transport induced by low intensity events. In fact, we observed that identical channel morphologies, subject to simultaneous events, are responding in different ways according to site-specific sediment supply conditions. Moreover, at Ussaia Creek, we observed that hydro-meteorological forcing for the November 2014 event was weaker compared to Grigno Creek, but triggered a debris flow.

An additional study site, the Strimm Creek, characterized by drier conditions, allows us to analyze bedload transport data across a latitudinal transect within the Eastern Italian Alps. Results showed that Strimm Creek, a formerly glaciated high-elevation basin, is strongly influenced by its position and by the limited sediment-supply conditions, with bedload transport chiefly associated to snowmelt events. Tracers travel distances showed site-specific hydro-climatic forcing. To assess quantitatively the effects of specific hydrological forcing, for each site we summed the travel distances driven by each typology of forcing, comparing it to the overall sum of displacement lengths. At Strimm Creek, snowmelt events account for more than 70% of travel distances, and only 20% are related to rainfall events. At Ussaia site we observe that 83% of travelled distances are induced by rainfall and the 16% by snowmelt-related events. At Grigno and Tolva Creeks, the 98% of mobilized tracers at these two sites have been displaced by rainfall-induced floods.

The methodologies adopted in the present thesis provide effective means for the estimation of bedload sediment transfer. As we observed, the degree of connectivity between the hillslopes and the channels

profoundly affects the observed rates of bedload transport. In mountain watersheds sediment is mainly transported by rivers as bedload, that affects the amount of sediment delivered to coastal environments. Since mountain rivers are elected for hydropower production, the presence of artificial reservoir dams disrupts the river hydro-geomorphic continuity, affecting downstream sediment delivery. The dammed flux of water and sediment, largely affects channel morphodynamics of upstream and downstream reaches, imposing for example, sediment-starving conditions in the latter, causing degradation of river channel bed and banks, affecting properties and timing of bedload and altering riverine habitat conditions. Thus, quantitative estimates of sediment evacuated from headwater catchments are important to solve problems in many fields such as those of coastal engineering, where processes such as coastal erosion and shoreline retreat are governed by inland sediment supply.

Fieldwork conducted in this study showed the efficiency of bedload tracking monitoring programs in quantifying bedload rates at various scales, from flood event to seasonal and annual scale. The low-cost, effective tools adopted for tagging stones (each PIT has an approximate cost of \$2.00) and tracking displacements, permits to release statistically significant amount of tracers within study reaches, to investigate bedload properties. The b-axis of tracers released at our study sites range from 45 to 128 mm. The lower limit is physically imposed by the size of PITs, but we could extend the upper limit, tagging and releasing larger clasts, to observe timing and displacement lengths associated to those elements.

In this thesis, we have evaluated flow resistance and colluvial sediment supply respectively in a semi-qualitative and qualitative fashion. In order to appraise fully the effects of these two variables on the morphodynamics of our study reaches, future work in the upcoming field season will aim at quantifying: (i) subaerial and submerged channel bed roughness; and (ii) contemporary colluvial sediment supply to the drainage network. The effects of channel roughness on tracers' displacements have been partly described in this study, adopting a proxy for roughness that we analyzed in terms of step height or pool depth. A quantitative estimate will be obtained by integrating topographic (total station surveys) and photogrammetric (structure-from-motion surveys) methodologies. Colluvial sediment supply to the channel network will be estimated by differencing two high-resolution, LiDAR-derived DTMs acquired by the Autonomous Province of Trento. One DTM was collected in 2005, the other, which is currently undergoing final post processing, was acquired between 2014 and 2015.

Bibliography

Aceti, A., Arpentì, E., Orombelli, G., Pini, R., and Ravazzi, C., Holocene climatic oscillations in the high mountains: new evidences and chronological constraints from the southern side of the Alps, in *Global Change in Mountain Regions*; Perth, Scotland, UK, 2-6 October 2005.

Agliardi, F., Crosta, G.B., Frattini, P., Integrating rockfall risk assessment and countermeasure design by 3D modelling techniques, *Nat. Hazards Syst. Sc.*, 9(2009), pp. 1059-1073, <http://dx.doi.org/10.5194/nhess-9-1059-2009>.

Allan, J.C., Hart, R., Tranquili, J.V., The use of Passive Integrated Transponder (PIT) tags to trace cobble transport in a mixed sand-and-gravel beach on the high-energy Oregon coast, *USA Marine Geology*, 232, 63-86. DOI: 10.1016/j.margeo.2006.07.00, 2006.

Andrews, E.D., Entrainment of gravel from naturally sorted riverbed material, *Geol. Soc. Am. Bull.*, 94, 1225-1231, 1983.

Armstrong, J. D., V. A. Braithwaite, and Rycroft, P., A flat-bed passive integrated transponder antenna array for monitoring behavior of Atlantic salmon parr and other fishes, *Journal of Fish Biology*, 48(3), 539-541, 1996.

Badoux, A., Turowski, J. M., Mao, L., Mathys, N., and Rickenmann, D.: Rainfall intensity–duration thresholds for bedload transport initiation in small Alpine watersheds, *Nat. Hazards Earth Syst. Sci.*, 12, 3091-3108, doi:10.5194/nhess-12-3091-2012, 2012.

Badoux, A., Andres, N., and Turowski, J.,M., Damage costs due to bedload transport processes in Switzerland, *Nat. Hazards Earth Syst. Sci.*, 14, 279-294, 2014.

Barth, S.; Oberli, F.; and Meier, M. 1994. Th-Pb versus U-Pb isotope systematics in allanite from cogenetic rhyolite and granodiorite: implications for geochronology, *Earth Planet. Sci. Lett.*, 124,149-159, 1994.

Belleudy, P., Valette, A., and Graff, B., Passive Hydrophone Monitoring of Bedload in River Beds: First Trials of Signal Spectral Analysis. In Gray, J. R., Laronne, J. B., and Marr, J. D. G., *Bedload-surrogate monitoring technologies: U.S. Geol. Surv. Scientific Investigations Report*, 2010-5091.

Bertrand, J., Chessex, R., Delaloye, M., Laurent, R., Vuagnet, M., Determinations, d'ages "plomb total" sur des zircons de la chaîne alpine, *Schw. Miner. Petr. Mitteil*, 45, pp. 317-326, 1965.

Bradley, D.N., and Tucker, G.E., Measuring gravel transport and dispersion in a mountain river using passive radio tracers, *Earth Surface Processes and Landforms*, 37, 1034-1045, 2012.

Braga G.P., Gatto G.O., Gatto P., Gregnanin P, Massari F, Medizza F., Nardin M., Perna G., Rossi D., Sacerdoti M., Semenza E., Somnavilla E., Zirpoli G., Zulian T. (1971), Note illustrative della Carta Geologica d'Italia. Foglio 022-Feltre. ISPRA, Servizio Geologico d'Italia.

Bunte, K. and Abt, S. R.: Sampling surface and subsurface particle size distributions in wadable gravel-and cobble-bed streams for analysis in sediment transport, hydraulics, and streambed monitoring, Gen. Tech. Rep. RMRS-GTR-74, U.S. Department of Agriculture, Forest Service, Rocky Mountain Research Station, Fort Collins, CO, USA, 428 pp., 2001.

Bunte, K., Abt, S., Effect of sampling time on measured gravel bed load transport rates in a coarse-bedded stream, *Water Resources Research*, 41, 2005.

- Butler, R.P., Movement of cobbles in a gravel bed stream during a flood season, *Geological society of America Bulletin*, 88, pp. 1072-1074, 1977.
- Caine, N., The Rainfall Intensity: Duration Control of Shallow Landslides and Debris Flows, *Geografiska Annaler. Series A, Physical Geography*, Vol. 62, No. 1/2 (1980), pp. 23-27, 1980.
- Camenen, B., Le Coz, J., Paquier, A., Lagouy, M., An estimation of gravel mobility over an alpine river gravel bar (Arc en Maurienne , France) using PIT-tag tracers. *5th International Conference on Fluvial Hydraulics (River Flow 2010)*, Braunschweig, Germany, 8-10 September 2010.
- Castellarin, A., Ipotesi paleogeografica sul bacino del Flysch sudalpino cretacico, *Boll. Soc. Geol. Ital.*, 95, pp. 501–511, 1977.
- Castellarin A., Selli L., Picotti V., and Cantelli L., La tettonica delle Dolomiti nel quadro delle Alpi Meridionali orientali, *Memorie della Società Geologica Italiana*, v. 53, pp. 133-143, 1998.
- Castellarin, A., Vai, G.B., Cantelli, L., The Alpine evolution of the Southern Alps around the Giudicarie faults: A Late Cretaceous to Early Eocene transfer zone, *Tectonophysics*, [Volume 414, Issues 1–4](#), pp. 203-223, 2006.
- Cavalli, M., Trevisani, S., Comiti, F., and Marchi, L., Geomorphometric assessment of spatial sediment connectivity in small Alpine catchments, *Geomorphology*, 188, 31-41, 2013.
- Chacho, E.F. Jr., Burrows. R.L., and Emmett, W.W., Detection of coarse sediment movement using radio transmitters, In: *Proceedings of the XXIII Congress on Hydraulics and the Environment*, IAHR, Ottawa, Canada, pp-B-367-B-373, 1989.
- Chapuis M., Bright C. J., Hufnagel J., and MacVicar B., Detection ranges and uncertainty of passive Radio Frequency Identification (RFID) transponders for sediment tracking in gravel rivers and coastal environments, *Earth Surf. Process. Landforms*, 39, 2109–2120, doi: [10.1002/esp.3620](https://doi.org/10.1002/esp.3620), 2014.
- Chin, A. and Wohl, E., Toward a theory for step pool in stream channels, *Progress in Physical Geography*, 29: 275-296, 2005.
- Church, M., Channel morphology and typology, in *The rivers Handbook*, v.1, edited by Calow, P. and Petts, G.E., pp. 126 – 143, Blackwell Science, Oxford, 1992.
- Comiti F., and Mao, L., Recent advances in the dynamics of steep channels, in *Gravel-bed Rivers: Processes, Tools, Environments*, John Wiley&Sons, Chichester, UK, 351-377, 2012.
- Comiti, F., Marchi, L., Macconi, P., Arattano, M., Beroldi, G., Borga, M., Brardinoni, F., Cavalli, M., D'Agostino, V., Penna, D., Theule, J., A new monitoring station for debris flows in the European Alps: first observations in the Gadria basin, *Natural Hazards*, Volume 73, [Issue 3](#), pp 1175-1198, 2014.
- Crevaschi, M., and Sevink J., Micromorphology of paleosol chronosequences on gravelly sediments in Northern Italy. In Fedoroff N., Bresson L.M. e Courty M.A., *Soil Micromorphology*, Paris, pp. 577-584, 1987.
- Dal Piaz, G., Castellarin, A., Martin, S., Selli, L., Carton, A., Pellegrini, G.B., Casolari, E., Daminato, F., Montessor, L., Picotti, V., Prosser, G., Santuliana, E., Cantelli, L., Note Illustrative della Carta Geologica d'Italia alla scala 1:50000, foglio 042, "Malè", APAT, Dipartimento Difesa del Suolo, 2007.
- Dell'Agnesse, A., Brardinoni, F., Toro, M., Mao, L., Engel, M., and Comiti, F., Bedload transport in a formerly glaciated mountain catchment constrained by particle tracking, *Earth Surf. Dynam.*, 3, 527-542, doi:10.5194/esurf-3-527-2015, 2015.

- Diakakis, M., Rainfall thresholds for bedload triggering: The case of Marathonas in Greece, *Nat. Hazards*, 60, 789-800, 2012.
- Dogliani, C., 1987, Tectonics of the Dolomites (Southern Alps-Northern Italy), *Journal of Structural Geology*, v. 9, pp. 181-193. Prosser, 2000
- Einstein, H. A., The bedload transport as probability problem. Mitteilung der Versuchsanstalt fuer Wasserbau an der Eidgenössischen Technischen Hochschule. Zürich; 110, 1937.
- Ferguson, R. I., & Wathen, S. J., Tracer-pebble movement along a concave river profile: Virtual velocity in relation to grain size and shear stress. *Water Resources Research*, 34(8), 2031–2038. doi:10.1029/98WR01283, 1998.
- Ferrara, G., Hirt, B., Leonardi, P., Longinelli, A., Datazione assoluta di alcune rocce del massiccio intrusivo di Cima d'Asta, *Atti Soc. Toscana Sc. Nat., A*, 69, fasc. 2, pp. 585-597, 1962.
- Florineth, D. and Schlüchter, C., Reconstructing the Last Glacial Maximum (LGM) ice surface geometry and flowlines in the Central Swiss Alps, *Eclogae Geologicae Helveticae*, 91: 391–407, 1998.
- Froehlich, W., The mechanisms of fluvial transport and waste supply into the stream channel in a mountainous flysch catchment, *Polska Akademia Nauk*, 143, Warsaw, 1982.
- Green, K.C., Brardinoni, F., and Alila, Y., Channel morphology and bed-load yield in fluvial, formerly-glaciated headwater streams of the Columbia Mountains, Canada, *Geomorphology*, 188, 96-109. doi: 10.1016/j.geomorph.2012.05.004, 2013.
- Green, K.C., Alila, Y., and Brardinoni, F., Patterns of bedload entrainment and transport in forested headwater streams of the Columbia Mountains, Canada, *Earth Surf. Process. Landforms*, 40, 427-446. doi: 10.1002/esp.3642, 2015.
- Habersack, H. M., Radio-tracking gravel particles in a large braided river in New Zealand : a field test of the stochastic theory of bed load transport proposed by Einstein, 391(March 2000), 377–391, 2001.
- Habler, G., Thöni, M., and Grasemann, B.: Cretaceous metamorphism in the Austroalpine Matsch Unit (Eastern Alps): the interrelation between deformation and chemical equilibration processes, *Miner. Petrol.*, 97, 149–171, 2009.
- Ham, D.,G., and Church, M., Bed-material transport estimated from channel morphodynamics: Chilliwak River, British Columbia, *Earth Surface Processes and Landforms*, 25: 1123-1142, 2000.
- Haschenburger, J.K., Church, M.A., Bed material transport estimated from the virtual velocity of sediment. *Earth Surface Processes and Landforms*, 23, pp. 791 – 808, 1998.
- Haschenburger, J.K., Tracing river gravels: Insights into dispersion from a long-term field experiment. *Geomorphology*, 200, 121–131. doi:10.1016/j.geomorph.2013.03.033, 2013.
- Hassan, M.A., Schick, A.P., and Laronne, J.B., The recovery of flood-dispersed coarse sediment particle, a three dimensional magnetic tracing method. In: Schick, A.P., ed., Channel Processes – Water, Sediment and Catchment Controls, *Catena Supplement 5*, pp. 153-162, 1984.
- Hassan, M. and Church, M., Size and distance of travel of unconstrained clasts on a streambed. *Water Resources Research*, vol. 28, n. 1, 299 – 303, 1992.
- Hassan, M.A., Schick, A.P., and Shaw, P.A., The transport of gravel in an ephemeral sandbed river. *Earth Surface Processes and Landforms*, 24, 623-640, 1999.

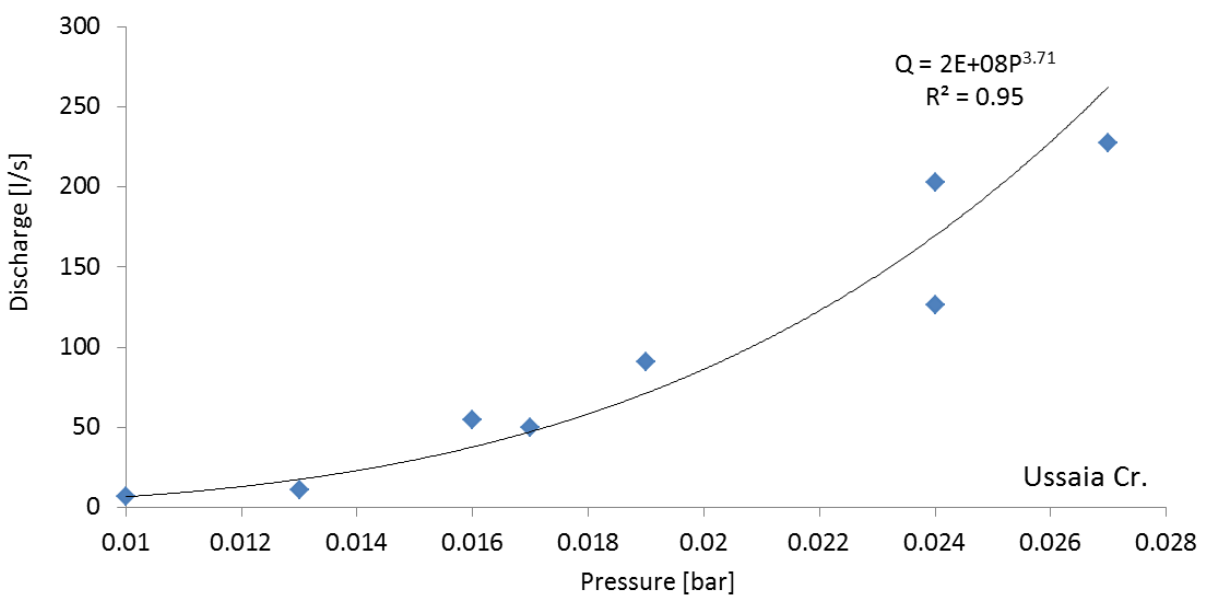
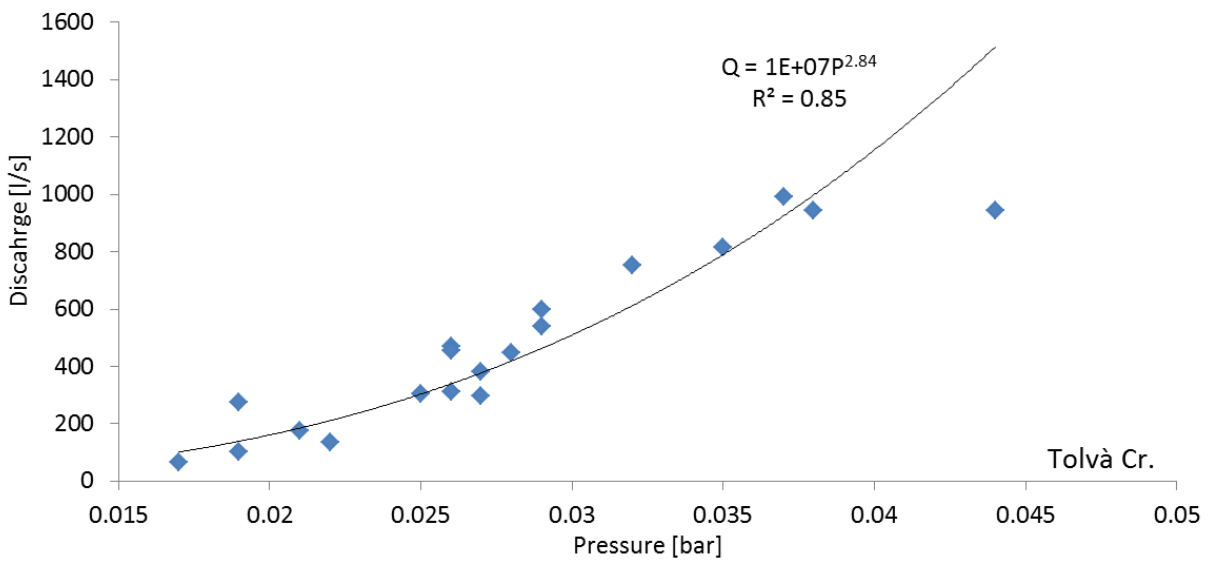
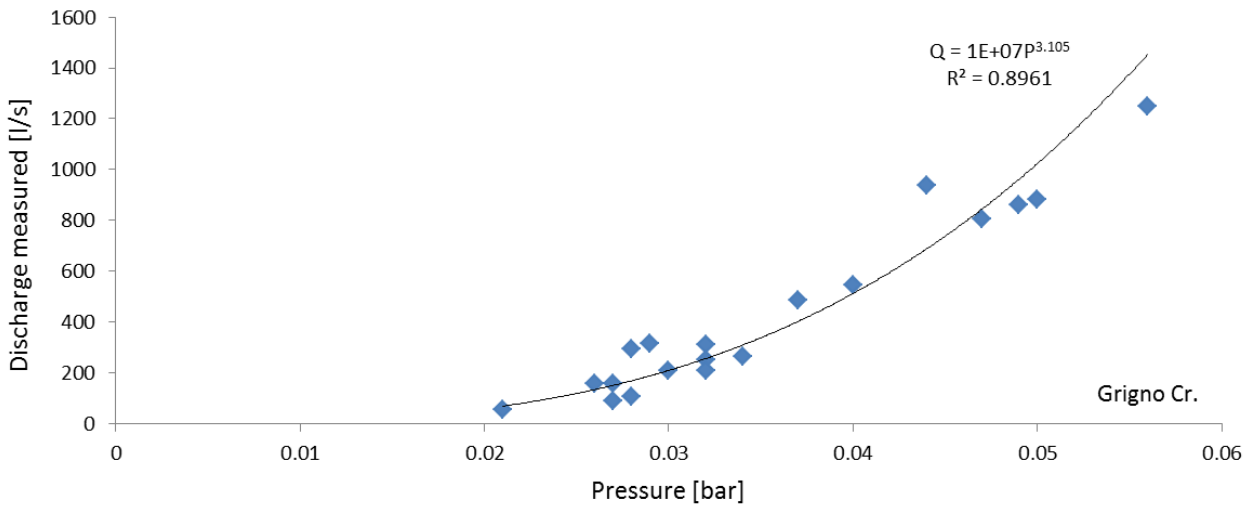
- Hassan, M., Ergenzinger, P., Use of tracers in fluvial geomorphology. In *Tools in Fluvial Geomorphology*, edited by Kondolf, G.M. and Piégay, H., pp. 397 - 423, John Wiley and Sons, 2002.
- Hassan, M. A., Egozi, R., and Parker, G., Experiments on the effect of hydrograph characteristics on vertical grain sorting in gravel bed rivers, *Water Resour. Res.*, 42, W09408, doi:10.1029/2005WR004707, 2006.
- Hassan, M. A., Voepel, H., Schumer, R., Parker, G., and Fraccarollo, L., Displacement characteristics of coarse fluvial bed sediment. *Journal of Geophysical Research: Earth Surface*, 118(1), 155–165. doi:10.1029/2012JF002374, 2013.
- Hayward, J.A. and Sutherland, A.J., The Torlesse stream vortex-tube sediment trap, *Journal of Hydrology (N.Z.)*, Vol. 13(1), pp. 41-53, 1974.
- Heiss, A. G., Kofler, W., and Oegg, K.: The Ulten Valley in South Tyrol, Italy: Vegetation and Settlement History of the Area, and Macrofossil Record from the Iron Age Cult Site of St. Walburg, *Palyto-Bull.*, 1, 63–73, 2005.
- Heritage G.L., Milan D.J., Large A. and Fuller I.C., Influence of survey strategy and interpolation model on DEM quality, *Geomorphology (112)*, 2009.
- Hicks D.M., and Gomez B., Sediment transport. In *Tools in Fluvial Geomorphology*, edited by Kondolf, G.M. and Piégay, H., pp. 105 - 134, John Wiley and Sons, 2003.
- Houbrechts, G., Van Campenhout, J., Levecq, Y., Hallot, E., Peeters, A. and Petit, F., Comparison of methods for quantifying active layer dynamics and bedload discharge in armored gravel-bed rivers. *Earth Surface Processes and Landforms*, 37, 1501-1517. Doi:10.1002/esp.3258, 2012.
- Ivy-Ochs, S., Kerschner, H., Kubik, P.W., and Schlüchter C., Glacier response in the European Alps to the Heinrich event 1 cooling: the Gschnitz stadial, *Journal of Quaternary Science*, v. 21, pp. 115-130, doi: 10.1002/jqs.955, 2006.
- Johnston, P., F. Bérubé, and Bergeron, N.E., Development of a flatbed passive integrated transponder antenna grid for continuous monitoring of fishes in natural streams, *Journal of Fish Biology*, 74(7), 1651-1661, 2009.
- Kelly, M.A., Buoncristiani, J.F., and Schlüchter C., A reconstruction of the Last Glacial Maximum (LGM), ice-surface geometry in the western Swiss Alps and contiguous Alpine regions in Italy and France, *Eclogae Geologicae Helveticae*, 97: 57-75, 2004.
- Knighton, D., *Fluvial forms and processes*. Arnold, 1998.
- Krumbein, W. C, and Pettijohn, F. J., *Manual of sedimentary petrography*: New York, D. Appleton-Century Co., 549, 1938
- La Brentana: l'alluvione del 1966 nella Valsugana Orientale. A cura di Attilio Pedenzini, Editore Le Croxarie, 2006.
- Lamarre, H., MacVicar, B., Roy, A.G., Using Passive Integrated Transponder (PIT) tags to investigate sediment transport in gravel-bed rivers. *Journal of Sedimentary Research*, 2005, v. 75, pp. 736 – 741, 2005.
- Lamarre, H., Roy, A.G., The role of morphology on the displacement of particles in a step–pool river system. *Geomorphology*, 99, pp. 270 – 279, 2008.
- Lambeck, K., Yokoyama, Y., and Purcell, T., Into and out of the Last Glacial Maximum: sea-level change during Oxygen Isotope Stages 3 and 2. *Quaternary Science Reviews* 21, 343–360, 2002.

- Laronne, J.B., Outhet, P.N., Duckham, J.L., McCabe, T.J., Determining event bedload volumes for evaluation of potential degradation sites due to gravel extraction, Erosion and sediment transport monitoring programmes in river basins, Proceedings of the Oslo Symposium, August 1992. IAHS Publ. No. 210, 1992.
- Laronne, J.B., Alexandrov, Y., Bergman, N., Cohen, H., Garcia, C., Habersack, H., Powell, D.M. and Reid, I., The continuous monitoring of bedload flux in various fluvial environments, Erosion and transport measurements in rivers: technological and methodological advances, Proceedings of the Oslo Workshop, June 2002, IAHS Publ. No. 283, 2003.
- Lenzi, M. A., L. Mao, and F. Comiti, Magnitude-frequency analysis of bed load data in an Alpine boulder bed stream, *Water Resour. Res.*, 40, W07201, doi:10.1029/2003WR002961, 2004.
- Leopold, L.B., Maddock, T., The hydraulic geometry of stream channels and some physiographic implication, *US Geological Survey Professional Paper*, 252, 1953.
- Leopold, L.B., Emmett, W.W., and Myrick, R.M., Channel and hillslope processes in a semi-arid area, New Mexico, *US Geological Survey Professional Paper* 352G, pp. 193-253, 1966.
- Liébault, F., Bellot, H., Chapuis, M., Klotz, S. and Deschâtres, M., Bedload tracing in a high-sediment-load mountain stream, *Earth Surf. Process. Landforms*, 37, 385–399. doi: 10.1002/esp.2245, 2012.
- Mao, L., Cavalli, M., Comiti, F., Marchi, L., Lenzi, M.A., Arattano, M., Sediment transfer processes in two Alpine catchments of contrasting morphology settings, *J. Hydrol.* 364, 88–98, 2009.
- Martin, Y., and Ham, D., Testing bedload transport formulae using morphologic transport estimates and field data: Lower Fraser River, British Columbia, *Earth Surface Processes and Landforms*, 30: 1265-1282, 2005.
- Micheletti N., Chandler J.H., Lane S.N., Structure from Motion (SfM) Photogrammetry, *Geomorphological Techniques*, 2015.
- Mizuyama, T., Laronne, J.B., Nonaka, M., Sawada, T., Satofuka, Y., Matsuoka, M., Yamashita, S., Sako, Y., Tamaki, S., Watari, M., Yamaguchi, M., Tsuruta, K., Calibration of a passive acoustic bedload monitoring system in Japanese mountain rivers. *U.S. Geological Survey Scientific Investigations Report*, 2010-5091, 2010.
- Montgomery D.R., and Buffington J.M., Channel-reach morphology in mountain drainage basins. *Geol. Soc. Am. Bull.*, v. 109, no. 5, pp. 596–611, 1997.
- Mueller, E. R., and J. Pitlick, Sediment supply and channel morphology in mountain river systems: 1. Relative importance of lithology, topography, and climate, *J. Geophys. Res. Earth Surf.*, 118, 2325–2342, doi:10.1002/2013JF002843, 2013.
- Nathan Bradley, D. and Tucker, G. E., Measuring gravel transport and dispersion in a mountain river using passive radio tracers. *Earth Surf. Process. Landforms*, 37, 1034–1045. doi: 10.1002/esp.3223, 2012.
- Nichols, M.H., A radio frequency identification system for monitoring coarse sediment particle displacement. *Applied Engineering in Agriculture*, 20(6), 783–787. doi:10.13031/2013.17727, 2004.
- Nir, D., Le processus érosifs dans le Nahal Zine (Neguev Septentrional) pendant le saisons pluvieuses, *Annales de géographie*, 73, pp. 8-20, 1964.
- Parker, G., and P. C. Klingeman, On why gravel bed streams are paved, *Water Resour. Res.*, 18(5), 1409–1423, doi:[10.1029/WR018i005p01409](https://doi.org/10.1029/WR018i005p01409), 1982.

- Pelpola, C. & Hickin, E.J. 2004. Long-term bed-load transport rate based on air photo and ground-penetrating radar surveys of fan-delta growth, Coast Mountains, British Columbia. *Geomorphology*, 57,169-181.
- Philips, C.B., Jerolmack, D.J., Willenbring, J.K., The threshold of motion filters extreme climatic fluctuations in gravel bedded alluvial and bedrock rivers resulting in near-threshold and transported-limited systems, *American Geophysical Union, Fall Meeting 2014*, abstract #EP31D-3585, 2014.
- Piégay, H., Schumm, S.A., System approaches in fluvial geomorphology. In *Tools in Fluvial Geomorphology*, edited by Kondolf, G.M. and Piégay, H., pp. 105 - 134, John Wiley and Sons, 2003.
- Reid, I., and Laronne, J.B., Bed load sediment transport in an ephemeral stream and a comparison with seasonal and perennial counterparts, *Water Resources Research*, 31(3), pp. 773-781, 1995.
- Rigon, R., G. Bertoldi, and T. M. Over, GEOFtop: a distributed hydrological model with coupled water and energy budgets, *J. Hydromet.*, 7, 371–388, 2006.
- Sayre, W.W., and Hubbell, D.W., Transport and dispersion of labeled bed material: North Loup River, Nebraska, *US Geological Survey Professional Paper*, 433-C, 48 p., 1965
- Schmidt, K.H., & Ergenzinger, P., Bedload entrainment, travel lengths, step lengths, rest periods—studied with passive (iron, magnetic) and active (radio) tracer techniques. *Earth Surface Processes and Landforms*, 17(2), 147–165. doi:10.1002/esp.3290170204, 1992.
- Schneider, J., Hegglin, R., Meier, S., Turowski, J.M., Nitsche, M., Rickenmann D., Studying sediment transport in mountain rivers by mobile and stationary RFID antennas. In *River Flow 2010*, edited by Dittrich, Koll, Aberle & Geisenhainer, pp. 1723 – 1730, 2010.
- Schneider, J.M., Turowsky, J.M., Rickenmann, D., Hegglin, R., Arrido, S., Mao, L., and Kirchner, J.M., Scaling relationships between bedload volumes, transport distances, and stream power in steep mountain channel, *J. Geophys. Res.-Earth*, 119, 533-549, 2014.
- Schumm S.A., *The Fluvial System*. Wiley, New York, 338 pp, 1977.
- Sear, D.A., Sediment transport processes in pool-riffle sequences, *Earth Surface Processes and Landforms*, 21, 241-262, 1996.
- Selli, R., Il Lineamento della Valsugana fra Trento e Cima d’Asta: cinematica neogenica ed eredit. strutturali permo-mesozoiche nel quadro evolutivo del Sudalpino Orientale (NE-Italia), *Mem. Soc. Geol. It*, 53, pp. 503–541, 1998.
- Sölva, H., Grasemann, B., Thöni, M., Thiedem R. and Habler, G. (2005) - The Schneeberg Normal Fault Zone: Normal faulting associated with Cretaceous SE-directed extrusion in the Eastern Alps (Italy/Austria). *Tectonophysics*, 401 (3-4), 143-166.
- Syvitsky, J.P.M., and Milliman, J., D., Geology, geography and humans battle for dominance over the delivery of fluvial sediment to the coastal ocean, *The Journal of Geology* 115(1), 1-19, 2007.
- Takayama, S., Bedload movement in torrential mountain streams, *Tokyo Geographical Paper*, 9: 169-188 (in Japanese), 1965.
- Tinner, W., Kaltenrieder, P. 2005. Rapid responses of high-mountain vegetation to early Holocene environmental changes in the Swiss Alps, *Journal of Ecology*, Vol. 93-5, 936–947.
- Totschnig, R., Sedlacek, W., and Fuchs, S., A quantitative vulnerability function for fluvial sediment transport for fluvial sediment transport, *Nat. Hazards*, 58, 681-703, 2011.

- Turowsky, J.M., Rickenmann, D., Measuring the Statistics of Bed-Load Transport Using Indirect Sensors. *Journal of Hydraulic Engineering*, Vol. 137, No. 1, January 1, 2011.
- Unfer, G., Hauer, C., and Lautsch, E., The influence of hydrology on the recruitment of brown trout in an Alpine river, the Ybbs River, Austria, *Ecol. Freshw. Fish*, 20, 438-448, 2011.
- Vericat, D., M. Church, and R. J. Batalla, Bedload bias: comparison of measurements obtained using two (76 and 152 mm) Helley-Smith samplers in a gravel bed river. *Water Resources Research*, 42, 2006.
- Vescovi, E., Ravazzi, C., Arpentì, E., Finsinger, W., Pini, R., Valsecchi, V., Wick, L., Ammann, B., and Tinner, W., Interactions between climate and vegetation during the Lateglacial period as recorded by lake and mire sediment archives in Northern Italy and Southern Switzerland, *Quaternary Sci. Rev.*, 26, 1650–1669, 2007.
- Westoby, J.M., Brasington, J., Glasser, N.F., Hambrey, M.J., Reynolds, J.M., ‘Structure- from-Motion’ photogrammetry: a low-cost, effective tool for geoscience applications, *Geomorphology*, 179, pp. 300-314, 2012.
- Williams R., Brasington J., Vericat D., Hicks M., Labrosse F. and Neal M., Monitoring braided river change using Terrestrial Laser Scanning and Optical Bathymetric Mapping, *Developments in Earth Surface Processes (15)*, 2011.
- Wilson, E.M., *Engineering Hydrology*. London, , UK: Macmillan Publ., 1983.
- Wolman, M.G., A method for sampling coarse river-bed material, *Transactions, American Geophysical Union, Volume 35*, Number 6, 1954.
- Yarnell, S.M., Mount J.F. and Larse E.W., The influence of relative sediment supply on riverine habitat heterogeneity, *Geomorphology*, 80, 310-324, 2006.

Appendix A3.1 – Stage-discharge curves

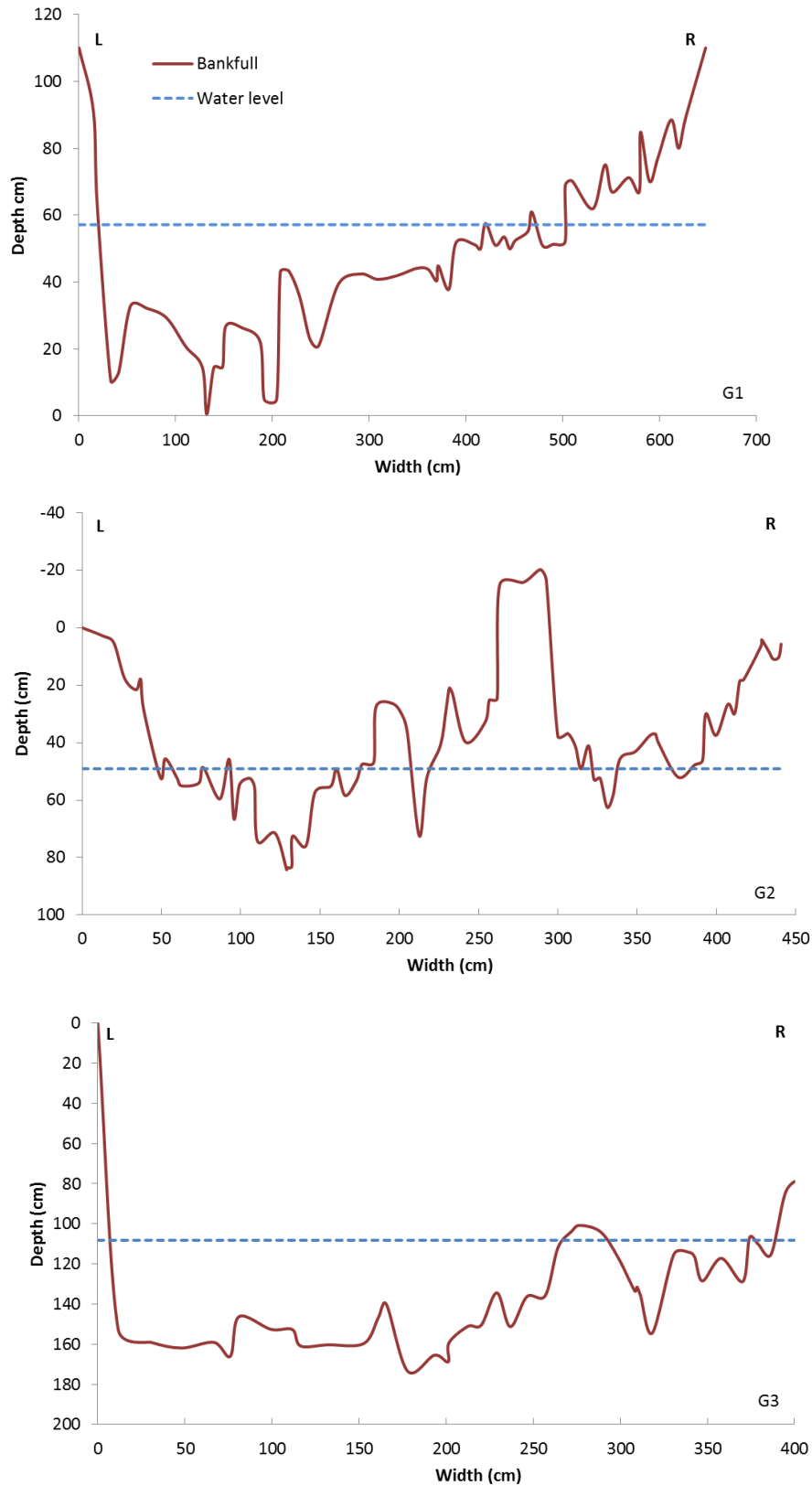


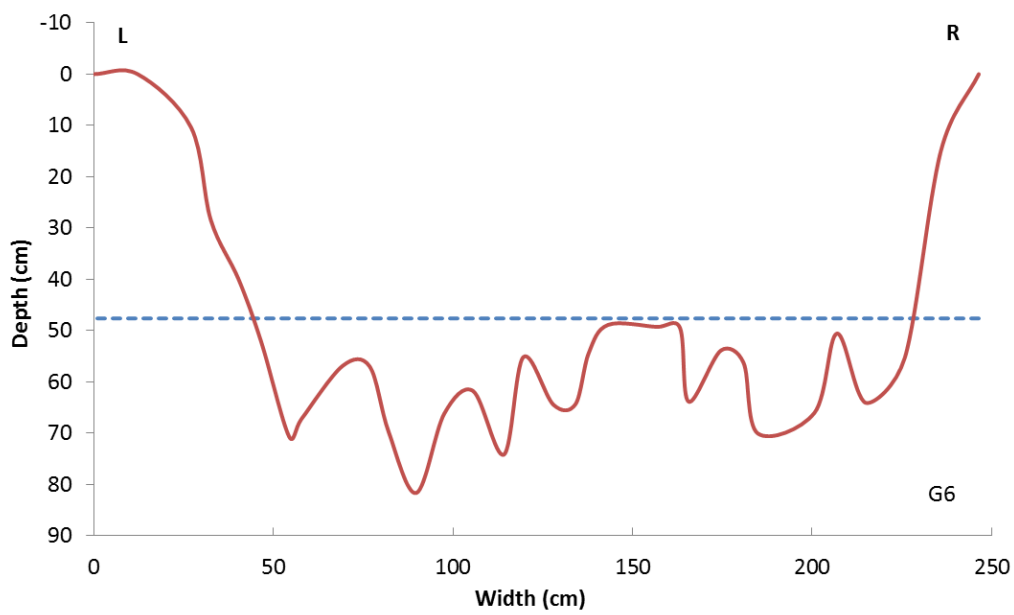
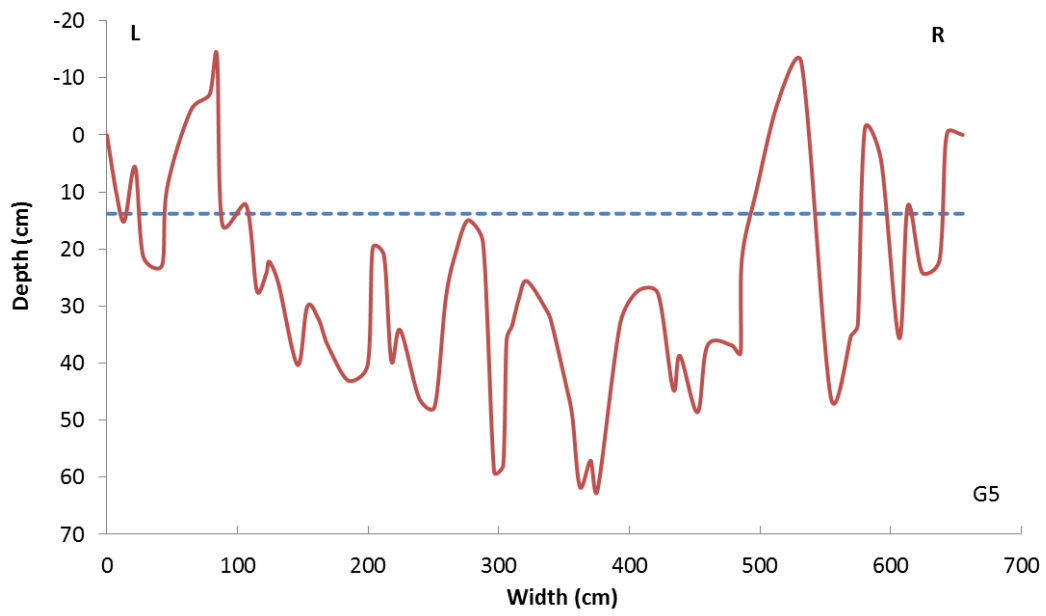
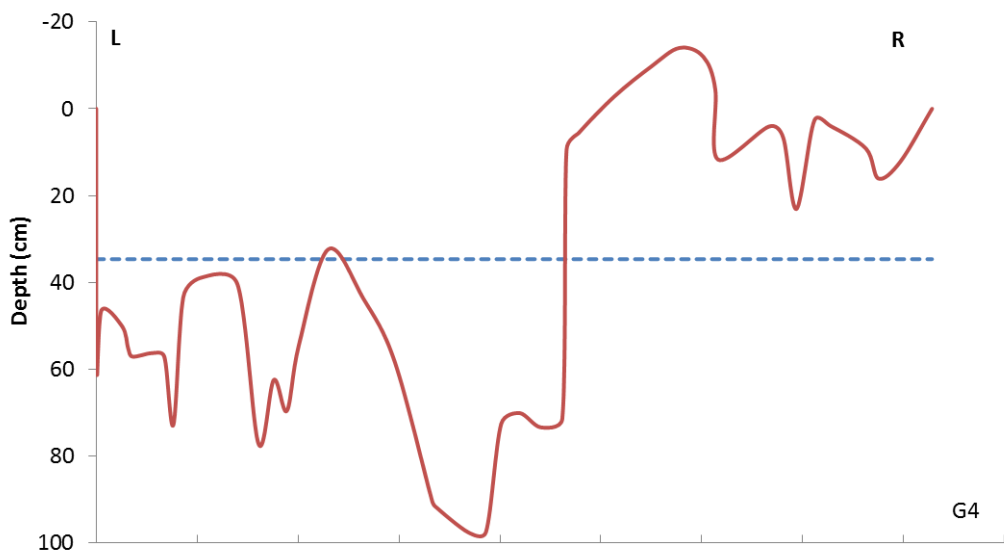
Stage-discharge curves constructed at Grigno, Tolvà and Ussaia Creek monitoring site. (Q = water discharge ($l s^{-1}$), P = hydrostatic pressure (bar)).

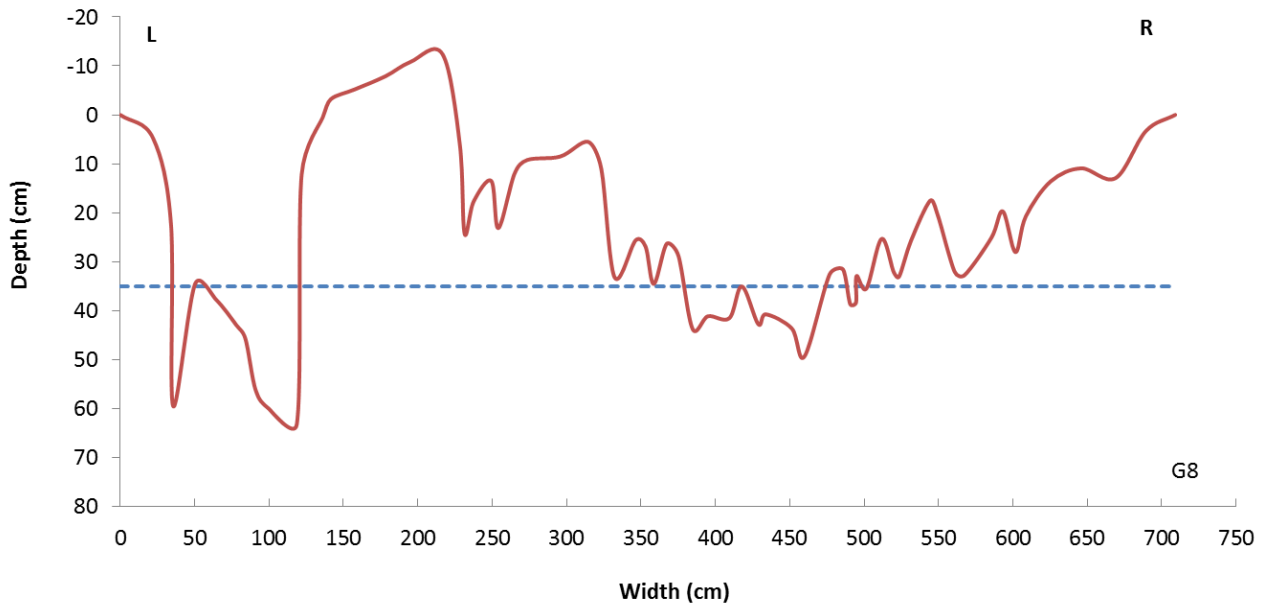
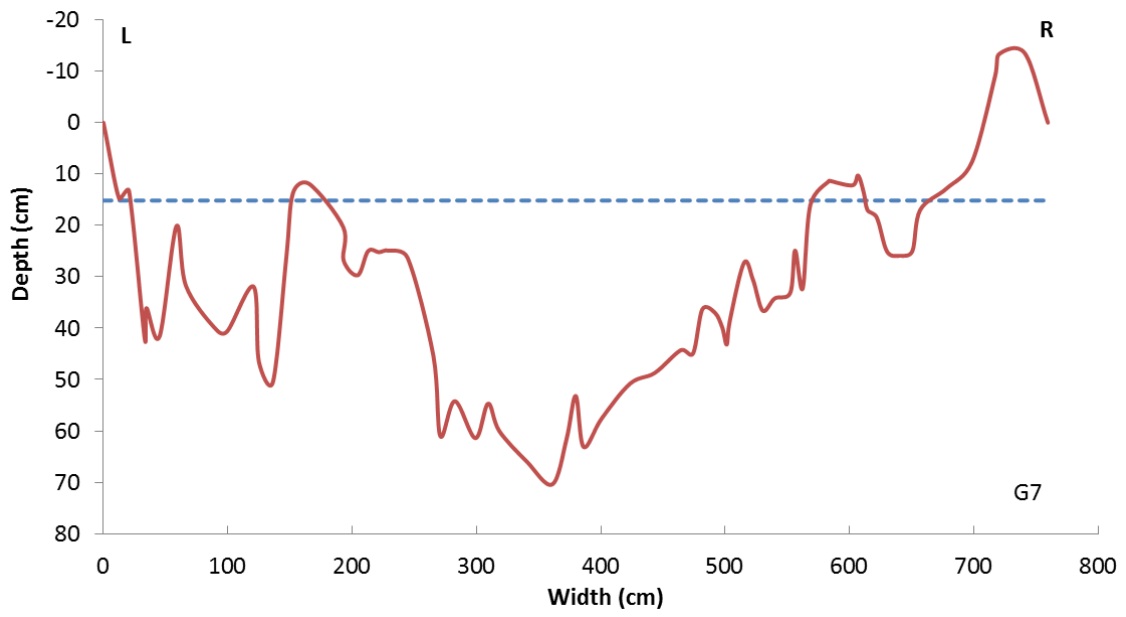
Appendix 4.1.1.2

Cross sections

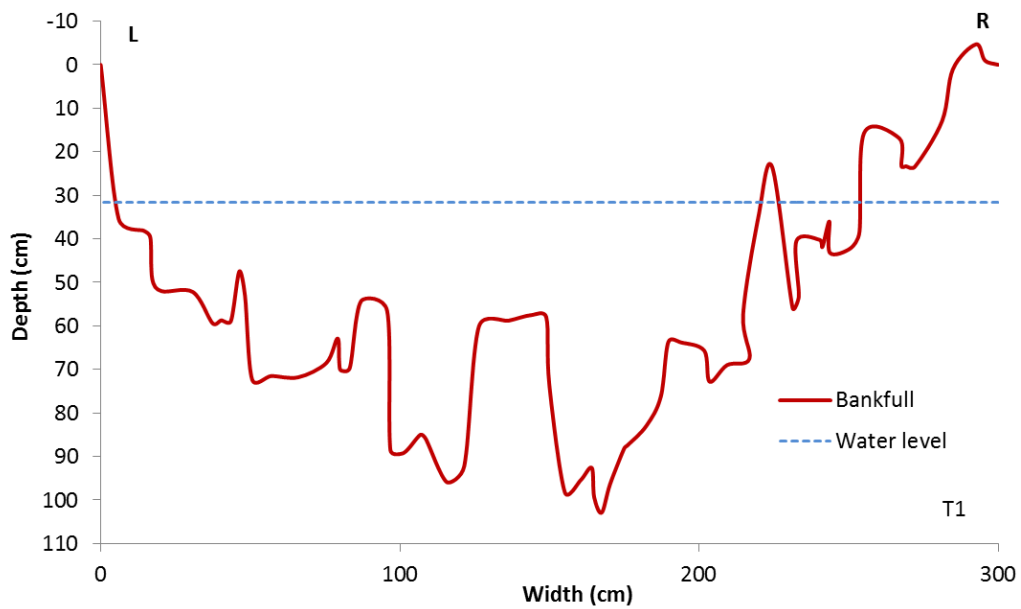
Grigno Creek

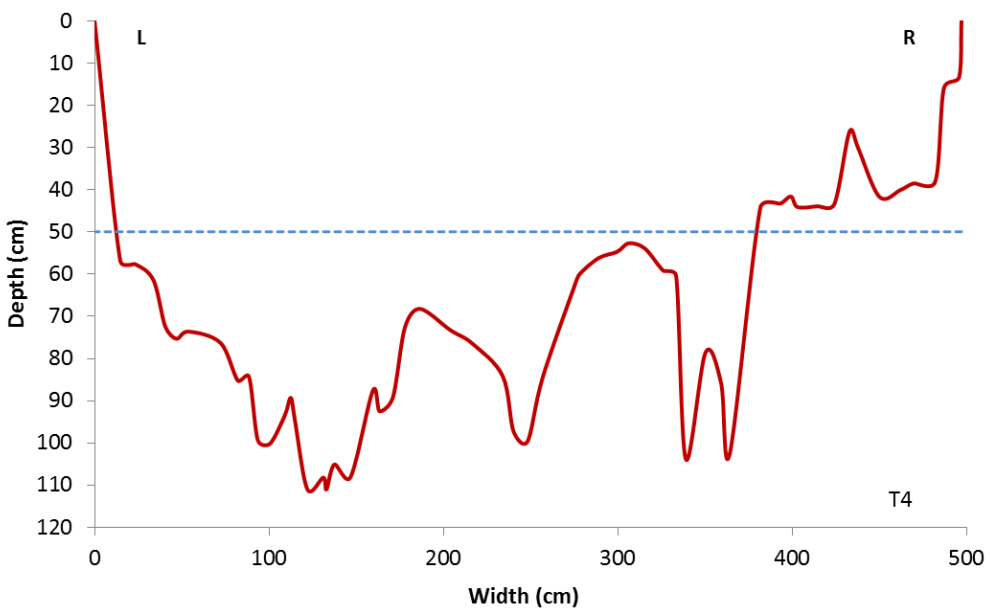
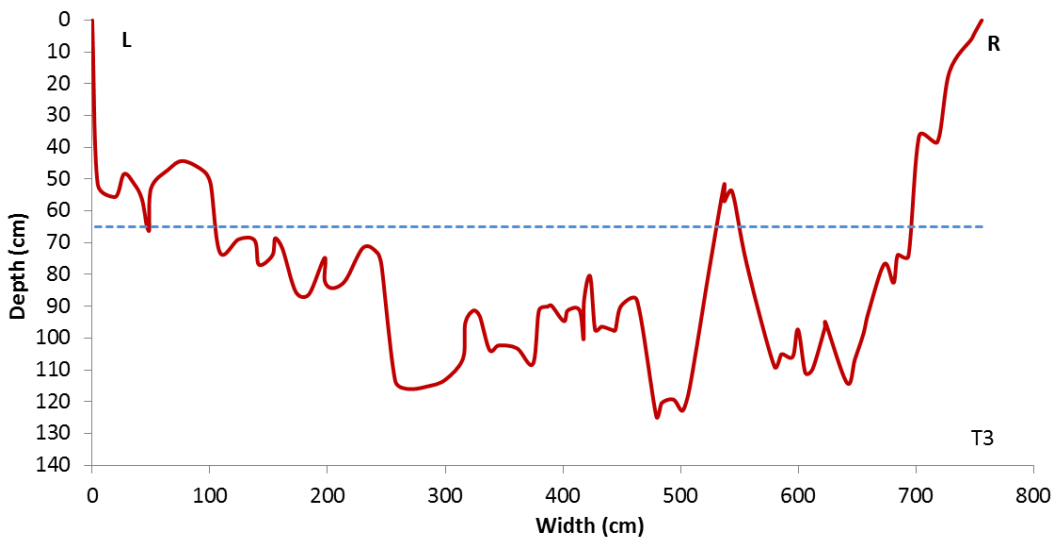
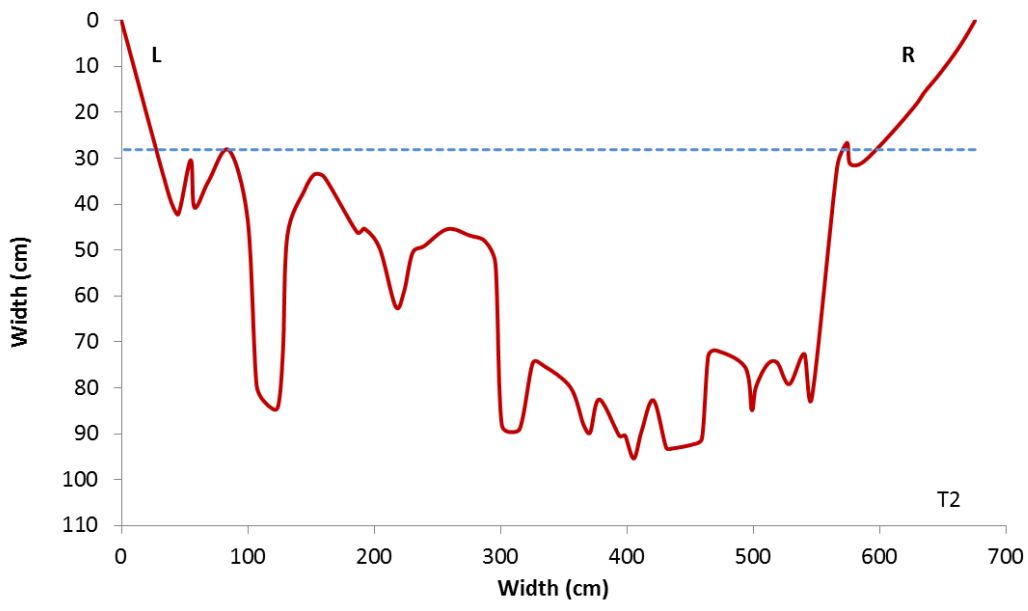


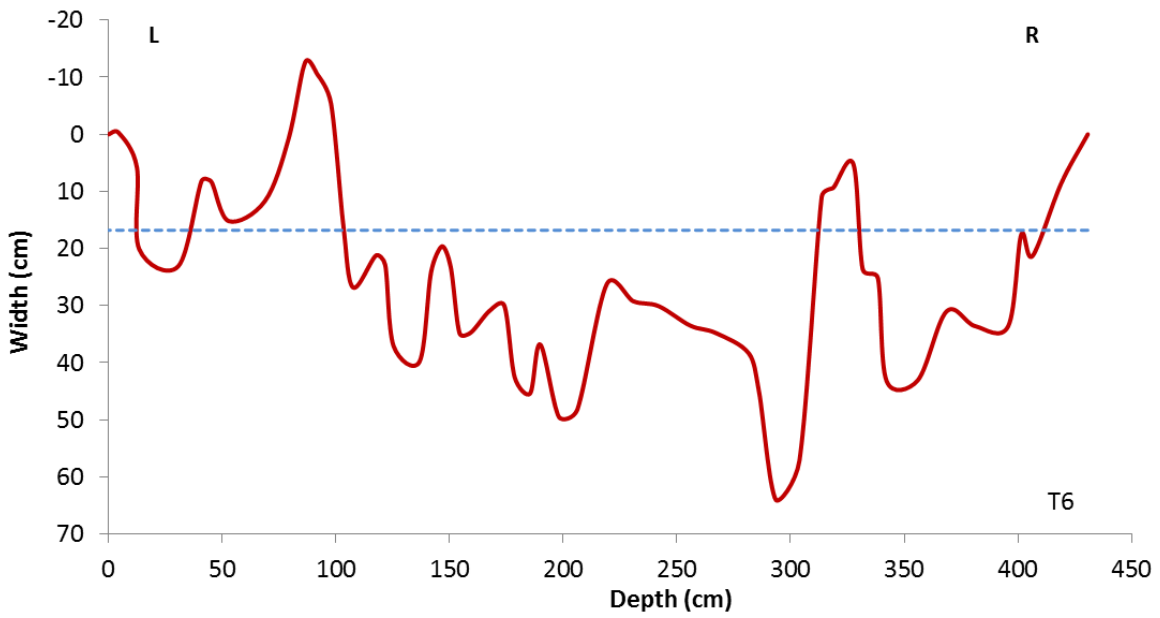
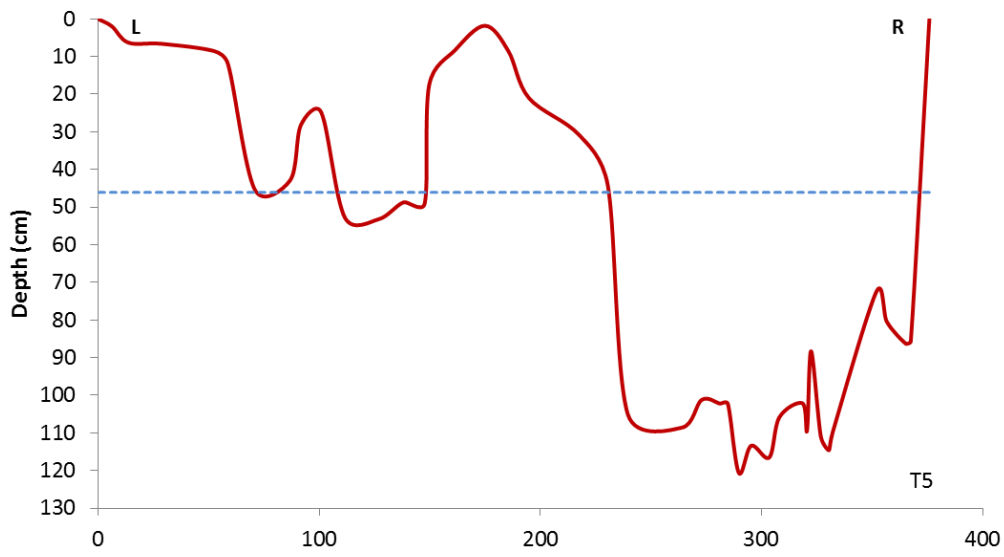




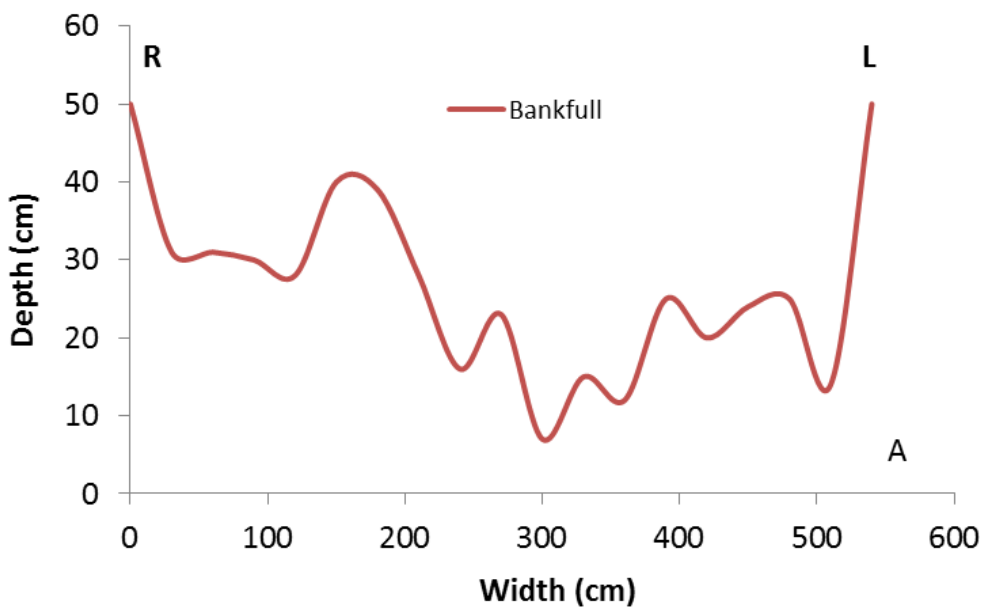
Tolvà Creek

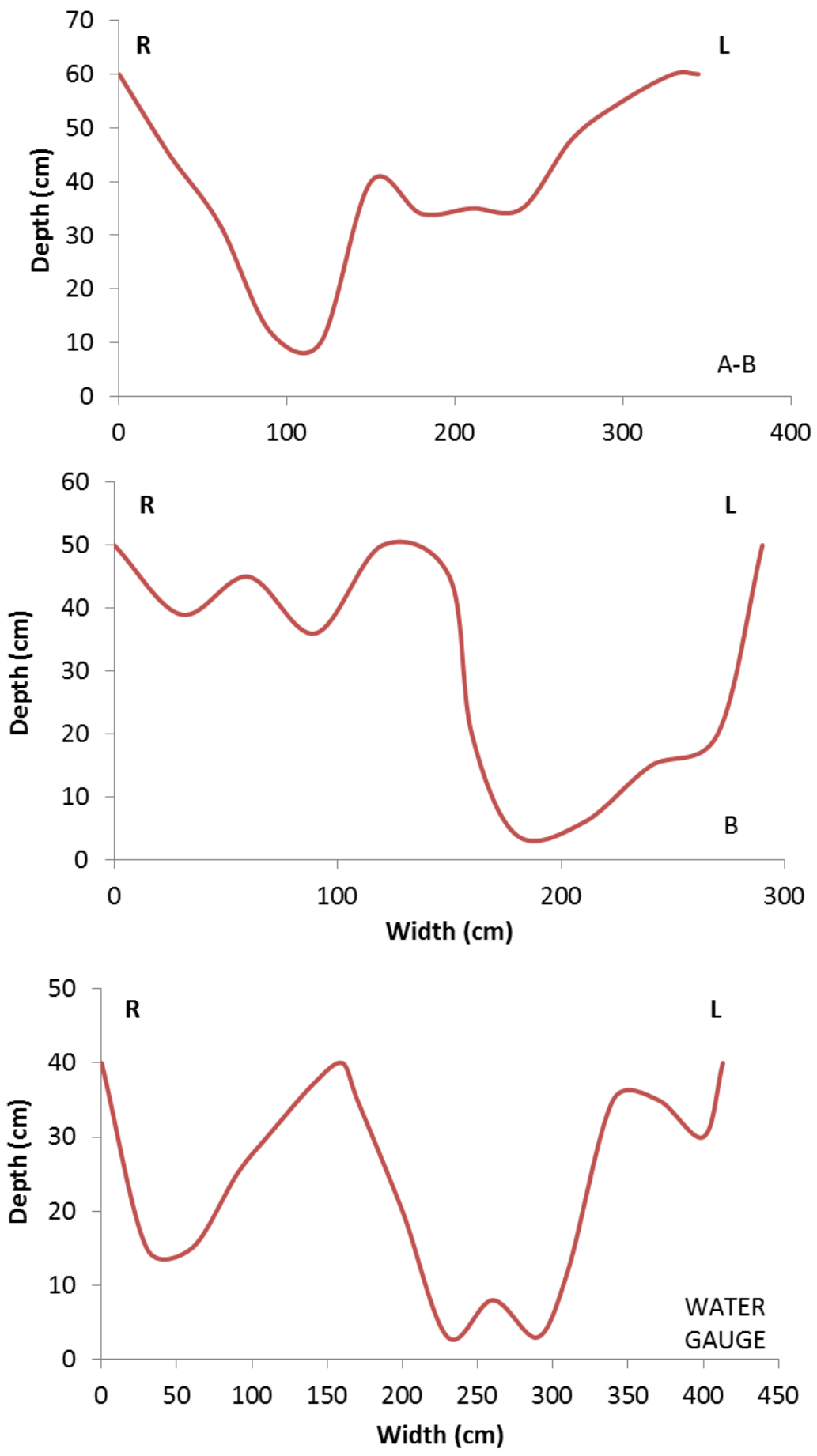


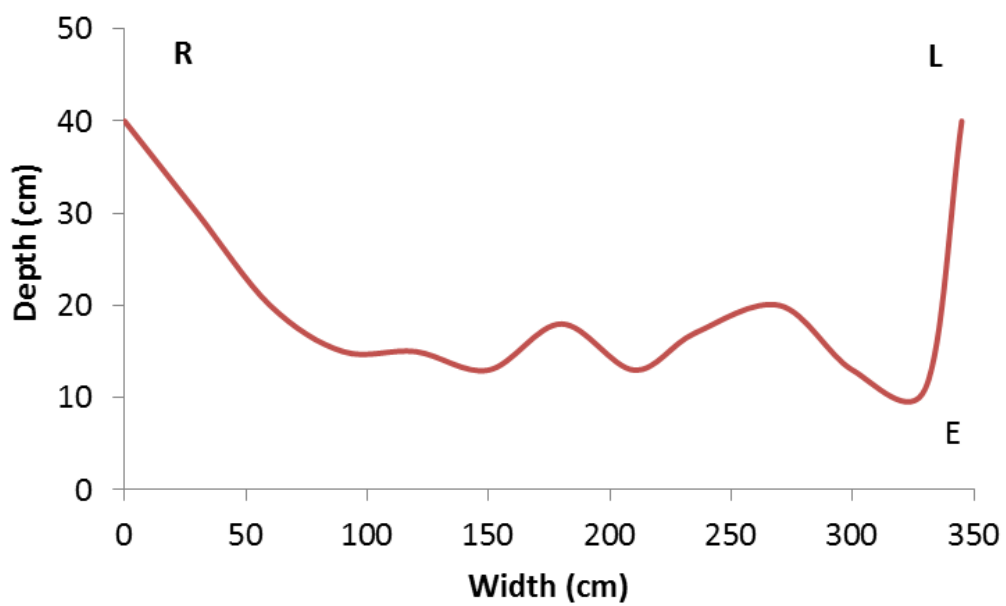
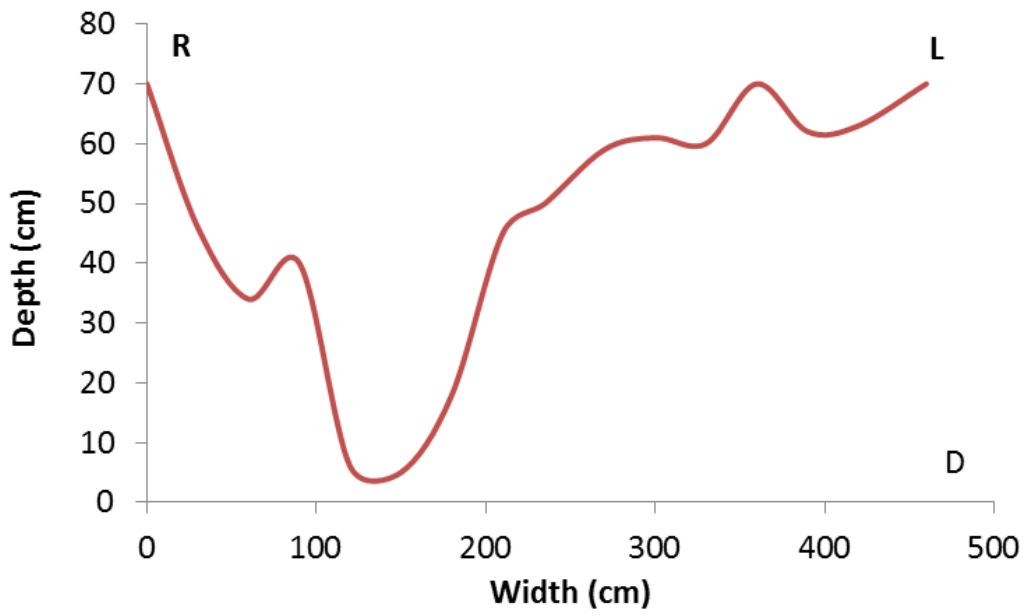
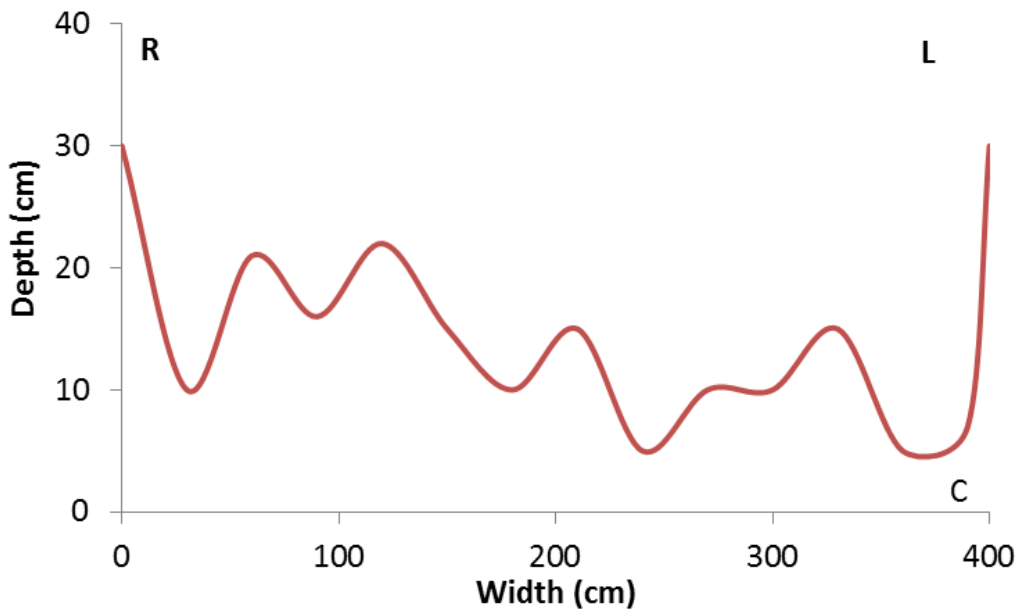


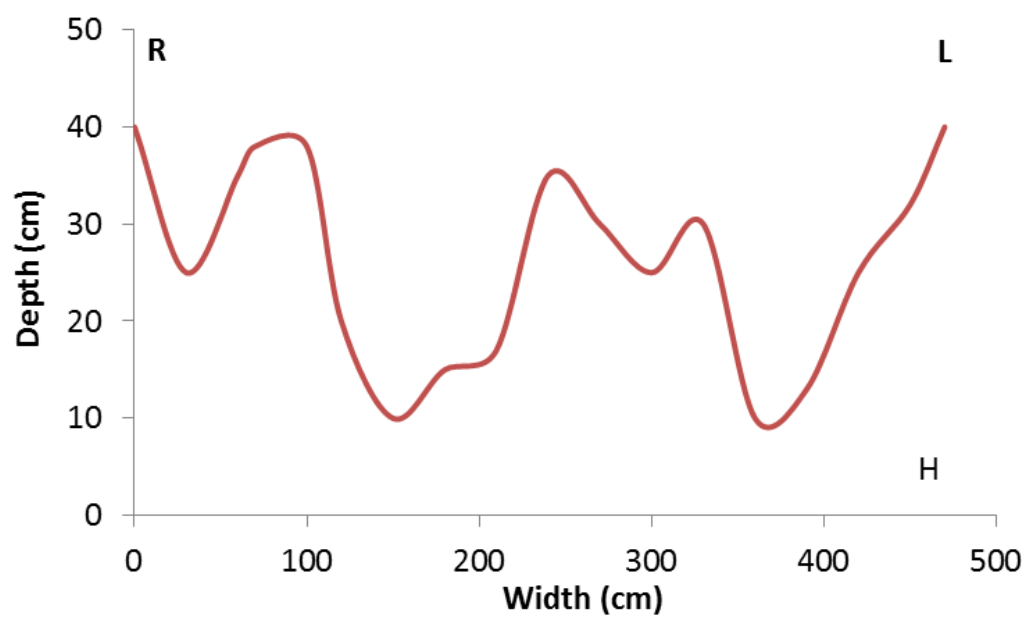
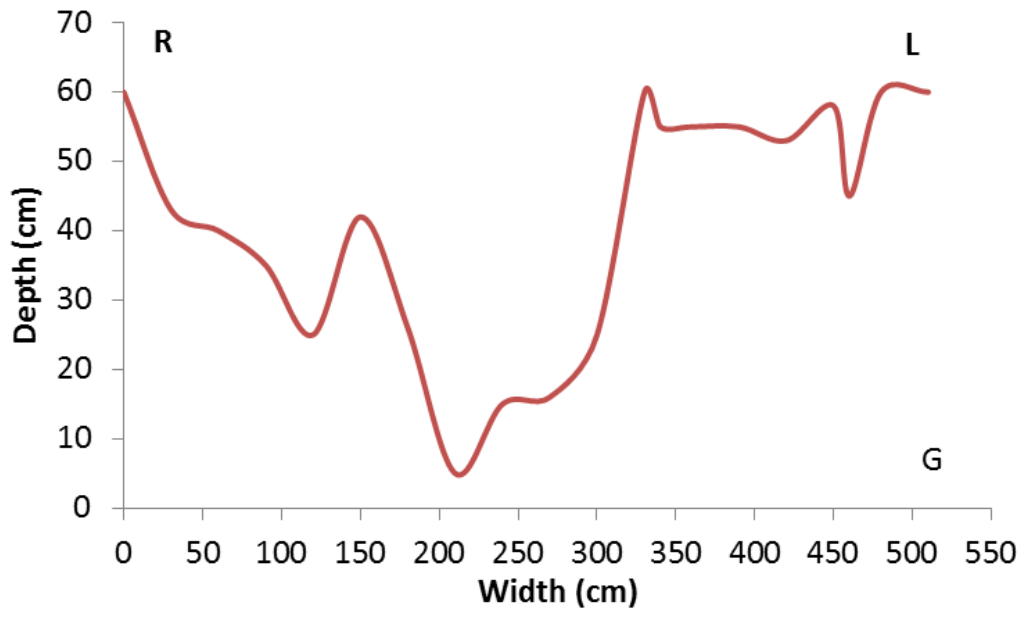
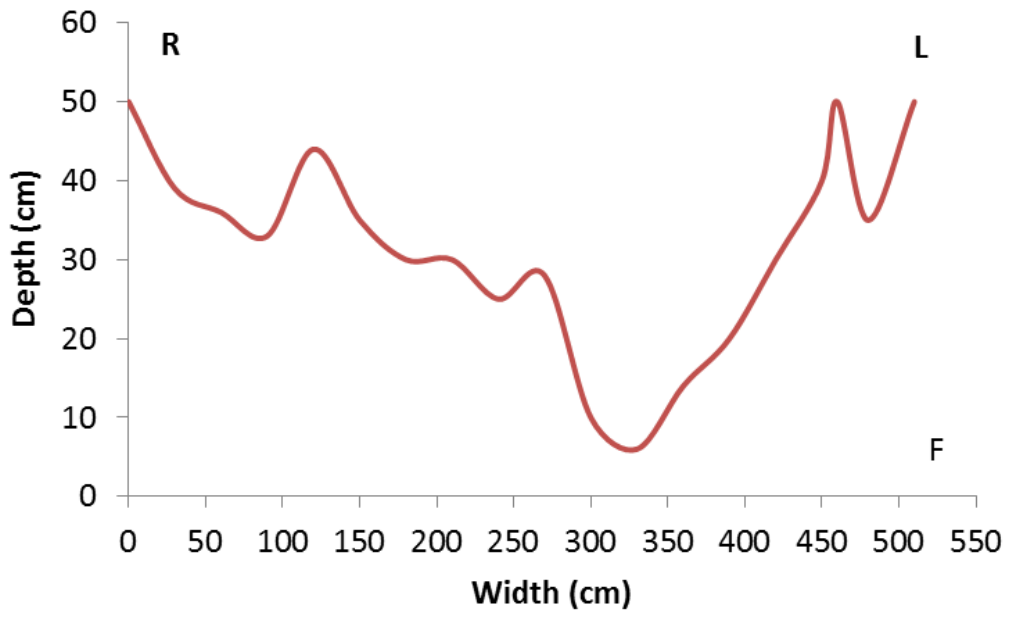


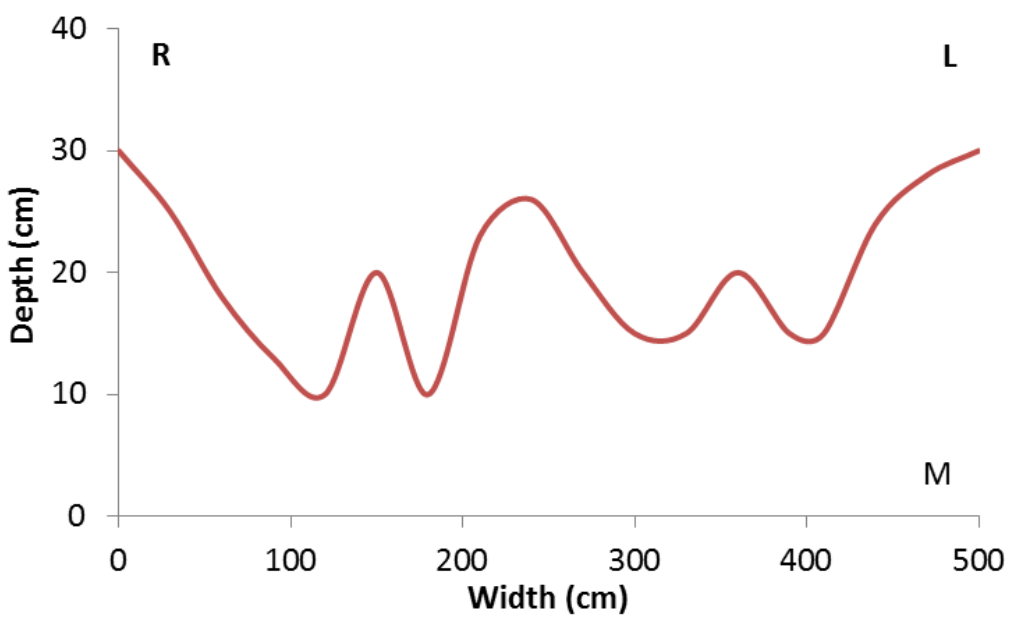
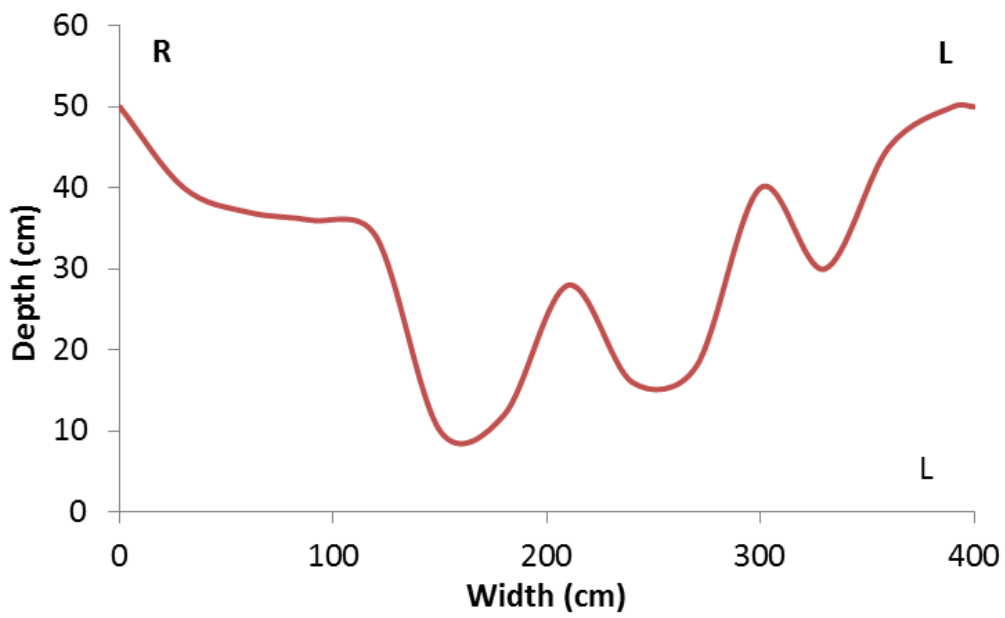
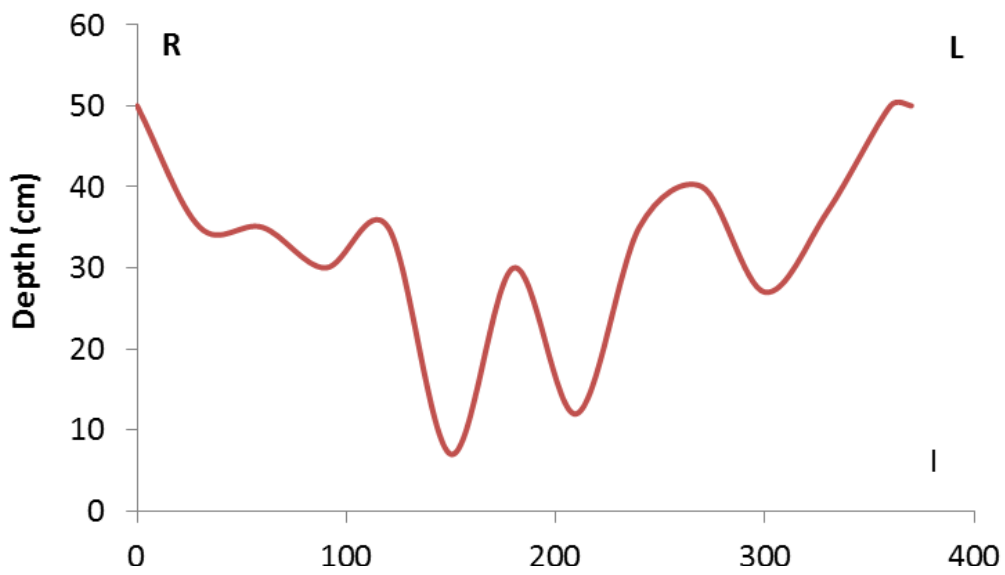
Ussaia Creek

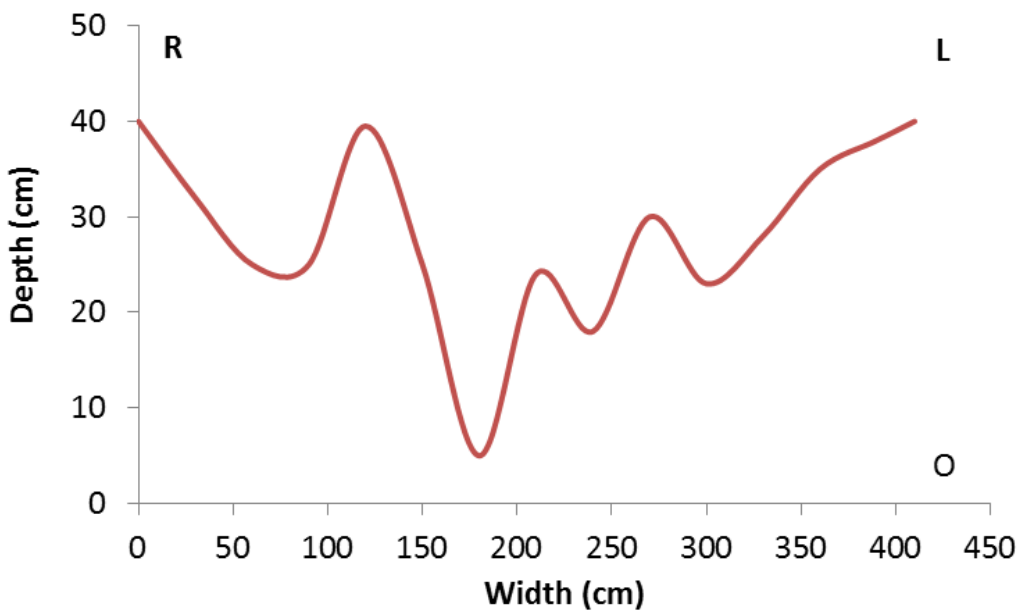
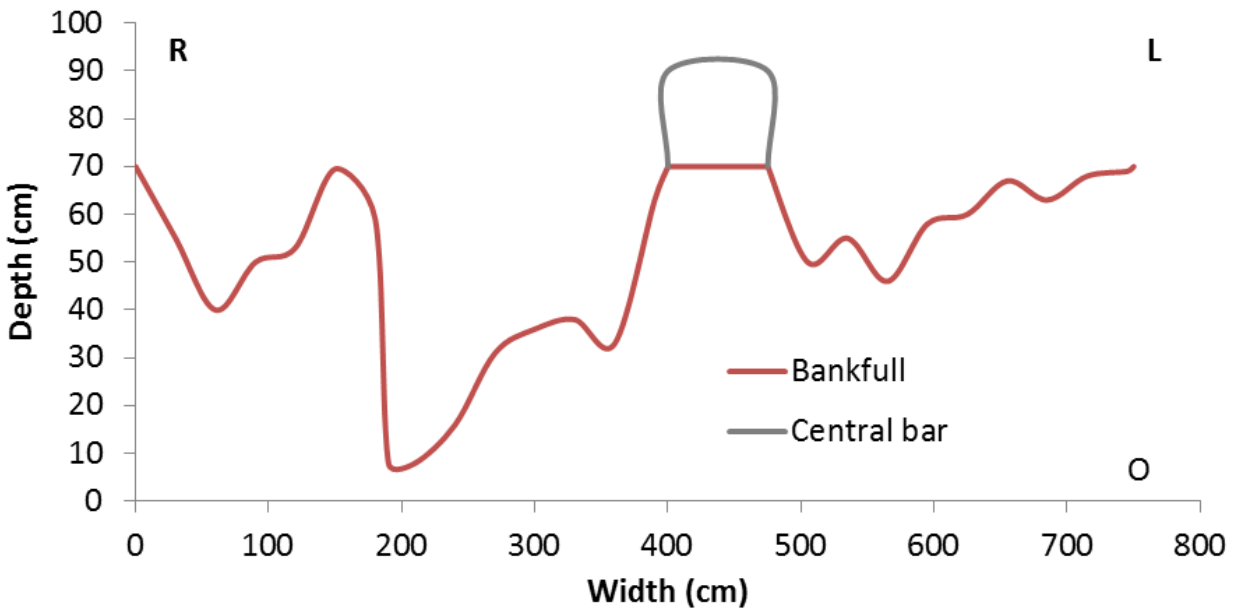
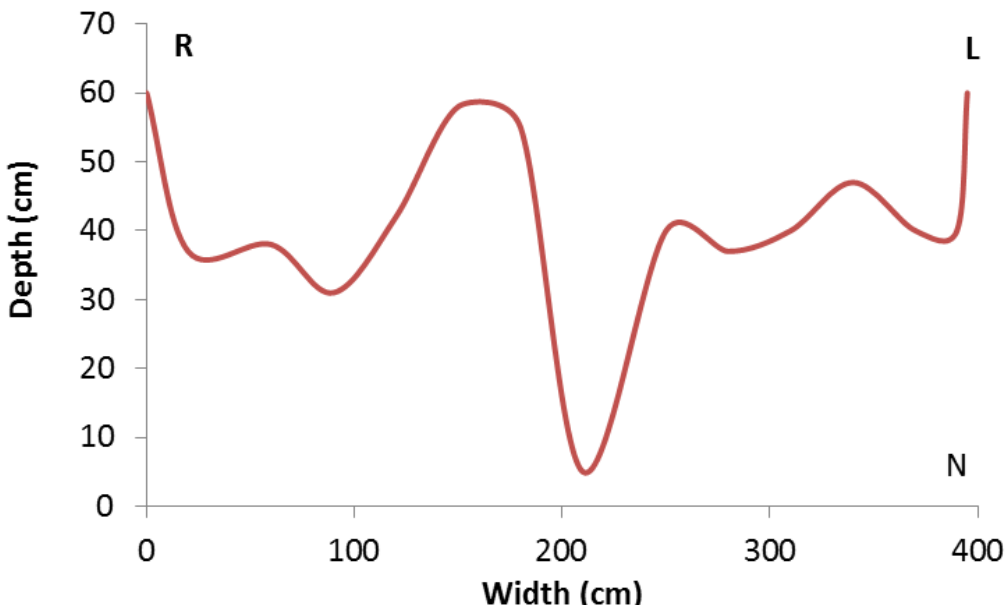


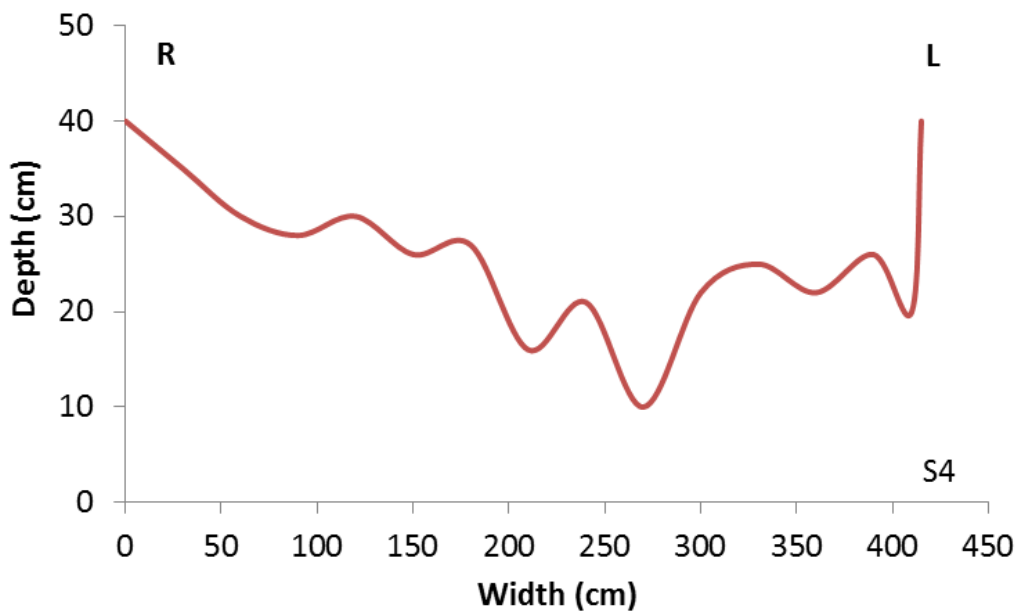
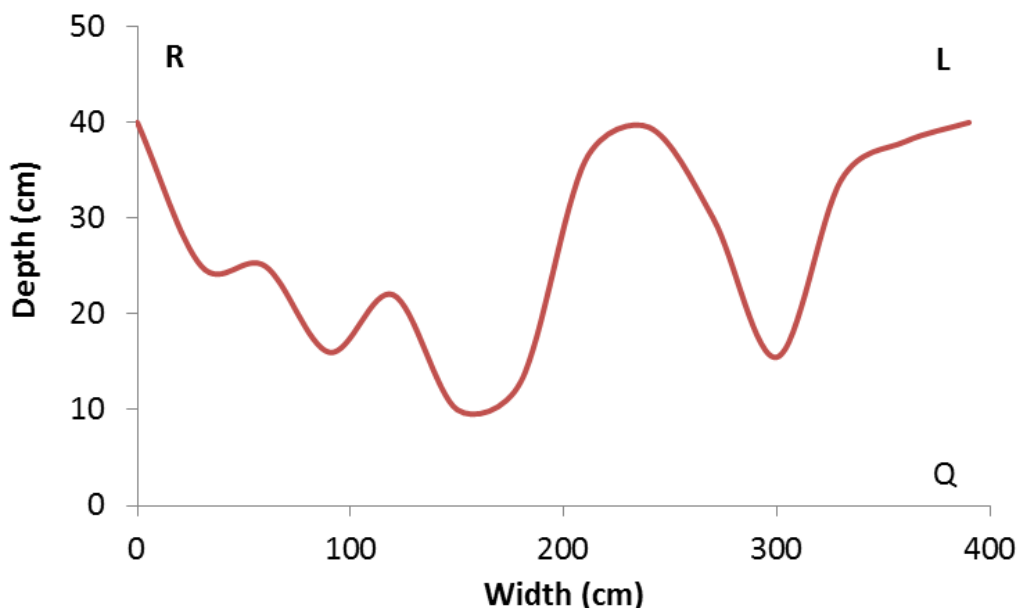
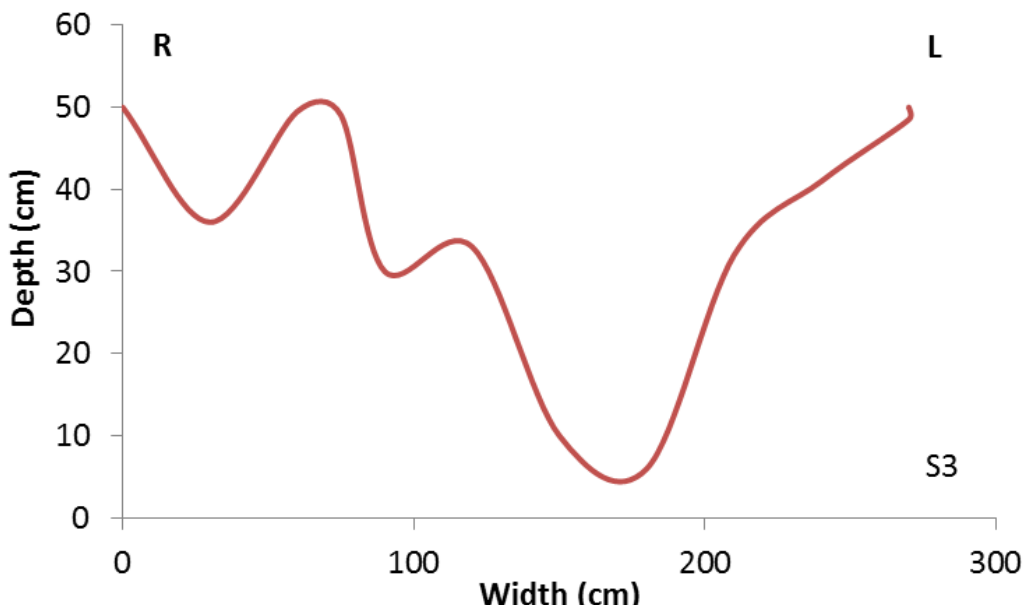


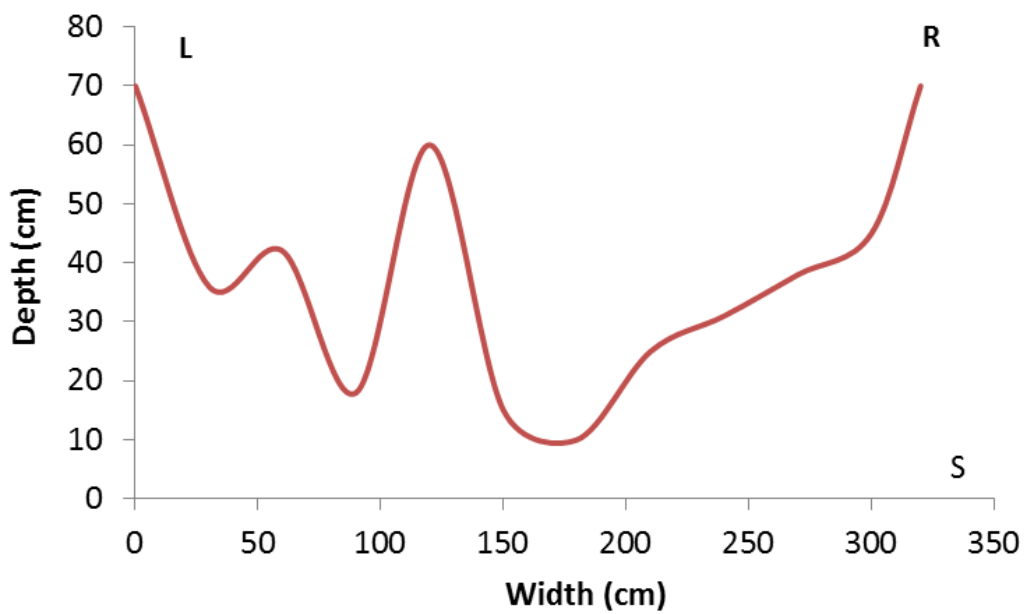
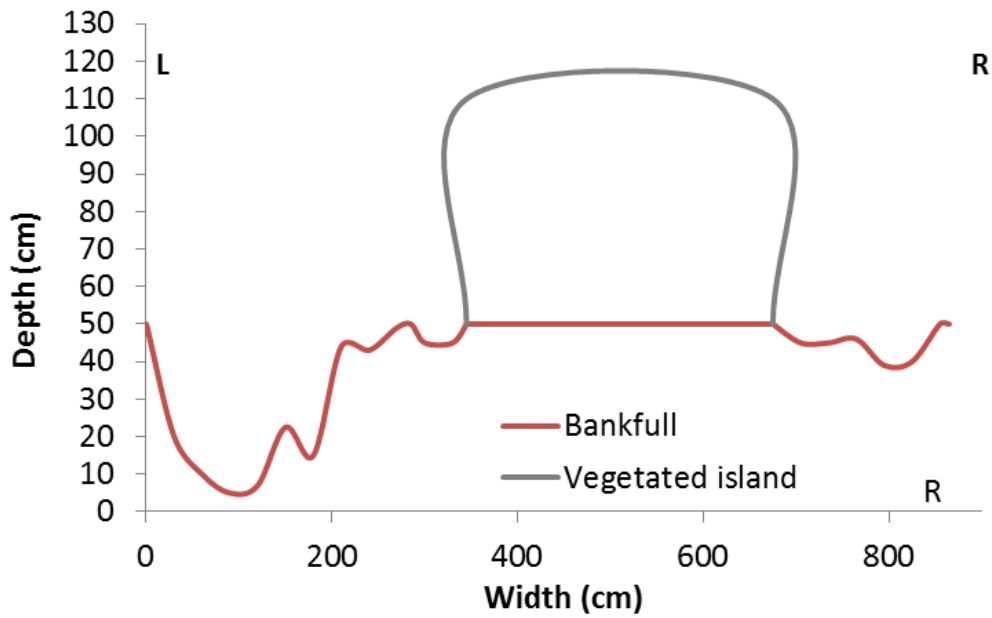
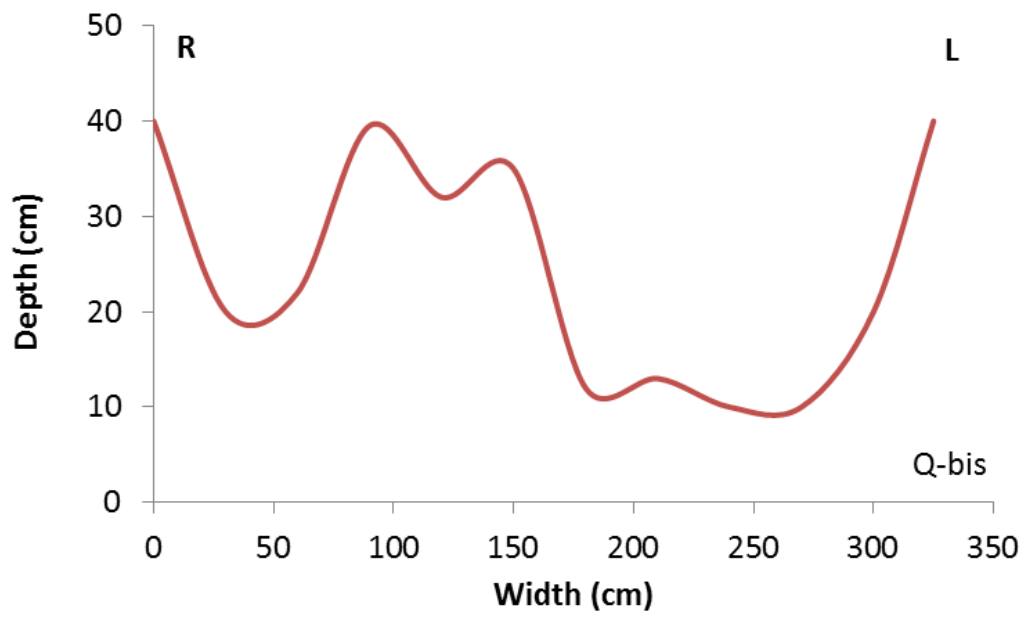


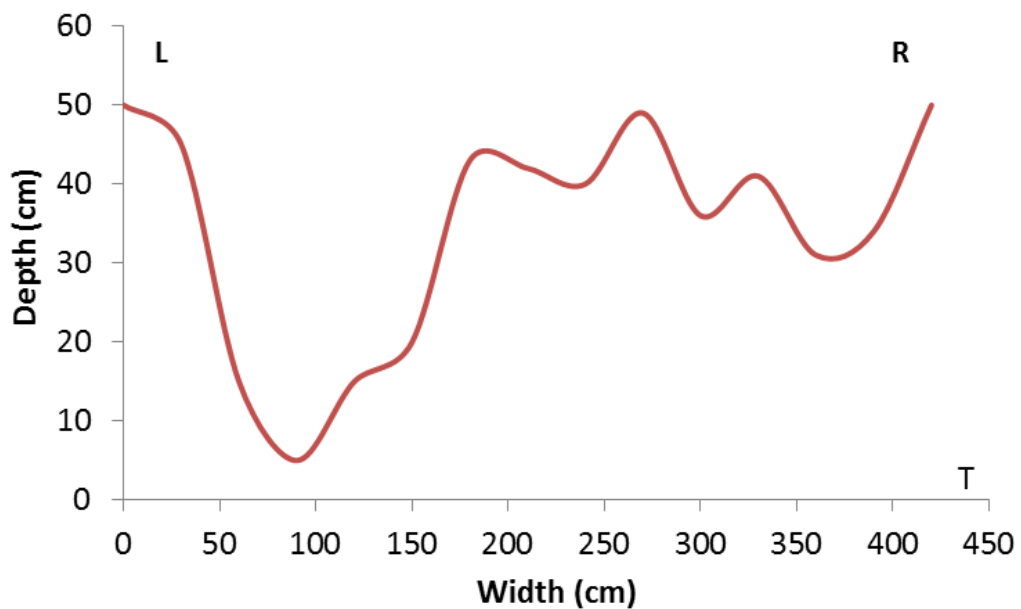
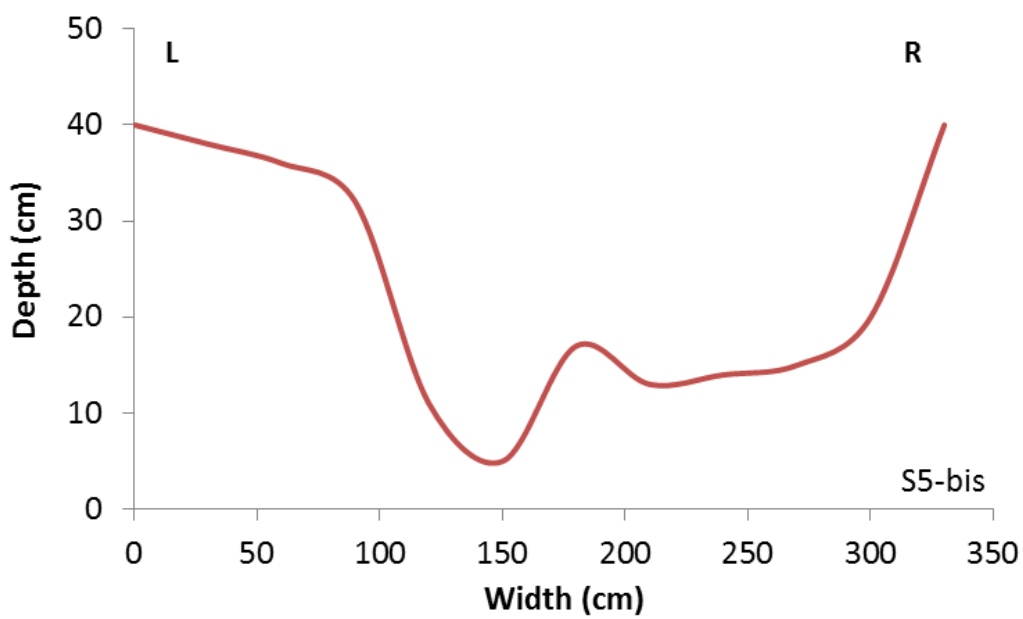
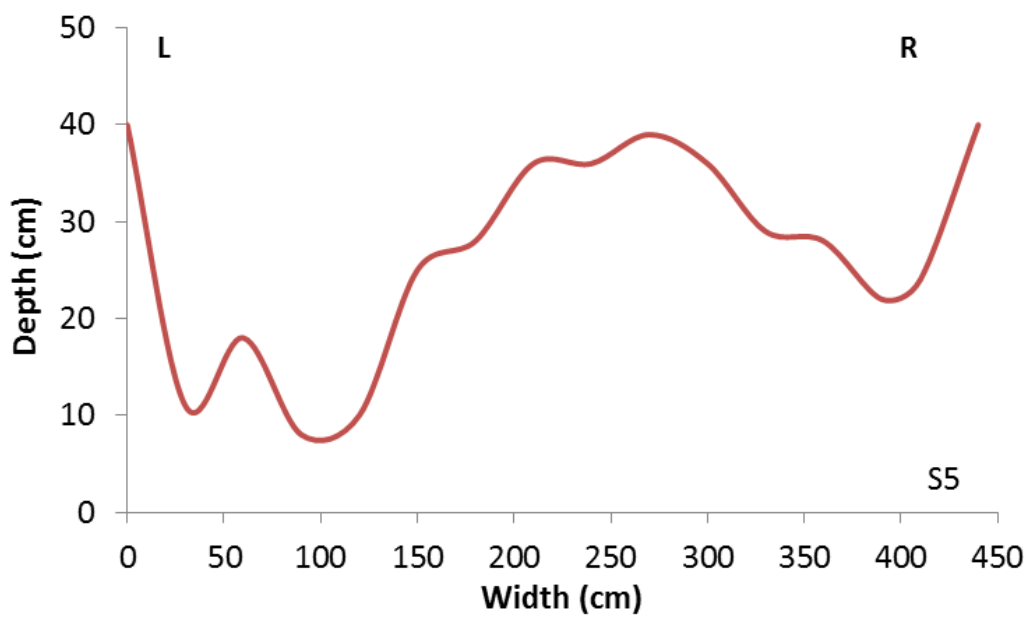


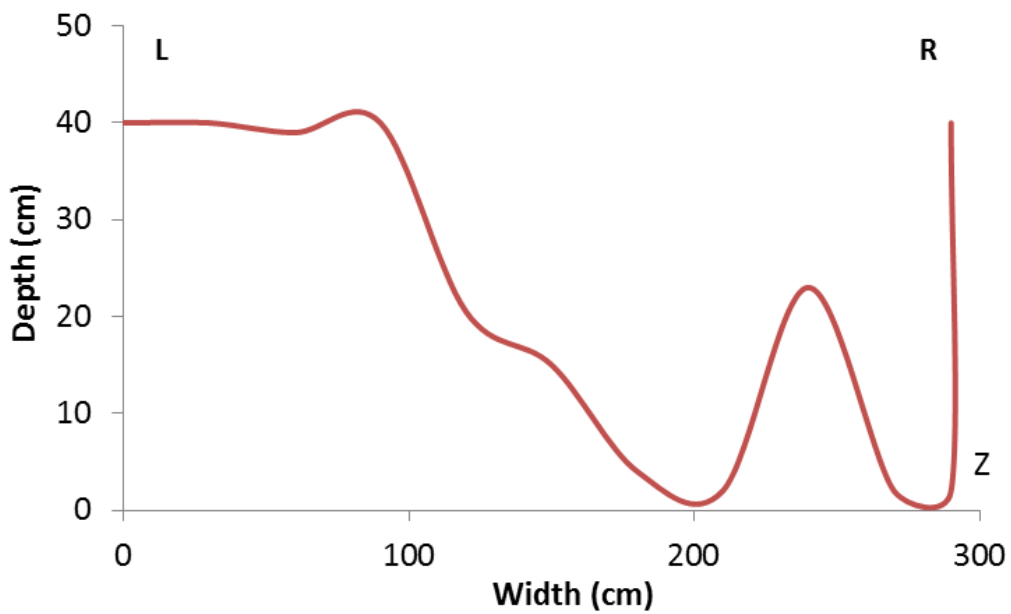
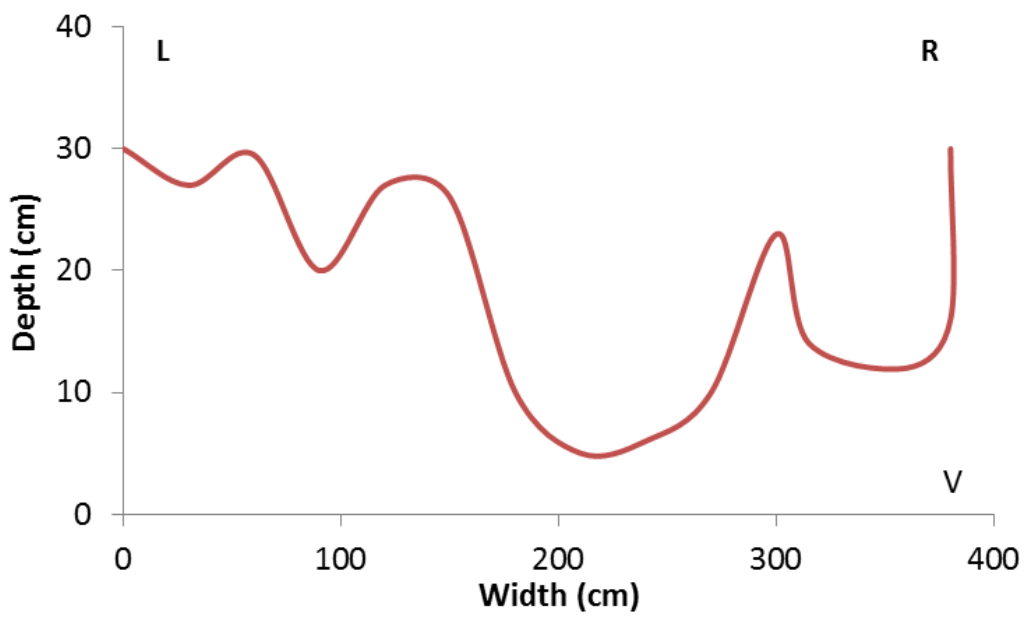
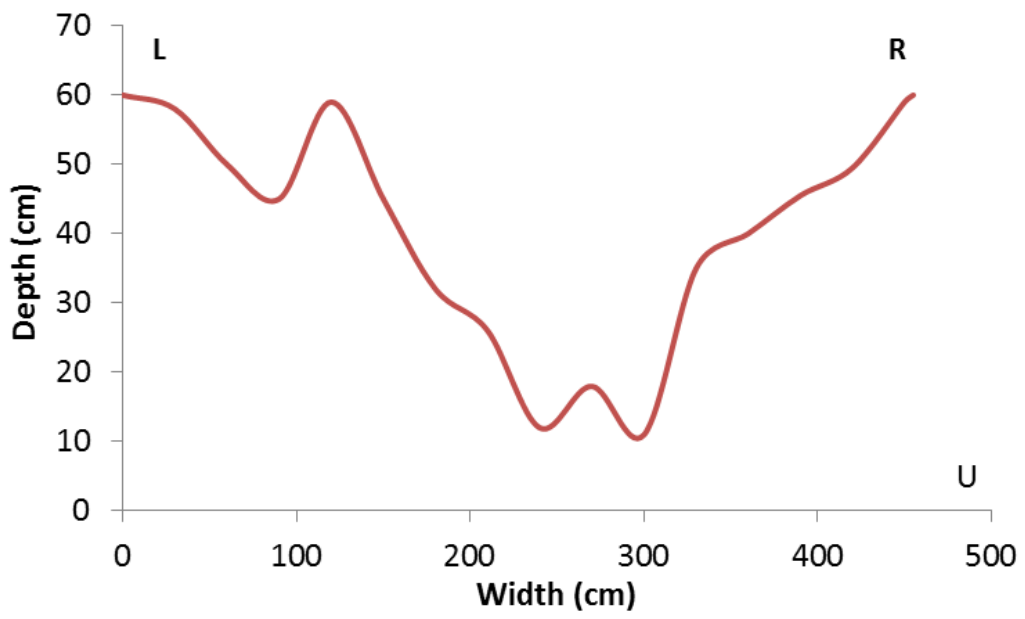


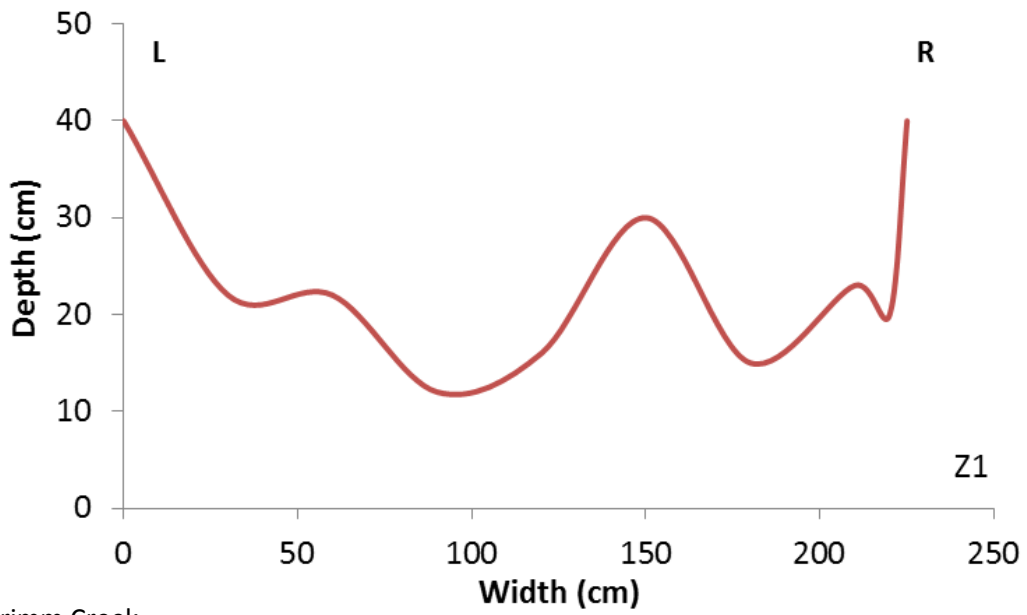




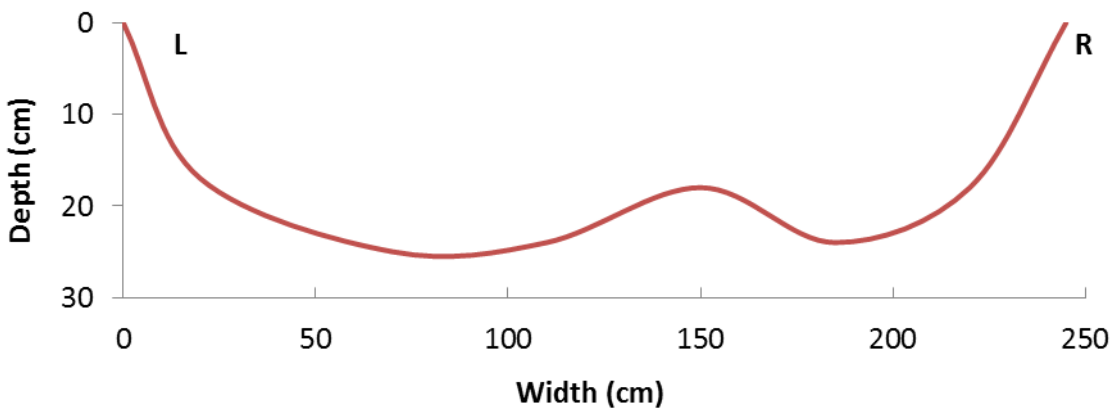
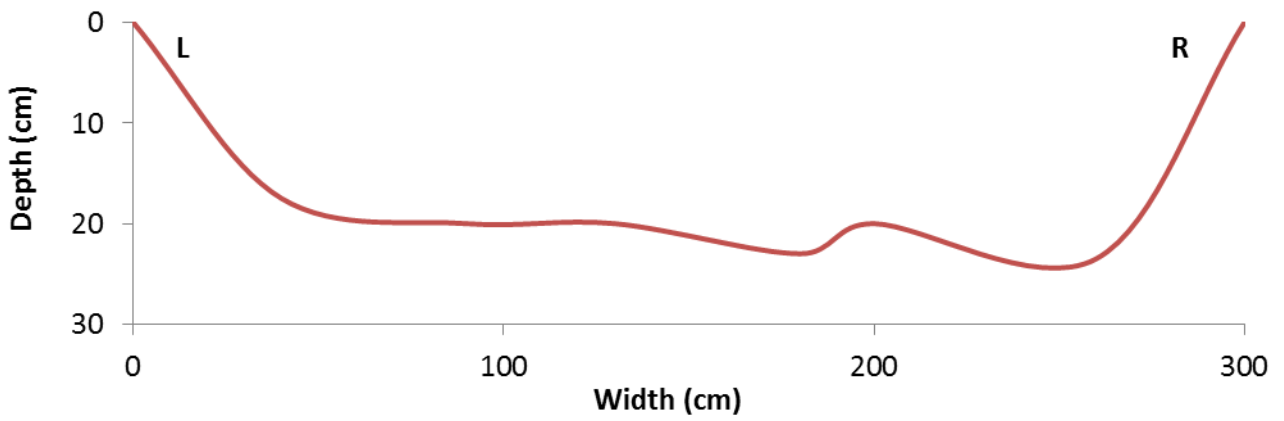


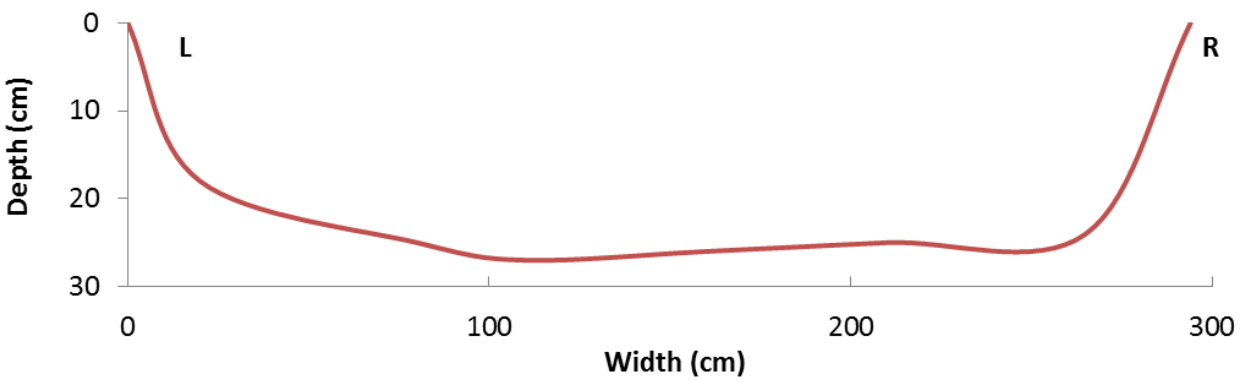
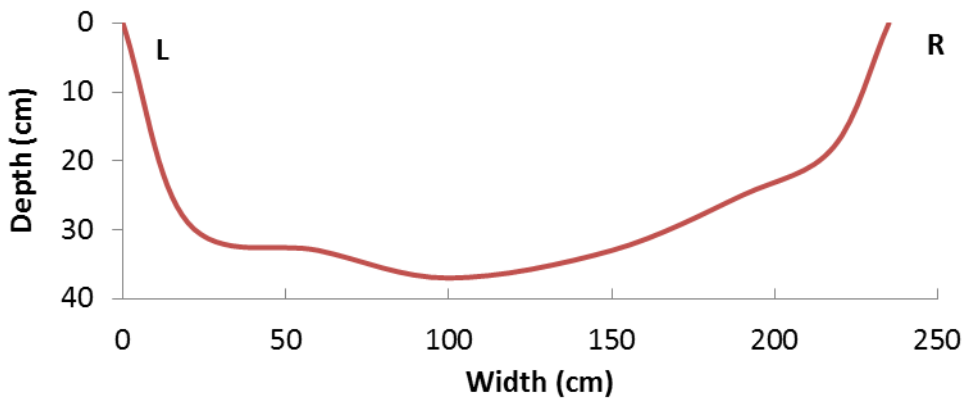
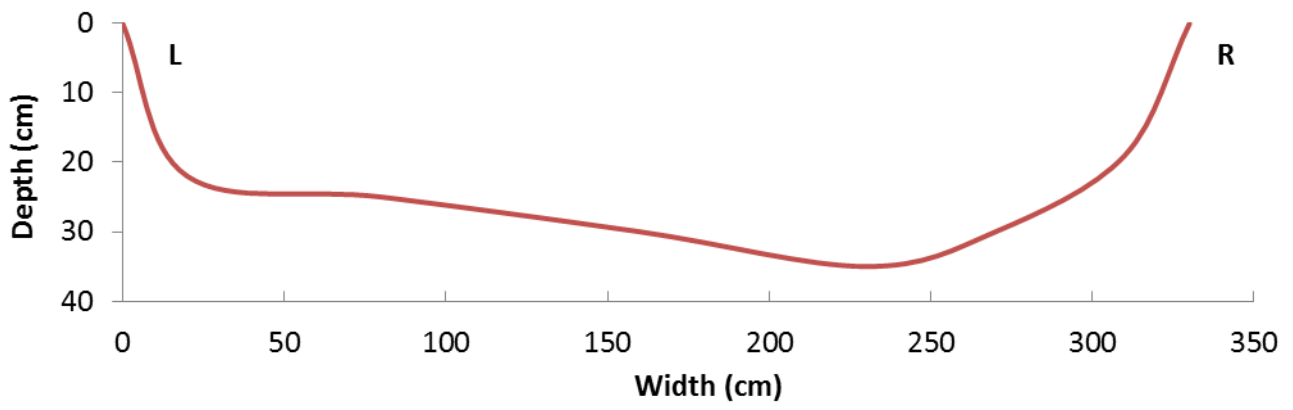
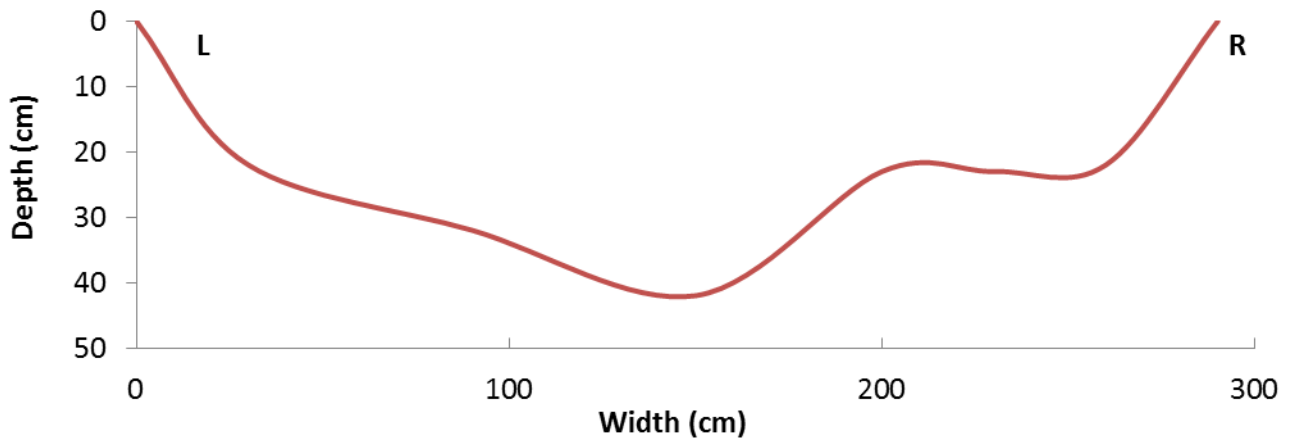


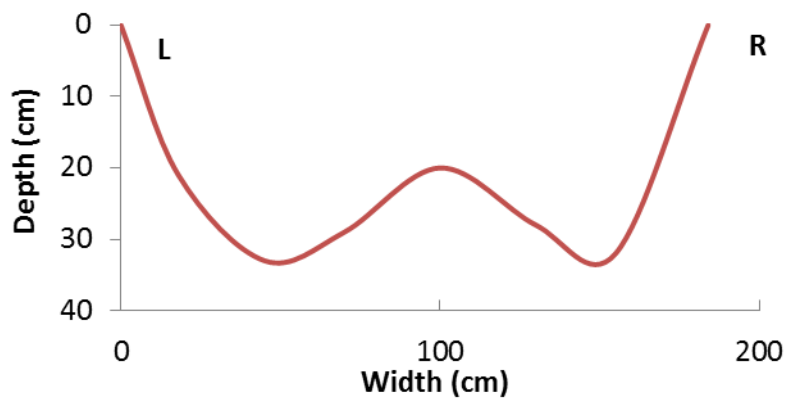
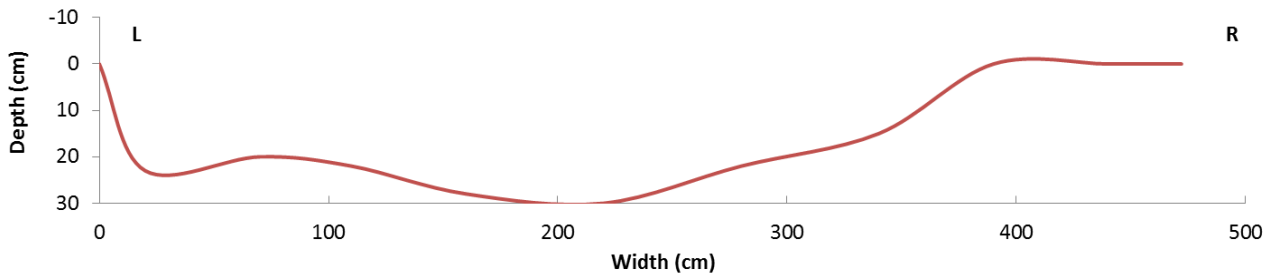
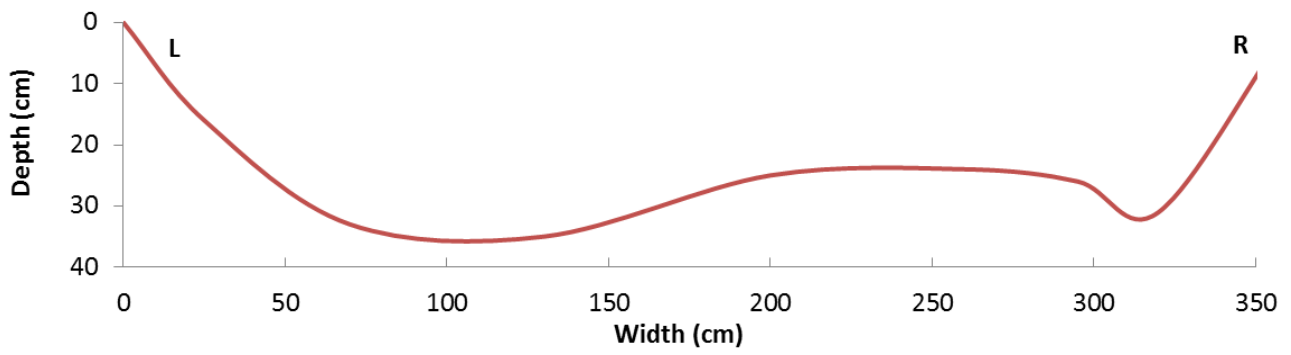
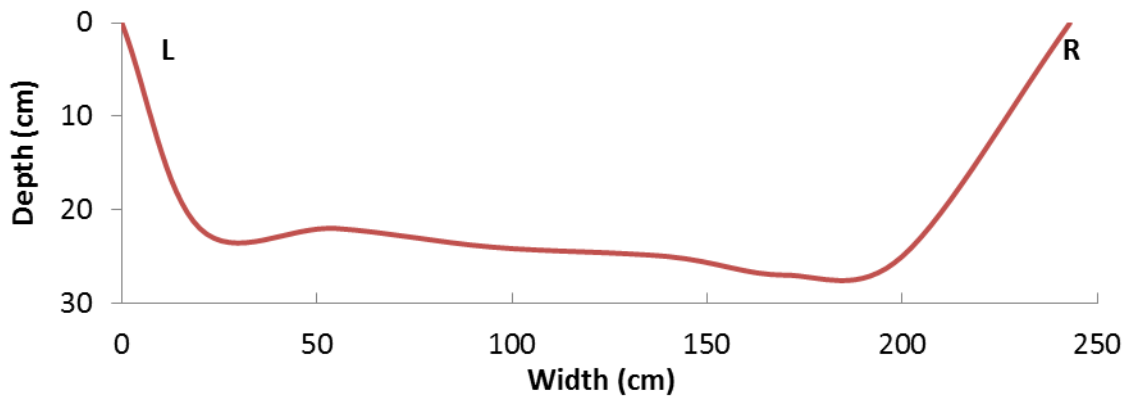


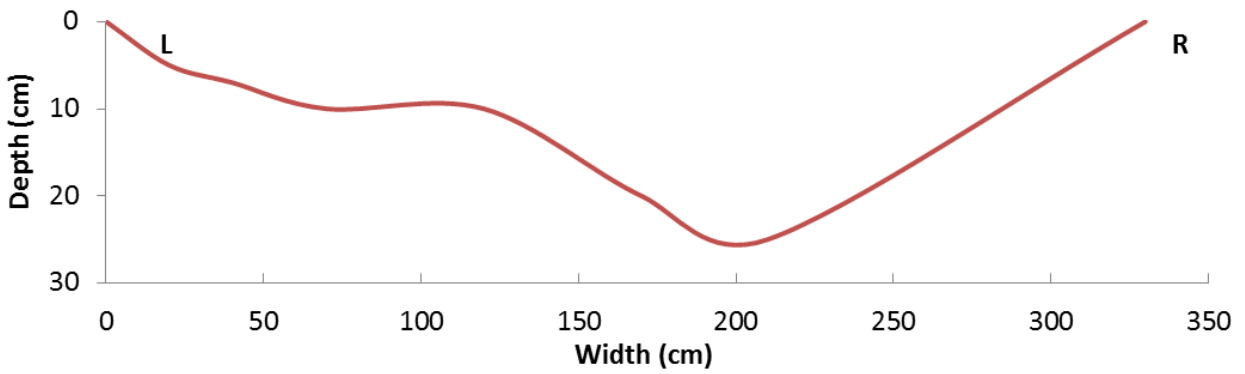
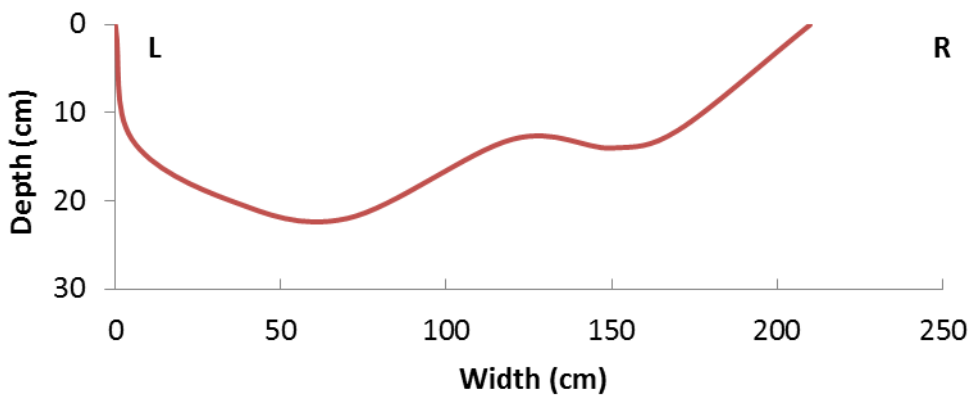
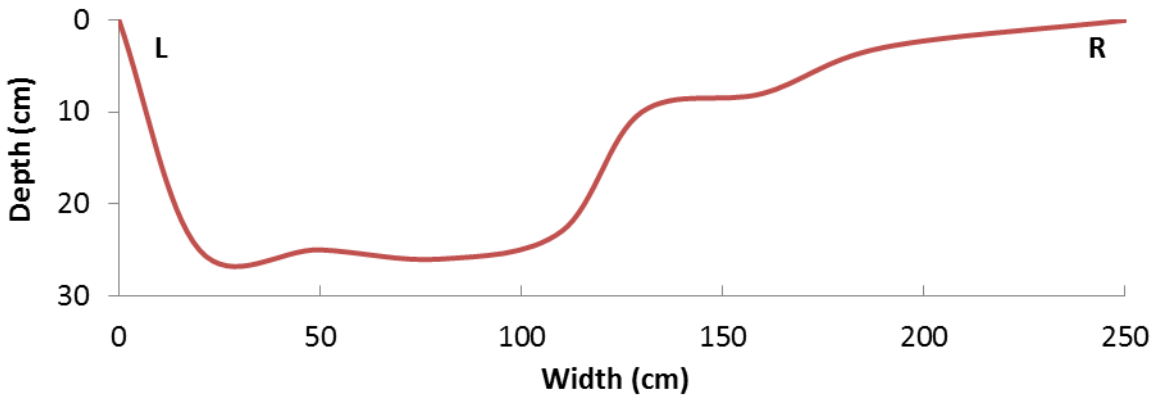
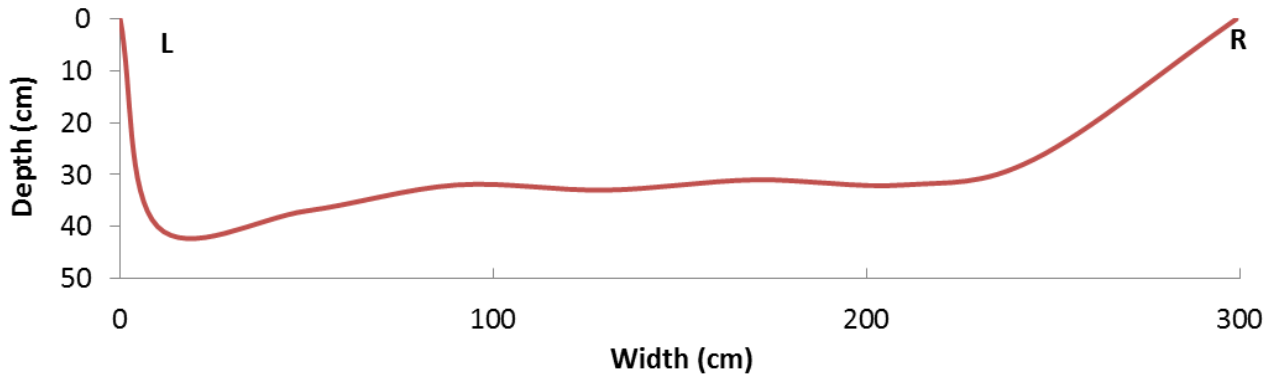


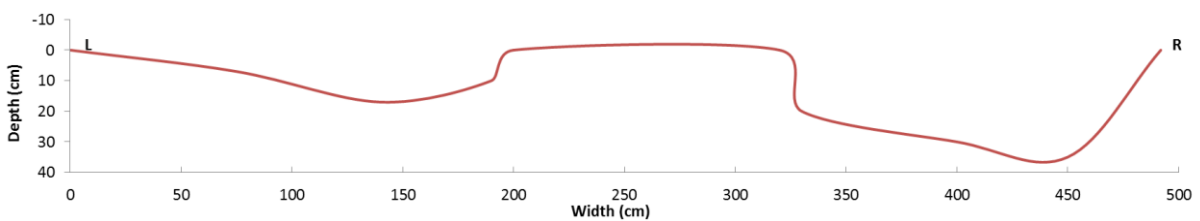
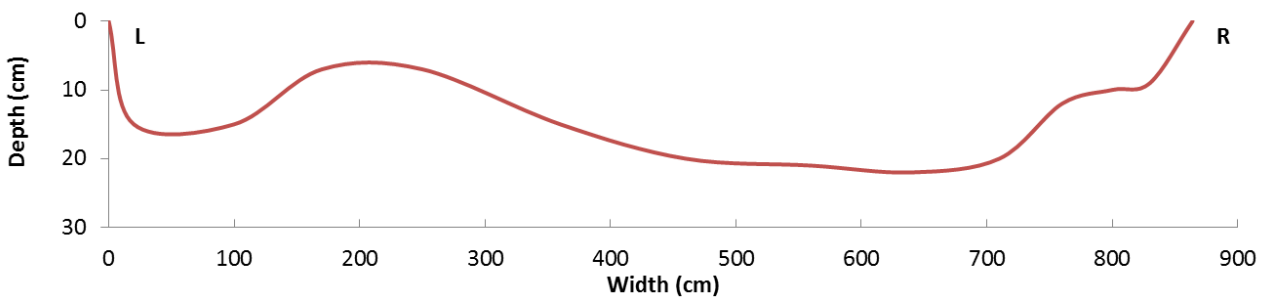
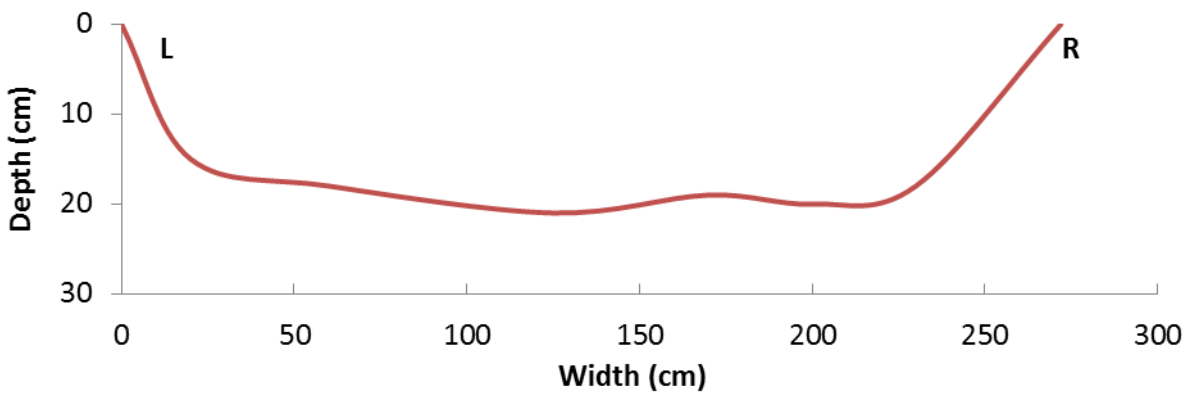
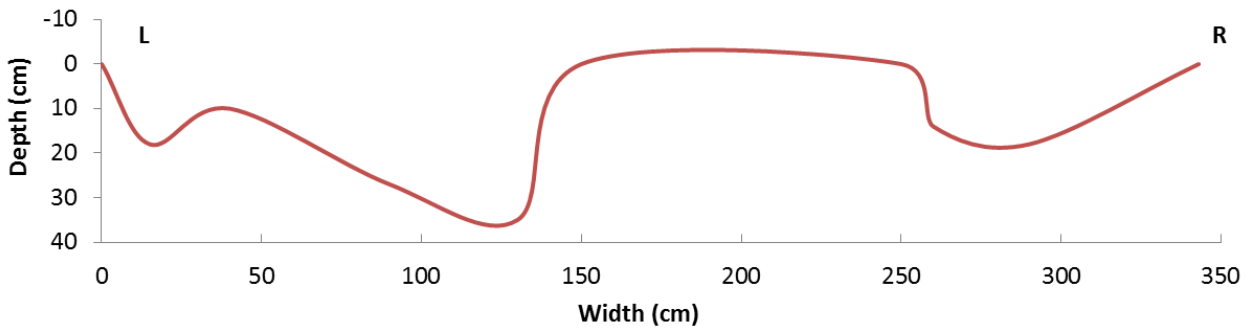
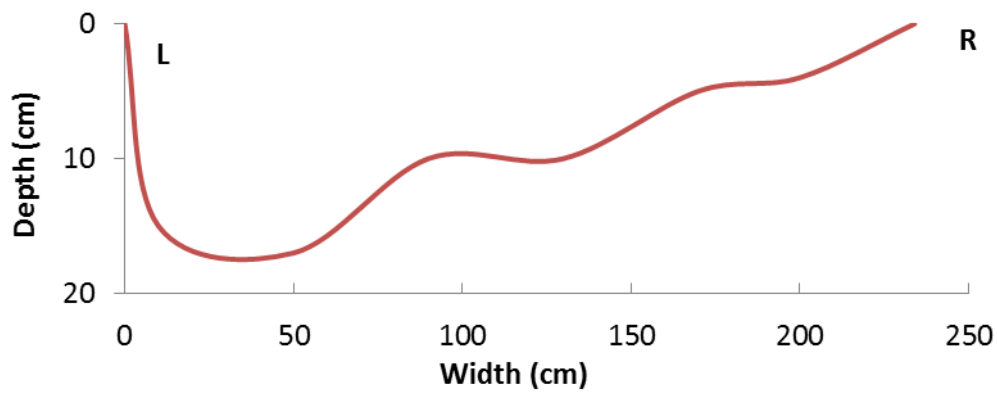
Upper Strimm Creek

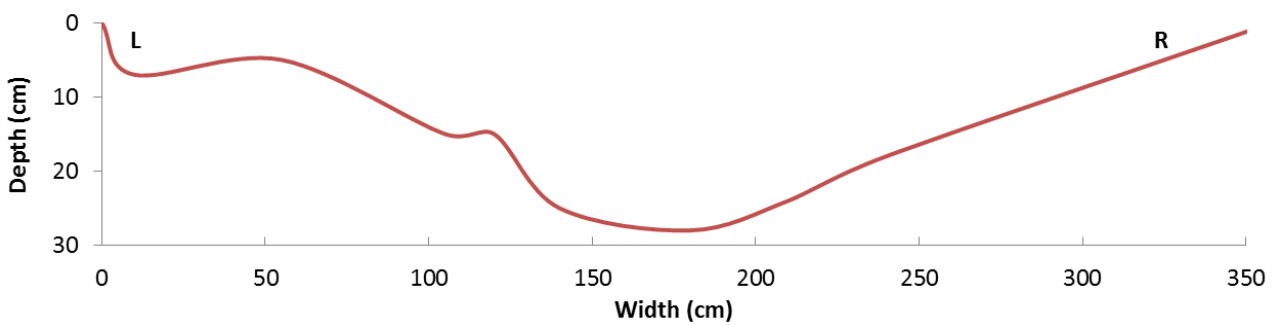
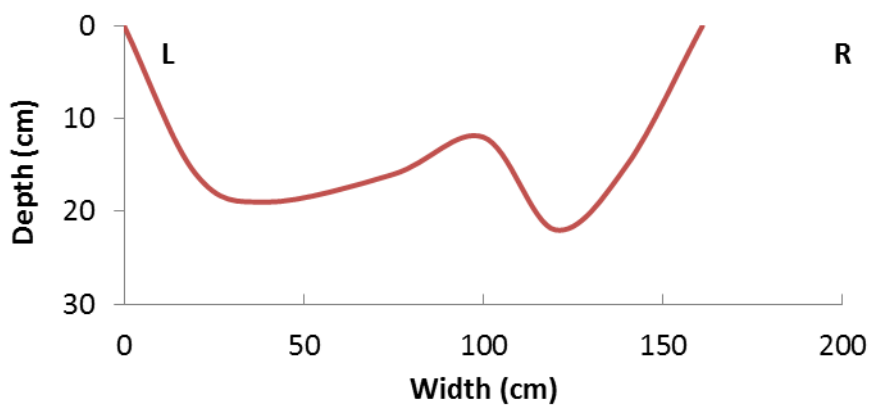
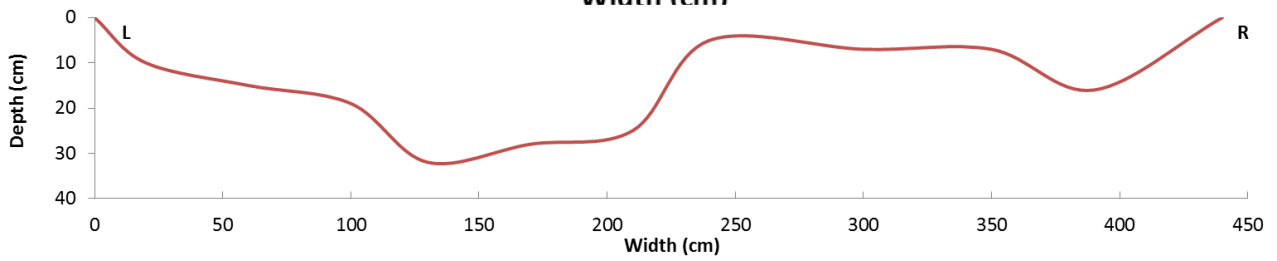
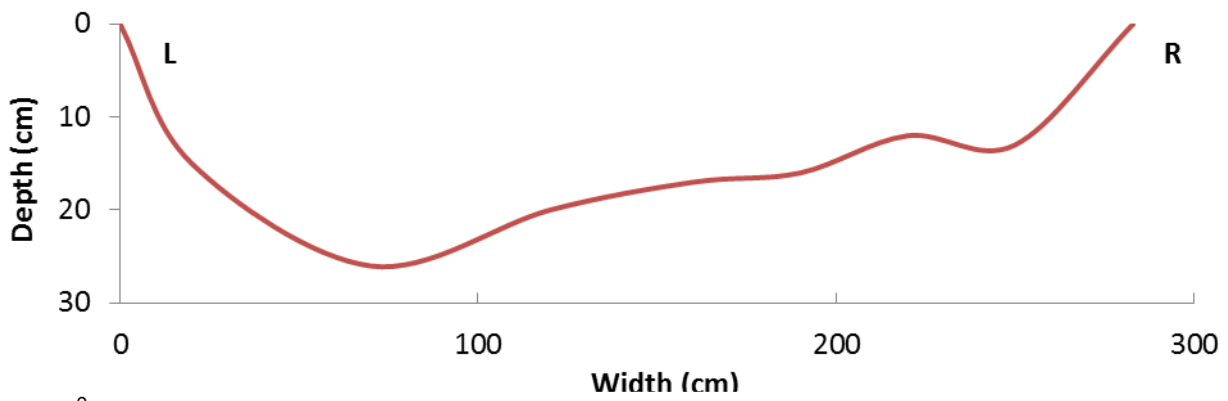
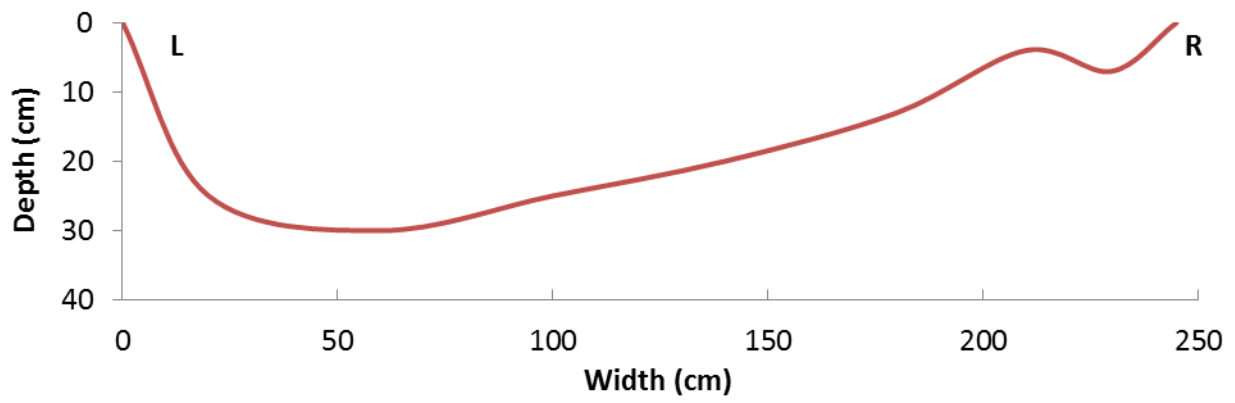


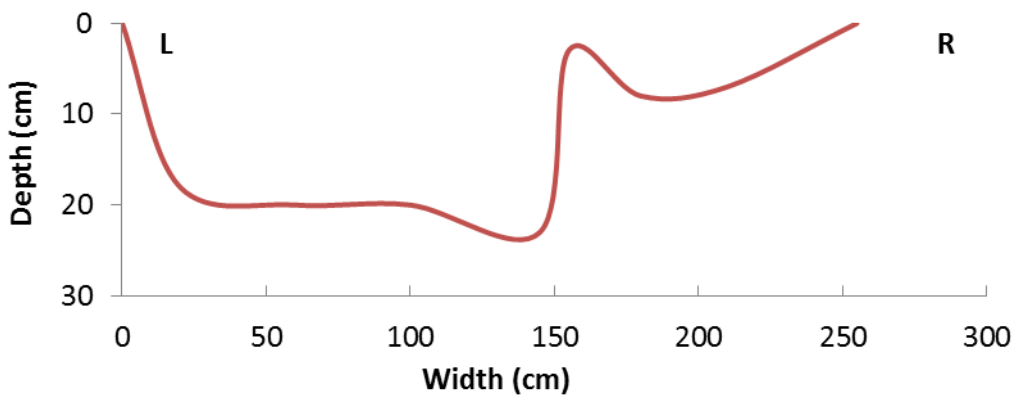
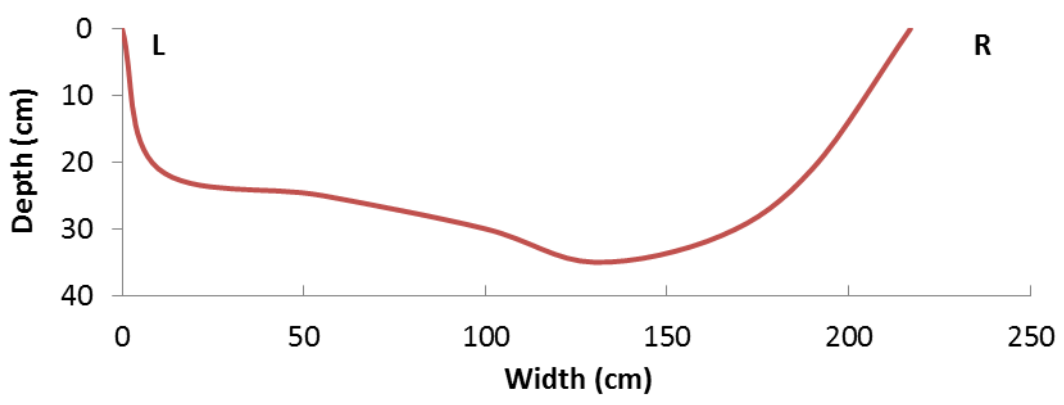
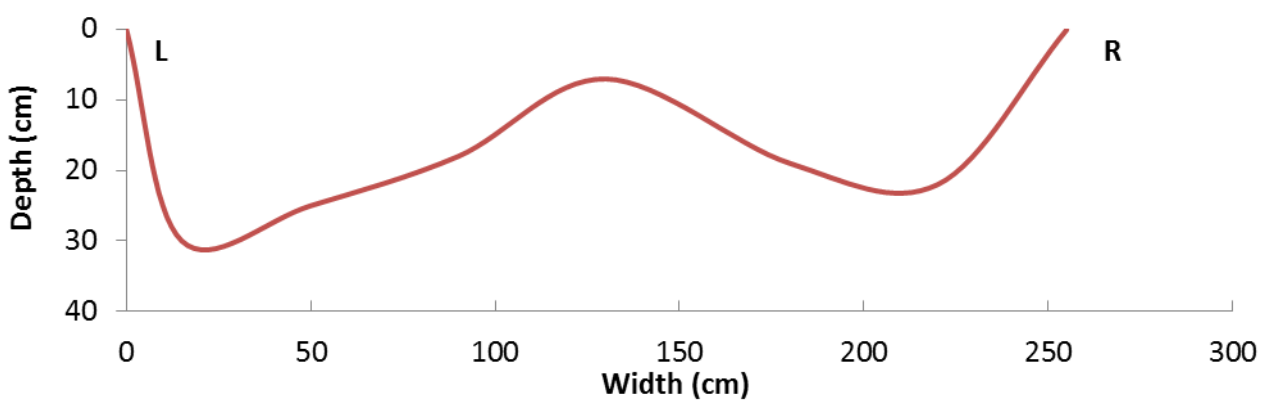
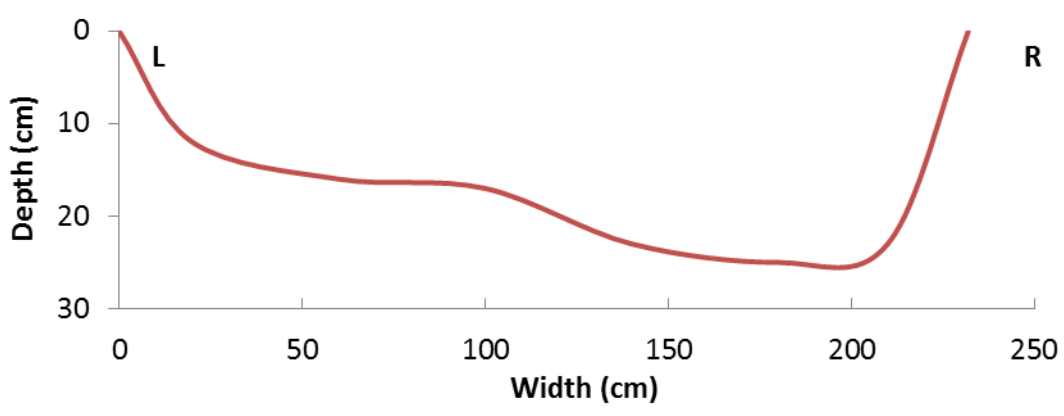


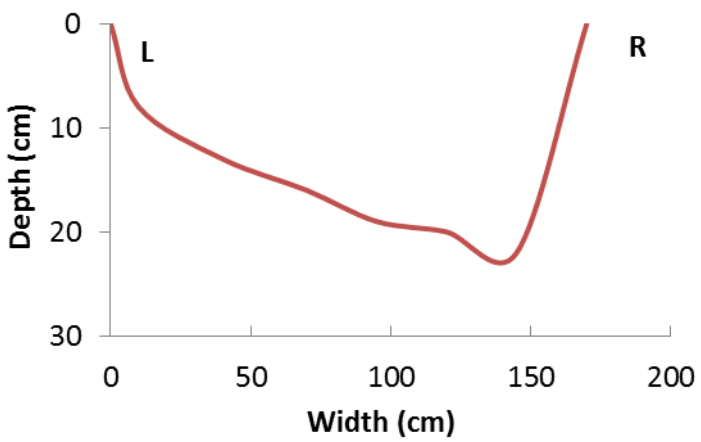
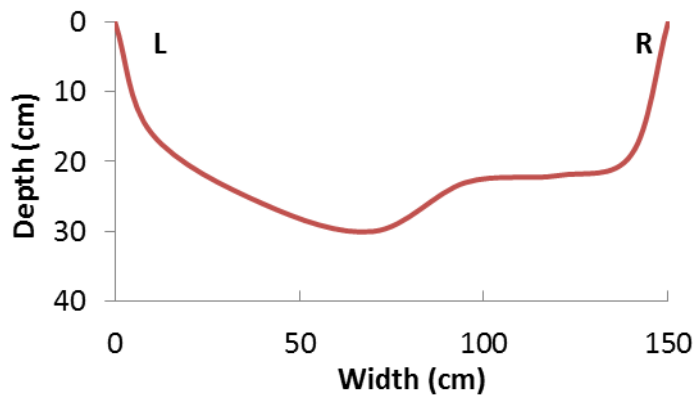
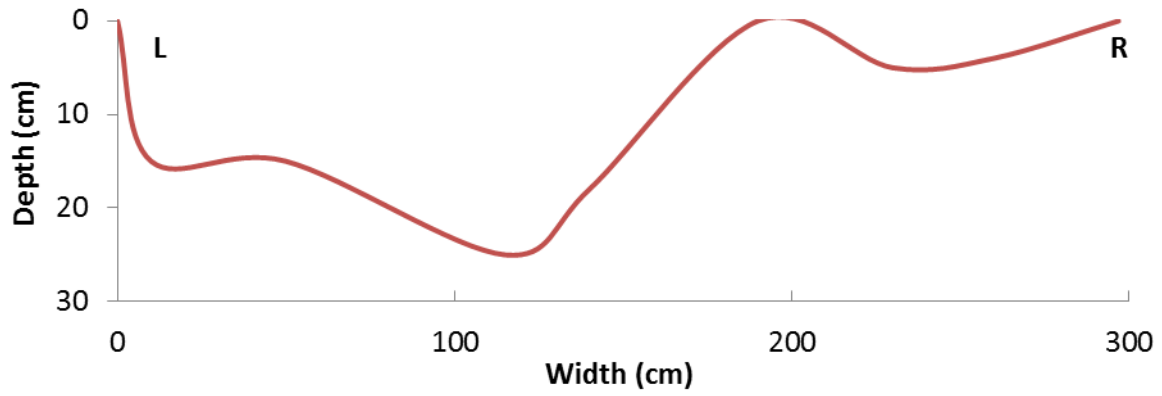
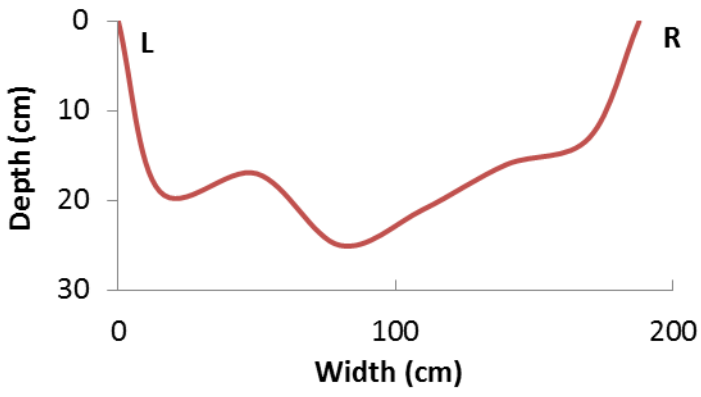


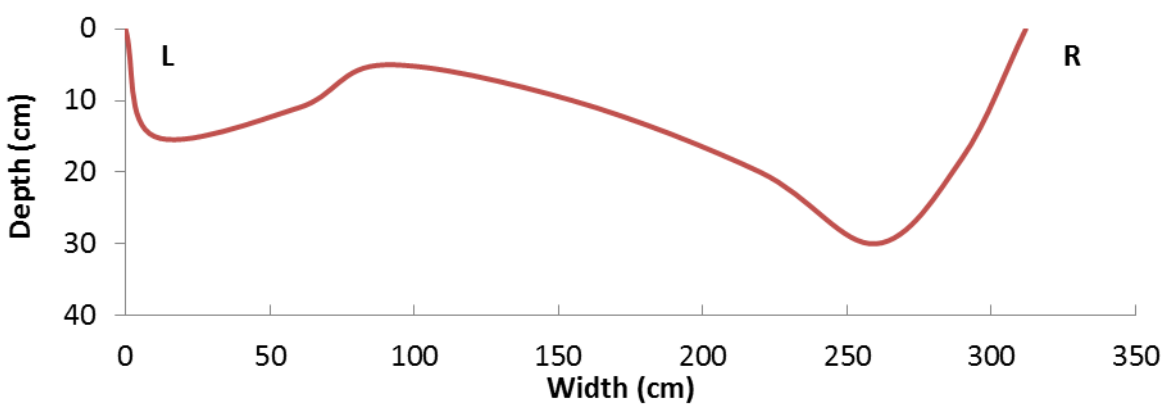
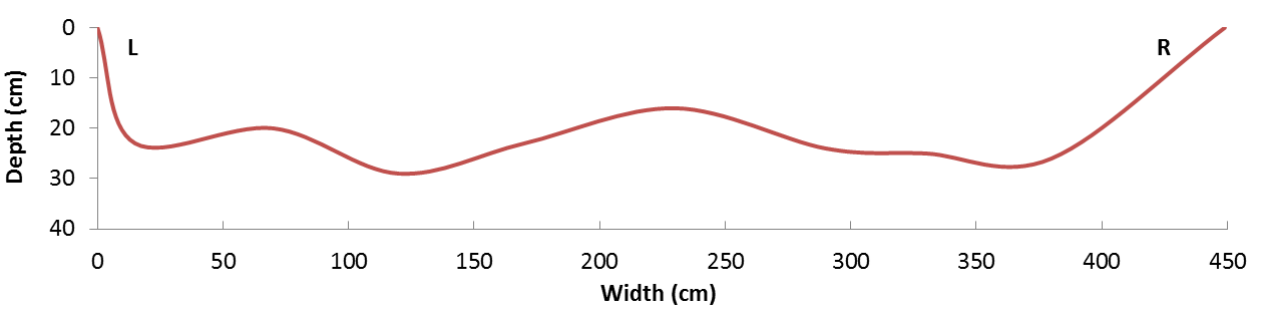
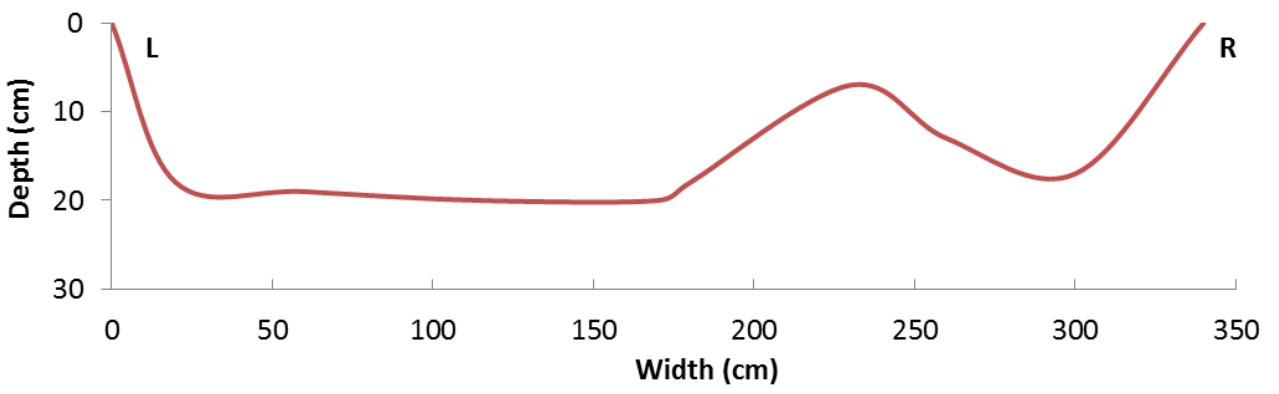
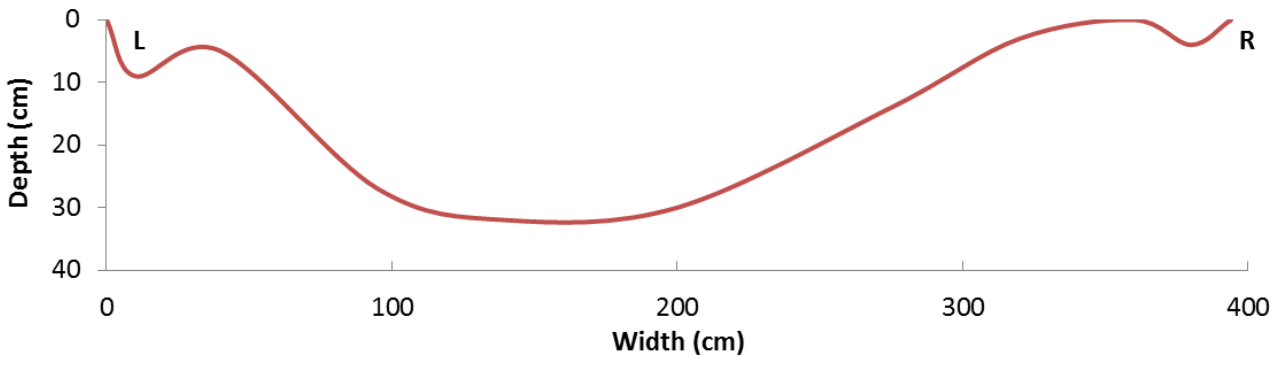
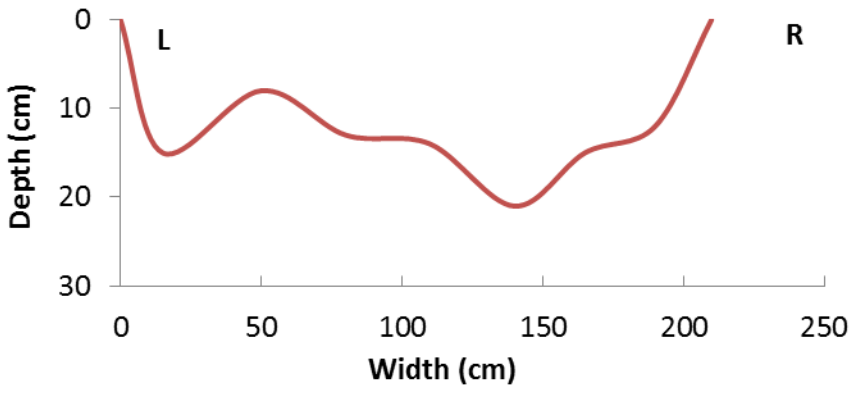


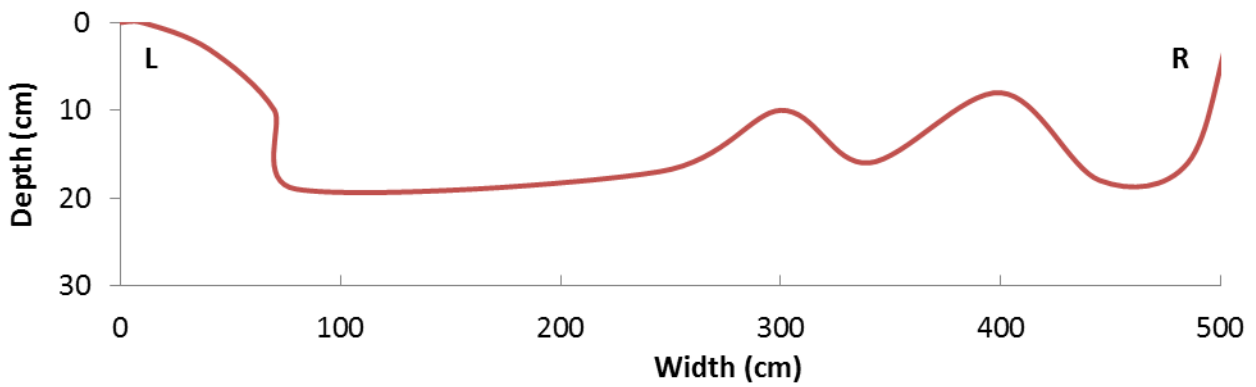
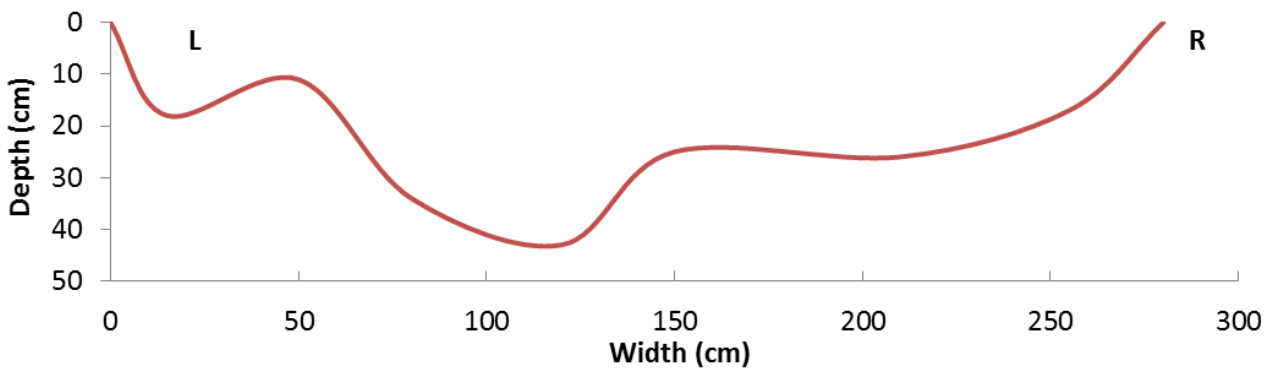
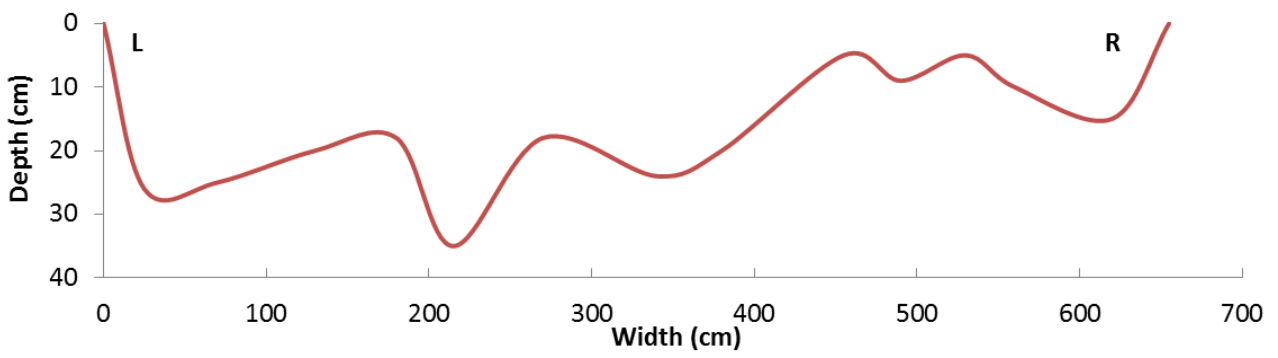
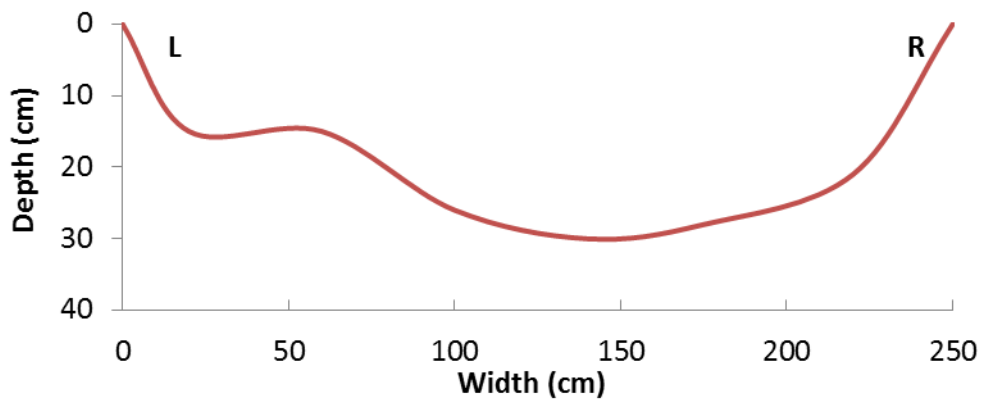


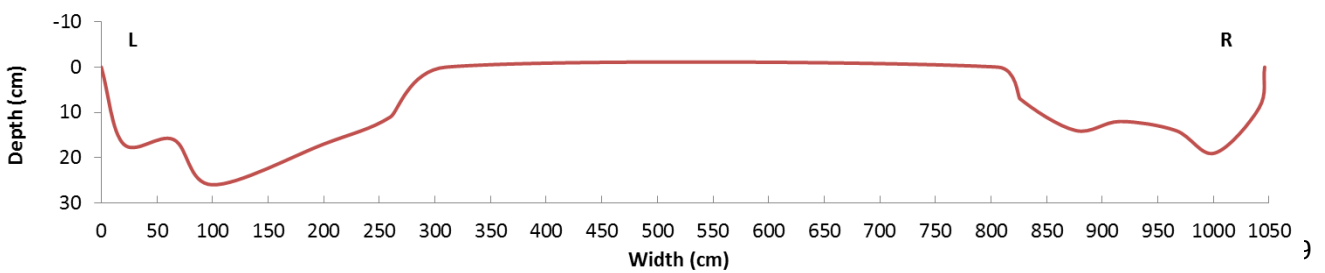
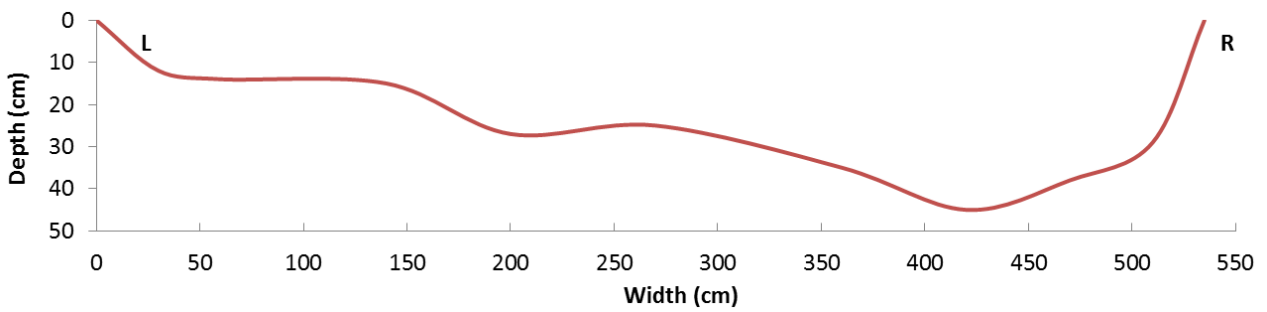
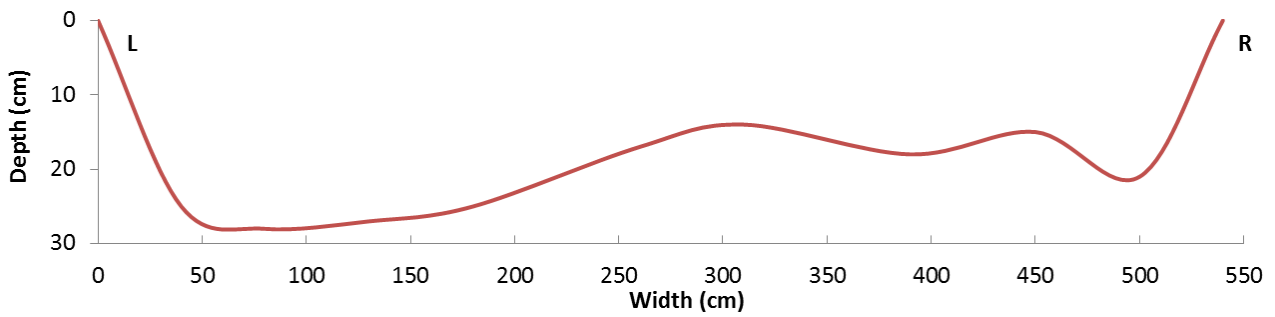
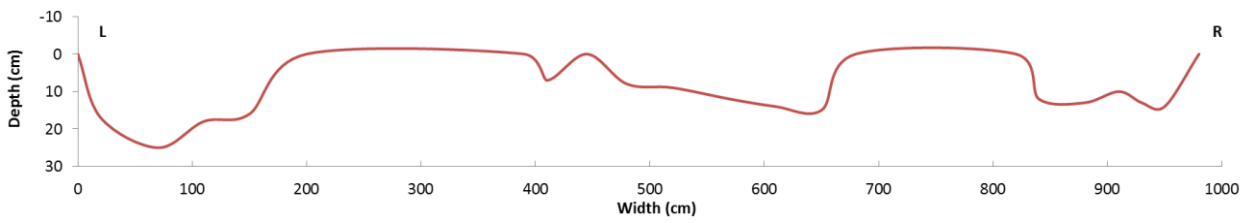
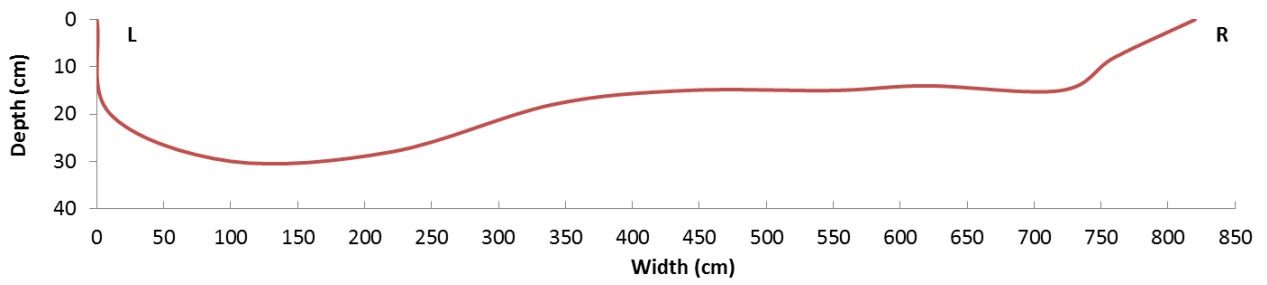


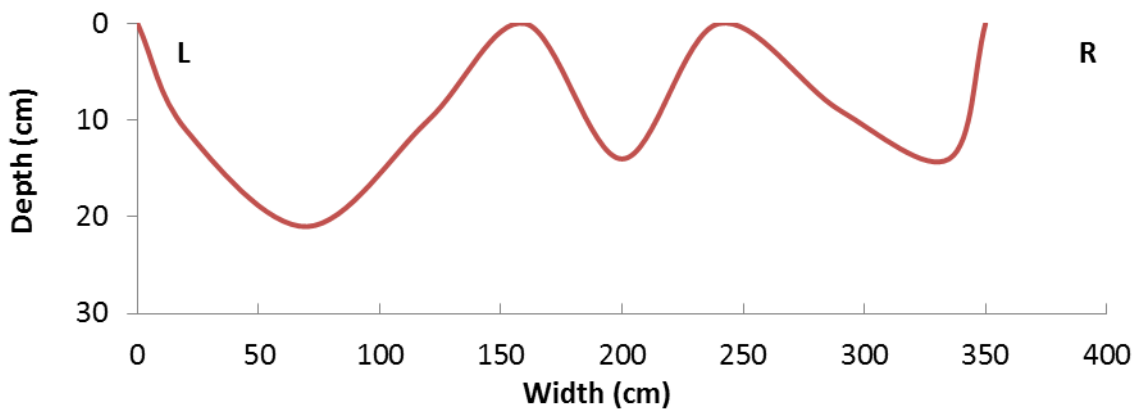
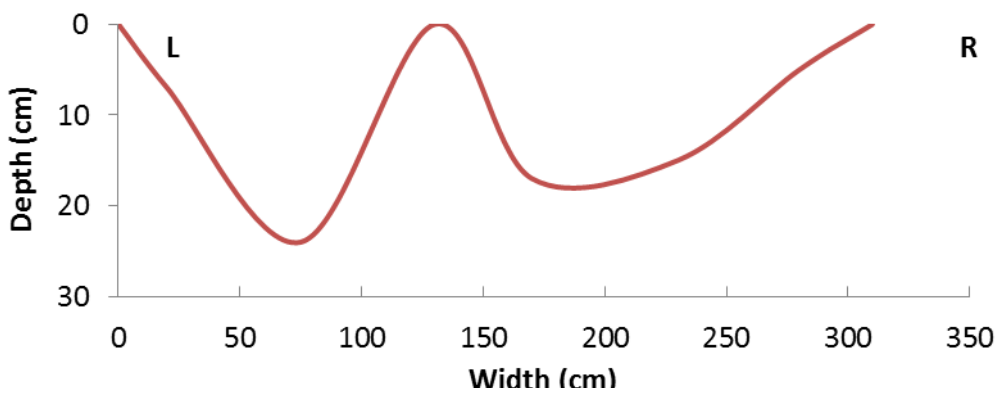
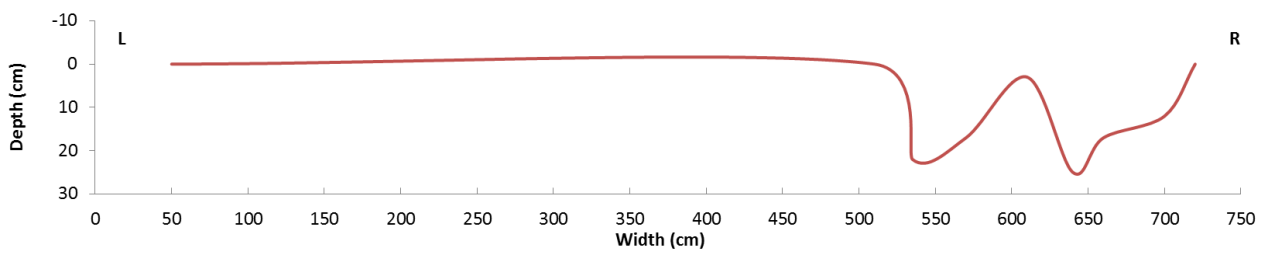
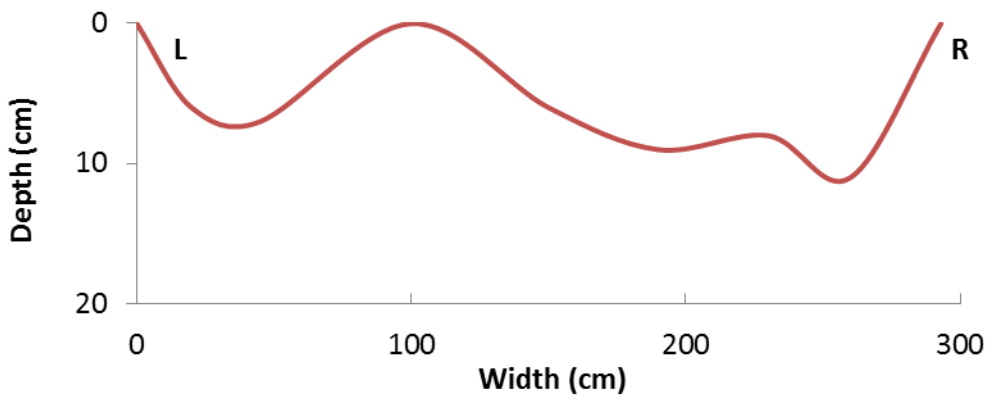








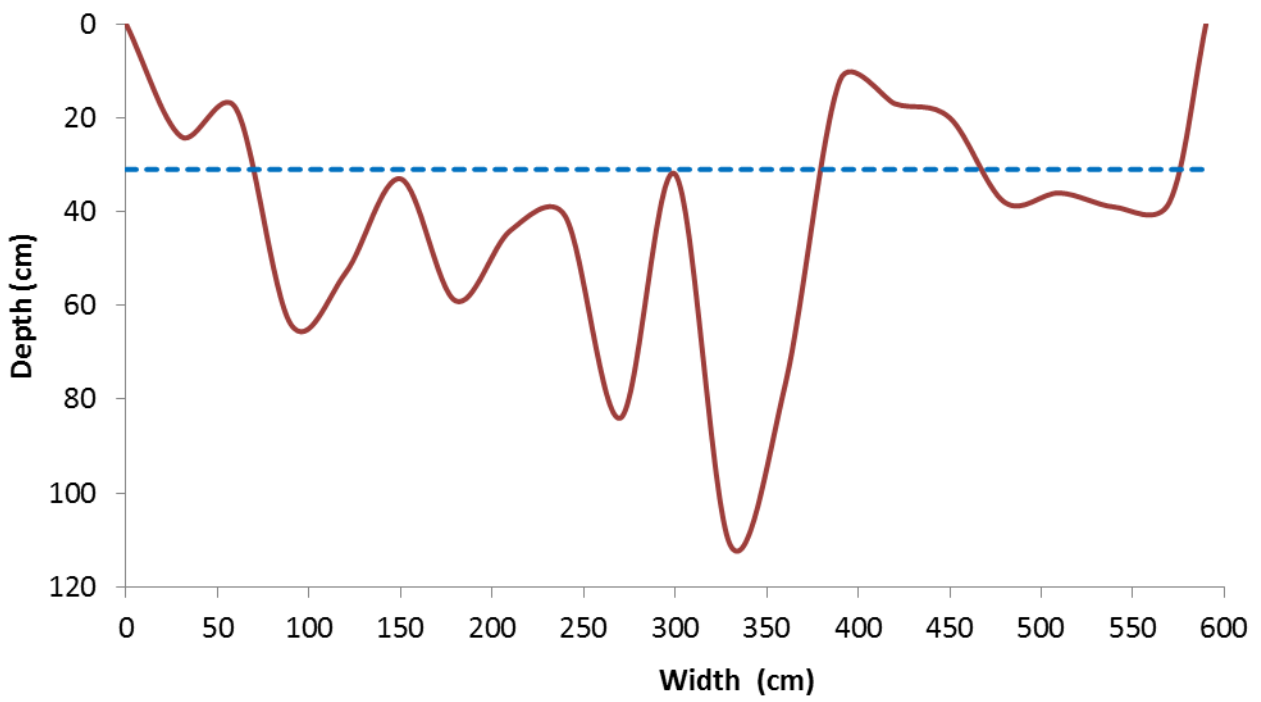
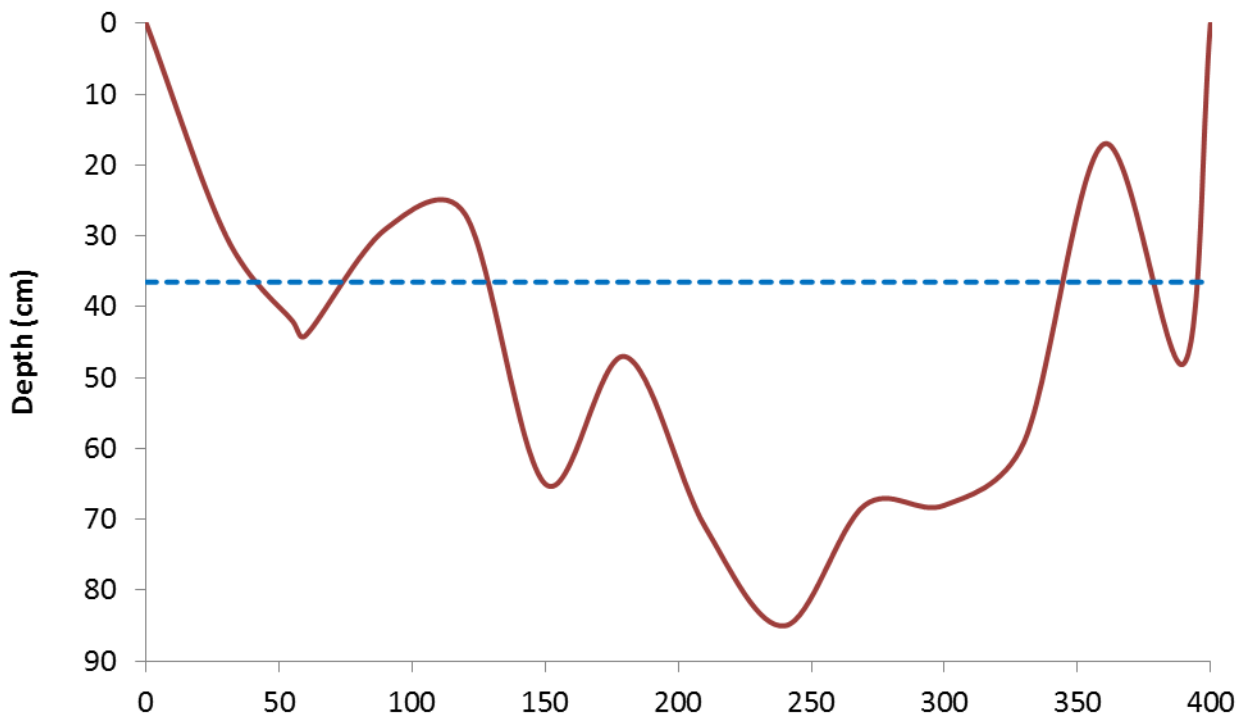


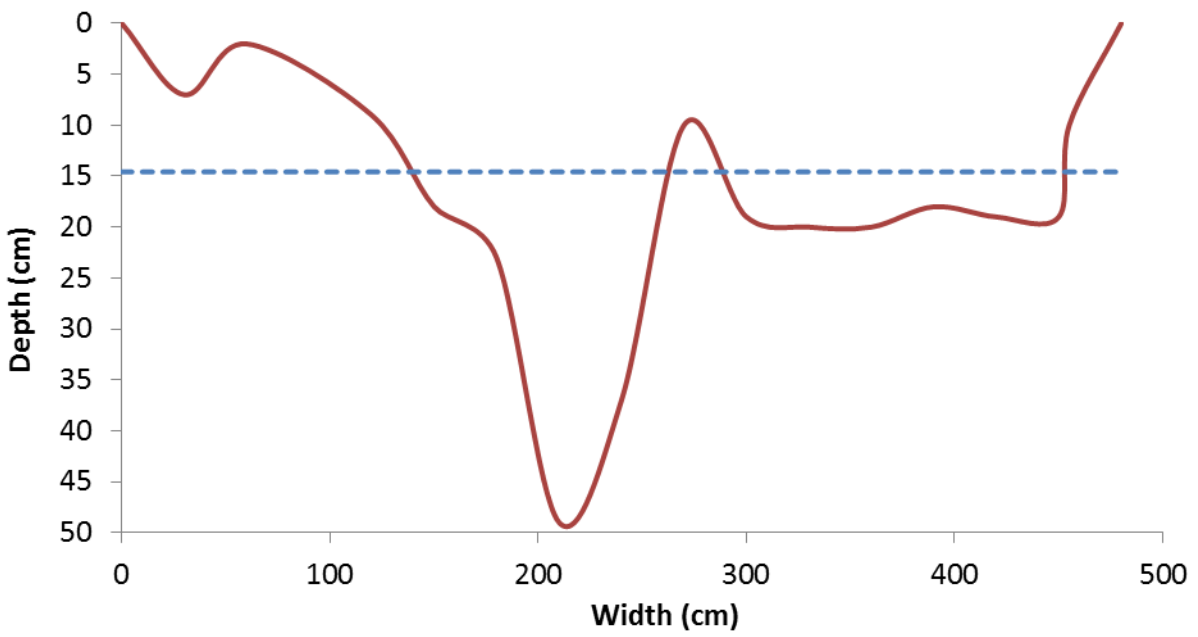
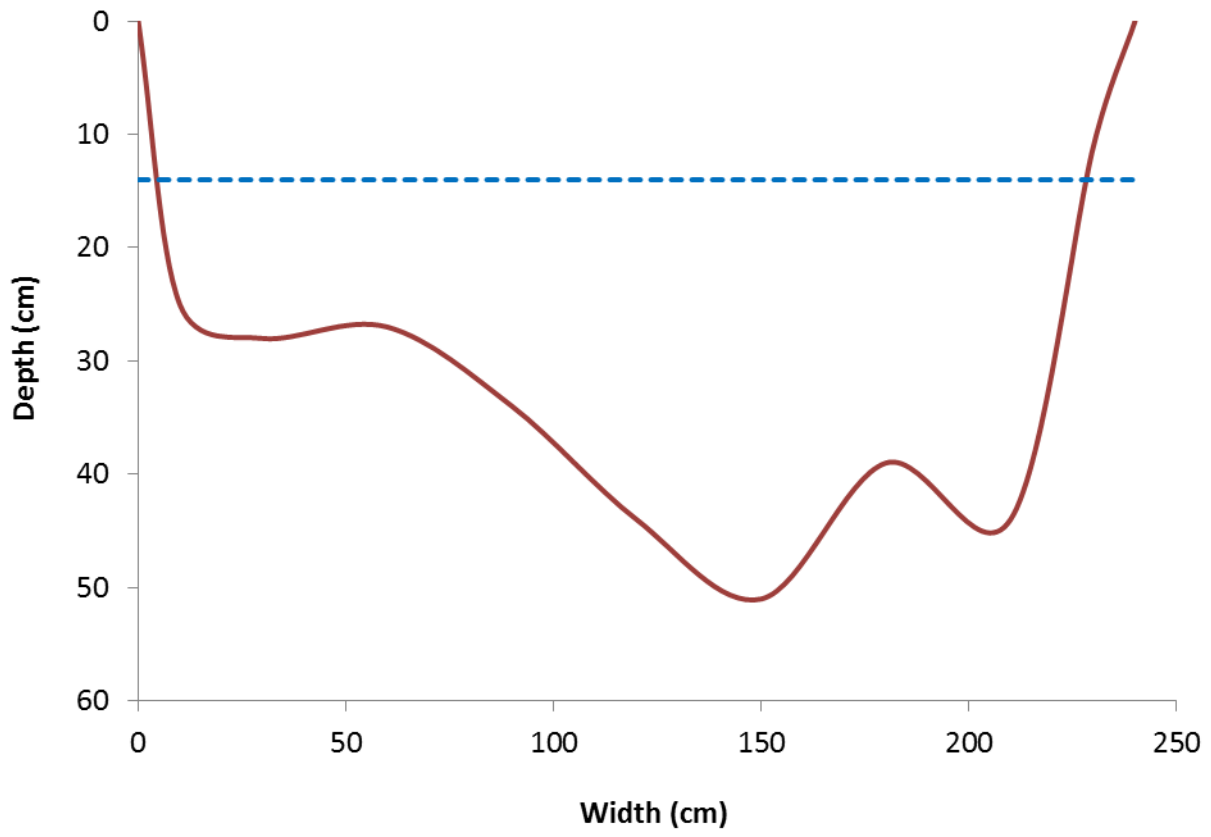


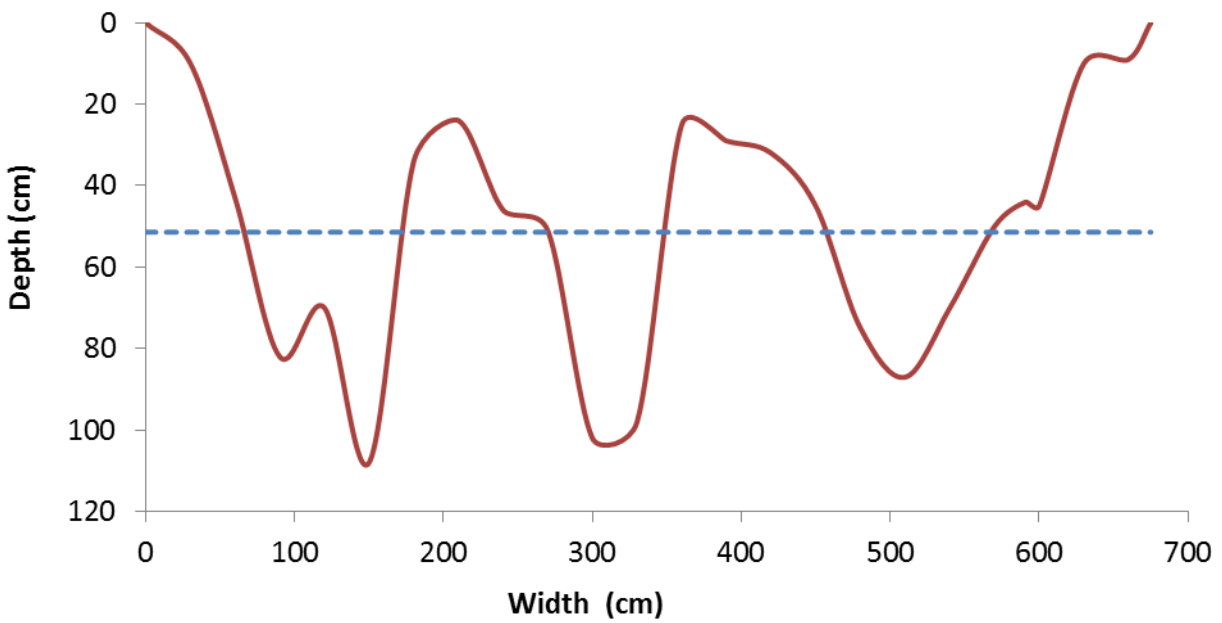
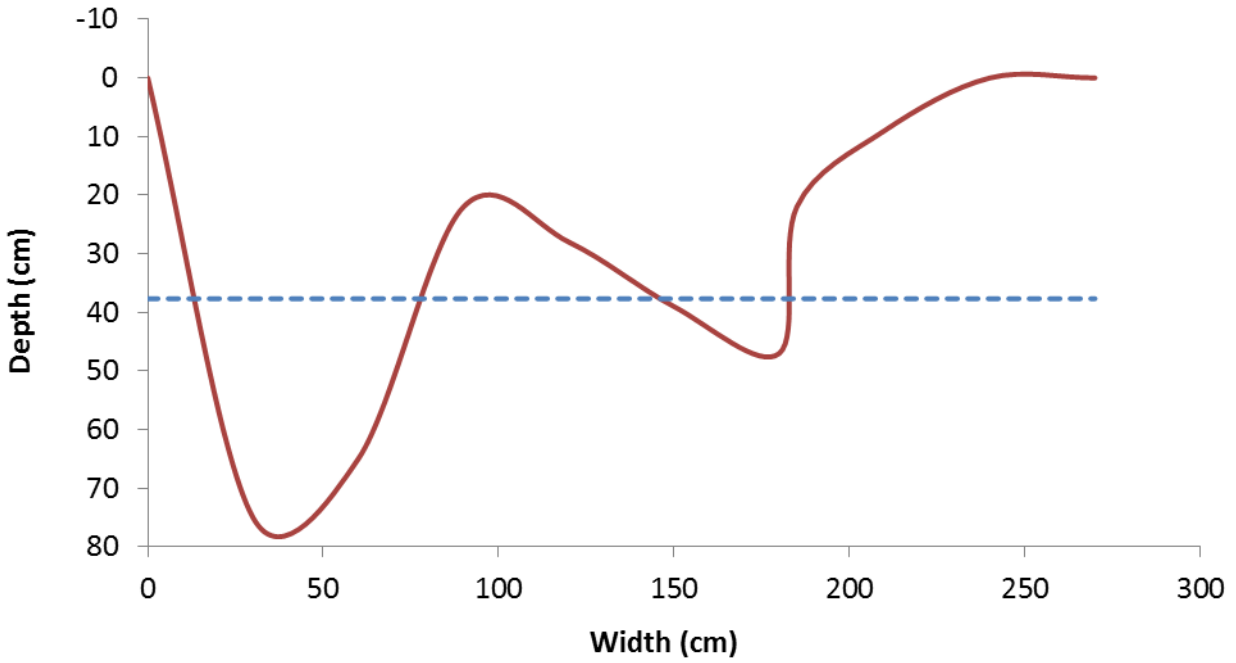
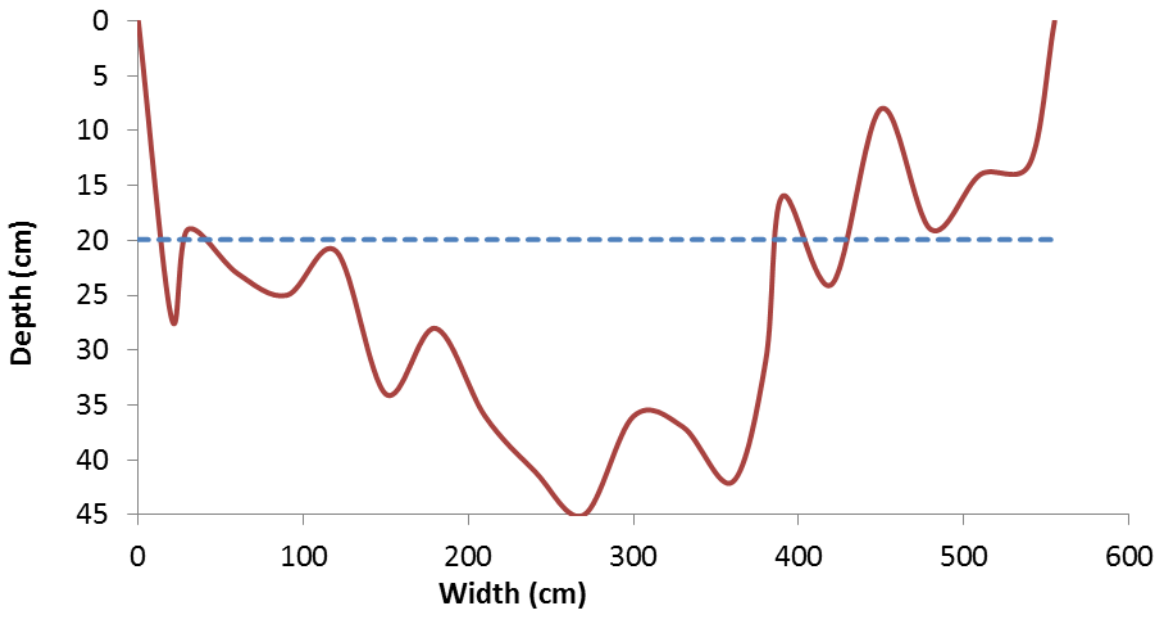
Appendix 4.1.2

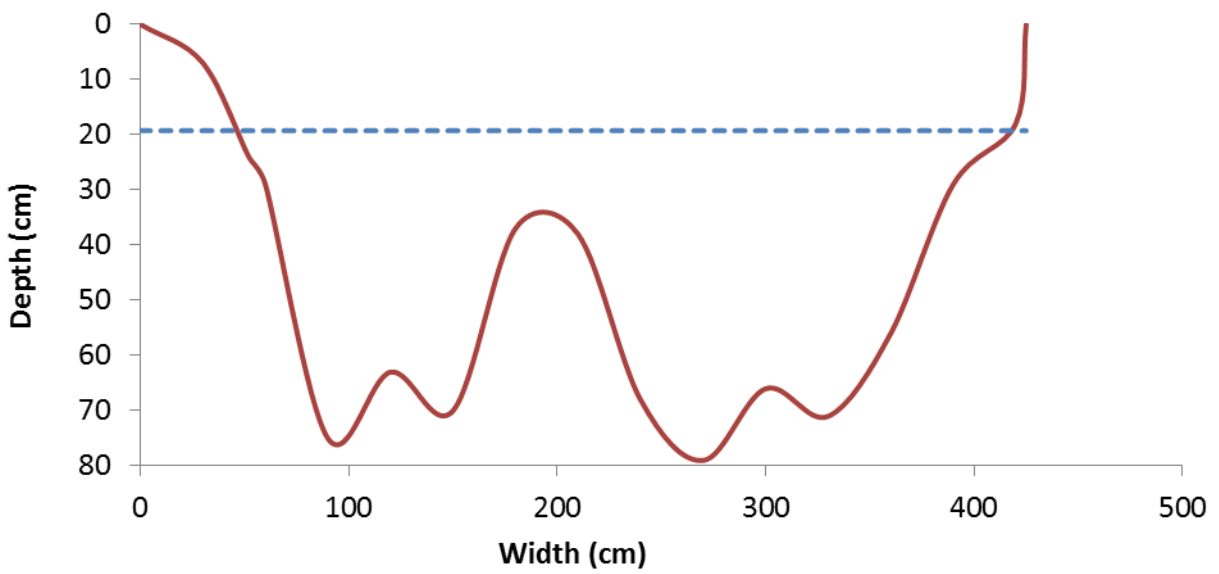
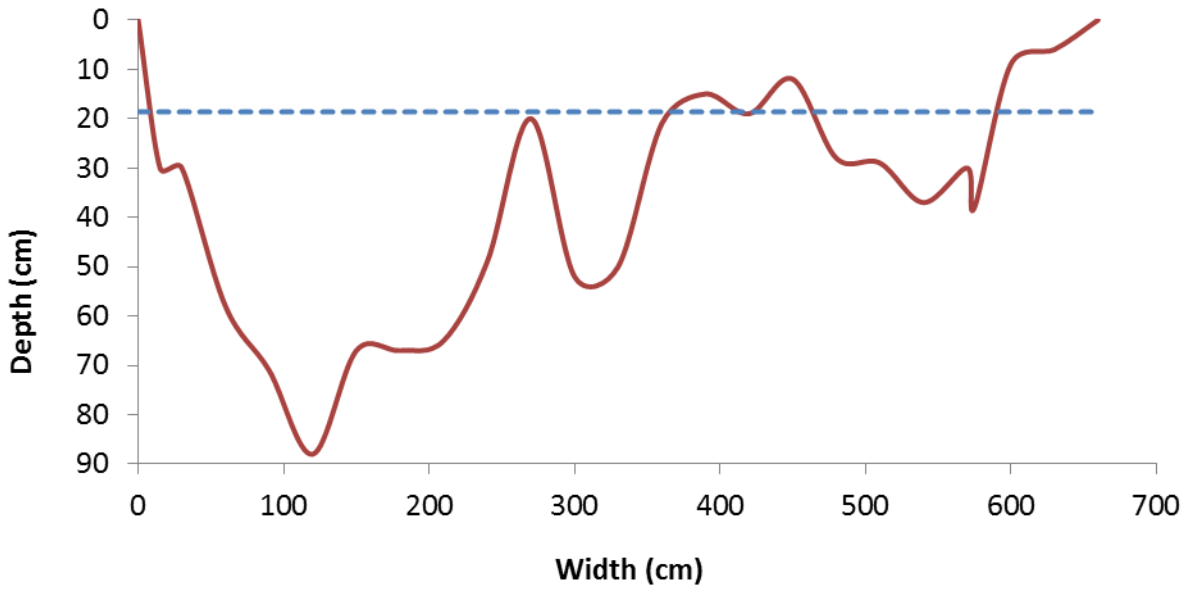
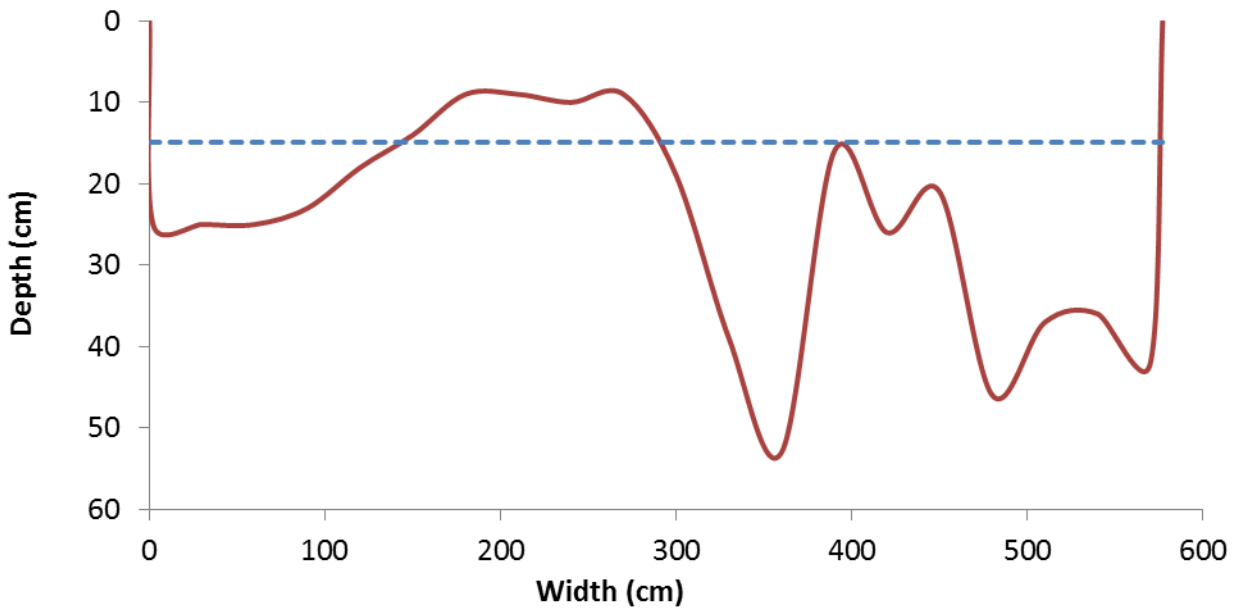
Downstream hydraulic geometry

Grigno Creek – G1

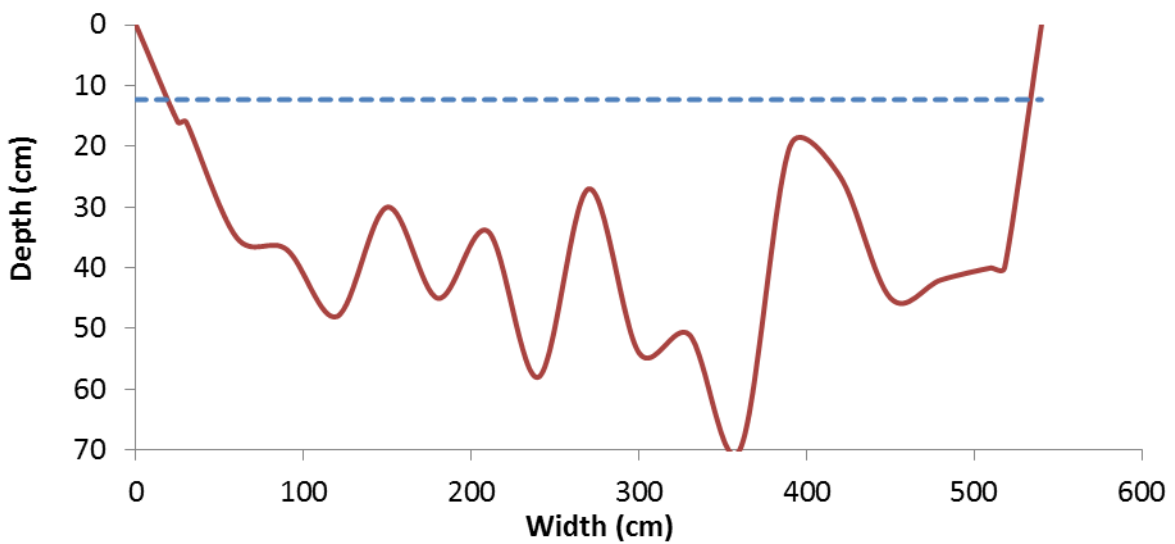
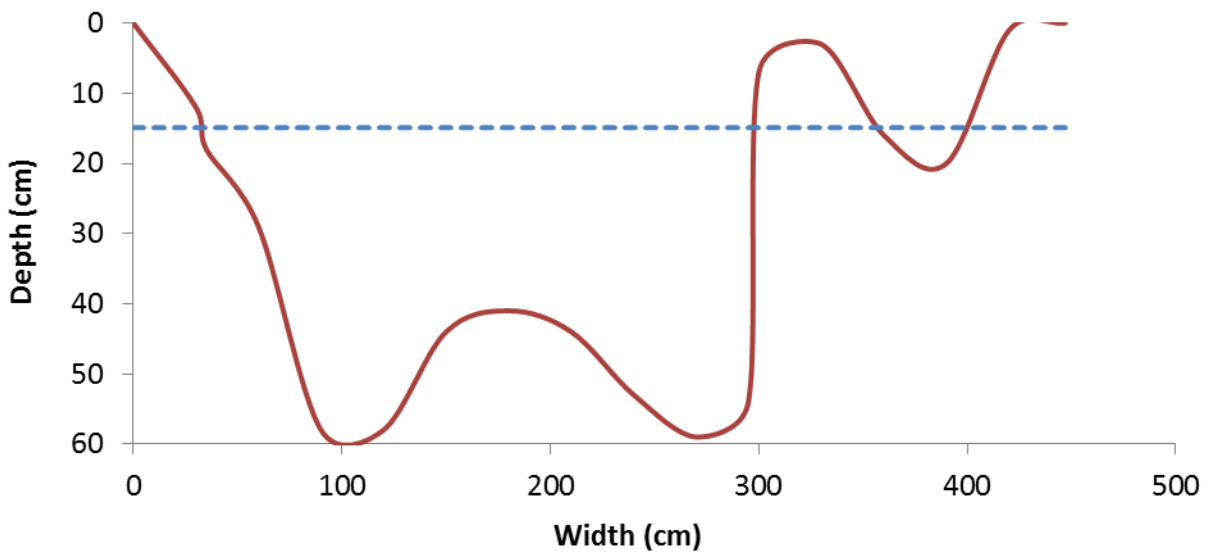
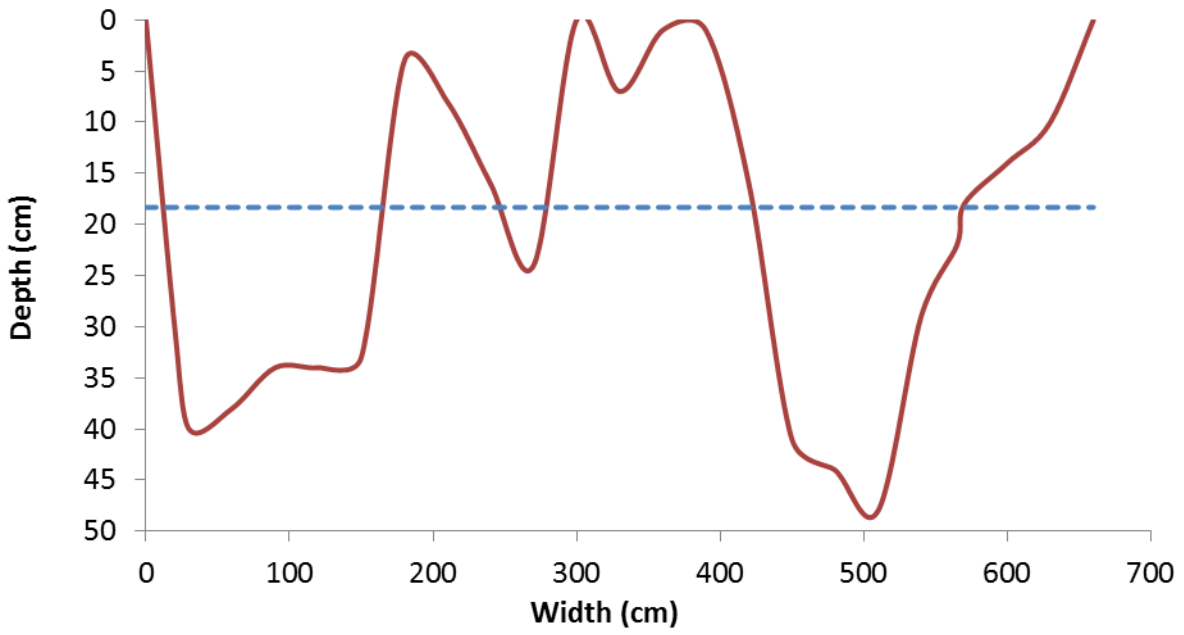


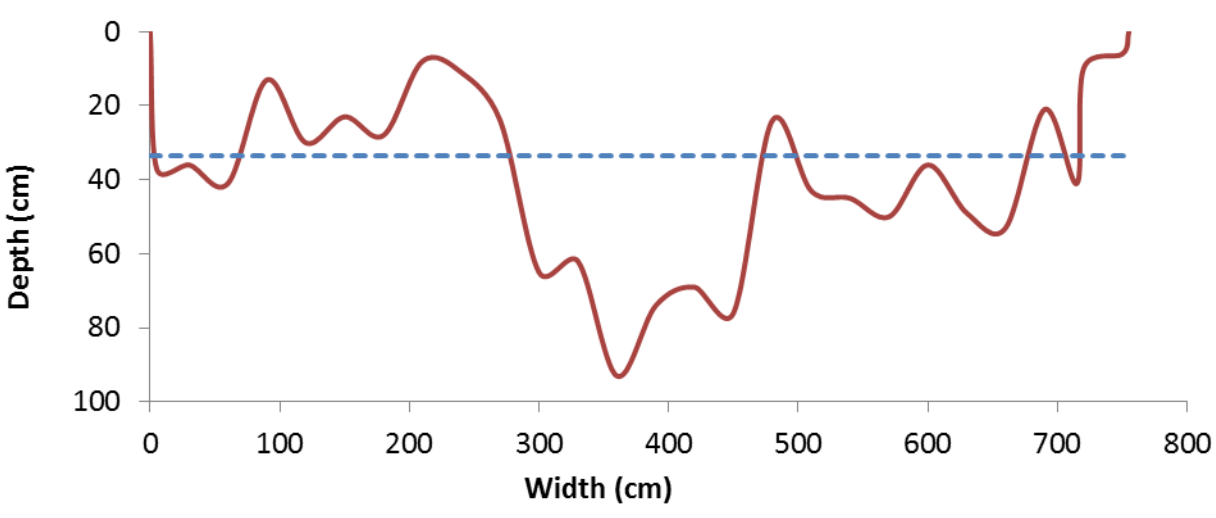
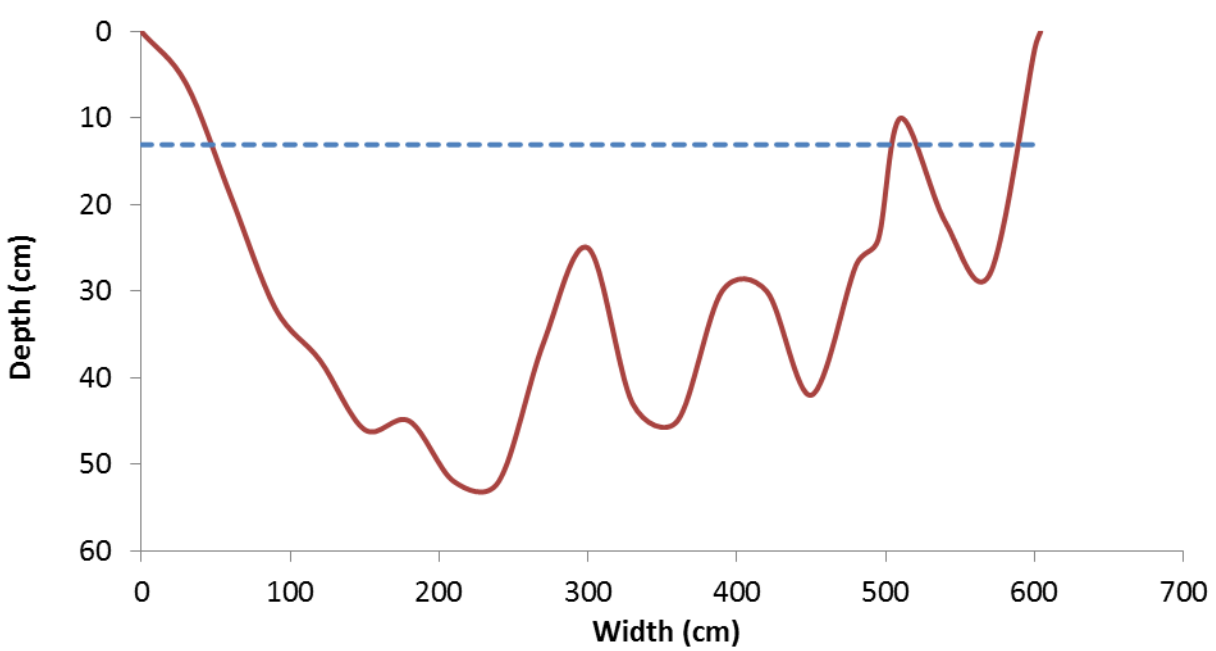
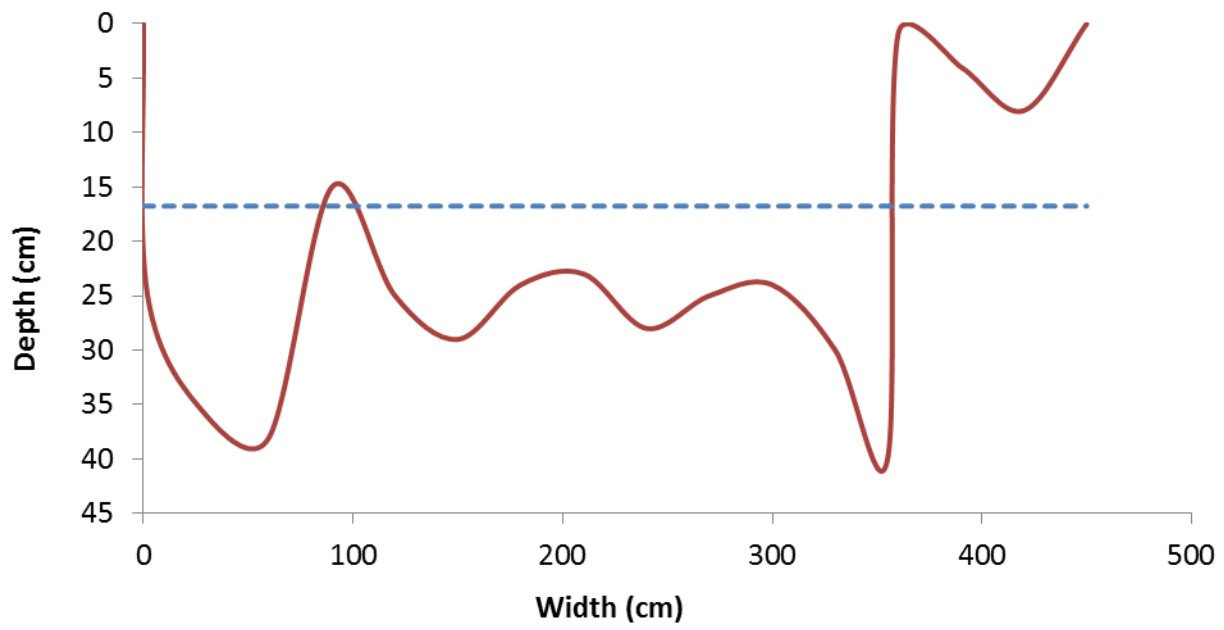


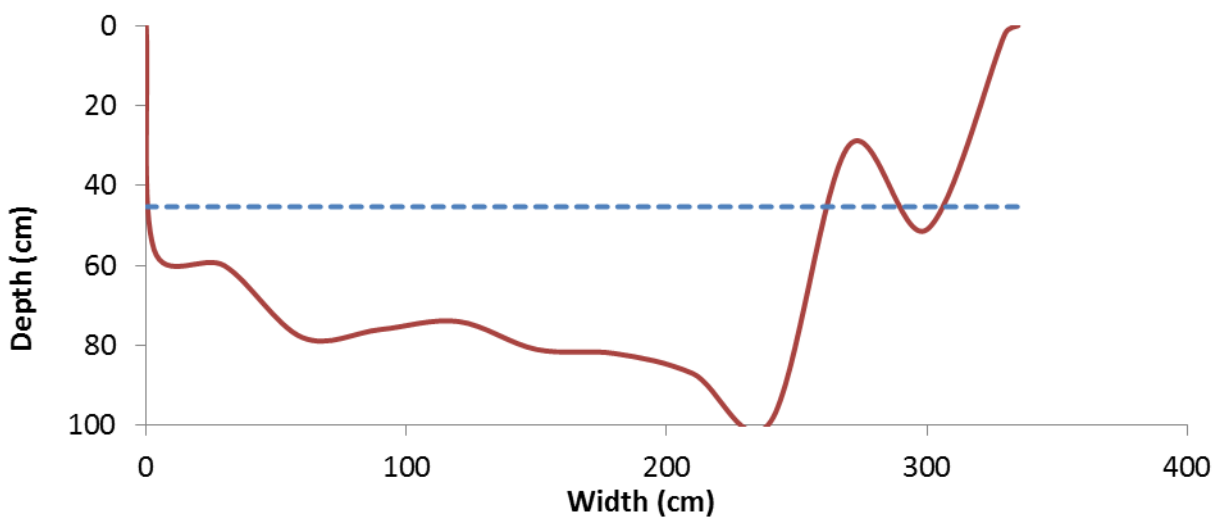
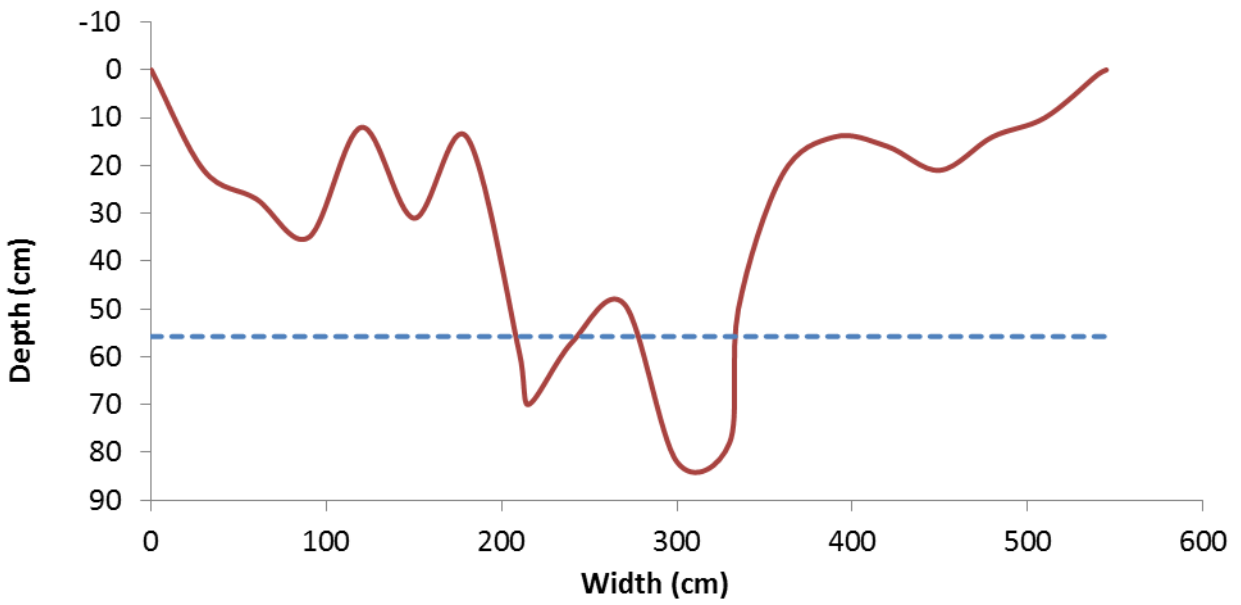
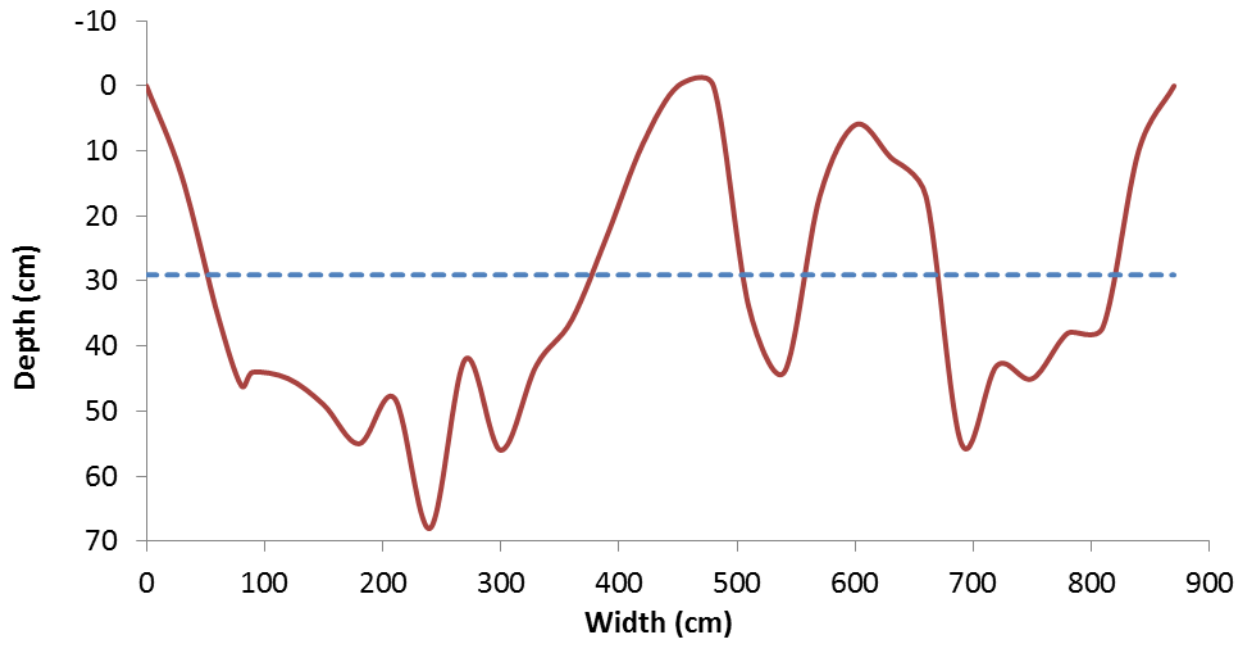


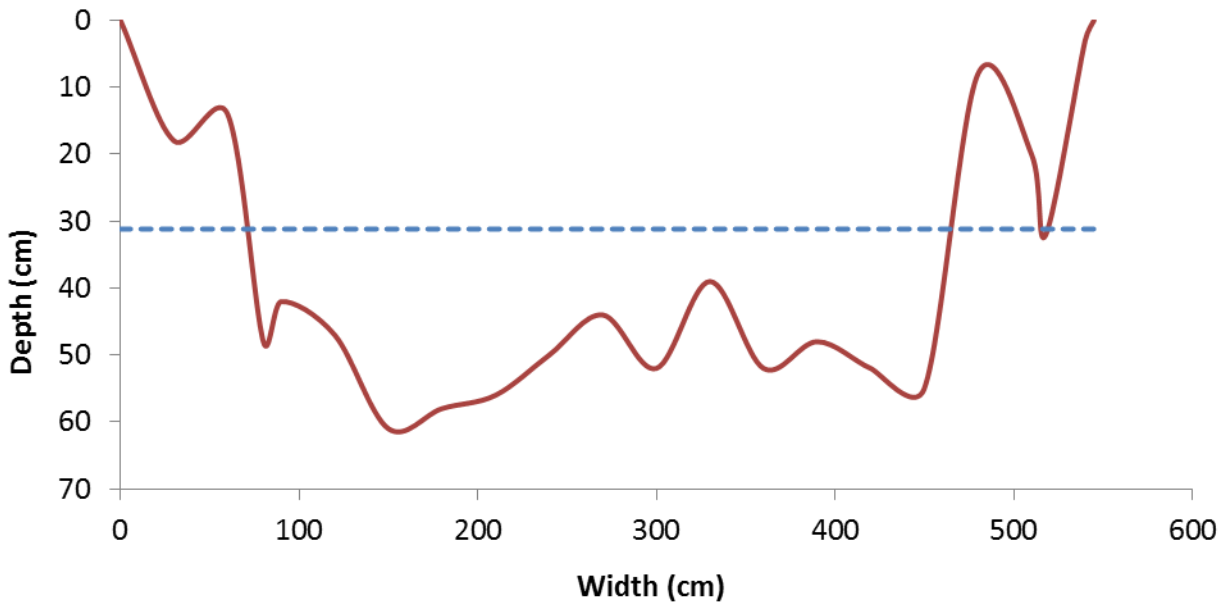


Grigno Creek – G2

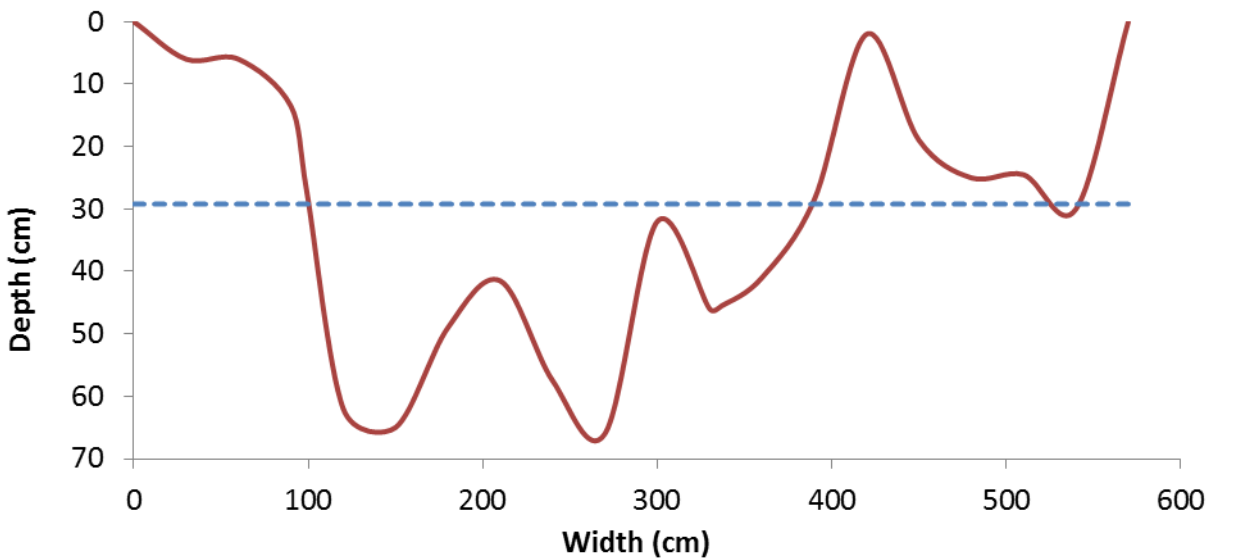
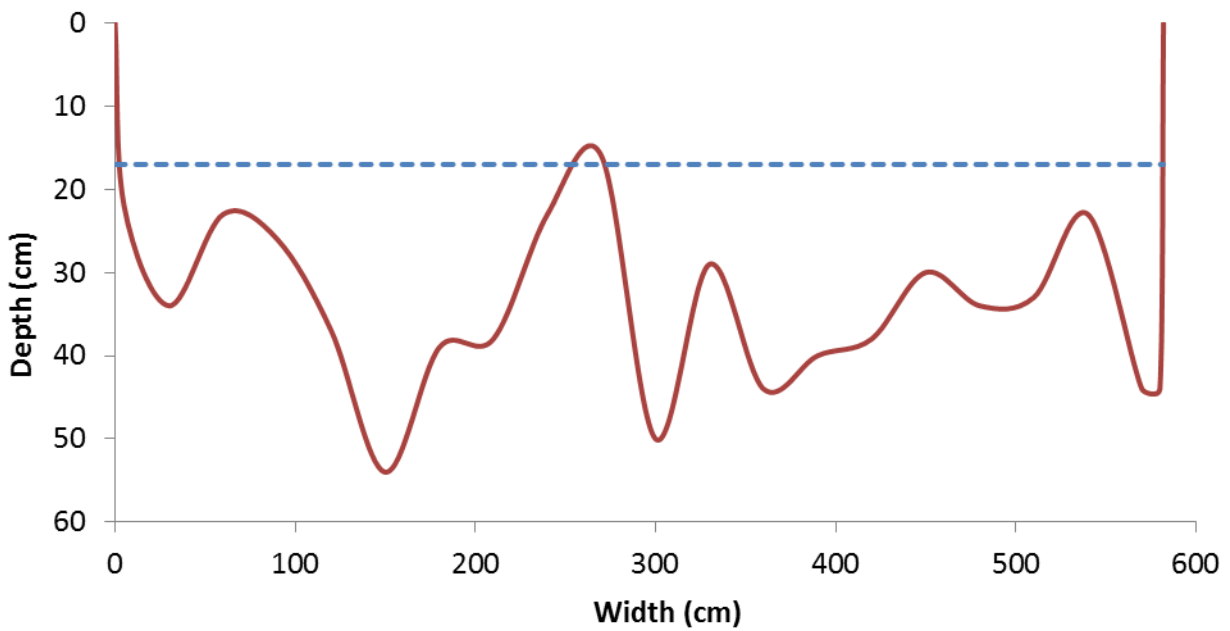


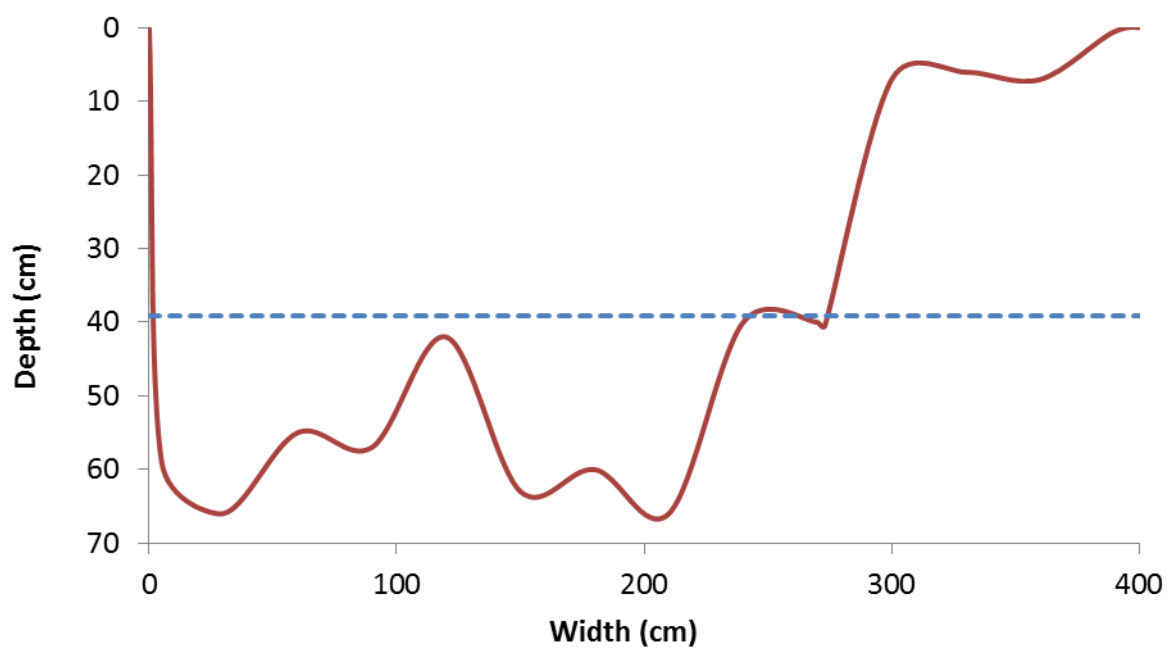
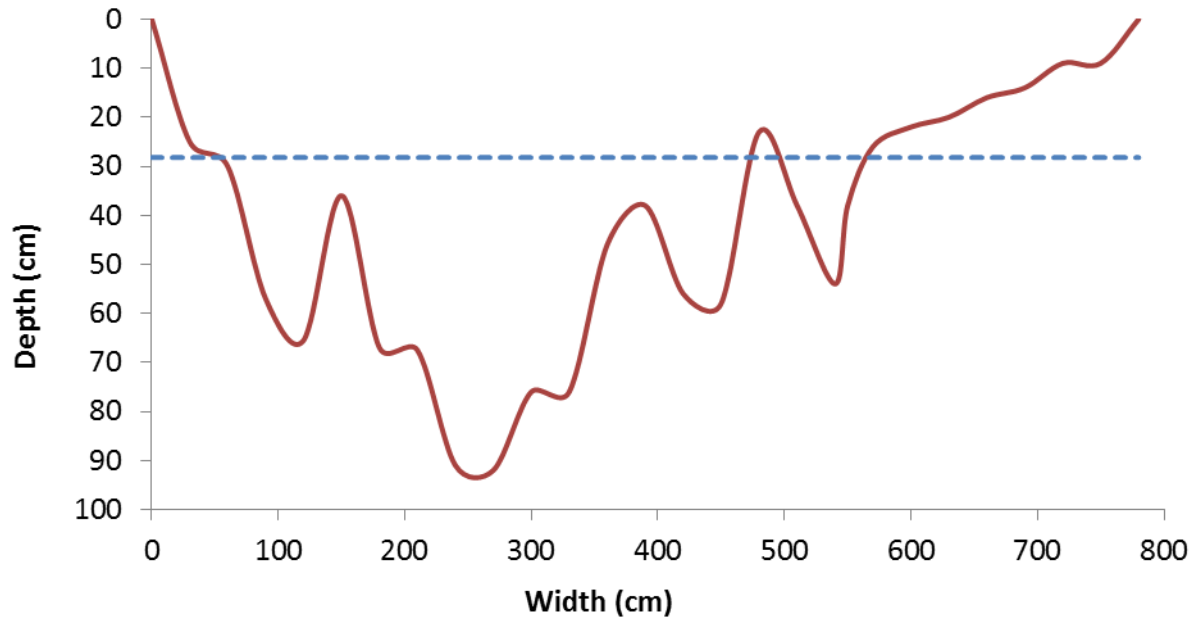
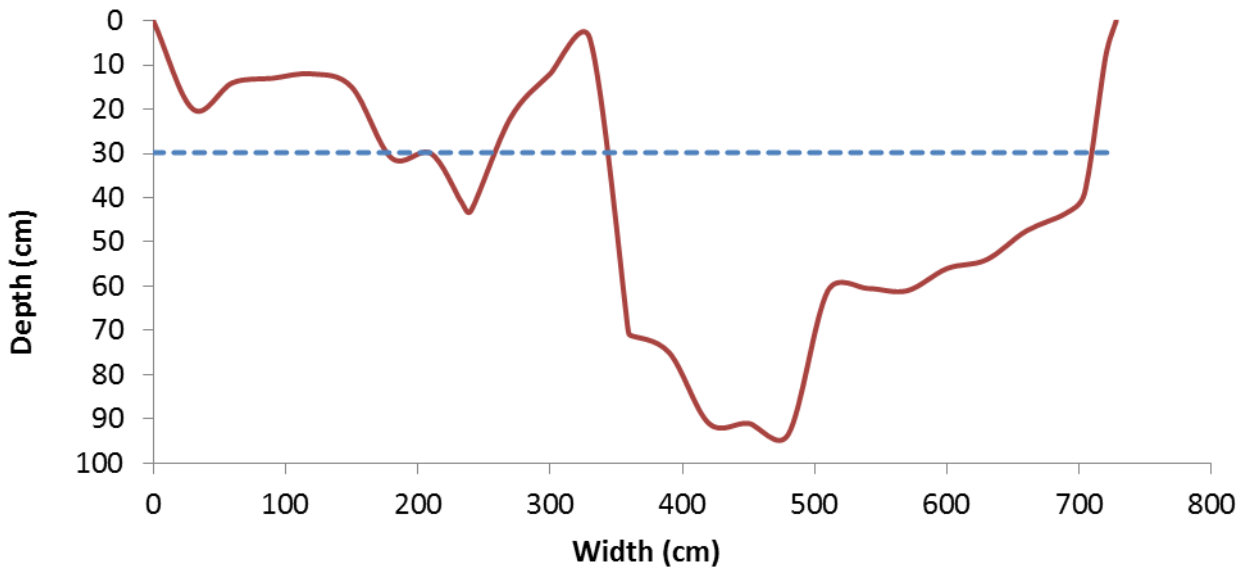


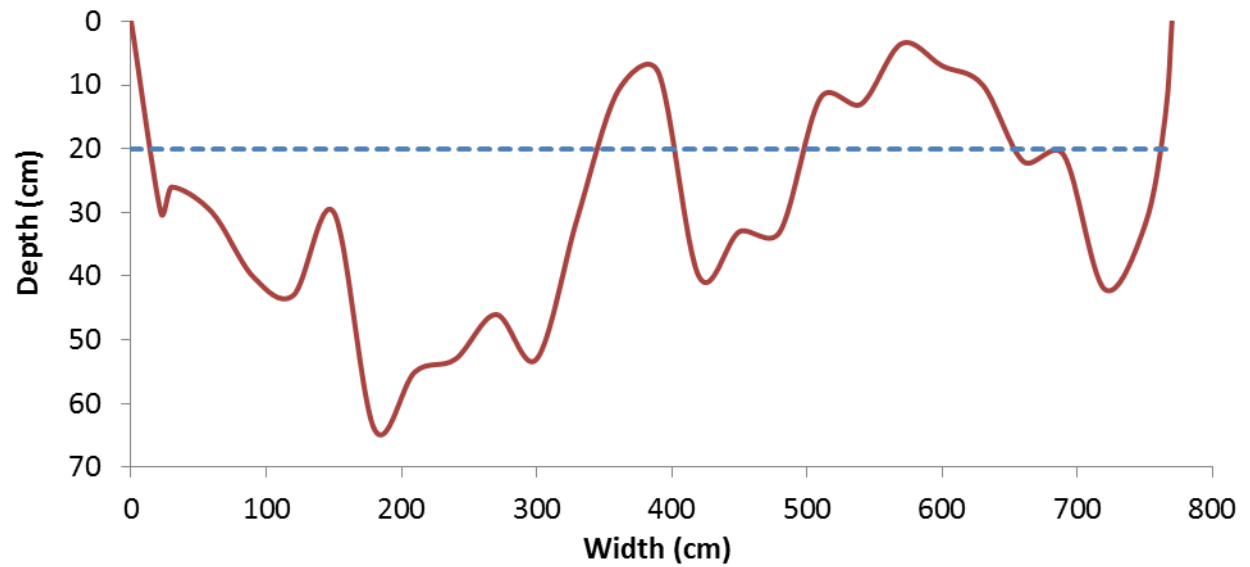
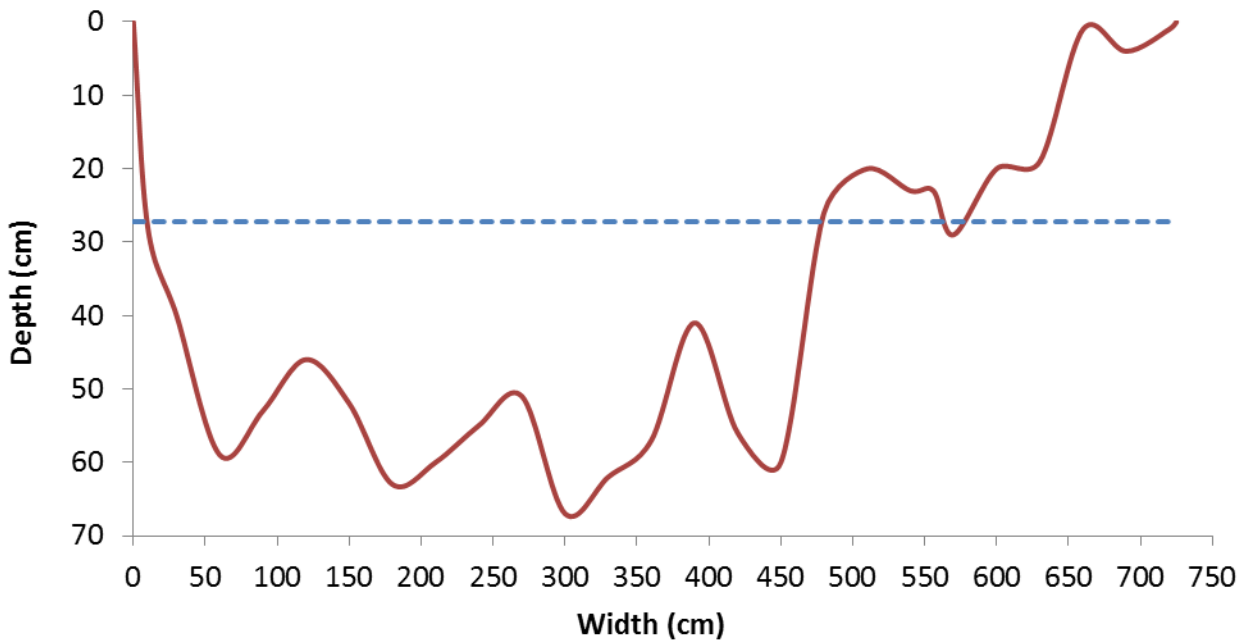
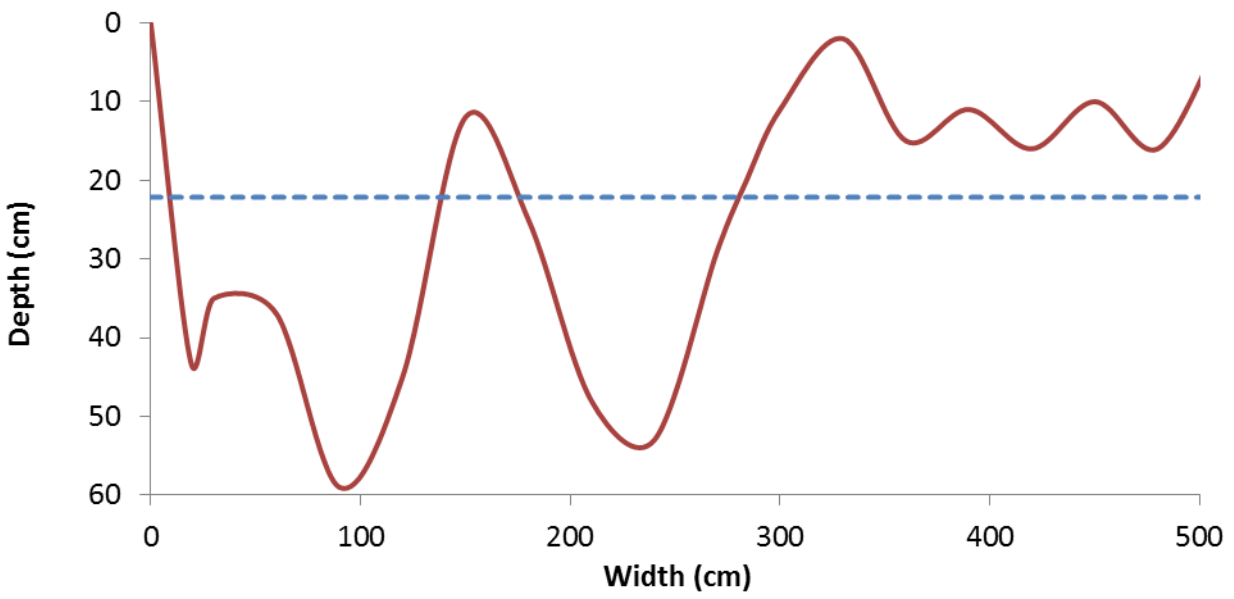


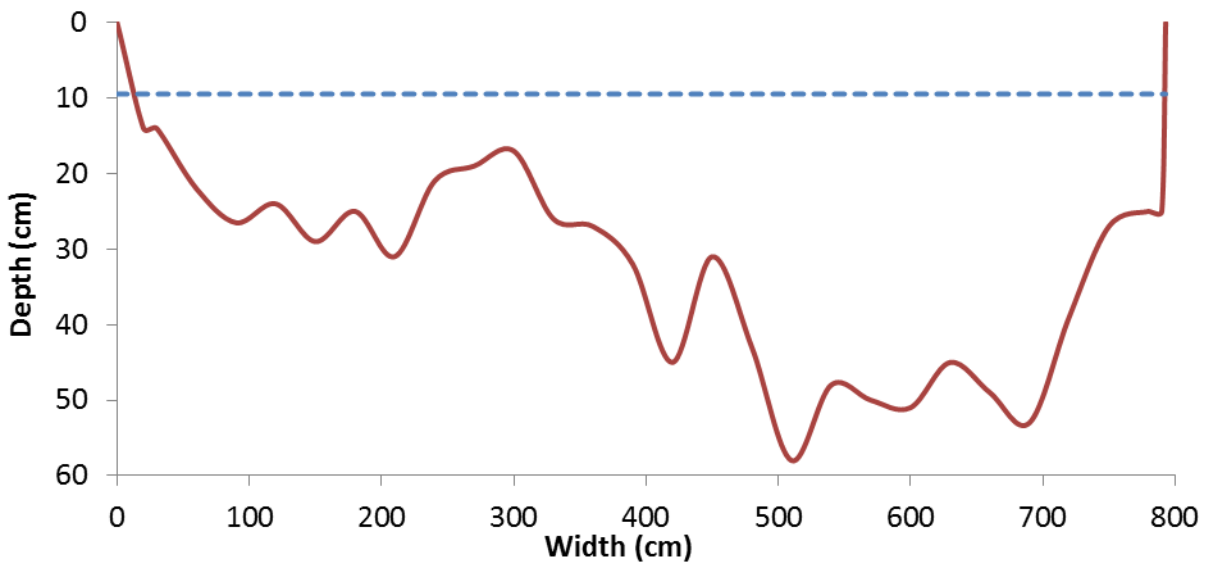
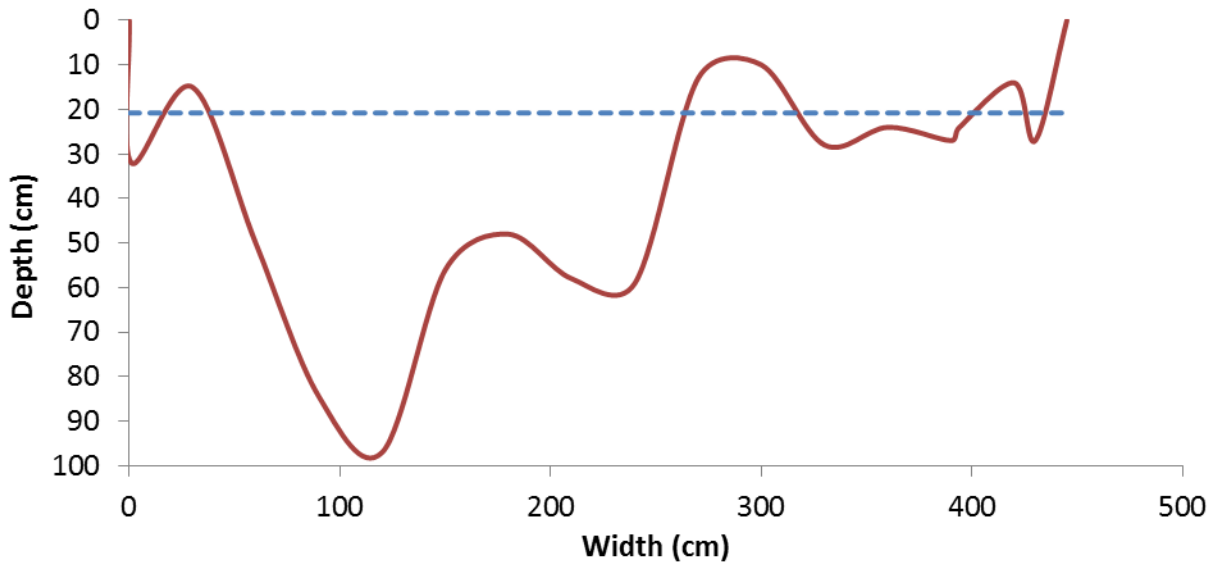


Grigno Creek – G3

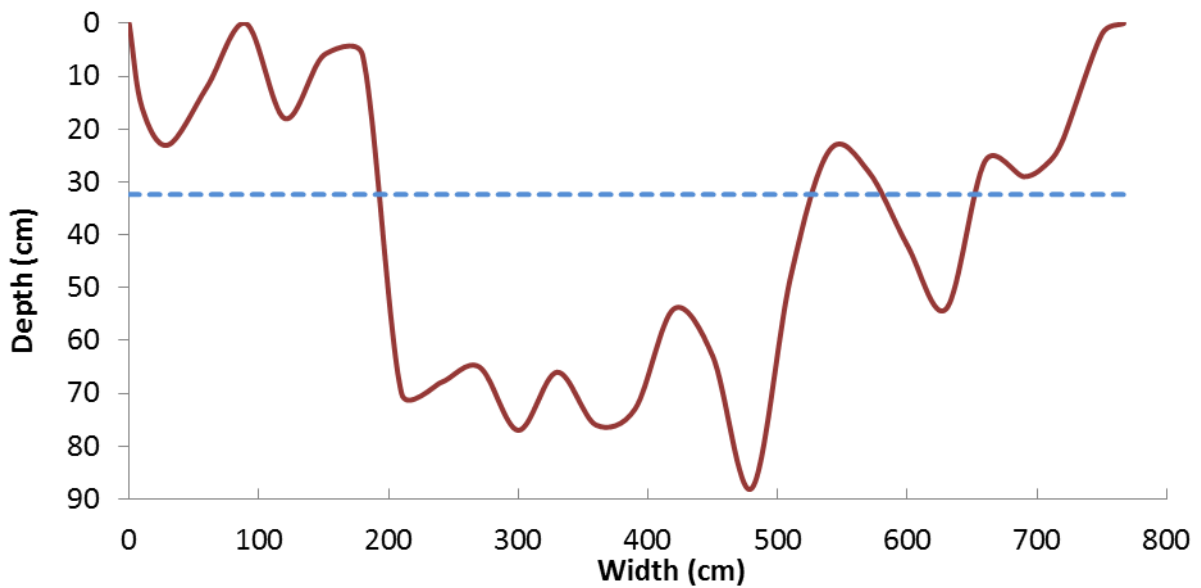


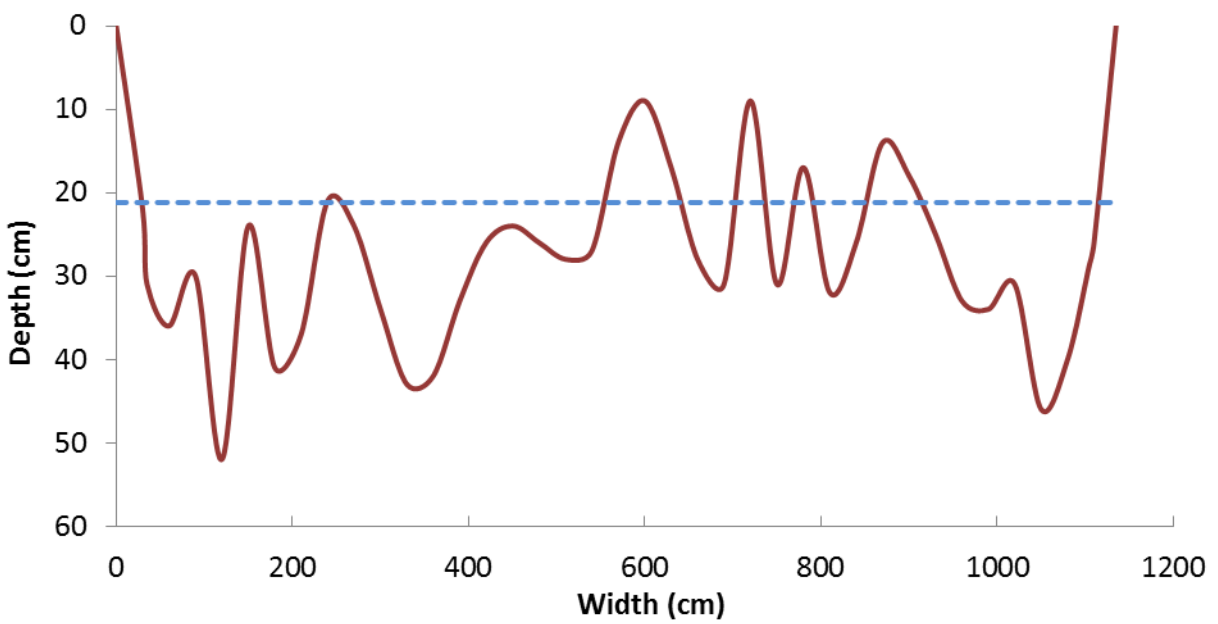
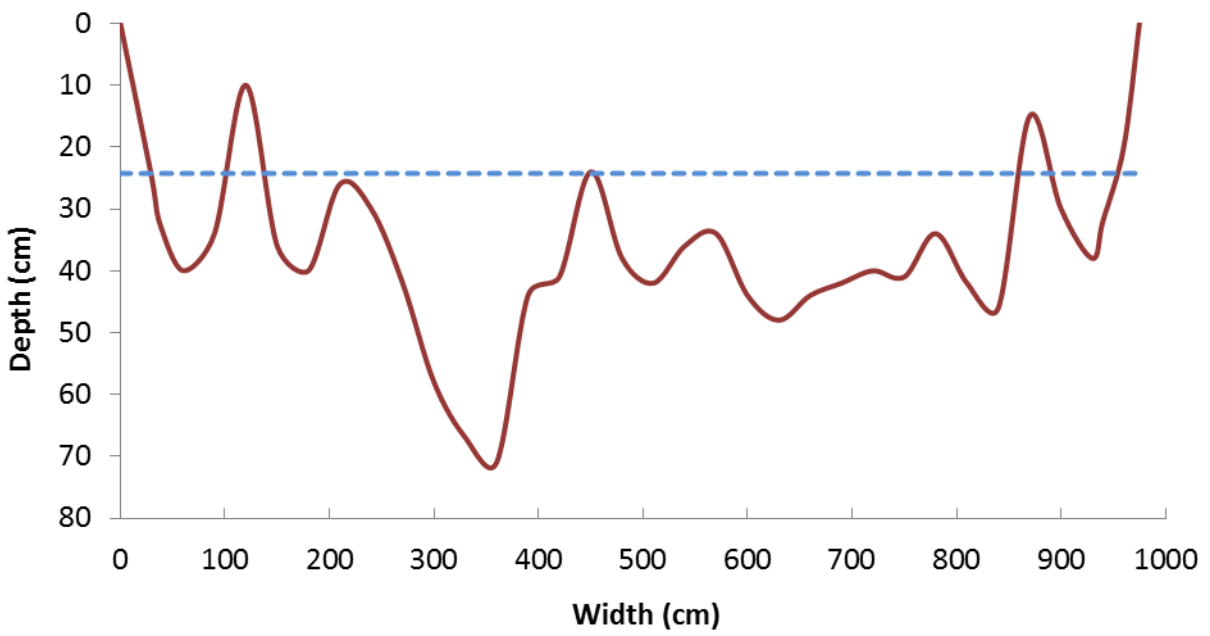
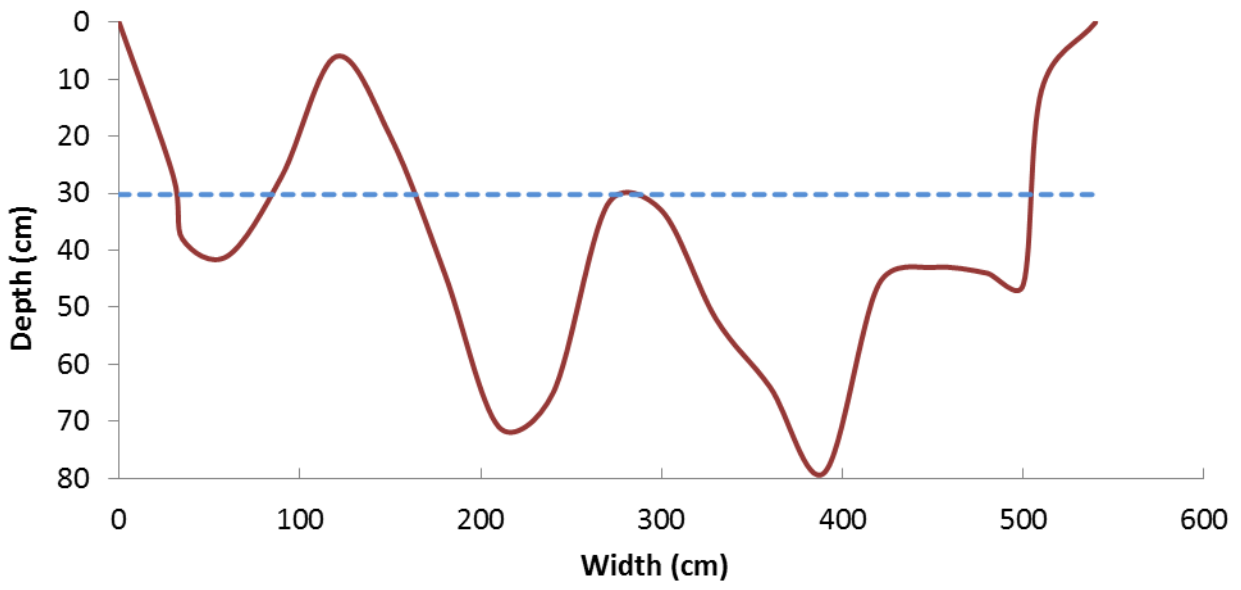


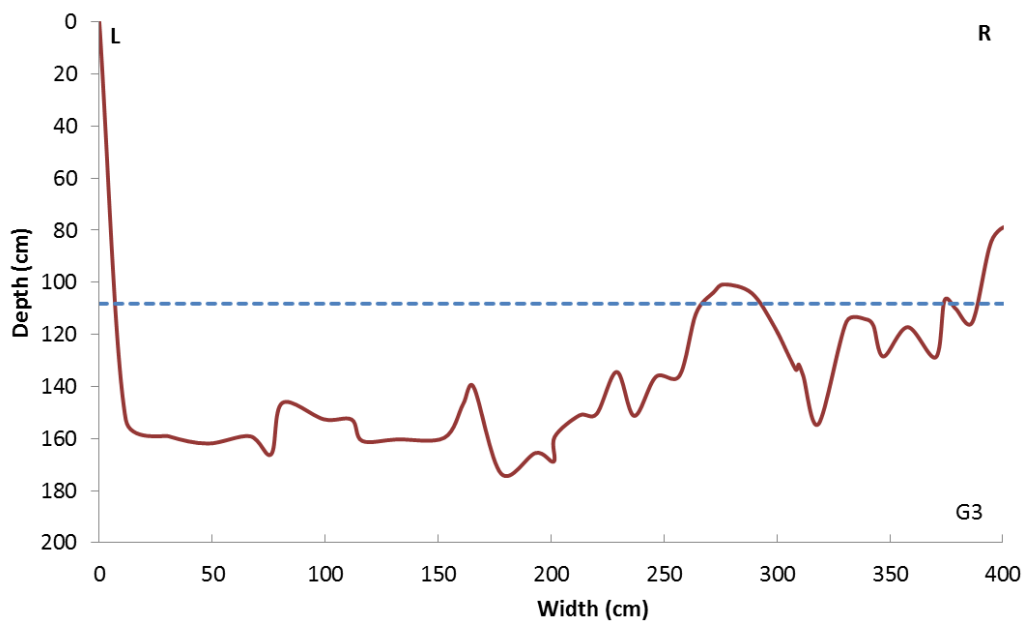
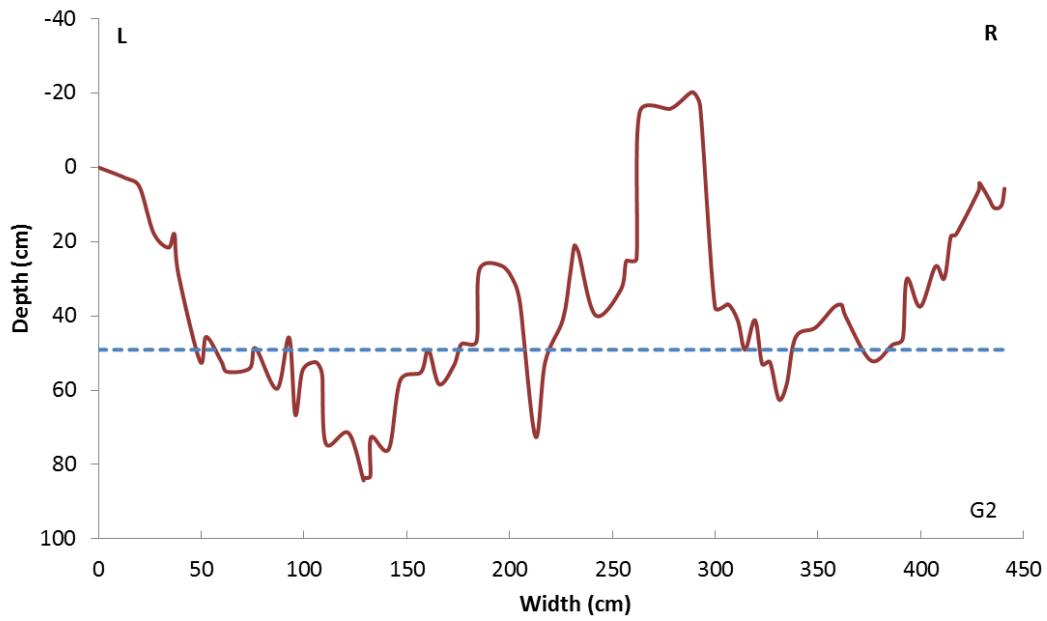
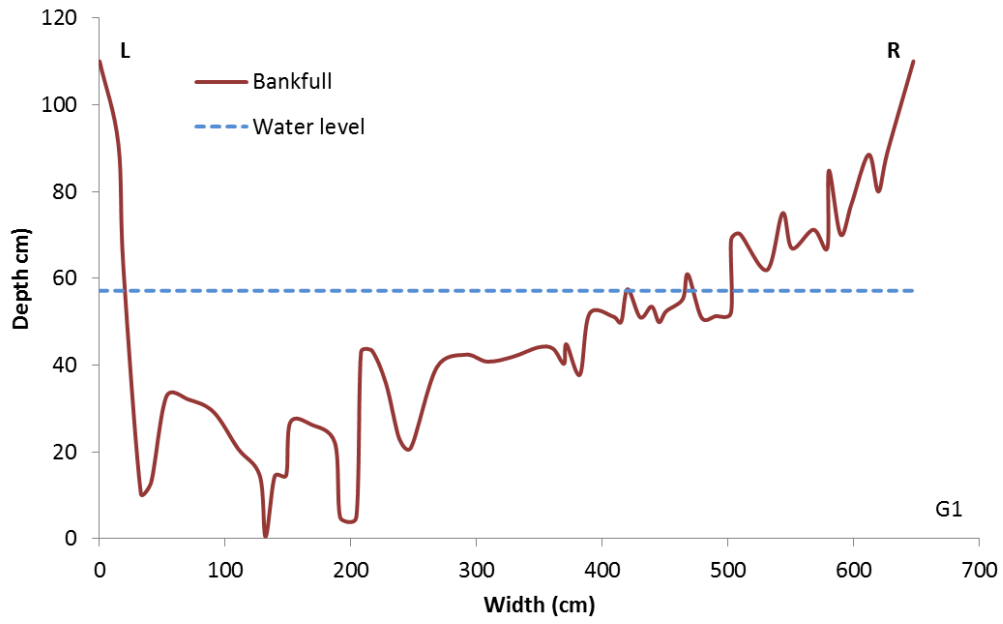


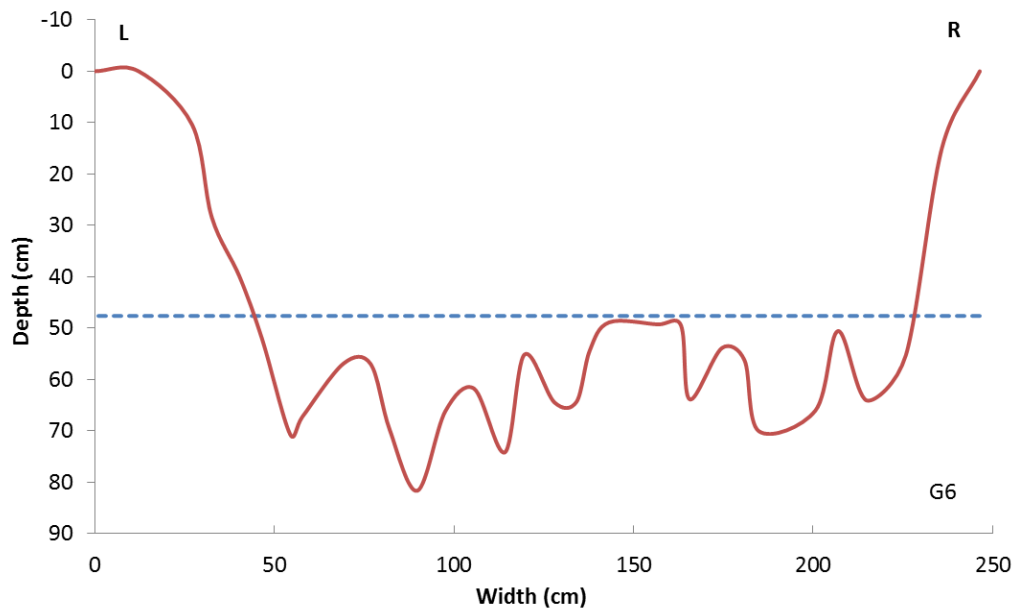
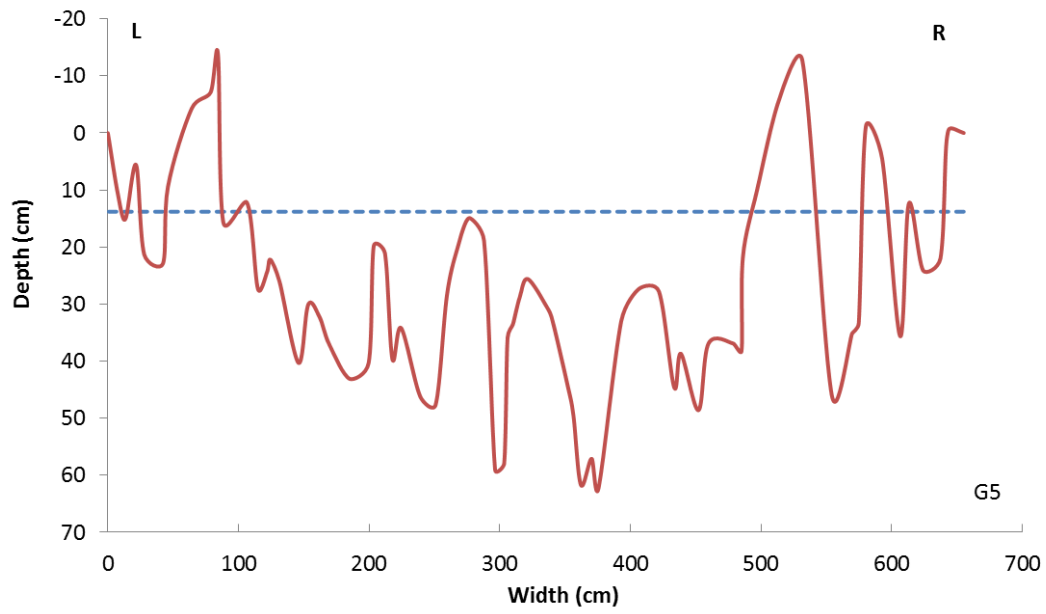
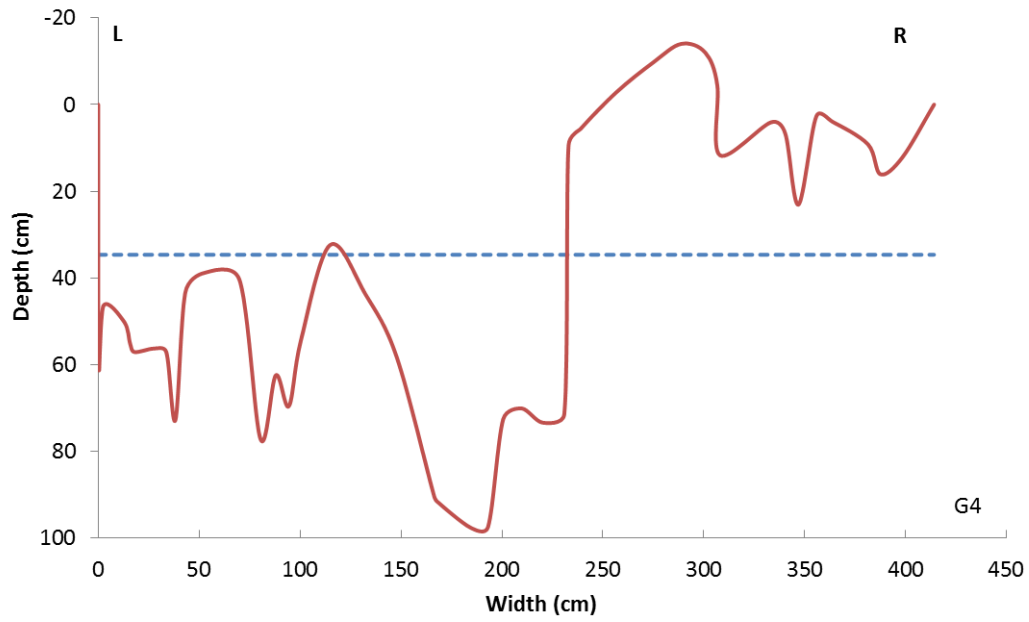


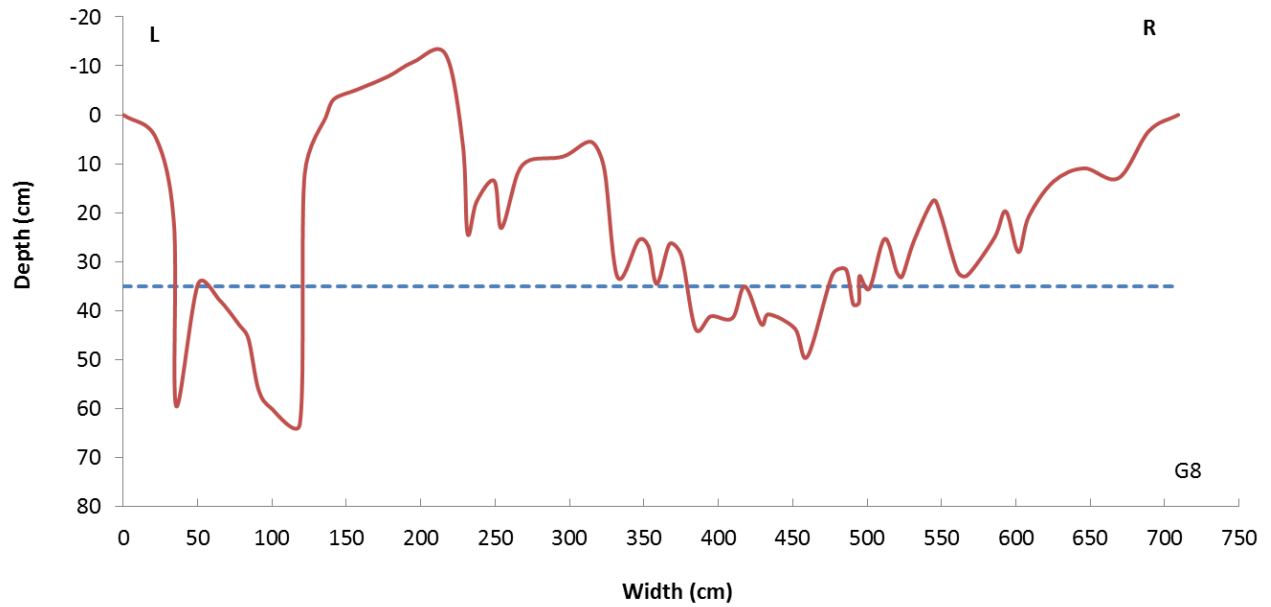
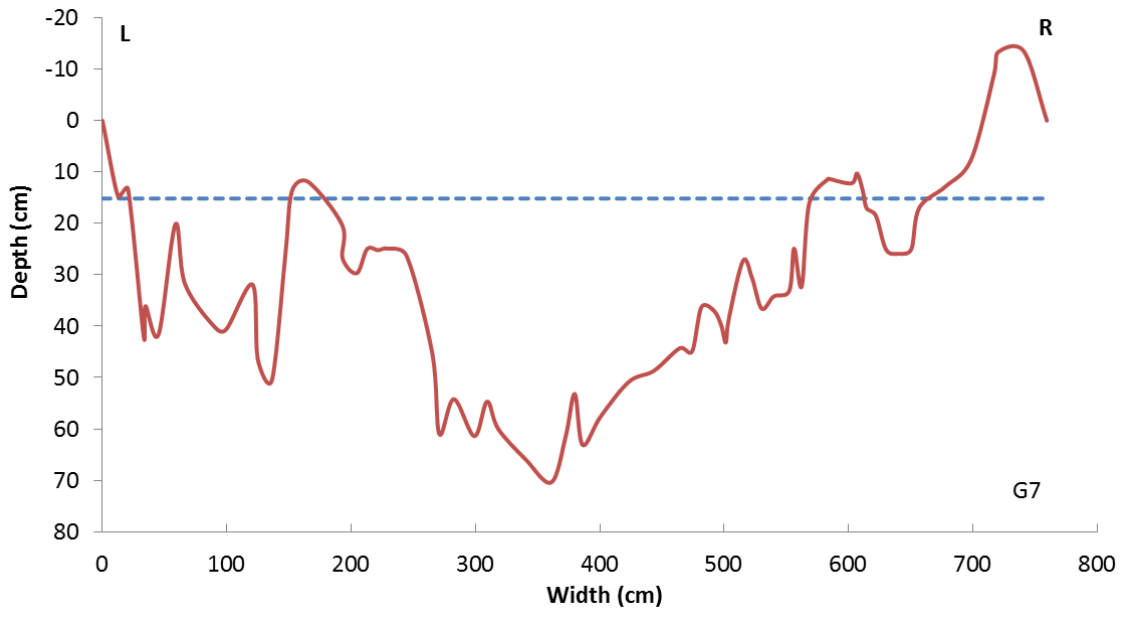
Grigno Creek – G4



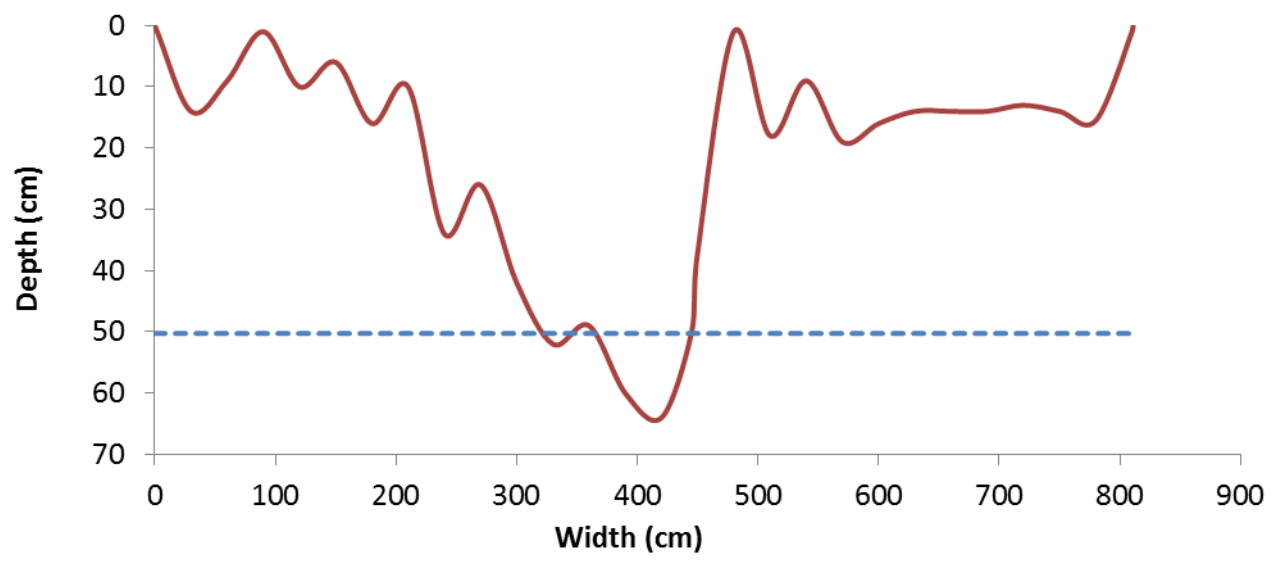


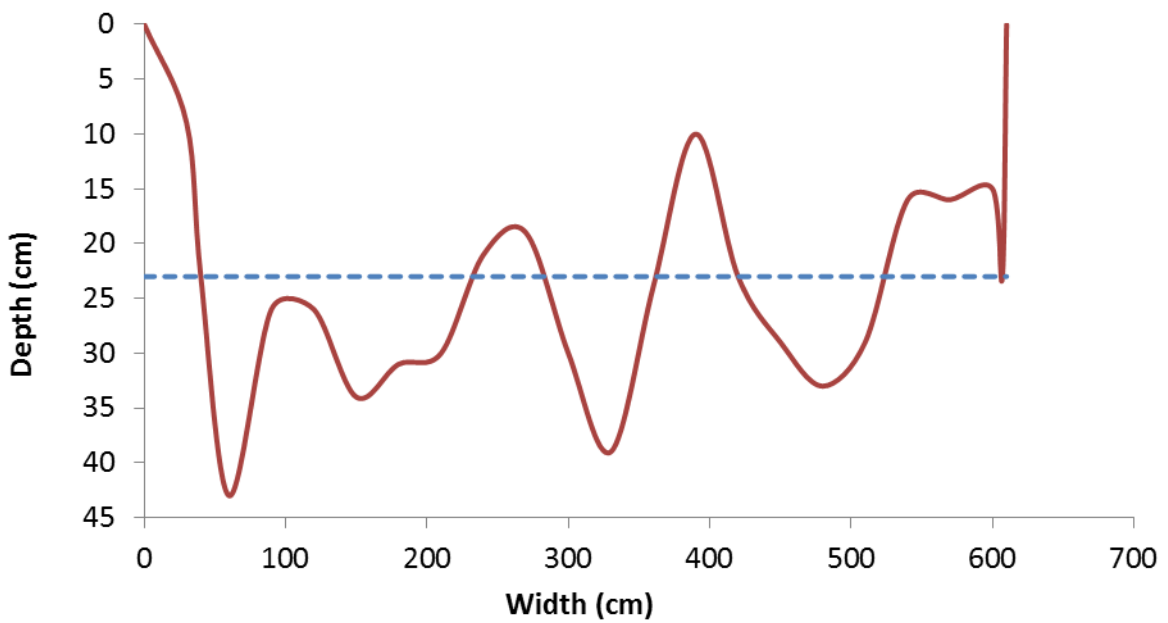
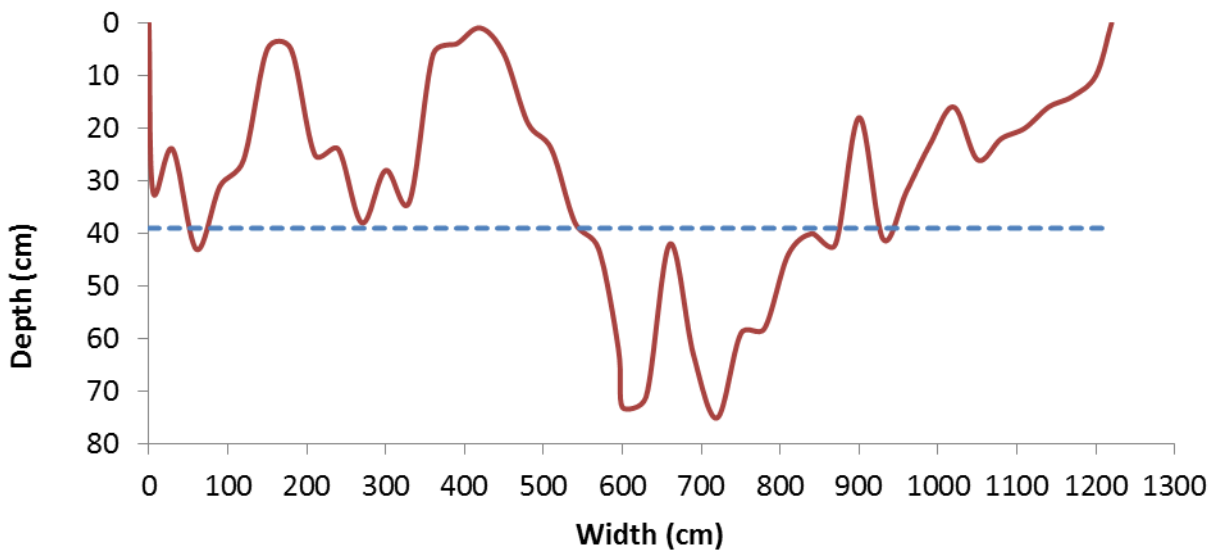
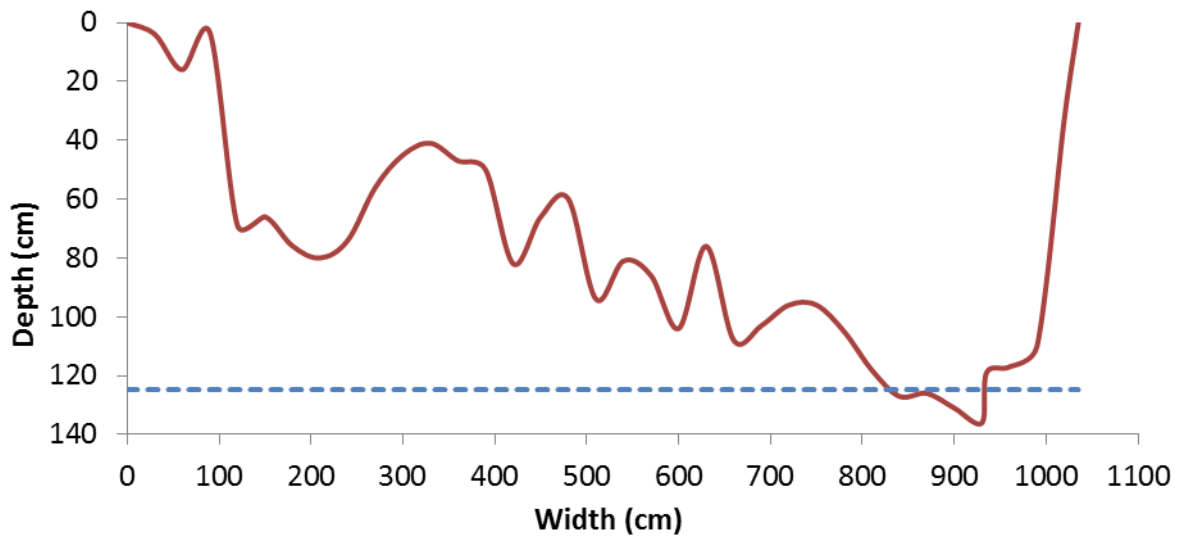


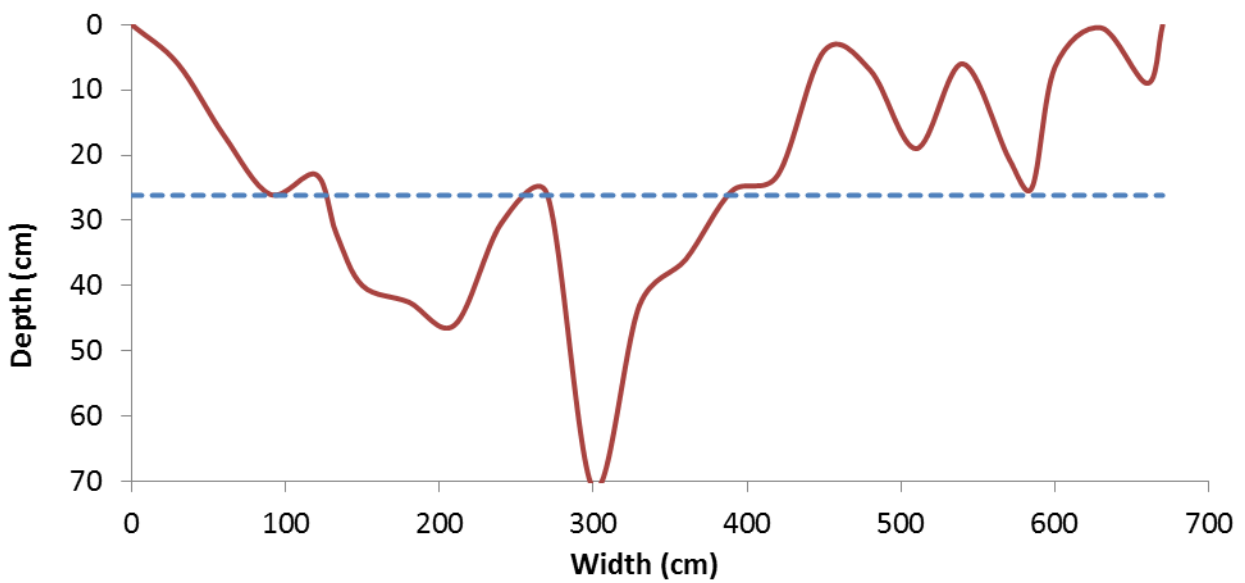
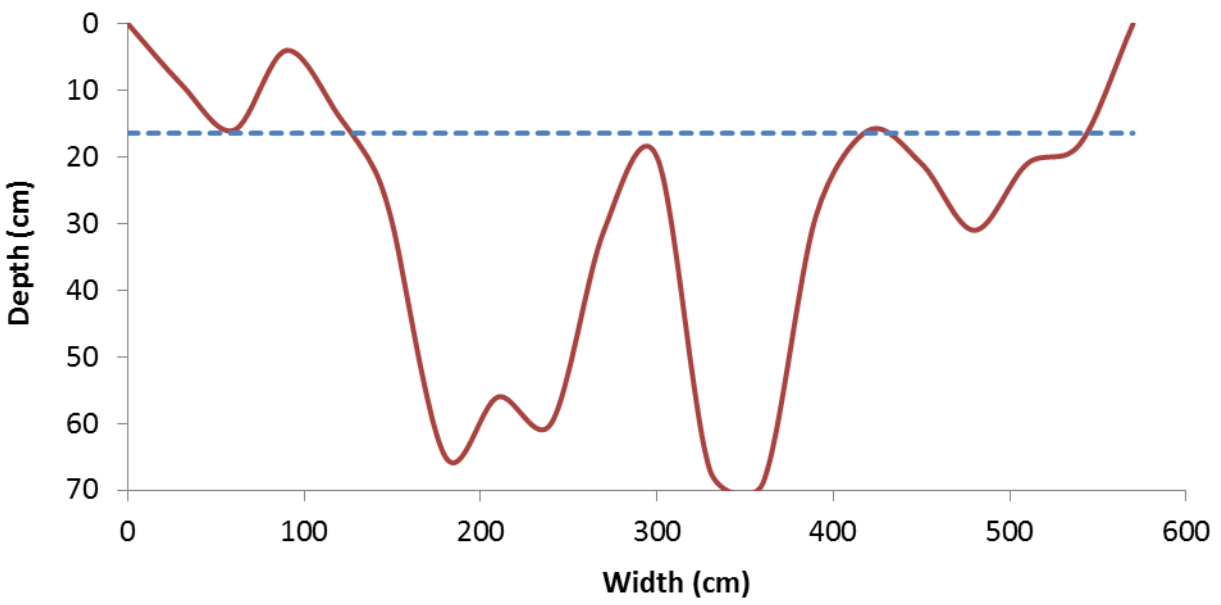
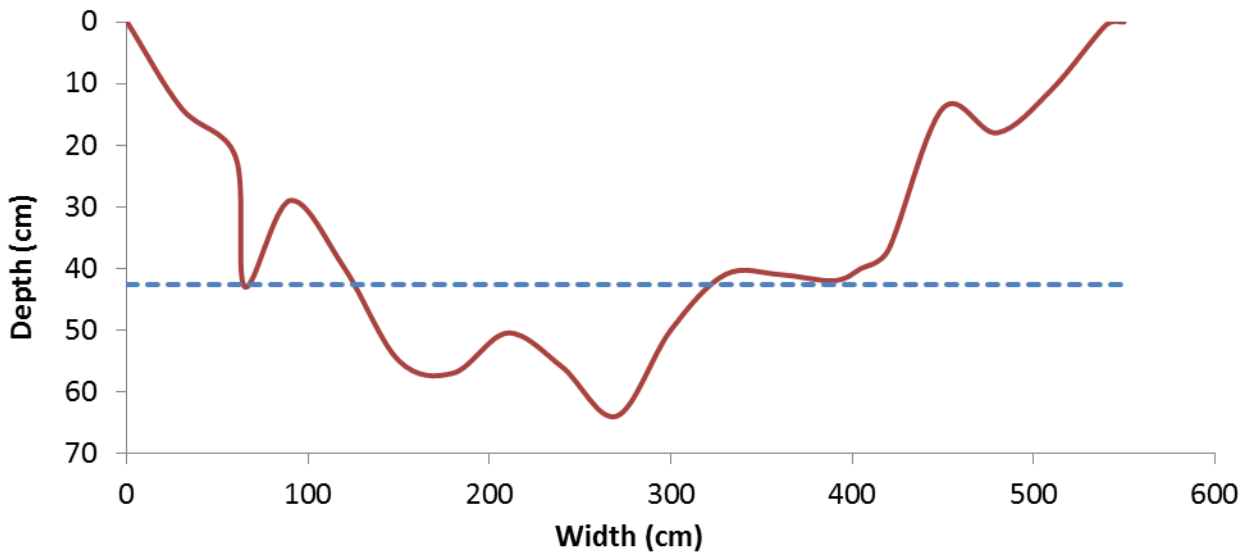


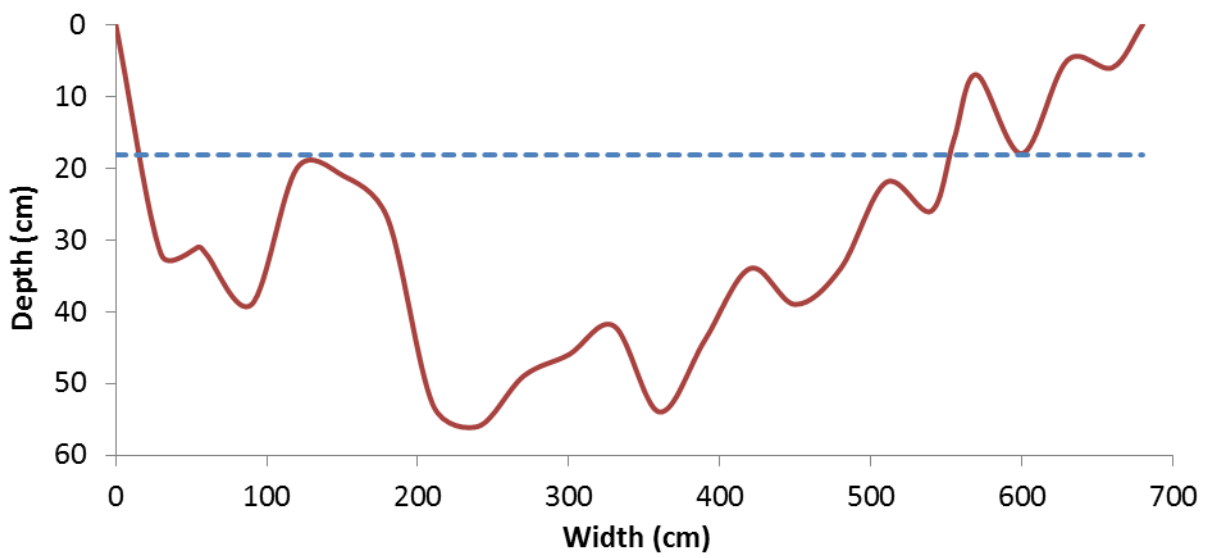
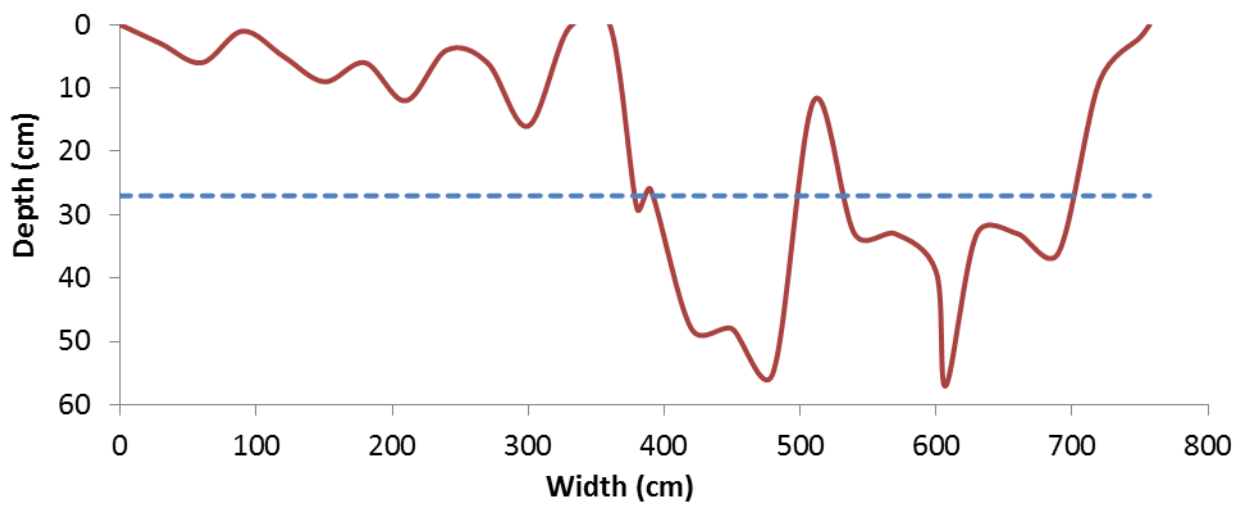
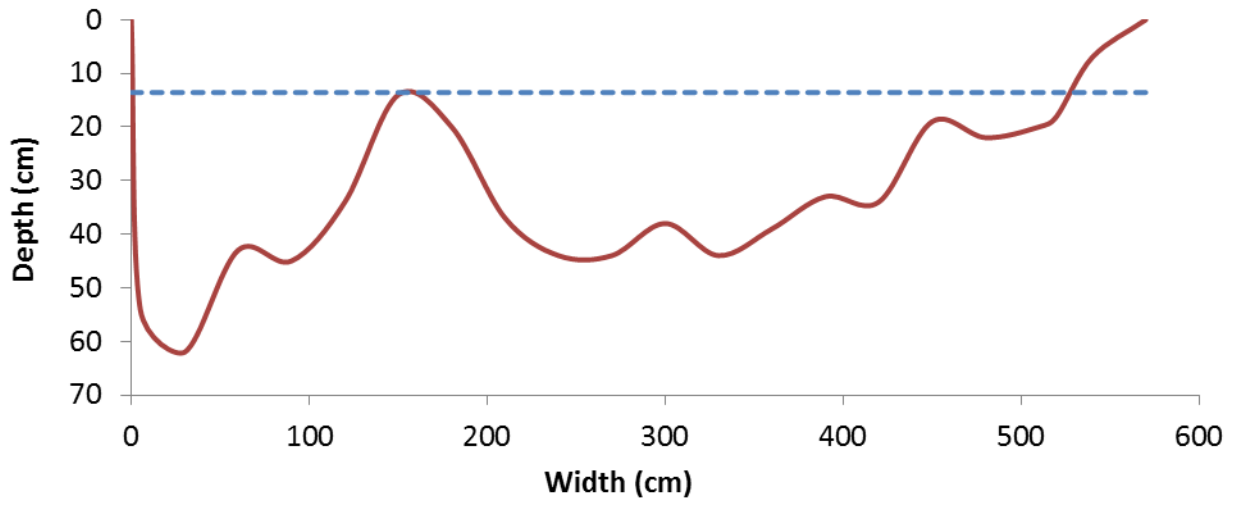


Grigno Creek – G5

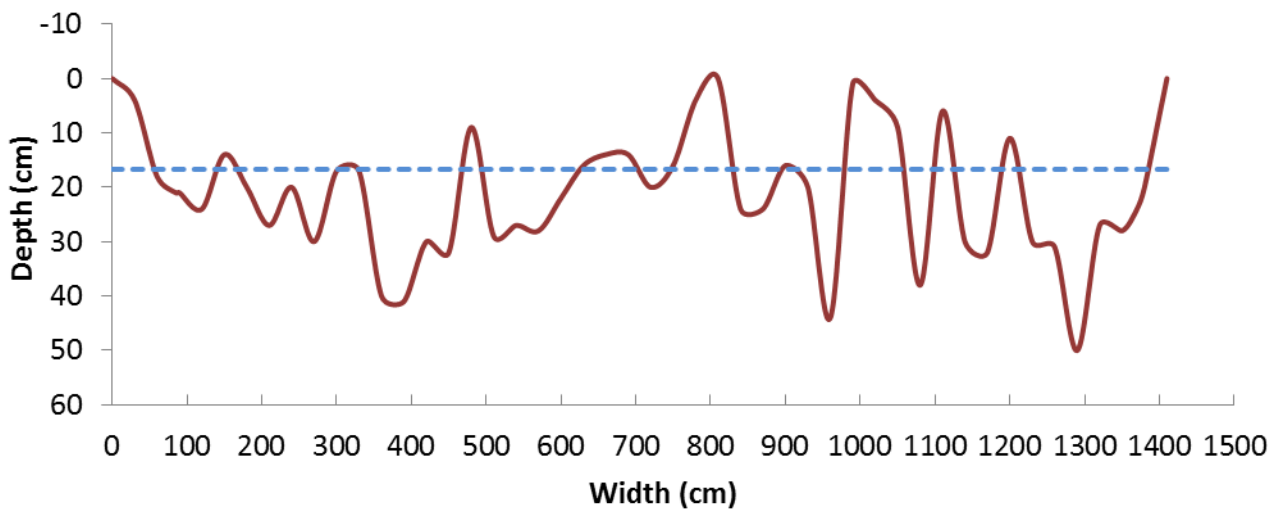
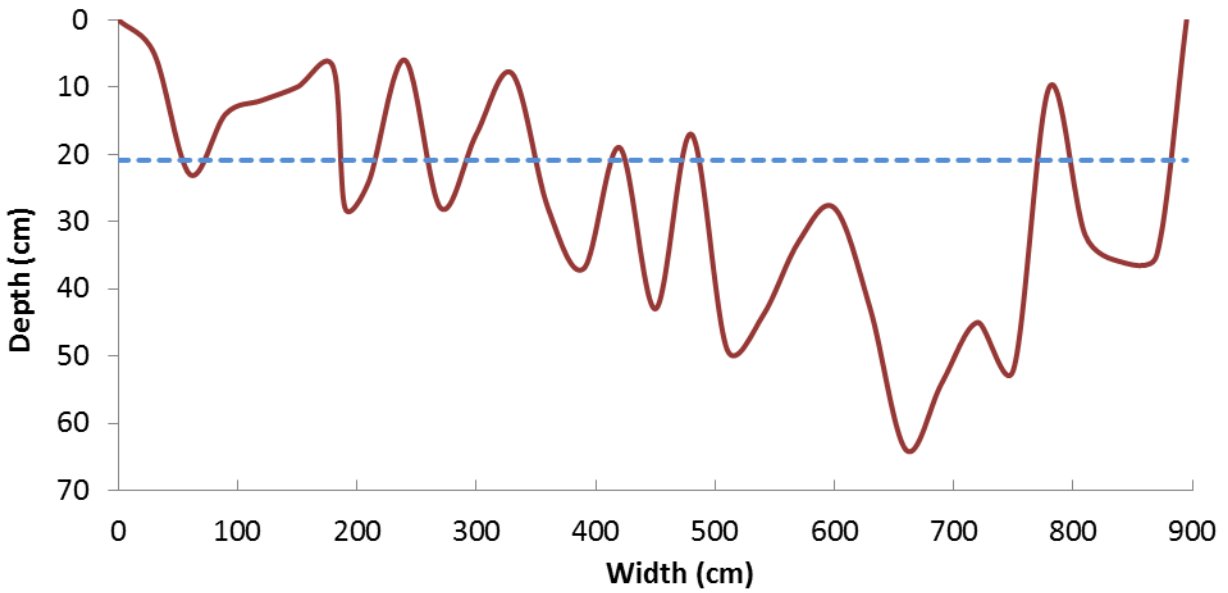
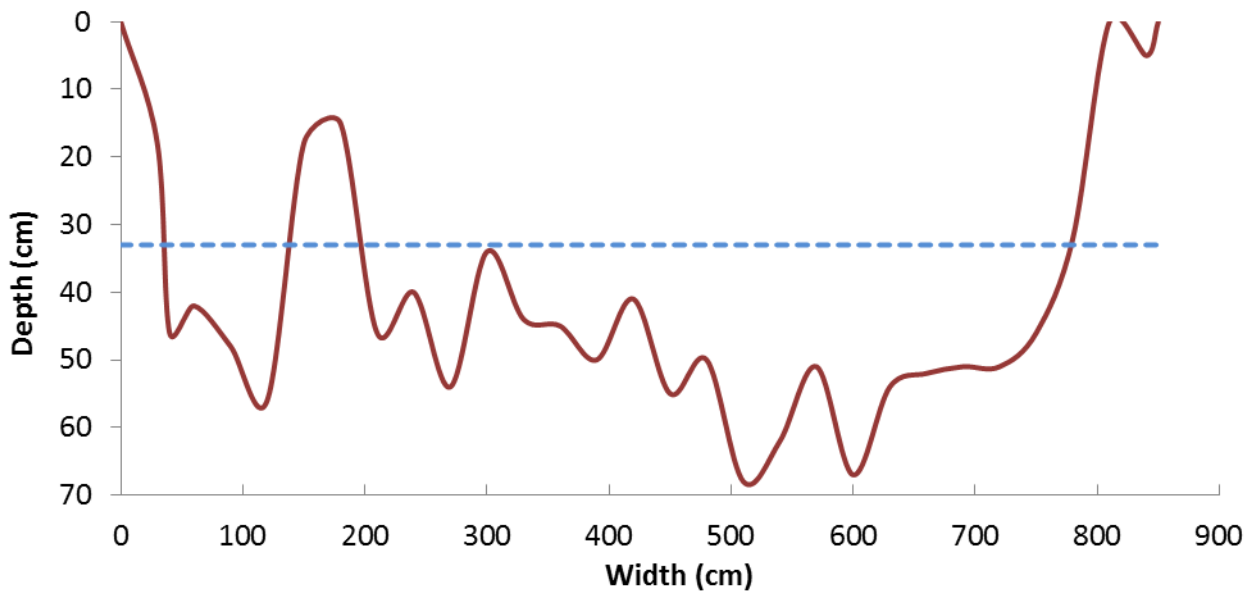


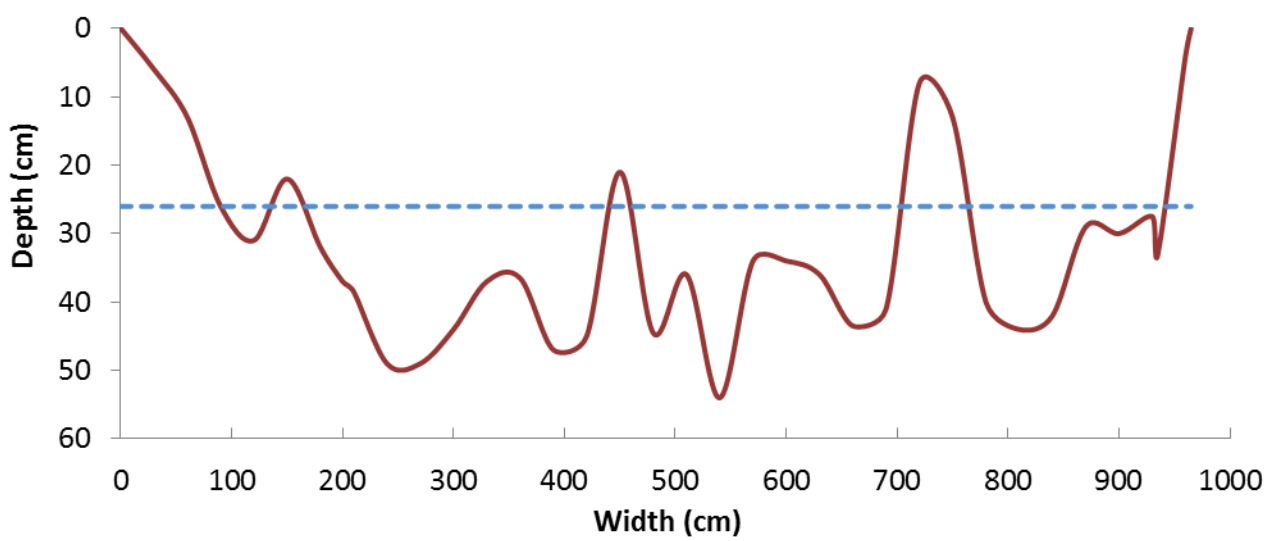
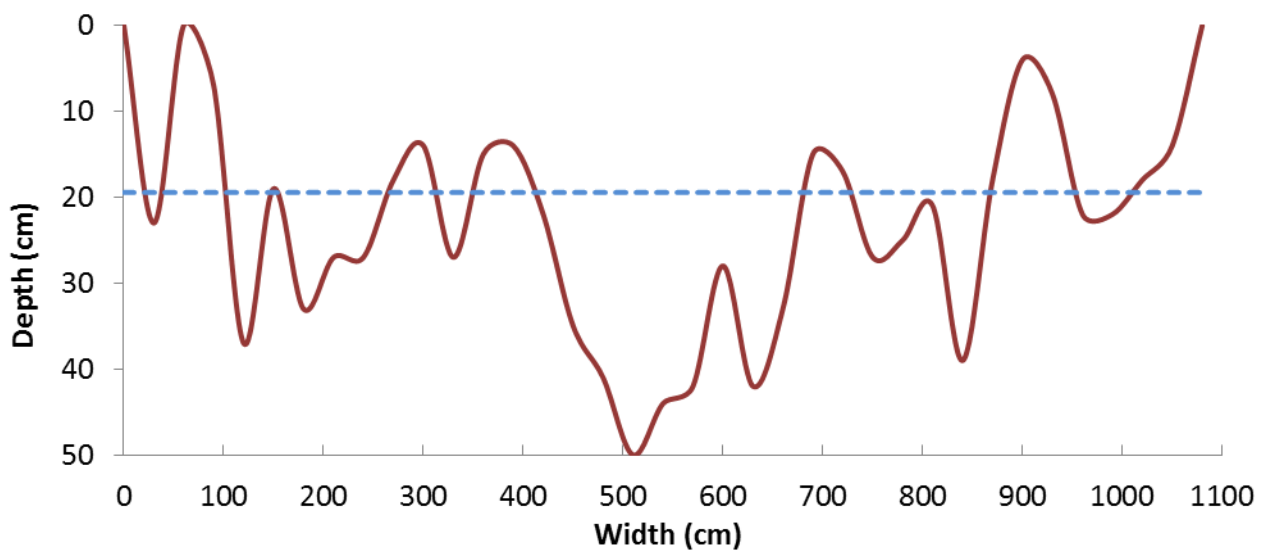
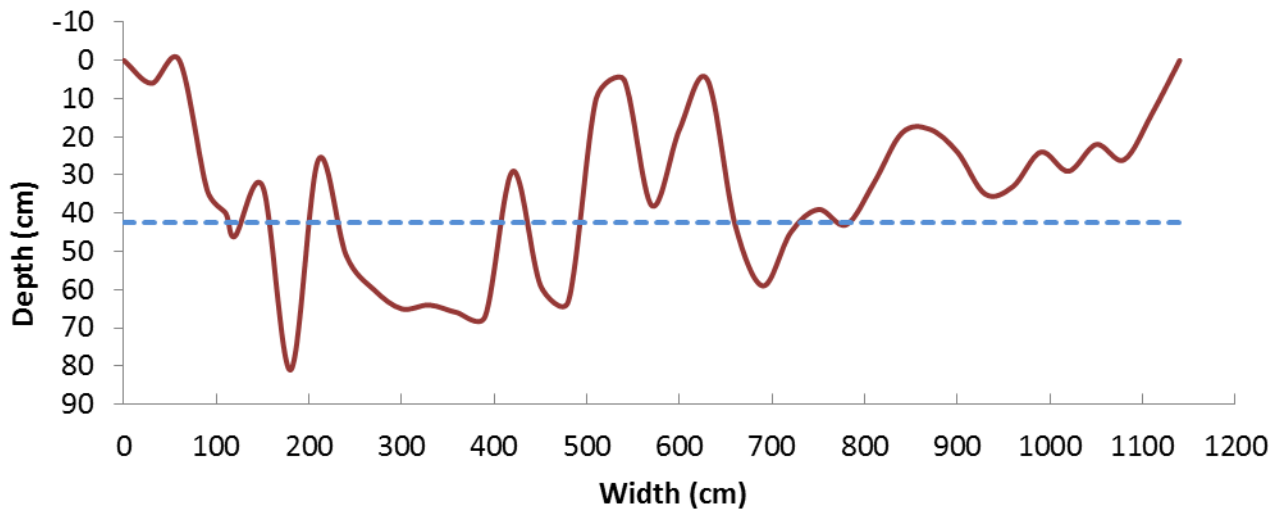


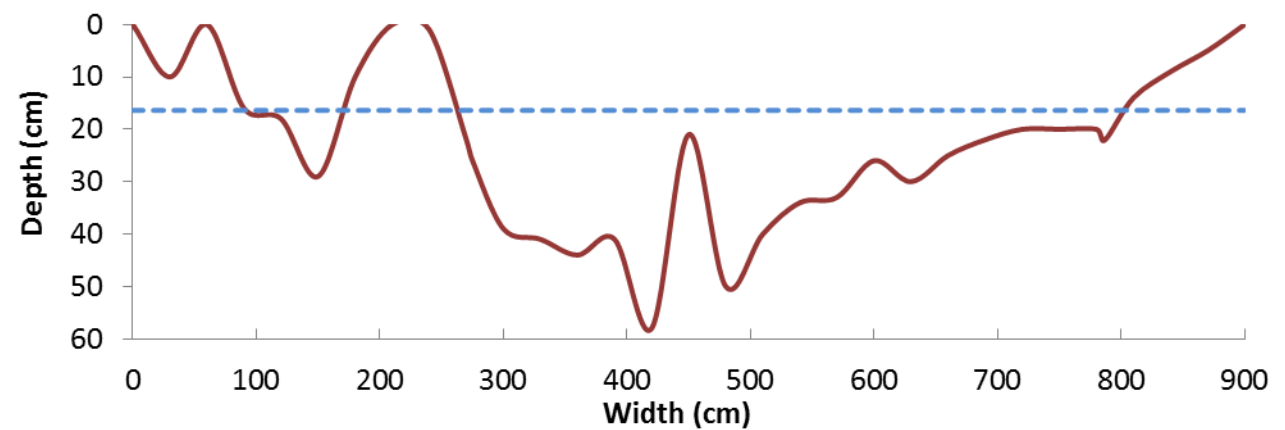
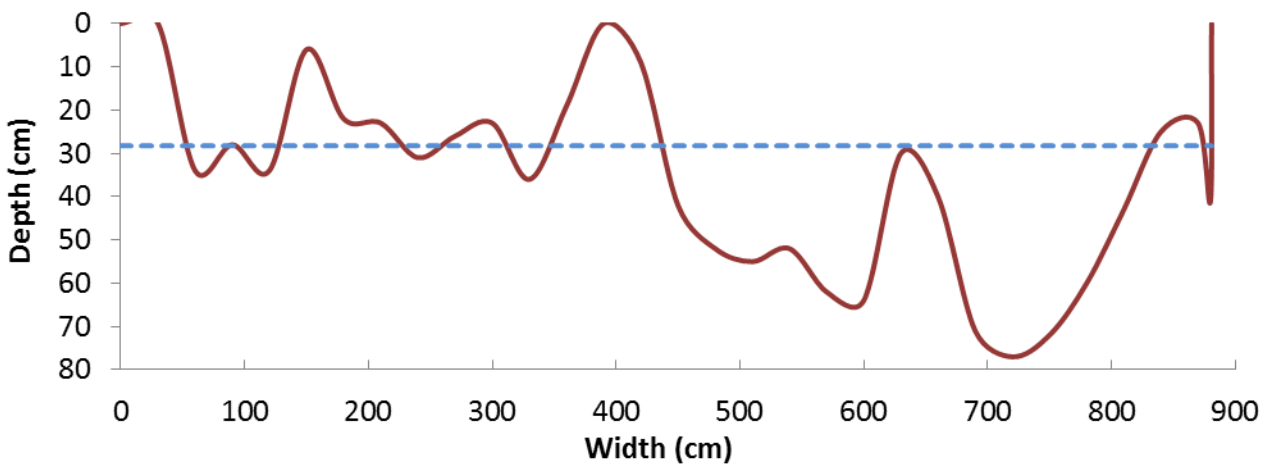
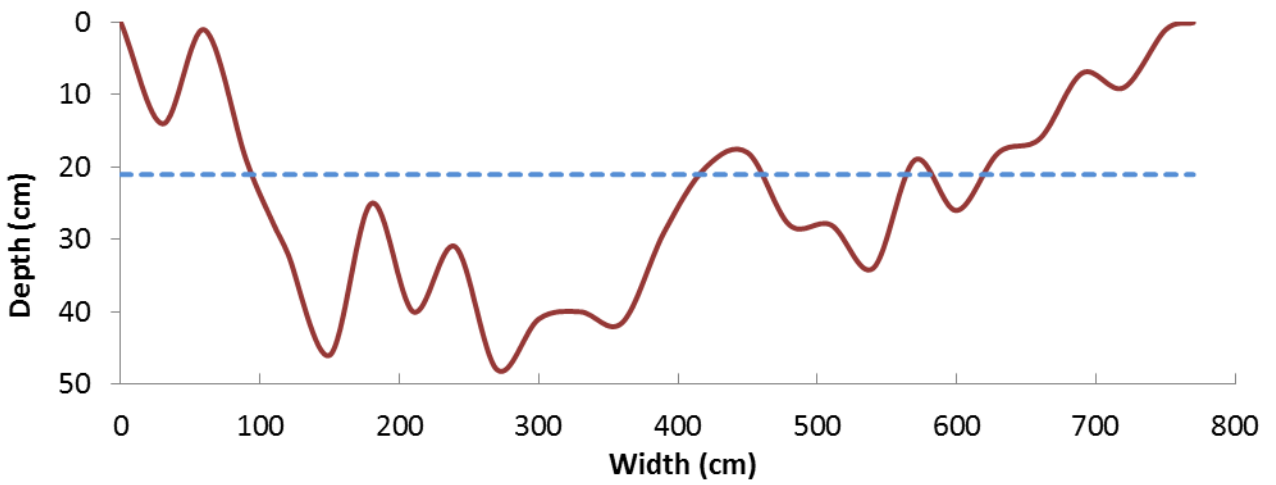
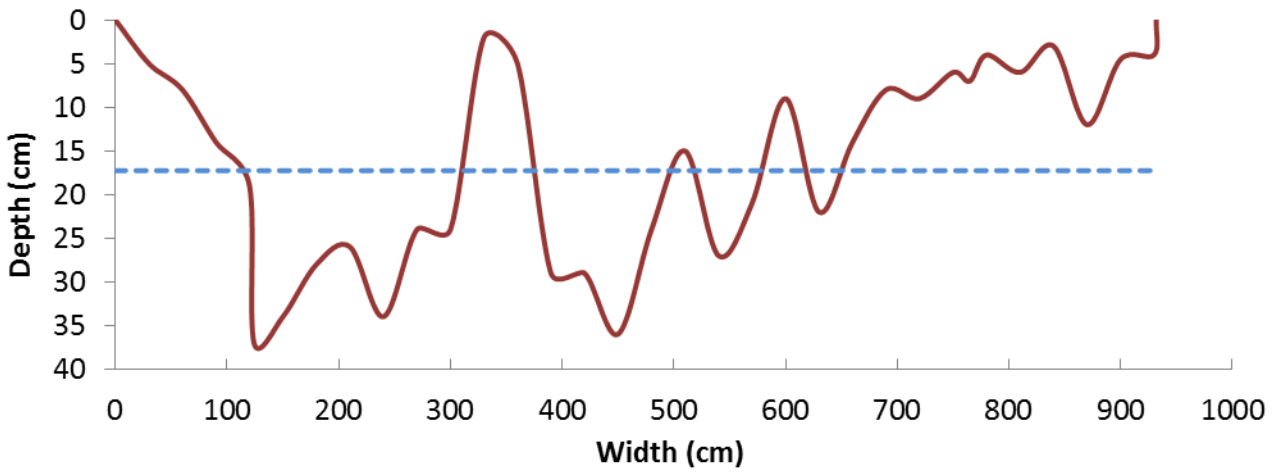




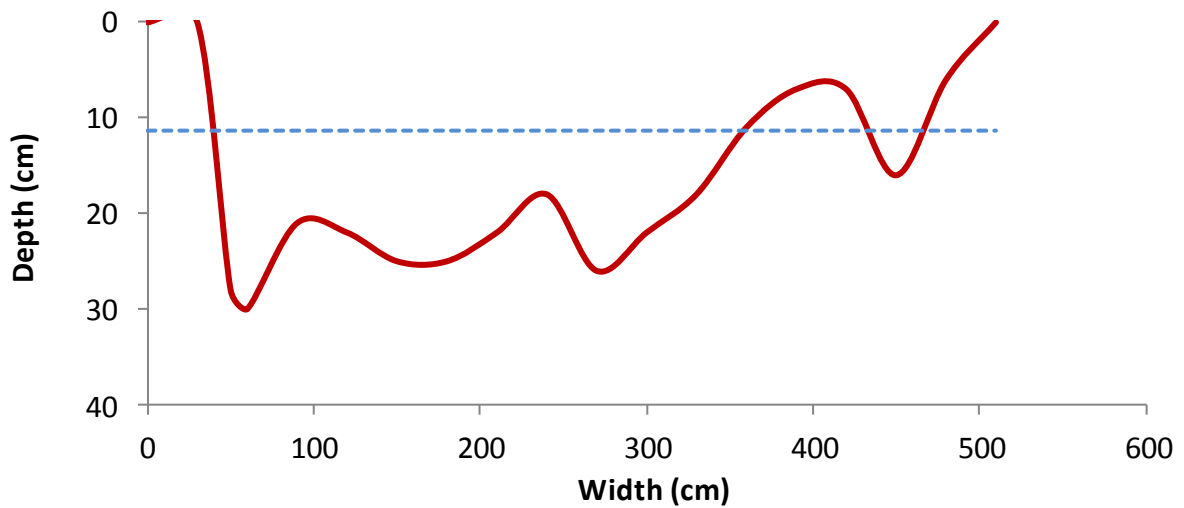
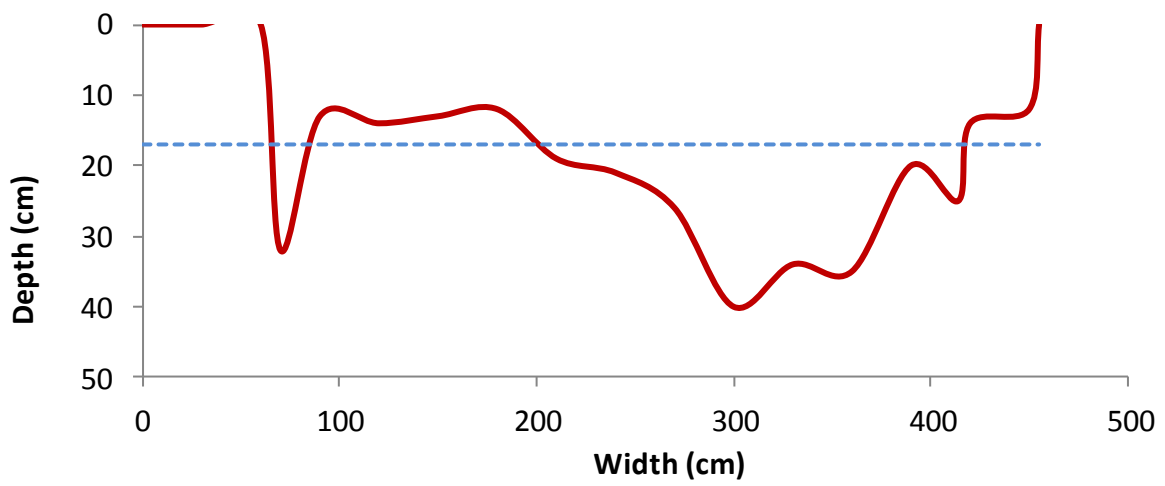
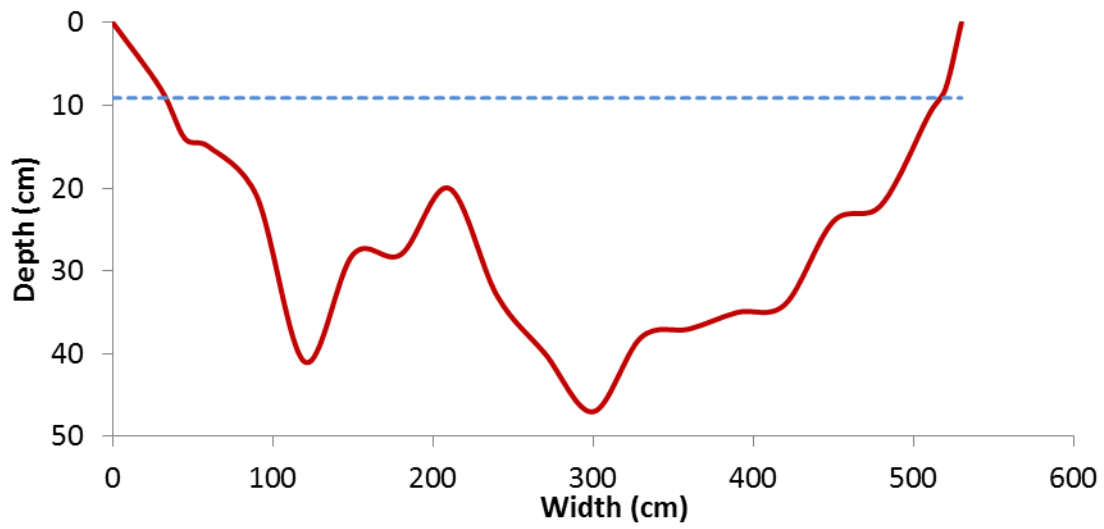
Grigno Creek – G7

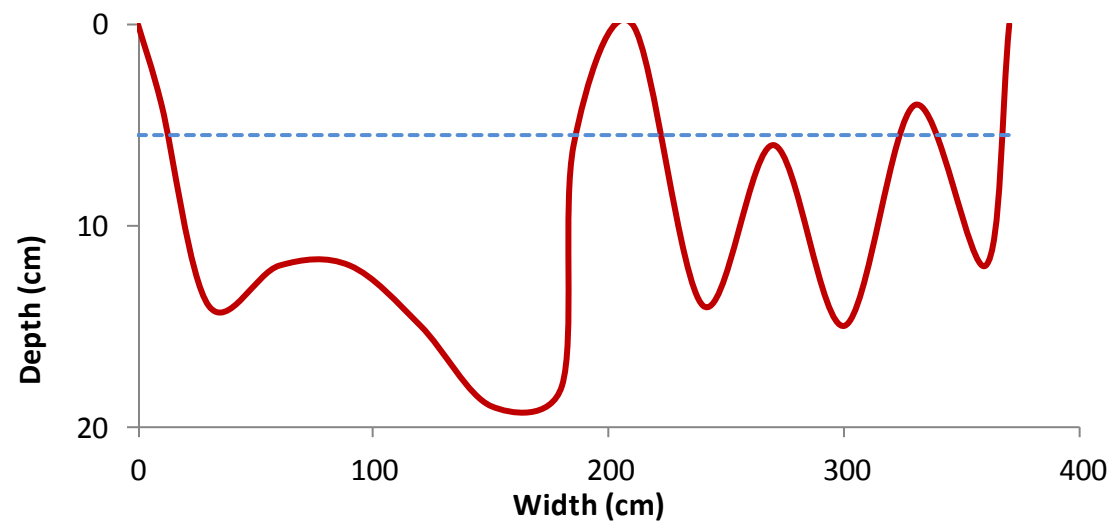
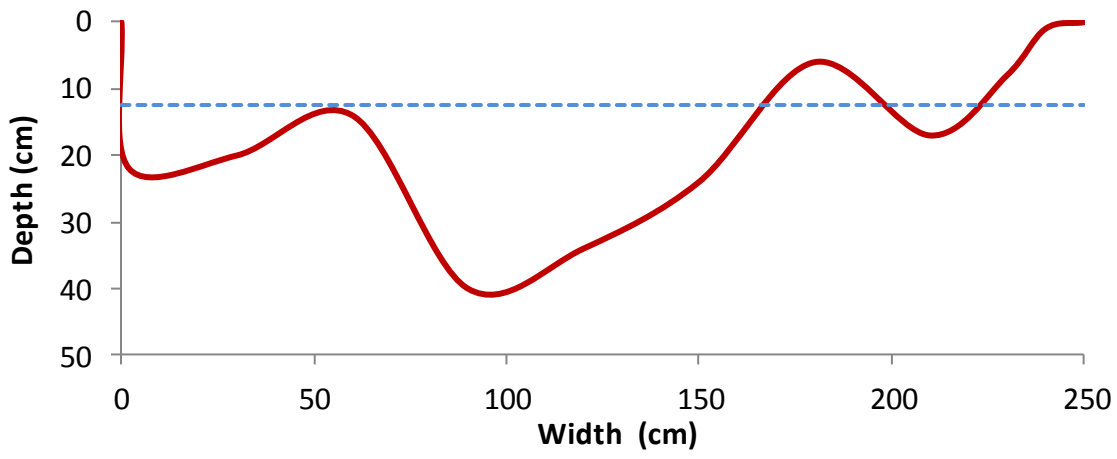
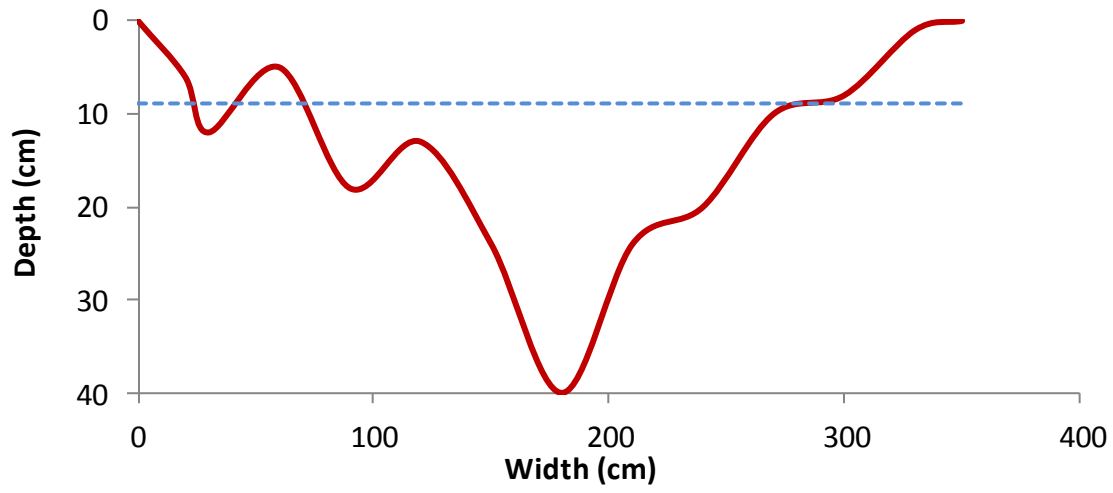




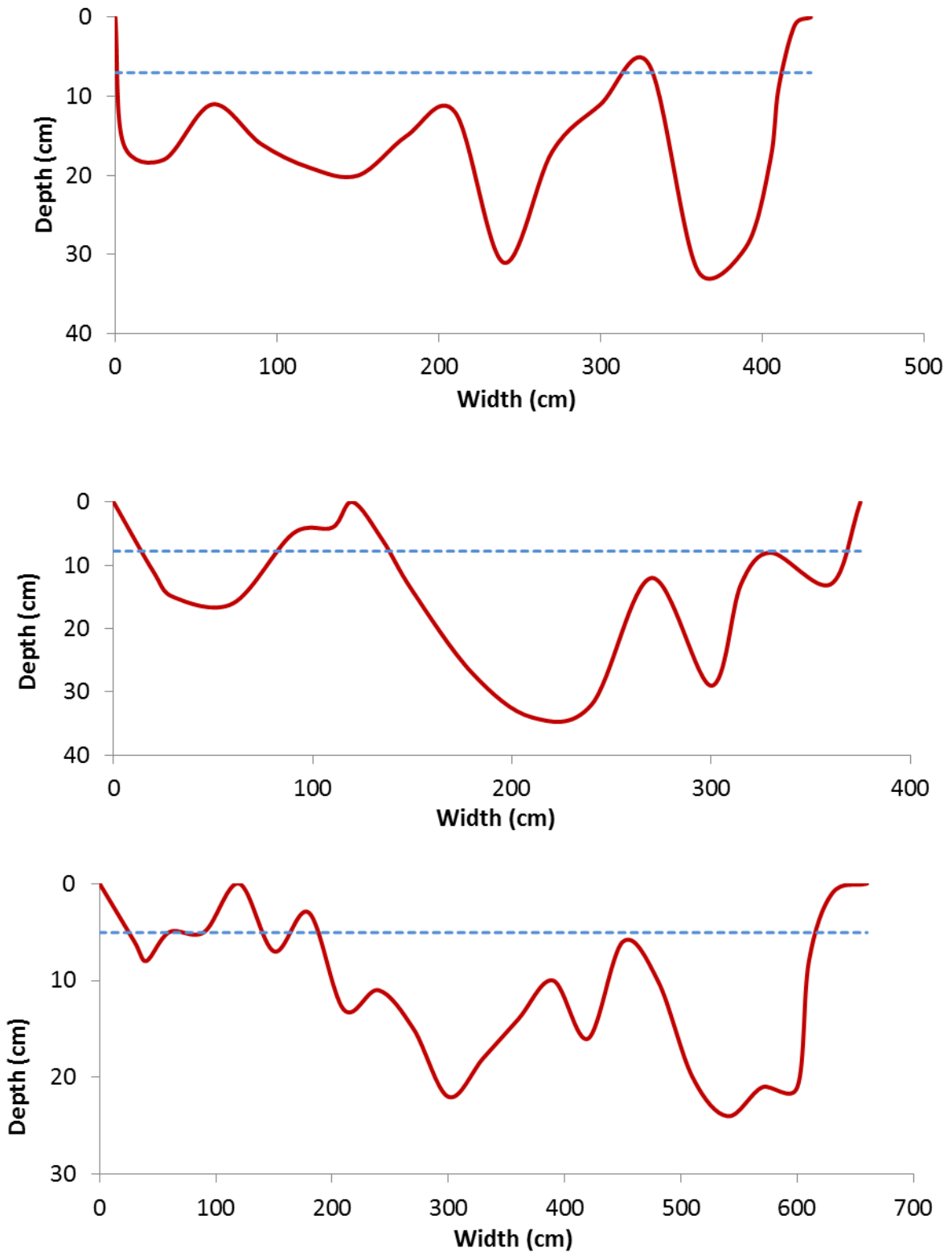


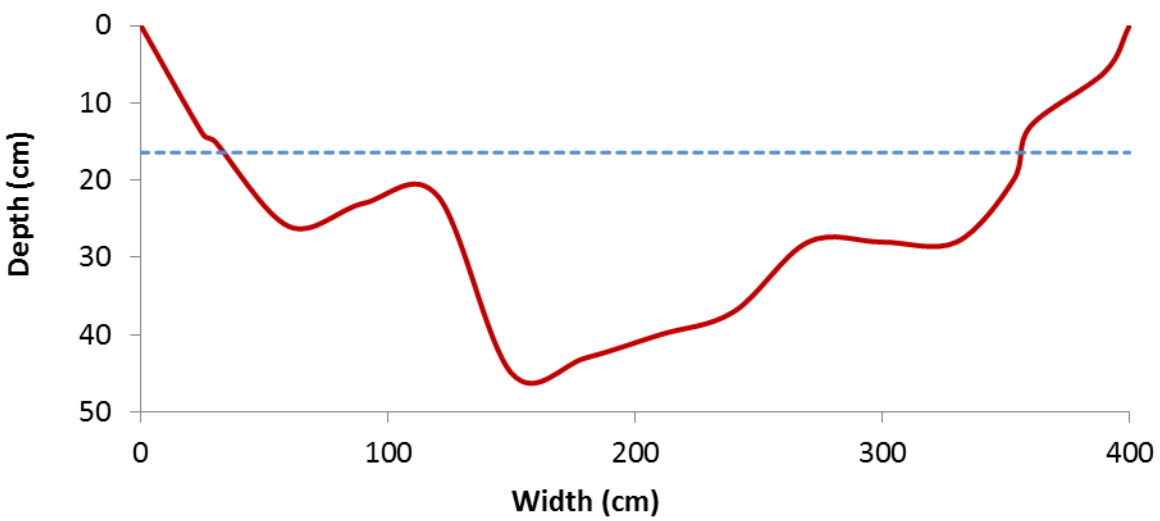
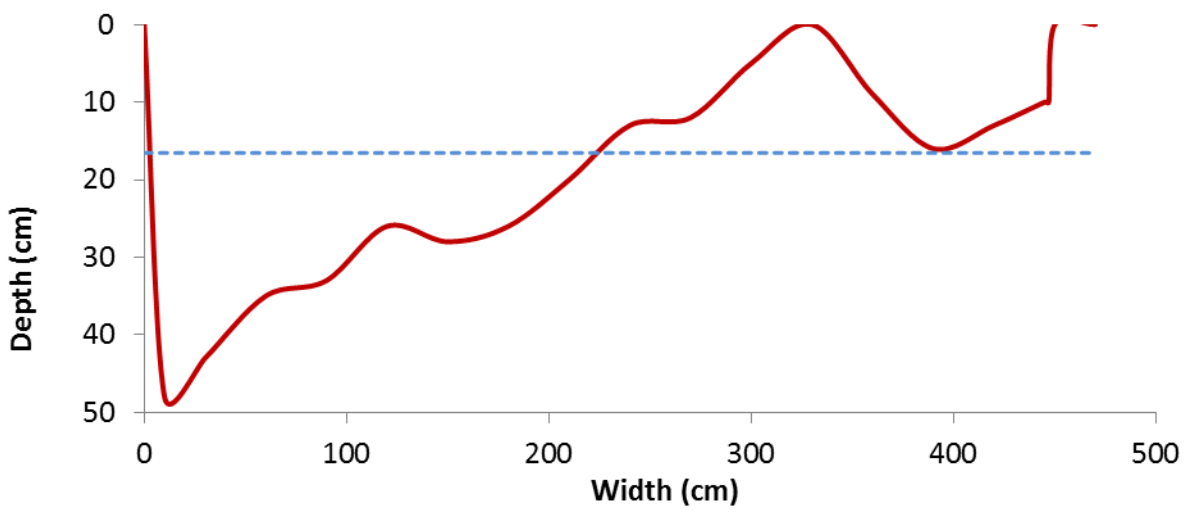
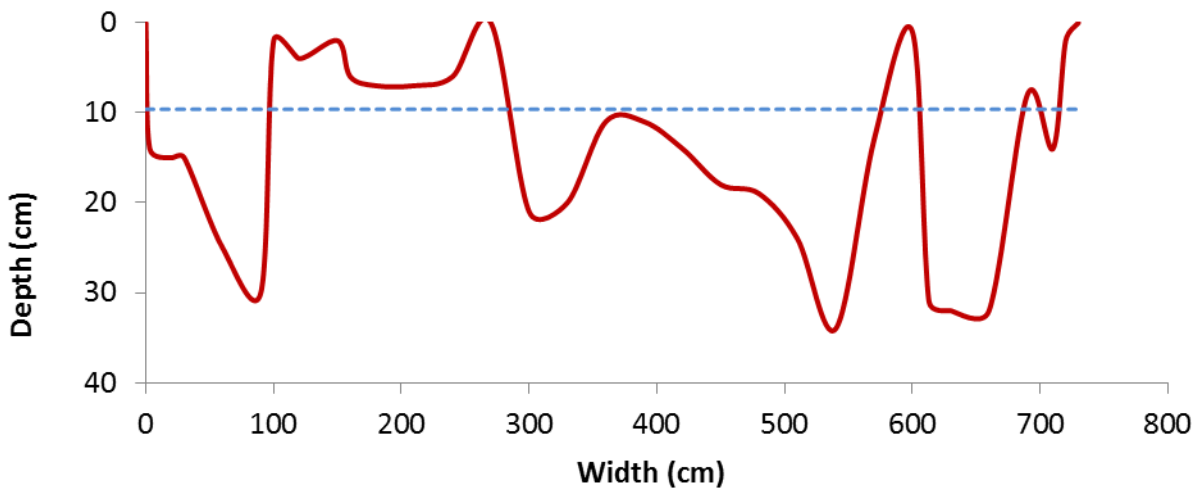
Tolvà Creek – T1

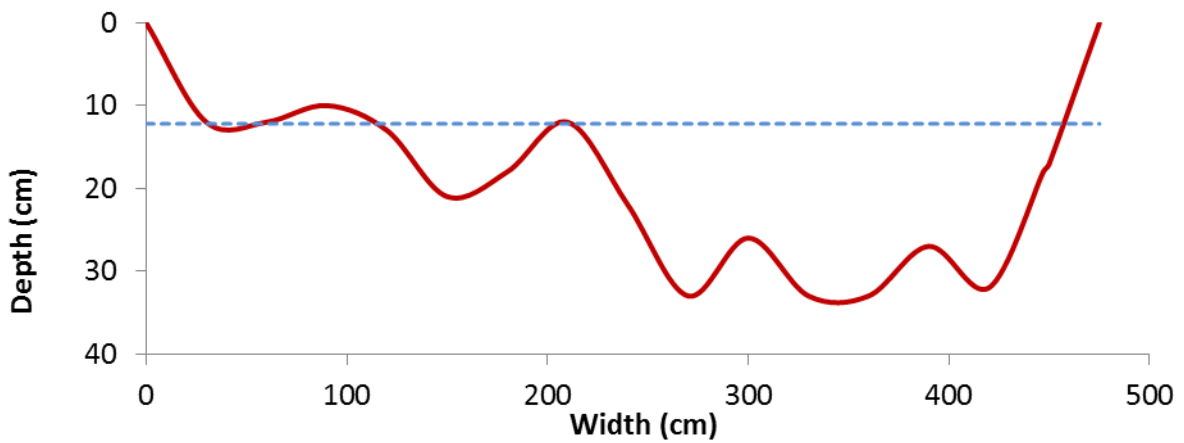
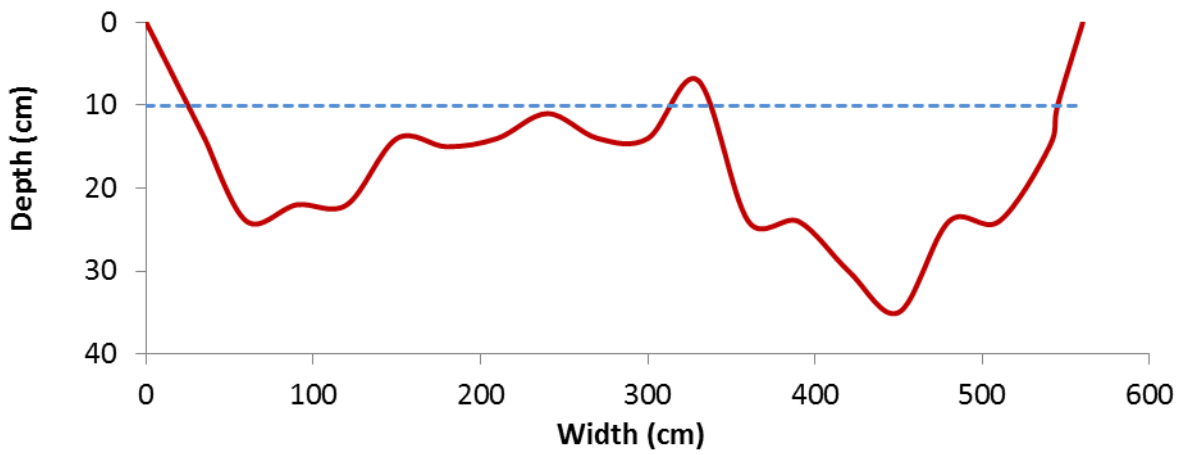
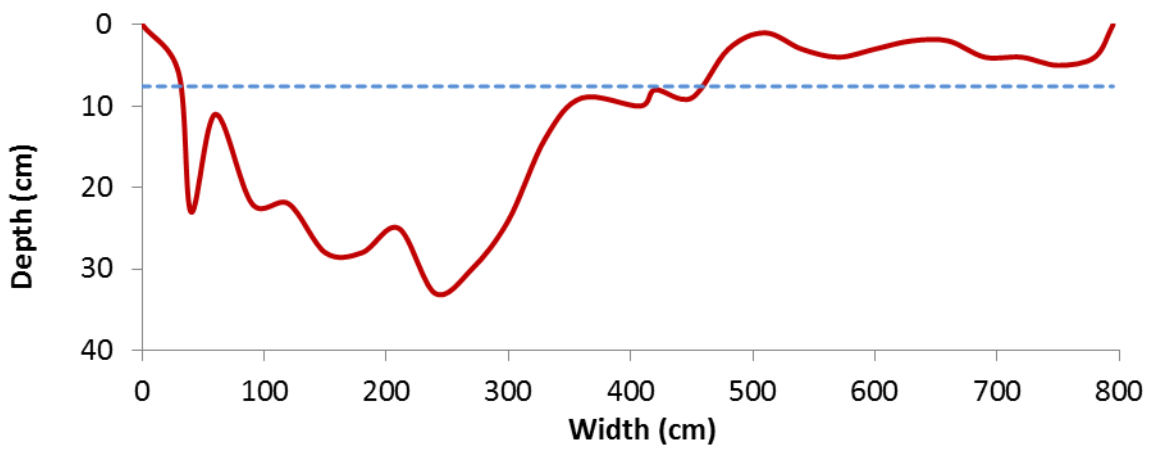
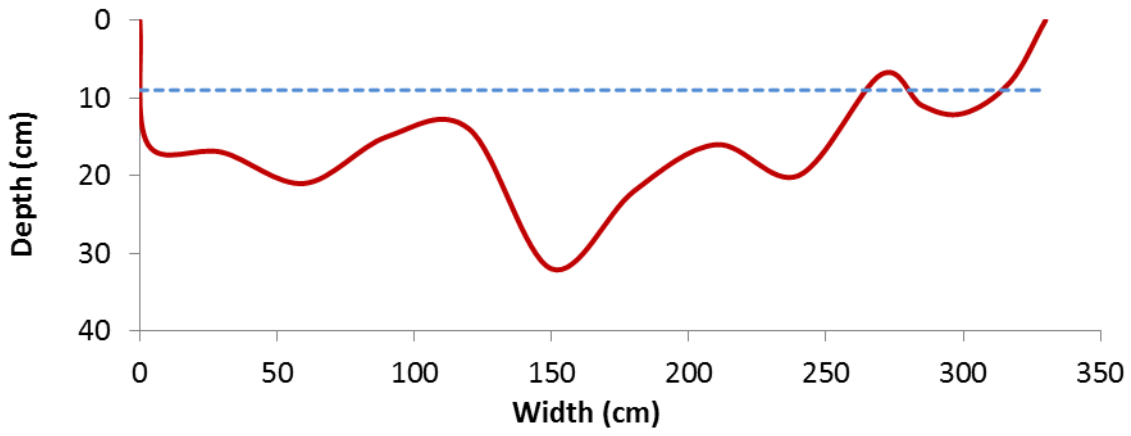




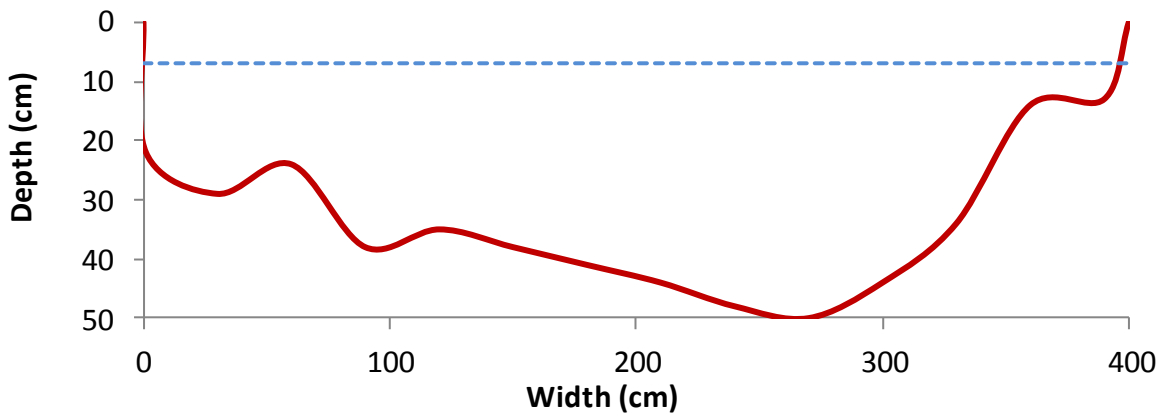
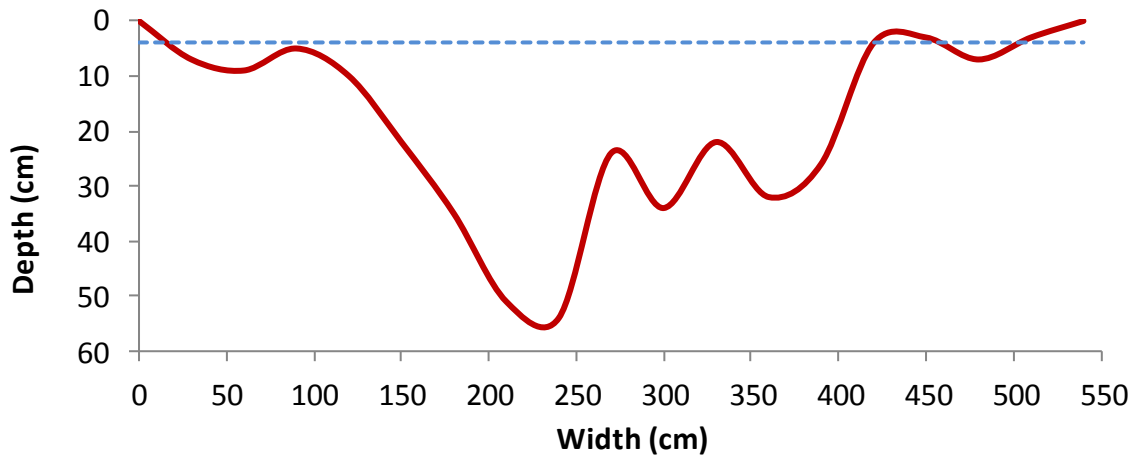
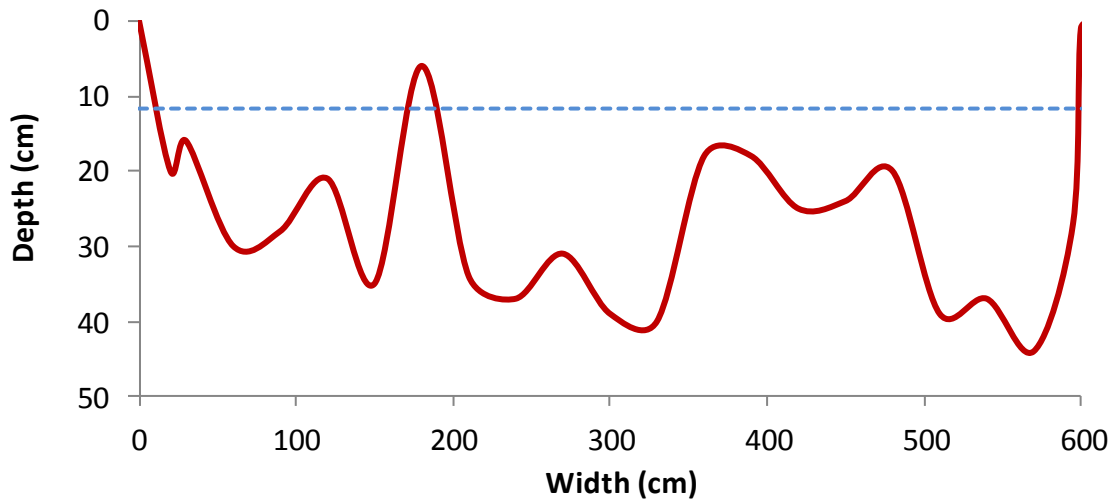
Tolvà Creek – T2

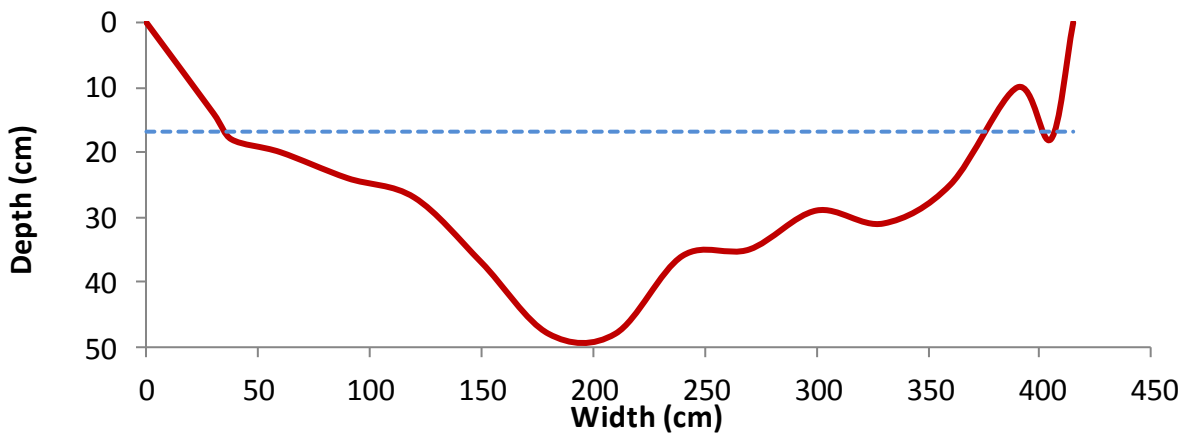
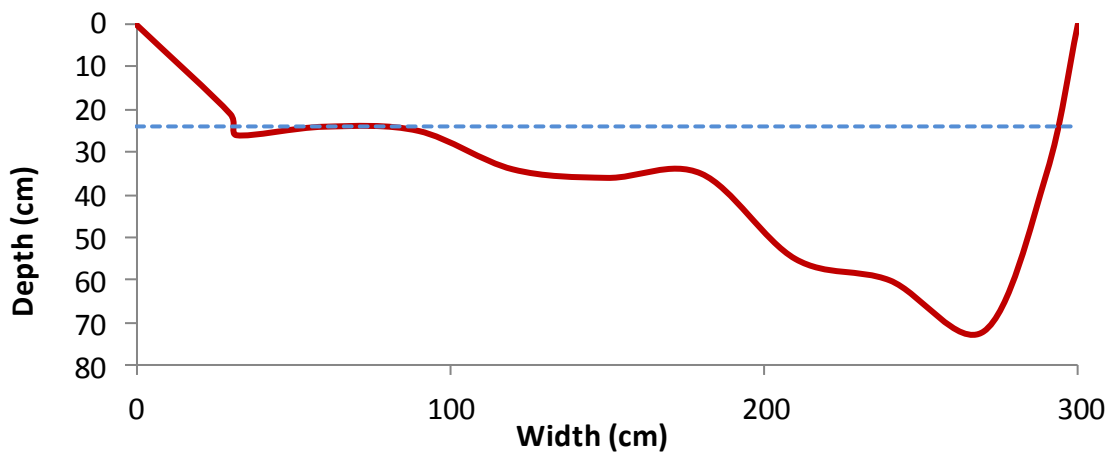
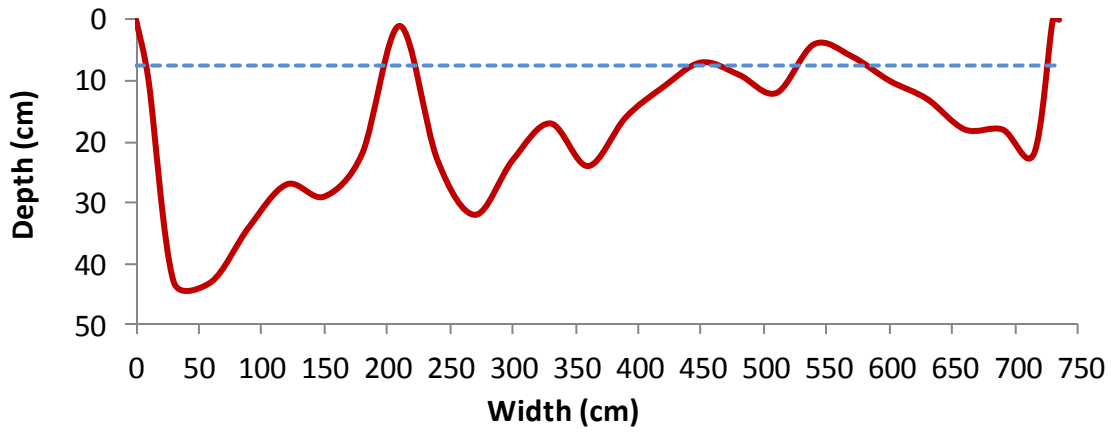


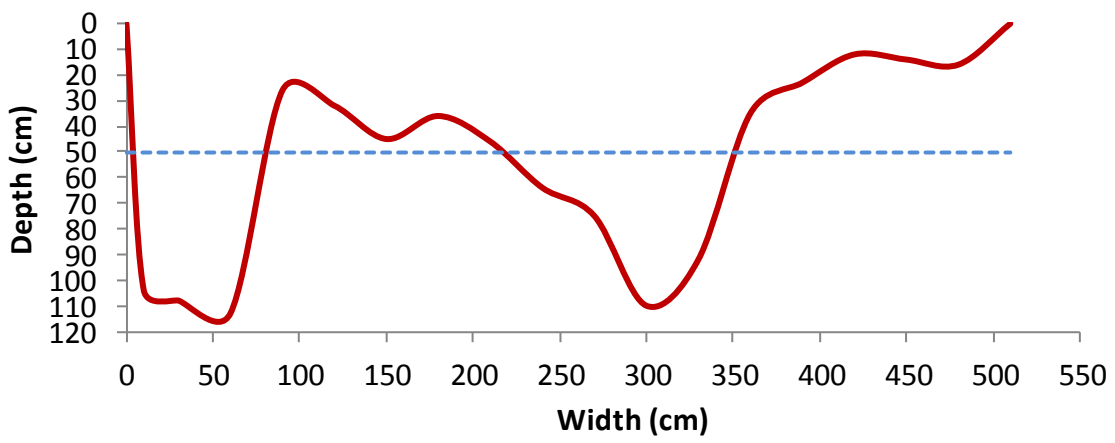
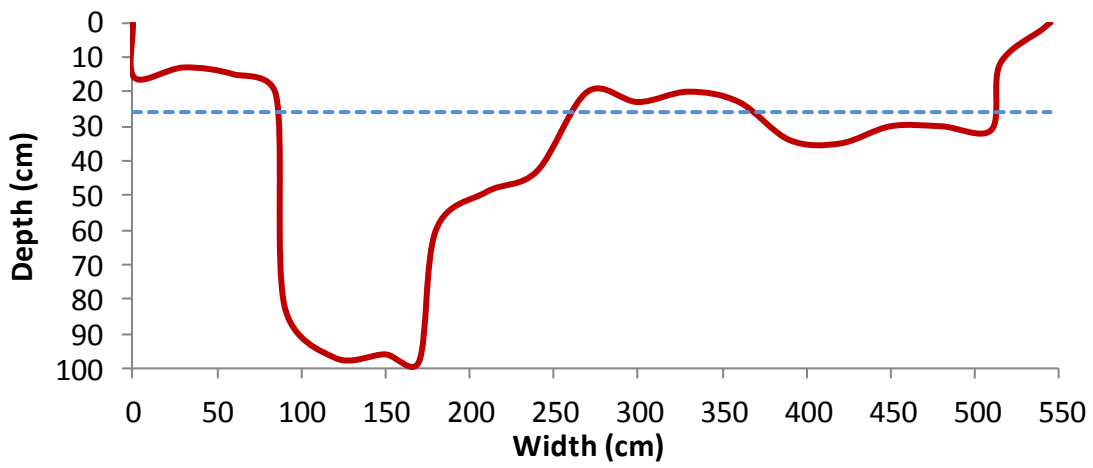
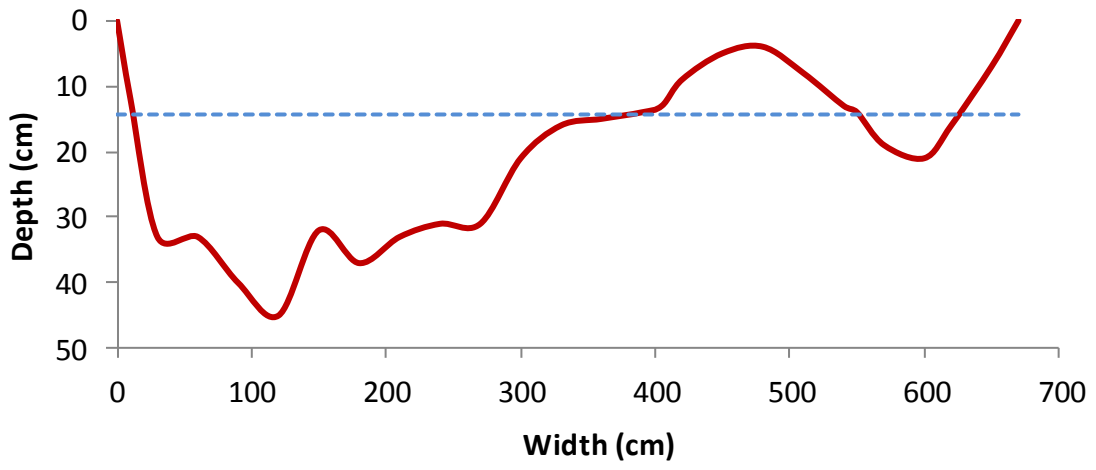


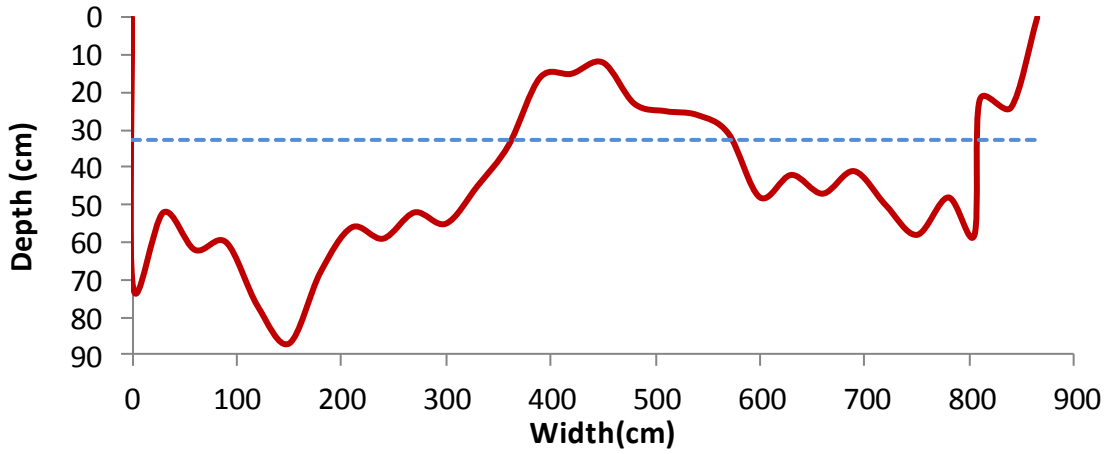


Tolvà Creek – T3

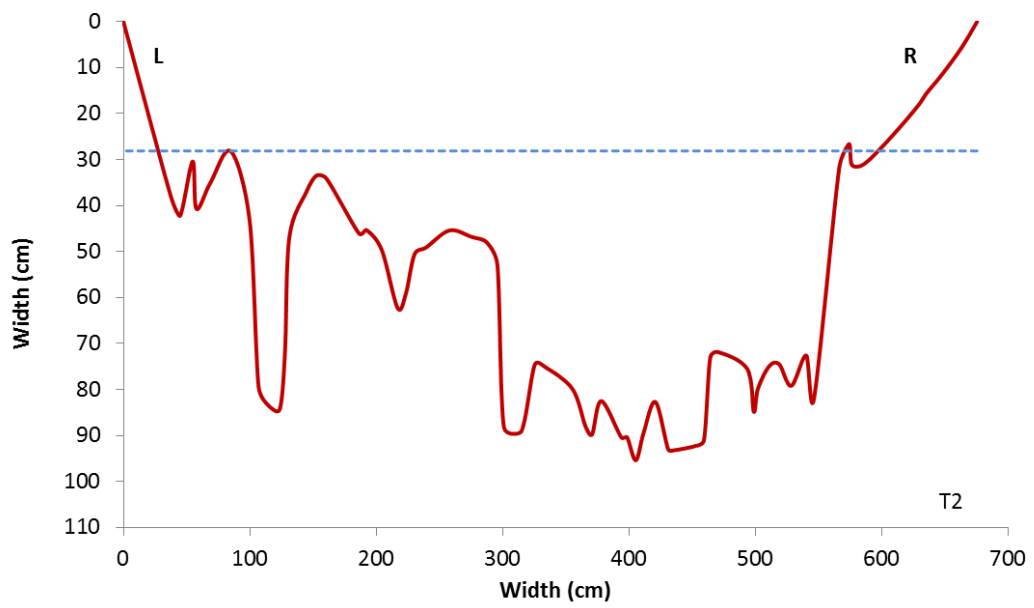
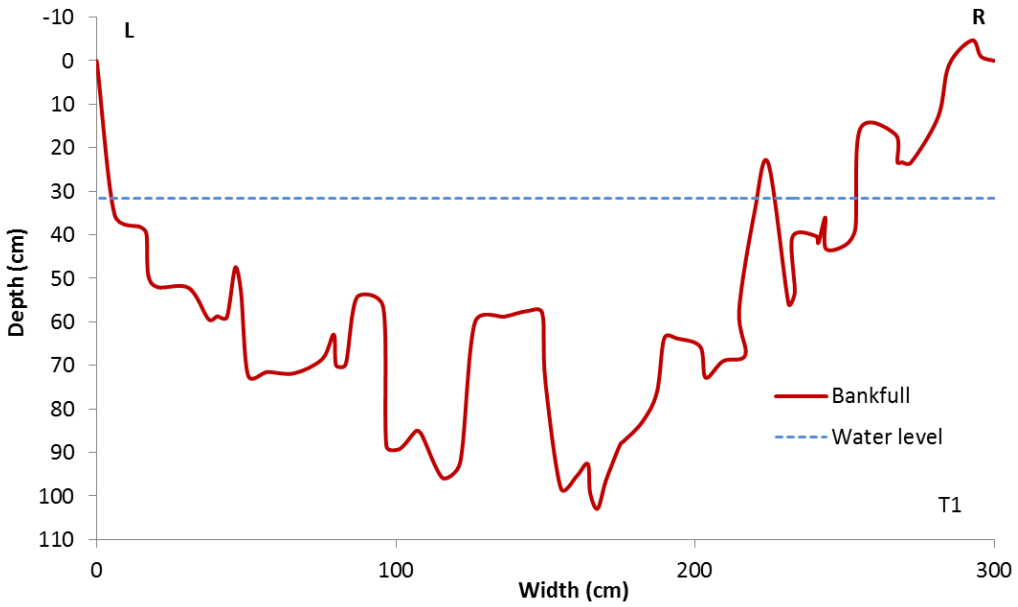


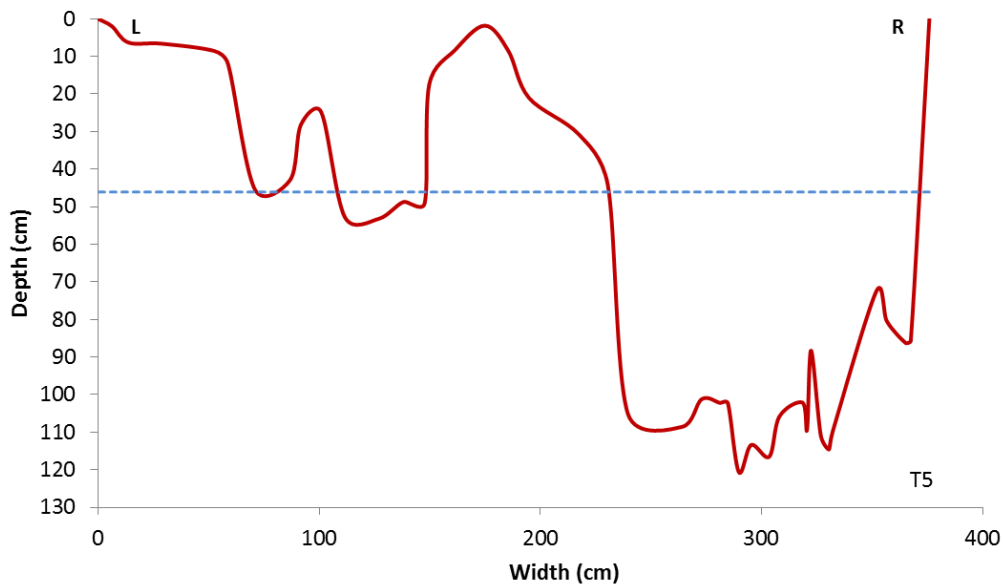
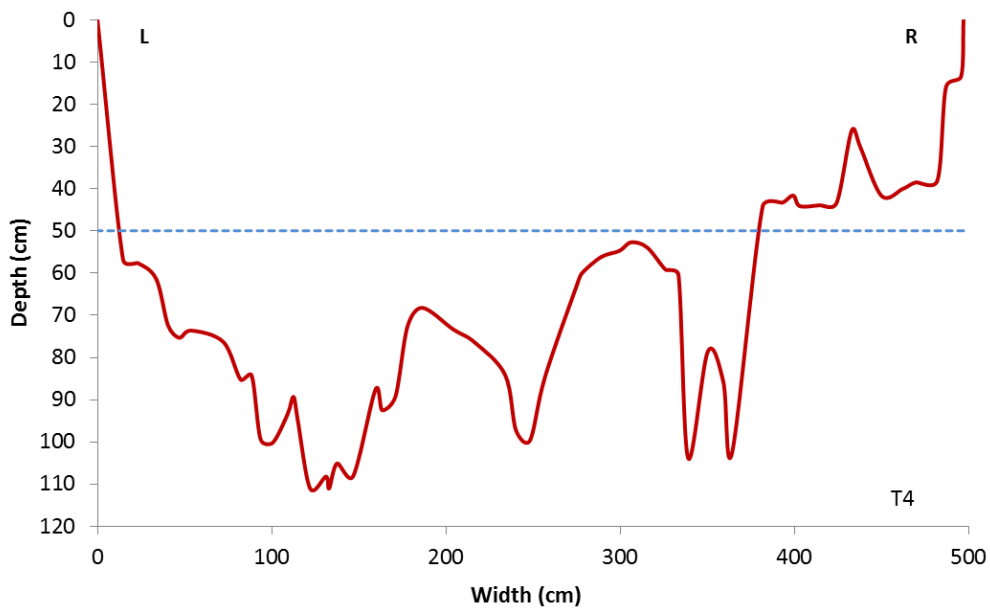
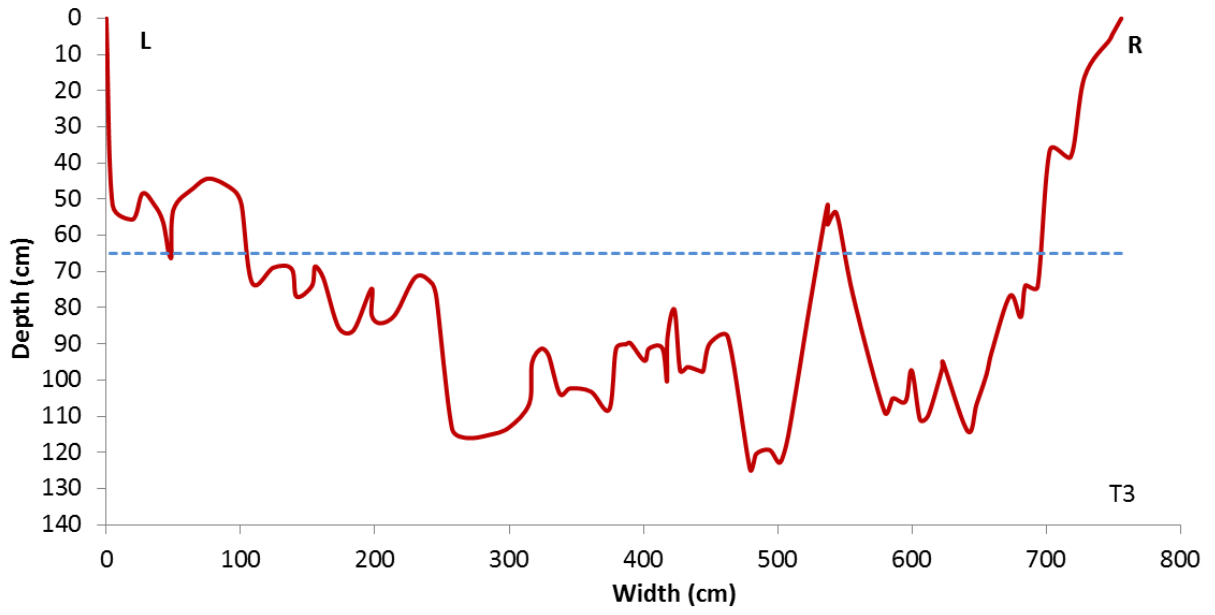


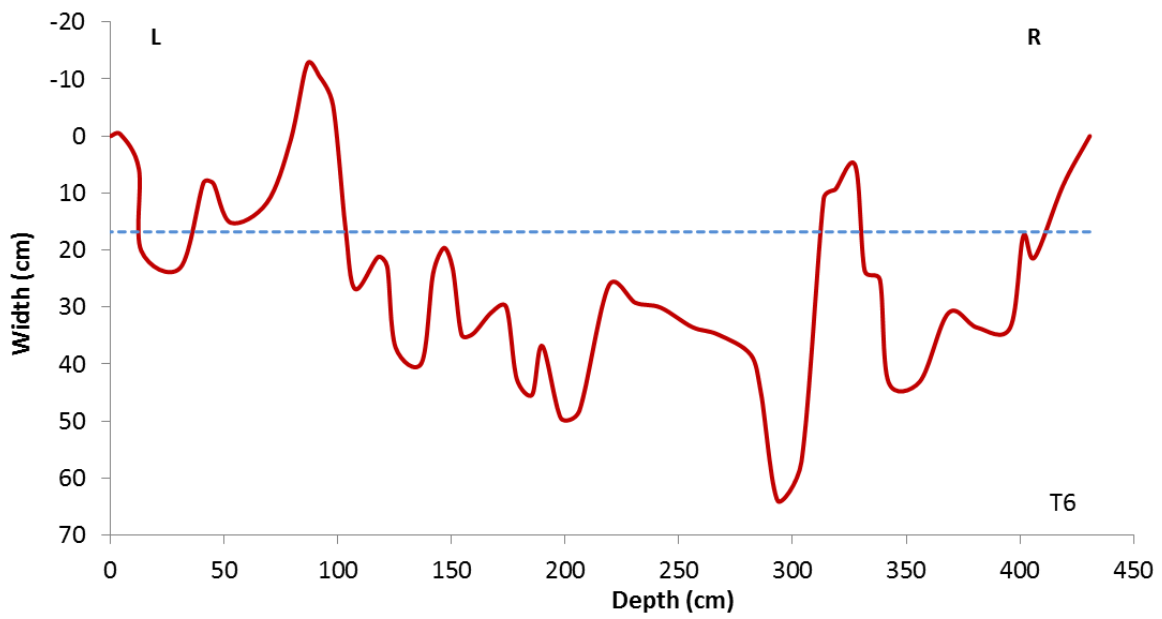




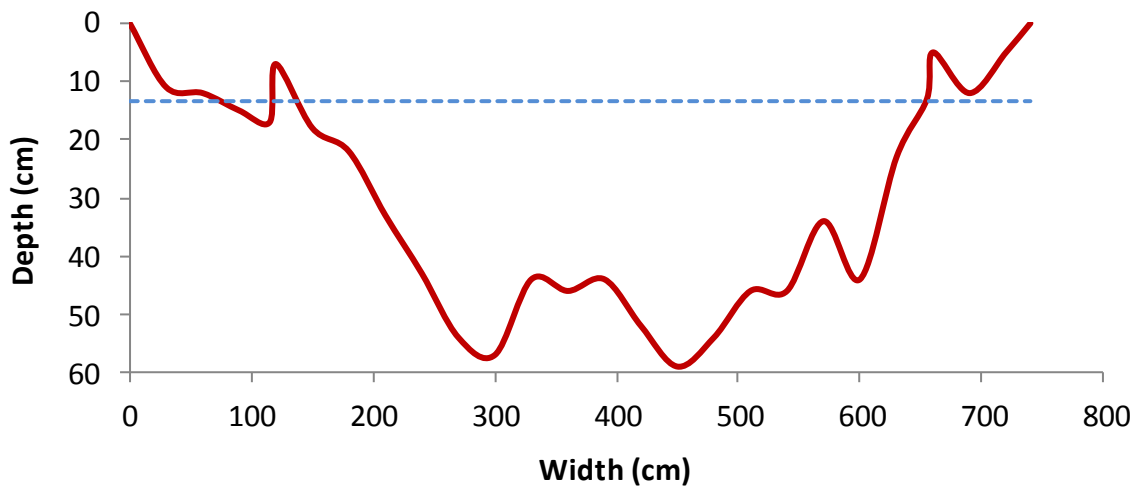
Tolvà Creek – T4



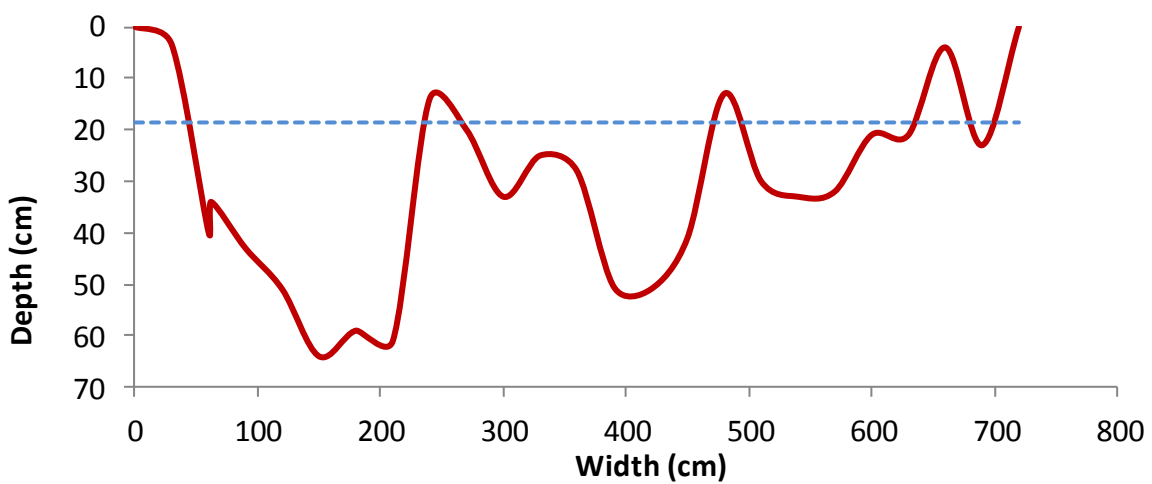




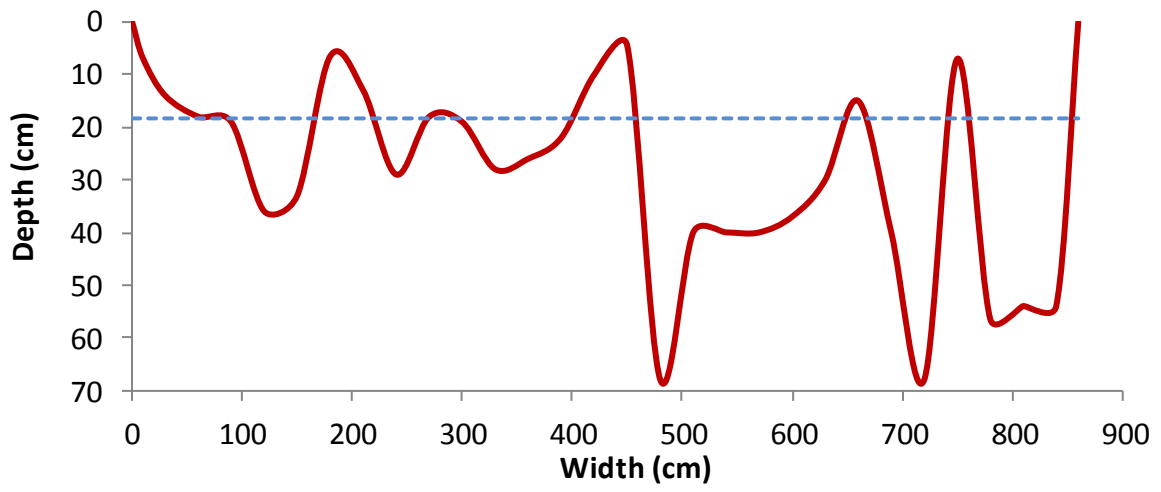
Tolva Creek – T5



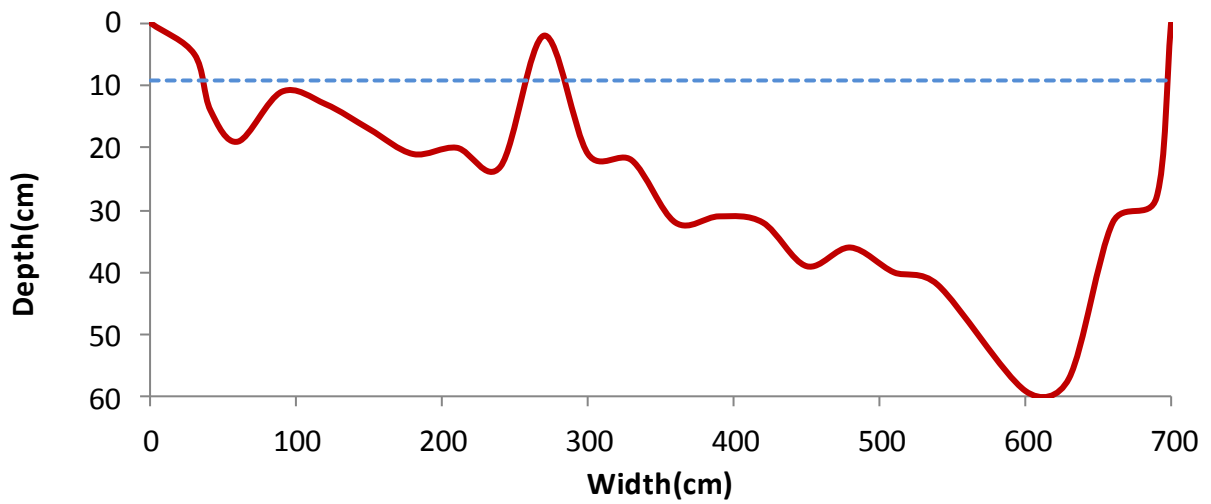
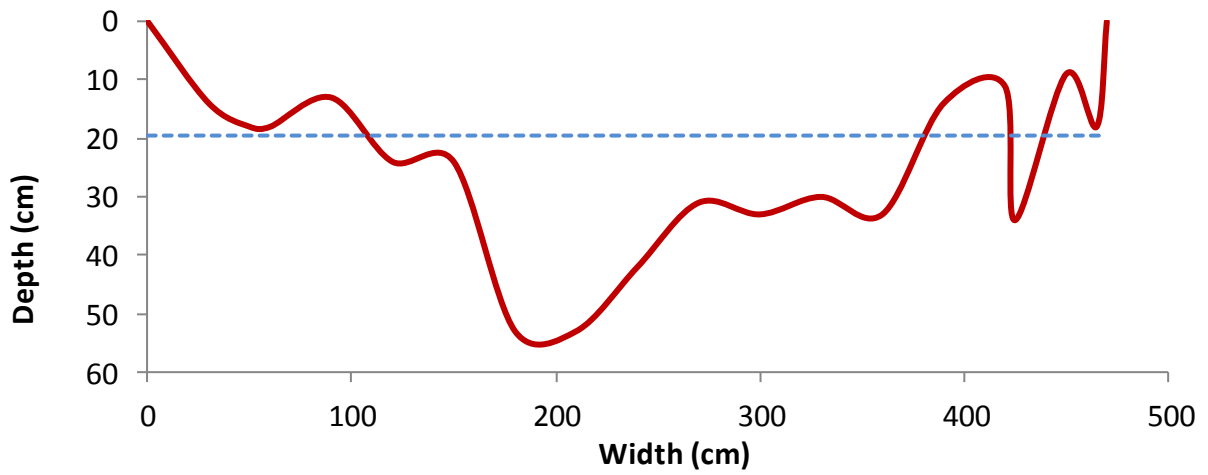
Tolva Creek – T6

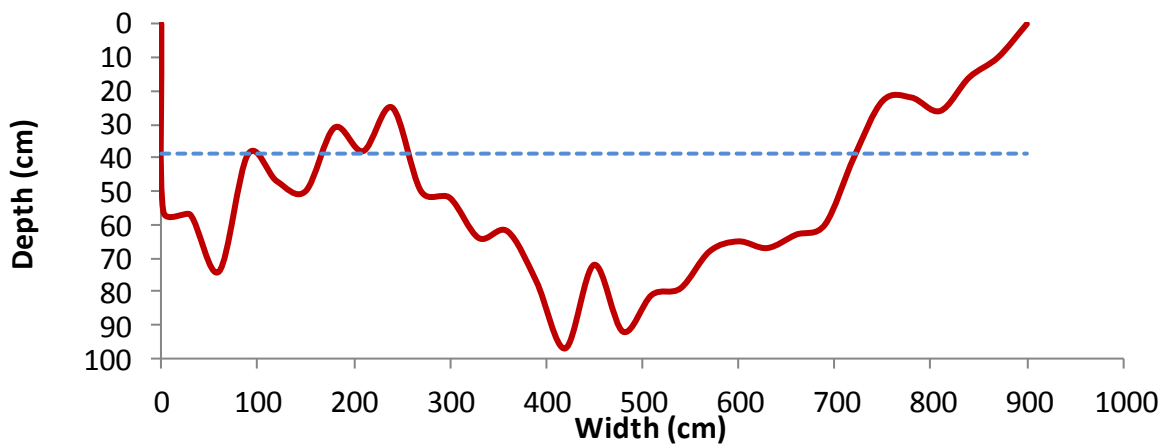
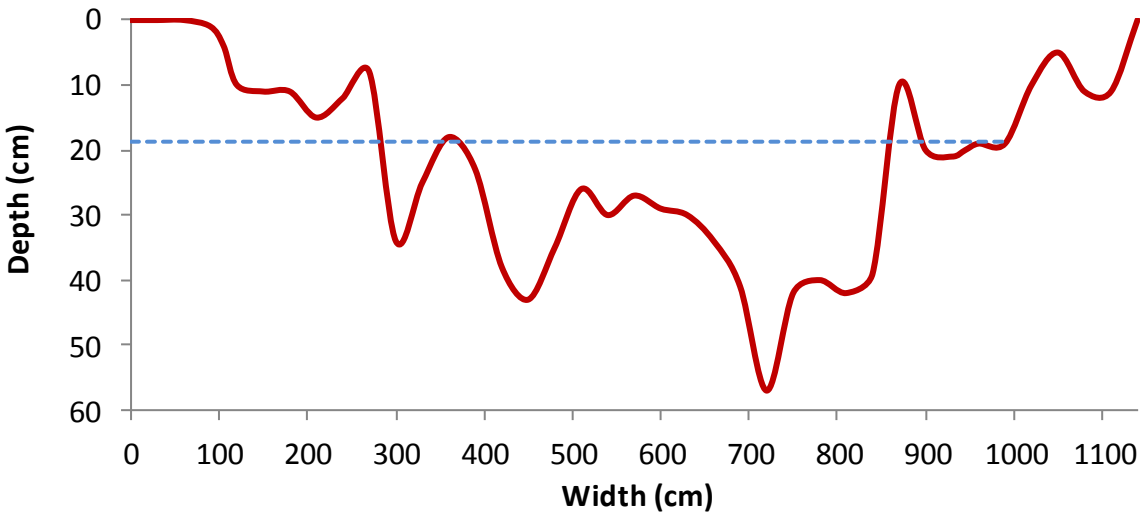
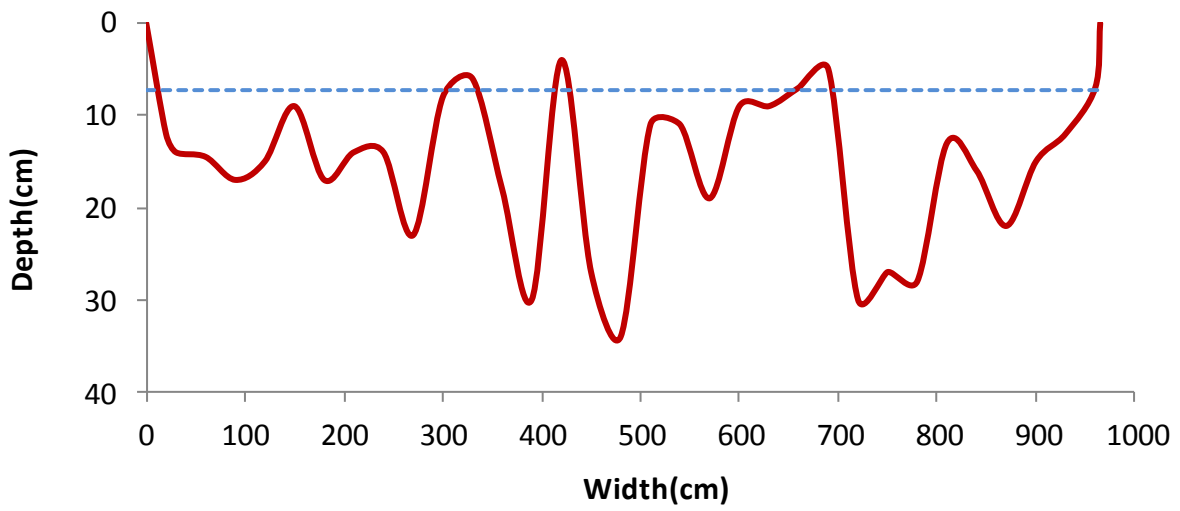


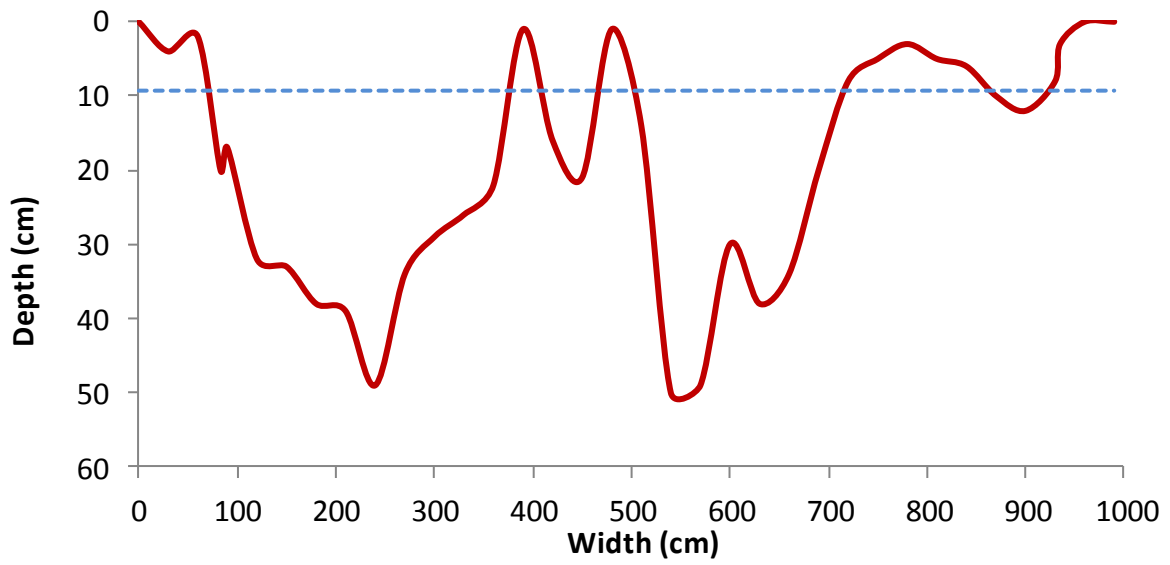
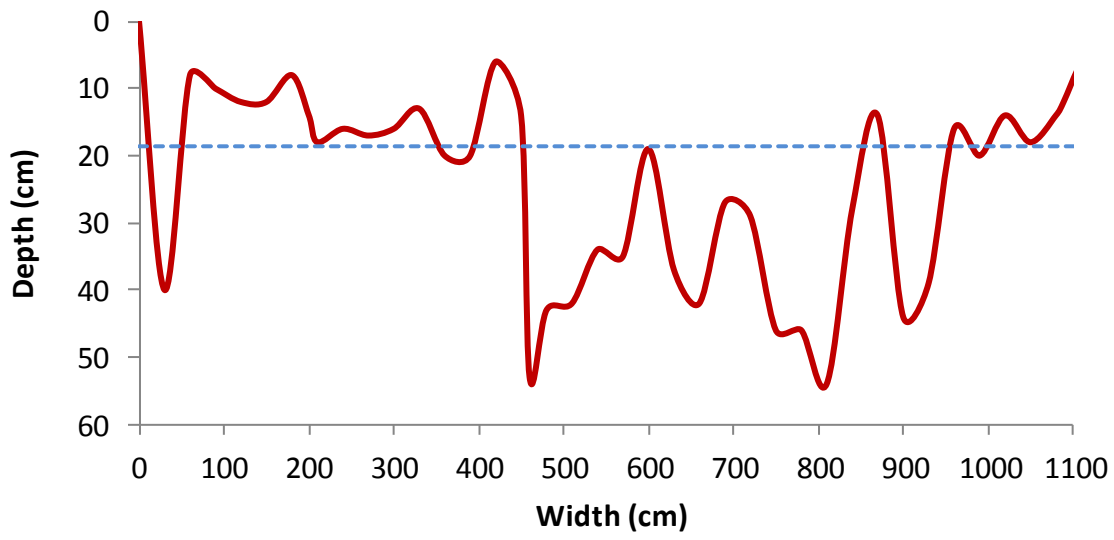
Tolvà Creek – T7



Tolvà Creek – T8







Appendix A4.2 - Characteristics of hydro-meteorological forcing events

Table A4.2.1. Characteristics of hydro-meteorological forcing events recorded at the Grigno Creek monitoring site and Malga Sorgazza weather station in 2014.

<i>Date</i>	<i>Duration</i> [h]	<i>Max</i> <i>intensity</i> [mm/h]	<i>Mean</i> <i>intensity</i> [mm/h]	<i>Median</i> <i>intensity</i> [mm/h]	<i>Total</i> <i>rainfall</i> [mm]	<i>Forcing</i> <i>type</i>	<i>Q_p</i> [l/s]	<i>Δt</i> [h]
08.04.14	6	3.8	1.60	1.20	9.8	Snowmelt	2772	4
30.04.14	15	4.8	2.54	2.30	35.6	Snowmelt	1593	12.5
11.05.14	6	7.6	2.60	1.00	13	Snowmelt	2499	4
24.06.14	19	14.6	3.68	1.80	62.6	Mixed	8414	3
7-9.07.14	34	9.8	2.10	1.50	63.2	Rainfall	3889	27.5
21- 22.07.14	19	17.4	5.40	3.80	91.8	Rainfall	9691	-
13- 14.08.14	4	17.8	8.40	7.60	33.6	Rainfall	10731	1.5
13- 14.10.14	10	9.4	4.08	4.40	40.8	Rainfall	3065	3
4-8.11.14	66	16.4	5.01	4.60	325.4	Rainfall	19172	4.5

Q_p is the peak discharge related to meteorological event; Δt represents the time lag between the peak intensity of rainfall and the peak discharge.

Table A4.2.2. Characteristics of hydro-meteorological forcing events recorded at the Grigno Creek monitoring site and Malga Sorgazza weather station in 2015.

<i>Date</i>	<i>Duration</i> [h]	<i>Max</i> <i>intensity</i> [mm/h]	<i>Mean</i> <i>intensity</i> [mm/h]	<i>Median</i> <i>intensity</i> [mm/h]	<i>Total</i> <i>rainfall</i> [mm]	<i>Forcing</i> <i>Type</i>	<i>Q_p</i> [l/s]	<i>Δt</i> [h]
14.04.15	0	0	0	0	0	Snowmelt	501	na
08.05.15	8	6.6	2.43	2.10	19.4	Mixed	1899	6.5
20.05.15	9	12.4	3.88	2.90	31	Mixed	3379	1.5
23.06.15	2	10.8	9.10	9.10	18.2	Rainfall	4071	3

24.07.15	4	20.2	9.7	7.5	38.8	Rainfall	419	9
15.08.20 15	2	11.4	9.6	9.6	19.2	Rainfall	421	2.5
14.09.15	8	11	6.25	8.25	49.4	Rainfall	11847	2.5
13- 16.10.15	88	6.4	1.36	1.10	120	Rainfall	389	5.5

Q_p is the peak discharge related to meteorological event; Δt represents the time lag between the peak intensity of rainfall and the peak discharge.

Table A4.2.3. Characteristics of hydro-meteorological forcing events recorded at the Tolvà Creek monitoring site and Passo Brocon weather station in 2014.

<i>Date</i>	<i>Duration [h]</i>	<i>Max intensity [mm/h]</i>	<i>Mean intensity [mm/h]</i>	<i>Median intensity [mm/h]</i>	<i>Total rainfall [mm]</i>	<i>Forcing Type</i>	<i>Q_p [l/s]</i>	<i>Δt [h]</i>
26.07.14	5	13.6	8.08	7.60	40.4	Rainfall	1330	2
03.08.14	4	37	11.9	4.2	47.6	Rainfall	995	3
09.08.14	3	2	1	0.8	3	Rainfall	727	2.5
13.08.14	3	26.6	13.30	11.00	39.8	Rainfall	8106	3
10.09.14	2	18.2	10.2	10.2	20.4	Rainfall	341	8.5
13.10.14	11	13.4	3.92	3.40	43.2	Rainfall	917	4.5
4- 8.11.14	60	17.8	6.31	5.40	378.4	Rainfall	28510	9
15.11.14	13	18.8	6.6	4.6	85.8	Rainfall	6023	4

Q_p is the peak discharge related to meteorological event; Δt represents the time lag between the peak intensity of rainfall and the peak discharge.

Table A4.2.4. Characteristics of hydro-meteorological forcing events recorded at the Tolva Creek monitoring site and Passo Brocon weather station in 2015.

<i>Date</i>	<i>Duration</i> [h]	<i>Max</i> <i>intensity</i> [mm/h]	<i>Mean</i> <i>intensity</i> [mm/h]	<i>Median</i> <i>intensity</i> [mm/h]	<i>Total</i> <i>rainfall</i> [mm]	<i>Forcing</i> <i>Type</i>	<i>Q_p</i> [l/s]	<i>Δt</i> [h]
15.04.15	0	0	0	0	0	Snowmelt	380	-
24.04.15	24	3	1.17	0.8	25.8	Mixed	464	9
8- 9.05.15	9	8.2	3.38	2.80	30.4	Mixed	995	3.5
15.05.15	18	8.4	1.7	0.8	30.6	Mixed	1070	7.5
20.05.15	9	7.2	3.48	2.50	27.8	Mixed	1070	3.5
23.06.15	3	10	4.87	3.80	14.6	Rainfall	854	1.5
24.07.15	4	20.2	9.7	7.5	38.8	Rainfall	419	9
15.08.20 15	2	11.4	9.6	9.6	19.2	Rainfall	421	2.5
14.09.15	8	11	6.25	8.25	49.4	Rainfall	4322	2.5
13- 16.10.15	88	6.4	1.36	1.10	120	Rainfall	1921	3

Table A4.2.5. Characteristics of hydro-meteorological forcing events recorded at the Ussaia Creek monitoring site and Mezzana weather station in 2013.

<i>Date</i>	<i>Duration</i> [h]	<i>Max</i> <i>intensity</i> [mm/h]	<i>Mean</i> <i>intensity</i> [mm/h]	<i>Median</i> <i>intensity</i> [mm/h]	<i>Total</i> <i>rainfall</i> [mm]	<i>Forcing</i> <i>Type</i>	<i>Q_p</i> [l/s]	<i>Δt</i> [h]
02.04.13	30	10.6	2.85	2.10	85.4	Rain on snow	3097	2
25.04.13	49	8.8	1.99	1.2	95.4	Rain on snow	8218	7
12.06.13	36	6.4	2.23	1.8	71.4	Rainfall	1877	3
23.07.13	4	6.8	3.25	3.00	13	Rainfall	3210	11
22.08.13	6	5.8	3.90	4.10	23.4	Rainfall	245	3

07.09.13	4	6.4	3.25	2.5	13	Rainfall	1003	0
15.10.13	22	9.0	2.48	1.4	52	Rainfall	1104	0
26.10.13	24	7.8	2.89	2	66.4	Rainfall	8683	9
16.11.13	33	5.2	1.58	1	50.4	Rainfall	1727	3

Q_p is the peak discharge related to meteorological event; Δt represents the time lag between the peak intensity of rainfall and the peak discharge.

Table A4.2.6. Characteristics of hydro-meteorological forcing events recorded at the Ussaia Creek monitoring site and Mezzana weather station in 2014.

<i>Date</i>	<i>Duration [h]</i>	<i>Max intensity [mm/h]</i>	<i>Mean intensity [mm/h]</i>	<i>Median intensity [mm/h]</i>	<i>Total rainfall [mm]</i>	<i>Forcing Type</i>	<i>Q_p [l/s]</i>	<i>Δt [h]</i>
29.04.14	48	4.80	1.08	0.80	43.20	Snowmelt	714	8.50
06.05.14	17	3.8	1.88	1.90	30	Snowmelt	976	2.5
03.06.14	14	6	1.8	0.6	23.6	Snowmelt	1187	3
30.06.14	21	5	1.6	0.9	29.8	Mixed	507	3.5
11.07.14	26	3.4	1.2	0.8	26.4	Rainfall	167	13.5
27.07.14	9	6.4	3.5	3.8	31.6	Rainfall	347	4
18.08.14	6	8.8	4.0	3.3	24	Rainfall	396	4
20.10.14	21	6.4	2.2	1.8	46.5	Rainfall	-	-
08.11.14	75	7.4	2.1	1.4	158	Rainfall	26405	4.5

Q_p is the peak discharge related to meteorological event; Δt represents the time lag between the peak intensity of rainfall and the peak discharge.

Table A4.2.7. Characteristics of hydro-meteorological forcing events recorded at the Ussaia Creek monitoring site and Mezzana weather station in 2015.

<i>Date</i>	<i>Duration</i> [h]	<i>Max intensity</i> [mm/h]	<i>Mean intensity</i> [mm/h]	<i>Median intensity</i> [mm/h]	<i>Total rainfall</i> [mm]	<i>Forcing Type</i>	<i>Q_P</i> [l/s]	<i>Δt</i> [h]
19.05.15	16	14.8	3.9	2.5	55	Mixed	329	7
20.05.15	20	7	1.7	1.2	34.8	Mixed	367	6
16.06.15	6	9.4	3.7	2.1	22.4	Rainfall	180	3.5
07.08.15	6	12	5.17	3.2	31	Rainfall	96	3
22- 23.08.15	8	4	1.6	1.8	12.2	Rainfall	67	1.5
14.09.15	16	5.4	2.7	1.6	42.6	Rainfall	2107	2
23.09.15	13	9.3	3.3	2.8	42.8	Rainfall	306	4
14- 15.10.15	44	4.2	1.1	0.5	49.2	Rainfall	321	6.5

Appendix A4.3 – Bedload monitoring surveys and tracers’ travel distances

Table A4.3.1. Summary information on PIT surveys.

Site	Survey date	Recovered tracers	Recovery rate	Q _{max}	Rainfall duration	
			(%)	(m ³ s ⁻¹)	(h)	
Grigno Cr.	S1	16 Apr 2014	98	88	2.7	5
	S2	5 May 2014	110	99	1.6	13
	S3	25 May 2014	84	76	2.5	7
	S4	1 Jul 2014	64	58	8.4	17
	S5	18 Jul 2014	108	97	3.9	33
	S6	31 Jul 2014	111	98	9.7	18
	S7	29 Aug 2014	128	98	10.7	4
	S8	18 Oct 2014	128	98	3.1	10

S9	25 Nov 2014	116	81	19.2	65	
S10	14 Apr 2015	148	90	3.71	0	
S11	14 May 2015	147	90	1.9	8	
S12	25 May 2015	147	90	3.38	9	
S13	25 Jun 2015	147	90	4.07	2	
S14	28 Jul 2015	148	90	1.24	4	
S15	19 Sep 2015	153	94	11.85	8	
S16	21 Oct 2015	145	89	3.89	88	
<hr/>						
Tolvà Cr.	S1	28 Jul 2014	94	100	1.3	18
	S2	19 Aug 2014	92	98	8.1	4
	S3	21 Oct 2014	93	99	1.32	11
	S4	27 Nov 2014	75	80	28.5	65
	S5	14 Apr 2015	127	84	0.38	0
	S6	14 May 2015	127	84	0.99	9
	S7	25 May 2015	127	84	1.07	9
	S8	25 Jun 2015	127	84	0.85	3
	S9	28 Jul 2015	127	84	0.34	4
	S10	19 Sep 2015	127	84	4.3	8
	S11	21 Oct 2015	126	83	1.9	93
<hr/>						
Ussaia Cr.	S1	29 Apr 2014	108	100	0.7	49
	S2	6 May 2014	107	99	0.97	16
	S3	30 May 2014	62	57	1.2	14
	S4	3 Jun 2014	104	96	1.2	14
	S5	30 Jun 2014	103	95	0.5	13
	S6	11 Jul 2014	106	98	0.17	25
	S7	27 Jul 2014	104	96	0.35	8
	S8	18 Aug 2014	104	96	0.4	6

S9	20 Oct 2014	104	96	1.1	18
S10	8 Nov 2014	31	29	26.4	81
S11	19 May 2015	179	60	0.33	19
S12	26 May 2015	179	60	0.37	20
S13	18 Jun 2015	173	58	0.18	6
S14	29 Jul 2015	175	59		
S15	18 Aug 2015	175	59	0.1	6
S16	28 Aug 2015	176	60	0.07	8
S17	15 Sep 2015	176	60	2.1	16
S18	25 Sep 2015	176	60	0.31	13
S19	22 Oct 2015	176	60	0.32	44

Table A4.3.2. Recovery rates per survey at Grigno Creek.

	Survey (GRIGNO CR.)	Q _{max} [m ³ s ⁻¹]	Mobilized clasts [%]	Mobilized classes	Max travel distance [m]	Inter-survey dominant regime	Recovery rate [%]
S1	16 Apr 2014	2.7	4	W1, W3,W6	0.6	Snowmelt	88
S2	5 May 2014	1.6	10	W1 to W4, W6	2.5	Snowmelt	99
S3	25 May 2014	2.5	14	W1 to W3, W6	1.75	Snowmelt	76
S4	1 Jul 2014	8.4	15	W1 to W6	4.5	Mixed	58
S5	18 Jul 2014	3.9	38	W1 to W6	9	Rainfall	97
S6	31 Jul 2014	9.7	46	W1 to W6	18	Rainfall	98
S7	29 Aug 14	10.7	75	W1 to W6	40	Rainfall	98

S8	18 Oct 2014	3.1	24	W1 to W6	3.3	Rainfall	98
S9	25 Nov 2014	19.1	86	W1 to W6	89.6	Rainfall	81
S10	14 Apr 2015	1.9	6	W1, W4 to W6	0	Snowmelt	90
S11	14 May 2015	3.4	4	W1, W2, W6	0.5	Mixed	90
S12	25 May 2015	4.1	3	W3, W4, W5	0.3	Mixed	90
S13	25 Jun 2015	4.07	2	W2, W4	0.4	Rainfall	90
S14	28 Jul 2015	1.24	0	--		Rainfall	90
S15	19 Sep 2015	11.85	29	W1 to W6	4.9	Rainfall	94
S16	21 Oct 2015	3.89	23	W1 to W6	8.3	Rainfall	89

Table A4.3.3. Recovery rates per survey at Tolvà Creek.

	Survey (TOLVA' CR.)	Qmax [m ³ s ⁻¹]	Mobilized clasts [%]	Mobilized classes	Max travel distance [m]	Inter-survey dominant regime	Recovery rate [%]
S1	28 Jul 2014	1.3	22	W1 to W6	1.25	Rainfall	100
S2	19 Aug 2014	8.1	25	W1 to W6	1.70	Rainfall	98
S3	21 Oct 2014	1.32	17	W1 to W6	4.70	Rainfall	99
S4	27 Nov 2014	28.5	94	W1 to W6	225	Rainfall	80
S5	14 Apr 2015	0.38	6	W1 to W6	0.6	Snowmelt	84

S6	14 May 2015	0.99	5	W1 to W6	0.7	Mixed	84
S7	25 May 2015	1.07	3	W1, W5	0.9	Mixed	84
S8	25 Jun 2015	0.85	0	--	0	Rainfall	84
S9	28 Jul 2015	0.34	0	--	0	Rainfall	84
S10	19 Sep 2015	4.3	26	W1 to W6	22.60	Rainfall	84
S11	21 Oct 2015	1.9	24	W1 to W6	5.40	Rainfall	83

Table A4.3.4. Recovery rates per survey at Ussaia Creek.

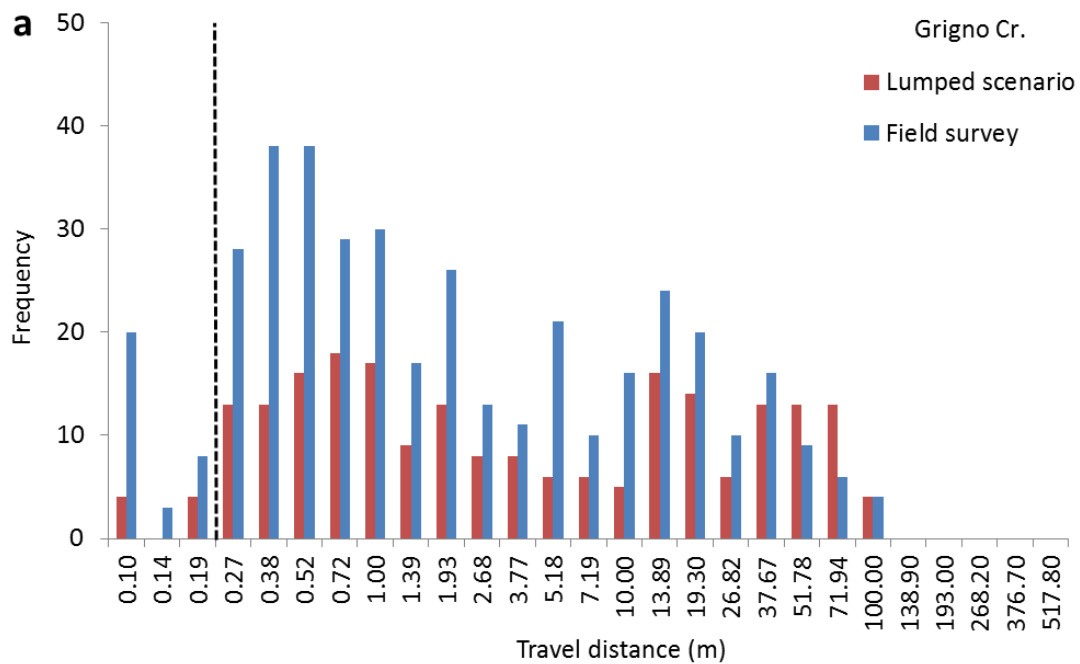
	Survey (USSAIA CR.)	Q _{max} [m ³ s ⁻¹]	Mobilized clasts [%]	Mobilized classes	Max travel distance [m]	Inter-survey dominant regime	Recovery rate [%]
S1	02/04/2013	3.1	29	W1 to W5	219	Mixed	33
S2	25/04/2013	8.2	13	W1 to W5	180	Mixed	21
S3	12/06/2013	1.8	10	W1 to W4	36	Rainfall	26
S4	23/07/2013	3.2	2	W2, W4 to W6	0.2	Rainfall	58
S5	22/08/2013	0.2	1	W2, W6	0.15	Rainfall	58
S6	07/09/2013	1	1	W5, W6	0.2	Rainfall	56
S7	15/10/2013	1.1	17	W1 to W6	11	Rainfall	52
S8	26/10/2013	8.7	19	W1 to W6	332	Rainfall	21
S9	16/11/2013	1.7	Clasts not found	W1 to W6	Clasts not found	Rainfall	22
S10	29/04/2014	0.7	5	W1 to W6	10.3	Snowmelt	48

S11	06/05/2014	1	8	W1 to W6	2.6	Snowmelt	49
S12	03/06/2014	1.2	21	W1 to W6	265	Snowmelt	49
S13	30/06/2014	0.5	3	W1 to W3, W5, W6	3.1	Mixed	40
S14	11/07/2014	0.2	8	W1 to W6	3.1	Rainfall	32
S15	27/07/2014	0.3	11	W1 to W6	1.3	Rainfall	39
S16	18/08/2014	0.4	6	W1 to W6	63	Rainfall	38
S17	20/10/2014	--	5	W1 to W6	206	Rainfall	38
S18	08/11/2014	26	13	W1 to W6	376	Rainfall	13
S19	19/05/2015	0.3	7	W1 to W6	5.8	Mixed	60
S20	26/05/2015	0.4	4	W1 to W4, W6	2.3	Mixed	60
S21	18/06/2015	0.2	2	W1 to W4, W6	0.4	Rainfall	60
S22	29/07/2015	0.1	--	--	--	Rainfall	60
S23	18/08/2015	0.1	--	--	--	Rainfall	60
S24	28/08/2015	0.07	--	--	--	Rainfall	60
S25	15/09/2015	2.1	27.2	W1 to W6		Rainfall	60
S26	25/09/2015	0.31	20.7	W1 to W6		Rainfall	60
S27	22/10/2015	0.32	2	W3, W4, W6		Rainfall	60

Table A4.3.5. Recovery rates per survey at Strimm Creek.

	Survey (STRIMM CR.)	Qmax [m ³ s ⁻¹]	Mobilized clasts [%]	Mobilized classes	Max travel distance [m]	Inter-survey dominant regime	Recovery rate [%]
S1	28 Sep 2011	0.36	3.8	W2, W3, W5	1.2	Rainfall	100
S2	14 Jun 2012	0.66	27.7	W1 to W6	4.5	Snowmelt	100
S3	3 Jul 2012	0.55	4.6	W1, W2	3.4	Snowmelt	100
S4	11 Sep 2012	0.33	17.3	W1 to W5	3.9	Rainfall	98.5
S5	4 Oct 2012	0.32	4.3	W1 to W3	1.6	Rainfall	97.7
S6	27 Jun 2013	1.13	50.8	W1 to W6	35	Snowmelt	93.4
S7	1 Oct 2013	0.72	38.1	W1 to W6	12	Mixed	92.3
S8	13 Jun 2014	0.95	40.6	W1 to W6	23.9	Snowmelt	90.3

Appendix A5.1



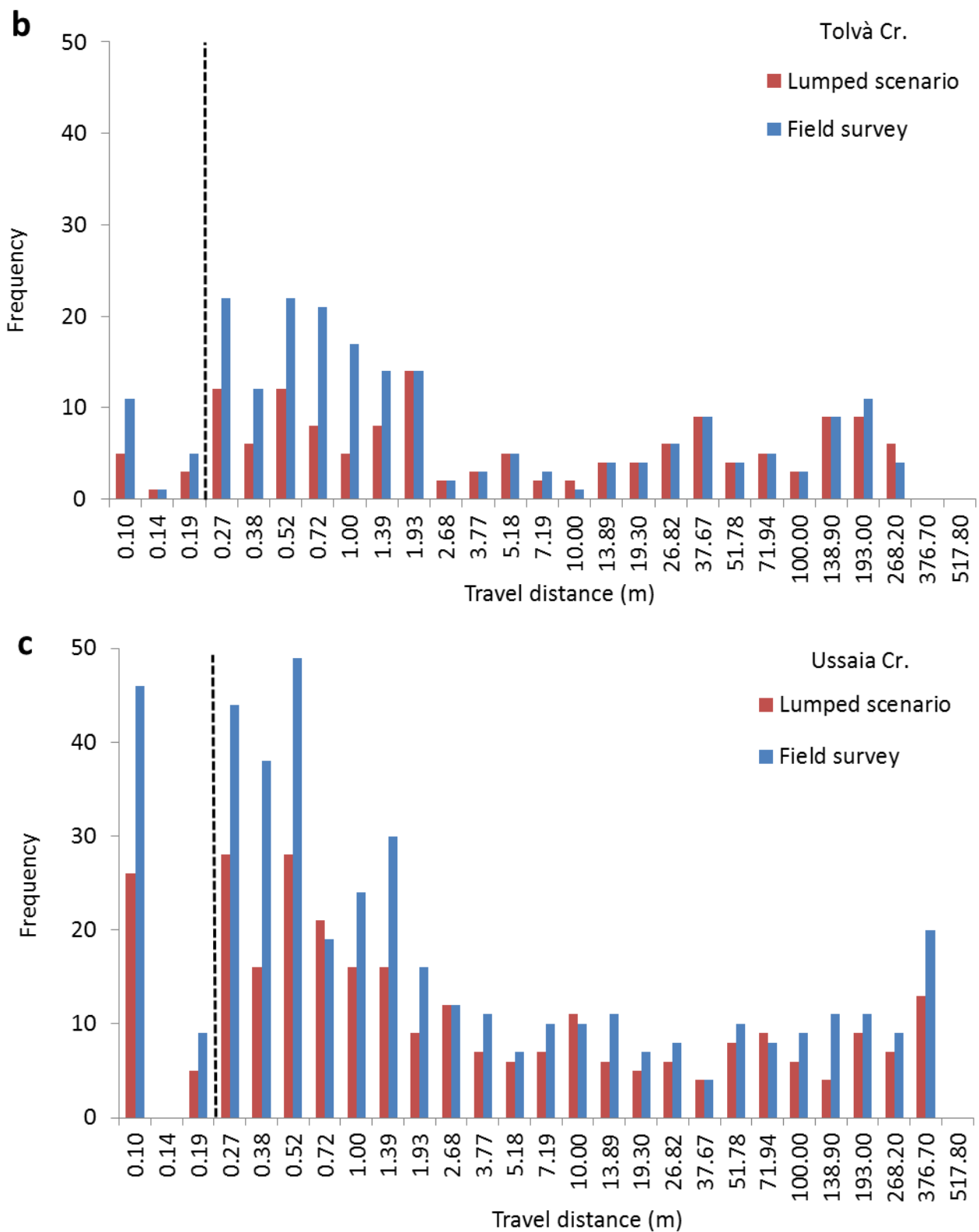
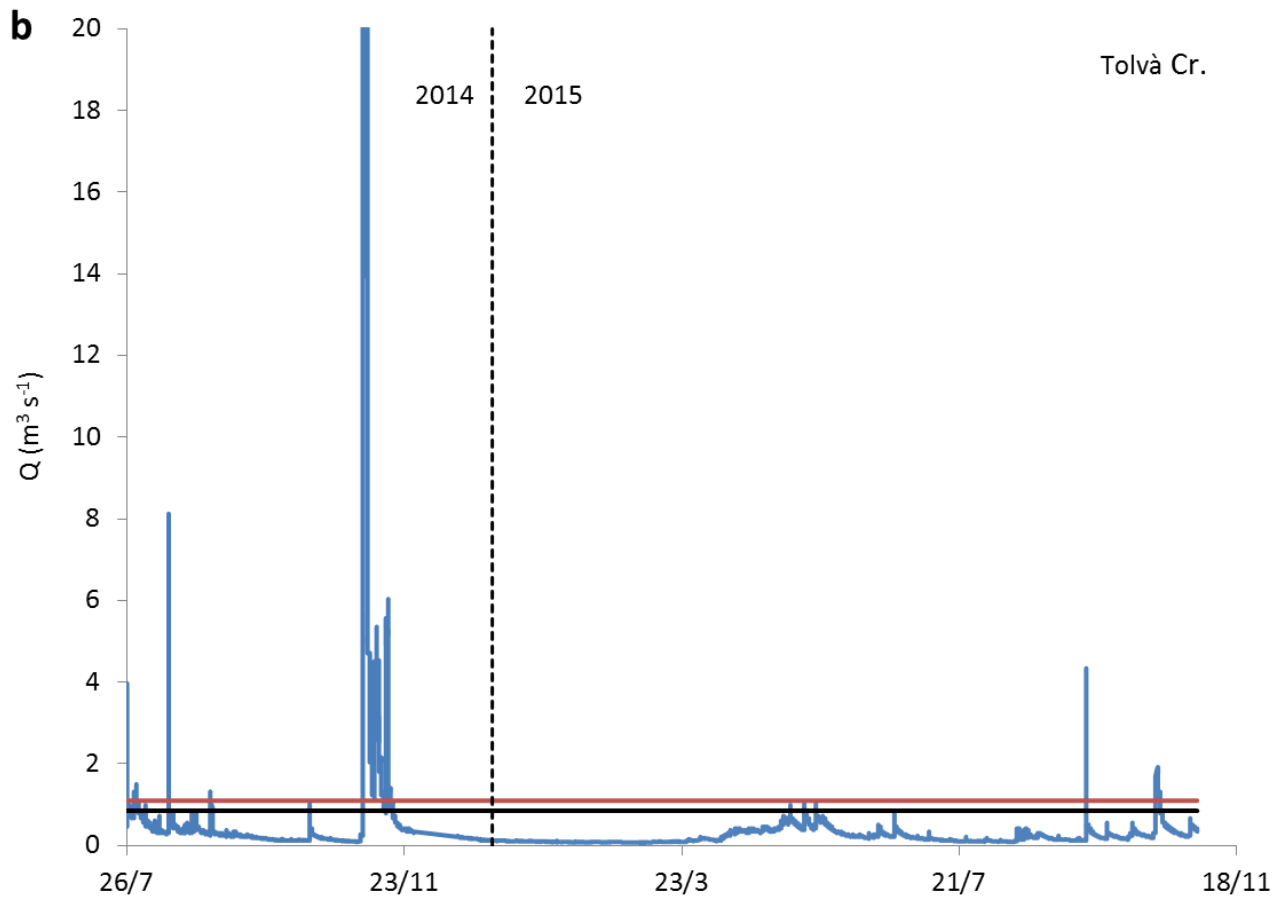
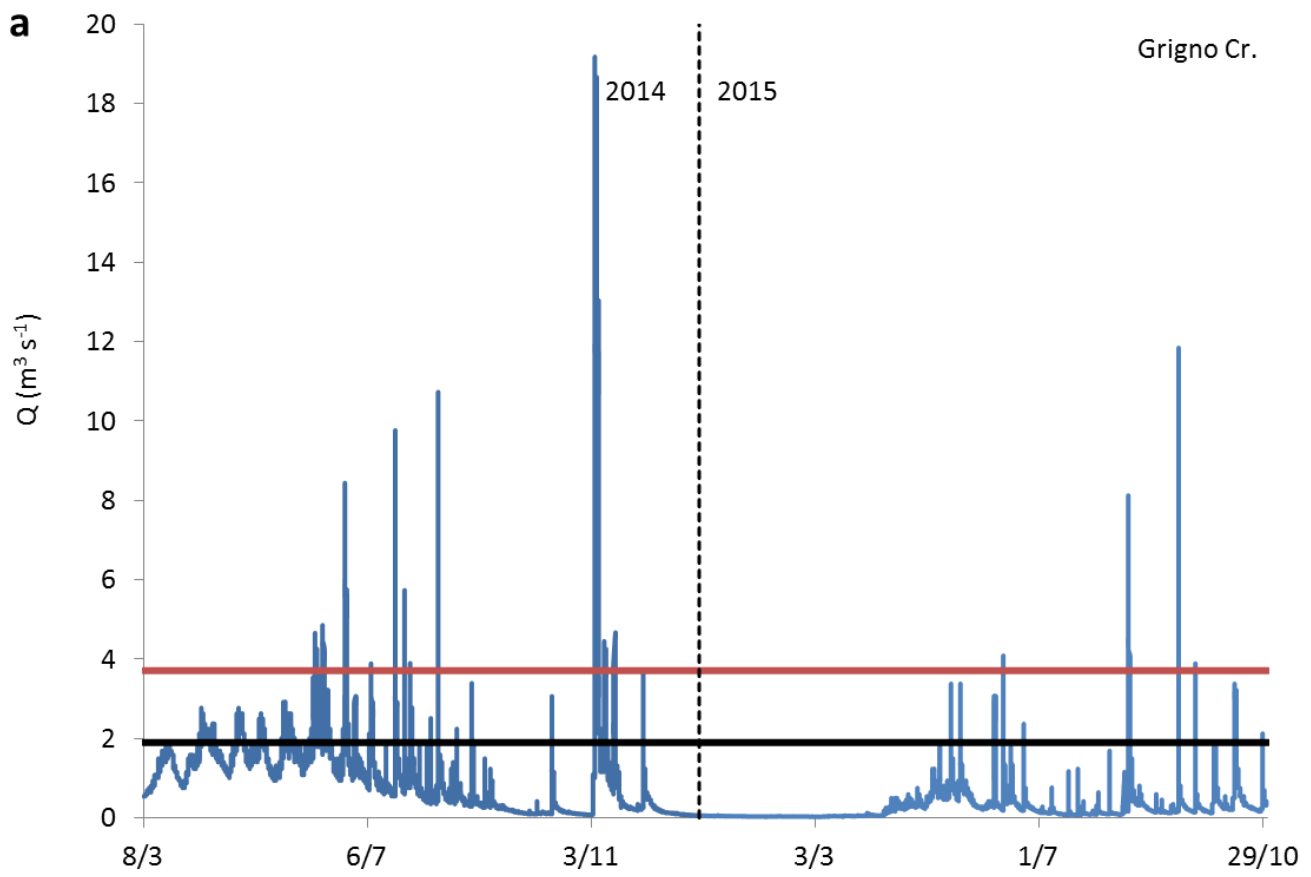


Figure A5.1. Frequency distributions of tracers' travel distance obtained from the actual field surveys and from the seasonally lumped scenario) at: (a) Grigno Creek; (b) Tolvà Creek; and (c) Ussaia Creek.



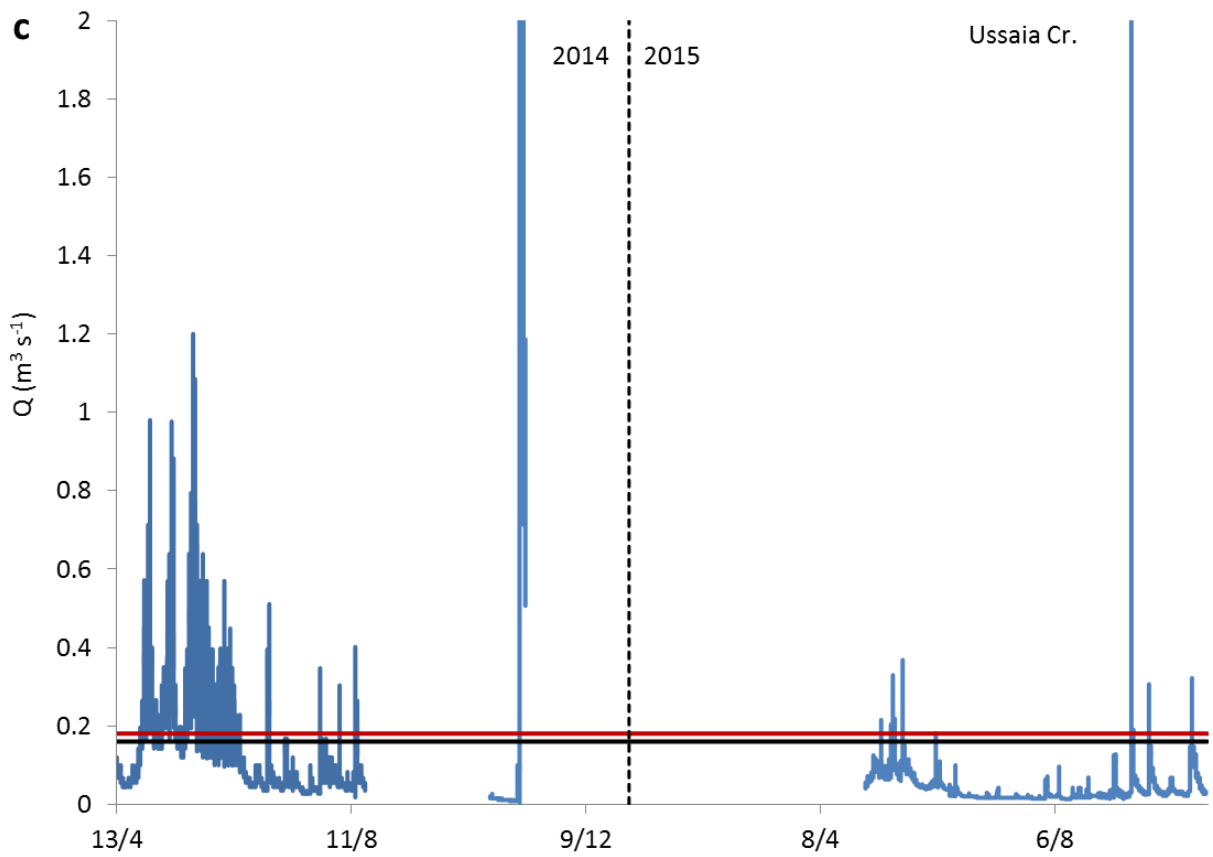
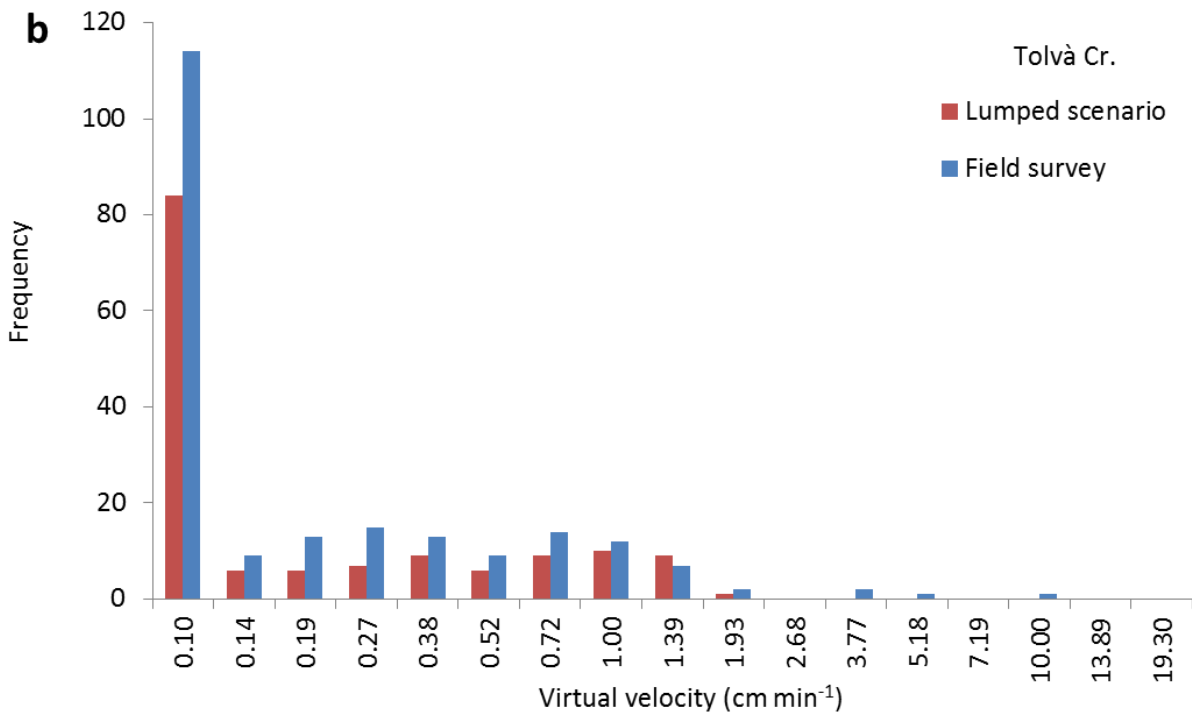
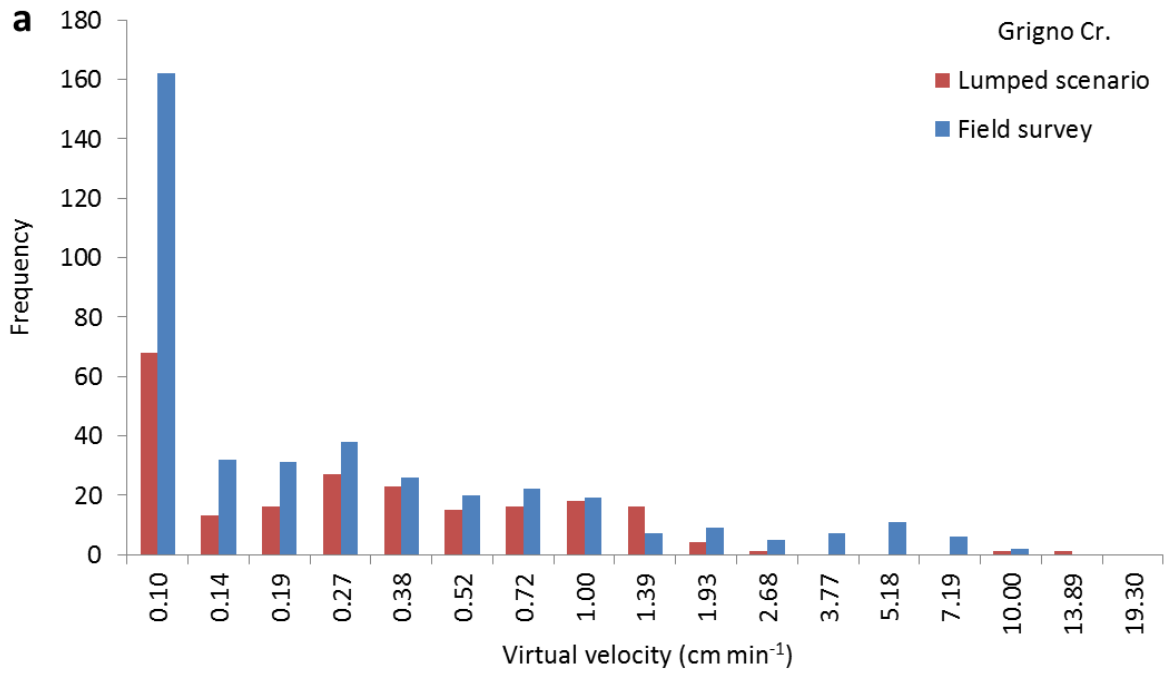


Figure A5.2. Example of threshold discharges obtained from the actual field surveys (black line) and from the seasonally lumped scenario (red line) at (a) Grigno; (b) Tolvà Creek; and (c) Ussaia Creek.



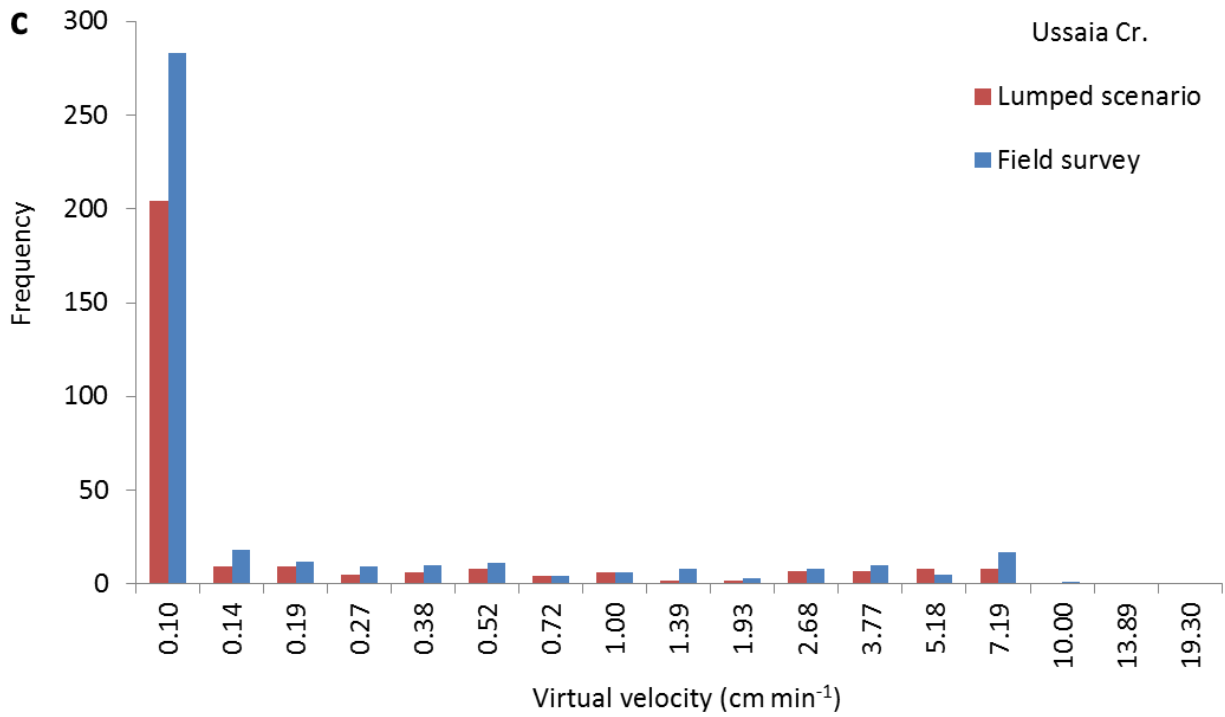


Figure A5.3. Frequency distributions of tracers' travel distance obtained from the actual field surveys and from the seasonally lumped scenario) at: (a) Grigno Creek; (b) Tolvà Creek; and (c) Ussaia Creek.